

Design and Synthesis of Multifunctional Dopamine D₂/D₃ and Histamine H₃ Receptor Ligands

Inaugural-Dissertation

zur Erlangung des Doktorgrades
der Mathematisch-Naturwissenschaftlichen Fakultät
der Heinrich-Heine-Universität Düsseldorf

vorgelegt von

Milica Elek
aus Bajina Basta

Düsseldorf, 2021

aus dem Institut für Pharmazeutische und Medizinische Chemie
der Heinrich-Heine-Universität Düsseldorf

Gedruckt mit der Genehmigung der
Mathematisch-Naturwissenschaftlichen Fakultät der
Heinrich-Heine-Universität Düsseldorf

Printed and published with the support of German Academic Exchange Service.

Berichterstatter:

1. Univ. Prof. Dr. Dr. h.c. Holger Stark

2. Univ. Prof. Dr. Holger Gohlke

Tag der mündlichen Prüfung: 20.12.2021

To my grandmother

Acknowledgments

This PhD project was carried out under Prof. Dr. Dr. h.c. Holger Stark's supervision at the Institute for Pharmaceutical and Medicinal Chemistry at Heinrich - Heine University Duesseldorf, Germany.

I would like to express my deepest gratitude to:

- Prof. Dr. Dr. h.c. Holger Stark for providing me constant support in challenging and exciting projects and always giving me new ideas, motivation, and constructive criticism. I am delighted that I could be part of his working group, where I could broaden my knowledge and horizons and develop myself as a scientist.
- German Exchange Academic Service (DAAD), which scholarship I hold, for providing financial support.
- Dr. Aleksandra Zivkovic for her outstanding support during the entire time of the PhD. Her suggestions and critics helped me expand not only my chemical but also my life knowledge! Thank you for your tough love and for being my dearest friend and support. HVALA!
- Prof Dr. Holger Gohlke, my mentor, for reading and evaluating this PhD thesis.
- Associate Professor Katarina Nikolic, and Assistant Professor Slavica Filipic for their assistance in obtaining DAAD Scholarship and performed molecular modeling, together with my dear colleague Nemanja Djokovic.
- Prof Dr. Thomas J.J. Müller and Laura Mayer for determination of optical properties of compounds.
- All my old and new colleagues for providing such a nice working atmosphere and joyful moments. Dr. David Reiner-Link, Dr. Annika Frank, and Mariam Dubiel for carrying out *in vitro* experiments. Kathrin Grau, for her outstanding support over the years and always fun and interesting conversation. Dr. Stefanie Hagenow for scientific discussion and reading this thesis. My lab colleagues: Dr. Jens Hagenow and Dr. Markus Falkenstein, for providing an ideal working environment in the laboratory. Dr. Kiril Lutschenko, Sicheng Zhong, Cristian di Biase, Dr. Hjördis Brückmann, Luisa Leitzbach, Lars Seiffet, Markus Schultes, Patrick Krolikowski. It was a pleasure working with you.
- My friends Ivana and Nikolina, who were great support in the last years.

- My family in Serbia, and my best friends, especially to Milena, Ljilja, Milan, and Djuka, for their believing in me.
- And my most enormous thanks go to my mom, my most significant support for everything. Hvala ti Kokice, bez tebe nista od ovoga ne bi bilo moguće!

Affidavit

Ich versichere dass an Eides Statt, dass die Dissertation von mir selbständig und ohne unzulässige fremde Hilfe unter Beachtung der Grundsätze zur Sicherung guter wissenschaftlicher Praxis an der Heinrich-Heine-Universität Düsseldorf erstellt worden ist.

M. Fleck

Contents

ACKNOWLEDGMENTS	i
AFFIDAVIT	iii
ABBREVIATIONS	vi
1 INTRODUCTION	1
1.1 DOPAMINE	2
1.1.1 Biosynthesis and Metabolism	2
1.1.2 Dopamine Pathways in the Human Brain	5
1.1.3 Dopamine Receptors	8
1.1.4 Dopamine D ₂ Receptor	12
1.1.5 Dopamine D ₃ Receptor	17
1.2 SCHIZOPHRENIA	23
1.3 PARKINSON'S DISEASE	27
1.4 HISTAMINE	32
1.4.1 Histamine Receptors	32
1.4.2 Histamine H ₃ Receptor	34
1.5 SLEEP-WAKE DISORDERS	38
1.6 MULTI-TARGET-DIRECTED LIGANDS	39
1.7 OBJECTIVES	43
2 CHEMISTRY	45
2.1 STANDARD REACTION AND CHEMICAL APPROACHES	46
2.2 D ₃ R LIGANDS WITH THE ANTAGONIST MOIETY	46
2.2.1 Amide Synthesis	51
2.3 D ₂ R AND D ₃ R BITOPIC LIGANDS	52
2.3.1 D ₂ R and D ₃ R Ligands with Amide Moiety	52
2.3.2 D ₂ R and D ₃ R Ligands Connected with Methylene Groups as Spacer	55
2.3.3 Reductive Amination	57
2.3.4 Optimization of Bitopic Ligands	58
2.4 D ₂ R AND H ₃ R MULTITARGETING LIGANDS	64
2.5 D ₃ R AND H ₃ R RECEPTOR LIGANDS	69
2.6 FLUORESCENT DOPAMINE AND HISTAMINE RECEPTOR LIGANDS	76
2.6.1 D ₃ R Fluorescent Ligands	77
2.6.2 H ₃ R Fluorescent Ligands	79
2.7 DETERMINATION OF FLUORESCENT PROPERTIES	81
2.7.1 Fluorescent Dyes and their Field of Application	81
2.7.2 Dopamine Receptor Fluorescent Ligands	85
2.7.3 Histamine Receptor Fluorescent Ligands	90
2.8 SUMMARY OF CHEMISTRY PART	93
3 COMPUTER-AIDED DRUG DESIGN	95
3.1 MOLECULAR DOCKING SIMULATIONS	97
3.2 QM/MM CALCULATIONS	100
3.3 NON-COVALENT INTERACTION ANALYSIS	102

4	PHARMACOLOGY AND DISCUSSION	105
4.1	PHARMACOLOGICAL EVALUATION	106
4.2	IN VITRO BINDING AFFINITY DETERMINATION	106
4.3	ANTIOXIDATIVE CAPACITY MEASUREMENT	110
4.4	DRUG-LIKENESS EVALUATION.....	111
4.5	STRUCTURE-ACTIVITY RELATIONSHIPS OF SELECTIVE D ₃ R LIGANDS	113
4.6	STRUCTURE-ACTIVITY RELATIONSHIPS OF BITOPIC D ₂ R AND D ₃ R LIGANDS	119
4.7	STRUCTURE-ACTIVITY RELATIONSHIPS OF BIOSOSTERIC COMPOUNDS	126
4.8	STRUCTURE-ACTIVITY RELATIONSHIPS OF MULTITARGETING D _{2/3} R AND H ₃ R LIGANDS	131
4.9	STRUCTURE-ACTIVITY RELATIONSHIPS OF MULTITARGETING D ₃ R AND H ₃ R LIGANDS	137
4.10	STRUCTURE-ACTIVITY RELATIONSHIPS OF FLUORESCENT LIGANDS	141
5	SUMMARY	147
6	EXPERIMENTAL SECTION.....	153
6.1	CHEMICAL EXPERIMENTS	154
6.2	GENERAL PROCEDURES	158
6.3	MOLECULAR DOCKING SIMULATION	209
6.3.1	Protein Preparation	209
6.3.2	QM/MM Calculations.....	209
6.3.3	Non-Covalent Interaction Calculations.....	210
6.4	PHARMACOLOGICAL EXPERIMENTS	211
6.4.1	Cell Culture and Membrane Preparation of CHO-K1 Cells expressing the hD _{2s} R and the hD ₃ R.....	211
6.4.2	Radioligand Displacement Assay at D _{2short} R and D ₃ R on CHO-K1 Cell Line Preparation	211
6.4.3	hH ₃ R [³ H]-N ^α -methylhistamine Binding Assay on HEK-293 Cell Membrane Preparation	212
6.4.4	Oxygen Radical Absorbance Capacity Assay.....	213
7	REFERENCES	215
8	LIST OF PUBLICATIONS	245
9	CURRICULUM VITAE	247

Abbreviations

3-MT	3-methoxytyramine
5-HT	5-hydroxytryptamine
AAAD	aromatic amino acid decarboxylase
AAPH	2,2'-azobis(2-amidinopropane) dihydrochloride
AC	adenylyl cyclase
AChE	scetylcholinesterase
AUC	area under the curve
ACN	acetonitrile
AD	Alzheimer's disease
ADHD	attention deficit hyperactivity disorder
ADME	absorption, distribution, metabolism, and excretion
ALDH	aldehyde dehydrogenase
BBB	blood/brain barrier
BDNF	brain-derived neurotrophic factor
B-PE	B-phycoerythrin
B-PE	B-phycoerythrin
BRET	bioluminescence resonance energy transfer
BOC	<i>tert</i> -butyl carbamate
CADD	computer-aided drug design
cAMP	3',5'-cyclic adenosine monophosphate
CDI	<i>N,N'</i> -carbonyldiimidazole
CHO	Chinese hamster ovary
CI	confidence interval
CNS	central nervous system
COMT	catechol- <i>O</i> -methyltransferase
D ₂ R	dopamine D ₂ receptor
D ₃ R	dopamine D ₃ receptor
DAT	dopamine transporter
DCE	1,2-dichloroethane
DCM	dichloromethane
DIPEA	<i>N,N</i> -diisopropylethylamine
DHB	dihydrobiopterine
DMEM	Dulbecco's Modified Eagle Medium-high glucose
DMF	<i>N, N</i> -dimethylformamide
DMSO	dimethyl sulfoxide
DOPA	3,4-dihydroxyphenylalanine
DOPAC	3,4-dihydroxyphenylacetic acid
DOPAL	3,4-dihydroxyphenylacetaldehyde
DSM	Diagnostic and Statistical Manual of Mental Disorder

EBP	extended binding pocket
ECT	electroconvulsive therapy
EDC	1-Ethyl-3-(3-dimethylaminopropyl)carbodiimide
EL2	extracellular loop 2
EMA	European Medicines Agency
EPS	electrostatic potentials
Et ₃ N	triethylamine
EtOH	ethanol
ERK	extracellular signal-regulated kinase
ESP	electrostatic potentials
FBS	fetal bovine serum
FDA	Food and Drug Administration
FGA	first-generation antipsychotics
FRET	Förster resonance energy transfer
GABA	γ-aminobutyric acid
GDP	guanosine diphosphate
GIRK	G-protein-regulated inwardly rectifying potassium channel
GPCR	G-protein coupled receptor
GRK	G-protein kinases
GSK	glycogen synthase kinase 3
GTP	guanosine triphosphate
HR	histamine receptors (H ₁ R-H ₄ R)
HAC	hydrogen bond acceptor
HDC	histamine decarboxylase
HDO	hydrogen bond donor
HEK	human embryo kidney
HNMT	histamine N ^α -methyltransferase
HOBt	1-hydroxy-1 <i>H</i> -benzotriazole hydrate
HOMO	highest occupied molecular orbital
HTS	high-throughput screening
HVA	homovanillic acid
INN	international nonproprietary name
<i>i.v.</i>	intravenous
<i>i.p.</i>	intrapertioneal
IP3	inositol-1,4,5-trisphosphate
LB	ligand-based
LC	liquid chromatography
LID	<i>L</i> -Dopa-induced dyskinesia
LUMO	lowest unoccupied molecular orbital
MAO	monoamine oxidase

MAPK	mitogen-activated protein kinase
MD	molecular docking
MDS	Movement Disorder Society
MeOH	methanol
MDS	International Parkinson and Movement Disorder Society
MPTP	1-Methyl-4-phenyl-1,2,3,6-tetrahydropyridinium
MTDL	multi-target-directed ligands
MS	mass spectrometry
MSN	medium spiny neurons
MW	molecular weight
NAM	negative allosteric modulator
NCI	non-covalent interaction
NDDO	neglect of differential diatomic overlap
NIR	near-infrared spectroscopy
NMR	nuclear magnetic resonance
OBS	orthosteric binding site
ORAC	Oxygen Radical Absorbance Capacity
PAM	positive allosteric modulator
PET	positron emission tomography
PD	Parkinson's disease
PI3K	phosphatidylinositol 3-Kinase
PKA	protein kinase A
PKC	protein kinase C
PMB	<i>p</i> -methoxybenzyl
PP	primary pharmacophore
PP1	protein phosphatase 1
PP2A	protein phosphatase 2A
PPHT	phenylethyl-propyl-hydroxytetraline
PSA	polar surface area
QM/MM	quantum mechanic/molecular mechanic
REM	rapid eye movement
Ro5	Lipinski's rule of five
ROS	reactive oxygen species
SAR	structure-activity relationships
SB	structure-based
SBP	secondary binding pocket
<i>s.c.</i>	subcutaneous
SCF	self-consistent field
SCR	structurally conserved regions
SD	standard deviation

SGA	second-generation antipsychotics
SF ₅	pentafluorosulfanyl
SI	selectivity index
SN	substantia nigra
SNpc	substantia nigra pars compacta
SP	secondary pharmacophore
SPECT	single photon emission computed tomography
TBDMS	<i>tert</i> -butyldimethylsilyl
THB	tetrahydrobiopterin
THF	tetrahydrofuran
TLC	thin-layer chromatography
TM	transmembrane domaine
TSA	total surface area\
VMAT 2	vesicular monoamine transporter 2
VTA	ventral tegmental area
WHO	World Health Organisation

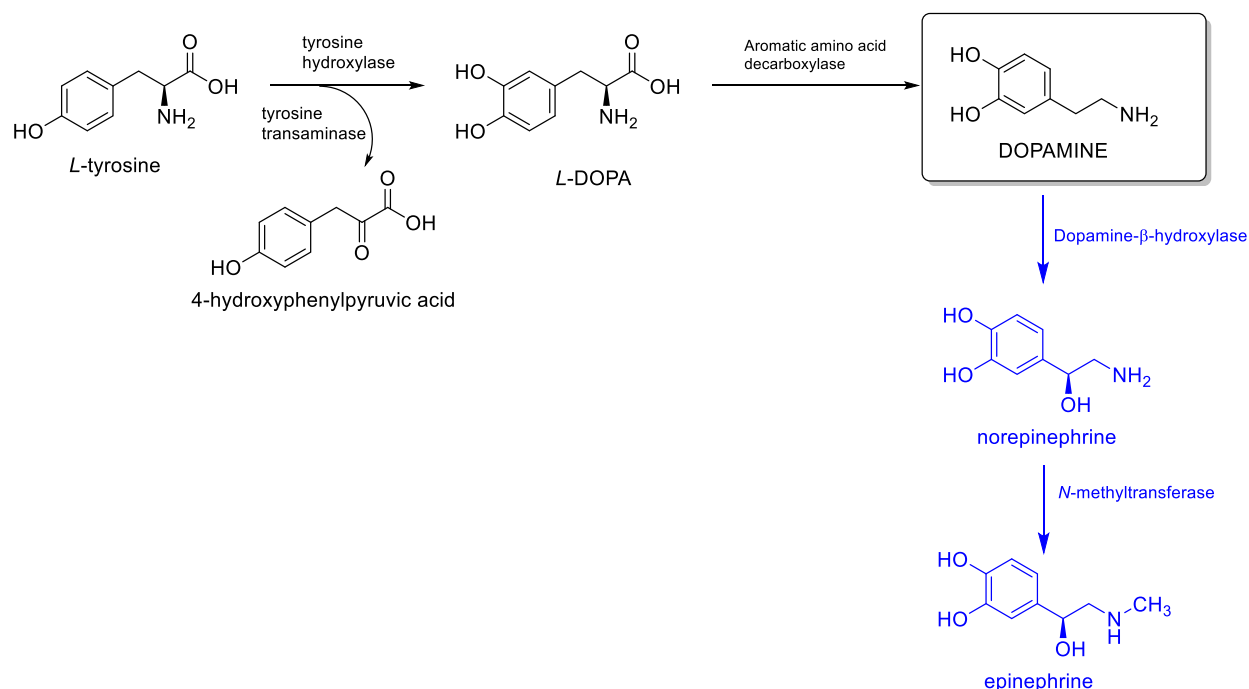
1 Introduction

1.1 Dopamine

1.1.1 Biosynthesis and Metabolism

Dopamine is one of the essential neurotransmitters in the human brain that regulates processes like motor function, emotion, reward, or cognition. Therefore, the altered dopamine concentration and consequently modified signal transduction can lead to severe pathophysiological conditions such as Parkinson's disease (PD), restless legs syndrome, addictive behavior, schizophrenia, attention deficit hyperactivity disorder (ADHD), Huntington's chorea, or obesity. Even though dopamine was described at the beginning of the 19th century,¹ it was first recognized as an independent neurotransmitter in the early 1960s by Carlsson et al. This working group observed the effect of 3,4-dihydroxyphenylalanine (DOPA) injection in mice, as well as their antagonizing effects on reserpine.² This scientific breakthrough granted Carlsson together with Kandel, and Paul Greengard the Nobel Prize for Physiology and Medicine in 2000.

The biosynthesis of dopamine and other catecholamines (epinephrine and norepinephrine) starts from *L*-tyrosine (Scheme 1). Tyrosine is firstly hydroxylated by tyrosine hydroxylase to *L*-DOPA, in the rate-limiting step in biosynthesis.² Tyrosine can, however, partly undergo transamination by tyrosine transaminase to 4-hydroxyphenylpyruvic acid. Tyrosine hydroxylase is an enzyme with four catalytical subunits that expresses a high level of short-term and long-term regulation.³ By phosphorylation of serine residues, the enzyme is activated, and it is inhibited by *L*-phenylalanine.⁴ Tyrosine hydroxylase specifically converts tyrosine to *L*-DOPA, while tryptophan, phenylalanine, or substituted tyrosine are not substrates of this enzyme. *L*-DOPA is an essential precursor and nowadays widely used as a therapeutic agent in PD. *L*-DOPA is further decarboxylated by aromatic amino acids decarboxylase (AAAD, sometimes referred to as DOPA decarboxylase) to dopamine. DOPA decarboxylase is a non-specific enzyme that decarboxylates almost all amino acids like phenylalanine, tryptophan, or tyrosine. It is both pre and post-translationally regulated (e.g., by dopamine agonists or antagonists).⁵⁻⁷ Even though this reaction step is not rate-limiting under physiological conditions, it is crucial in PD patients.⁷ Dopamine can be further converted by the dopamine- β -hydroxylase, in the presence of ascorbic acid, to norepinephrine. Dopamine- β -hydroxylases are inhibited by various chelating agents.⁸ Norepinephrine is consequently converted by *N*-methyltransferase to epinephrine,⁹ with *S*-adenosyl methionine as methyl group donor. Dopaminergic neurons, however, do not express dopamine- β -hydroxylases, and therefore dopamine is the final product of the catecholamine synthesis in these neurons.¹⁰

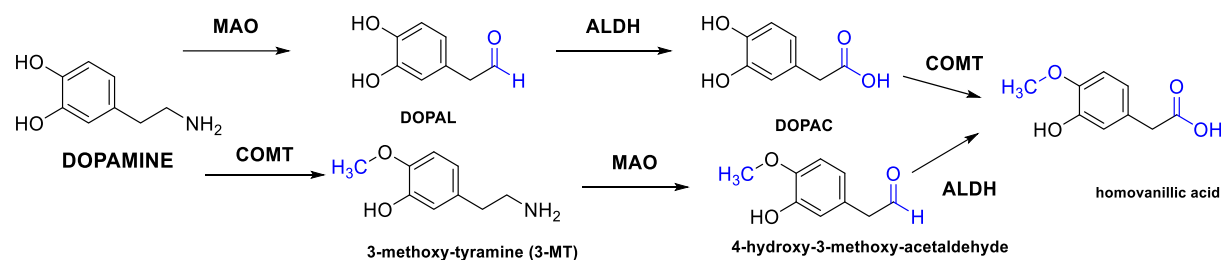


Scheme 1: Biosynthesis of catecholamines. Adapted from Daubner et al.,² Berry et al.⁶

The degradation of dopamine is mediated by monoamine oxidase (MAO) and catechol-*O*-methyl transferase (COMT, Scheme 2). MAO converts dopamine to 3,4-dihydroxyphenylacetaldehyde (DOPAL),¹¹ and in this reaction, one molecule of hydrogen peroxide is generated. The aldehyde can be further either reduced to the corresponding alcohol or oxidized to 3,4-dihydroxyphenylacetic acid (DOPAC).^{12,13} MAO is found in mitochondria and exists in two isoforms MAO A and MAO B, that differ in coding genes,¹⁴ expressions, and affinity to substrates.¹⁵ For instance, serotonin is mainly metabolized by the MAO A isoforms, which are inhibited by commercially available antidepressants (e.g., moclobemide).¹⁶ On the other hand, biogenic amines like dopamine, are substrates for the MAO B isoforms. MAO B inhibitors are established agents in the treatment of PD (e.g., rasagiline, selegiline).

It was long hypothesized that oxidative deamination by MAO is the only way of catecholamine degradation. However, Axelrod et al. reported that catecholamines could also be metabolically converted by the enzyme that transfers methyl group,^{17,18} hypothesizing a new metabolic pathway. In this reaction, COMT converts dopamine to 3-methoxytyramine (3-MT). Different COMT isoforms are products of genetic polymorphism. Several studies hypothesized that this enzyme is involved in dopamine regulation, as the COMT valine allele can increase the risk for cognitive

impairments or developing schizophrenia.¹⁹ The inactive dopamine metabolic products, DOPAC and 3-MT, are converted to homovanillic acid (HVA). The latter can be further used as a marker to determine dopamine metabolism rate,²⁰ or as a biomarker in neurological diseases, due to decreased HVA levels that were *post mortem* confirmed in patients with dementia and Alzheimer's disease (AD).²⁰ All dopamine metabolic products enter phase II metabolism (glucuronidation, sulfo-conjugation) and are excreted.



Scheme 2: Metabolic pathway of dopamine. ALDH: aldehyde dehydrogenase; COMT-catechol-*O*-methyltransferase; DOPAC: 3,4-dihydroxyphenylacetic acid; MAO-monoamine oxidase. Adapted from Meiser et al.¹¹

The presented pathway is considered the main metabolic pathway for dopamine. However, other metabolic routes were proposed. Funae et al.²¹ suggested direct tyramine conversion to dopamine via CYP2D6, and the hypothesis was *in vivo* confirmed by Bromek et al. more than a decade later.²² The biosynthesis of dopamine can, to a lesser extent, begin from essential amino acid *L*-phenylalanine, brought into the organism by dietary intake, converted by phenylalanine hydroxylase to tyrosine. Nevertheless, this conversion occurs only at low tyrosine levels. Altered dopamine concentration and metabolic pathway changes are associated with numerous neurological diseases such as PD, AD, Huntington's chorea, schizophrenia, or addictive behavior. Hydrogen peroxide, formed in the metabolic pathway, is further converted to a highly toxic hydroxyl radical (OH^\bullet), which belongs to the reactive oxygen species (ROS). ROS are usually neutralized by defending cell mechanisms like glutathione, citrulline, or dismutase. The catecholamine group displays antioxidant properties itself and can be oxidized by ROS.²³ When scavengers' capacities are exhausted, ROS accumulate in the cell and this can lead to oxidative stress, consequent neuroinflammation, and cell denaturation. These processes play significant roles in neurodegeneration and cognitive impairments as observed in PD or AD.²⁴ In order to determine catecholamine ration and their metabolic rate, which can further influence above mentioned processes in the brain, catecholamines can be labeled with hydrogen or carbon

isotopes.²⁵ Dopamine can also be converted in the presence of metal ions²⁶ to quinone, a yellow substance that undergoes rearrangement to leucoaminochrome²⁷ and finally to neuromelanin, the dark pigment responsible for the coloring in the *substantia nigra* or the *locus ceruleus*.²⁸

1.1.2 Dopamine Pathways in the Human Brain

Dopamine exerts its action both centrally and peripherally. Dopamine is peripherally synthesized in sympathetic neurons or adrenal medulla and cannot cross the blood-brain barrier (BBB). It is hypothesized that dopamine is involved in several processes such as immune response reactions (it is present in T and B lymphocytes),²⁹ Na⁺ transport and consequent blood pressure regulation,³⁰ mesenteric modulations,³¹ or regulation of pancreatic hormones.³² Dopamine can peripherally be found only in the form of sulfo- or glucurono-conjugates and to a lesser extent in an unbound form.³³ There are four dopamine pathways in the central nervous system (CNS) (Figure 1). Nigrostriatal, mesolimbic, and mesocortical originate from the mesencephalon, whereas tuberoinfundibular stretches out from the diencephalon.

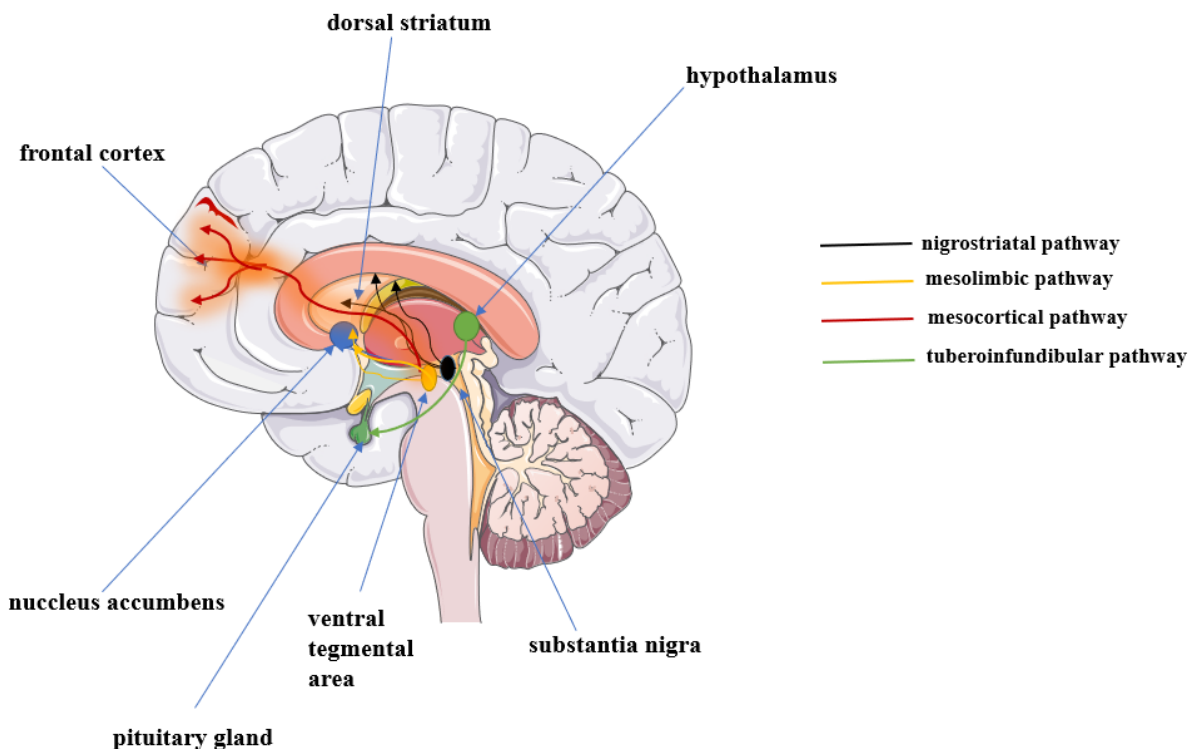


Figure 1: Dopamine pathways in the human brain.

The nigrostriatal pathway extends from *substantia nigra pars compacta* (SNpc) to the *dorsal striatum* (*caudate nucleus* and *putamen*). SN is translated from Latin as the black substance due to the high neuromelanin concentration. Dopamine neurons in the CNS are grouped into different nuclei, and in the SNpc, they form nucleus A9.³⁴ SNpc is located in the midbrain (Greek *meso* = middle, *enkephalos* = brain) and besides dopaminergic exhibits γ -aminobutyric acid (GABA) neurons,³⁵ that suppress dopamine release³⁶ and control dopamine concentration in the synaptic cleft. This initial hypothesis was later confirmed by the administration of GABA antagonists that resulted in increased dopamine release.³⁷ The nigrostriatal pathway is associated with voluntary movement and sensory stimuli. In PD, over 80% of dopamine neurons in SNpc are degenerated before symptoms manifest, and the remaining dopamine neurons are infiltrated with neuronal inclusions-Lewy bodies.³⁸ Consequently, typical PD-associated motor symptoms such as tremor, rigidity, or bradykinesia occur.

Involvement of the nigrostriatal pathway in schizophrenia has been recently hypothesized. Patients suffering from schizophrenia demonstrated a high level of striatal dopamine, proven by *post mortem* analyses.^{39,40} Elevated biosynthesis of dopamine can be one reason for this phenomenon, as an elevated level of rate-limiting enzyme tyrosine hydroxylase was confirmed in patients suffering from psychosis.⁴¹ In the literature, however, inconsistent results are reported, and involvement of nigrostriatal pathway in schizophrenia etiology is yet to be thoroughly examined.

The mesolimbic pathway extends from the ventral tegmental area (VTA) in the midbrain to the basal ganglia in the forebrain. (*nucleus accumbens* and the olfactory bulb). It is associated with the processes such as pleasure, reward, emotional, and seeking behavior. It is often referred to as the "reward pathway". Reward induces pleasure feeling and increases interest in learning about the stimulus, and can ultimately lead to craving or seeking behavior.⁴² Hyperactivation of the mesolimbic pathway can lead to aggressive behavior, as shown by Anstorm et al., where dopamine firing is more frequent in a life-threatening situation.⁴³

Different emotions (pleasure, reward, fear) lead to the dopamine burst firing, extensive and fast dopamine release in the synaptic cleft. This process is highly regulated via cellular mechanisms involving glutamate⁴⁴ and acetylcholine,⁴⁵ when awake and asleep.⁴⁶ Dopamine released in burst firing undergoes fast reuptake,⁴⁸ (phasic dopamine release) in a process that is limited to the synaptic cleft. On the other hand, tonic dopamine release is a slow process that occurs

extrasynaptically and spontaneously.⁴⁷ Dopamine neurons in the mesolimbic pathway release dopamine in a burst firing manner, with high frequency as a reaction to stimuli (somatosensory, visual, or audible) or as preparation for the reward observed by substance abuse.⁴⁸

Positive stimuli (e.g., cocaine) initiate a reward cascade and consequent intense reaction via hypersensitization of dopaminergic receptors.⁴⁹ This leads to neuroadaptation and neuroplasticity closely associated with recurring cocaine relapse.⁵⁰ Substance abuse is a chronic disorder with a high relapse rate. Hence, various efforts have been centered around designing novel ligands that target the mesolimbic pathway and can be used as pharmacological tools in treating addictive behavior.

According to the "mesolimbic hypothesis" hyperactivity in this region leads to the positive symptoms of schizophrenia such as delusions, hallucinations, disorganized thinking, and speech. Dopamine involvement in schizophrenia was postulated decades ago.⁵¹ All commercially available antipsychotics act as dopamine D₂ receptor (D₂R) antagonists or partial agonists. Antagonism at D₂R leads ultimately to their desensitization, confirmed with the bioimaging techniques (e.g., PET or SPET).⁵² However, due to their lack of selectivity, dopamine D₂R antagonism in other dopamine pathways leads to serious side effects such as extrapyramidal syndrome (EPS), hyperprolactinemia, or sexual dysfunction.

The mesocortical pathway stretches out from the *ventral tegmentum* to the *prefrontal cortex* and is associated with cognition, working memory, motivation, attention, emotional behavior, learning, and decision making.^{53,54} It is often described together with a mesolimbic pathway as mesocorticolimbic. Besides dopaminergic, glutamatergic neurons that impact dopamine release are present in this pathway.⁵⁵ Receptor desensitization in the mesocortical pathway leads to negative symptoms of schizophrenia: apathy, loss of motivation, disinterest or lack of enjoyment in daily activities, or social withdrawal, which are more challenging to diagnose and treat.

Tuberoinfundibular pathway stretches out from the hypothalamus (*arcuate nucleus*) to median eminence and regulates prolactin release from the pituitary gland. Prolactin is a protein that triggers lactation, and in this pathway, dopamine inhibits prolactin release. Non-selective first-generation antipsychotics (FGA) block dopamine receptors in the tuberoinfundibular pathway and cause side effects like hyperprolactinemia, sexual dysfunction, galactorrhea, or amenorrhea.⁵⁶

However, second-generation antipsychotics (SGA) reduced risk of these side effects due to their improved selectivity.⁵⁷

1.1.3 Dopamine Receptors

Neurotransmitters are signaling molecules in the human brain, which release is triggered by chemical or electrical stimuli. Neurotransmitters are stored inside neurons and released by exocytosis. All known neurotransmitters can be divided into two different groups. Fast neurotransmitters (e.g., glutamate, glycine-excitatory, or GABA-inhibitory) transduce the signal to the target cell in milliseconds.⁵⁸ In contrast, slow neurotransmitters (e.g., biogenic amines or amino acids), which release is regulated by more complex processes, act through various second messenger (e.g., protein kinases or phosphatases, Ca^{2+}).⁵⁹ As biogenic amine, dopamine belongs to slow neurotransmitters synthesized both centrally and peripherally. Vesicular monoamine transporter 2 (VMAT-2)⁶⁰ stores dopamine in vesicles, releasing it upon stimulation in the synaptic cleft (Figure 2). The vesicular monoamine transporter was cloned at the beginning of the 1990s. It expresses two isoforms, where only VMAT-2 is located in neurons,⁶¹ and catecholamines show a higher affinity to this isoform.⁶² VMAT-2 is an antiporter that exchanges two hydrogen ions for a monoamine molecule.

When released, dopamine binds either to a postsynaptic or presynaptic receptor or undergoes reuptake by transporters located proximately to the synaptic junction border in the presynaptic neuron. Dopamine's reuptake is performed by the dopamine transporter (DAT), located only presynaptically. DAT undergoes post-translation modification and can be used as a potential biomarker in PD due to its low level in this neurodegenerative disorder. DAT is the biological target of addictive substances (e.g., cocaine or amphetamine), which prolong the time that dopamine stays in the synaptic cleft by blocking this transporter.⁶³ Dopamine reuptake, release, and storage are highly regulated processes, and their alteration can influence above mentioned neurological disorders.

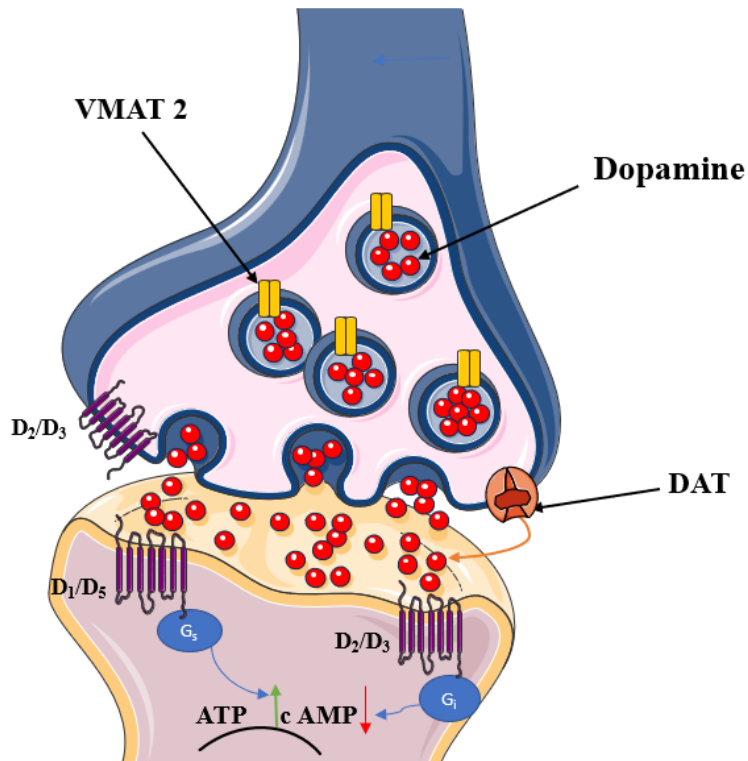


Figure 2: Dopamine release in the synaptic cleft. ATP, adenosine triphosphate; cAMP, cyclic adenosine monophosphate, D₁-D₅R, dopamine receptors; DAT, dopamine transporter; VMAT-2, vesicular monoamine transporter 2.

Dopamine receptors belong to the rhodopsin-like G protein-coupled receptors (GPCR). GPCRs are characterized by seven transmembrane domains (α helices). In 2012 the Nobel prize for chemistry was granted to Lefkowitz and Kobilka for their extraordinary work in the GPCRs field. GPCRs are a large family of receptors that transduce signals via G-protein heterotrimers or G-protein independent pathways as G-protein kinases (GRK), and they are targets of numerous commercially available drugs (30-50%). GPCRs activate heterotrimeric G-protein, consisting of α , β , and γ subunit. When a ligand binds to a GPCR, the G protein undergoes a conformational change, and the α subunit exchanges guanosine diphosphate (GDP) for guanosine triphosphate (GTP), resulting in its dissociation from the $\beta\gamma$ complex. There are three types of α subunits $G\alpha_s$, $G\alpha_i$ and $G\alpha_q$. In $G\alpha_s$ the α subunit further activates adenylate cyclase (AC) that hydrolyses adenosine triphosphate (ATP) to the second messenger cyclic adenosine monophosphate (cAMP). cAMP activates protein kinase A (PKA), which further activates phosphoprotein DAPP32, protein

phosphatase 1 (PP1), and regulates many cell processes. On the other hand, the $G\alpha_i$ subunit inhibits adenylate cyclase and induces opposite cell responses. $G\alpha_q$, upon ligand binding, activates phospholipase C (PLC), and further inositol 1,4,5-trisphosphate (IP3), leading to an increase of intracellular calcium levels. $\beta\gamma$ Units interact with GRK, mitogen-activated protein kinases (MAPK), or voltage-dependent K^+ and Ca^{2+} channels.⁶⁴

Dopamine receptors can be divided according to the difference in their genes or DNA into two different subclasses: D₁-like, which include D₁ and D₅, and D₂-like, which include D₂, D₃, and D₄ receptors^{65,66} (Table 1). Dopamine receptors can be found both presynaptically and postsynaptically. An important residue for binding dopamine and other catecholamine is the aspartate residue in the third loop in both D₁-like and D₂-like receptors. D₁-like and D₂-like receptors overlay functionally and cannot be strictly divided (e.g., D₁ and D₂ in the *striatum* are both involved in the regulation of motor movement).⁶⁷

The D₁ receptor (D₁R) is the most abundant subtype in the CNS.⁶⁸ D₁-like receptors are $G\alpha_s$ receptors, leading to an increase in cAMP concentration. These receptors can also activate PLC in the brain, which lead to phosphatidylinositol hydrolysis to IP₃, affecting Ca^{2+} mobilization from intracellular structures.^{68,69} D₁R share an 80% level of homology with D₅ receptors (D₅R),⁷⁰ and do not have introns in their coding area.⁷¹ D₁-like receptors are widely expressed in the *corpus striatum*,⁷² *nucleus accumbens*, *SNpc*,⁷³ *olfactory burb*,⁷⁰ *frontal cortex*,^{74,75} and *hypothalamus*, located predominantly postsynaptically. D₁-like receptors have a long intracellular carboxyl tail (seven times longer than in D₂-like). This receptor subtype is associated with cognition, substance abuse., and motor control.⁷⁶ Even though D₁R was well described subtype over the years D₁R selective and clinical ligands are not numerous. Phenyltetrahydrobenzazepines were recognized as a beneficial scaffold for binding to D₁R, which enabled developing D₁R selective ligands.⁷⁷

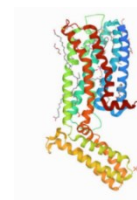
D₅R has a higher affinity (up to 10-fold) to dopamine than D₁R.⁷⁸ Due to the high homology level between D₁-like receptors, precise localization of D₅R was more challenging to determine.^{79,80} Nevertheless, slight different coupling to G-protein was suggested by Kimura et al.⁸¹ Even though there are two isoforms of these receptors, they display almost identical pharmacological profiles, and there has not yet been introduced to the market a selective compound that will target only one isoform. Both D₁R and D₅R receptor are involved in high cortical processes, such as memory consolidation.⁸²

On the other hand, D₂-like receptors belong to the G α_i receptor subclass, leading to a decrease in cAMP concentration,⁸³ and an increase of intracellular calcium,⁸⁴ which will be explained later in detail. D₂-like receptors can be found presynaptically and postsynaptically in *SNpc*,⁷³ *hypothalamus*, *ventral striatum*, *nucleus accumbens*,⁸⁵ *amygdala*, and *hippocampus*.⁸⁶ Presynaptic dopamine D₂-like autoreceptors regulate dopamine release by the negative feedback principle. Dopamine itself expresses a higher affinity at D₂R than at D₁R.⁸⁷ D₂-like receptors have the long third intercellular loop, a common characteristic for G α_i receptors, short carboxyl tail.^{74,88} and introns in their coding area.

D₄ receptor (D₄R) was cloned shortly after D₃ receptor (D₃R) and expresses at least three human isoforms.⁸⁹ It expresses the highest homology of all dopamine receptors to α_2 adrenergic receptors. D₄R is distributed in the frontal core and is upregulated under treatment with antipsychotics over two weeks.⁹⁰ Moreover, clozapine that belongs to the second-generation antipsychotics (SGA) expresses up to 10-fold higher affinity at D₄R than at D₂R, which could mediate their therapeutic and side effects as agranulocytosis.⁹¹ Recent studies confirmed the involvement of D₄R in glutamatergic transmission regulation,⁹² and an effect on stress-induced cognitive function.⁹³ This sparked the interest for further investigation of this receptor subtype. The crystal structure revealed in 2019⁹⁴ enabled the design of selective D₄R ligands

Table 1: Dopamine receptor subtypes and their characteristics

	D₁R	D₂R	D₃R	D₄R	D₅R
Cloning	1990 ⁹⁵	1988 ⁹⁶	1990 ⁹⁷	1991 ⁹⁸	1991 ⁹⁸
Introns⁷¹	no	yes	Yes	yes	no
G-protein⁶⁶ coupling	G α_s	G α_i	G α_i	G α_i	G α_s
Signal transduction⁶⁶	↑c AMP	↓c AMP	↓c AMP	↓c AMP	↑c AMP
Receptor	SKF 89626 ⁹⁹	pramipexole ¹⁰²	pramipexole ¹⁰²	A-412997 ¹⁰⁶	SKF83959 ¹⁰⁸
Agonists	SKF 8961 ¹⁰⁰ SKF-82958 ¹⁰¹	bromocriptine ¹⁰³	BP897 ¹⁰⁴ (partial agonist) ML417 ¹⁰⁵	PD168,077 ¹⁰⁷	
Antagonist	SCH 39166 ¹⁰⁹ SCH 23390 ¹¹⁰	risperidone ¹¹¹ haloperidol ¹¹¹	SB-277011A ¹¹² F17464 ¹¹³	PNU- 101387G ⁹³ , L-745, 870 ¹¹⁴	SCH-23390 ¹¹⁰ SCH-39166 ¹¹⁵
Crystal structure	/	2018 ¹¹⁶	2010 ¹¹⁷	2019 ⁹⁴	/



1.1.4 Dopamine D₂ Receptor

Dopamine D₂ receptor was the first dopamine receptor subtype to be cloned by Bunzow et al. in 1988.⁹⁶ However, the crystal structure of the human D₂R in complex with the atypical antipsychotic risperidone was described three decades later by Wang et al.¹¹⁶ This scientific breakthrough enabled a better understanding of the binding mode of already commercially available ligands, as well as the design of potent, novel ligands. Some differences to D₃R and D₄R were observed. For instance, the extracellular loop 2 (EL2) is oriented from the top of the receptor, and the extended binding pocket (EBP) is more flexible due to the transmembrane domain VII (TMVII) movement to outer space. This further resulted in revealing the structure of D₂R in the phospholipid membrane when the agonist is bound.¹¹⁸ D₂R has six introns and can be divided into two isoforms, generated by alternative intron splicing: D_{2S}-short isoform or the D_{2L}-long isoform, located mainly pre- and postsynaptically, respectively. Presynaptic D₂R regulates dopamine release and concentration.⁷¹ All dopamine D₂-like receptors share a high homology level of 78%

between D₂R and D₃R and 53% between D₂R and D₄R.^{70,117} D₂R can be either in the high or low-affinity state, and dopamine itself shows *in vitro* a higher affinity to the high state whereby neuroleptics do not express any preference.^{119,120}

D₂R belongs to GPCRs, coupled with the G α_i subunit (Figure 3). Stimulation of this receptor subtype leads to an adenylyl cyclase inhibition and a decrease in cAMP concentration. Consequently, PKA and protein DARP332 are deactivated, whereas protein phosphatase 1 (PP1) is activated. However, D₂R also signals through the G-protein independent pathway by recruiting β -arrestin. This process is involved in both cell desensitization and signaling.¹²¹ To be activated, GPCR needs to be phosphorylated by G-protein-coupled serine or threonine kinases (GRK), which exhibit seven different isoforms in humans.¹²² Phosphorylation happens at intracellular loops at the C-terminal. When phosphorylated, the receptor undergoes conformational changes and can recruit β -arrestin (β -arrestin 1 and 2). Upon their recruitment, they transduce signals that initiate receptors' desensitization, and ultimately their internalization.¹²³ Internalized receptors can be either restored in the cell membrane or degraded by lysosomes.¹²⁴ Desensitization is a claritin-mediated protective mechanism that prevents overresponse to the stimulus. Except for desensitization, D₂-like receptors can also signal through β -arrestin 2. Dopamine leads to Akt kinases' dephosphorylation and their consequent inactivation. This further results in the activation of glycogen synthase kinase 3, alpha and beta (GSK α/β). The hypothesis was confirmed by Beaulieu et al., where both isoforms were significantly reduced in mice lacking the DAT gene (DAT-KO mice).^{125,126} β -Arrestin recruitment is connected with cell movement as chemotaxis or endocytosis.¹²¹ When dopamine binds to D₂R, it forms complexes with β -arrestin 2, Akt, and protein phosphatase 2A (PP2A). PP2A dephosphorylates Akt, resulting in its inactivation and consequently elevated concentration of GSK α/β .¹²³

Both D₁R and D₂R can regulate the extracellular signal-regulated kinase pathway (ERK, member of MAPK). This pathway is associated with reward, confirmed by the MAPK stimulation when the drug is abused (e.g., cocaine).¹²⁷ In addition, dopamine acting on D₂-like receptors can activate PLC and increase the calcium level in cells by releasing it from storage.¹²² All D₂-like receptors can activate G-protein-regulated inwardly rectifying potassium channel (GIRK) and inactivate L, N, and P/Q-type calcium channel, via $\beta\gamma$ subunit.¹²⁸ Signaling through D₂R is highly regulated and associated with enhanced cognitive flexibility.¹²⁹

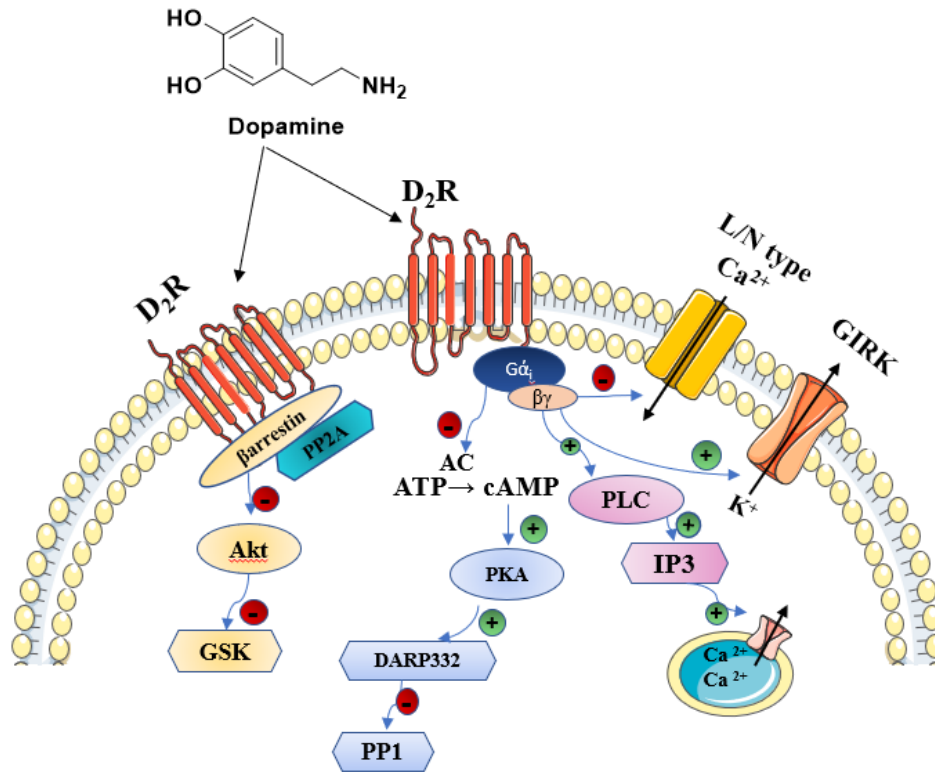


Figure 3: Dopamine signaling via D₂-like receptors on the example of D₂R. D₂R, Dopamine D₂ receptor. Akt, Akt kinase; cAMP, cyclic adenosine monophosphate; ATP, adenosine triphosphate; GIRK, G protein-regulated inwardly rectifying potassium channel. GSK, glycogen synthase kinase; IP₃, inositol-1,4,5-trisphosphate; PKA, protein kinase A; PKB, protein kinase B; PLC, protein kinase C; PP1, protein phosphatase 1; PP2A protein phosphatase 2A. Adapted from Beaulieu et al.,¹²⁵ Neve et al.¹²⁸

Dopamine D₂R is a primary therapeutic target in PD and schizophrenia.¹³⁰ According to the mesolimbic hypothesis, increased dopamine release in this pathway leads to the development of positive symptoms confirmed by numerous studies. In patients suffering from schizophrenia, hypersensitization of dopamine receptors is observed. Patients are susceptible to dopamine agonists or dopamine-releasing substances. Therefore, D₂R was first referred to as the “antipsychotic receptor”, after a revelation by Van Rossum et al., who hypothesized that this receptor is a biological target for neuroleptics. The assumption was *in vivo* confirmed by Seeman et al., who identified that all commercially available antipsychotics bind to in the same manner to the D₂R as haloperidol.¹³¹

D₂R can form homo- or heterodimers in the cell membrane and, therefore, be the target of bitopic (bivalent) ligands. These ligands can bind either to orthosteric and allosteric sites in one receptor

or to orthosteric sites in two different receptors.¹³² This presumption was confirmed by D₂R interaction with Gq-coupled orphan receptor GPR139^{133,134} due to their coexpression in the mesolimbic and tuberoinfundibular pathway.¹³⁵ Bitopic ligands with appropriate linker length (up to 92C atoms) can bind into the D₂R orthosteric binding site (OBS). D₂R dimerization can be facilitated by amphetamine,¹³⁶ and elevated D₂R dimer concentration is observed in patients suffering from schizophrenia.

The involvement of D₂R in motor control and, therefore, in PD was confirmed almost three decades ago.^{137,138} High ROS levels, increased risk for neuroinflammation, and consequently, PD was confirmed in D₂R knock-out mice.¹³⁹ D₂Rs are significantly decreased in PD,¹⁴⁰ and their polymorphism is connected with pharmacotherapy response in PD, confirmed by a large clinical study with MAO B inhibitor rasagiline.¹⁴¹ D₂R is involved in cognitive impairment as confirmed by numerous studies,^{53,129} and its density declines with age, especially in caudate and *putamen*, regions closely associated with cognition.¹⁴²

Developing selective D₂R ligands has been a prerequisite due to the side effects of commercially available D₂R ligands that are consequences of off-target binding. Synthesis of novel ligands can be knowledge-based, optimizing already marketed structures, or based on *in silico* experiments. Selective D₂R ligands have become a potent pharmacological tool in the treatment of PD or schizophrenia. It has been shown that the majority of commercially available antipsychotics occupy 60-80% of D₂R in the brain.¹³⁰ Novel generation antipsychotic as aripiprazole occupies D₂R up to 96%,¹⁴³ and leads to less off-target side effects.

The 4-phenylpiperazine moiety has been identified as one of the prerequisites for receptor interaction, even before the crystal structures of D₂R and D₃R were described.¹⁴⁴ Soon after revealing crystal structures, molecular docking (MD) simulations confirmed the optimal binding mode of this privileged scaffold. Basic piperazine nitrogen interacts with the OBS in D₂R and D₃R. OBS in both receptors is structurally conserved. Therefore, selectivity to one receptor subtype must be achieved with moieties that bind to the secondary binding pocket (SBP), which is more flexible in D₂R than in D₃R. Higher flexibility could interfere with MD simulations and make them less reliable. However, the distance between the OBS and the extended binding pocket (EBP) is longer in D₂R compared to D₃R,¹⁴⁵ and compounds with longer linkers could be potential D₂R selective ligands (Figure 4). Therefore, bivalent ligands with high molecular weight have gained

attention recently. These ligands could target both homomers as well as heteromers and therefore could represent new therapeutic options, as reported by Ullman et al.^{132,146} Structured-based virtual screening led to developing selective dopamine D₂R agonists **O₄SE₆**, and **O₈LE₆** by Fan et al.¹⁴⁵ These small molecules show high affinity and selectivity towards D₂R and could be further used as potential tools for further optimization. Knowledge-based ligand development optimizes already marketed drugs to improve their characteristics and decrease the risk of severe side effects. In line with this, Merck has developed dopamine D₂R selective antagonist **L-741626** due to the optimization of well-known FGA haloperidol.¹⁴⁵ Optimization of new SGA (e.g., aripiprazole or cariprazine) led to developing selective D₂R ligands that show 50-fold affinity over D₃R as reported by Vangveravong et al.¹⁴⁷ Further optimization on caripirazine led to compound **MS 1768**, selective D₂R agonist, both *in vitro* and *in vivo*.¹⁴⁸ As previously described, dopamine transduces signal via the G-protein independent pathway, recruiting β-arrestin. This represented a promising field in the synthesis of biased ligands. Aripiprazole-based derivatives **UNC9975**, and **UNC9994** are developed as biased ligands, less potent but more efficient than SGA Aripiprazole, showed promising results in the treatment of negative symptoms in schizophrenia in mice.¹⁴⁹

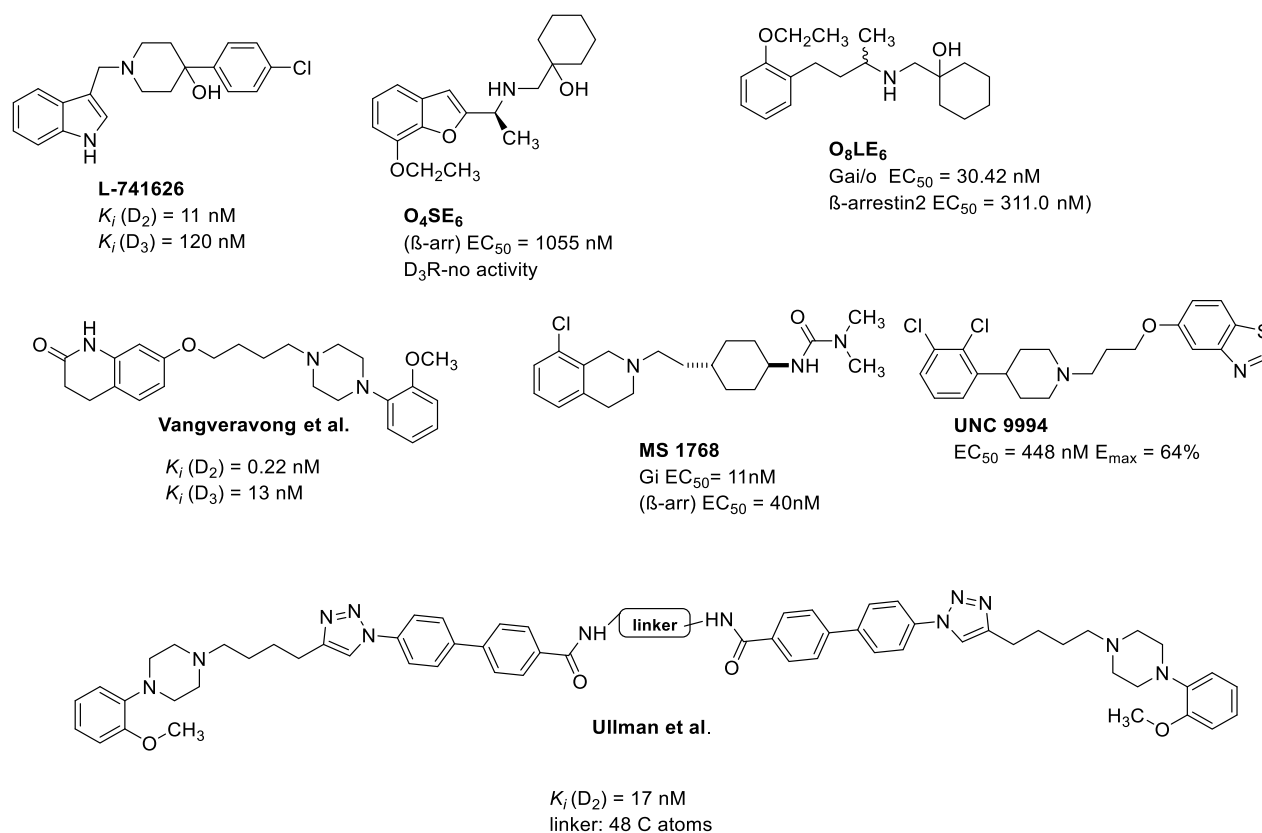


Figure 4: D₂R preferring ligands. EC₅₀ half-maximal effective concentration; E_{max}, maximal efficacy; K_i, inhibition constant.

1.1.5 Dopamine D₃ Receptor

Dopamine D₃ receptor (D₃R) was cloned in the early 1990s by Sokoloff et al.,⁹⁷ via the homology approach.⁷⁴ D₃R gene has five introns and six exons and is highly regulated (e.g., by the brain-derived neurotrophic factor (BDNF)).¹⁵⁰ It gained attention due to its focal localization¹⁵¹ (Figure 5), and high dopamine affinity to this receptor subtype.¹⁵² The crystal structure of D₃R was described by Chen et al. almost three decades later.¹¹⁷ As already described, the synthesis of selective D₃R ligands remained up to date a challenge due to the high homology between D₂R and D₃R.^{117,153,154} Nevertheless, D₃R compared to D₂R or D₄R, has a longer third intracellular loop that interacts with the ligand.¹⁵⁵ D₃R is localized only in the CNS,⁶⁸ and restricted to the limbic region: *nucleus accumbens*, *ventral pallidum*, islands of Calleja, *hippocampus*, *prefrontal cortex*, *hypothalamus*, and *striatum*. The highest D₃R density is observed in Calleja and medium spiny neurons (MSN) island of the rostral and ventromedial shell of the *nucleus accumbens*.¹⁵² D₃R mRNA is mainly found in the island of Calleja and *nucleus accumbens*.¹⁵⁶

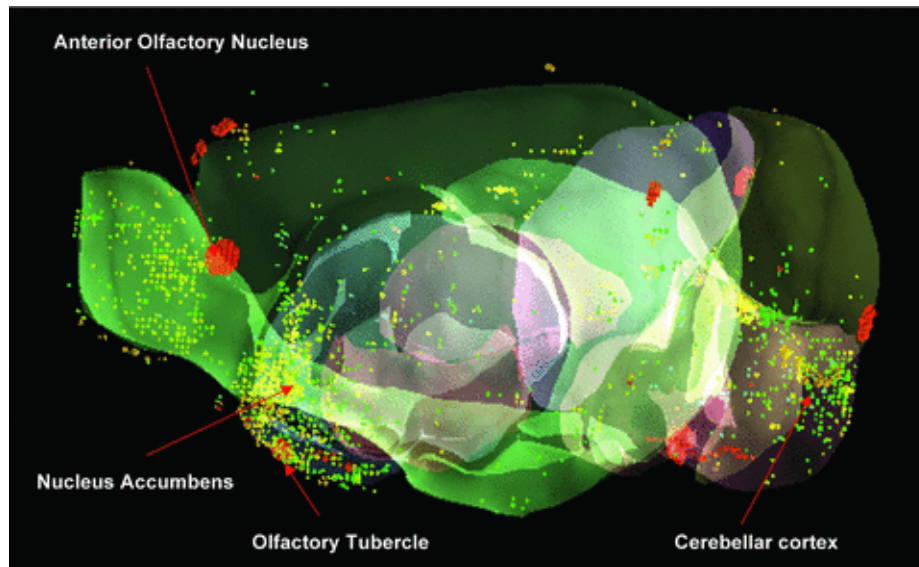


Figure 5: D₃R in the mouse brain, 3D reconstruction.¹⁵¹ Reprinted with permission from Heidbreder, C. A.; Newman, A. H. Current Perspectives on Selective Dopamine D₃ Receptor Antagonists as Pharmacotherapeutics for Addictions and Related Disorders. *Ann. N. Y. Acad. Sci.* 2010, 1187, 4–34. License obtained through Copyright Clearance Center (Order License ID: 1139647-1, ISSN: 0077-8923).

The dopamine D₃ receptor is an interesting target due to its association with schizophrenia and PD. Recent studies reported that D₃R and D₃R mRNA could be early biomarkers in PD due to quantitative and qualitative changes in D₃R signaling in PD patients (e.g., D₃R gene expression was decreased in lymphocytes in patients with PD).¹⁵⁷ Nevertheless, D₃R sparked controversy about its involvement in PD. Human T-cells contain VMAT-2,¹⁵⁸ D₃R, and tyrosine hydroxylase, the rate-limiting enzyme in dopamine's biosynthesis.¹⁵⁹ An elevated D₃R levels lead to the activation of CD4⁺T-cells and their differentiation to effector phenotype TH₁¹⁶⁰ and TH₁₇.¹⁶¹ Effector T-cells cross BBB and interact with antigen-presenting microglia cells. Activation of antigen-presenting cells leads to the release of inflammation mediators and consequent neuroinflammation, confirmed *in vitro* and *in vivo* in mice.¹⁶² Even though D₃R levels are elevated in the early stage PD, D₃R is downregulated in a later phase of the disease, even in patients that did not receive prior therapy. Downregulation can be explained with an adaptive mechanism or different T-cell subtypes in blood and brain that act differently (proinflammatory function in the brain, anti-inflammatory in the blood). D₃R gene deletion leads to decreased levodopa-induced

dyskinesia (LID),¹⁶³ and D₃R antagonist **PG01037** improved motor symptoms.¹⁶⁴ Taken all together, the fundamental role of D₃R in PD pathology remains to be clarified.¹⁶⁵

According to the "mesolimbic hypothesis", schizophrenia symptoms occur due to altered dopamine concentration and signaling.¹⁶⁶ Positive symptoms of schizophrenia occur as a result of hyperactivation of the mesolimbic brain region. On the other hand, negative symptoms of schizophrenia are connected with decreased dopamine release in the mesocortical pathway.¹⁶⁷ All commercially available antipsychotics block dopamine D₂-like receptors (Section 1.1.4). Radiotracers were developed to localize dopamine receptor subtypes and estimate their distribution and occupancy in different brain regions.¹⁶⁸ Up to now, four D₂R/D₃R radiotracers are described,¹⁶⁹ and [¹¹C]-(+)-PHNO¹⁷⁰ is a PET-ligand with preference to D₃R.¹⁷¹ Brain-imaging studies with this ligand confirmed high D₃R occupancy after acute treatment with antipsychotics,¹⁷² while the occupancy in chronic pharmacotherapy is not significant. D₃R mRNA was not upregulated after two-week or extended treatment with antipsychotics (e.g., haloperidol) or labeled ligands.^{90,166} However, elevated D₃R mRNA concentrations were found in T-cells in schizophrenia patients.¹⁷³ Therefore, antagonism at D₃R is not sufficient to control clinical symptoms of schizophrenia; D₂R needs to be occupied, which is the case with all currently available neuroleptics. The most recent approved antipsychotic, cariprazine, is D₃R, preferring antipsychotic that addresses negative symptoms.¹⁷² Bupirone, another D₃R preferring antagonist used in the treatment of anxiety, showed an excellent impact on negative symptoms of schizophrenia, raising interest for D₃R involvement in the mesocortical pathway regulation.¹⁷⁴

Focal localization of D₃R in a region closely connected with the reward, reinforcement, and seeking behavior makes this receptor subtype a possible target in addiction therapy. All addictive substances increase dopamine concentration in the shell of the *nucleus accumbens*.¹⁵² In cocaine users, D₃R is upregulated in a time-dependent manner.^{151,152} Neisewander et al. confirmed an increase in D₃R concentration after 31 days before last cocaine administration, which is closely connected to the *nucleus accumbens* core.¹⁷⁵ It is involved in the second-order schedule reinforcement.¹¹² D₃R association with addictive behavior was confirmed with the development of the selective D₃R partial agonist **BP 897**, that decreased hyperactivity produced by cocaine.¹⁷⁶ Another D₃R antagonist **SB-277011A** blocked induced second-order schedule reinstatement of

cocaine¹¹² and nicotine seeking behavior.¹⁷⁷ Buspirone also antagonize alcohol-seeking behavior,¹⁷⁸ and **YQA14** inhibited morphine sensitization.¹⁷⁹

Considering all the facts, D₃R represents a very interesting target, and the synthesis of selective D₃R ligand could provide a better understanding of this receptor subtype. 7-hydroxy-2-(*N,N*-dipropylamino)tetralin (**7-OH-DPAT**),¹⁸⁰ was the first compound synthesized shortly after D₃R cloning that showed excellent nanomolar affinity ($K_i = 0.57$ nM). *R*-enantiomer showed over 200-fold affinity at D₃R and served as a marker for this receptor subtype visualization. The general pharmacophore for selective D₃R ligand was proposed in the early 2000s.¹⁸¹ It can be divided into four regions: a basic center connected with an **aryl substituent**, an **arylamide moiety** (H bond acceptor), and a **linker** of appropriate length (Figure 6).

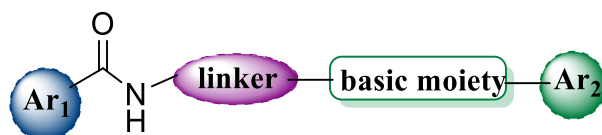


Figure 6: General pharmacophore for D₃R selective ligand.¹⁸¹

Over time, all four prerequisites have been modified and optimized (Figure 7). To date number of new publications and patents regarding D₃R ligands is constantly increasing. Linkers that contain four methylene groups between the aryl amide moiety and the basic center grant interaction with receptor of interest. The linker's stereochemistry significantly impacts the binding mode of both the primary pharmacophore (PP) and the secondary pharmacophore (SP), confirmed by tetrahydroisoquinoline derivatives.¹⁸² Introducing OH, F, or a double bond into the linker increased rigidity and led to higher selectivity. Introducing bulky basic moieties as in **SB-207711A** and **S33084** lead to remaining affinity to D₃R and increasing selectivity.^{183,184} Replacement with 6-methoxy-1,2,3,4-tetrahydroisoquinoline-7-ol leads to increasing solubility and better drug-likeness.¹⁸⁵ Amide moiety replacement with cyclopropyl amine derivatives did not diminish D₃R affinity, as recently reported by Tan et al.¹⁸⁶ emphasizing once more enantioselectivity and different binding modes of enantiomers (*S*-enantiomers were agonist and *R*-enantiomers antagonists). Aryl amide moiety replacement with thiocarbamate and indole moiety resulted in promising ligands as reported by Kumar et al., Basha-Shaik et al. (**R-VK4-40**), and Sun et al. (**Y-QA31**), respectively.¹⁸⁷⁻¹⁸⁹ On the other hand, by merging the aryl amide moiety with the basic

moiety and introducing linker in the eastern part of the basic moiety, Moritz et al. reported **ML417** that showed excellent results as D₃R agonist in β -arrestin recruitment.¹⁰⁵ Therefore, optimization in the eastern part of the molecule could lead to agonist synthesis and can be a potential tool in treating PD. As pramipexole shows higher affinity at D₃R than at D₂R, pramipexole derivatives were introduced as aryl moiety as reported by Chen et al. **CJ 1037** was full *in vivo* D₃R agonist with moderate affinity at D₂R.¹⁹⁰

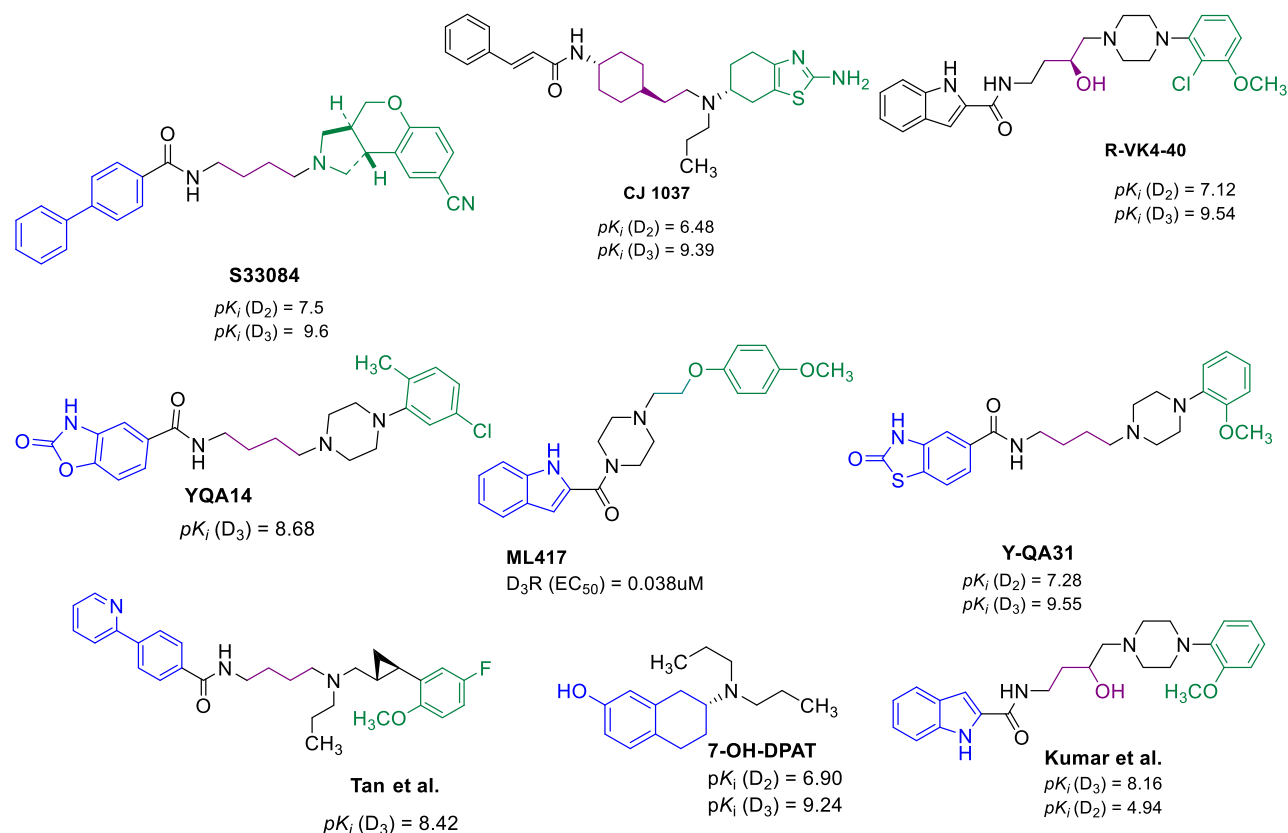


Figure 7: D₃R preferring preclinical candidates. pK_i obtained from inhibition constant K_i .

Above mentioned efforts resulted in reporting D₃R preferring partial agonist **BP 897** (Figure 8) by Bioprojet.^{104,191} It was the first D₃R ligand to enter clinical trials for addictive behavior and schizophrenia. **BP 897** contains 4-phenylpiperazine moiety, which is recognized as a promising scaffold for the interaction with the receptor. 4-Phenylpiperazine derivatives were recognized as potent moieties for designing D₃R preferring ligands by different working groups,¹⁹² especially *o*-methoxy or *o,m*-dichloro substituted derivatives. Interaction within the receptor was confirmed by *in silico* studies. Recently reported antipsychotics as cariprazine,^{111,193,194} brexpiprazole,¹⁹⁵ or

aripiprazole¹⁹⁶ share this scaffold. These second-generation antipsychotics (SGAs) also address negative symptoms, which is a considerable advantage compared to first generation antipsychotics (FGAs) or other SGAs. Replacement of the naphthyl moiety (as observed in **BP 897**) with the tetrahydroisoquinoline moiety led to another clinical candidate, **SB-277011A**,^{177,197} that showed promising results in the treatment of addictive behavior.^{198,199} Introducing bulky oxygen derivatives led to another clinical candidate, D₃R preferring antagonist-**F17464** by Pierre Fabre. Besides affinity at D₃R **F17464** acts as a 5HT_{1A}R agonist. This derivative completed phase II in a clinical trial for schizophrenia.^{113,200,201} Bioisosteric replacement of methylene group with sulfur in the linker and introducing highly lipophilic and electrophilic trifluoromethyl substituents (CF₃) in aryl amide moiety lead to two D₃R preferring clinical candidates: **GSK598809** and **ABT-925**.^{202,203} Both ligands showed more than 100-fold selectivity to D₃R.²⁰⁴ **GSK598809** showed promising results in reward anticipation,²⁰⁵ although it can cause a risk of acute blood pressure increase when co-administered with cocaine.²⁰⁶ However, the main drawback of D₃R preclinical and clinical candidates is their poor solubility and low bioavailability.²⁰⁷ Therefore, efforts should be centered around the design of compounds that can cross BBB and exert their action in the CNS, but still be good drug-like candidates in terms of hydrophilicity and consequent pharmacokinetic characteristic, which up to date was not a successful mission.

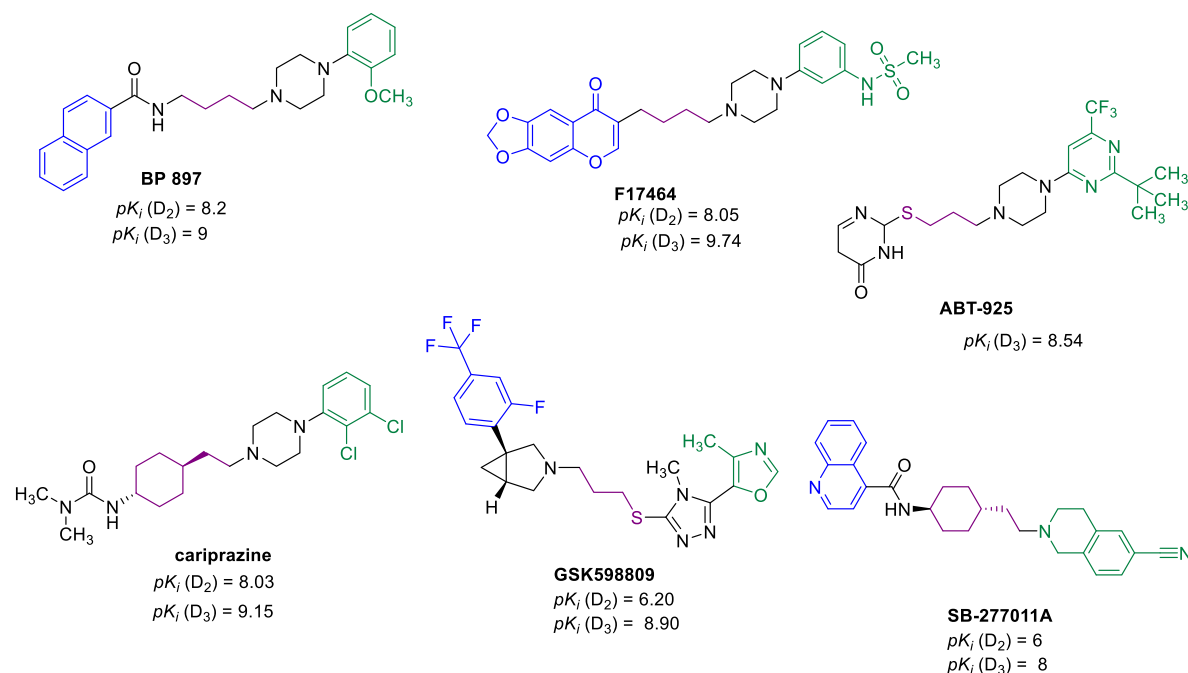


Figure 8: D₃R preferring clinical candidates. pK_i obtained from inhibition constant K_i .

1.2 Schizophrenia

According to the WHO: "Schizophrenia is a chronic and severe mental disorder affecting 20 million people worldwide". The word schizophrenia originates from Greek (*skhizein* = to split *phren* = mind). It is typically diagnosed in the late teen years up to the early thirties, with the later onset in women. People suffering from schizophrenia are 2-3 times more likely to die in comparison to the general population. Patients with schizophrenia interpret reality abnormally, lose touch with reality, which further causes severe distress. In general, all schizophrenia symptoms can be divided into three groups:

- Positive: hallucinations, delusions, disorganized thinking and speech, extremely disorganized motor behaviors (e.g., motor agitation).
- Negative: loss of motivation, disinterest, or lack of enjoyment in daily activities, social withdrawal. They can be classified as primary (a consequence of schizophrenia) or secondary (more complex, dependent on other factors as substance abuse, depression). These symptoms are more challenging to diagnose and not well addressed by current therapeutic options.
- Cognitive: impairment as deficits in working memory, attention, or critical thinking.

To diagnose schizophrenia, according to the Diagnostic and Statistical Manual of Mental Disorders (DSM), at least two of the following symptoms need to be present for at least one month: delusion, hallucination, or disorganized speech. They need to be accompanied by decreased functioning levels in work, personal relations, or self-care.²⁰⁸ Schizophrenia is a recurrent disease and, therefore, requires lifelong treatment, even when patients are in remission. Schizophrenia is often associated with other pathophysiological conditions as substance abuse, depression, or anxiety.

Unfortunately, the cause of schizophrenia remains up to now unknown, and this mental illness can only be symptomatically treated. However, some risk factors have been recognized, one of them being heritability. This phenomenon was observed by Bleuler in 1910,^{209,210} and confirmed in later studies, where heritability was up 83% in twins.²¹¹ People with this mental disorder in the family have an increased risk of developing schizophrenia. Up to now, over 40 risk genes have been identified, where mutations of rare, common inherited, and *de novo* alleles were observed.²¹⁰ Recently, genetic engineering generated pluripotent cells that can further differentiate into various cell types.^{212,213} This cutting-edge technology can provide answers about genetics involvement in

schizophrenia. Besides genetic factors, environmental factors such as migration,²¹⁴ ethnic origins,²¹⁵ addiction,²¹⁶ neonatal,²¹⁷ and adult vitamin D deficiency,^{218,219} upbringings in the urban environment,^{220,221} unemployment, birth complication, childhood trauma maltreatment,²²² and even prenatal exposure to infections could be potential risk factors for psychosis.²²³

Besides mesolimbic and mesocortical pathway involvement in the pathology of schizophrenia (Section 1.1.2), striatal and the association of other neurotransmitters (e.g., glutamate). has recently been confirmed.²²⁴ The latter is confirmed by the fact that NMDA agonists (e.g., ketamine) can induce psychosis.^{225,226} Besides, excessive glutamate concentration can have toxic effects and accelerate cognitive impairment.^{227,228}

Both pharmacotherapy and psychotherapy (individual therapy, social skills training, family therapy, vocational rehabilitation) need to be implemented to address the symptoms. Schizophrenia is principally a dopamine disorder, confirmed by the fact that dopamine agonists can induce schizophrenia-like symptoms or that dopamine antagonists express antipsychotic activity.²²⁹ Antipsychotics reached the market in the second half of the 20th century, are still a central pharmacological tool for schizophrenia treatment. In general, antipsychotics can be divided into two generations: first and second generation, depending on their discovery time. All currently available antipsychotics show D₂R occupancy between 60-80% (excluding cariprazine). First-generation antipsychotics (FGA, Figure 9) are so-called "dirty drugs" that do not selectively target dopamine D₂-like receptors but also exert their action on other "off-targets" as muscarine, histamine, and acetylcholine receptors. Due to their lack of selectivity, they express severe side effects as EPS (which is expressed as tremor or dystonia leading to tardive dyskinesia), reduced libido, or hyperprolactinemia. These are consequences of hyperactivation of dopamine receptors in nigrostriatal and tuberoinfundibular ways, respectively (Section 1.1.2). FGAs do not address negative symptoms. This group includes antipsychotics such as chlorpromazine, fluphenazine, haloperidol, perphenazine, and thioridazine.

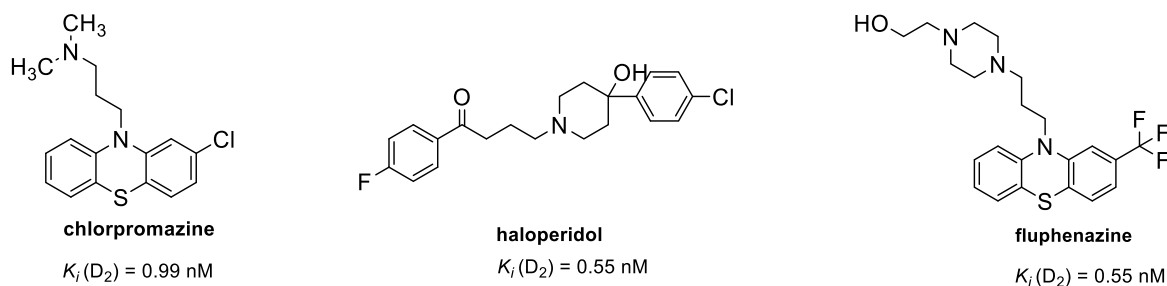


Figure 9: First-generation antipsychotics, K_i inhibition constant.

The second-generation antipsychotics (SGA, Figure 10) include atypical antipsychotics as aripiprazole, asenapine, brexpiprazole, cariprazine, clozapine, lurasidone, olanzapine, paliperidone, quetiapine, risperidone, and ziprasidone. SGA have increased selectivity compared to the first generation and, therefore, fewer side effects, resulting in better patient adherence. They are more efficient regarding negative symptoms than FGA, also acting on 5HT_{2A} receptors.²³⁰ They bound loose and dissociate more rapidly.^{231,232} However, metabolic side effects as weight gain, hyperglycemia, or dyslipidemia occur more often when compared to that of FGA.^{233–235} Clozapine is SGA related with severe side effect-agranulocytosis.²³⁶

SGAs (all except clozapine) present the first therapeutic option in the treatment of schizophrenia. New 4-phenylpiperazine derivatives as aripiprazole, brexpiprazole and cariprazine were developed and marketed to increase selectivity and overcome mentioned SGA side effects. Cariprazine is D₃R preferring partial agonist¹⁷² that effectively addresses negative symptoms. It is metabolized via CYP3A4 to active metabolites desmethyl and didesmethyl cariprazine, leading to a total half-life of cariprazine of 3 days.^{111,194} Consequently, the efficacy and the relapse time, are prolonged and symptom exacerbation is ameliorated.²³⁷ As negative symptoms have a significant impact on life quality, cariprazine is suggested as the first therapeutic option.²³⁰

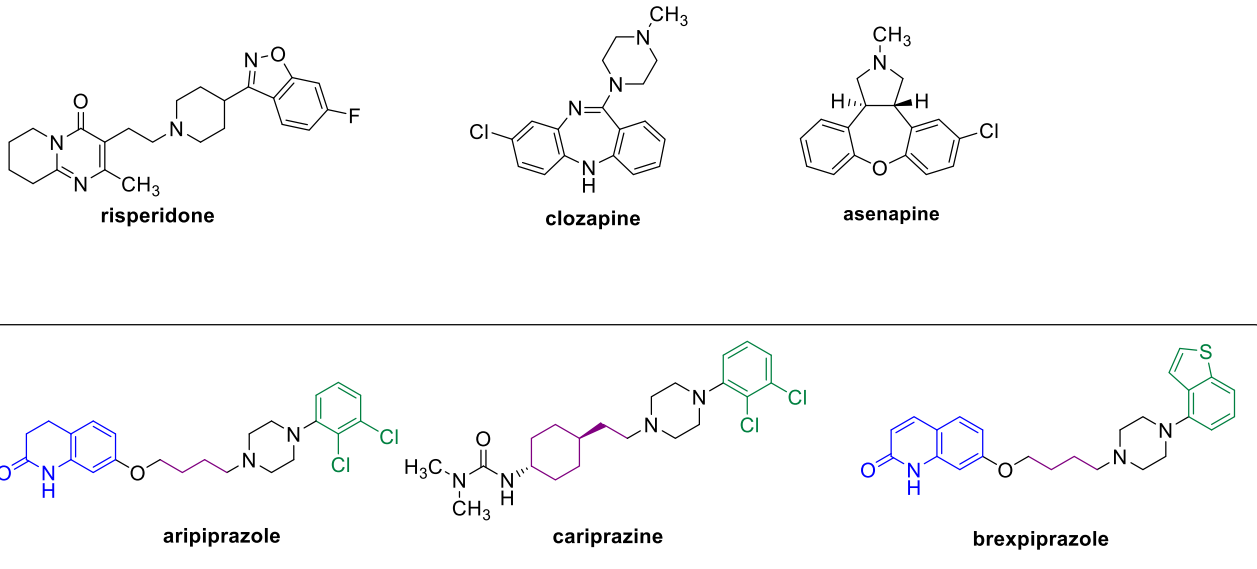


Figure 10: Second-generation antipsychotics

Taken all together, schizophrenia should firstly be treated with SGA as monotherapy, and if not effective in combination with other SGA. FGA should be administered only when therapy with SGA did not provide efficient results.²³⁸ Guidelines for schizophrenia treatment have been shown in Figure 11.

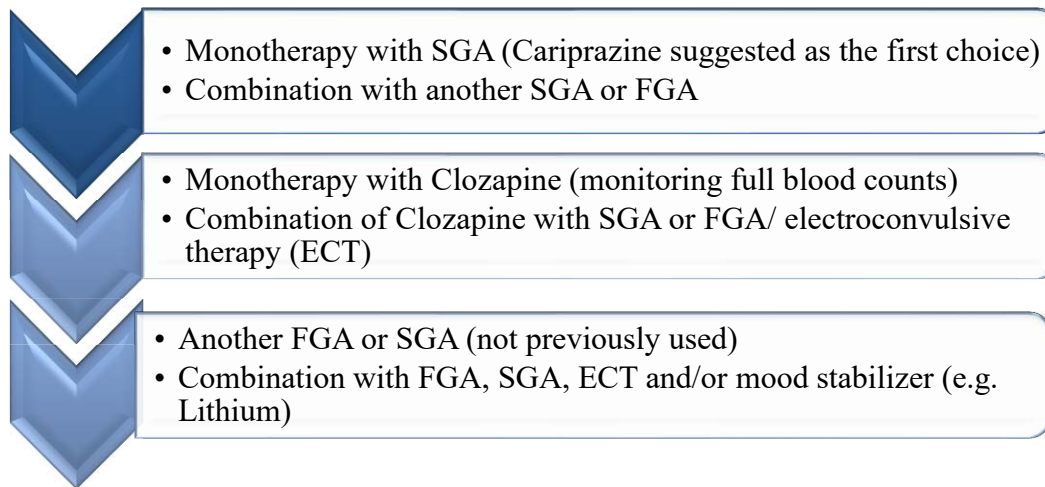


Figure 11: Guidelines for treatment of schizophrenia.²²⁶

1.3 Parkinson's Disease

Parkinson's disease (PD) is a progressive neurodegenerative disease characterized by the loss of the dopamine neurons, especially in *SNpc* that project to the *striatum* (nigrostriatal pathway, Section 1.1.2). PD was first described in 1817 by James Parkinson as the "shaking palsy" phenomenon, and soon after, named after him. It is the second most common neurodegenerative disease after AD and affects 1 % of the population older than 60.^{239,240} Prevalence increases with age up to 3 % in people older than 80.^{241,242} The mean on-set age is 55,²⁴³ and only in 5% the on-set is under 40 years.²³⁹

The exact cause of PD are unknown, the disease is mainly diagnosed, when 60-80% of dopaminergic neurons have degenerated.²⁴³ The late diagnosis occurs due to the adaptive mechanisms as decreased reuptake of dopamine, increased biosynthesis in non-dopaminergic neurons, or increased number of postsynaptic receptors.^{244,245} Degeneration is not restricted to the dopaminergic neurons and also affects the noradrenergic, serotonergic, cholinergic, glutamatergic neurons, but not histamine neurons.²⁴⁶ Neuron loss causes denervation and formation of α -synuclein-containing Lewy bodies in the surviving dopaminergic neurons. Depigmentation is also observed in the *SNpc* in PD patients occurs due to the loss of pigment neuromelanin.²⁴⁷ Therefore, causal therapy is not a therapeutic option, and PD can actually only be symptomatically treated.

However, it has been hypothesized that both genetic and environmental factors can lead to PD. This disorder can be in general divided into genetically inherited and idiopathic PD.²⁴⁸ Five risk genes (PARK 1,2,6-8)^{248,249} and more than 24 risk loci²⁵⁰ have been associated with developing hereditary PD. Gene therapy gained recognition in the last 15 years as a potential tool for treating PD and other diseases. By targeting disease-modifying and disease non-modifying transgenes, the etiology of PD should be better understood. Targeting non-modifying transgenes have not been successful up to now, as neuriturin was the only examined agent. However, several clinical trials are still ongoing.²⁵¹⁻²⁵³

Oxidative stress, protein aggregation, mitochondrial dysfunction, or exposure to exogenous and endogenous neurotoxins can be additional risk factors for developing PD.²⁴³ The latter was encouraged by findings that 1-methyl-4-phenyl-1,2,3,6—tetrahydropyridine (MPTP), precisely their toxic metabolite MPP^+ ,^{245,254} causes neurodegeneration, confirmed in *post mortem* analysis. Age, exposure to herbicides and pesticides, smoking, or coffee consumption have been extensively

studied as risk factors in PD. For the two latter, numerous studies confirmed a negative association with PD.²⁵⁵⁻²⁵⁸ Even though PD prevention cannot be made, dietary intake of non-fatty acids or antioxidants due to their protective role is strongly suggested.

Parkinsonism is a broad concept that describes changes in the brain due to dopaminergic neuron loss. However, this may not always be due to the PD (although in 80% of cases, PD is the main cause of Parkinsonism), it can occur due to toxin exposure or head trauma. Typical PD motor symptoms are tremor that occurs in rest, rigidity, bradykinesia (slowed movement), and postural disturbances. Motor symptoms (Figure 12) are accompanied by non-motor symptoms such as facial hypomimia, sleep disorder, swallowing problems, depression, cognitive impairments, sexual dysfunction, micrographia (difficulty in writing), obstipation, bladder problems, or respiratory impairments.^{246,259} Since there is no specific biomarker, diagnosis is based on the clinical picture. For a long time, the diagnosis was confirmed when two out of four motor hallmarks were present.²⁴⁰ Parkinsonism is diagnosed when bradykinesia is present with rigidity or tremor in rest, or both. According to the recent guidelines, motor symptoms remain a prerequisite for the diagnosis, but non-motor symptoms also need to be included. To determine if parkinsonism is a consequence of PD, at least two supportive criteria defined by Movement Disorder Society (MDS), without absolute exclusion criteria or red flags, need to be observed.²⁶⁰ PD is often confirmed only at autopsy when denervation and Lewis bodies are observed.²³⁹ Symptoms start gradually and exacerbate progressively. Motor symptoms may not be highly expressed in the initial disease phase, but if left untreated or appear in the late phase, they could exacerbate and express a high impact on the life quality. An exacerbation can be triggered by infections or emotional stress.²⁶¹ Progressive motor and non-motor symptoms lead ultimately to dependency. Patients need assistance in the regular daily activity (e.g., patients remain "stuck," cannot commit voluntary movement, and are prone to falls).

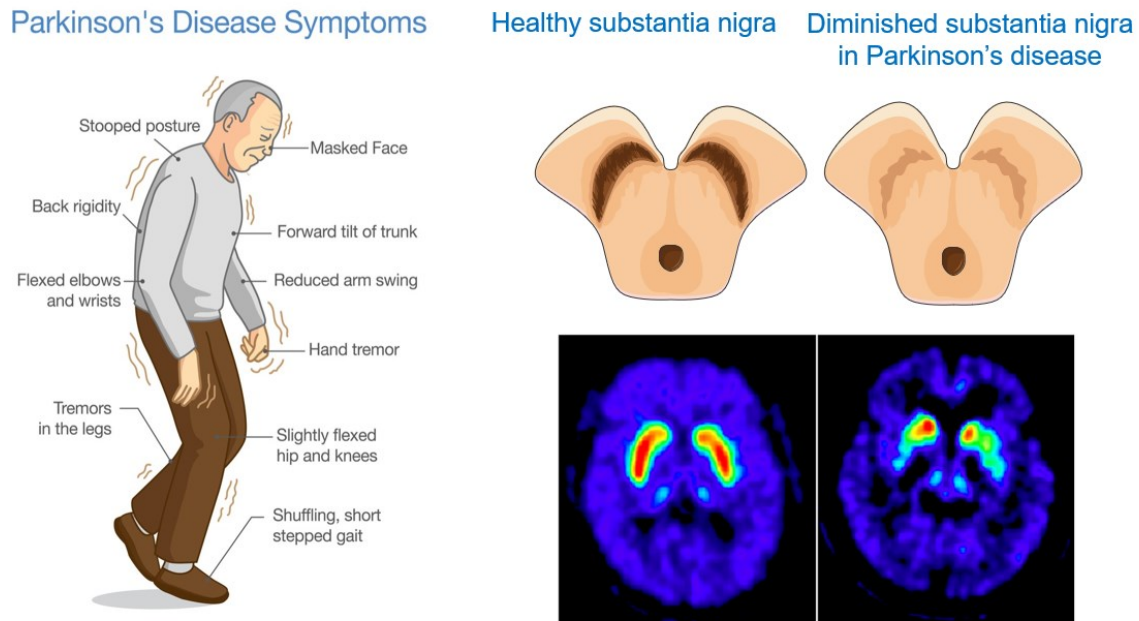


Figure 12: Left: Typical motor symptoms in PD (source: Shutterstock license Nr Nummer: 763720675). Right: Neurodegeneration in *SNpc*: schematic (up) and PET scan (down) (Source: Center for Neuroscience at the Feinstein Institut for Medical Research).

PD requires lifelong therapy due to its progressivity and chronicity. PD treatment includes pharmacotherapy, surgical procedures (deep brain stimulation, lesional stimulation, restorative operation), and rehabilitation (speech, physical and occupational therapy). The majority of the currently marketed drugs for PD target the dopaminergic system. However, there has been an increased interest in drugs that impact other neurotransmitter pathways: cholinergic,²⁶² glutamatergic,²⁶³ or serotonergic,²⁶⁴ due to increasing evidence of their involvement in PD pathogenesis.

Levodopa, the precursor of dopamine, revealed in the early beginning of the 20th century, gained overall recognition in the 1970s, still represents the gold standard in PD treatment.²⁶⁵ However, after several years of treatment (average onset six and a half years), levodopa can lead to motor side effects. These side effects include levodopa-induced dyskinesia (LID, prevalence increase with age),²⁶⁶ or “on-off” phenomenon (cyclic good and inadequate response to the medication or “wearing-off”- effect disappears before the following doses).²⁴⁶ Levodopa is always combined with aromatic amino acid decarboxylase inhibitors (benserazide and carbidopa). These inhibitors

prevent peripheral degradation of levodopa and enable crossing BBB. The usual doses of levodopa are 300 mg per day (usually divided into three doses).²⁶⁷

Another therapeutic option in PD are D₂R agonists: ergot derivatives (bromocriptine and pergolide) and non-ergot derivatives as pramipexole, ropinirole, rotigotine, and apomorphine. The latter is efficiently used for the treatment of “off-episodes” induced by levodopa.²⁶⁸ Ergot derivatives are almost abandoned in PD pharmacotherapy due to the numerous side effects such as heart valve or pulmonary fibrosis.^{269,270} Non-ergot dopamine agonists, on the other hand, can be used as a monotherapy or in combination with levodopa. They represent the first choice in younger patients.²⁶⁷ Dopamine agonists have a longer half-life than levodopa,²⁷¹ leading to better patient adherence. Side effects of dopamine agonists occur as a direct consequence of their mechanism of action. Hallucinations, nausea, dizziness, somnolence, constipation, asthenia, or impulse control disorder (as in impulsive gambling or compulsive buying)²⁷² are often observed side effects.

Pramipexole is a dopamine D₃R preferring agonist (K_i (D₃R) = 0.5 nM), acting on both presynaptic and postsynaptic receptors, with no affinity at D₁R.²⁷³ Pramipexole occupies dopamine receptors in *substantia nigra*, *globus pallidus*, temporal and frontal cortex.²⁷⁴ It was marketed in 1997 to treat PD and nowadays is also used in the therapy of restless legs syndrome.^{275,276} It is rapidly absorbed and metabolized only up to 10%.²⁷³ Bioavailability is over 90%, the half-life is 8-12 hours, and pramipexole is renally excreted.²⁷⁷ The dose range is 0.375 - 4.5 mg per day.²⁷⁸ It has neuroprotective effects,²⁷⁹ also in different extended-release dosage forms as in transdermal patch.²⁸⁰ Pramipexole decreases the risk of motor complications, whereas increases the risk of somnolence and hallucinations, compared to levodopa.²⁸¹ Moreover, it acts positively on depressive PD patients,²⁸² and major,²⁸³ or treatment-resistant depression.²⁸⁴ Pramipexole served as a lead compound to synthesize novel, potent dopamine ligands in this PhD project.

As described in Section 1.1.1, dopamine degradation is mediated by MAO B and COMT. These two enzymes served as therapeutic targets for developing drug classes in PD that inhibit dopamine metabolic degradation. MAO B inhibitors can be divided into irreversible inhibitors as rasagiline and selegiline, and reversible such as recently approved safinamide (Xadago®).²⁸⁵ Rasagiline and selegiline are used either as a monotherapy or in combination with other agents. They both contain propargyl amine moiety, which enables irreversible, covalent binding to the enzyme.²⁸⁶ On the

other hand, safinamide was approved in 2015 and is used as an adjuvant to treat "off" episodes during levodopa therapy,²⁸⁷ alone or in combination with other PD drugs. It is administered in dose range 50-100 mg per day²⁸⁸ and mainly used to treat advanced PD.²⁸⁹ MAO B inhibitors act as neuroprotective agents, inhibiting the formation of ROS in the dopamine metabolism (Section 1.1.1).

Another therapeutic class is COMT inhibitors such as entacapone, tolcapone, or opicapone, that are always used in combination therapy. Tolcapone is, however, avoided nowadays due to its potential hepatotoxic effects.²⁹⁰ This resulted in market withdrawal, but it was reintroduced after conducting safety analyses.²⁹¹

Dopamine and acetylcholine are in balance in the physiological brain. In PD, dopamine loss affects the cholinergic system hyperactivation, which results in further complications. Anticholinergics such as benztropine, trihexyphenidyl, biperiden, orphenadrine, procyclidine are therefore used in PD therapy. Amantadine, an NMDA receptor antagonist, was initially marketed as an antiviral agent and is now used to treat dyskinesia.²⁹² PD treatment options are summarized in Figure 13.

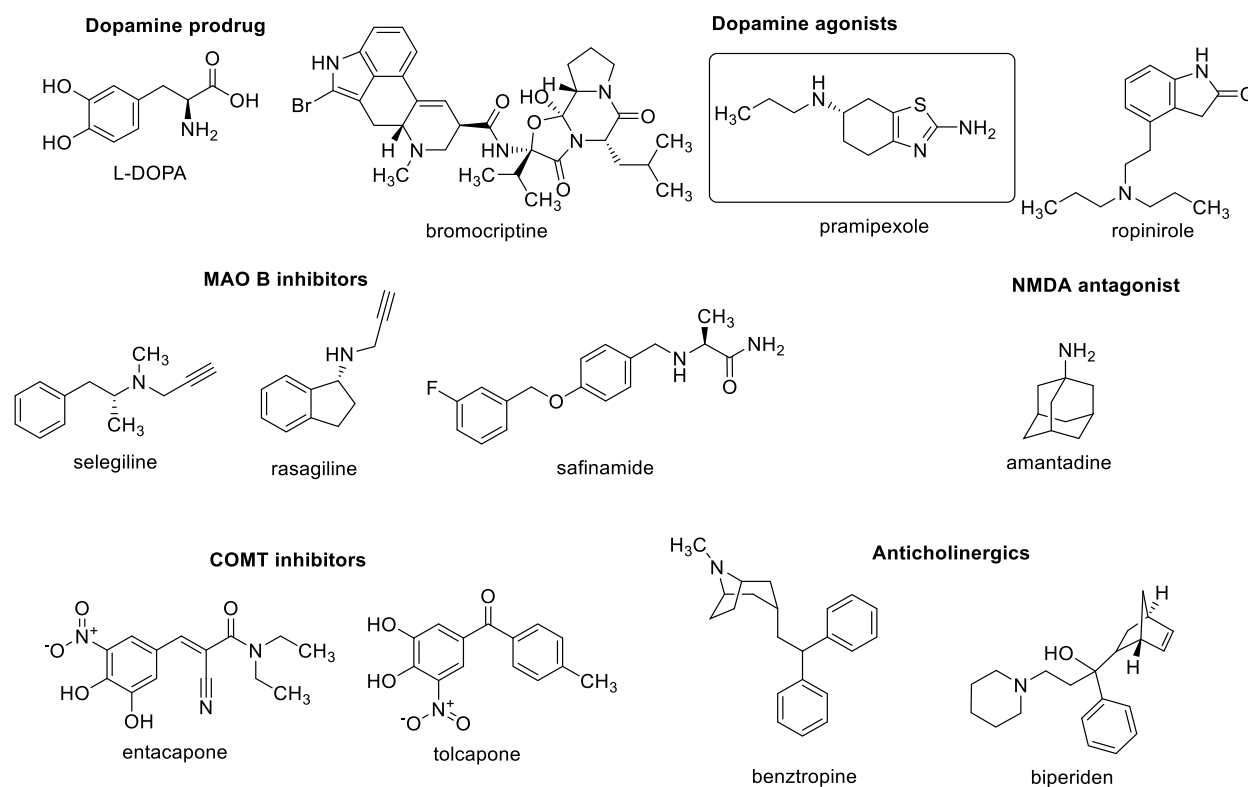
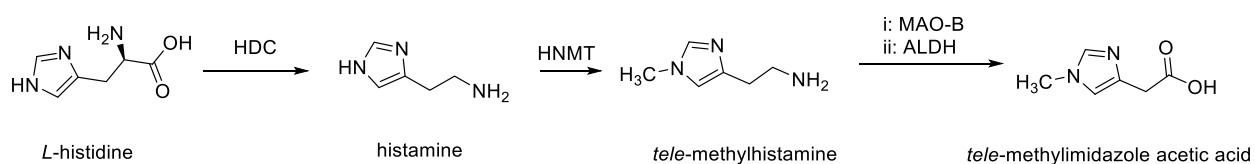


Figure 13: Commercially available drugs for PD treatment.

1.4 Histamine

Histamine is a biogenic amine discovered at the beginning of the 20th century by Sir Henry Dale.²⁹³ Soon after, its connection with gastric secretion and smooth muscle stimulation has been established. It is synthesized in the tuberomammillary nucleus within the hypothalamus and mast cells.²⁹⁴ Biosynthesis of histamine (Scheme 3) starts from *L*-histidine that undergoes decarboxylation via histamine decarboxylase (HDC). Histamine metabolism is dependent on three enzymes: histamine *N*-methyltransferase (HNMT) that methylates histamine to *tele*-methyl histamine, in which *S*-adenosylmethionine serves as methyl group donor. *Tele*-methyl histamine further undergoes oxidative deamination via MAO B to the corresponding aldehyde and consecutive oxidation via aldehyde dehydrogenase (ALDH) to *tele*-methylimidazole acetic acid.



Scheme 3: Biosynthesis and metabolism of histamine.

Histamine is stored in mast cells and basophils,²⁹⁵ enterochromaffin-like cells,²⁹⁴ neurons in the CNS and the PNS. Like numerous other neurotransmitters, histamine is stored in neurons via VMAT 2, which serves as an antiporter and exchanges two protons for one histamine molecule.²⁹⁶ There is no specific reuptake transporter for histamine. It acts as a neurotransmitter in the CNS and PNS and as a mediator in the gut or immune system.²⁹⁵

1.4.1 Histamine Receptors

Histamine's role is complex. Its altered concentration relates to numerous diseases: AD, gastric ulcers, immune diseases, or allergies. Histamine acts on four receptor subtypes: H₁₋₄R (Table 2), all of which belong to the rhodopsin A, like GPCR receptors (Section 1.1.3). Histamine activates receptor subtypes in different concentrations and generally has a higher affinity at H₃R and H₄R in comparison to H₁R and H₂R.²⁹⁵ Histamine H₁ receptor (H₁R) was first discovered over half a century ago. Agonism at H₁R, which belongs to the G_{αq} receptors, leads to PLC and IP₃ activation. This further activates protein kinase C (PKC), leading to calcium mobilization from intracellular storages, and finally to contraction of smooth muscle and histamine release from mast cells.²⁹⁷

H₁Rs are localized ubiquitously in the human body. However, the highest density in the CNS is in the *hypothalamus* and *thalamus* nuclei and cortical regions.^{298,299} Antihistamines acting as H₁R antagonists reached the blockbuster status as potent antiallergic agents. Histamine transduce signal also via H₂R, which belongs to the G α_s receptor,²⁹⁷ and stimulates gastric secretion. H₂Rs are distributed in the stomach, brain, smooth muscle cells, and immune system.³⁰⁰ Therefore, H₂R antagonists were widely used in the therapy of gastritis, gastroesophageal reflux disease, or ulcer. However, nowadays, they are almost abandoned in therapy and replaced with more potent and safer proton pump inhibitors. H₄R presents the most recently discovered histamine receptor subtype (the early 2000s).³⁰¹ It expresses 40% homology with the H₃R and is not expressed in the brain.³⁰² It signals through the G α_i subunit, leading to a decrease in cAMP concentration. It is associated with chemotaxis, but its precise role is yet to be thoroughly determined. However, its association with allergies or immune reactions was confirmed.

Table 2: Main characteristics of histamine H₁₋₄ receptors

	H ₁ R	H ₂ R	H ₃ R	H ₄ R
Discovery	1919 ²⁹³	1972 ³⁰³	1983 ³⁰⁴	1977 ³⁰⁵
Cloning	1991 (cattle) ³⁰⁶ 1993 (human) ³⁰⁷	1991 ³⁰⁸	1999 ³⁰⁹	2000 ³⁰²
GPCR²⁹⁵	Gq	Gs	Gi	Gi
Cell effect²⁹⁵	↑phospholipase C ↑ c AMP	↑ c AMP	↓c AMP	↓c AMP
Role³⁰⁰	sleep-wake cycle regulation, vasoconstriction, bronchodilatation	gastric acid secretion	sleep-wakefulness cognition, memory	allergy, autoimmune disorders
Receptor agonists³⁰⁰	histamine, suprahistaprodifen	amtamine impromidine, UR-AK 24	N ^α -methyl histamine imepip, imetit, ciproxifan thioperamide	ST-1006 ³¹⁰ 4-methylhistamine ³¹¹ VUF-8430 ³¹²
Receptor antagonists³⁰⁰	mepyramine, doxepin loratadine, cetirizine levocetirizine	ranitidine, cimetidine, famotidine	pitolisant ³¹³ , ABT-239 ³¹⁴ DL-77 ³¹⁵	JNJ-7777120 ³¹⁶ ; SENS-111 ³¹⁷ , JNJ-3975879 ³¹⁸
Distribution²⁹⁵	epithelial cells, smooth vascular cells, neuronal, glial cells ²⁹⁶	parietal cells, smooth muscle vascular cells, immune system	<i>nucleus accumbens</i> , <i>cortex</i> , <i>hippocampus</i> , <i>striatum</i> , <i>basal</i> <i>ganglia</i>	hematopoietic cells

1.4.2 Histamine H₃ Receptor

It was long hypothesized that histamine acts only through H₁R and H₂R. A new receptor isoform, histamine H₃ receptor (H₃R), was discovered at the beginning of the nineties by Arrang et al., who confirmed histamine release inhibition via the new subtype.³⁰⁴ It was cloned a decade later by Lovenberg et al.³⁰⁹ H₃R has four exons and three introns, and 445 amino acids.^{295,319} It expresses only up to 31% homology with other GPCRs, (α_1 and α_2 adrenergic and muscarine M1 receptor) and only up to 21% and 22% with H₁R and H₂R, respectively.³²⁰ H₃R is an auto and heteroreceptor, located mainly presynaptically and expressed almost exclusively in the CNS. The highest H₃R density was observed in the *striatum*, olfactory tubercle, *locus ceruleus*, *dorsal raphe nucleus*, Purkinje cells, *tuberomammillary nucleus*, and *globus pallidus*.^{298,321,322} It has at least twenty human isoforms due to alternative splicing.^{322,323} As an autoreceptor, H₃R leads to inhibition of histamine synthesis via negative feedback.³²⁴ As a heteroreceptor, it affects dopamine and noradrenergic release.^{300,325} It was, however, confirmed that H₃R could also be located postsynaptically, especially in *striatum*.³²⁶ Even though H₃R crystal structure is not resolved yet, it is hypothesized that conserved GPCR residue Asp 114^{3,32} in the third transmembrane domain is essential for ligand interaction as in other GPCR (e.g., dopamine receptors).³²⁷ H₃R displays high constitutive activity- producing a biological response when the ligand is not bonded.³²⁸ It is G α_i coupled (Figure 14), and upon activation consecutive inhibition of adenylate cyclase, a decrease in cAMP concentration and reduced PKA activity occur.³²⁹ H₃R also transduce signals through other pathways such as mitogen-activated protein kinase (MAPK). Histamine and imepip, H₃R agonist, phosphorylate ERK 2 (a member of MAPK family) and activate MAPK cascade via G $\beta\gamma$ subunit.³²¹ ERK activation in the *hippocampus* impacts the memory of fear and plays an important role in neuroplasticity development and neuroprotection.^{330,331} ERK 2 activation is H₃R specific, confirmed by H₄R antagonist, JNJ-7777120 administration, that had no impact on this pathway.³³¹ H₃R leads to PLC and IP₃ activation and further releases Ca²⁺ from intracellular depots.³³² H₃R can furthermore inhibit the Na⁺/H⁺ pump that exchanges one hydrogen ion for sodium ion. This is an especially important mechanism for maintaining intracellular pH. Increased intracellular sodium concentration activates the Na⁺/Cl⁻ noradrenaline dependent channel and promotes norepinephrine release from the cell. By inhibiting this exchanger, H₃R activation can have protective impact in the ischemic state due to noradrenalin induced arrhythmias.^{325,333} G $\beta\gamma$ subunit leads to phosphatidylinositol-3-kinase (PI3K) activation and Akt activation by phosphorylation

and consequent decreased concentration of glycogen synthase kinase 3 β , major tau kinase (GSK 3 β).³³⁴ Besides activation of H₃R lead to activation of phospholipase A₂ (PLA₂) and formation of arachidonic acid.

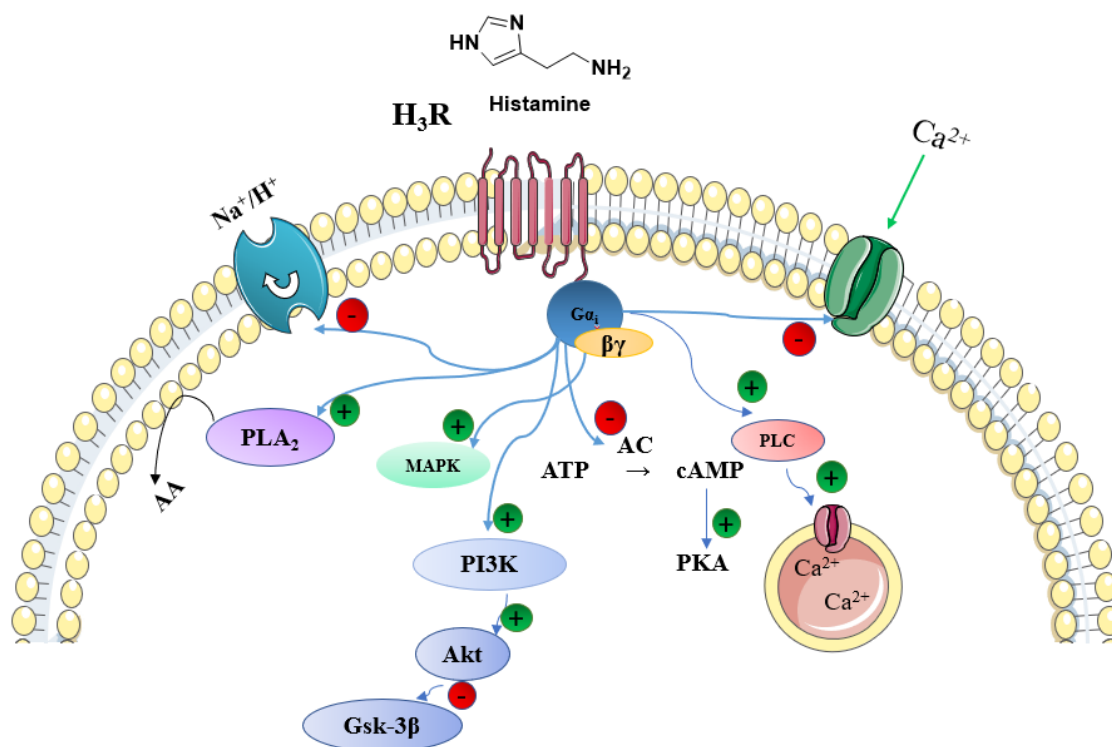


Figure 14: H₃R mediated signaling. AA, arachidonic acid; Akt, Akt kinase; cAMP cyclic adenosine monophosphate, AC adenylyl cyclase; ATP adenosine triphosphate; GSK 3 β , glycogen synthase kinase 3 β , MAPK, mitogen-activated protein kinase; PKA protein kinase A; PKB, protein kinase B; PLA₂ phospholipase A₂; PLC phospholipase C. Adapted from Bongers et al.³³⁴

Since its revelation, H₃R has raised interest due to its involvement in the etiology of diseases such as AD, cognitive impairment, ADHD, narcolepsy, neuropathic pain, alcohol addiction, and epilepsy, representing an interesting target for developing new potent ligands.^{300,322} Several studies have confirmed a positive association between histamine and cognitive processes. Moreover, in *post mortem* analysis in AD patients, decreased histamine levels have been found.³³⁵ Rizk et al. confirmed its involvement in high cognitive processes, with mice lacking H₃R that showed improved spatial learning³³⁶ both in short and long-term memory.³³⁷

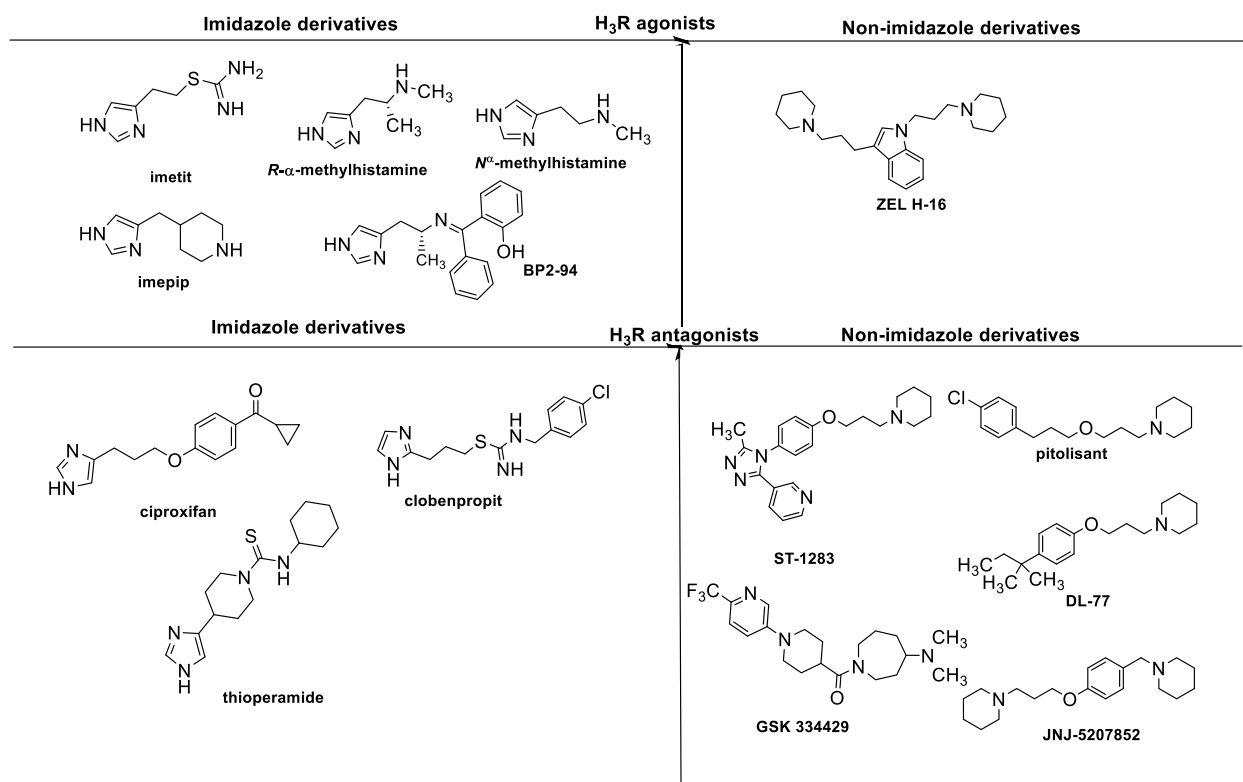
H₃R association with the higher cortical processes and high histamine affinity towards this receptor subtype raises interest in investigating H₃R as a potential CNS target.²⁹⁸ Current H₃R ligands can

be roughly divided into two groups: imidazole and non-imidazole derivatives. The imidazole moiety incorporated in histamine represents important moiety for binding to the receptor by forming hydrogen bonds. Histamine and its structurally closed derivatives *R*- α -methylhistamine (Figure 15) and *N* ^{α} -methylhistamine are potent but not selective H₃R agonists. (*R*- α -methylhistamine shows affinity at H₄R and *N* ^{α} -methylhistamine at H₁R and H₂R).³⁰⁰ Nevertheless, *N* ^{α} -methylhistamine was investigated in migraine in clinical phase III, where its efficacy has been confirmed.³³⁸ H₃R agonists have been widely used in [³H]-labeled radioligand binding assays. Imepip and imetit are later developed H₃R agonists that show high H₃R and moderate H₄R affinity.³⁰⁰ *R*- α -methylhistamine prodrug, **BP2-94**,³³⁹ developed almost three decades ago, expressed anti-inflammatory activity, as well as antinociceptive characteristics.³⁴⁰ **Cipralisant** was initially developed as an H₃R antagonist, showed full and partial agonism *in vitro*, while full antagonism *in vivo*.³⁴¹ Cipralisant is in a clinical trial for ADHD.³⁴² All described ligands lack selectivity and show moderate to high affinity to histamine H₄R. Moreover, imidazole is metabolized via CYP450 isoenzymes and can interact with CYP450 inhibitors and inductors and cause drug-drug interaction. Non-imidazole derivatives were developed to overcome this obstacle. Recently developed H₃R agonist **ZEL-H16** showed nanomolar affinity ($K_i = 2.07$ nM) and a 20-fold higher affinity to H₃R than to H₄R,³⁴³ is up to date the only non-imidazole H₃R agonist.

H₃R antagonists present a promising field regarding potential therapy. As in the development of agonists, the imidazole moiety was also the key scaffold for optimizing and developing new H₃R antagonists. First H₃R imidazole-containing antagonists were **thioperamide**, which also shows an affinity at H₄R and expressed promising results in epilepsy³⁴⁴ and cognitive behavior therapy.³⁴⁵ **Clobenpropit** is another imidazole H₃R antagonist that also shows an H₄R affinity.³⁴⁶ It showed anticonvulsive activity,³⁴⁷ but also possible antidepressant effects.³⁴⁸ **Ciproxifan** is a very potent H₃R antagonist/inverse agonist that promotes attention, confirming its role in high cognitive processes.³⁴⁹ However, non-imidazole derivatives were developed to address the potential metabolic interactions caused by imidazole moiety.³⁰⁰ Replacement of the aromatic imidazole ring with the aliphatic piperidine resulted in the synthesis of potent H₃R ligands that do not interfere with the CYP450 metabolic pathway.³⁴² This breakthrough further led to designing novel non-imidazole H₃R ligands, resulting in high affine compounds as **JNJ-5207852**,^{350,351} **ST-1283** with promising effects in alcohol abuse³⁵² and **DL 77** in autistic behavior³¹⁵ epilepsy³⁵³ and in improving memory.³⁵⁴

Introducing thiazole as in recently reported derivatives resulted in H₃R affinity that remained in low nanomolar concentration range.^{355,356} Introducing azepane ring in **GSK 189254**³⁵⁷ lead to obtaining a high affine compound efficient in neuropathic pain therapy.

The most significant success in the field of H₃R ligands was the development of **pitolisant**. The only marketed selective H₃R antagonist/inverse agonist (Wakix®) for treating excessive daytime sleepiness in adult narcolepsy patients with or without cataplexy. Pitolisant was designed by Bioproject and approved by EMA in 2016 and by FDA in 2019. It shows a high affinity to H₃R ($K_i = 0.16$ nM)³⁵⁸ and is more potent in humans than in rodents.³⁴² Usually, it is dosed one time per day (in the morning), is fast absorbed, metabolized via CYP3A4, and CYP2D6, and renally eliminated.³¹³ It successfully decreased both excessive daytime sleepiness as well as cataplexy episodes when compared to placebo. Pitolisant is an interesting target for cognitive impairment, epilepsy, Prader Willi syndrome, and obesity.³⁵⁹⁻³⁶² Due to its low abuse potential, it does not have the status of controlled drug in the USA.³⁵⁸ Pitolisant is well-tolerated,³⁴² and the most common side effects are insomnia or headache, but both do not affect the quality of life and are relatively moderate. pitolisant was also influential in balancing sleep-wake disorders that accompany other neurological diseases as PD.³⁴² Procognitive effects of pitolisant can be promising for developing novel potent pharmacological tools for the drug development for diseases characterized by cognitive impairment as PD, AD, or schizophrenia. Taken all together, pitolisant was chosen as a lead compound to synthesise multitargeting ligand in this PhD project.

Figure 15: Preclinical and clinical H₃R ligands

1.5 Sleep-Wake Disorders

Narcolepsy is a chronic sleep-wake disorder characterized by sudden sleep attacks. The prevalence of narcolepsy is 20 to 60 in 100 000.³⁶³ The etiology of the diseases remains unknown, and therefore is only symptomatically treated.³⁶⁴ It is a chronic disease and requires lifelong therapy. Narcolepsy can be divided into two types. Type I is caused by selective loss of orexin, and characterized with cataplexy (sudden loss of muscle tonus), followed by fall.³⁶⁵ Cataplexy is mainly triggered by strong positive or negative emotions. In type II, cataplectic fall does not occur, and this type is more challenging to diagnose.³⁶⁶ Symptoms of narcolepsy are excessive daytime sleepiness (EDS), fragmented nocturnal sleep, cataplexy (type I), hypnagogic hallucinations, and “sleep paralysis” during awakening or falling to sleep.³⁶⁷ Narcolepsy diagnosis is based on EDS, which should last for at least three months.

The histamine pathway is involved in the sleep-wake cycle. Histaminergic neurons originated from the posterior hypothalamus, and together with orexinergic neurons, take part in sleep-wake regulation.³⁶⁸ Hypocretin activates histaminergic neurons, and in narcolepsy type I, as a consequence of hypocretin loss, histaminergic levels are significantly decreased.³⁶⁹ The only approved H₃R inverse agonist Wakix® (INN: pitolisant, Section 1.4.2) acts on presynaptic H₃Rs and leads to a consequent increase in histamine concentration.

Sleep-wake disorders exist as isolated disorders but can often accompany other neurological diseases, as PD. Up to 40% of PD patients have abnormal sleep-wake behavior, characterized by EDS.³⁴² Moreover, drugs used in PD treatment can induce somnolence (e.g., dopamine agonists as described in Section 1.3), excessive daytime sleepiness, and poor sleep quality in PD patients.^{370,371} The latter is also observed in newly diagnosed PD patients.³⁷² Unbalanced sleep-wake cycles have a significant negative impact on life quality. Besides, cognitive impairment has been observed in patients with PD more often if they suffer from EDS.³⁷³

1.6 Multi-Target-Directed Ligands

Numerous CNS diseases have multifactorial etiology, and the “single drug → single disease” approach is often not a practical option for their treatment. The traditional method was focused on the development of selective ligands (often referred to as “magic bullet”)³⁷⁴ that interacts with a specific biological target of interest. Nevertheless, this process expresses several limitations. Lack of selectivity leads to interactions with “off-targets”, resulting in decreased efficacy or severe side effects. This phenomenon, however, was used for repurposing drugs and their “off-label” use. For instance, Sildenafil was initially developed to treat angina pectoris but repurposed for sexual dysfunction, and currently, its use in oncology is hypothesized.³⁷⁵

Lack of selectivity and severe side effects shifted drug development to other therapeutic approaches. There are three approaches for multifactorial disease treatment:^{376,377}

- drug cocktails or **polypharmacy**: administering multiple dosage forms, each with active ingredient, which often results in low patient adherence

- combining two or more active ingredients in one dosage form (e.g., Stalevo® - levodopa, carbidopa, and entacapone)
- designing multitargeting ligand that will simultaneously target two or more biological on-targets, often referred as **polypharmacology**

The latter is particularly interesting and gained more attention in the last decades due to its advantages compared to the two former approaches. That further led to developing Multitarget-directed ligands (MTDL) (referred sometimes as “designed multiple ligands” (DML)), where two or more moieties are combined in one ligand, interact with at least two different on- targets.

MDL express several advantages when compared to the polypharmacy approach ^{374,378,379}

- ✓ Potential superior efficacy (additive or synergistic effects)
- ✓ Better patient adherence (one dosage form instead of polypharmacy)
- ✓ Improved pharmacokinetic characteristics (easier to predict when compared to the multiple drugs)
- ✓ Reduced risk of dose-dependent side effects by rationally designed MTDLs
- ✓ Reduced drug-drug interaction
- ✓ Lower probability for resistance development (due to lower doses administered)
- ✓ Less complicated approval process (only one safety and efficacy study need to be conducted)
- ✓ Better cost/effectiveness

MTDLs should not be confused with “dirty drugs”. The latter interact with the target of interest and with numerous “off-targets” (e.g., FGAs). Dirty drugs often express severe side effects that can ultimately lead to the withdrawal from the market. However, MDTLs need to be rationally designed, enabling interaction only with the receptors of interest, their biological on-targets, and decreased risk of interaction with off-targets. This is particularly challenging when the target of interest and off-targets have high homology levels.³⁷⁴ Rational MTDLs design raised interest,

resulting in 21% of newly approved drugs by the FDA were MTDL in 2015-2017.³⁸⁰ Some commercially available drugs are, in essence, MDTLs, proven after their global approval. (e.g aripiprazole, cariprazine, safinamide).³⁸⁰

MTDLs should achieve targeted delivery and consequent allosteric and/or orthosteric interaction with the biological targets.³⁷⁶ They should express a good pharmacokinetic profile (absorption, distribution, metabolism, and excretion (ADME) properties). MDTLs can be designed based on prior synthetic knowledge and clinical observations in a particular field or using *in silico* methods. The latter enables high throughput screening (HTS), ligand-based (LB), and structure-based (SB) approaches to find the best moieties for the receptor interaction, optimal linker for coupling,³⁸¹ as well as their possible “off-target” effects.

MTDLs can be classified according to their architecture and arrangement (Figure 16). Two pharmacophores in MTDLs can be separated with a linker, which is either metabolically stable or cleavable, resulting in MTDLs with higher molecular weight.³⁷⁹ Conjugation of two pharmacophores without linker results in merged MTDLs. Fused MTDLs occur when moieties overlap, resulting in ligands with lower molecular weight.

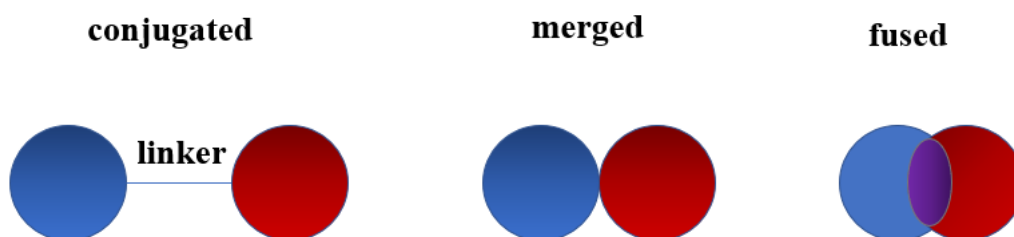


Figure 16: Different types of MTDLs by pharmacophore combination. Adapted from Proschak et al.³⁷⁶

A multitargeting approach was proposed for the treatment of cognitive diseases.³⁸¹ There is an increased interest in the synthesis of MTDLs to treat neurological diseases with complex pathology and etiology such as AD or PD.

In 2012 Besnard et al. reported high affine dual D₄R agonist and D₂R inverse agonist MDTLs based on donepezil (Figure 17). Obtained ligands showed a higher affinity to D₂R in comparison to donepezil.³⁸² Bolea et al. also reported donepezil derivatives combined with MAO B antagonist

moiety. This MTDL containing both benzopiperidine moieties, responsible for interaction with AChE) and a propargyl amine moiety, which inhibits MAO B.³⁸³ Jaitech et al. reporter novel MTDL which target both MAO B enzyme and adenosine A_{2A} receptor.³⁸⁴

Introducing H₃R antagonistic moiety and combining it with amitriptyline derivatives has been a promising approach in the design and synthesis of MTDLs (von Coburg et al.).³⁸⁵ Moreover, recent MTDLs, containing both an adenosine moiety and a MAO B moiety, can be potential tools in treating PD,³⁸⁶ as xanthine derivatives reported by Koch et al.³⁸⁷ Cao et al.³⁸⁸ combining SGAs moieties like in aripiprazole, brexpiprazole, and cariprazine displays multitargeting properties to obtain novel ligands with better pharmacokinetic profiles.

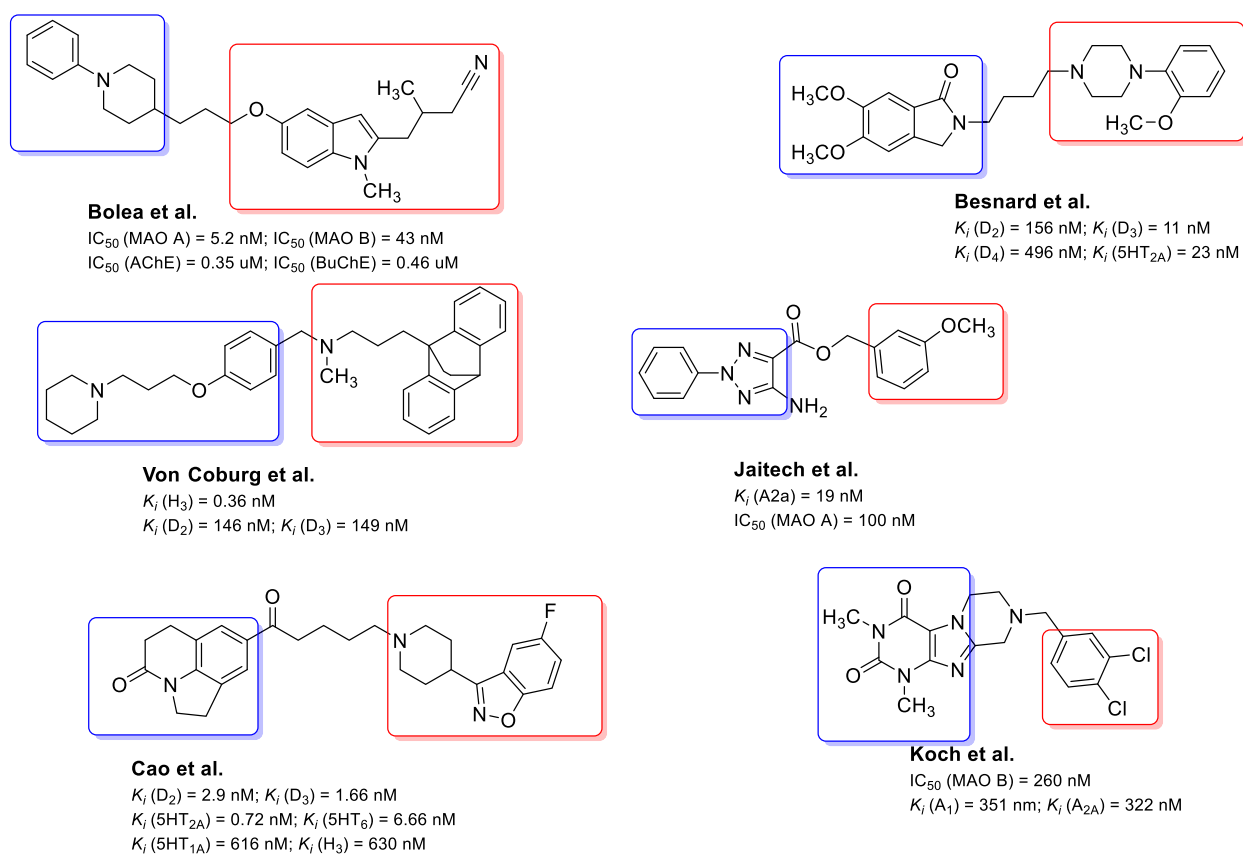


Figure 17: Cherry-picked MTDLs. IC_{50} half-maximal inhibitory concentration; K_i inhibition constant.

1.7 Objectives

The main objective of this PhD project was to develop potent, novel dopamine multifunctional D_{2/3}R and H₃R ligands that can be further used in the therapy of various neurological diseases connected with the altered concentration of dopamine and histamine such as Parkinson's disease, schizophrenia, drug addiction, Huntington's chorea, sleep-wake disorders, or ADHD.

Even though dopamine receptors are well-known targets, the design of selective ligands has remained a challenge up to now due to the high homology between the different receptor subtypes. In the last decades, the crystal structures of D₂R and D₃R were resolved, providing better insight into structural properties, and thereby providing valuable information for the design and synthesis of novel, selective dopamine ligands. However, up to date, no selective ligands have been introduced to the market. Therefore, it is still unclear whether clinical effects occur due to the interaction with on-target, off-target receptors, or both. The lack of selectivity can lead to severe side effects and lower patient adherence, as observed in commercially available antipsychotics. Moreover, the currently employed drug regime barely addresses negative symptoms, and room for improvement in this research field is left. D₃R presents a particularly interesting target due to its limited localization and implications in severe neurological disorders as schizophrenia or addictive behavior. Over the years, efforts have been centered around the design of selective D₃R receptor ligands, and **BP 897** was the first described, selective D₃R partial agonist. Therefore, this compound served as a lead molecule to design and synthesize the first set of selective dopamine D₃R ligands. By connecting the primary pharmacophore with a various moiety that interacts with the second binding pocket, better selectivity can be achieved. Molecular docking simulations were performed to examine potential binding mode.

More recently, it was confirmed that D₂-like receptors exist as homo- or heterodimers. Their formation is highly regulated and can impact ligand binding as well as signal transduction. Attention has been drawn to synthesize bitopic ligands with a higher molecular weight that would target these dimers and occupy the receptor's orthosteric binding site. However, developing low molecular weight ligands that can target single receptor or homo- or heterodimers and have better drug-like properties can be highly interesting. Currently available dopamine receptor ligands for PD treatment cause side effects and express moderate to low selectivity. In line with these results, the synthesis of low molecular dopaminergic D₂R and D₃R bitopic ligands was conducted.

Histamine H₃R represents an attractive target ever since it was cloned at the end of millennia. It is associated with high cortical processes like attention, cognition, sleep-wake cycle, or memory regulation. Due to the complexity of the above-mentioned neurological diseases, MTDLs were developed, wherein one moiety, dopamine, and histamine receptor pharmacophores were combined. The rational design of MTDLs can lead to a more practical approach and improved pharmacokinetics and pharmacology. As shown in numerous studies, PD is often followed by sleep disturbances. Therefore, pramipexol analogues (D_{2/3}R pharmacophores) were combined with pitolisant analogues (H₃R pharmacophores). Not only pitolisant can reduce excessive daytime sleepiness, but this combination may reduce the side effect of pramipexole-based somnolence and, therefore, can provide a potent agent that will overcome the disadvantages of currently available PD medicaments. Cognitive impairment often accompanies neurological disorders such as PD or schizophrenia and can significantly reduce patients' quality of life. Considering the positive effect that H₃R antagonists express on cognitive impairment, it would be beneficial to synthesize D_{2/3}R and H₃R multifunctional ligands and, from the start of the therapy, try to reduce the risk of cognitive impairment.

Even though receptor localization is mainly revealed, it is still not resolved where the exact receptor subtypes are located due to their high homology. Designing selective fluorescent ligands will enable better insight into receptor distribution and localization and, consequently, their physiological role closely connected to their distribution. Coupling both D_{2/3}R and H₃R pharmacophores with highly stable and recently reported fluorophore was conducted, resulting in ligands with beneficial fluorescent properties.

To summarize, by designing and combining dopamine and histamine receptor ligands for each receptor subtype, their effects on the receptor and receptor occupancy can be followed, which can further result in resolving signal cascade and explaining their pharmacological roles, leading to rationally designed, novel drug-like candidates.

2 Chemistry

2.1 Standard Reaction and Chemical Approaches

The main objective of this PhD project is the rational design and synthesis of multifunctional dopamine D₂R, D₃R, and histamine H₃R ligands to develop new, potent mono-, and multitargeting small molecules. These ligands could be further applied in treating numerous neurological diseases or receptor visualization. In this chapter, the main chemical principles and reaction mechanisms for designing and synthesizing desired ligands will be described. *In silico* studies, determination of pharmacological properties, and SAR studies will be explained in Chapters 3 and 4, respectively. Synthesis description follows the experimental timeline during PhD with overlapping of few projects that are mentioned and explained in corresponding sections. This chapter is divided according to the moieties that were introduced.

2.2 D₃R Ligands with the Antagonist Moiety

Since the revelation of dopamine D₃ receptor¹⁵⁶ different efforts have been centered around designing selective, novel, and potent D₃ receptor ligands. Various working groups struggled to develop selective ligand, mainly due to the high homology level between the D₂R and D₃R receptors (up to 88% in structurally conserved regions (SCR)³⁸⁹ and almost identical orthosteric binding site (OBS) interaction within two receptors subtypes).^{116,117,154}

General D₃R pharmacophore was described almost twenty years ago (Section 1.1.5).¹⁸¹ It can be divided into four regions: aromatic moiety, amide moiety, linker, and basic heterocycles with aryl substitution. First, potent ($K_i = 0.92$ nM) D₃R partial agonist, **BP 897** (Figure 18), was developed parallel with the description of general pharmacophore.^{390,104} **BP 897** entered several clinical trials (for schizophrenia, ADHD, and addictive behavior) but up to date was not marketed. This D₃R preferring ligand served as a blueprint for synthesizing the first compound set.

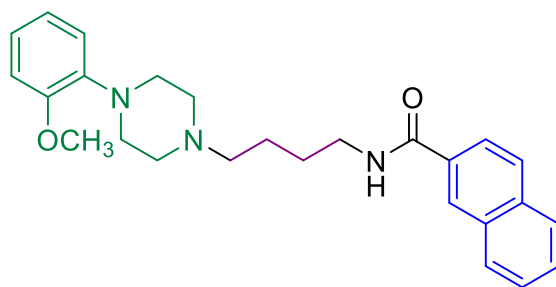
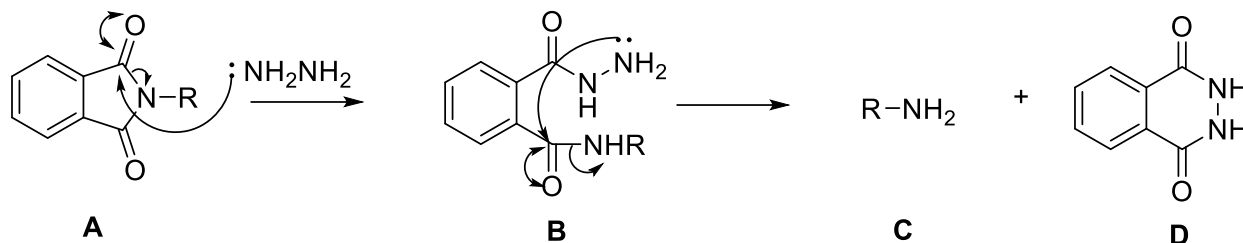


Figure 18: **BP 897**, a blueprint for the synthesis of the first compound set

After **BP 897** complete characterization, various efforts were made to optimize D₃R selective ligands. This resulted in reporting 1-(2-methoxyphenyl)piperazine and 1-(2,3-(dichlorophenyl)piperazine as D₃R primary pharmacophore (PP)^{144,391,392} that bind to the OBS in both D₂R¹¹⁶ and D₃R.¹¹⁷ Besides, arylamide moiety binds to the SBP and represents one of the prerequisites for obtaining selectivity between these two receptor subtypes.^{393–395} First compound set consists of ten dopamine D₂R and D₃R receptor ligands (**1-10**) that display all necessary elements for interaction with the D₃R: basic nitrogen incorporated in piperazine, amide moiety, different aromatic moieties, and linker. The main goal was to evaluate linker length and further optimize arylamide moiety to increase selectivity towards D₃R. Firstly, the linker was varied from two to five methylene groups to achieve optimal distance between PP and SP. Secondly, naphthyl moiety in **BP 897** was replaced with 3-bromo-4-methoxyphenyl, coumarin, or pentafluorosulfanyl moiety (SF₅). The latter presents a novel chemical entity and displays high values of electrophilicity and lipophilicity. SF₅ is chemically and thermally stable.^{396,397} This group is considered as bioisosteric replacement of trifluoromethyl (CF₃) and, under some conditions *tert*-butyl moiety.³⁹⁸ This novel chemical entity was recently incorporated in benzodiazepine derivatives.³⁹⁹ Hence this moiety has beneficial physicochemical properties, it was incorporated into the four compounds (**7-10**) to increase selectivity towards D₃R and to examine its impact on the binding mode.

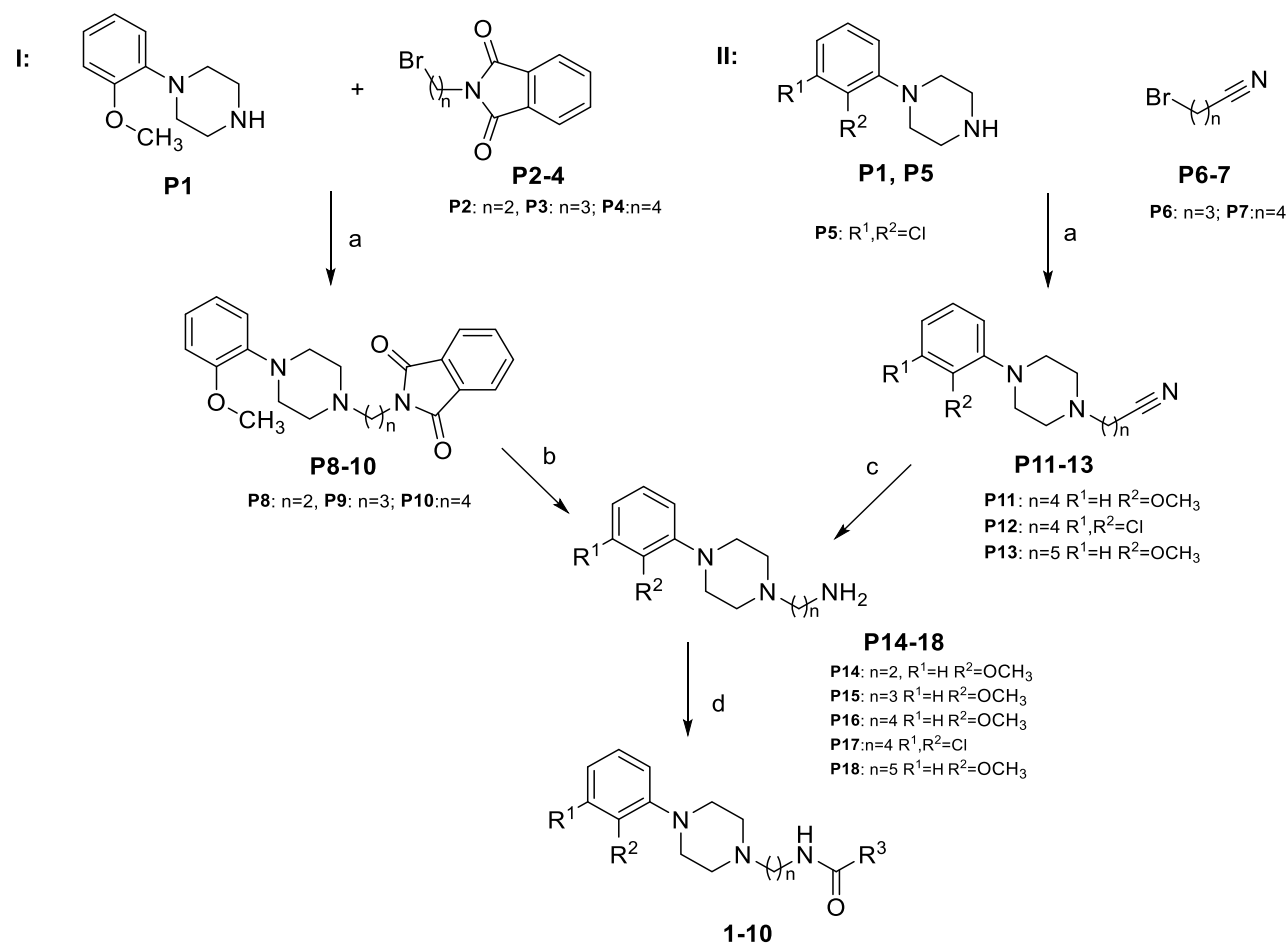
As a precursor for this and several other synthetic routes, amines that contain D₃R moiety were synthesized (Scheme 5). Two different approaches were developed and compared, to obtain amines.⁴⁰⁰ In the first synthetic route (**Route I**), 1-(2-methoxyphenyl)piperazine (**P1**), well-described dopamine D₃R pharmacophore in S_N2 reaction undergoes alkylation with corresponding *N*-(ω -bromoalkyl)phthalimide derivatives (**P2-4**) to obtain protected amines (**P14-16**). Potassium carbonate provides basic conditions, and potassium iodide in catalytic amount enables FINKELSTEIN exchange.⁴⁰¹ As the amino group is prone to alkylation and oxidation, various protecting groups can be introduced, including phthalimide. Alkyl phthalimide (**P8-10**) is obtained through Gabriel synthesis,^{402,403} serves as H₂N-synton and can be efficiently cleaved by hydrazinolysis.⁴⁰⁴ Thereupon, in the next reaction step, hydrazine was used as a deprotection agent to obtain crude amines (**P14 -P16**).

In the hydrazinolysis partially positively charged imide carbon (**A**) undergoes two consecutive nucleophilic attacks (**B**), which results in amine deprotection (**C**) and 2,3-dihydrophthalazine-1,4-dione (**D**) that can be easily removed by extraction (Scheme 4).

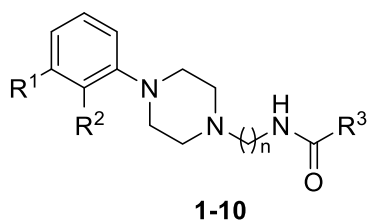


Scheme 4: Mechanism of hydrazinolysis

Despite efficient cleavage, the formation of side products can often lead to low yields. To obtain higher yields, scale up, and decrease costs of the synthesis, more economically second synthetic approach (**Route II**) was developed (Scheme 5). In this approach, precursors (**P1**, **P5**), again following $\text{S}_{\text{N}}2$ mechanism, undergo alkylation with commercially available nitriles: 4-bromobutanenitrile (**P6**) and 5-bromovaleronitrile (**P7**). Nitriles can be further reduced by several reagents (e.g., LiAlH_4 , NaBH_4). However, the simplest reducing agent is hydrogen (H_2) itself. Due to the lack of its nucleophilicity, hydrogen cannot be used to reduce carbonyl compounds. Thus, it represents excellent reducing agents for weaker bonds (e.g., triple). This process, known as catalytic hydrogenation, takes place on the metal surface. Firstly, chemical absorption of hydrogen on the metal surface occurs, resulting in H-H bond breakage. Secondly, nitriles bond to the metal surface and come into direct contact with a reducing agent, enabling hydrogen transfer. In the second synthetic approach, Raney Nickel was prepared as described in the literature,⁴⁰⁵ (from 500 mg nickel alloy), and the reduction took place in methanol saturated with ammonia to obtain crude amines (**P16-P18**). Amines were further coupled with a corresponding activated carboxylic acid in dichloromethane to obtain amides as final compounds (**1-10**, Table 3).



Scheme 5: Two synthetic approach for the synthesis of the first compound set (1-10) a: K₂CO₃, KI, reflux 16h; b: H₂NNH₂, MeOH, reflux, 2h; 2M HCl, reflux, 1h; c: Raney-Ni, NH₃/MeOH, H₂ 5bar, 12h; d: DCM, HOOC-R³, HOBt, EDC, R.T., 16h.

Table 3: Compounds that contain D₃R antagonist moiety (1-10)

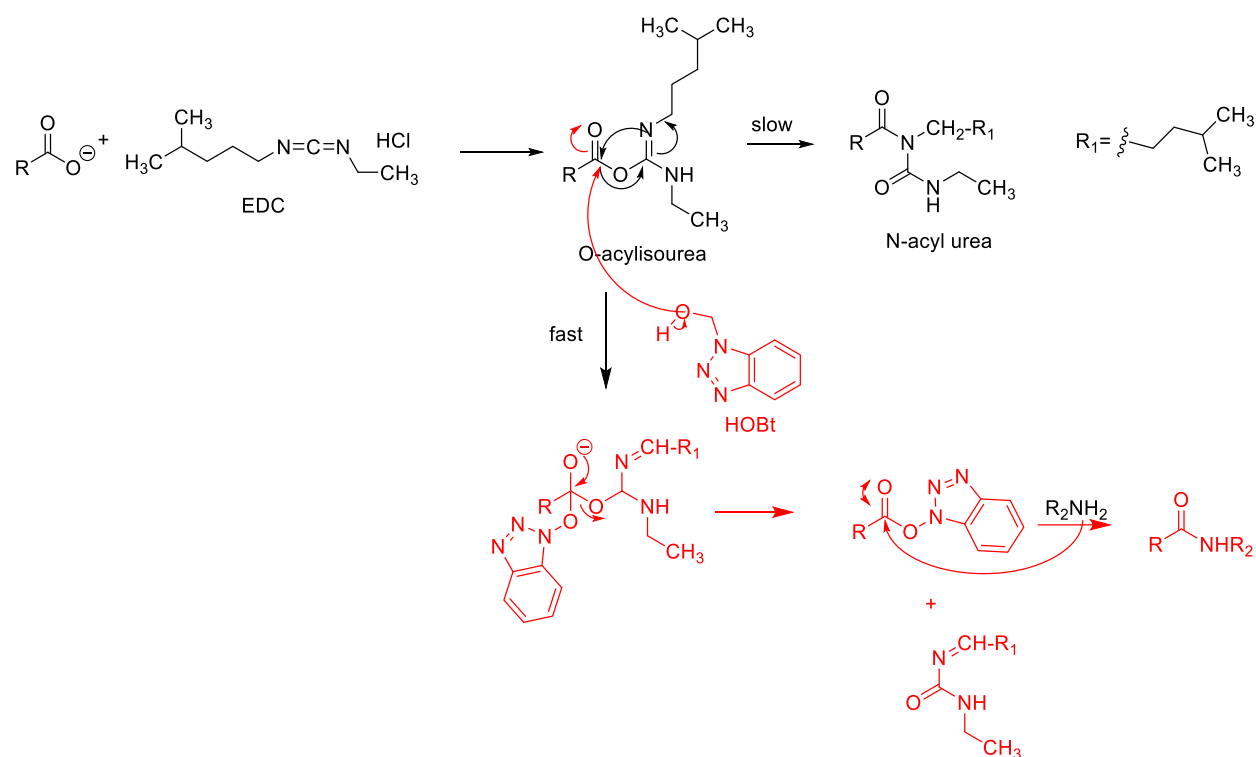
Nr.	n	R ¹	R ²	R ³
1	2	H	OCH ₃	
2	3	H	OCH ₃	
3	4	H	OCH ₃	
4	5	H	OCH ₃	
5	4	H	OCH ₃	
6	4	H	OCH ₃	
7	4	H	OCH ₃	
8	4	Cl	Cl	
9	4	Cl	Cl	
10	4	H	OCH ₃	

2.2.1 Amide Synthesis

Compounds **1-10** contain an amide functional group, as previously described prerequisite for interaction with D₃R. Amide bond formation is one of the crucially important synthetic approaches in medicinal chemistry. Not only amide bond is broadly present in macromolecules such as proteins, but also within numerous preclinical, clinical candidates and commercially available drugs. This functional group itself represents a potential tool due to its resistance to hydrolyses and high temperature. It can form hydrogen bonds or π -interactions within the receptor's active site.

Amides are formed from carboxylic acids and corresponding amines. This reaction, however, does not occur spontaneously and requires a high temperature. This can further lead to several problems as low yields, complex purification, or racemization. Carboxylic acids need to be activated, to avoid these difficulties. Activation can be achieved in several ways. One of the oldest, but up to date very common way, is converting carboxylic acid to halides (mostly chlorides) with thionyl, oxalyl chloride, or phosphorus trichloride. Carboxylic acids could be further converted to anhydrides, azides, acylimidazoles, or esters. The main goal of activation is to form a better leaving group, leading to an unstable tetrahedral intermediate.

Taken environmental issues into consideration, coupling reagents (e.g., DCC, CDI, EDC) present facile way to obtain amides, often resulting in high yield, and cost-effective one-pot synthesis (Scheme 6). However, soluble side product *N*-acyl urea is often observed when coupling reagents are used. Even though this side product can be removed by filtration or extraction, it can significantly decrease yield. By adding nucleophile that reacts faster than acyl transfer (e.g., HOBt, HOAt) and still leads to active intermediate that can be coupled with an amine, yields can be increased.^{406,407} In the last reaction step in the synthesis of the first compound set, EDC was chosen as a coupling reagent in the presence of additive HOBt.



Scheme 6: Mechanism of one-pot amidation approach using EDC as coupling reagent and HOBT as an additive. Adapted from Montalbetti et al., Valeur et al.^{406,407}

2.3 D₂R and D₃R Bitopic Ligands

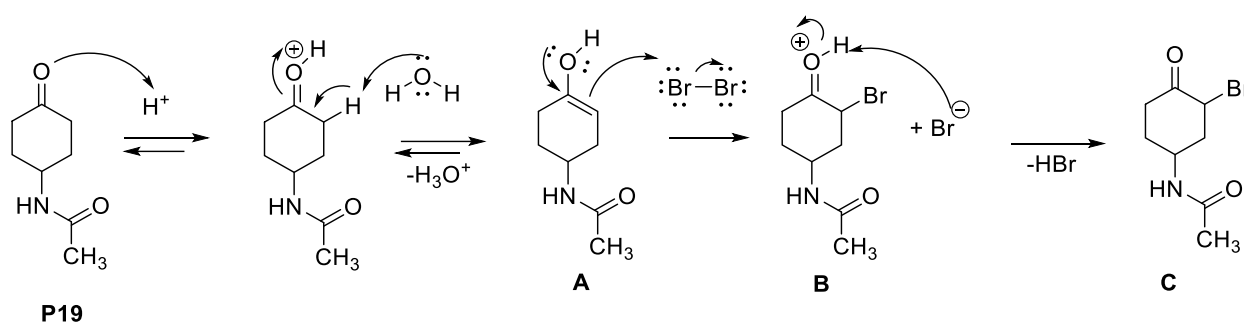
2.3.1 D₂R and D₃R Ligands with Amide Moiety

Recently described D₂R crystal structure¹¹⁶ revealed OBS positioned deeper in D₂R than in D₃R. A new mechanism of aripiprazole-induced-fit binding to D₂R was proposed by Agren et al., where is hypothesized that aripiprazole first reversibly bind to OBS, following by receptor conformational changes, that enables irreversibly binding to SBP.⁴⁰⁸ This further encourages the development of bitopic or bivalent ligands that incorporate pharmacophore that occupy both orthosteric and allosteric binding sites and can act as orthosteric, positive or negative allosteric modulators (PAM and NAM, respectively).⁴⁰⁹ Length of the linker coupling these two entities is of crucial importance for binding mode and selectivity.⁴¹⁰ Moreover, some of the selective commercially available drugs could be categorized as bitopic ligands. Rationally designed bitopic

ligands can be designed as biased ligands, which will help resolving signaling cascades and their involvement in (patho)physiological processes.

Considering all the facts, compounds **11-17** contain already described D₃R pharmacophore and newly introduced D₂R pharmacophore, pramipexole derivative. Pramipexole is a well-known full dopamine D₂R antagonist currently used in PD and restless legs syndrome therapy.²⁷⁶ It shows a higher affinity at D₃R when compared to that at D₂R.^{411,412} It is often the first therapeutic choice for people younger than 65 and is used either as monotherapy or in combination with levodopa.⁴¹³

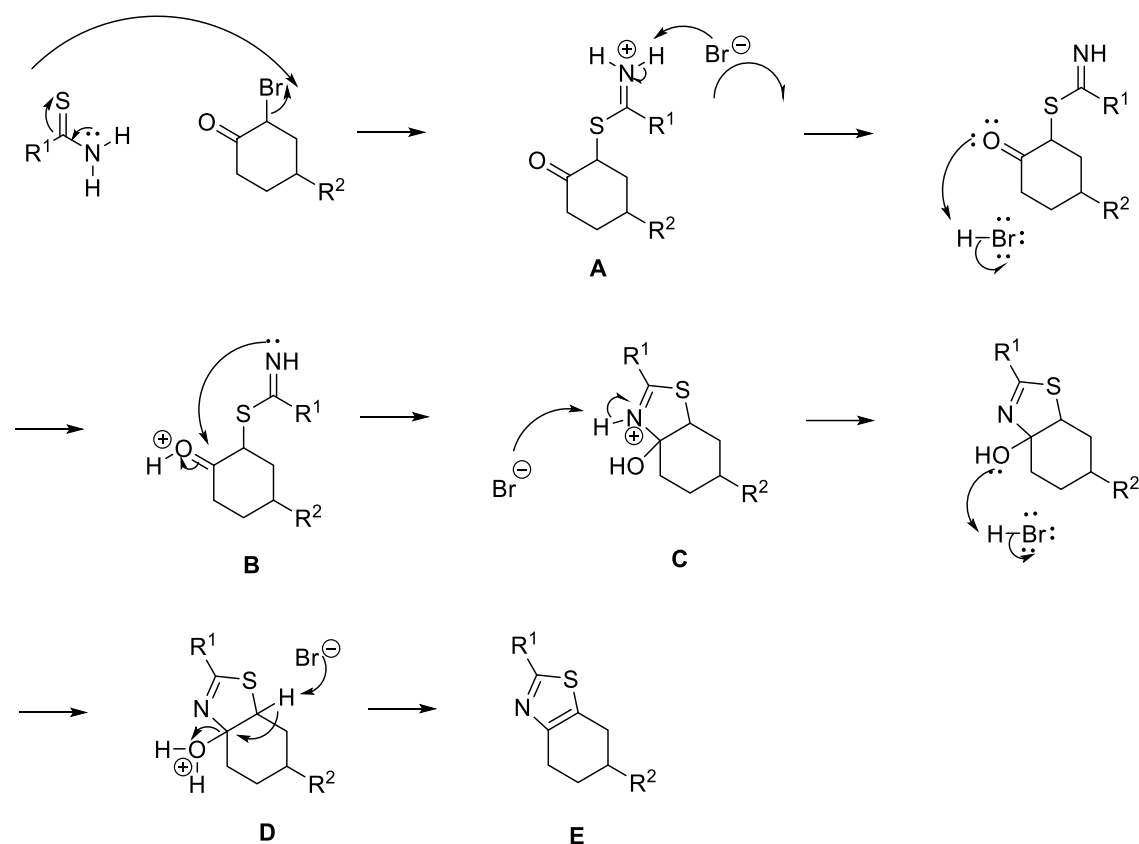
Precursor **P19** was dropwise brominated in glacial acetic acid until the solution changed color from red to yellow.⁴¹⁴ α -Bromination of aliphatic ketones can be performed in the presence of an acid that catalyzes the first reaction step if it occurs slowly. Acid-catalyzed α -bromination leads to the protonation of carbonyl oxygen and enables forming enol (**A**). Enol further undergoes nucleophilic attack by bromine (**B**) with the following deprotonation (**C**) (Scheme 7).



Scheme 7: Mechanism α -bromination of aliphatic ketones on the example 4-acetamidocyclohexanone.

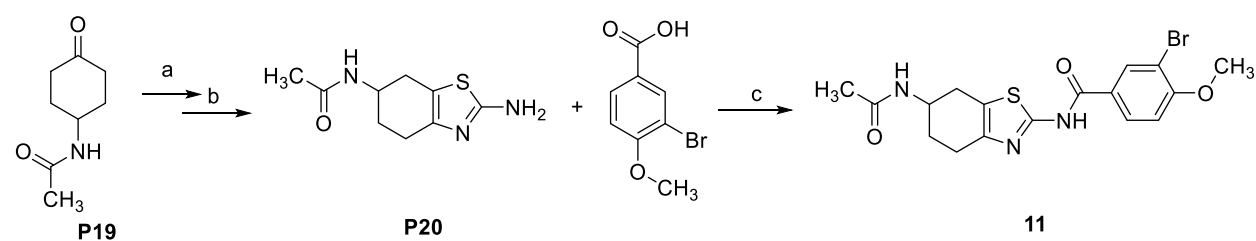
The reaction was carried out at different temperatures to obtain higher yields, resulting in the highest yield (~ 70%) when conducted at 65 °C for two hours. Subsequently, thiourea was added, and HANTZSCH THIAZOLE synthesis was performed to obtain **P20**. HANTZSCH THIAZOLE reaction (Scheme 8), first described in 1889, still represents the main procedure for obtaining thiazoles. Thiazoles are formed from thioamides and corresponding α -bromo ketones. α -Bromo ketones are firstly nucleophilic attacked by thioamide resulting in imino-thiol formation (**A**). Partially positive carbon, which is protonated under acidic conditions, undergoes a second nucleophilic attack (**B**) that further results in cyclization (**C**). After consecutive dehydration (**D**), thiazole (**E**) is formed.

HANTZSCH THIAZOLE reaction is conditions sensitive, and several intermediates (e.g., elimination products or disubstituted derivatives) could lead to lower yield.^{415,416}



Scheme 8: Mechanism of HANTZSCH THIAZOLE synthesis on the example of 2-bromocyclohexanone

The highest yields were obtained when the reaction mixture was refluxed for 1 hour in DMF. Prolongation of reaction time led to the formation of various side products and made purification more difficult. Finally, **P20** has been coupled with activated 3-bromo-4-methoxy benzoic acid to obtain **11** (Scheme 9).



Scheme 9: Synthesis of compound **11**. a: Br₂, CH₃COOH, 2h 60 °C; b: thiourea, 1h, reflux; c: DCM, HOBt, EDC, R.T., 10h.

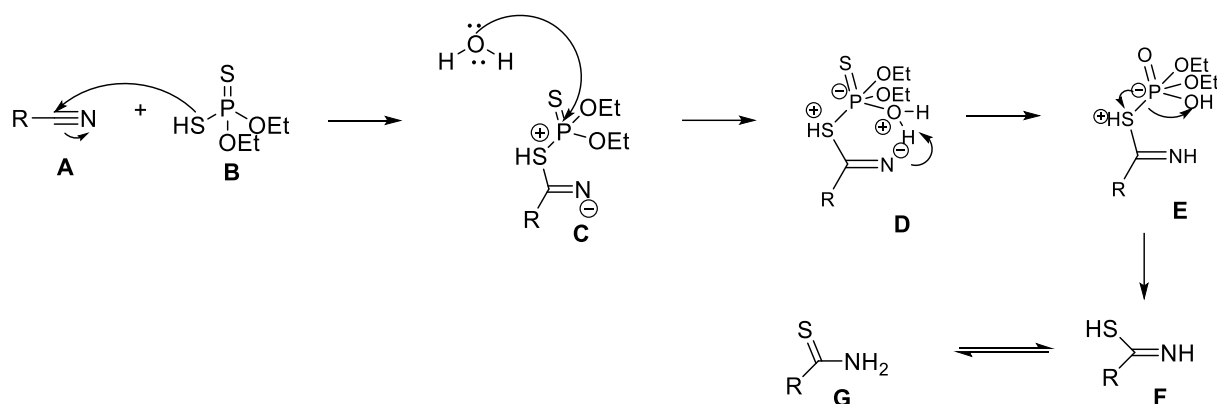
2.3.2 D₂R and D₃R Ligands Connected with Methylene Groups as Spacer

After successfully conducted amide synthesis, the next compound set was expanded to ligands that incorporate D₃R antagonistic pharmacophore and newly introduced pramipexole, connected with methylene groups as linker. Since this synthesis is conducted shortly after the optimization of synthesis in Section 2.4, detailed optimization will be mentioned in the following section.

In the first step, precursor **P1** underwent nucleophilic substitution (S_N2 mechanism) by **P6** and **P7** to obtain nitriles **P11** and **P13**. Nitriles were further converted to thioamides, with *O,O'*-diethyl-dithiophosphate. Thioamides have broad application in organic chemistry and can be obtained by several procedures from different sulfide sources: as with carbon disulfide, sodium sulfide,⁴¹⁷ resin-sulfide,⁴¹⁸ phosphorous sulfide,⁴¹⁹ thioacetic acid,⁴²⁰ Lawesson reagent,⁴²¹ etc. Nevertheless, all mentioned procedures have several disadvantages: toxicity, gas formation, prolonged reaction time, high applied pressure, and/or complex purification. *O,O'*-diethyl-thiophosphate⁴²² is a mild reagent for thioamides synthesis and therefore expresses several advantages compared to the above mentioned reagents. Even though microwave-assisted thioamide synthesis provided good yields as reported by Kaboudin et al.⁴²³ and Bachman et al.⁴²⁴ in this case, thionation in the microwave at 80 °C in water led to only 4% yield. Thioamide synthesis was performed under acidic conditions (in both 4M HCl in 1,4-dioxane and 4M HCl in EtOAc) to increase yield. These synthetic approaches provided excellent yields (up to 95%, LC-MS purity 90-100 %) (**P21-22**).

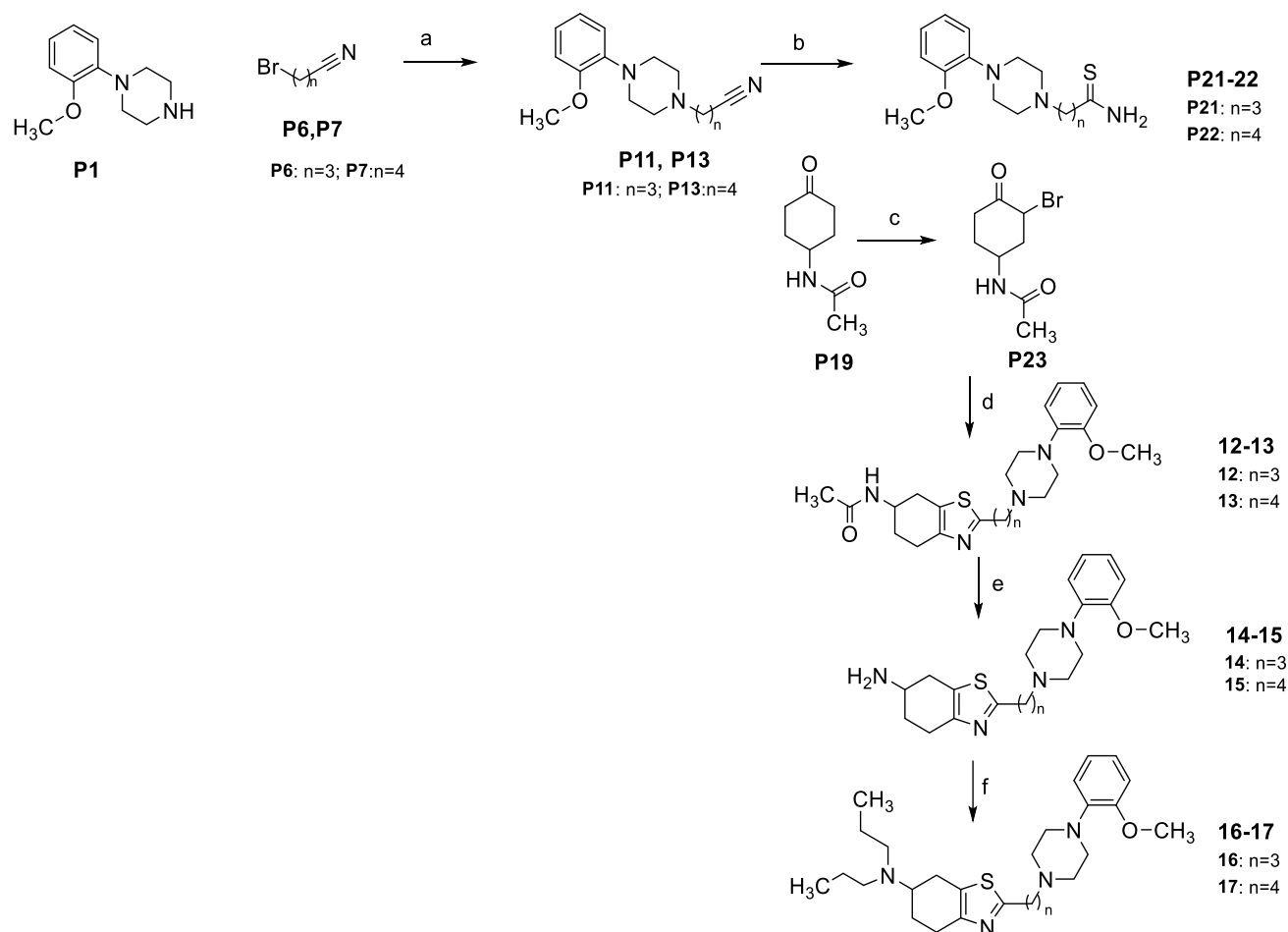
A plausible mechanism of thioamide formation under acidic conditions has been shown in Scheme 10.^{423,425} Nitriles(**A**) are firstly directly nucleophilic attacked by *O,O'*-diethyl-dithiophosphate (**B**), and secondly by water (**C**). After proton transfer (**D**) and dehydration (**E**), iminothiols were formed (**F**), tautomers of thioamides (**G**).

II:



Scheme 10: Plausible mechanism for thioamide synthesis under acidic conditions. Adapted from Kaboudin et al., Yadav et al.^{423,425}

In the following reaction step, thioamides (**P21-22**) and α -bromo ketones (Scheme 11) led to thiazole formation (HANTZSCH THIAZOLE synthesis, Section 2.3.1) in DMF at 65 °C for 2 hours, to obtain 6-acetamide-4,5,6,7-tetrahydrobenzothiazol derivatives (**12-13**). Amides are poor nucleophiles and not basic, in contrast to amines. Therefore, the main goal was to examine impact of different groups (such as amides, primary, and tertiary amines) on the binding affinity to the receptor of interest. Even though the acetyl group is widely used as protecting group for amines, it requires harsh conditions for deprotection (usually presence of strong acid and base with/without catalyst).⁴²⁶ Recently, mild conditions for *N*-deacetylation have been reported, for instance, with Schwarzman reagent up to 5 minutes⁴²⁷ or with transamidation-acyl group transfer from one amine to another.⁴²⁸ Since all of the compounds contain sulfur, which interferes with several chemical processes (e.g., sulfur poisoning of metal catalysts⁴²⁹), harsh conditions were chosen from the beginning and consequently optimized (Section 2.4). *N*-Deacetylation was performed in refluxing hydrochloric or hydrobromic acid over two days to obtain primary amines (**14, 15**). Obtained amines were reductively aminated, resulting in tertiary amines as final products (**16, 17**).

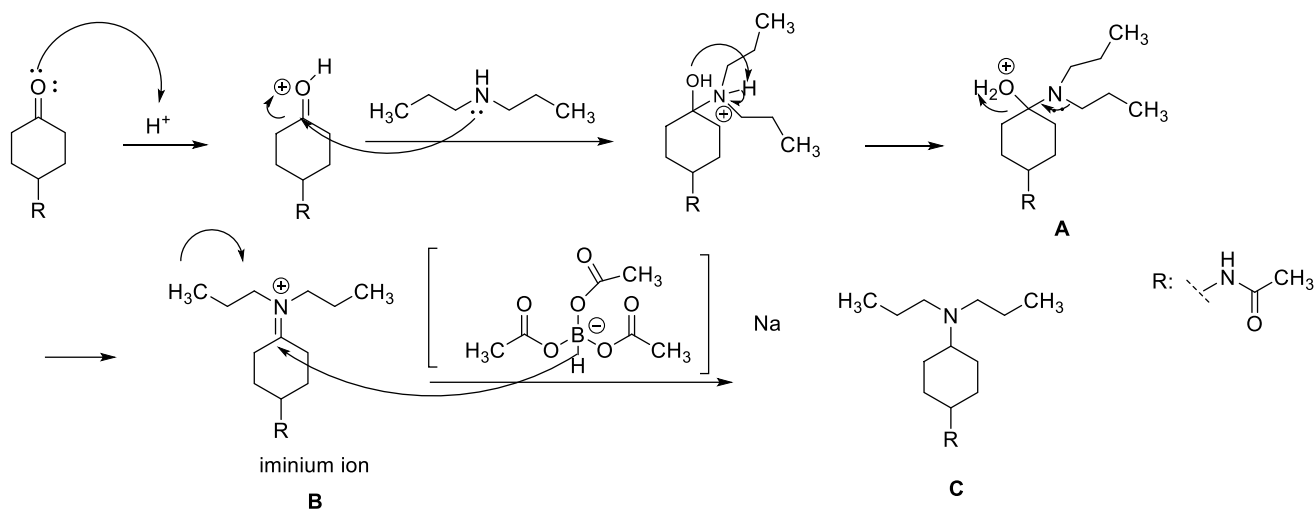


Scheme 11: Synthesis of bitopic dopamine D₂R/D₃R ligands. a: K₂CO₃, KI, acetone, reflux 10h; b: *O,O'*-diethyl-dithiophosphate, 4M HCl/1,4-dioxane, R.T., 1h; c: Br₂, CHCl₃, R.T. 1h; d: DMF, 65 °C, 2h; e: c. HBr, reflux, 48h f: Na[BH(CH₃COO)₃], propanal, DCM, R.T., 10h.

2.3.3 Reductive Amination

Reductive amination is a commonly used procedure in organic chemistry for fast and efficient amine synthesis. In this procedure, compounds containing either aldehyde or ketone groups react with corresponding amines, often using acids as catalysts (Scheme 12).⁴³⁰ The initial step is the formation of the carbinol amine intermediate (**A**). This hemiaminal is under acidic conditions protonated to iminium ion (**B**) and further reduced under mild conditions to corresponding amine (**C**). Reductive amination can be performed with palladium,⁴³¹ or hydrides like sodium cyanoborohydride⁴³² or sodium borohydride.⁴³³ These reagents, however, express various limitations as high toxicity, functional group intolerance, complex purification, product impurity

by the cyanide rest, or the long reaction time. On the other hand, sodium triacetoxyborohydride represents mild and selective reagent and results in higher yields,⁴³⁰ and therefore was chosen as a reducing agent in all of conducted reductive aminations.



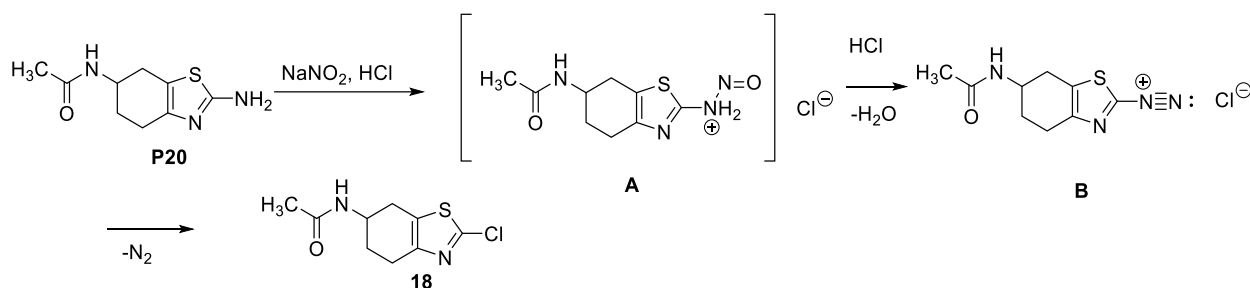
Scheme 12: Mechanism of reductive amination on the example of 4-acetamidocyclohexanone.

2.3.4 Optimization of Bitopic Ligands

After successfully conducted synthesis of D_{2/3}R bitopic ligands (11-17) further modifications were made to examine their impact on the binding affinity. Therefore, methylene groups in spacer were replaced with ether derivatives. Oxygen is more nucleophilic than carbon and can interact with the receptor of interest in a different manner (e.g., forming hydrogen bonds). Recent patents have shown that ligands containing short oxy linkers expressed subnanomolar affinities to both D₂ and D₃ receptors,⁴³⁴ can be considered promising drug-like candidates. On the other hand, 4-phenylpiperazine moiety in the eastern part of the molecule was replaced with other aromatic, bulky and non-bulky aliphatic moieties to examine their effect on the affinity and selectivity of synthesized ligands.

To obtain ether derivatives, 2-aminothiazole derivatives needed to be deaminated and converted into 2-halogen derivatives. Halides are better leaving groups than amines and therefore are more prone to nucleophilic attack by alkoxides. Deamination of 2-aminothiazoles can be achieved in several ways but is mainly done with sodium nitrite and various nitrites. Two latter procedures

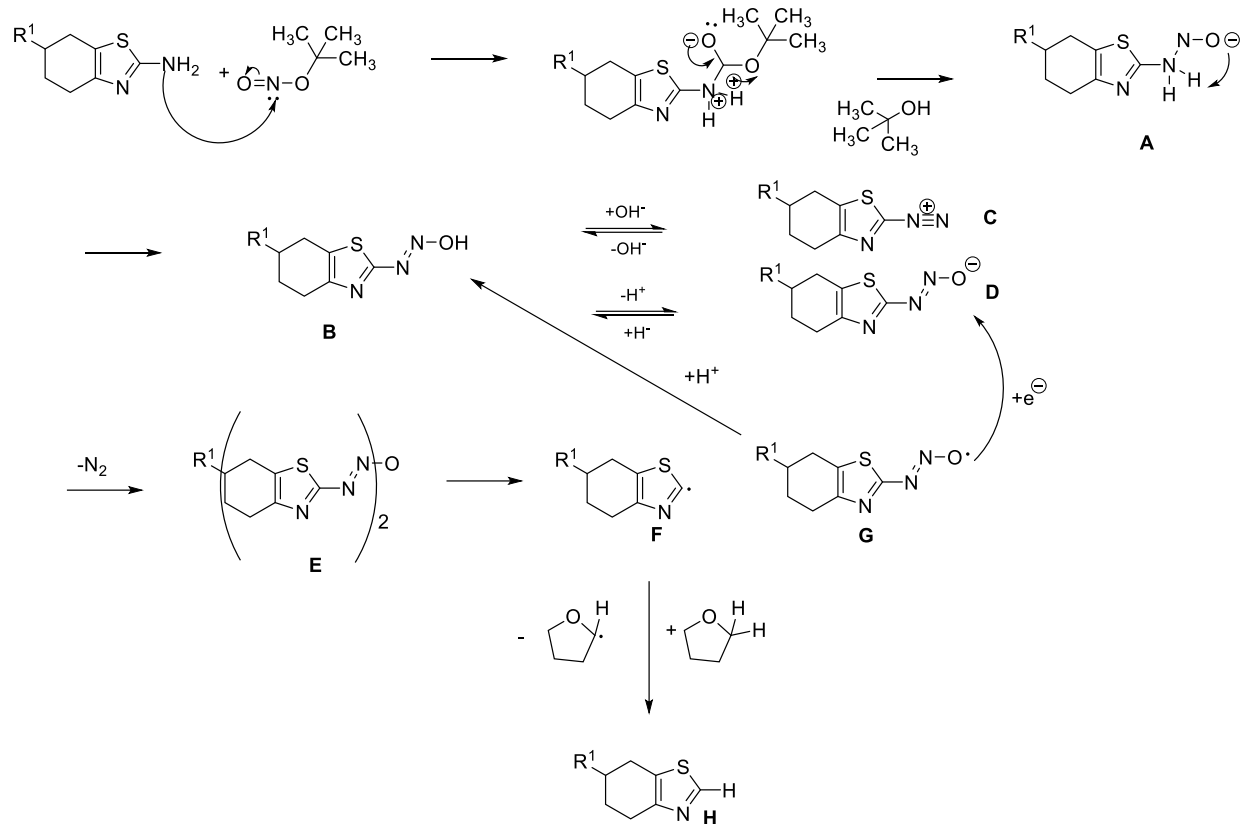
were performed to obtain as high yields as possible. In the first procedure previously described, precursor **P20** was dissolved in concentrated hydrochloric acid, and the solution was cooled down to the $-30\text{ }^{\circ}\text{C}$. Consequently, 1M solution NaNO_2 (in H_2O) was dropwise added over 15 minutes resulting in forming diazotate (**A**) that under acidic conditions was converted to nitrosonium cation (**B**) (Scheme 13). Due to this cation's instability in hydroxylic solvents,⁴³⁵ where it tends to build nitrous acid, the reaction needs to be performed at very low temperatures ($-80\text{ }^{\circ}\text{C}$). As a reductive agent commonly used, hypophosphorous acid (50% in H_2O) was carefully added, enabling nitrogen cleavage out of the molecule and formation of 2*H*-thiazol derivative. The reaction mixture was stirred overnight at ice bath temperature. After 12h reaction, the mixture was cooled down to $-30\text{ }^{\circ}\text{C}$ and dropwise neutralized with NaOH solution (40%). The crude product was extracted with chloroform and methanol, resulting in 100% LC-MS pure 2-chlorothiazol derivative **18** in 10% yield.



Scheme 13: Synthesis of compound **18**.

The second synthetic approach started from different precursors due to the poor solubility of **P20** in solvents commonly used for deamination (e.g., EtOH , ACN , THF).⁴³⁶⁻⁴³⁸ In the first step, the 1,4-cyclohexanedione monoethylene acetal (**P24**) underwent reductive amination with dipropyl amine to obtain tertiary amine (**P25**). Acetal is another stable, not reactive, and commonly used protecting group in organic chemistry, cleaved only under acidic conditions. Therefore, acetal was cleaved in concentrated HBr over two days, as cleavage over 24h did not lead to the desired yield. The cleaved product was not isolated and was used without further purification. Bromine was added in chloroform solution at $0\text{ }^{\circ}\text{C}$, dropwise over 30 minutes until the reaction mixture became light yellow. After heating up to the room temperature and stirring for another hour, urea was added to the reaction mixture and it was heated up to $90\text{ }^{\circ}\text{C}$, resulting in the formation of *N,N*-dipropyl-4,5,6,7-tetrahydrobenzo[*d*]thiazole-2,6-diamine (**P26**).

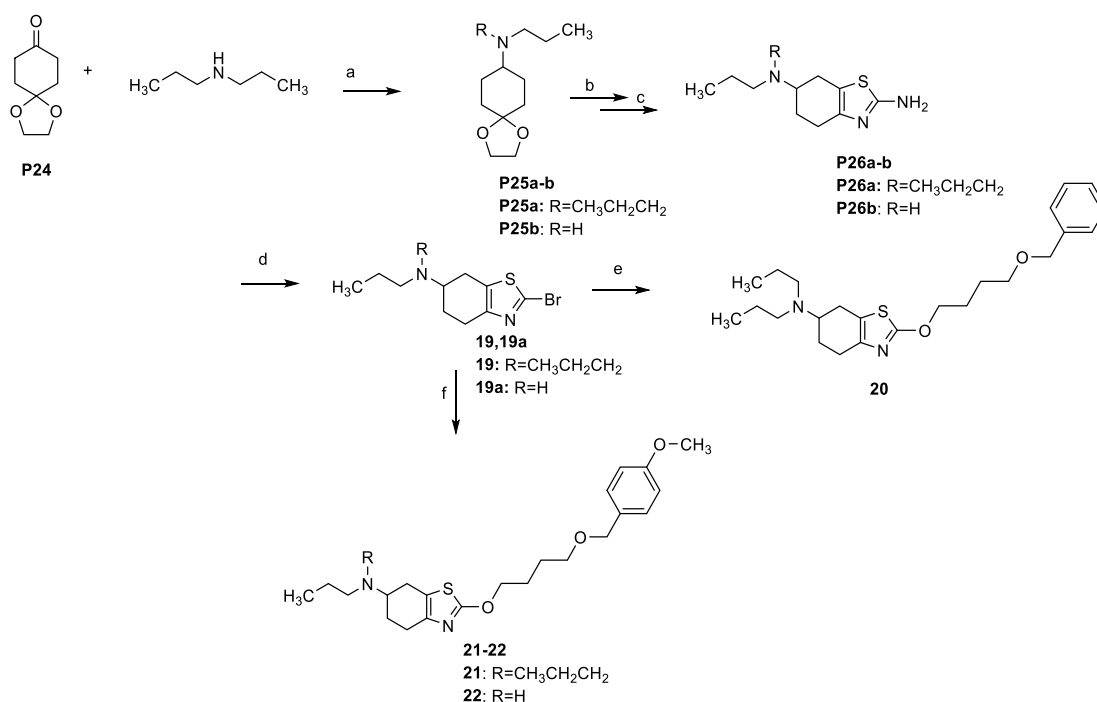
A deamination procedure of 2-aminothiazole was conducted in several low boiling solvents, resulting in the highest yield (up to 60%) when performed in dimethyl sulfoxide (DMSO). The plausible radical mechanism of this reaction by Doyle et al. and Ek et al. is shown in Scheme 14.^{439,440} The intermediate (**A**) is formed in the reaction between *tert*-butyl or isopentyl nitrite and corresponding 2-aminothiazole derivative, followed by the elimination of *tert*-butanol. Hydroxydiazonium salt (**B**) is in equilibrium with diazonium salt (**C**) and diazotate (**D**), depending on the pH of the solution. Both of those intermediates result in forming diazoanhydride (**E**). Consequently, nitrogen cleavage occurs, resulting in 2-thiazole radical (**F**) and nitroso radical (**G**). Nitroso radical (**G**) can be reduced to diazotate (**D**) or protonated to diazoanhydride (**B**). The 2-thiazol radical (**F**) further removes hydrogen from solvent THF resulting in 2*H*-thiazole (**H**). The yield was optimized up to 60% yield, and therefore this procedure was chosen over the procedure shown in Scheme 13. Obtained 2-bromothiazole derivatives (**19**), expressed excellent stability even after several months, which was confirmed by LC-MS measurements and further facilitated workflow.



Scheme 14: Plausible radical mechanism of deamination of 2-aminothiazoles in THF. Adapted from Doyle et al, Ek et al.^{439,440}

The following reaction step was a nucleophilic aromatic substitution, resulting in ether synthesis (Scheme 15). This reaction step follows a two-step, addition-elimination mechanism, and its rate is determined by the first, slow step and not by properties of leaving group. In this reaction, alcoholate formation is a crucial step, and the entire reaction flow is dependent on the yield of formed alcoholate. Different alcohols were therefore introduced to obtain as high yields as possible. The first introduced alcohol was lipophilic benzyl alcohol. Introducing aromatic moiety led to lipophilicity increasing and additionally to a higher probability for passing BBB. Benzyl represents a commonly used group in organic chemistry for the protection of free hydroxyl groups. It is usually cleaved by catalytic hydrogenation⁴⁴¹ or via electrochemical oxidation.⁴⁴² Deprotonation was first conducted at 0 °C due to its exothermic nature, but no alcoholate was observed under these conditions. To overcome difficulties, the temperature was increased up to 40 °C, and deprotonation was conducted for 3 hours, resulting in **20**. Prolongation of deprotonation time up to 10 hours did not lead to a significant increase in yield. As the most suitable solvent

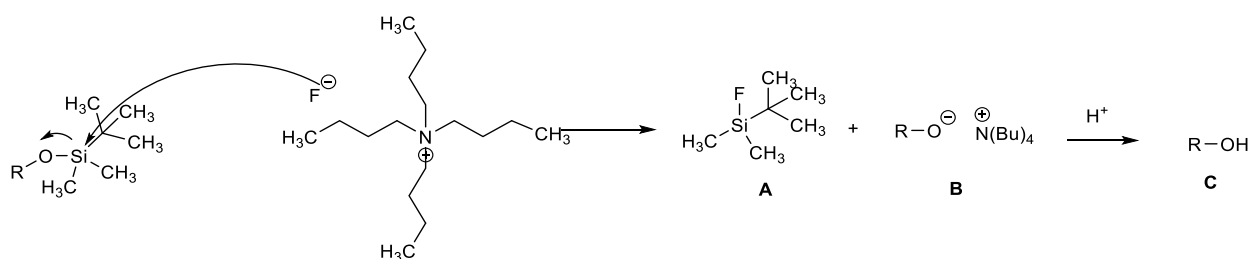
alternatives, 1,4-dioxane and THF were chosen, leading to better yield when compared to DMF. *p*-Methyl benzyl alcohol was another aromatic moiety that was introduced in the eastern part of the molecule. This moiety is another commonly used protective group in organic chemistry, mainly to protect phenols or carbohydrates.⁴⁴³ PMB is efficiently and selectively cleaved by acids,⁴⁴⁴ oxidative agents,⁴⁴⁵ or even under visible light.^{446,447} Introducing PMB in the molecule led to a significant increase in lipophilicity, and compounds that contain PMB moiety could be further examined as prodrugs, and their metabolic pathway and rate could be determined. Interestingly, in the final reaction step (f), both tertiary amine **21** and secondary amine **22** could be isolated. It was practically determined the presence of monopropyl derivative **P26b**,^{448–450} already in the third reaction step (c), which further led to monopropyl derivative **19a** formation, confirmed with LC-MS measurements. Even if present to a lesser extent, **P26b** has very similar properties to **P26a** (in LC-MS no baseline differences have been observed), interfering with purification.



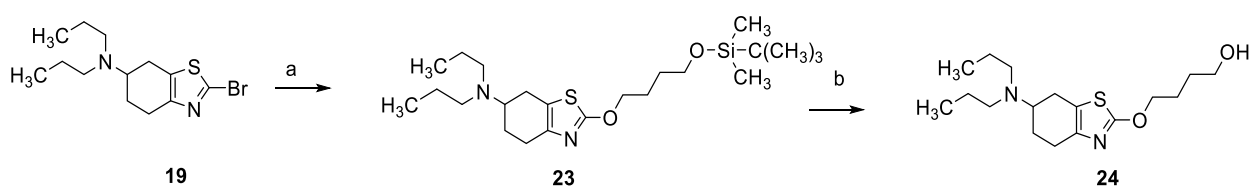
Scheme 15: Synthesis of bitopic ligands connected with oxygen linker. a: Na[BH(CH₃COO)₃], DCM, R.T 10h; b: conc.HBr, R.T., 48h; c: thiourea 1.5h. 90 °C; d: *tert*-butyl/isopentyl nitrite, DMSO, 0 °C, CuBr₂ 10h; e: I: 4-(benzyloxy)butanol, 1,4 dioxane, NaH 40 °C 3h II: 10h THF 40 °C; f: 4-((4-methoxybenzyl)oxy)butanol, THF, reflux 48h.

To examine if aromatic moiety in the eastern part of the molecule is a prerequisite for interaction with the receptor, bulky and non-bulky aliphatic substituents were introduced (Scheme 17).

Therefore, deprotection of **20-22** was tried to obtain primary alcohol. Sulfur is a well-known catalyst poison, and deprotection of benzyl or PMB group through catalytic benzylation remained a challenge. Therefore, a new protecting group was introduced -*tert*-butyl dimethylsilyl (TBDMS as part of TBDMS alcohol). Deprotonation of TBDMS alcohol with NaH in THF for 4 hours and consequent aromatic nucleophilic substitution in refluxing THF for 10 hours resulted in forming **23**. Silyl ether has been widely used to protect the hydroxy groups under basic conditions.⁴⁵¹ Nevertheless, silicon expresses a great affinity for electronegative elements such as oxygen, forms strong covalent bonds, and could contribute to the irreversible binding to the receptor of interest. This group is selectively removed by fluoride anion (Scheme 16) incorporated in tetrabutylammonium fluoride (TBAF). This leads to forming of *tert*-butylfluorodimethylsilane (**A**) and tetrabutyl ammonium alkoxide (**B**) that in under acidic conditions converted to corresponding alcohol (**C**),⁴⁵² resulting in forming of **24**.



Scheme 16: Cleavage of TBDMS with TBAF



Scheme 17: Synthesis of bitopic ligands connected via ether. a I: NaH, *tert*-butyldimethylsilanol THF. 4h R.T. II: reflux, 10h; b: TBAF, R.T.

2.4 D₂R and H₃R Multitargeting Ligands

H₃R pharmacophore 1-propyl-piperidine was introduced to novel, potent multi-targeting ligands (Section 1.6). This moiety is part of only up-to-date commercially available H₃R antagonist/inverse agonist- Wakix® (INN: pitolisant). for the treatment of narcolepsy with or without cataplexy in adults.^{313,358} Numerous SAR studies confirmed the benefits of this moiety for obtaining high H₃R affinity.^{300,453,454} MTDLs can be designed as coupled, merged, or fused (Figure 16). The main objective of this part was to develop optimal coupled D_{2/3}R-H₃R multitargeting ligands connected with the appropriate length linker. Linker length is crucially important by combining two or more different pharmacophores and could lead to a significant increase in affinity, depending on the receptor distribution.

In order to synthesize H₃R moiety, piperidine firstly underlaid nucleophilic substitution following S_N2 mechanism to obtain nitriles under standard conditions (in the presence of potassium carbonate as base and potassium iodide in catalytic amount) for FINKELSTEIN exchange.⁴⁰¹ Obtained nitriles (**P29-P32**) were used in the next reaction step with or without purification by distillation. When distilled, they can be isolated in high yield (up to 90%) which facilitated further workflow. Nitriles were further converted to thioamides (**P33-P36**) under acidic conditions (both in 4M HCl in 1,4-dioxane and 4M HCl in ethyl acetate) with *O,O'*-diethyl-dithiophosphate, as thionation reagent (Section 2.3.2). Thioamides (**P33-P36**) were additionally coupled with α halogenated ketones in HANTZSCH THIAZOLE synthesis (Scheme 8).

These two consequent steps presented crucial reaction steps and were fully optimized (Tables 4 and 5, respectively). Obtained bromo derivates were characterized by mass and NMR spectra and were not isolated. Bromination follows zero-order kinetics,⁴⁵⁵ whereby the rate-determining step is dependent on tautomer formation. Several procedures were conducted to gain product and avoid side product (dibrominated derivative) formation. Due to poor solubility of starting material in different solvents (e.g., water, methanol, toluene, diethyl ether), this reaction was conducted in chloroform and acetic acid as solvents. Bromination in acetic acid (Section 2.3.1) led to yields up to 70% when thiourea is used as a nucleophile. Unfortunately, due to the lower nucleophilicity of thioamides compared to thiourea, the product cannot be obtained (entry 1). In other attempts, bromine was dissolved in chloroform and slowly added to 4-acetamidocyclohexanon (**P19**) solution in the same solvent, carefully monitoring color change (from red to light yellow). In

entries **2** and **3** elementary bromine was added over 20 minutes at room temperature⁴⁵⁶ and 40 °C, respectively. The best result, however, was obtained when bromine was added at once and stirred at room temperature for an hour (entry **4**), as described by Dennone et al.⁴⁵⁷ This led to forming almost no side (dibrominated) product and highest yields when compared to other entries.

Table 4: Optimization of α -bromination of 4-acetamidocyclohexanon

Entry	Solvent	Time (h)	Temperature (°C)	Br ₂ addition
1	CHCl ₃	2	R.T.	dropwise >20 min
2	CHCl ₃	2	30-40	dropwise >20 min
3	CH ₃ COOH	2	65	dropwise >20 min
4	CHCl ₃	1	R.T.	Immediately

The second step of HANTZSCH THIAZOLE synthesis is ring closure, resulting in thiazole formation. Firstly, the reaction was conducted in low-molecular alcohols (entries **1-3**), used as common solvents for HANTZSCH THIAZOLE synthesis (HANTZSCH conditions), at room and reflux temperature. However, the desired product could be obtained only in very low yields. Acetic acid used as a solvent described in Section 2.3.1 (entry **4**) led to a slight increase in yield (10%) that was still not sufficient for further reaction steps. As most promising solvents DMF and 1,4-dioxane were used, whereby compounds expressed better solubility in DMF when compared with that in 1,4-dioxane. The addition of chloroform to 1,4-dioxane and heating the reaction mixture to the 40 °C increased solubility and lead to a slight increase in yield (entry **6**). Depending on the temperature, different side products were obtained. Interestingly, one of the main side products at higher temperatures (e.g., DMF reflux) was paracetamol (entries **5, 7**). This product was characterized with NMR, MS and directly compared on the TLC plate with chemical reference substance. Paracetamol formation proved that dibrominated product was obtained, even though in a small percentage, and high temperatures and prolonged reaction time lead to aromatization to paracetamol. Paracetamol has a very similar R_f value as the desired product (R_f difference 0.01), which interfered with purification. Purification was further complicated due to the formation of paracetamol and 4-aminophenol colored oxidation and degradation products that could be easily spotted at the TLC plate, and therefore this reaction step required purification by a minimum of three different column chromatography. Paracetamol degradation occurs at temperatures higher than 160 °C,⁴⁵⁸ which corresponds to reflux at DMF (boiling point DMF 153 °C, entry **7**).

Another side product formed at higher temperatures was the elimination product, with another double bond in tetrahydrobenzothiazole ring (entries **9,10**). Dehydration of 2-aminothiazole derivatives occurs at high temperatures and is favored under acidic conditions.⁴¹⁵ This product was confirmed with LC-MS measurement and naturally had a very similar retention time as the desired product. Share of this side product linearly increased with the reaction time prolongation. This led to further optimization, DMF was chosen as the primary solvent, and the temperature was decreased. Finally, the best reaction conditions (entry **11**) for conducting HANTZSCH THIAZOLE synthesis were: DMF, stirring at room temperature for one hour and at 80 °C for another two hours to obtain amides **25-28**. These reaction conditions were used in all HANTZSCH THIAZOLE synthesis (also in Section 2.3.2). Yield over two steps was increased up to 53%.

Table 5: Optimization of HANTZSCH THIAZOLE synthesis

Entry	Solvent	Conditions	Time (h)	Yield (%)	Specials
1	EtOH	Reflux	10	3	
2	EtOH	130 °C MW, 6 bar	1	2	
3	isopropanol	Reflux	4	4	
4	CH ₃ COOH	Reflux	16	<10	
5	1,4-dioxane	R.T.→80 °C	1,2	25	Poor solubility, paracetamol
6	1,4-dioxane/CHCl ₃	R.T.→40→80 °C	10	27	↑ solubility by adding CHCl ₃
7	DMF	Reflux	16	13-18	
8	DMF	Reflux	2,5	18	
9	DMF	R.T.→80 °C	1;2	31	60% product 30% elim. product
10	DMF	80 °C	16	30	After 2h-75 % elim. product
11	DMF	80 °C	2	53	

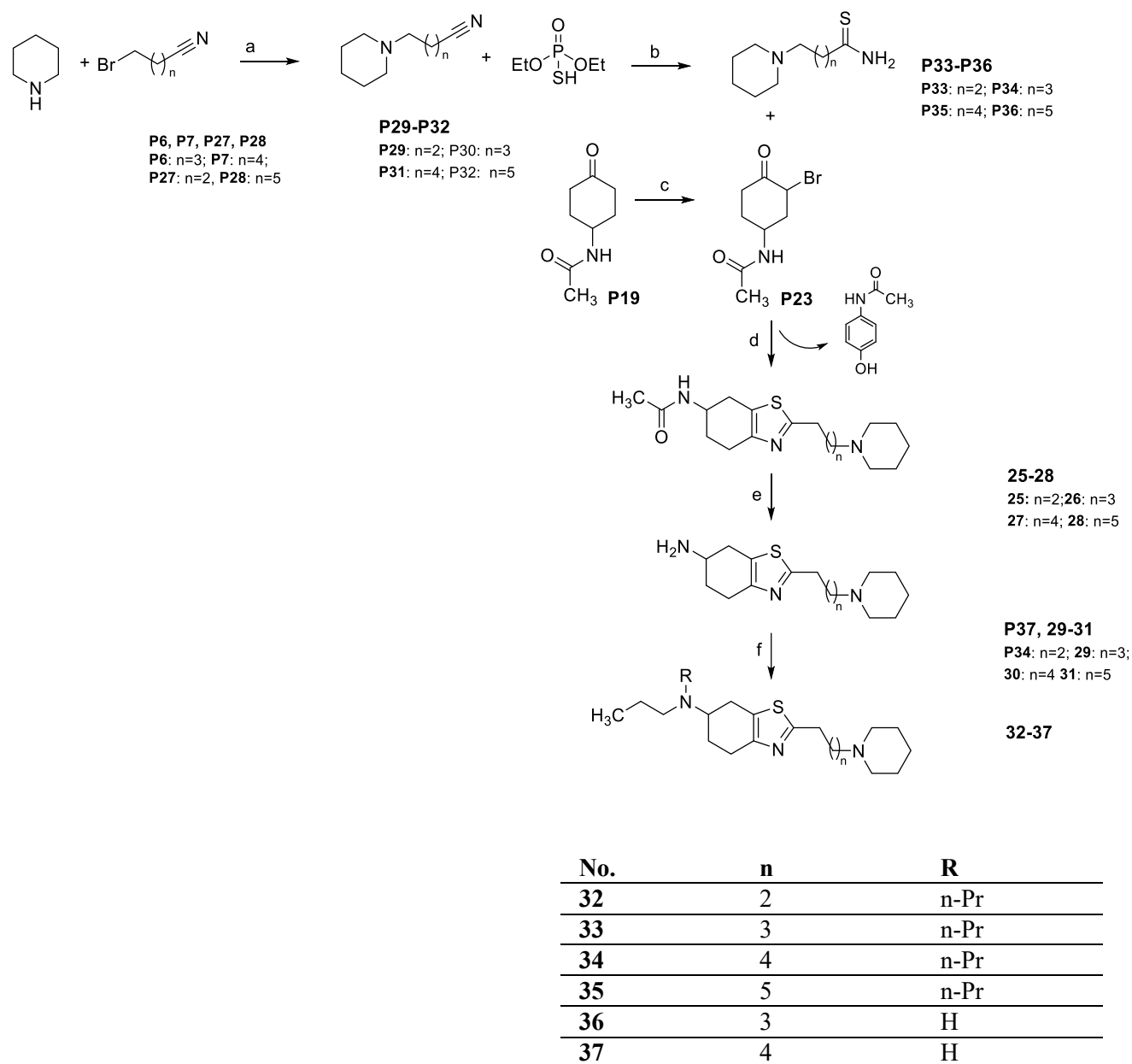
Consequently, obtained amides (**25-28**) were deacetylated to obtain primary amines (**P37, 29-31**). As described in Section 2.3.2 this chemical reaction should be conducted under harsh conditions. Firstly conducted basic *N*-deacetylation as by cariprazine and its derivatives,⁴⁵⁹ only resulted in the isolation of starting material (entry **1**, Table 6). Reflux in concentrated hydrochloric acid for 24 hours leads to isolating only starting material (confirmed by LC-MS measurements, entry **2**). Therefore, prolongation of the reaction time, as well as a solvent change to more acidic-concentrated HBr, were the next steps in the synthesis optimization. After 48 hours in refluxing,

concentrated HCl, 70% product, was formed (entry **3**). After the same time in refluxing concentrated HBr 75% product was obtained (entry **5**). This reaction time and both of mentioned acids were chosen as the best alternative for *N*-deacetylation and used in further reactions of this type.

Table 6: Optimization of *N*-deacetylation

Entry	Solvent	Temperature	Time (h)	Yield (%)
1	LiOH/MeOH	reflux	6	x
2	c. HCl	reflux	24	x
3	c. HCl	reflux	48	50-80
4	c. HBr	reflux	24	22
5	c. HBr	reflux	48	75

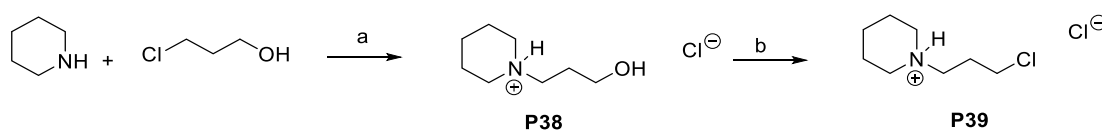
The final step included reductive amination of primary amines (**P37, 29-31**) with propionaldehyde to get secondary and tertiary amines as final products (**32-37**), depending on the molar ratio. Reductive amination was performed as described previously (Section 2.3.3), with sodium triacetoxyborohydride as a reducing agent without adding an acid due to aldehydes' higher reactivity than that of ketones. Reductive amination was carried out in 1,2-dichloroethane at room temperature, overnight. Crude products were purified with column chromatography. Overall yield over seven synthetic steps was 18% (Scheme 18).



Scheme 18: Synthesis of multitargeting D_{2/3}R and H₃R ligands. n-Pr - *N*-propyl; K₂CO₃, KI, acetone, reflux, 10h; b: 4M HCl in 1,4 dioxane/EtOAc, R.T, 10h; c: Br₂, CHCl₃ 1h, R.T; d: DMF, 2h, 80 °C; e: conc. HBr, reflux, 48h; f: Na[BH(CH₃COO)₃], propanal, DCE, R.T. 10h.

2.5 D₃R and H₃R Receptor Ligands

After successfully conducted synthesis of multitargeting ligands containing both D₂R agonistic and H₃R antagonistic pharmacophore, the next aim was expanding this compound set with multitargeting ligands that, besides H₃R pharmacophore, display D₃R antagonist moieties. Newly reported multitargeting D₃R-H₃R ligands showed encouraging results in autism spectrum disorder.⁴⁶⁰ Recently, the benefits of piperazine derivatives in the histamine H₃R field have been recognized.⁴⁶¹ To develop these multitargeting ligands, typical H₃R moiety 1-(3-phenoxypropyl)piperidine had to be introduced.^{462,463} Synthesis of this precursor was carried out as described in the literature.^{462,464,465} Under an inert atmosphere, piperidine underwent S_N2 alkylation with 3-chloropropanol in the presence of potassium carbonate as a base to obtain primary alcohol (**P38**). FINKELSTEIN exchange was carried out (Scheme 19)⁴⁰¹ with potassium iodide in a catalytic amount to improve the leaving group properties. Consequently, alcohols were obtained quantitatively and converted to chloride (**P39**) with thionyl chloride in toluene. Obtained chlorides were crystalized as hydrochloride salts and were used as starting materials for syntheses requiring H₃R pharmacophore.

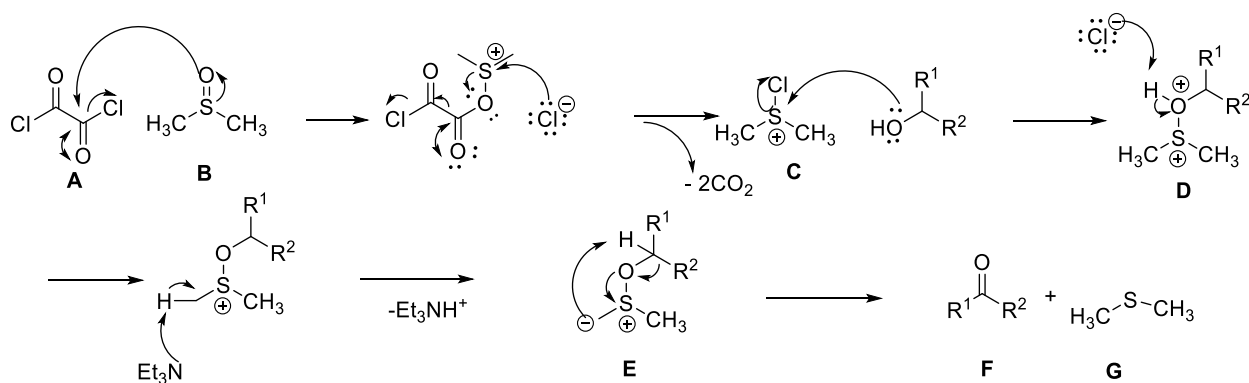


Scheme 19: Synthesis of H₃R precursors **P38-39**. a: I: K₂CO₃, KI, acetone, R.T. 72h II: HCl, 2-Propanol; b: SOCl₂, toluene, 0 °C →60 °C.

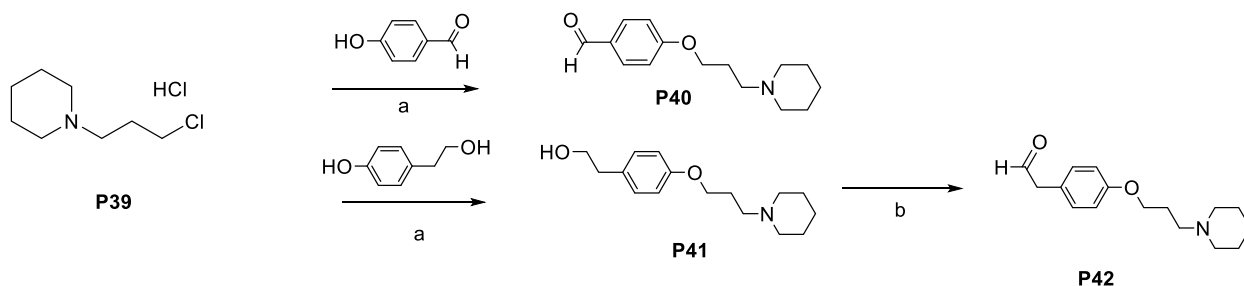
To obtain H₃R pharmacophore for different reaction types H₃R precursor **P39** have further undergone WILLIAMSON ETHER synthesis, resulting in **P40** and **P41** (Scheme 21). Even though WILLIAMSON ETHER synthesis is first described in the mid-19th century, it still presents a fast and efficient way to obtain ethers, both at the laboratory and the industrial scale.^{466,467} This reaction occurs under basic conditions,⁴⁶⁸ with an alkyl halide and follows S_N2 mechanism. Additives (metal salts, crown reagents) are often used for reaction promotion. The reaction results in the highest yield when performed with primary alkyl halides since secondary or tertiary halides are more sterically hindered and nucleophilic attack is more difficult to occur. Moreover, a second order (E2) elimination reaction is favored instead. To overcome this obstacle, WILLIAMSON ETHER

is performed in aprotic solvents such as acetone or acetonitrile, due to its effect of stabilization of reactive species⁴⁶⁹ or on the solid phase.⁴⁷⁰

SWERN oxidation was performed to obtain another precursor, aldehyde **P41**. SWERN oxidation, firstly described by Daniel Swern,⁴⁷¹ is a facile way of synthesizing aldehydes and ketones from primary and secondary alcohols with activated dimethyl sulfoxide (DMSO) as an oxidizing agent. (Scheme 20). The reaction is performed at low temperatures (-80 °C) due to the exothermic reaction between oxalyl chloride (**A**) and DMSO (**B**), resulting in forming dimethylchlorosulphonium ion (**C**) that further underlay nucleophilic attack from alcohol, resulting in alkoxy-sulphonium ion (**D**). Alkoxy-sulphonium ion is then deprotonated by the base (Et₃N), resulting in Sulphur ylide (**E**). Sulfur ylide is fragmented to corresponding aldehyde (**F**) and gaseous dimethyl sulfide (**G**).



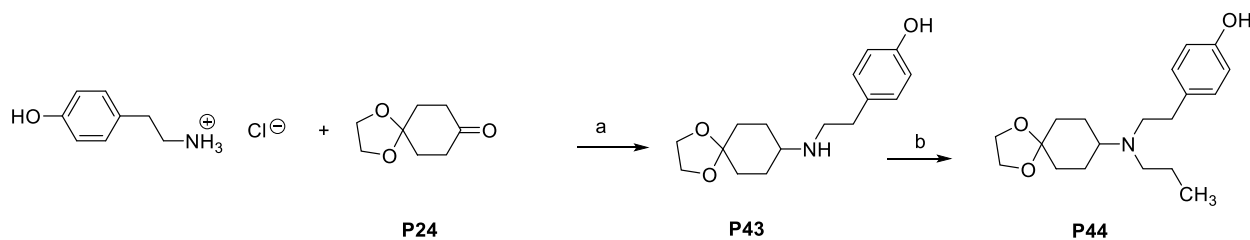
Scheme 20: Mechanism of SWERN oxidation



Scheme 21: Synthesis of precursors **P40-42**. a: K₂CO₃, KI, acetone reflux, 16h; b: SWERN oxidation: I: oxalyl chloride, DCM, DMSO, -80 °C, 3 h II: alcohol, Et₃N -80°C→R.T. 2h.

All mentioned precursors were used in the synthesis of multitargeting D₃R-H₃R receptor ligands. Biosynthesis of dopamine starts from tyrosine (Scheme 1),¹⁰ and the reaction catalyzed by tyrosine hydroxylase represents a rate-limiting step.² Therefore, as the starting material for the synthesis of these multitargeting ligands, tyramine was used. Tyramine shows a good affinity at the D₂R itself⁴⁷² and is considered as a dopaminergic agonist.⁴⁷³

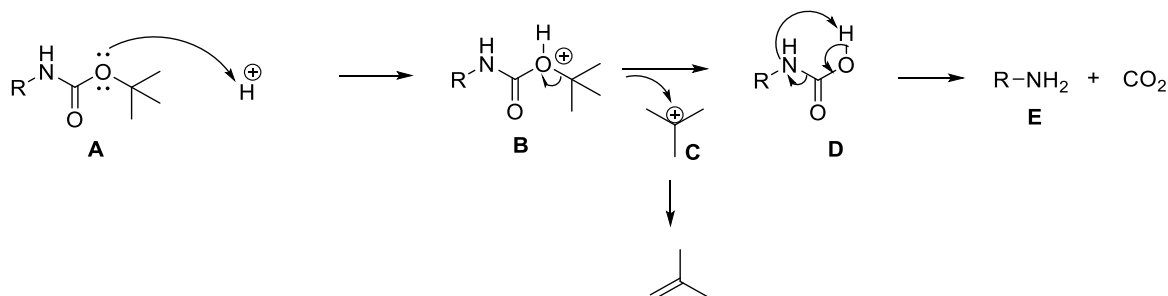
Firstly, tyramine was directly reductively aminated with 1,4-cyclohexanedione monoethylene acetal (**P24**) under standard reaction conditions to obtain **P43** (Scheme 22). This reaction resulted in low yield (10%) due to the poor solubility of tyramine salts in commonly used solvents for reductive amination (e.g., DCE and DCM). Ion exchange and conversion of hydrochloride into freebase resulted in slightly better yield (up to 15%), whereby azeotropic distillation in toluene resulted in a higher but still not significant increase in yield (18%). Secondary amine (**P43**) was further reductively aminated to obtain tertiary amine **P44**.



Scheme 22: Synthesis of precursor **P43-P44**. a: Na[BH(CH₃COO)₃], DCM, R.T., 10h; b: propionaldehyde Na[BH(CH₃COO)₃], DCM, R.T., 10h.

A second synthetic approach was developed to address this challenge. In this approach the free amino group of tyramine hydrochloride was firstly protected with di-*tert*-butyl dicarbonate (BOC) resulting in carbamate formation (**P45**). The reaction was conducted in a methanol/water mixture (2:1) due to the good solubility of starting materials in the chosen solvent mixture. BOC is a commonly used protecting group in organic chemistry, primarily for amino group protection, especially by amino acids. It is stable under basic conditions towards nucleophilic attack and prevents overalkylation often observed when reductive amination is conducted.⁴⁷⁴ This protecting group can be easily cleaved by oxalyl chloride,⁴⁷⁵ CeCl₃,⁴⁷⁶ or under acidic conditions (HCl in 1,4-dioxane or EtOAc) as in the case of synthesis of this compound set⁴⁷⁷ (Scheme 23). Carbamate (**A**) is firstly protonated under acidic conditions, which leads to electrophilicity increasing. After

rearrangement (**B**) and cleavage of tertiary carbocation (**C**), carbamic acid (**D**) is formed. Carbamic acid, under acidic conditions, decarboxylates to corresponding amine (**E**).

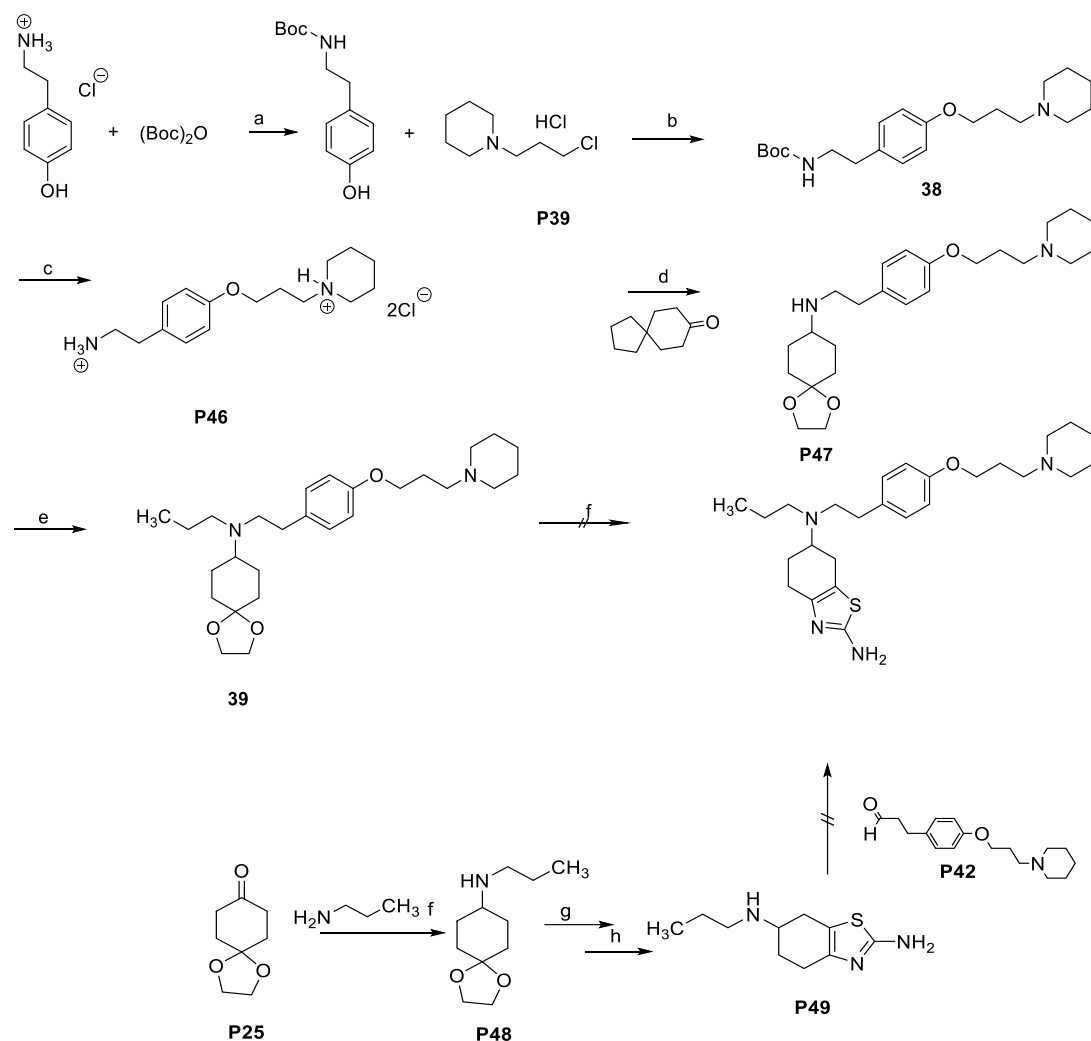


Scheme 23: Mechanism of cleavage of BOC protecting group.

After successfully conducted amino group protection, obtained derivatives underlaid WILLIAMSON ETHER synthesis with 1-(3-chloropropyl)piperidine (**P39**) under standard conditions resulting in ether formation (**38**). Obtained ether derivative was deprotected in 4M HCl in 1,4-dioxane, resulting in primary amine (**P46**), which further underlaid two consecutive reductive aminations to obtain secondary (**P47**) and tertiary amine (**39**) (Scheme 24). The latter was also obtained from **P44**. First reductive amination was performed in the presence of acetic acid, which enhances electrophilicity. In the second reaction, acid was not necessary due to the higher reactivity of aldehydes compared to ketones.⁴³⁰ Introducing rigid spiro moiety in the molecule could potentially impact binding affinity and selectivity towards dopamine receptor subtypes. Spiro scaffold is a common motif in medicinal chemistry that gain more recognition lately.⁴⁷⁸ Recently reported diazaspino ligands showed low nanomolar affinities toward D₃R.⁴⁷⁹ Due to this functional group's rigidity, it has been hypothesized that dopamine receptor could be modulated,⁴⁸⁰ and therefore conformational changes could be decelerated or controlled. Spiro derivatives (**39**) were deprotected under acidic conditions. Consequently, they were brominated at 0 °C and HANTZSCH THIAZOLE synthesis with thiourea was performed. Unfortunately, this led to the obtaining the desired compound in very low yield, no matter which molar ratio was used. The reaction was performed in various low molecular alcohols (e.g., methanol, ethanol, isopropanol) at different temperatures. LC-MS measurements confirmed the formation of only up to 4% of the product.

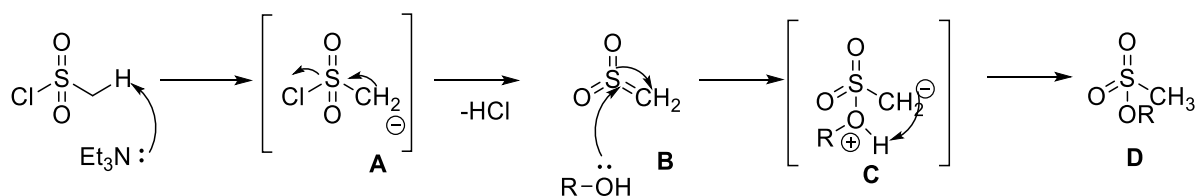
Another synthetical approach was therefore introduced. Starting from 1,4-cyclohexanedione monoethylene acetal (**P25**) that underlaid reductive amination with propylamine to obtain

secondary amine (**P48**). This reductive amination was performed with palladium on activated carbon, hydrogen at 4bar in an autoclave in methanol saturated with ammonia.^{481,482} Secondary amine (**P48**) consequently underlaid bromination and HANTZSCH THIAZOLE to obtain dexpramipexole derivative (**P49**). Dexpramipexole derivative was reductively aminated by **P37**. This synthetic approach also did not result in the desired product. One possible reason could be the high similarity between precursors and desired compounds, especially in basicity, due to the three basic centers. One-pot synthesis can result in various side products due to the different side reactions (e.g., elimination, aromatization, described in Section 2.4). As a potential difficulty, steric hindrance (**39**) can be discussed, which disables nucleophilic attack by thiourea.



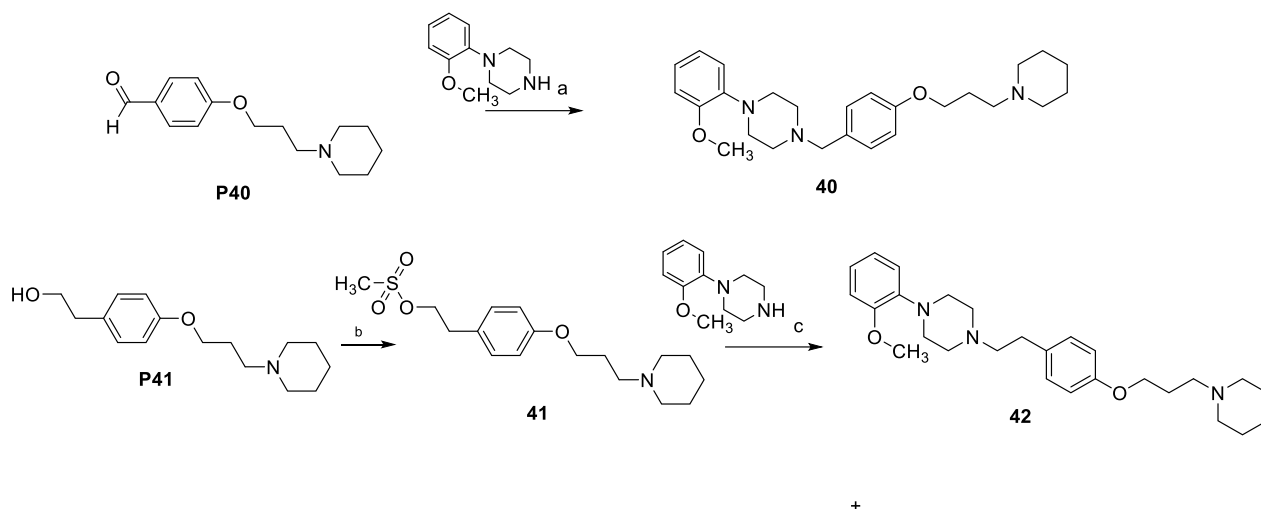
Scheme 24: Synthesis of multi-targeting dopamine D₃R and histamine H₃R ligands. a: MeOH, H₂O (2:1), R.T., 2h; b: K₂CO₃, KI, acetone, reflux 10h; c: 4M HCl/1,4-dioxane R.T. 10h; d: Na[BH(CH₃COO)₃], CH₃COOH DCE, R.T. 10h; e: Na[BH(CH₃COO)₃], CH₃COOH, DCE, R.T. 10h; e: Pd/C MeOH/NH₃, 4bar, R.T., 10h; f: I: HBr, R.T 48h II: Br₂ 0 °C → R.T CHCl₃, 2h g: thiourea, 90 °C, 1.5h.

Consequently, D₃R privileged scaffold 1-(2-methoxyphenyl)piperazine was introduced. Two compounds with various linker lengths bridging D₃R and H₃R moieties were developed (Scheme 26). In the first synthetic approach, obtained precursor **P40** was reductively aminated with 1-(2-methoxyphenyl)piperazine to obtain **40** as a final compound. In the second approach precursor, **P41** was firstly activating via mesylation to obtain **41**. Methanesulfonyl chloride is a commonly used reagent for activating alcohol groups. It is a better leaving group than the hydroxyl group since the negative charge is better distributed throughout three oxygen atoms. The procedure for preparing mesylates from alcohols is optimized and rarely lasts more than two hours⁴⁸³ (Scheme 25). Mesyl esters are among the most common ways for alcohol activation. In mesylation, a terminal methyl group is firstly deprotonated under basic conditions (**A**) and consequently nucleophilic attack by the alcohol (**B**). After charge redistribution (**C**), sulfonyl esters (**D**) are formed whereby. the poor leaving hydroxyl group is converted to good leaving. Mesylation was performed at ice bath temperature in dichloromethane. Triethylamine (Et₃N) was dropwise added, and the reaction mixture was stirred for one hour at 0 °C. Subsequently, Methanesulfonyl chloride was added, the reaction mixture was stirred for further 15 minutes at ice bath temperature and left to heat up to room temperature,



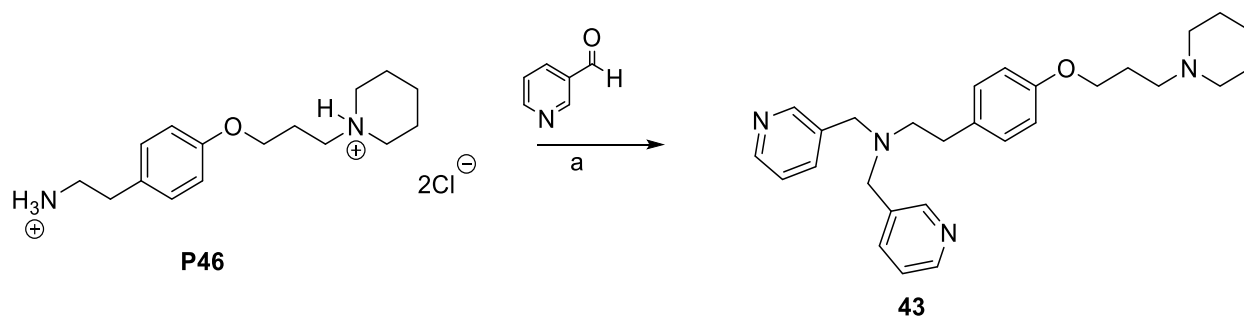
Scheme 25: Mechanism of mesylation

After activating alcohol group mesyl esters (**41**) undergo alkylation with 1-(2-methoxyphenyl)piperazine with potassium carbonate as base and potassium iodide in a catalytic amount to obtain **42**.



Scheme 26: Synthesis of compounds **40-42**. a: $\text{Na}[\text{BH}(\text{CH}_3\text{COO})_3]$, DCE, R.T. 10h; b: I: Et_3N , DCM, 0°C , II: methanesulfonyl chloride, $0^\circ\text{C} \rightarrow \text{R.T.}$; c: K_2CO_3 , KI, acetone, reflux 10h.

In order to investigate optimal moiety for the synthesis of $\text{D}_3\text{R}/\text{H}_3\text{R}$ multitargeting ligands, another basic moiety 1-(3-pyridinyl)piperazine was introduced (Scheme 27). The basic center forms a salt bridge in the OBS in both D_2R and D_3R and is therefore essential. Several pharmacological entities containing pyridine or pyrazolopyridine⁴⁸⁴ were developed. Precursor **P46** was reductively amination with pyridine 3-carboxaldehyde to obtain final compound **43**.



Scheme 27: Synthesis of compound **43**. a: $\text{Na}[\text{BH}(\text{CH}_3\text{COO})_3]$, DCE, R.T., 10h.

2.6 Fluorescent Dopamine and Histamine Receptor Ligands

Fluorescence labeling has been up to date most used technique to estimate receptor distribution and localization. Ever since its revelation in 1968,³⁷⁸ BODIPY presented a standard in fluorescence bioimaging due to its versatility and stability.^{485,486} BODIPY is a difluoro-boraindacene derivative and can be synthesized via different procedures: from pyrroles and halides or anhydrides, from ketopyrroles, or pyrroles and aldehydes. BODIPY can be substituted in 8-(*meso*) position. Substitution in position 8 with different moieties does not affect spectral characteristics of this dye (e.g., absorption or emission maxima) but enhances the rigidity in the molecule. BODIPY dyes can be synthesized by click chemistry approach via HUISGEN 1,3-dipolar cycloaddition, that occurs between azides and unsaturated carbon derivatives (e.g., alkyne). BODIPY expressed weak fluorescence in solid states and therefore, new more stable alternatives were developed. Aldehydes, used in synthesis of BODIPY derivatives are almost always substituted, to avoid polymerization. Treibs and Kreuzer concluded that BODIPY derivatives that are not substituted in position 2 and 6 could undergo electrophilic attack, and this presented initial step for other working groups to develop more stable and versatile fluorescent derivatives, resulting in symmetrical F₂ derivative by Tamgho et al. in 2014 abbreviated as BOPHY⁴⁸⁷ and unsymmetrical bis BF₂ derivatives by Yu et al. abbreviated as BOPPY⁴⁸⁸ (Figure 19).

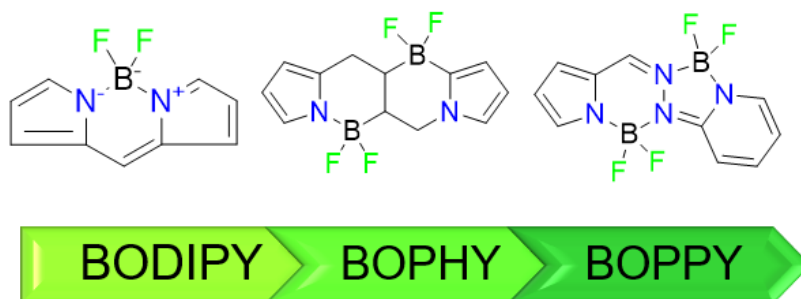
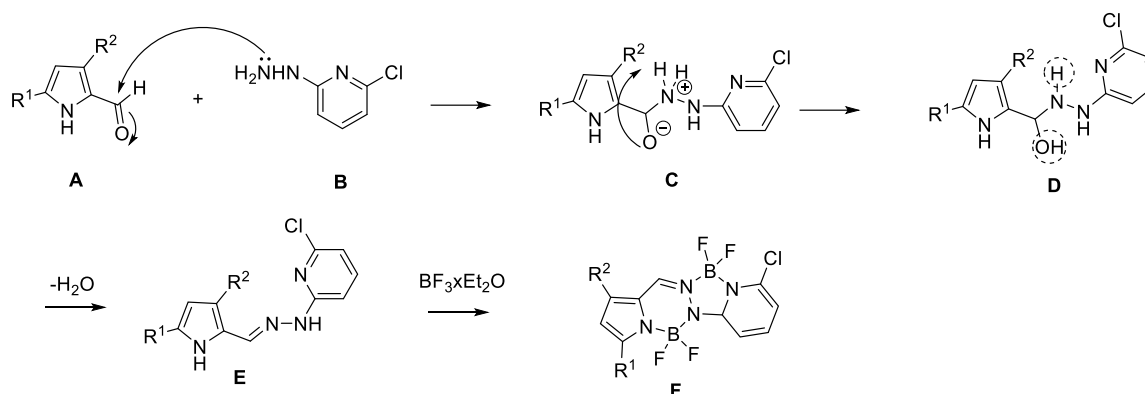


Figure 19: BODIPY and its analogues BOPHY and BOPPY.

The first step in the BOPPY synthesis is pyrrole condensation, often used in porphyrin synthesis⁴⁸⁹ (Scheme 28). Carbonyl compound, in this case, aldehyde (**A**) undergoes nucleophilic attack by 2-chloro-6-hydrazinopyridine (**B**). After proton rearrangement (**C**) and dehydration (**D**), diazo compound (**E**) is formed. This intermediate further complex Lewis acid (borontrifluoride-

diethyletherat) which promotes nucleophilic addition of strongly basic substrates to form two different unsymmetrical cores (**F**).



Scheme 28: Synthesis of unsymmetrical BOPPY core.

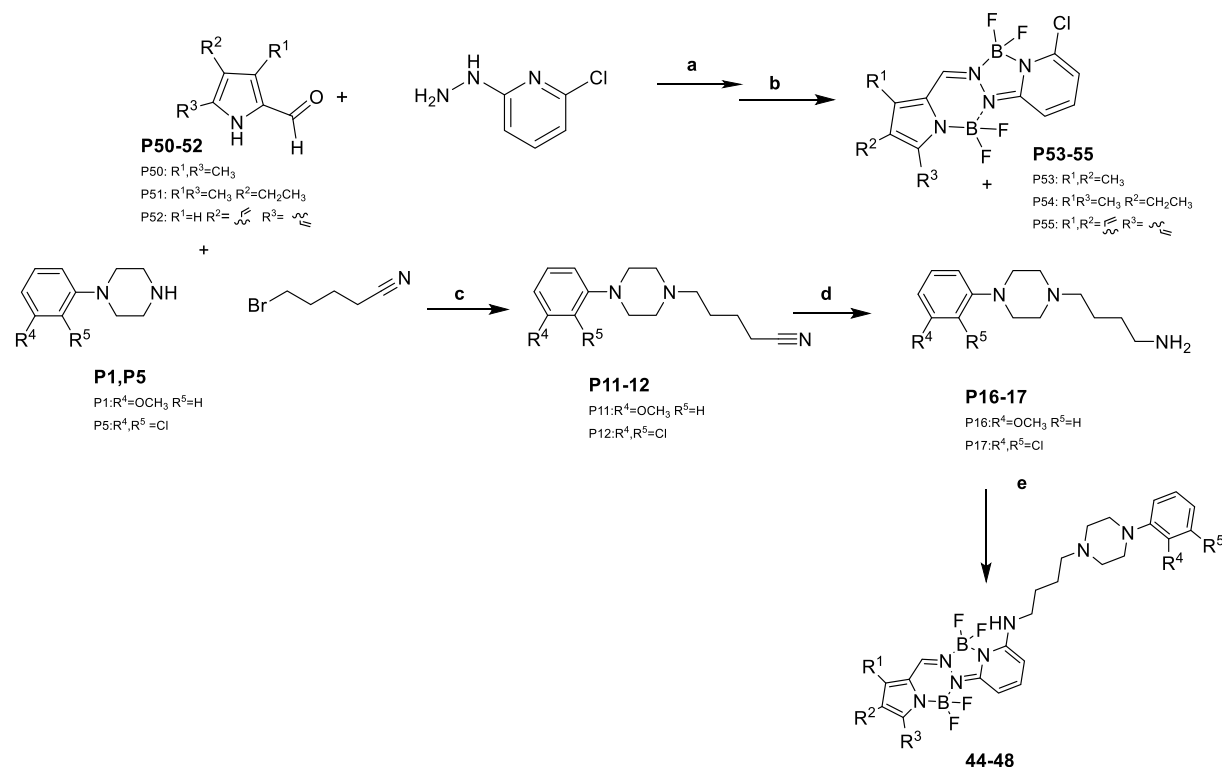
BOPPY fluorophore was coupled for the first time with dopamine D₃R and histamine H₃R moiety to gain potent, novel fluorescent ligands, further enlightening receptor distribution, and localization.

2.6.1 D₃R Fluorescent Ligands

Dopamine D₃R represents an interesting target due to its relatively focal localization and distribution.^{490,491} Even though dopamine receptor ligands have been long studied and developed, and dopamine involvement in numerous neurological diseases is a well-known fact, only a few fluorescent dopamine ligands have been up to date designed. These ligands sustain from commercially available or one-pot synthesized ligands, like fluorescein,⁴⁹² biotin,⁴⁹³ BODIPY,⁸⁵ or most recent dansyl derivatives.¹²⁵

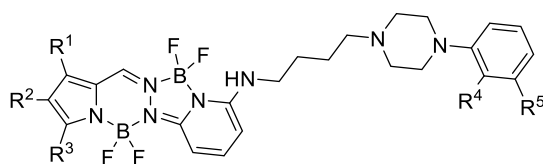
To a stirring solution of pyrrole 2-carboxaldehyde derivatives (**P50-52**) in 1,2-dichloroethane (DCE) with 6-chloro-2-hydrazinopyridine and a catalytic amount of *p*-toluene sulfonic acid were added, and the reaction mixture was refluxed overnight (Scheme 29). After 12h, diisopropylethylamine was added and the reaction mixture was stirred for 14 minutes. Consequently, boron trifluoride-diethyletherate (BF₃·xEt₂O) was added and the reaction mixture was refluxed for another four hours, resulting in fluorophore **P53-55**. Precursors **P16** and **P17** were prepared as described before (Section 2.2). Halogen group at BOPPY fluorophore can be easily functionalized as reported by Yu et al.⁴⁸⁸ It can undergo SUZUKI MIYAUARA coupling as reported

by Hayashi et al.⁴⁹⁵ In this case fluorophores (**P53-55**) undergo nucleophilic substitution by corresponding amines (**P16-17**) in DCE with the presence of triethylamine (Et₃N), to obtain final compounds **44-48**. All synthesized dopamine receptor fluorescent ligands are summarized in Table 7.



Scheme 29: Synthesis of compounds **44-48**: a: PTSA, DCE, 16h; b: BF₃·xEt₂O, DIPEA; c: K₂CO₃, KI, acetone, reflux 10h; d: Raney-Ni, MeOH/NH₃ 10h, H₂ 5bar; e: **P53-55**, DCE, Et₃N, DCE 10h.

Table 7: Dopamine receptor fluorescent ligands **44-48**



No.	R ¹	R ²	R ³	R ⁴	R ⁵
44	CH ₃	H	CH ₃	Cl	Cl
45	CH ₃	H	CH ₃	OCH ₃	H
46	CH ₃	CH ₂ CH ₃	H	OCH ₃	H
47	CH ₃	CH ₂ CH ₃	H	Cl	Cl
48	H	CH ₂ =CH ₂ -	CH ₂ =CH ₂ -	OCH ₃	H

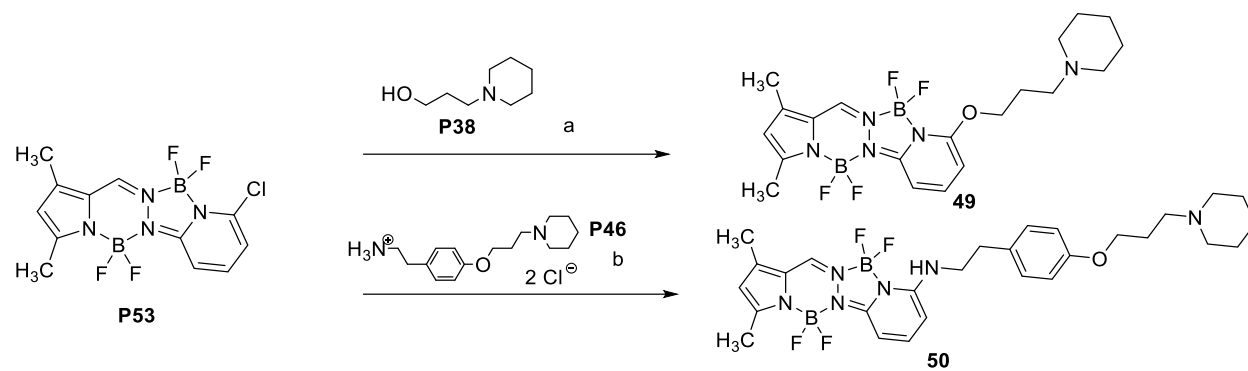
2.6.2 H₃R Fluorescent Ligands

Different H₃R ligands with fluorescent properties were developed in our working group to visualize H₃R. Among them are chalcone, ciproxifane,⁴⁶⁵ or BODIPY derivatives.⁴⁹⁶ However, all these fluorophores display several disadvantages when compared to BOPPY. Therefore, the synthesis of ligand containing BOPPPY linked with H₃R pharmacophore has been conducted. The length of the linker was varied, precisely the presence of phenyl moiety, which acts as a central core and is important for hydrophobic interaction with H₃R. 1-(3-phenoxypropyl)piperidine moiety, incorporated in pitolisant, is not the utmost prerequisite, as it can be replaced with different moieties without loss of affinity. Therefore, two fluorescent H₃R ligands with and without phenyl moiety were developed (Scheme 30). Firstly, BOPPY fluorophore undergoes aromatic nucleophilic substitution by 3-(piperidin-1-yl)propanol (**P38**). Alkoxide formation was optimized (Table 8). As solvents were chosen THF, DMF, and 1,4-dioxane due to the good solubility of starting material in those solvents. Deprotonation is commonly performed at ice bath temperature due to its exothermic nature. Deprotonation at 0 °C for one hour in both THF and DMF (entries **1** and **2**) did not result in the desired product. Prolongation of deprotonation time up to 3 hours and increasing temperature up to 40 °C led to yield of 19% (entry **3**). Therefore, deprotonation should be conducted at 40 °C. Deprotonation reactions were conducted simultaneously, in both THF and 1,4-dioxane, at chosen temperature for 3 hours, and aromatic nucleophilic substitution took place under reflux. No product was formed when the reaction was conducted in 1,4 dioxane (entry **4**), while yield was up to 58% when the reaction was conducted in THF, resulting in **49** (entry **5**).

Table 8: Optimization of deprotonation and aromatic nucleophilic substitution

Entry	Solvent	Reactants	Temperature	Time	Yield (%)
1	THF	NaH	0 °C/R.T.	1h/overnight	<1
2	DMF	NaH	0 °C /R.T.	1h/overnight	x
3	THF	NaH	40 °C	3h/overnight	19
4	1,4-dioxane	NaH	40 °C /reflux	3h/overnight	x
5	THF	NaH	40 °C /reflux	3h/overnight	58

In the second approach BOPPY fluorophore (**P53**) underlaid aromatic nucleophilic substitution by precursor **P46** in the presence of triethylamine as a base in 1,2-dichloroethane at 40 °C, resulting in **50** as final compound.



Scheme 30: Synthesis of fluorescent histamine H₃R ligands. a: I: NaH, THF, 40 °C, 3h II: THF, 40 °C overnight; b: DCE, Et₃N, 40 °

2.7 Determination of Fluorescent Properties

2.7.1 Fluorescent Dyes and their Field of Application

Fluorescent labeling is a commonly used technique in bioimaging that expresses several advantages compared to radiolabeling. Assays performed with fluorescence-labeled derivatives are sensitive and selective, can be performed in real-time, do not generate radioactive waste, and enable high throughput.⁴⁹⁷ Organic fluorophores bind covalent or non-covalent to the target of interest and therefore enable their visualization. Fluorophore needs to be appropriately chosen, taking into account excitation and emission wavelength and experiment type that needs to be performed (e.g., single-molecule or group of molecules targeting).⁴⁹⁸ Ideally, fluorophores should be chemically and thermally stable small molecules with high Stokes shift, quantum, and fluorescent time (time spent in an excited state).^{498,499}

Fluorescence bioimaging could be divided into two categories, depending on the affinity of fluorescent ligands. In non-targeted bioimaging, fluorophores are internalized in the cells. They bind non-specifically and serve as biomarkers. On the other hand, in targeted bioimaging, fluorophores that show high affinity towards the receptor of interest are generated (e.g., the pharmacophore for the specific receptor is incorporated in the fluorophore). Those fluorophores can selectively target cells and tissues that express receptors of interest.⁵⁰⁰ In targeted bioimaging, pharmacophores can be incorporated or coupled to a fluorophore with different length linkers. Fluorescence-based assays are the most convenient method to obtain results fast and efficiently. Moreover, they have gained recognition lately due to developing modern techniques for target visualization as bioluminescence resonance energy transfer (BRET) or Förster resonance energy transfer (FRET). FRET is a sensitive, cutting-edge technology developed in the last two decades that provide information about the range and approximate distance of two fluorescent-labeled ligands. It is commonly used for determining dynamic interactions between macromolecules (e.g., protein-protein or protein-DNA interactions). Fluorescent-labeled acceptor and donor are sufficiently close and participate in energy transfer, which is consequently measured.⁵⁰¹ Energy transfer does not occur due to photon emission and absorption but instead through dipole coupling. The radiating energy is quantified.⁵⁰²

Various efforts have been centered around designing novel, potent and stable fluorophores, which will selectively target receptors of interest. Different heterocycles and their bioisosteres were

introduced in fluorophores (e.g., oxygen, nitrogen, or sulfur derivatives), and their properties were extensively studied over the decades. For instance, coumarin is a natural product (a secondary metabolite of plants) that was first isolated almost two centuries ago. Coumarins can be used for fluorescent labeling, especially for metal ions, as they can form chelate complexes.^{497,503} Fluorescein is another widely used fluorophore with emission maxima around 500 nm and high molar absorptivity. Due to its safety, it is commonly used in human biomaging.⁵⁰⁴

Firstly reported by Treibs and Kreuzer,³⁷⁸ BODIPY (Figure 20) did not gain popularity until the nineties, but then almost fully commuted fluorescein. BODIPY, 4,4-difluoro-4-bora-3a,4a-diaza-*s*-indacene, is abbreviated from BORone DIPYromethenes. BODIPY was the most versatile and stable fluorophore up to then, regarding polarity or stability at different pH, relatively triple-state formation, good solubility, considerably high molar absorption coefficients,⁴⁸⁵ high quantum yield, and Stokes shift.⁵⁰⁵ BODIPY synthesis is carried out in inert solvents (e.g., pyridine, DCM) via acid-catalyzed condensation of the corresponding aldehyde with pyrrole, which results in dipyrromethane.⁴⁸⁵ The latter can also be synthesized from acyl pyrroles⁵⁰⁶ with pyrrole excess or oxalyl chloride for condensing two pyrrole units.⁵⁰⁷ Dipyrromethane further complex boron to obtain BODIPY. BODIPY is a chemically robust bor-aza-indacene derivative with a rigid backbone, substituted in the *meso* position (position 8). This substitution pattern improves rigidity and does not affect spectral characteristics. BODIPY and its derivatives were extensively used as a highly versatile agent in the pharmaceutical industry to enable processes like drug delivery (e.g., coupled with POSS units),⁵⁰⁸ lasers dyeing,⁵⁰⁹ or in biomolecular imaging.^{510 511}

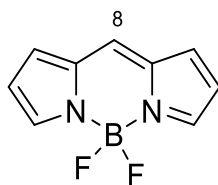


Figure 20: 4,4-Difluoro-4-bora-3a,4a-diaza-*s*-indacene (BODIPY)

Various modifications on the BODIPY core were reported to improve its photophysical and physicochemical characteristics and obtain derivatives that will fluorescence strongly at different wavelengths (Figure 21). Fluorescent derivatives that emit near IR range (NIR) can be used in live tissue bioimaging due to maximal light penetration. They are noninvasive and enable deep tissue

visualization.⁵¹² One of the first modifications, therefore, was enriching electronic density in the fluorophore core. By substitution with phenyl moieties, especially in position 3 and 5, delocalization of π -Electrons is extended,⁵¹³ resulting in bathochromic (red) shifting to IR spectral ranges and higher molecular extinction coefficients as reported by Chen et al.⁵¹⁴ or Ortiz et al.⁵¹⁵ Further modification on aryl substituents and more rigid derivatives as reported by H.Kim et al., expressed redshift and up to 5-fold higher quantum yield, compared to the parent molecule.⁵¹⁵ Modification on isoindole moiety can lead to bathochromic shift up to 700 nm as reported by Yu et al.⁵¹⁶ On the other hand, blue-emitting dyes can be interesting for *in vivo* imaging. New compound class 8-amino BODIPY, reported by D. Kim et al., expressed bathochromic (blue) shift and can be used for protein labeling and further examining of protein dynamics.⁵¹⁷

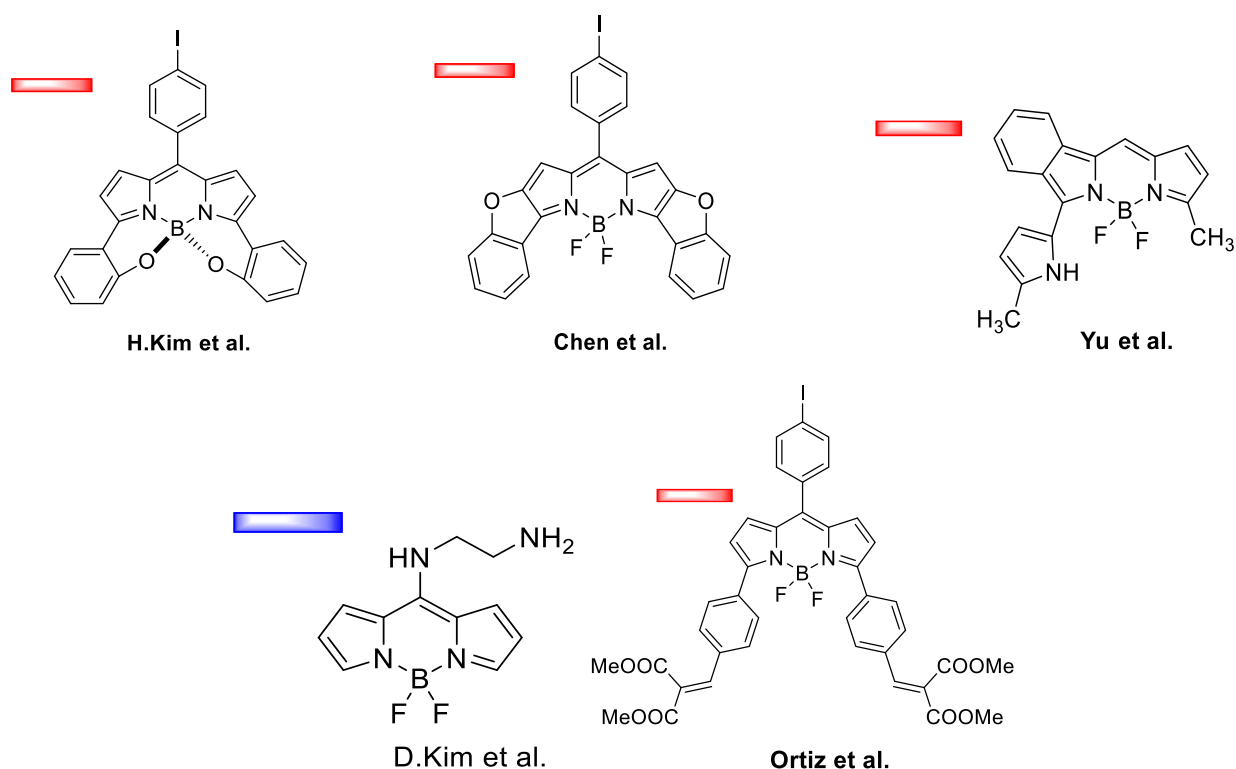


Figure 21: Structural modification on BODIPY core

However, BODIPY expressed a few disadvantages: it expresses weak fluorescence in solid state⁵¹⁸ solvent-dependent fluorescence,⁵¹⁹ unsubstituted derivatives are prone to polymerization,⁴⁸⁵ and bioimaging studies in humans occasionally reported inconsistent results.⁵²⁰ In line with these results, BODIPY core was further modified. This led to extending BODIPY core by developing

hydrazine -Schiff base linked bipyroles that chelate BF_2 unit and form new symmetric planar derivatives reported almost at the same time by Yu et al.⁵¹⁸ and Tamgho et al.⁴⁸⁷ (abbreviated as BOPHY, Figure 22). Both of two reported series can be easily synthesized in one-pot synthesis, expressed larger Stokes shift, slight solvent-dependence of optical properties, and expressed two well-split absorption as well as emission maxima. Most of reported BOPHY derivatives expressed high quantum yield (close to one).

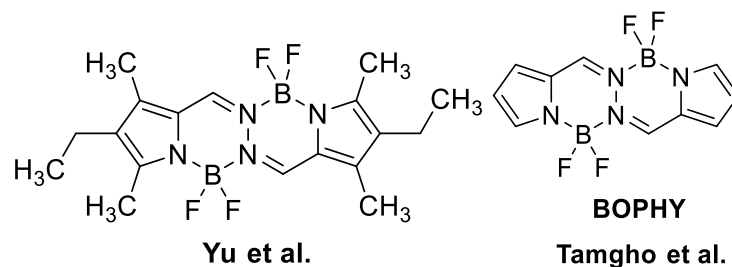


Figure 22: Symmetric BODIPY analogues.^{487,518}

Modifications on symmetrical derivatives further led to developing unsymmetrical bis BF_2 derivative, abbreviated as BOPPY by Yu et al. in 2018⁴⁸⁸ (Figure 23). BOPPY fluorophores express excellent optical properties are up to now the most stable dyes (to oxidation, hydrolysis, or photodegradation). They express fluorescence also in solid-state, which represents a considerable advantage when compared to BODIPY. BOPPY expresses two well split absorption maxima at 393 nm and 413 nm in DCM with high molar absorption coefficients of 4.48×10^4 and $4.43 \times 10^4 \text{ M}^{-1} \text{ cm}^{-1}$. These derivative exhibit two emission maxima at 432, and 462 nm, respectively, and the quantum yield of 0.79. Yu et al. also reported solvatochromic effects, where quantum yield was lower in polar solvents such as methanol and higher when observed in a lyophilic solvent like hexane. The highest occupied molecular orbital (HOMO) and lowest unoccupied molecular orbital (LUMO) are well split with a high HOMO-LUMO gap. HOMO and LUMO energies of substituted derivatives are higher when compared to unsubstituted derivatives. This further explain the electron-donating effect of alkyl substituents (ethyl or methyl). BOPPY fluorophore has been coupled with corresponding dopamine and histamine receptor

pharmacophores to obtain novel, potent, fluorescent ligands that can be further used to estimate receptor localization and distribution.

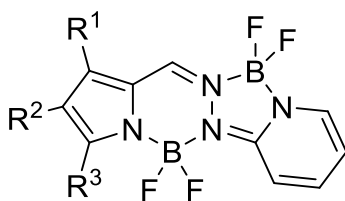


Figure23: BOPPY fluorophore, that served as a starting material for compounds **44-50**.

2.7.2 Dopamine Receptor Fluorescent Ligands

Even though dopamine is involved in numerous physiological and pathophysiological processes, only a few dopamine ligands with fluorescent properties have been fully characterized. Dopamine receptor pharmacophores were coupled with different fluorescent moieties such as coumarin, Cascade blue, Texas red, BODIPY,⁴⁹² fluoresceins,⁵²¹ and rhodamines.⁴⁹² These fluorescent derivatives have a broad field of application as shown by Sykes et al., who performed kinetic experiments with commercially available phenylethyl-propyl-hydroxytetraline (PPHT)-red to examine the binding mode of currently marketed antipsychotics.⁵²² Fluorescence-labeled ligands which bind to the biological target should express affinity at the receptor of interest. This can be particularly challenging, as bulky fluorophores can sterically hinder interaction with the receptor and interfere with the binding affinity. All mentioned fluorescent markers express disadvantages compared to new fluorophores developed in the recent five years. Even though Alliklait et al. in 2020 reported promising dansyl labeled ligands with subnanomolar affinities at both D₂R and D₃R as potential ligands in the NanoBRET assay,⁴⁹⁴ it remains imperative to develop highly potent and affine fluorescent dopamine receptor derivatives.

Compound **44-50** were synthesized as described in Section 2.6. Determination of the absorption and emission maxima and quantum yield was determined at the Institute of Organic Chemistry at the Heinrich-Heine University, Duesseldorf, in the working group of Prof. Dr. Thomas J.J. Müller by Laura Mayer. Coumarin was used as a reference due to its similar optical characteristics (absorption and emission maxima wavelengths)^{497,523} as described BOPPY derivatives. Measurements were performed in DCM, in five different concentrations, as shown in graphics (Figure 24-28). All dopamine receptor fluorescent ligands except **48** expressed two well-split emissions and four well-split absorption maxima (Table 9). Two absorption maxima in the range

of 252-258 nm and 293-297 nm correspond to substituted phenylpiperazine moiety. Two remaining maxima in the range of 423-425 nm and 444-448 nm belong to BOPPY moiety. Extinction coefficients were in a range of $1.5\text{-}3.01 \times 10^4 \text{ M}^{-1}\text{cm}^{-1}$, which is in line with previously published results.⁵²⁴ These four compounds (**44-47**) exhibit two well-split emission maxima at 461-465 nm and 489-490 nm, respectively. Compound **45** expressed moderate (0.19), **44** exemplary (0.49), while **46** and **47** excellent (0.63 and 0.69, respectively) quantum yields. The two latter compounds are substituted in position 3 with ethyl substituent, indicating an optimal substitution pattern for the synthesis of potent fluorescent ligands. Besides, dichloro substituted derivatives expressed higher quantum yield when compared to that of their methoxy substituents analogues. The moderate quantum yield of compound **45** compared to other compounds of this set should be further explored, and conformational studies need to be performed to estimate the exact orientation of compounds. Compounds **46** and **47** stood out from this compound set as the most promising candidates for further *in vitro* imaging studies.

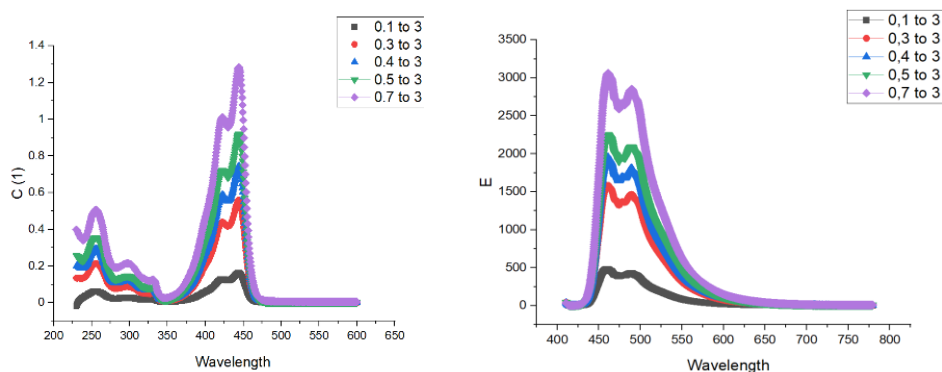


Figure 24: Absorption (C, left) and emission (E, right) spectra of compound **44**. Wavelength is expressed in nm. Different concentrations of solution are presented in different colours.

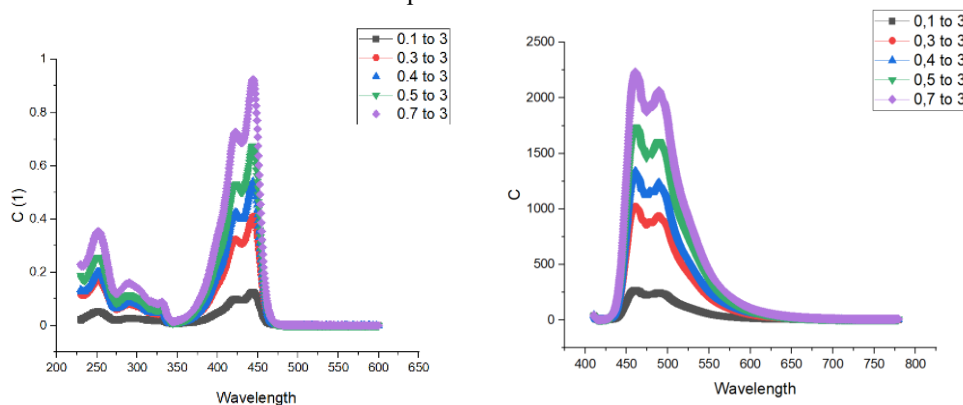


Figure 25: Absorption (C, left) and emission (E, right) spectra of compound **45**. Wavelength is expressed in nm. Different concentrations of solution are presented in different colours.

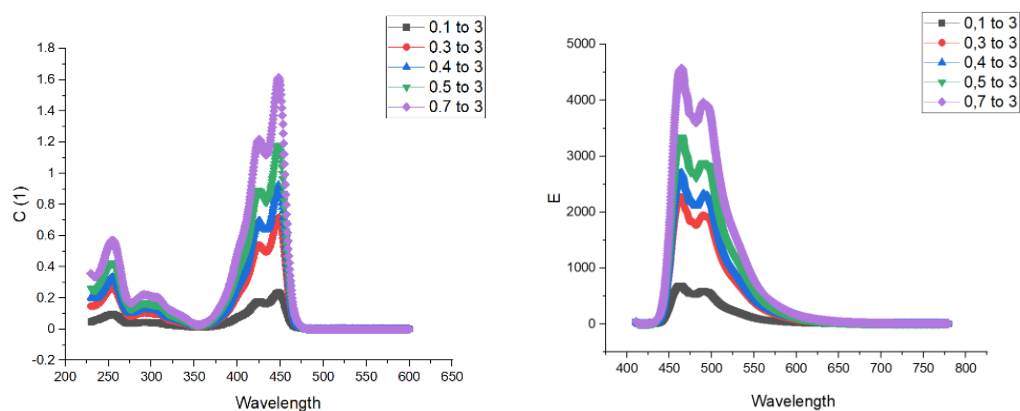


Figure 26: Absorption (C, left) and emission (E, right) spectra of **46**. Wavelength is expressed in nm. Different concentrations of solution are presented in different colors.

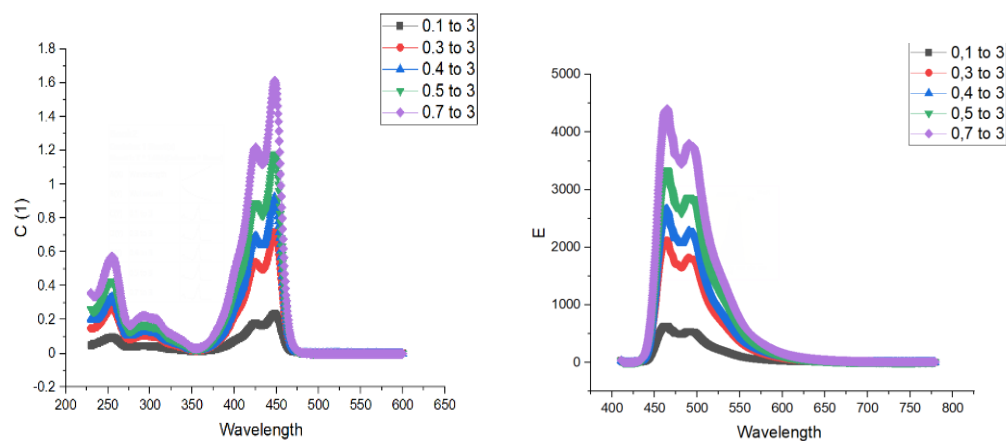


Figure 27: Absorption (C, left) and emission (E, right) spectra of compound **47**. Wavelength is expressed in nm. Different concentrations of solution are presented in different colors.

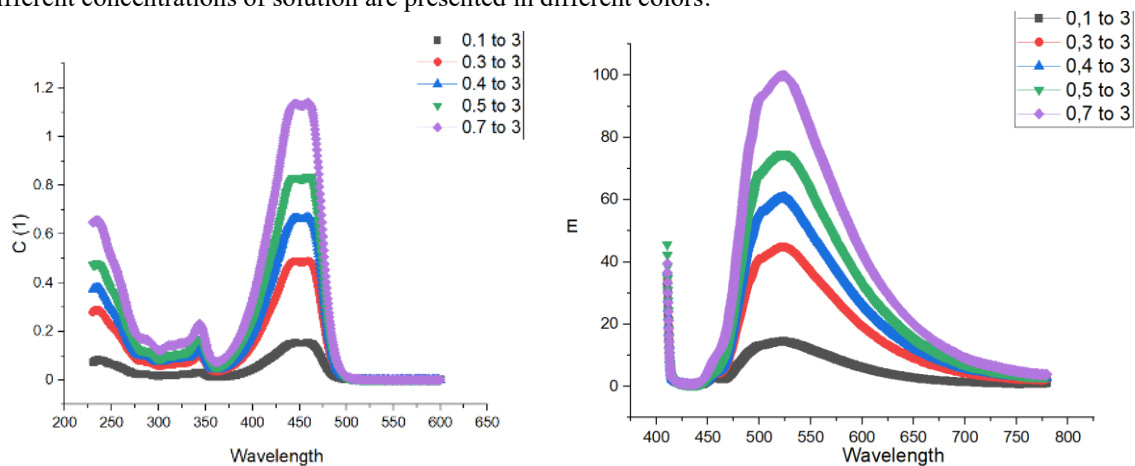
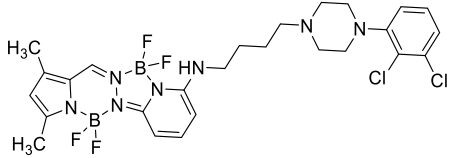
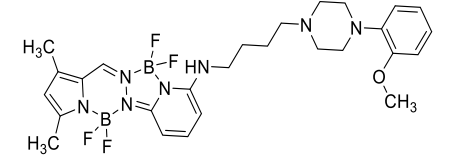
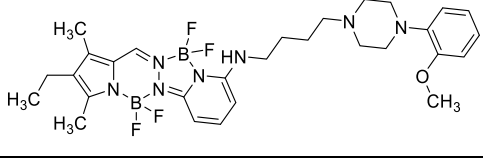
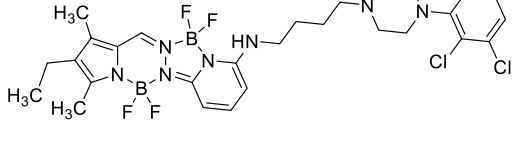
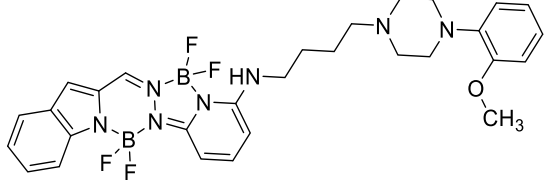


Figure 28: Absorption (C, left) and emission (E, right) spectra of compound **48**. Wavelength is expressed in nm. Different concentrations of solution are presented in different colors.

Table 9: Spectral characteristics of dopamine D₃ receptor fluorescent ligands **44-48**.

No.	Structure	Absorption	Emission
		λ_{\max} [nm] (ϵ [$M^{-1} cm^{-1}$])	λ_{\max} [nm] (Φ_F [au])
44		256 (16300), 297 (6800), 423 (32800), 444 (41700)	461, 490 (0.49)
45		252 (12500), 291 (5700), 423 (25600), 444 (32500)	461, 489 (0.19)
46		252 (12500), 291 (5700), 423 (25600), 444 (32500)	464, 490 (0.63)
47		258 (21000), 305 (8000), 425 (44100), 448 (58700)	465, 490 (0.69)
48		343 (9000), 445 (44300), 459 (44500)	523 (0.03)

λ_{\max} - absorption/emission maximum; Φ_F -quantum yield

Compound **48** structurally differs from the above-mentioned dopamine receptor ligands, as it has incorporated another phenyl moiety. As previously described, higher electronic densities can lead to bathochromic shifts and emissions in the near IR range. Compound **48** expressed three absorption maxima at 343, 445, and 449 nm, respectively, with an extension coefficient of $1.7 \times 10^4 M^{-1} cm^{-1}$ and one emission maxima at 523 nm. Nevertheless, the quantum yield was very low (0.03), and this compound cannot be considered a fluorescent marker. Low quantum yield can be explained with the photoinduced electron transfer process (PET), as reported by isoindole derivatives.⁵²⁵ As observed, introducing heterocycles led to enriched electronic density, resulting

in redshift and bathochromic effect. On the other hand, heterodimers enable PET and, therefore, can lead to low quantum yield.⁵²⁶ In this case, electronic transitions occur from HOMO of the fluorophore to HOMO of the substituent and LUMO of the substituent to LUMO of the fluorophore, electron transfer is then in direct competition with radioactive decay resulting in fluorescence quenching. This process is already observed between amino acids like tryptophan and nucleic basis like guanine.^{525,527}

Solvatochromism is a complex phenomenon where spectral characteristics of a compound (wavelength intensity, shape of absorption, and emission band) change depending on the solvent, resulting in the color change.⁵²⁸ Solvatochromic effects are consequences of different intermolecular interactions between ground and excited state and their environment in a particular moment.⁵²⁹ Solvatochromic effect especially affects emission spectra.⁵³⁰ These effects can lead either to a bathochromic (red) shift to higher wavelengths and lower frequency or to hypochromic (blue) shifts to lower wavelengths and higher frequency. Previously described measurements were conducted in dichloromethane, a lipophilic (dielectric constant 9.1) aprotic solvent. On the other hand, methanol is polar, protic solvent that can form hydrogen bonds and lead to different intermolecular interactions. 2D Excitation and emission spectra of compounds **44-48** were measured in methanol in Stark's lab to examine the solvatochromic effect of these two different solvents (concentration of Stock solution 0.1 mg/mL). 2D Excitation and emission spectra of **47**, as a representative, is shown in Figure 29.

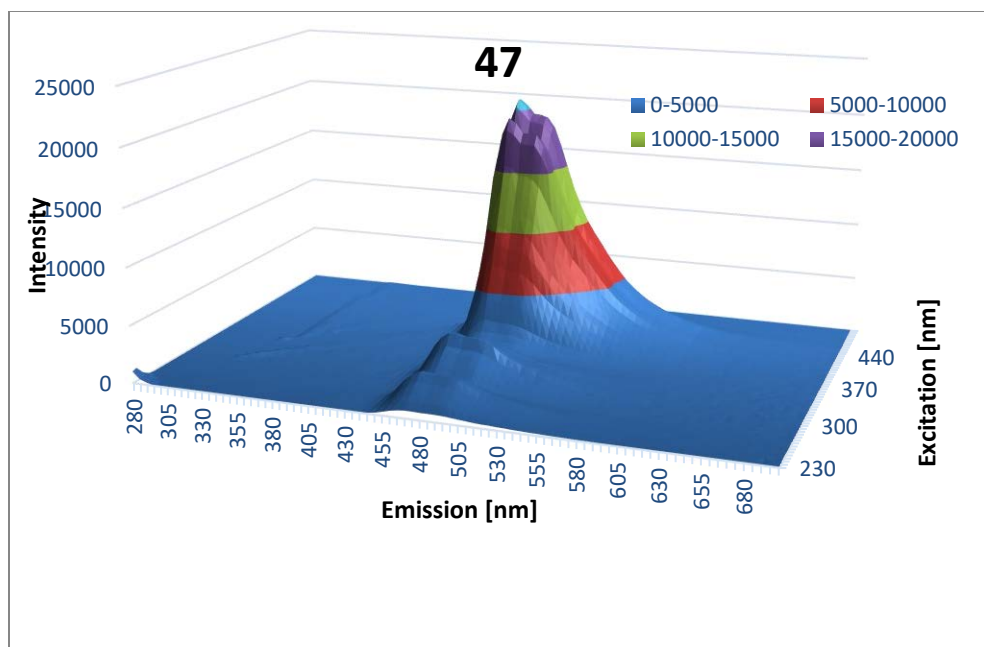


Figure 29: 2D Excitation/Emission spectra of compound **47** in MeOH (0.1 mg/mL).

Slight hypsochromic shift was confirmed for all the observed compounds. Emission maxima were shifted towards lower wavelengths. Even though shifts were only up to 10 nm, these results suggest intermolecular reactions between ligands **44-48** and polar protic solvents as methanol. These results are in agreement with previously reported by Yu et al. where BOPPY derivative itself expressed a blue shift when spectral characteristics were obtained in more polar solvents. The blue shift was linearly increased from hexane to methanol, and quantum yields were decreased.⁴⁸⁸

2.7.3 Histamine Receptor Fluorescent Ligands

The histamine H₃ receptor represents an interesting target due to its involvement in various neurological diseases such as sleep-wake disorder, Parkinson's disease, and severe cognition impairments such as Alzheimer's disease (Section 1.4.2). Potent fluorescent ligands need to be developed to gain better insight into the role of this receptor in disease etiology. Non-imidazole fluorescent, oxygen containing⁵³¹ H₃R fluorescent derivatives are described as pyrrolidine or piperidine-containing fluorophore coupled with cyano, nitrobenzo,^{532,533} chalcone,⁴⁶⁵ or recently

reported Py-5-labeled derivatives.⁵³⁴ H₃R pharmacophore was coupled with BODIPY, resulting in Bodilisant, which expresses a high quantum yield (0.92).⁴⁹⁶ However, as already described, BOPPY represents a more stable alternative compared to all so far described fluorophores, and therefore two histamine ligands coupled with this fluorophore were developed. Compound **49** is coupled via ether to BOPPY core, while compound **50** is coupled via amino group. Compound **50** contains phenyl moiety as central core, as part of H₃R pharmacophore 1-(3-phenoxypropyl)piperidine. On the other hand, BOPPY core imitates hydrophobic central core in compound **49**. Therefore, the goal was to examine if central core is an absolute prerequisite for the interaction with receptor, if bulky BOPPY fluorophore can mimic these effects, and to determine if differences between these compounds impact the binding mode and spectral characteristics. Both synthesized histamine H₃R ligands exhibited two well split absorption maxima and two well split emission maxima with comparable quantum yield (0.56 and 0.60, respectively, Figure 30-31). Introducing benzyloxy moiety in compound **50** led to a slight hypsochromic shift compared to that of **49** but resulted in a slightly lower quantum yield (Table 10). Spectral characteristic did not change, by introducing benzyl moiety. However, binding affinities significantly differ, which will be in detail explained in Section 4.

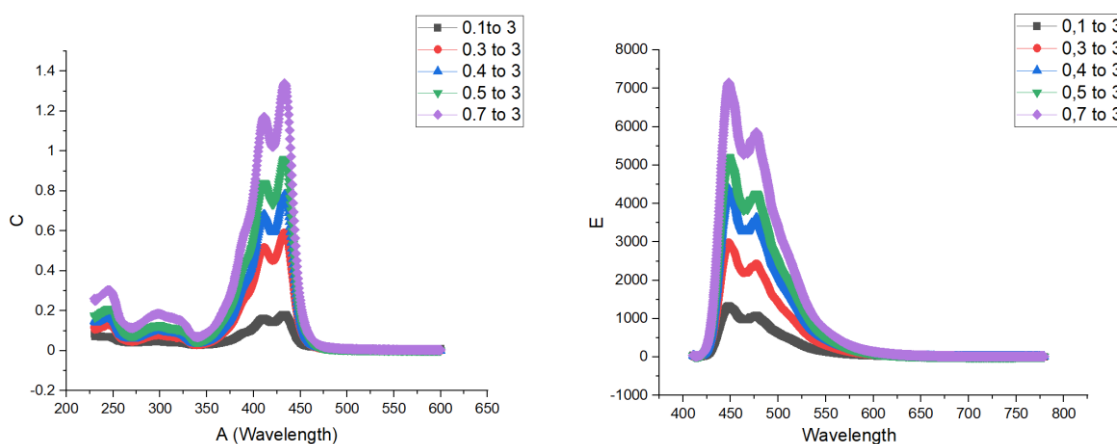


Figure 30: Absorption (C, left) and emission (E, right) spectra of compound **49**. Wavelength is expressed in nm. Different concentrations of solution are presented in different colors.

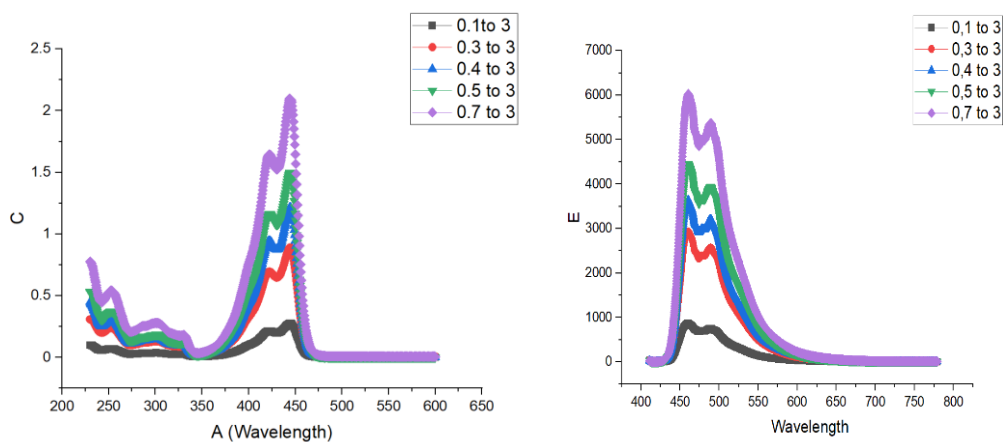
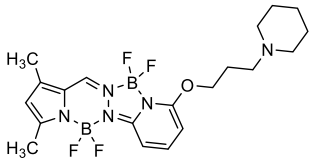
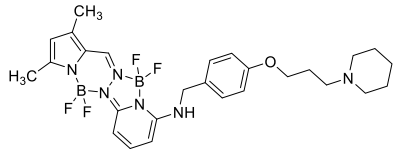


Figure 31: Absorption (C, left) and emission (E, right) spectra of compound **50**. Wavelength is expressed in nm. Different concentrations of solution are presented in different colors.

Table 10: Summarized spectral characteristics of histamine fluorescent ligands **49-50**.

No.	Structure	Absorption	Emission
		λ_{\max} [nm] (ϵ [$M^{-1} cm^{-1}$])	λ_{\max} [nm] (Φ_F [au])
49		245 (9400), 299 (5700), 411 (36800), 433 (42100)	448, 477 (0.60)
50		254 (16600), 301 (8500), 422 (50800), 444 (65000)	461, 489 (0.56)

λ_{\max} - absorption/emission maximum; Φ_F -quantum yield

2.8 Summary of Chemistry Part

Ten D₃R ligands in the three-step synthesis were developed in the first compound set (Scheme 5, **1-10**). This synthetic route was successfully optimized to reduce costs and obtain a higher yield, resulting in a yield of over 60% over three steps. (**Route II**). Amide synthesis was conducted with mild coupling reagent EDC and additive HOBt, resulting in facile, one-pot synthesis and shortening of reaction time.

In the second compound set (**11-17**), bitopic D₂R and D₃R ligands were developed. To obtain amide **11**, HANTZSCH THIAZOLE synthesis was conducted and optimized, leading to 70% yield over two reaction steps and resulting in a fast and effective way for the synthesis of 2-aminothiazole derivatives that could further be effectively functionalized and undergo different reaction types. Bitopic ligand was further modified with bioisosteric replacement of methylene groups with ether as well as derivatization of arylamide moiety. A new compound set (**18-24**) connected via ether was developed. This synthetic route was optimized, leading to an increase in yield of up to 60% when deamination of 2-aminothiazoles derivatives was performed in DMSO at 0 °C, with tert-butyl isopentyl- nitrite. Ether synthesis was performed in various solvents (THF, 1,4-dioxane, DMF) and resulted in the highest yield when performed in 1,4-dioxane (deprotonation for three hours and ten hours at 40 °C) for **20** and THF (deprotonation for three hours at 40 °C and refluxing for 48 hours) for compounds **21-22**.

Compounds **25-37** were designed as multitargeting D₂R/H₃R ligands. This six-step synthesis was optimized, resulting in an overall yield of over 18%. α -Bromination of ketones and ring closure in HANTZSCH THIAZOLE synthesis were crucial steps that had to be rationally optimized to obtain the highest possible yield. This cyclization led to no product when conducted in low boiling alcohols, typical solvents for HANTZSCH THIAZOLE synthesis, and to low yields (10%) when performed in acetic acid. Numerous side products were observed, depending on the reaction conditions (e.g., temperature, solvent, time). Paracetamol was isolated as a side product, when the reaction was conducted at high temperatures for more than ten hours (e.g., reflux in DMF overnight). Paracetamol had a very similar R_f value as desired products, making the purification more difficult. Elimination products (with another double bond in 4,5,6,7-tetrahydrobenzothiazole ring) interfered with purification were in addition observed at higher temperatures. Nevertheless, optimized reaction conditions were chosen (chloroform, room temperature, 15-30 minutes for α -

keto bromination and DMF, room temperature, stirring for one hour and then heating up to 80 °C and stirring for two hours for HANTZSCH THIAZOLE synthesis). This led to a 53% yield over two reaction steps. Next reaction step, *N*-deacetylation of amides was conducted, resulting in yields up to 75% if conducted in concentrated hydrochloric or hydrobromic acid over two days. This optimization led to compounds **25-37** and, in the same manner, compounds **12-17**.

In compounds **38-43** D₂R and D₃R were coupled with H₃R pharmacophore. Due to the poor solubility of starting material (tyramine and tyramine hydrochloride) in various solvents, the procedure had to be optimized to achieve a better yield. Ion exchange and azeotropic distillation did not lead to the desired yield, and another synthetic approach had to be introduced. BOC protection of tyramine hydrochloride increased solubility in lipophilic organic solvents as DCM, DCE, resulting in **38** and further in **39**. Compounds **41-43** were obtained through reductive amination as described in Section 2.3.3.

Finally, dopamine D₃R and histamine H₃R fluorescent ligands were developed. These ligands contain recently reported BOPPY fluorophore that expresses excellent fluorescent properties (good quantum yield, high Stokes shift, chemical, and thermal stability to different agents). BOPPPY fluorophore was further coupled with D₃R pharmacophore resulting in **44-48**, and with H₃R pharmacophore, resulting in **49-50**. Ether synthesis in the case of **49** has been optimized, resulting in the highest yield (58%) when conducted in THF (deprotonation for 3 hours, further refluxing overnight).

In this PhD project, 50 final compounds were obtained from 10 synthetical routes that had been fully developed and optimized in different steps. This led to a significant increase in yield, cost-effective synthesis, and successful troubleshooting resulting in the highest possible yield with minimum side products that could interfere with purification. Those ligands present a potent pharmacological tool that will further be *in vitro*, *in silico*, and potentially *in vivo* examined.

3 Computer-Aided Drug Design

Computer-aided drug design (CADD) presents one of the crucial factors in rational drug design. Carefully conducted *in silico* experiments lead to an efficient design of potent novel ligands and shortened the entire process by choosing only a few affine, selective, potential drug-like candidates. CADD developed alongside the first computer in the last half of the 20th century and is a rapidly growing chemistry field. CADD optimized and reviewed different postulates (e.g., Hartree-Fock⁵³⁵ and Born-Oppenheim approximation,⁵³⁶ or Schrodinger equation⁵³⁷). Newly developed technology provided support for theoretical chemists to conduct experiments and broaden knowledge. In medicinal chemistry, CADD can predict the binding mode of ligands towards receptors of interest. These predictions reveal novel chemical entities that can be incorporated in the molecule of interest, receptor interaction of so far commercially available medicaments or preclinical and clinical candidates, and consequent explanation of side effects (e.g., that arise as a consequence of different binding kinetics)⁵²², lack of affinity, selectivity, or reason their off-label use.

Molecular docking simulations have been used to examine precise binding mode towards receptor of interest in structure-based design, where the target of interest is the already known structure, and compounds library can be screened to find the optimal ligand. However, when this is not the case, suitable ligands can be found only by ligand-based virtual screening and other *in silico* methods.⁵³⁸ Active and inactive compounds, structurally characterized and optimized, were screened to develop pharmacophore and perform virtual off-target screening. Crystal structure of dopamine D₃R in complex with dopamine D₃R selective antagonist eticlopiride was resolved in 2010 by Chien et al.¹¹⁷ D₂R crystal structure in complex with D₂R inverse agonist risperidone was described later in 2018 by Wang et al.¹¹⁶ Even though D₂R and D₃R express a high homology^{539,540} this two receptor subtypes also exhibit striking differences, especially in surrounding of the secondary binding pocket (Val/Phe^{2,61}, TrpEL1, Phe/Leu^{3,28}, and Tyr/Val^{7,35} residues),¹¹⁶ raising hope for developing highly selective dopamine D₂R ligands. Since both crystal structures were described, the main objective was to conduct rational structure-based design, determine the precise binding mode, and possible interaction with protein residues that could further lead to higher ligands' affinity and selectivity between these two receptor subtypes.

3.1 Molecular Docking Simulations

In silico studies described in this chapter were performed with the first set of synthesized ligands (**1-10**) at the Department for Pharmaceutical and Medicinal Chemistry at Belgrade University, Serbia.⁴⁰⁰ Dopamine D₃R pharmacophore was described in the early 2000s¹⁸¹ and is corroborated with *in silico* examination. Primary pharmacophore that contains basic moiety occupies OBS. Simultaneously, aryl amido rest interacts with SBP and in both D₂R and D₃R.^{117,541} Basic center is a prerequisite as it forms a crucially important salt bridge with Asp 110,^{3,32} and enables interaction within the receptor.^{395,542} D₂R and D₃R express almost the same structurally conserved regions and identical OBS, and therefore differences and desired selectivity are consequences of different binding modes to SBP. Extracellular loop 2 (EL2) in SBP is open into the outer space and exposed to solvent in D₃R forms hydrogen bonds with aryl-amido head. Therefore this interaction is one of the prerequisites for selective binding.¹⁸⁵ However, extracellular loops are more flexible,⁵⁴³ able to change conformation,⁵⁴⁴ and therefore, synthesis of highly selective ligand targeting only one receptor subtype remains a challenge.

Ten ligands (**1-10**) were firstly docked into co-crystal structures of D₂R and D₃R (Figure 32). Validation of docking protocol for D₃R was confirmed by redocking eticlopride and calculating an RMSD score of 0.67Å. To estimate the correlation between docking results and experimental obtained p*K_i* values, Spearman rank correlation coefficient *r_s* and Pearson correlation coefficient *R*² were calculated. (*R*² = 0.92; *r_s* = 0.97.) These high values validated binding modes of obtained ligands. In the case of D₂R, Spearman rank correlation coefficient and Pearson correlation coefficient were lower when compared to D₃R but remained in the moderate range (*R*² = 0.32; *r_s* = 0.73).⁵⁴⁵ Lower values are according to the literature, where a more flexible extended binding pocket in D₂R was observed. Extracellular loop 2 makes additional space for the extended binding pocket in D₂R, resulting in more difficult conformations to predict.¹⁴⁵

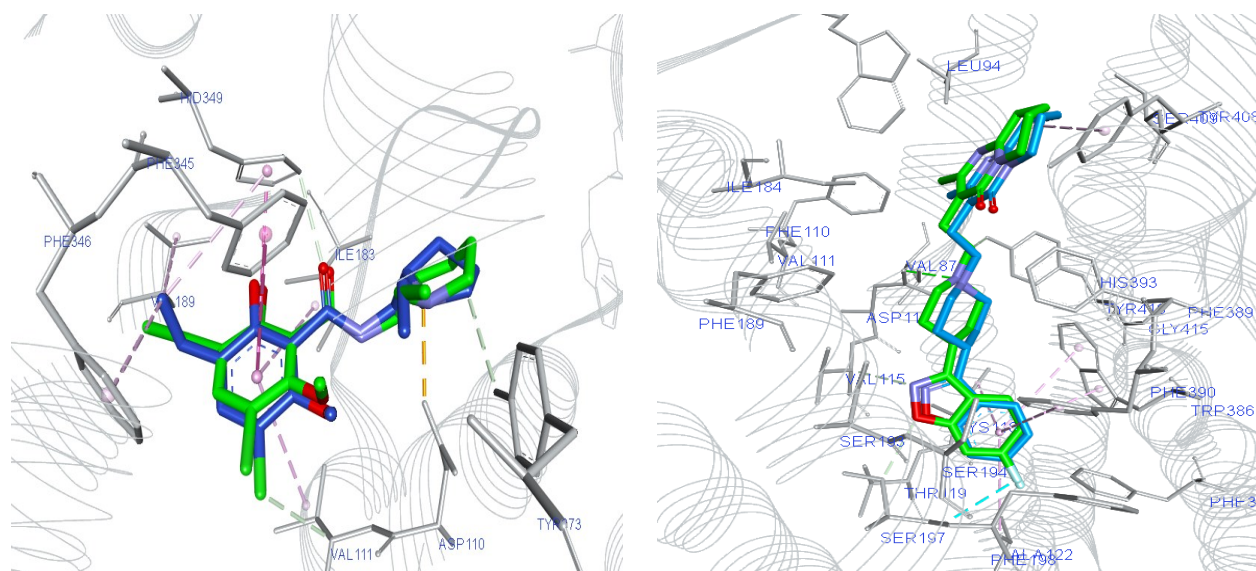


Figure 32: Comparison of binding poses of eticlopride obtained by redocking (blue sticks) and from X-ray structure (green sticks) – PDB ID: 3PBL, D₃R (left) RMSD = 0.67Å and in PDB ID: 6CM4, D₂R (right) RMSD = 0.62Å. Interacting residues are depicted in gray sticks.

Molecular docking (MD) simulations in D₃R confirmed that PP 1-(2,3 dichlorophenyl)piperazine or 1-(2-methoxyphenyl)piperazine binds to OBS and positively charged nitrogen forms a salt bridge Asp 110^{3,32}, while arylamide moiety interacts with SBP. These results correlated with previously reported.^{182,395,543} Compound **9** showed the highest affinity and selectivity *in vitro* (Section 4.5, SI = 20.5), displaying a similar binding profile as that of eticlopride in OBS (Figure 33). However, compound **9** forms additional π -alkyl interaction with Cys 114^{3,36} which is not observed in eticlopride. This residue is located at the third transmembrane segment, physically near, Asp 110^{3,32} and is prone to oxidation. Mutations on this residue led to the lower affinity of commercially available D₂R and D₃R ligands as confirmed by Alberts et al.⁵⁴⁶ Moreover, Ericksen et al. highlighted its importance for binding of benzamide moiety.⁵⁴⁷ Arylamide moiety of **9** is surrounded in SBP by Val 86^{2,60}, Leu 89^{2,63}, Gly 93, Ser 366^{7,35} in SBP Tyr 36^{1,39} Glu 90². Two latter residues are reported to be important for binding **GSK598809**, a D₃R preferring antagonist that has been examined in the therapy of addictive behaviour.^{205,543}

MD simulations in D₂R confirmed binding 4-phenylpiperazine moiety to OBS and arylamido moiety to the extended binding pocket. (EBP) and forming a salt bridge between Asp 110^{3,32} and positively charged piperazine nitrogen.

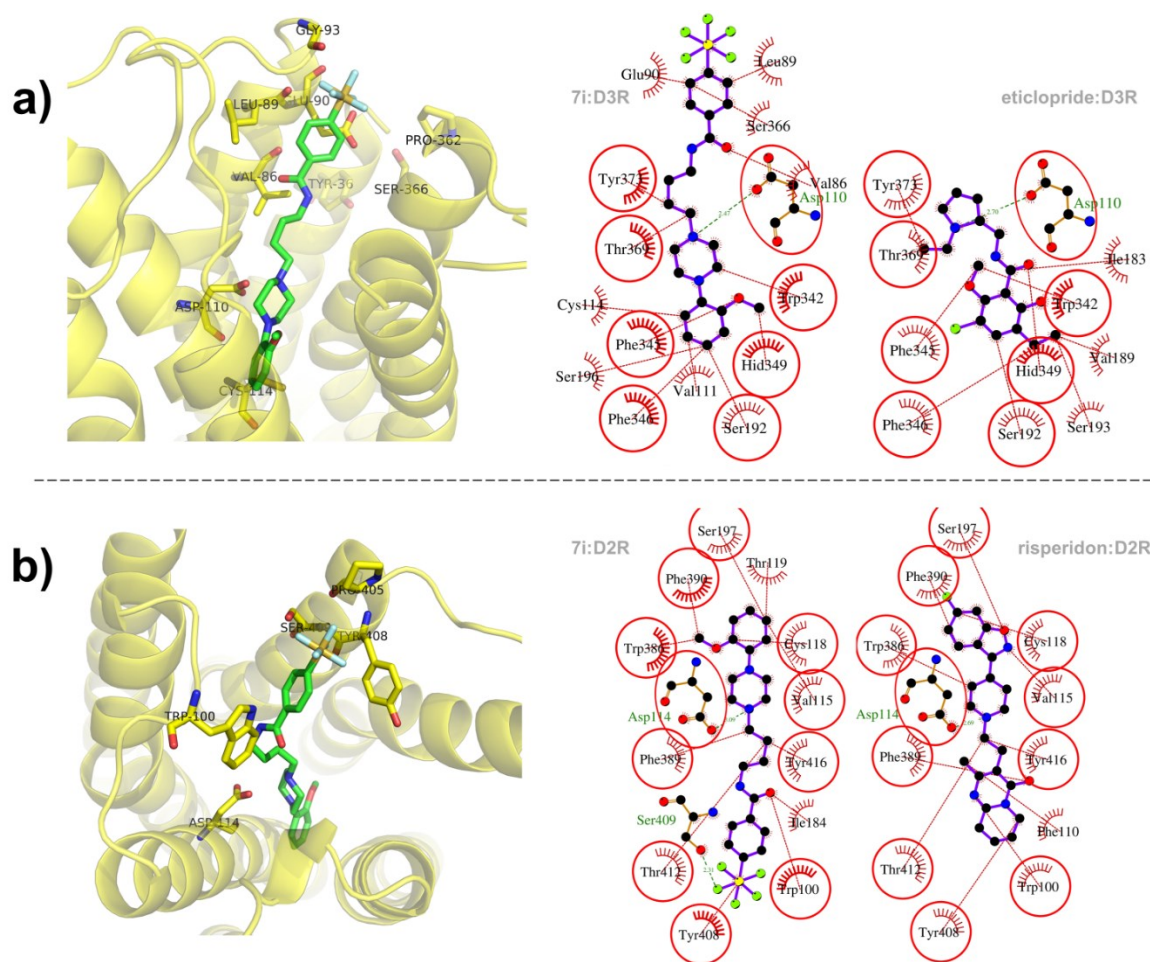


Figure 33: Docking results of **9** into the binding site of a) D₃R and b) D₂R. Left: 3D representation of binding sites Right: 2D interaction plots obtained for **9** and co-crystal ligands (eticlopride – a), risperidone –b). Encircled are engaged interact with both ligands. Adapted from Elek et al., **7i** corresponds to **9**.⁴⁰⁰

Novel chemical entity- SF₅ was introduced in *m*- or *p*- position in compounds **7-10**, as described in Section 2.2. Molecular docking simulations confirmed that *m*-substituted compounds achieve interaction with Tyr408^{7,34} On the other hand, *p*-substituted derivatives tend to decrease affinity towards D₂R due to steric hindrance (Figure 34). At the same time, this substitution pattern does not diminish affinity towards D₃R. These results are in accordance with the literature, where ligands are positioned deeper in the OBS in D₂R and higher in the OBS in D₃R and D₄R.¹⁴⁵

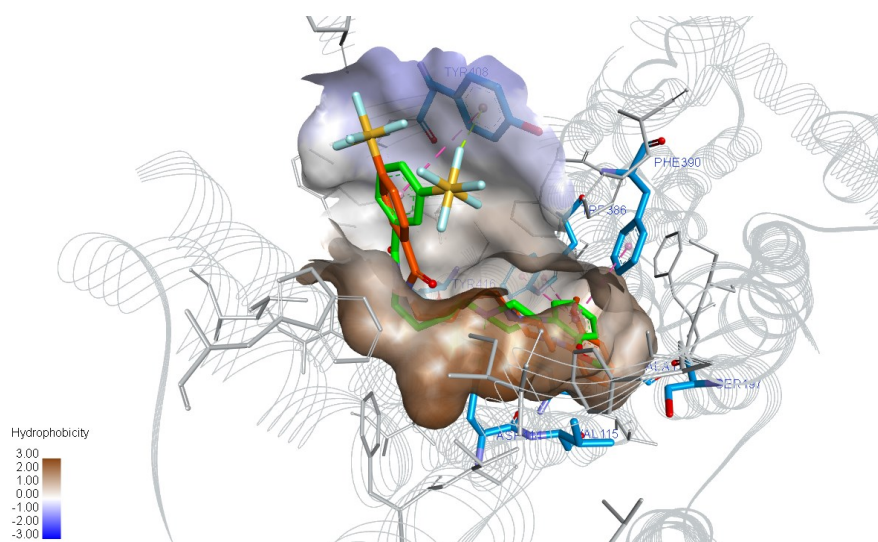


Figure 34: Comparison of binding modes obtained for *p*-substituted SF₅ derivative **9** (red sticks) and *m*-substituted SF₅ **7** (green sticks) into D₂R. SF₅ moiety is marked in yellow.

3.2 QM/MM Calculations

In order to determine the precise binding mode of the lead compound **9** from the first compound set (**1-10**), and the impact of the novel chemical entity SF₅, hybrid quantum mechanics molecular mechanics (QM/MM) simulations were performed by Professor Katarina Nikolic and coworkers at the Belgrade University, Serbia. SF₅ moiety is highly lipophilic and electrophilic and therefore can be an interesting factor in drug design, especially by improving their bioavailability.^{396,397} Common CADD fields (e.g., CHARM and AMBER) do not recognize hypervalent sulfur atom type; therefore, classical molecular dynamics could not be conducted. The QM/MM approach was first introduced by Warschell and Levitt back in the seventies.⁵⁴⁸ According to this principle, the entire system can be divided into two components that are treated differently. In the QM/MM approach, the specific region (here SF₅ moiety) is treated at an appropriate level of quantum chemistry while the rest of the system (non-interacting moieties, solvent, membrane) is described with the molecular mechanics. QM/MM approach enables analysis of biomacromolecule system (e.g., enzymes)⁵⁴⁹ in the reasonable time. As this system is too large for analyzing with *ab initio* theory, QM/MM approach was introduced to validate the predicted docking pose of compound **9**

by MD simulations. Firstly, semi-empirical theory (PM3) was conducted, and afterward more advanced and computationally demanding DFT calculations (M06-2X functional with def2-TZVP basis set) were used.^{550,551} Semi-empirical methods are simplified versions of Hartree-Fock using empirical correction to improve performance. PM3 is based on Neglect of Differential Diatomic Overlap (NDDO), which reduce the number of integral electron-electron repulsion, simplifying Hartree-Fock calculation.⁵⁵² M06-2X is density functional that calculates a gas-phase system's relative conformational energies that could not be fully characterized with spectroscopic techniques.^{553,554} This method predicts intermolecular interactions with high accuracy.⁵⁵⁵ During 100 ps of QM/MM simulations, posed obtained through molecular docking of **9** remained stable, which validates MD prediction. Compound **9** was stabilized through equilibrium between repulsive and attractive non-covalent interactions (NCIs) in both D₂R and D₃R. In D₂R position of SF₅ moiety did not change through QM/MM simulation, but the hydrogen bond between Ser409^{7.35} of D₂R and fluorine of SF₅ moiety predicted by MD could not be observed anymore. On the contrary, C-H···F-S interaction was instead observed. In D₃R, SF₅ moiety was slightly reoriented towards Pro362^{7.31} interacting with this protein residue. QM/MM simulation revealed precise position and surrounding of SF₅ in SBP and EBP in D₃R and D₂R, respectively (Figure 35). Compound **9** was positioned deep in the sub-pocket of D₂R consisting of Tyr408^{7.34}, Pro405^{7.31}, and Ser409^{7.35}, according to MD simulation. In contrast, in D₃R, compound **9** was surrounded with the interacting D₃R residues while the upper fluorine of SF₅ was free and exposed to solvent. QM/MM simulations validated docking obtained with MD simulations. To explain in detail how protein environment affected electronic density in ligand, electrostatic potentials (ESP) were obtained from electron densities and consequently plotted on molecular Van der Waals surfaces. ESP was obtained after single point calculation of lone ligands compared with ESP obtained after QM/MM calculations of QM regions of protein/ligand complexes (M06-2X level of theory). As a result, it was concluded that the protein environment affected the charge distribution of SF₅ moiety, pointing out possible intramolecular interactions. Fluorine atoms closer to protein residues displayed more negative electrostatic potential, which could be explained by intramolecular interactions between SF₅ moiety and protein residues.⁴⁰⁰

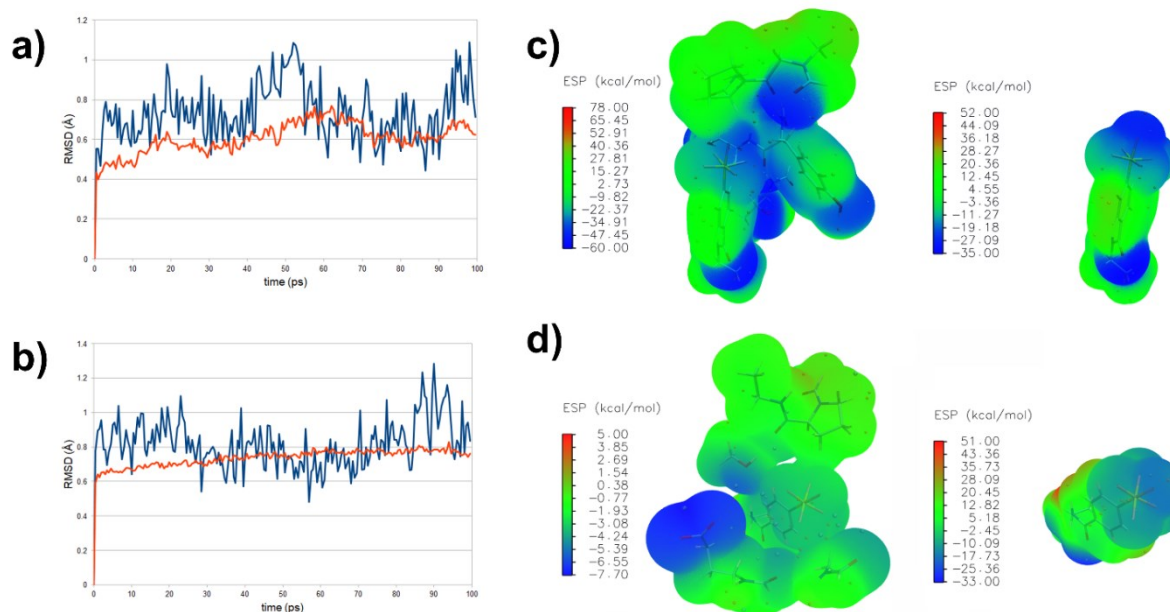


Figure 35: Root-mean-square deviation of atomic positions (RMSD) during 100 ps of QM/MM (PM3) simulations (a) D₂R:9- system and b) D₃R:9 system) and electrostatic potential (ESP) maps calculated on M06-2X level of theory for QM region after QM/MM minimizations (c) D₂R:9 system and d) D₃R:9 system) and after single-point calculations. Blueline (a) and b)) indicates RMSD calculated for ligand atoms, while the red line represents RMSD calculated for protein backbone.⁴⁰⁰

3.3 Non-covalent Interaction Analysis

Non-covalent interaction (NCI) analysis was performed to explain the precise interaction type between SF₅ moiety and protein residues and their orientation in space (Figure 36).^{556,557} Self-consistent field (SCF) densities were first derived from QM/MM calculations on the M06-2X level of theory. NCI analysis detected no strong stabilizing interaction and confirmed that interaction between SF₅ and both D₂R and D₃R are delocalized weak interactions. In D₂R, C-H⋯F-S and S-F⋯C=O were the most important interaction while C-H⋯F-S was most noticeable in D₃R reduced density gradient, $s \leq 0.3$). These results are in accordance with the literature, where it is stated that highly deshielded fluorine atoms mainly participate in F⋯C=O orthogonal interactions with carbons from carbonyl groups, and by deshielded fluorine atoms it this interaction type not common.⁵⁵⁸ To determine intermolecular reaction between the entire molecule and D₂R and D₃R promolecular approach was used. Hirschfield and Rostkowitz⁷³ first used the term promolecule, referring to the electron density before molecule forming. In the promolecular approach, total

electron density represents the sum of atomic density. Promolecular approach confirmed that compound **9** achieved a more significant number of interactions with D₂R through the SF₅ moiety, while D₃R interacted with compound **9** mainly through phenyl moiety. This is according to the results of molecular docking (Section 3.1), where steric effects of *-p* SF₅ moiety of **9** prevented interaction with Tyr 408^{7,34} in D₂R.

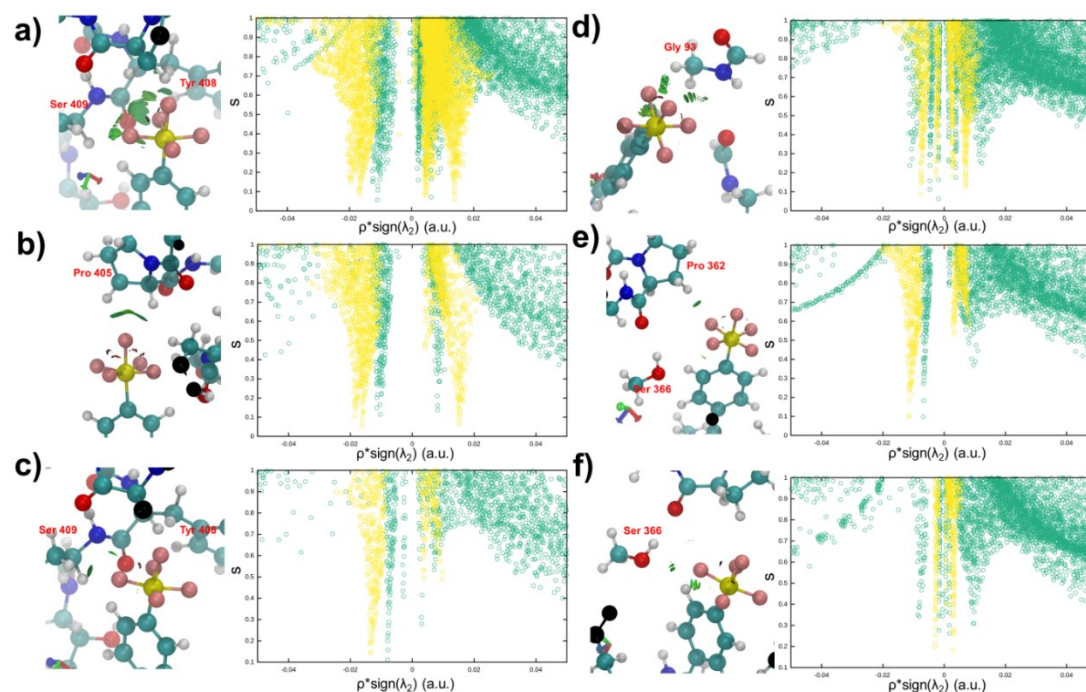


Figure 36: Results of the noncovalent interaction (NCI) analysis for D₂R: **9** (a–c) and D₃R: **9** (d–f) systems. On three-dimensional (3D) NCI plots, green isosurfaces represent delocalized weak attractive interactions (inter- and intramolecular), whereas red isosurfaces represent repulsive interactions calculated from self-consistent field (SCF) densities (quantum mechanics/molecular mechanics on M06-2× level of theory). On 2D NCI plots, $\text{sign}(\lambda_2)\rho(r)$ versus reduced density gradient (s), green points represent results from SCF densities for intra- and intermolecular interactions, whereas yellow points represent results from promolecular densities only for intermolecular interactions. Due to inherent limitations of the NCI approach, it was not possible to omit intermolecular interactions from analysis for SCF densities.⁴⁰⁰

4 Pharmacology and Discussion

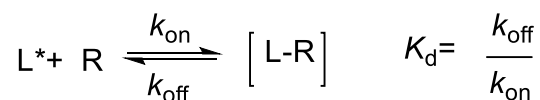
4.1 Pharmacological Evaluation

Synthesized dopamine and histamine receptor ligands were evaluated for their *in vitro* receptor binding properties to examine affinities for their intended targets. Consequently, selectivity to the target over other off-targets was examined. Only highly affine and selective ligands represent potent drug-like candidates and could be considered for further development (such as *in vivo* and later in clinical studies). All performed *in vitro* studies were conducted in Professor Holger Stark's working group, as previously reported, with slight modifications.^{355,559,560}

4.2 *In vitro* Binding Affinity Determination

Binding studies can be performed to determine receptor localization and distribution, characterize receptors of interest and their regulation, examine the ligands' kinetics, determine affinity to on- and off-targets, selectivity, and finally develop new, potent drug-like candidates. The ligand used for binding studies is mostly radio- or fluorescence-labeled (Section 2.7.1). These ligands should express high affinity and selectivity at the receptor of interest. High affinity at the receptor is associated with slow dissociation that provides favorable conditions for performing an assay. Furthermore, the selection of the model system is crucial. Using receptor overexpressing recombinant cell lines provides a focus on the interaction with the receptor of interest.⁵⁶¹

Assays carried out in the presence of antagonist, although very complex, could be simplified as a two-part system. They consist of ligand (L) and receptor (R), the target of interest. The homogenate and the desired biological target are mixed for empirically determined time (time of incubation), which enables collision and equilibration of binding. The binding to the receptor of interest follows the Law of Mass Action. The complex between free, unbound ligand (L*) and receptor (R) is formed until the equilibrium state is reached, resulting in the formation of bound ligand (L-R) (Equation 1). This reaction is reversible. In the binding assay, free ligands are mostly separated from the bound ligand by rapid filtration through a glass fiber filter, and the latter is consequently measured. Bound ligand is quantified by scintillation counting.⁵⁶¹



Equation 1: K_d : equilibrium binding constant; k_{off} : dissociation rate constant; k_{on} : association rate constant; L: ligand; R: receptor.

The unbound ligand concentration (L^*) determines the first reaction rate, while the second reaction rate is determined by the formed complex concentration ($L-R$). At equilibrium state, defined by K_d , the concentrations of bound and unbound ligand are constant. K_d , the binding constant, is calculated as a ratio of association (k_{on}) and dissociation rate (k_{off}) constants. The binding constant is expressed in molar units (e.g., nM or μ M). A low value of K_d indicates that ligand occupies the receptor of interest at low concentration, and therefore shows high affinity.

There are three major groups of radioligand binding assays: saturation, kinetic, and competition binding assays. In these assays separation of bound to the non-bound ligands happens at a different time, due to their different fields of application. In saturation assay, separation of bound to the non-bound ligand happens after forming an equilibrium state. In saturation assay (sometimes referred to as equilibrium) is essential to quantify formed complex to examine affinity. On the other hand, in the kinetic assay, separation happens at different times during complex formation, and the velocity of forming an equilibrium state is essential. Therefore, the association and dissociation constants (also referred to as forward and reverse rate constants, k_{on} and k_{off}) and consequently kinetics of the bimolecular reaction are observed.⁵⁶²

Even though radioligand binding studies express few disadvantages compared to newly introduced techniques (e.g., environmental issues, radioactive waste disposal), it remains up to date, the most common technique for facile, robust, and fast determination of ligands affinity and selectivity with high throughput.

In saturation binding assay, the receptor is incubated with increasing ligand concentrations until all exposed membrane receptors bind ligands and there are no more free receptor binding sites available for ligand binding. This point in the experiment is called saturation and is characterized by curve-flattening on the diagram (Figure 37). A finite number of receptors in the assay (B_{max}) can be occupied with a specific ligand. Further increase in ligand concentration upon saturation does not provide more bound receptor-ligand complexes. Specific binding describes ligand bound to the biological target of interest. The assay is considered reliable if there is at least 70% and excellent if it provides 90% specific binding over non-specific binding (signal/noise ratio).⁵⁶² Assays with specific binding less than 50% cannot provide reliable results. However, the radiolabeled ligand can interact with other cell membrane structures, glass-fiber filters and non-specifically bind to them, further interfering with results. Even though it was first speculated that

non-specific binding is not saturable, it was proven otherwise.⁵⁶³ Non-specific binding is measured in the presence of a high concentration of unlabeled ligand that occupies all receptors, leading to radioligand that can only be trapped by other cellular membrane parts and therefore non-specifically bind. The non-specific binding should be subtracted from the total binding. Fractional occupancy of receptors indicates a fraction of occupied receptors (bounded to ligand) in all of the receptors⁵⁶⁴ (Equation 2).

$$\text{fractional occupancy} = \frac{[L]}{[L] + K_d}$$

Equation 2: L: Ligand K_d : binding constant.

K_d and B_{\max} values can be obtained from the Scatchard plot⁵⁶⁵ using linear regression. However, nowadays, this is not performed due to the lack of accuracy and non-reliable results. In linear regression, the central assumption is that data are normally distributed, and the standard deviation is the same for every measurement, which is not the case. On the other hand, an alternative, more economical approach for obtaining K_d and B_{\max} are competition binding assays. Competition (often referred to as displacement) assays are performed with a constant concentration of labeled ligand and increased unlabeled ligand concentration, which competes for the biological target. In the displacement assay, the IC_{50} value is determined (Figure 37), representing the concentration of unlabeled ligand which displaces 50% of the labeled radioligand. Inhibition constant (K_i) values are further obtained from IC_{50} values via the CHENG-PRUSOFF equation (Equation 3).⁵⁶⁶ Data can be analyzed with non-linear regression, using specific mathematical software (e.g., GraphPad).

$$K_i = \frac{IC_{50}}{1 + \frac{[L]}{K_d}}$$

Equation 3: Cheng-Prusoff equation. L: ligand; K_d : binding constant, K_i inhibition constant.

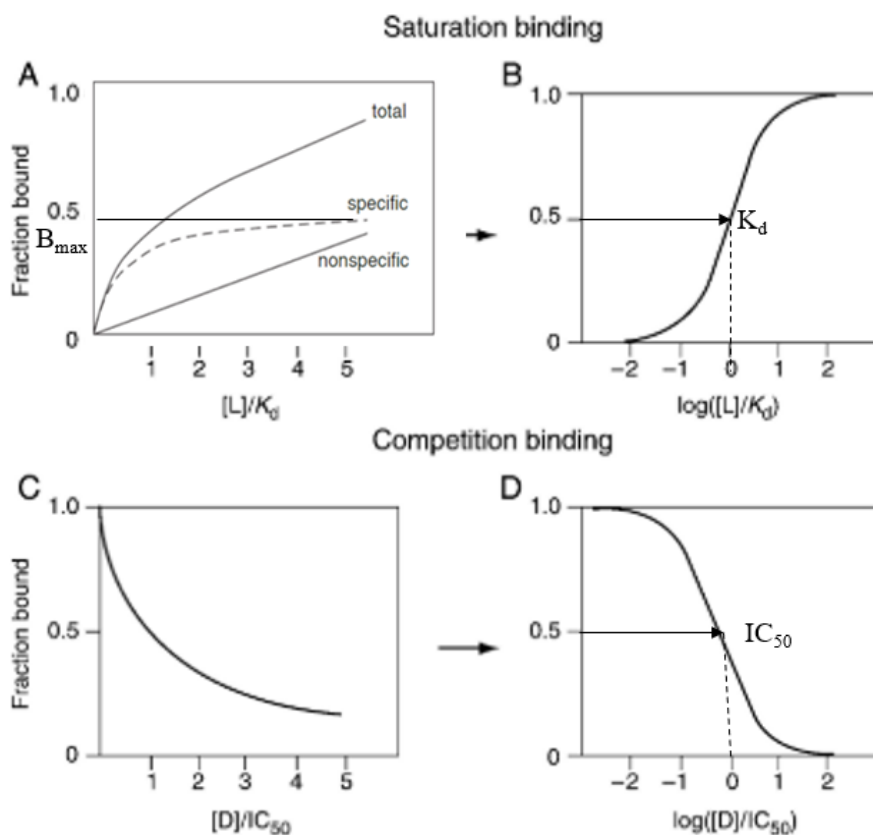


Figure 37: Saturation binding (A and B) and competition binding data (C and D), using different (not transformed (A and C) and semilogarithmic (B and D)) plotting methods; L = labeled ligand, D = unlabelled ligand, K_d = equilibrium binding constant of labeled ligand, B_{max} = maximal specific binding, IC_{50} = half-maximal binding concentration of test (unlabelled) ligand. Adapted from McKinney et al.⁵⁶¹

All final compounds (**1-50**) were examined for their affinities at dopamine D_2R , D_3R , and histamine H_3R . Cell lines, radioligands, and standards used in *in vitro* assays have been shown in Table 11. Obtained results will be presented in Sections 4.5-4.10.

Table 11 Cell-lines, radioligands, and standards used for assay conduction

Receptor	Cells	Radioligand	Reference compound
Dopamine D_2	CHO-K1	$[^3H]$ spiperone	haloperidol ^{559,560}
Dopamine D_3	CHO-K1	$[^3H]$ spiperone	haloperidol ^{559,560}
Histamine H_3	HEK-293	$[^3H]N^\alpha$ -methylhistamine	pitolisant ^{355,567}

4.3 Antioxidative Capacity Measurement

Compounds with antioxidative properties represent an increasing field in the modern drug pipeline. Oxidative stress is a consequence of forming reactive oxygen species (ROS) such as hydroxyl radical (OH^\bullet), hydrogen peroxide (H_2O_2), superoxide radical (O_2^\bullet), and singlet oxygen ($^1\text{O}_2$). ROS products of cell or drug metabolism can also be non-enzymatically formed upon external stressors (UV light, heavy metals, ionization). Even though they fulfill their physiological roles (e.g., in cellular messaging, or gene transcription), ROS accumulation can lead to irreversible cell damage and finally to apoptosis. These processes occur when defending cell mechanisms that trap and neutralize ROS (glutathione, arginine, citrulline, taurine, vitamins A, C, E) are exhausted, and this state is commonly referred to as oxidative stress. Several studies confirmed that numerous diseases (e.g., cardiovascular diseases,⁵⁶⁸ chronic obstructive pulmonary disease,⁵⁶⁹ diabetes,⁵⁷⁰ aging process,⁵⁷¹ muscle-specific diseases,⁵⁷² or neurological disorders⁵⁷³) are associated with increased ROS production and accumulation and ultimately oxidative stress.⁵⁷⁴

Oxygen Radical Absorbance Capacity (ORAC) was first established by Cao et al. at the beginning of the nineties (Figure 38).⁵⁷⁵ This assay presents a simple, fast, and precise assay for the determination of the antioxidant properties of examined compounds. It is hardly based on an assay developed by Glazer et al. a few years earlier.⁵⁷⁶ ORAC assay is built on the reaction between protective scavengers (such as vitamin C and E) and ROS, which results in their neutralization. The amount of protective scavenger is determined. 2,2'-Azobis(2-amidinopropane) dihydrochloride (AAPH) is used for the formation of peroxy radical generator and fluorescein as an indicator protein.⁵⁷⁷ Fluorescein express advantages when compared to other agents such as B-phycoerythrin (B-PE). B-PE is not photostable and can be easily photobleached, leading to non-reliable or false-negative results. Protein damage caused by radicals leads to a loss of fluorescence, which is quantified. In the ORAC assay, results are expressed as ORAC units. Each ORAC unit equals the net protection produced by 1 μM Trolox, a water-soluble vitamin E derivative and ORAC units are calculated based on the Trolox standard curve. Results are quantified with the area under the curve (AUC) due to the proportional relationship between total ORAC in the sample and kinetic curve.

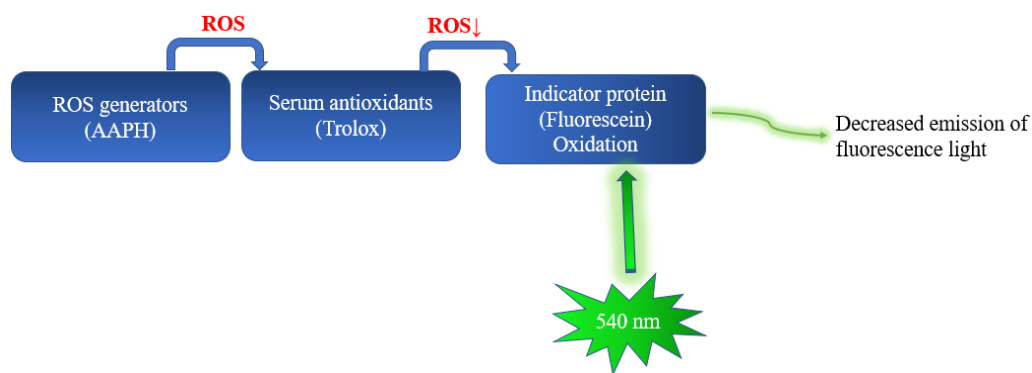


Figure 38: The main principle of ORAC assay. Adapted from Cao et al.⁵⁷⁵

4.4 Drug-likeness Evaluation

Back in the 15th century, Swiss pharmacist Paracelsus said: "*Alle Dinge sind Gift, und nicht ohne Gift. Allein die Dosis macht, das ein Ding kein Gift sei*" (all things are poisonous, and nothing is without poison, only the dosage determines whether something is poison or not).

Drug-likeness of all final compounds (**1-50**) was estimated by Data Warrior.⁵⁷⁸ Drug-likeness is a qualitative property of a drug that predicts all beneficial characteristics that are prerequisites for one compound to be further developed in a potential drug. For instance, each potential drug-like candidate should express important features to be considered for further development. Each candidate should not express toxic or mutagenic potential, and express good water solubility and optimal lipophilicity for BBB penetration (in the case of CNS drugs). These parameters enable fast and efficient high throughput screening (HTS) from various computer libraries to find hits, small molecules with optimal properties.⁵⁷⁹

Almost twenty years ago, Lipinski et al. observed a connection between permeability and solubility and potential drug-like candidates at Pfizer Research Center. Observing Pfizer data bank, they notice associations between physicochemical parameters and drug-like candidates and nondrug-like compounds. These observations further resulted in parameters that impact the drug-likeness of the molecule. Lipinski et al. defined the Rule of 5 (Ro5, sometimes referred to as Pfizer Ro5), stating that the molecule is less likely to be a promising drug-like candidate if it expresses following parameter:⁵⁸⁰

- Molecular weight greater than 500
- More than five H-bond donors (HDO)
- More than ten H-bond acceptors (HAC)
- Calculated log P is greater than 5

Lipinski's Ro5 is still widely accepted in both industry and academy for estimation of oral bioavailability. It enabled a better understanding of pharmacokinetics and pharmacodynamic profile and tremendously shortened the drug pipeline by carefully selecting promising drug-like candidates. However, Lipinski's Ro5 is not exclusive, and this rule only points out possible drug-like candidates based on statistical analyses. There are marketed drugs that violate this rule due to their higher molecular weight or high lipophilicity (e.g., bromocriptine, ivermectin, fosinopril). Lipinski's Ro5 mainly refers to the compounds that are not actively transported into the cell.⁵⁸¹ It still represents a golden standard, but it does not discriminate drug from non-drug candidates. Lipinski's Ro5 further encouraged scientists to expand this concept, tailoring to the specific subclasses of drugs (e.g., CNS drugs) by defining cut-off values for these subclasses, resulting in different modifications. These efforts further determined other parameters closely associated with CNS penetration and oral availability of drugs.

- Molecular weight should not exceed 450.⁵⁸²
- Polar Surface Area (PSA), the sum of all surfaces over polar atoms in the molecule, needs to be under 140 Å for the drug to cross the intestinal membrane and be absorbed.⁵⁸³ Drugs with < 60 Å. are entirely absorbed,⁵⁸⁴ while compounds that exert their action in CNS should have PSA < 90 Å. ⁵⁸²
- The sum of HDO and HAC should not exceed 12.⁵⁸³
- Optimal cLog P, which represents the calculated value of partition coefficient between n-octanol and water, should be between 2 and 5.⁵⁷⁹
- Moriguchi logP should be greater than 4.15.⁵⁸⁰
- Aqueous solubility is an important parameter for the ADME properties of drugs. For CNS drugs, it should be ~60µg/ ml.⁵⁸⁴ Here is aqueous solubility estimated as cLogS, a logarithm value of concentration measured in mol/L. Around 80% of marketed drugs have cLogS > -4. This value is the cut-off value in Data Warrior.⁵⁷⁸

Besides all mentioned parameter that affects drug-likeness, Data Warrior estimates drug-likeness itself as an own parameter. This program compares structures or their fragments with commercially available drugs. Commercially available drugs are compared with Fluka chemicals, nondrug-like candidates (Figure 39).⁵⁷⁸ Around 80% of commercially available drugs have positive drug-like values that suggest that molecules contain fragments present in the marketed drugs (vice versa by negative values).

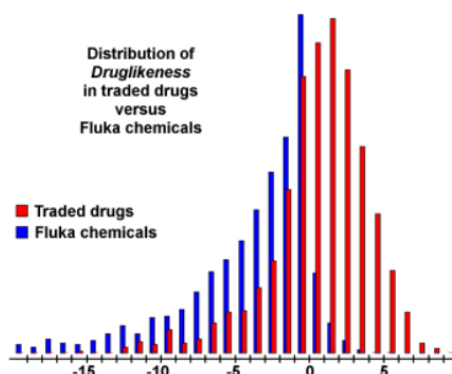


Figure 39: Distribution of commercially available drugs versus Fluka chemicals (non-drugs).⁵⁷⁸

Even though Ro5 gave insight into the solubility and permeability characteristics of chosen compounds, it did not reveal their potential toxic effects. Various programs incorporated parameters that estimate genotoxic, tumorigenic, or mutagenic potential of screened ligands. Data Warrior compares structures and their fragments with a database consisting of highly or potentially toxic compounds., estimating a potential, additional risk of the compound.⁵⁷⁸

4.5 Structure-Activity Relationships of Selective D₃R Ligands

Developing D₃R selective ligands can enable better insight into this receptor subtype and its involvement in the etiology and pathology of various above mentioned neurological disorders. Due to the high structural similarity between receptor subtypes (e.g., D₂R and D₃R, Section 1.1.5), the synthesis of high selective D₃R ligand remained a challenge. Moreover, the few promising candidates failed in clinical trials due to their low solubility, bioavailability, and poor drug-likeness. Design and synthesis of selective D₃R ligands have been particularly challenging processes. Drug-like properties as appropriate lipophilicity to penetrate BBB and good solubility, (enables disintegration, absorption, and bioavailability of orally administered drugs) need to be

balanced. So far, no dopamine D₃R selective ligand has reached the market, with several candidates being in the clinical trials for schizophrenia, addictive behavior, and ADHD. Design and development of the high affine D₃R partial agonist, **BP 897** ($K_i = 0.92$ nM, Figure), with over ~70-fold higher affinity to D₃R compared to that of D₂R, and very low affinity at D₁R and D₄R encouraged further design of D₃R selective ligands.³⁹⁰ In addition, **BP 897** shows affinities at 5HT_{1A}, α_1 , and α_2 receptors. The pharmacokinetic profile of **BP 897** is not available to the public, even though this ligand is in the clinical trials for schizophrenia, PD, and addictive behavior. However, it has been confirmed that **BP 897** reached the CNS when applied *s.c.*, *i.v.*, and *i.p.*³⁹⁰

This compound served as a blueprint for the design and synthesis of novel, potent, selective D₃R ligands. Privileged D₃R scaffold 4-phenylpiperazine and arylamide moiety were conserved in the first compound set (**1-10**). Positively charged nitrogen in 4-phenylpiperazine moiety at physiological pH forms a salt bridge in OBS, while amide moiety forms a hydrogen bond in SBP (Section 3.1). The linker length was varied, and aryl moiety in the western part of the molecule was modified to gain ligands that are as selective as possible (Figure 40). Introducing different substituents in arylamide moiety that can interact with SBP, can potentially increase selectivity over this receptor subtype and significantly impact binding affinity. Structural modifications in the linker, can lead to higher D₃R selectivity, as introducing OH or F in butyl linker, or introducing cyclopropyl linker.^{144,392} Therefore, different substituents patterns, were introduced to achieve better selectivity, like introducing SF₅ moiety. This group represents novel chemical moiety that acts as a bioisosteric replacement of CF₃ and under circumstances of *tert*-butyl. It is chemically, thermally stable, and highly lipophilic. These physicochemical properties can further impact binding mode and ADME properties, and therefore it would be particularly interesting to examine the effect of this functional group on the binding mode.

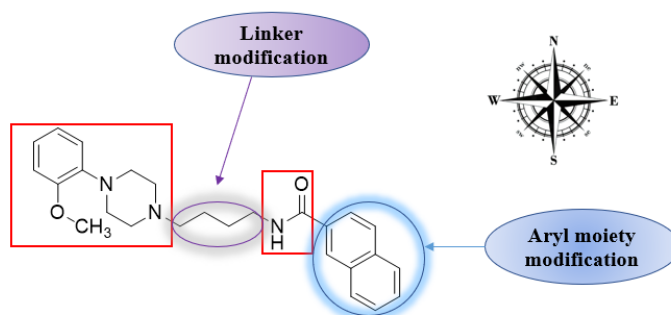
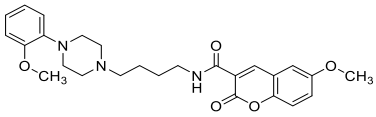
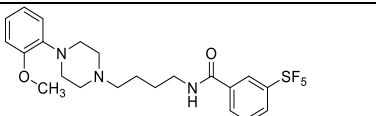
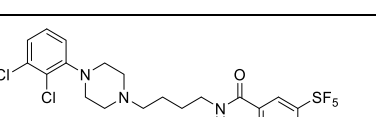
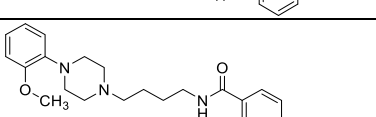
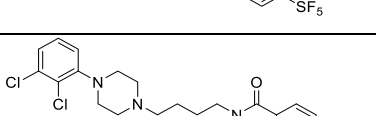


Figure 40: Modification in linker length and the aryl amide moiety in **BP 897**, that served as blueprint for compounds **1-10**.

Compounds **1-10** were *in vitro* examined in radioligand binding assay to determine affinities at receptors of interest (Table 12). Selectivity index (SI) determines the ratio of receptor affinities K_i (D_2R) / K_i D_3R . Binding constants are given as mean values with a corresponding confidence interval (CI).

Table 12: Binding affinities of compounds **1-10**.

Name	Structure	K_i (D_2R) [nM] [95% CI]	K_i (D_3R) [nM] [95% CI]	SI
Haloperidol		2.61 [2.02; 3.39]	13.5 [10.4; 17.4]	0.2
1		105.1 [76.5; 144]	184 [99.7; 339]	0.6
2		152 [68.2; 338]	127 [28.1; 570]	1.2
3		9.45 [4.71; 19.0]	5.67 [1.88; 17.0]	1.7
4		13.4 [9.16; 19.7]	30.7 [12.6; 75.3]	0.4
5		65.5 [42.6; 101]	9.04 [6.87; 11.9]	7.2

6		63.4 [36.5; 110]	3.90 [1.57; 9.70]	16.3
7		54.3 [28.2; 105]	4.96 [2.51; 9.79]	10.9
8		62.3 [25.5; 152]	9.34 [5.45; 16.0]	13.3
9		72.3 [31.3; 167]	3.52 [1.46; 8.74]	20.5
10		163 [90.2; 293]	12.2 [6.69; 22.4]	6.7

CI: confidence interval, SI, selectivity index (K_i (D₂R)/ K_i (D₃R)),

All obtained compounds (**1-10**) expressed affinities in nanomolar concentration ranges at both D₂R and D₃R. Naphthyl moiety in **BP 897** was replaced with 3-bromo-4-methoxy phenyl moiety in the eastern part of the molecule, and the linker length was varied (compounds **1-4**). 3-Bromo-4-phenyl moiety is not bulky as naphthyl, but the lipophilic substituents grant high logP values and enhance chances for crossing BBB. Compounds **1-4** contain this moiety as aryl amide moiety, 1-(2-methoxyphenyl)piperazine moiety as primary pharmacophore, and different linker-length from two to five carbon methylene groups. Among those, compound **3** that contains a four methylene groups as linker, showed tendency to the highest affinity at D₃R (pK_i (D₂R) = 8.02; pK_i (D₃R) = 8.25) as well as the highest selectivity (SI = 1.7). By increasing linker length to five methylene groups, affinity remained in the nanomolar concentration range, (compound **4** (pK_i (D₂R) = 7.87; pK_i (D₃R) = 7.51)), but selectivity decreased (SI = 0.4). Even though the distance between OBS and SBP is longer in D₃R than in D₂R, the latter expresses more flexible EBP.^{116,117} Dynamic and conformational changes are more difficult to predict in D₂R. Therefore, this could explain that compound **4** fits better into EBP of D₂R and showed higher affinity at this receptor subtype (Section 3.1). Shortening the linker to two methylene groups as in compound **1** or three-methylene groups as in compound **2** resulted in lower affinity at both D₂R and D₃R (compound **2**: pK_i (D₂R) = 6.98; pK_i (D₃R) = 6.74; compound **3**: pK_i (D₂R) = 6.82; pK_i (D₃R) = 6.90). Selectivity was up to

2-fold decreased with shortening the linker (SI = 0.6, compound **1**). In line with these results, it can be concluded that the favorable linker length for coupling PP and SP is a four methylene groups linker. Slight modifications in linker as prolongation or shortening for just one methylene group can lead to the loss of both affinity and selectivity, as observed in this compound set. Therefore, further modifications were conducted with a butyl linker. As a second modification, naphthyl moiety in **BP 897** was replaced with coumarin moiety in compounds **5** and **6**. Coumarins are secondary plant metabolites and are broadly distributed in the ecosystem. Coumarin derivatives act as antioxidants and can express neuroprotective properties,⁵⁸⁵ and therefore raised interest in the scientific community resulting in numerous publications reporting coumarin derivatives as potential drug-like candidates. Coumarin moieties were implemented in dopaminergic and serotonin pharmacophores. Teran et al. reported that coupling coumarin moiety with 4-phenylpiperazine leads to increasing affinity to both 5HT_{1A} and D₃R.⁵⁸⁶ Substitution in coumarin ring leads to the synthesis of highly affine serotonergic ligands as confirmed by Ostrowska et al.⁵⁸⁵ Coumarin moiety was incorporated in the eastern part of the molecule in compounds **5** and **6**. Replacement of the blueprint's naphthyl moiety with coumarin scaffold did not diminish affinity at both D₂R and D₃R. Substitution with the methoxy group in position 5 in compound **6** leads to a slight increase in affinity to D₃R and more than a 2-fold increase in selectivity (SI = 16.3) when compared with unsubstituted derivative **5**. Substitution in position 5 as observed in compound **6** can increase affinity and selectivity, suggesting stronger interaction within SBP through methoxy substituent. This substitution pattern can be considered beneficial for the design of the novel ligands. In compounds, **6-10** SF₅ moiety was introduced in the eastern part of the molecule. This moiety is chemically, thermally stable, highly lipophilic, and electronegative. It can serve as a bioisosteric replacement for CF₃ and *tert*-butyl moiety. CF₃ is a functional group that expresses high lipophilicity. It is well described and is part of highly affine D₃R preclinical candidates (Section 1.1.5). In contrast, SF₅ is a novel moiety that is up to date not fully characterized. Therefore, it would be interesting to examine the impact of this group on the receptor's binding affinity and pharmacokinetics profile of ligands that contain this scaffold. Increasing lipophilicity enhance chances for crossing BBB and reaching biological targets in CNS. However, high logP values can lead to poor solubility and permeability, and therefore compounds should be rationally designed. In compounds **6-10**, 1-(2-methoxyphenyl)piperazine and 1-(2,3-dichlorophenyl)piperazine were introduced as a PP. Compounds containing 1-(2-

methoxyphenyl)piperazine moiety (**7,9**) showed a tendency to increase affinity at D₃R (**7**: $pK_i = 8.30$; **9**: $pK_i = 8.45$) compared to 1-(2,3-dichlorophenyl)piperazine derivatives (**8**: $pK_i = 8.03$; **10**: $pK_i = 7.91$), favoring 2-methoxy over 2,3-dichloro substitution. Substitution in *p*-position with SF₅ leads to higher affinity at D₃R and lower affinity at D₂R, as confirmed in docking studies. In D₂R, the ligand is located deeper in OBS compared to D₃R. Compounds substituted in *m*-position (**7,8**) achieve optimal interaction with Tyr408^{7,34}, while *p*-substituted ligands (**9,10**) tend to decrease in affinity at D₂R due to steric hindrance, as described in Sections 3.1 and 3.2. Compound **9** was chosen as the lead compound for further evaluation as this compound showed the numerically highest affinity at D₃R and selectivity (SI = 20.5). Compounds were further examined to estimate the drug-like properties of synthesized ligands (Table 13).

Table 13: Drug-like properties of compounds **1-10**.

No.	MW	cLogP	cLogS	Drug-likeness	HAC	HDO	PSA	Ro5 Ø	TSA	Mut.	Tum.
1	448.36	2.957	-3.328	4.90	5	1	54.04	0	315.04	No	no
2	462.39	3.441	-3.598	6.70	6	1	54.04	0	328.80	No	no
3	476.41	3.866	-3.868	3.85	6	1	54.04	0	342.56	No	no
4	490.44	4.302	-4.138	1.97	6	1	54.04	0	356.32	No	no
5	435.52	2.727	-3.356	3.90	7	1	75.02	0	340.63	No	no
6	465.55	2.567	-3.374	3.90	8	1	84.25	0	362.89	No	no
7	493.54	8.294	-0.532	3.91	5	1	44.81	0	360.42	No	no
8	532.40	9.761	-1.986	4.01	4	1	35.57	2	369.00	No	no
9	493.54	8.294	-0.532	3.91	5	1	44.81	1	360.42	No	no
10	532.40	9.576	-1.986	4.01	4	1	35.57	2	369.00	No	no

* HAC: H-bond acceptor; HDO: H-bond donors; PSA-Polar Surface Area; Ro5Ø-Lipinski's rule violation; TSA: Total Surface Area; Mut.-mutagenic potential; Tum: tumorigenic potential.

None of the compounds showed mutagenic or tumorigenic potential. All compounds, except compound **5**, have PSA values under 60, indicating that they will be entirely absorbed, penetrate BBB, and reach the CNS. All synthesized ligands expressed high drug-likeness scores (positive values). A slightly lower value (1.97) was obtained for compound **4** due to its predicted poor water solubility ($cLog S < -4$), even though this compound showed higher affinity than those of **1** and **2**. Compounds **8** and **10** violate Lipinski's Ro5 twice due to their high lipophilicity ($cLogP > 5$) and high molecular weight (> 500), while compounds **7** and **9** have only one violation due to the high

clogP values. As already mentioned in Section 4.4, Lipinski's Ro5 is not exclusive, and it is rather guideline for rational design than a rule. Even though compound **9**, which *in vitro* showed the highest affinity, violates Lipinski's Ro5, it is predicted with a positive value (3.91) for drug-likeness by Data Warrior.

To summarize, the first compound set contains ten ligands **1-10** that all showed nanomolar affinity at both D₂R and D₃R with a slight preference at D₃R. Compound **3**, where PP and SP is coupled via butyl linker showed tendency to highest affinity at D₃R other synthesized compounds contain butyl linker. Replacement of naphthyl moiety in the eastern part of the molecule with 3-bromo-4-methoxyphenyl, coumarin, or SF₅ moiety did not diminish affinity, indicating that smaller, less bulky substituent can be well tolerated. This substitution pattern can further result in designing small molecules with lower molecular weight, better solubility, and bioavailability. Increasing lipophilicity in coumarin moiety led to increase in affinity at D₃R as well as selectivity, suggesting that rationally designed substitution patterns with small lipophilic substituents can lead to high affine D₃R preferring ligands. Compound **9**, the *p*-SF₅ derivative with the highest affinity and selectivity, was chosen as a lead compound from this compound set.

4.6 Structure-Activity Relationships of Bitopic D₂R and D₃R Ligands

Due to the high homology level between D₂-like receptor subtypes and their similar brain distribution, the synthesis of selective ligands remained a challenge. D₂-like receptor can exist in form of homo- or heterodimers, and these dimers represent actual targets of neurotransmitters. Dimerization of dopamine receptors requires transmembrane domains V and VI.⁸⁷ Nevertheless, it was recently confirmed that TM IV is crucial for forming D₂R homodimers, by Lee et al.,⁵⁸⁷ or Guo et al.⁵⁸⁸ Recent efforts have been centered around design of bitopic ligands, targeting one receptor or homo- and heterodimers (D₁R/D₃R, D₁R/H₃R, D₂R/H₃R, D₂R/5HT_{2A}).⁵⁸⁹ Bivalent (bifunctional) ligands (Figure 41) were firstly described by Phil Phortogese in 1982, describing ligands for opioid receptors.⁵⁹⁰ Bifunctional ligands can target two binding pockets (orthosteric sites) of the dimer.⁵⁹¹ However, recently developed bitopic ligands can target both orthosteric and allosteric site in one receptor.

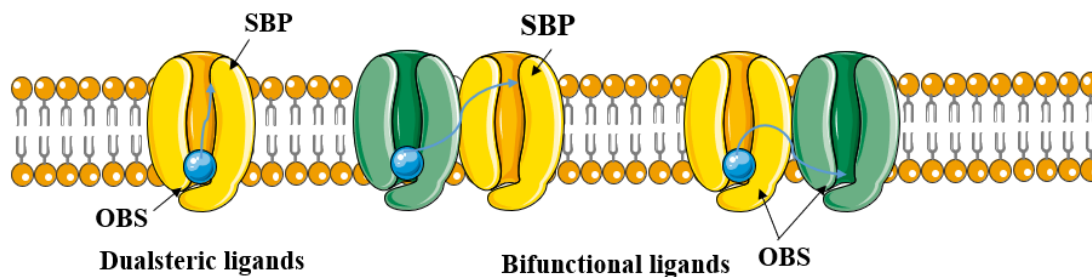


Figure 41: Bifunctional ligands. OBS, orthosteric binding site; SBP, secondary binding pocket. Adapted from Carli et al.⁵⁹¹

The latter approach developed from the classic bifunctional approach. Bitopic ligands contain primary pharmacophore (PP) that interacts with the orthosteric binding site (OBS), and secondary pharmacophore (SP) that interacts with allosteric binding site (in D₂-like receptors referred as secondary binding pocket, SBP). PP and SP are coupled via spacer that grants optimal distance for interaction with both sites at the receptor (Figure 42).¹³²

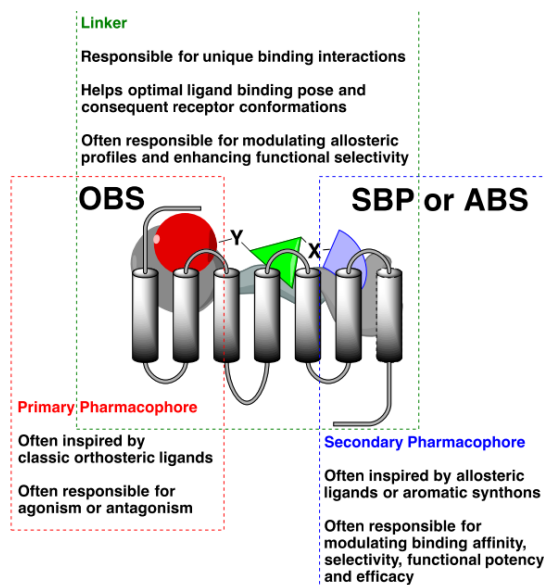


Figure 42: Rationally designed bitopic ligands.⁵⁹² Reprinted with permission from Newman, A. H.; Battiti, F. O.; Bonifazi, A. 2016 Philip S. Portuguese Medicinal Chemistry Lectureship: Designing Bivalent or Bitopic Molecules for G-Protein Coupled Receptors. The Whole Is Greater Than the Sum of Its Parts. *J. Med. Chem.* **2020**, *63* (5), 1779–1797. Copyright (2021) American Chemical Society.

The rational design of bitopic ligands can activate concrete signaling pathways and determine which exact signaling cascade provides therapeutic or side effects, or explain biased signaling.⁵⁹²

Therefore, it remains an urge to further develop novel, bitopic GPCR ligands as those receptors are targets of the majority of marketed drugs as well as preclinical and clinical candidates, and involved in many (patho)physiological processes.

Orthosteric binding sites are structurally conserved, and therefore selectivity cannot be obtained only by interaction within OBS.^{116,117} In contrast, allosteric binding sites changed over time and represent possible targets for highly selective ligands.⁵⁹³ D₃R sparked interest as a target for bitopic ligands to better understand its role in different (patho)physiological processes. Up to date, an increasing number of publications reported how different modifications in SP, linker length, or novel PP in bitopic ligands affect their affinity and selectivity in the GPCR field, particularly in D₂-like receptors.^{592,594,595} For instance, **SB269,652** (Figure 43) acts as negative allosteric modulator in D₂R/D₃R heterodimers, but as an negative orthosteric modulator in monomers.^{591,596} Newman et al. performed SAR studies to design several bitopic ligands, identifying morpholine derivatives as PP, resulting in **AB04-88** (K_i (D₂R) = 134 nM, K_i (D₃R) = 5.96 nM) and **FOB02-04A** (K_i (D₂R) = 87.8 nM, K_i (D₃R) = 1.85 nM).⁵⁹² Thereby they confirmed association between chirality and binding to receptor, previously confirmed also in 1-(2,3-dichlorophenyl)piperazine derivatives. Newman et al. also hypothesized that EL2 is significantly longer in D₃R than in other receptor subtypes, and that it can be responsible for the for the D₃ receptor selectivity.¹⁴⁴ Zou et al. reported sumarinole (D₂R/D₃R agonist) derivatives as potential PP, reporting derivatives with moderate affinities (K_i (D₂R) = 14700 nM; K_i (D₃R) = 2610 nM).⁵⁹⁷ Vaas et al. used fragment-based drug design to develop potent D₃R ligands K_i (D₂R) = 5.4 K_i (D₃R) = 0.63 nM.

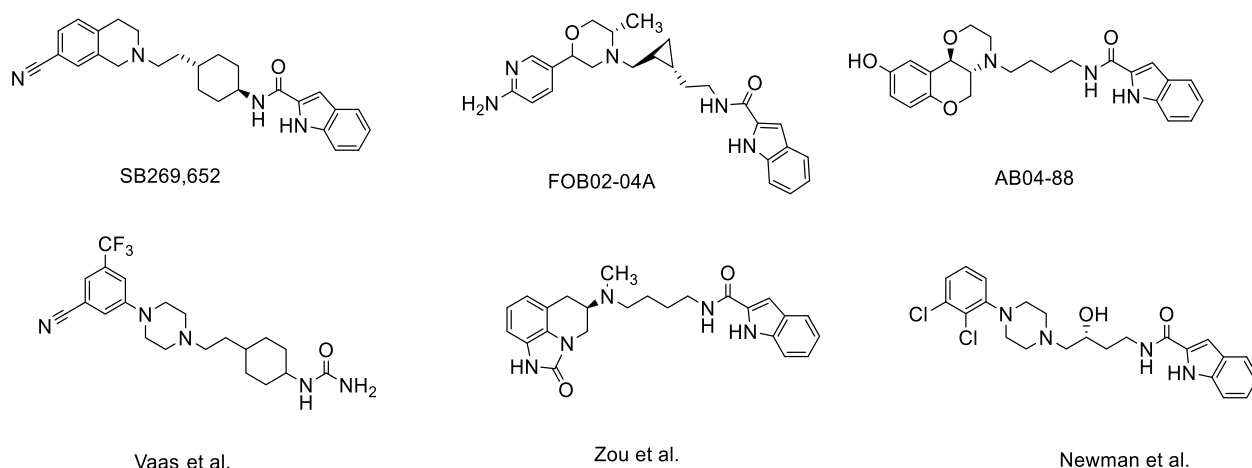


Figure 43: Recently designed D₂R and D₃R bitopic ligands.

Compounds **11-17** were designed as bitopic ligands by combining two D₃R pharmacophores, to enhance selectivity for this receptor subtype. To obtain compound **11** the D₃R preferring agonist pramipexole derivative was firstly coupled with 3-bromo-4-methoxy benzoic acid in a one-pot synthesis. 3-Bromo-4-methoxy-benzoic acid was already used for successful naphthyl replacement in compounds **1-10** and bound to SBP in both D₂R and D₃R, which was confirmed with molecular docking studies (Section 3.1). Two moieties were coupled via amide. However, this compound showed affinity neither at D₂R nor at D₃R ($> 10 \mu\text{M}$) (Table 14). Therefore, a second approach was conducted where both pramipexole derivatives and 1-(2-methoxyphenyl)piperazine were combined (Figure 44). Even though pramipexole contains secondary amine in position 6, modifications were made to examine how basicity impacts binding affinity. Linker length was optimized to determine the optimal distance between PP and SP for interaction with the receptor.

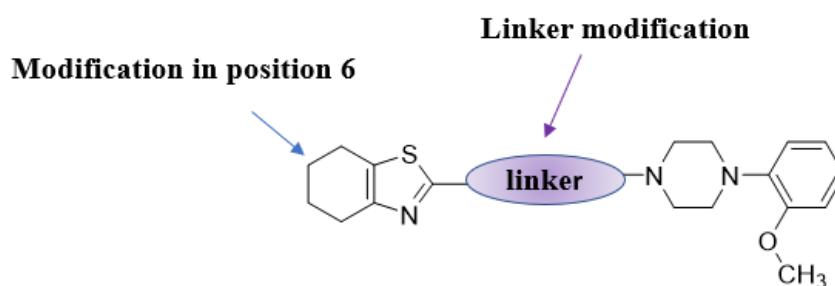
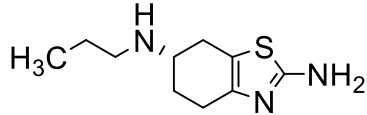
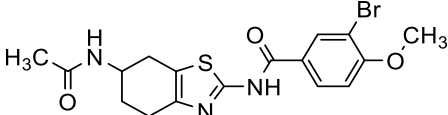
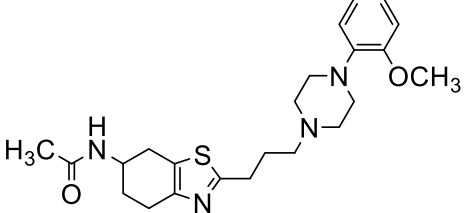
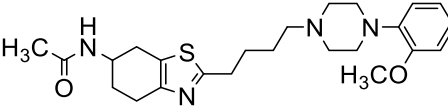
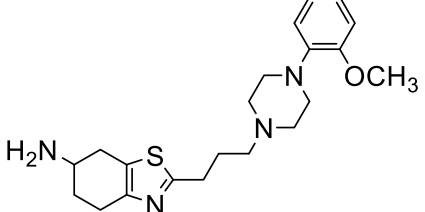
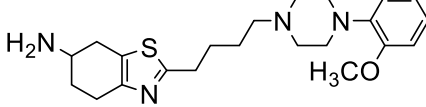
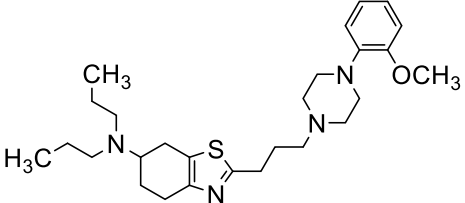
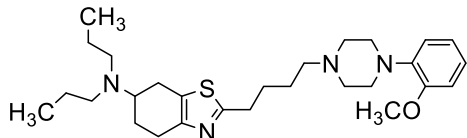


Figure 41: Modification in position six and linker length of bitopic D₂R/D₃R ligands in compounds **12-17**.

Compounds **11-17** were tested to examine their affinity to D₂R and D₃R and selectivity. Compounds have been tested in the ORAC assay to examine their antioxidative capacity. The results are shown as ORAC values (Section 4.3).

Table 14: Binding affinities of compounds 11-17.

No.	Structure	K_i (D ₂ R) [nM] [95% CI]	K_i (D ₃ R) [nM] [95% CI]	SI	ORAC- value [μ M] \pm SD
Pramipexole		3.3 \pm 0.3*	0.5 \pm 0.1*	6.6	n.d.
11		> 10 μ M	> 10 μ M	n.d.	n.d.
12		435 [393; 482]	562 [414; 764]	0.8	3.70 \pm 1.28
13		58.9 [27.0; 129]	40.2 [13.5; 120]	1.5	n.d.
14		190 [67.7; 535]	185 [81.4; 420]	1.0	6.00 \pm 0.83
15		5.61 [2.83; 11.1]	5.98 [0.57; 62.8]	0.9	5.81 \pm 0.11
16		203 [61.1; 677]	301 [93.9; 963]	0.7	1.18 \pm 2.26
17		5.12 [2.36; 11.1]	23.2 [5.86; 92.3]	0.2	0.29 \pm 0.39

*n.d not determined, CI: confidence interval, SI, selectivity index (K_i (D₂R)/ K_i (D₃R), SD, standard deviation, ORAC value: net protection produced by 1 μ M Trolox.⁵⁷⁵

Compounds **12-17** showed nanomolar affinities at both D₂R and D₃R. Ligands where 4-phenylpiperazine moiety was coupled via butyl linker to arylamide moiety expressed highest affinities at the receptor of interest, as described in Section 2.2. Therefore, ligands with butyl as well as propyl linkers were developed. Ligands containing butyl linkers (**13,15** and **17**) showed higher affinity at both D₂R and D₃R compared to ligands containing propyl linkers. (**12,14** and **16**), emphasizing once more the importance of the linker length. For instance, compounds **12** and **13** contain propyl and butyl linkers, respectively, and compound **13** showed a 14-fold higher affinity at D₃R ($pK_i(D_3R) = 7.4$) and more than 7-fold higher affinity to D₂R ($pK_i(D_2R) = 7.23$) when compared to those of **12** ($pK_i(D_2R) = 6.36$; $pK_i(D_3R) = 6.25$). The incorporation of the basic center in position 6 led to even bigger differences in terms of affinity. Compound **15** showed up to 39-fold higher affinity to D₃R and almost 40-fold higher affinity to D₂R when compared to compound **14**. Compound **17** showed a 15-fold higher affinity at D₃R and up to 40-fold higher affinity at D₂R (single digit nanomolar range) when compared to **16**. In line with these results, it can be concluded that butyl linker was favored over propyl linker for achieving optimal interaction with receptor of interest.

Modifications in position 6 were conducted to examine the effect of basic moieties on the binding mode. Pramipexole has secondary aliphatic amine in position 6 and less basic aromatic amine in position 2 that can interact with the receptor. In the D₃R receptor, the interaction in the OBS between positively charged piperazine nitrogen and the aspartate residue represents a prerequisite for forming a salt bridge. However, in **12-17**, effects of neutral amide functional group where lone pair are delocalized into the carbonyl group, basic primary amine, and tertiary amine were observed. In an aqueous state, secondary aliphatic amines show the highest basicity ($pK_a \sim 11$) followed by primary and tertiary amines ($pK_a \sim 9-10$). Compounds containing neutral amide moiety as **12** and **13** have lower affinity when compared to their derivatives that are substituted with basic moieties. Compound **15**, containing a primary amino group, tends to show a slight tendency to higher affinity at D₂R ($pK_i(D_2R) = 8.25$) and 3-fold at D₃R ($pK_i(D_3R) = 8.22$) than compound **17** that contain tertiary amino group. ($pK_i(D_2R) = 8.29$; $pK_i(D_3R) = 8.63$). Compounds **15** and **17** showed a slight preference for D₂R. These results indicate that basic moiety is favorable for the interaction with receptors, and that increasing basicity leads to potential higher affinity at the receptor of interest. Moreover, it can be hypothesized that the basic interaction is important in

both OBS and SBP, as the most potent compounds contain two basic centers, indicating potential basic interaction in SBP.

Pramipexole itself shows antioxidative properties and acts as a neuroprotective agent.^{598,599} Antioxidative properties can ameliorate neuroinflammation, which leads to neurodegeneration as observed in PD patients. Therefore, pramipexole derivatives **12-17** were tested to estimate their antioxidative capacity as described in Section 4.3. Data are presented as ORAC values. Positive results indicate that the compound's antioxidant capacity is superior to the antioxidant capacity of Trolox (vitamin E derivative). All compounds expressed positive ORAC values, indicating that all compounds can express antioxidant potential. Exceptionally high ORAC values showed compounds **15** and **16**, 5.81 and 6.00, respectively, and these two ligands can be considered the most promising antioxidative moieties. Prolongation of linker led to an increase in ORAC values, as shown in compounds **15** and **17**, that expressed higher values when compared with propyl linker analogues **14** and **16**. Compounds with the primary aliphatic amine in position 6 (**14** and **15**) expressed higher ORAC values than their dipropyl analogues, favoring substitution with primary over tertiary amine for antioxidant capacity.

Drug-likeness is associated with compound properties and their consequent pharmacokinetic and pharmacodynamic behavior in the human organism. By examining drug-like properties, absorption, distribution, metabolism, and elimination can be predicted (Table 15).

Table 15: Drug-like properties of compounds **11-17**.

No.	MW	cLogP	cLog S	Drug-likeness	HAC	HDO	PSA	Ro5 Ø	TSA	Mut.	Tum.
11	424.32	3.539	-4.814	-0.09	6	2	108.56	0	279.57	No	no
12	428.59	2.952	-3.075	7.25	6	1	85.94	0	335.15	No	No
13	442.63	3.406	-3.345	5.37	6	1	85.94	0	348.91	No	No
14	386.56	2.544	-2.877	7.60	5	1	82.86	0	302.20	No	No
15	400.59	2.998	-3.147	5.72	5	1	82.86	0	315.96	No	No
16	470.72	4.883	-3.571	8.37	5	0	60.08	0	383.54	No	No
17	484.75	5.338	-3.841	6.49	5	0	60.08	1	397.30	No	No

*HAC: H-bond acceptors; HDO: H-bond donors; PSA-Polar Surface Area; Ro5Ø-Lipinski's rule violation; TSA: Total Surface Area; Mut.-mutagenic potential; Tum: tumorigenic potential

None of the compounds **11-17** express neither mutagenic nor tumorigenic potential. None of the compounds **11-16** violate Lipinski Ro5; all of them have molecular weight lower than 500kDa, clogP values under 5, less than 10 H-bond acceptors, and less than 5 H-bond donors. Compound **17** expresses, however, clogP value slightly above 5 and has one violation. All compounds, except **11**, show positive drug-likeness scores and can be considered as potential drug-like candidates. Besides, compound **11** has poor water solubility and PSA value above 90, indicating that it will probably not reach CNS and its biological target. These results are in accordance with *in vitro* obtained data, where compound **11** shows no affinity at the receptor of interest, whereby all other ligands from this compound set showed affinities. in moderate to low nanomolar concentration ranges. In contrast, compounds **12-17** showed a high probability to penetrate BBB and exert their action in CNS, and all of them express good water solubility (cLogS > -4). Compound **16** that contains a propyl linker, showed an exceptionally high drug-likeness score (8.37). In general, compounds containing propyl linkers were predicted to be better drug-like candidates than their butyl linkers analogues due to their better aqueous solubility and lower lipophilicity. However, obtained *in vitro* data confirmed that the optimal interaction with the receptor requires four methylene groups and is favored over three methylene groups as spacer. Compound **15** showed *in vitro* highest affinity does not violate Ro5, has a good, predicted drug-likeness score (5.72), and an excellent ORAC value (5.81). Due to its promising profile, it was chosen as a lead compound from this set for potential further modifications and examination.

4.7 Structure-Activity Relationships of Bioisosteric Compounds

In order to further examine impact of different functional groups on the binding mode, bioisosteric replacement of methylene group with ether was performed. Bioisosters have different functional groups but similar physicochemical properties. They are developed to improve pharmacokinetics, pharmacodynamic characteristics of ligands, and their safety profile. Scaffold hopping is a technique for finding an efficient bioisosteric replacement to improve drug-like properties. By replacing the molecular core, new scaffolds are examined and compared. This approach is broadly used in both modeling and experimental chemistry.^{600,601} Due to the recent encouraging results reported by Stark's working group by Sauer and patented with Motac Neuroscience where pramipexole ether derivatives showed low nanomolar D₃R affinity, and promising *in vivo* results (Figure 45).^{434,602} In this patent, thiazole derivatives were substituted in position 2, with low molecular alcohols (methanol, ethanol, isopropanol). Moreover, Kozikowski et al. designed

thiazolone analogues of huperzine, alkaloid used in Chinese medicine due to its acetylcholinesterase inhibition, as potential targets in treatment of Alzheimer's disease.⁴³⁸

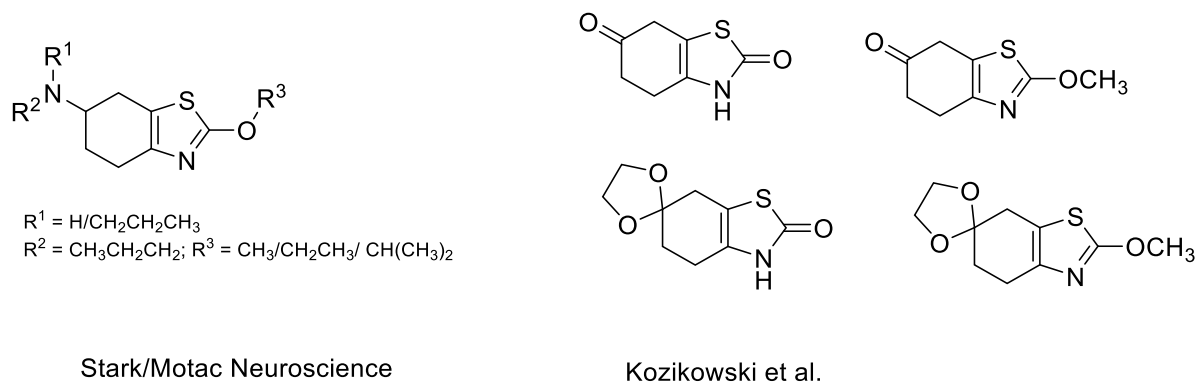


Figure 45: 2-oxothiazole derivatives that served as blueprints for compounds **18-24**.

In this set, methylene group linker was substituted with ether linker (Figure 46). Oxygen is more nucleophilic than carbon, and the oxygen incorporation enhances PSA in the molecule, which directly correlates with bioavailability and absorption. Oxygen itself can form hydrogen bonds and, therefore, bind to the receptor of interest differently when compared to the previously described carbon derivatives (**12-17**). While ligands reported in the literature contain small, not bulky substituents in position 2, we wanted to examine how the linker prolongation and substitution in the eastern part of molecule will impact binding mode. On the other hand, 4-phenylpiperazine moiety, incorporated in **12-17** is a privileged scaffold for the interaction with D₃R. This moiety was replaced with different aromatic and non-aromatic moieties to estimate its impact as well as the necessity of aromatic substituents on the binding mode (Table 16). Replacement of 4-phenylpiperazine moiety with non-basic moiety will enable pramipexole derivative binding to the OBS. (lack of a salt bridge between positively charged nitrogen and Asp110^{3,32}).

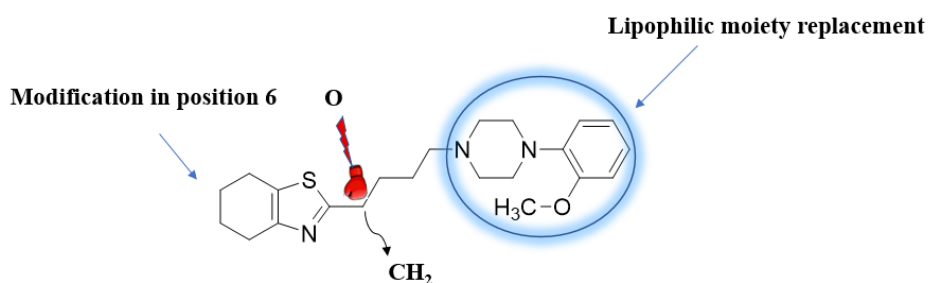
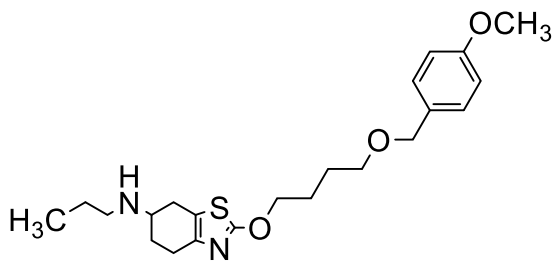
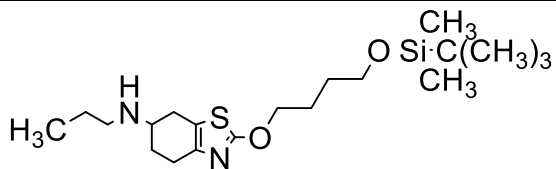
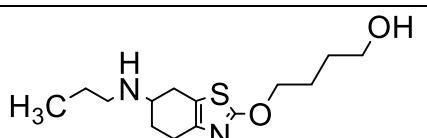


Figure 46: Structural modification in the compound set **18-24**; bioisosteric replacement in the linker, and introduction of various aromatic and aliphatic moieties in the ester part of the molecule

Table 16: Binding affinities of compounds **18-24**.

No.	Structure	K_i (D ₂ R) [nM] [95% CI]	K_i (D ₃ R) [nM] [95% CI]
Pramipexole (Ref)		3.3 ± 0.3*	0.5 ± 0.1*
18		>5 μM	>10μM
19		2503 [2660; 3169]	113 [31; 415]
20		>5 μM	2072 [1949; 2203]
21		>5 μM	1849 [714; 4788]

22		>5 μM	1710 [495; 5911]
23		>5 μM	1590 [587; 4312]
24		>10 μM	>10 μM

* Data were presented as mean value \pm standard deviation, obtained from Mierau et al.¹⁰² CI: confidence interval, SI, selectivity index, SD, standard deviation.

Halogen containing pramipexole derivatives **18** and **19** were synthesized as precursors for further derivatives. *In vitro* results indicate that basic moiety is necessary for interaction with the receptor, as was confirmed by compound **18** that contains amide moiety in position 6, showing no affinity at both D₂R and D₃R ($K_i > 10\mu\text{M}$). In contrast, compound **19** showed higher affinity at both D₂R (pK_i (D₂R) = 5.94) and D₃R (pK_i (D₃R) = 6.95), with over 20-fold selectivity at D₃R (SI = 25.6). Compound **19** was the most potent compound from this compound set. The exchange of 4-phenylpiperazine moiety with aromatic moieties as benzyloxy or *p*-methoxybenzyloxy moiety leads to a significant decrease in affinity compared to the compounds **12-17** as well as compound **19**. Derivatives **20-23** show a higher preference for D₃R, whereby compound **23** containing bulky *tert*-butyldimethylsilyl (TBDMS) substituent, showed very slight tendency at D₃R (pK_i = 5.8). On the other hand, compound **24** containing hydroxy group in the eastern part of the molecule showed no affinity at both D₂R and D₃R. These results indicate that replacement with small polar groups instead of either bulky aliphatic substituent or aromatic moieties led to complete loss of affinity at both D₂R and D₃R. The substituent in position 2 with aromatic, bulky and non-bulky aliphatic moieties led to decreased affinity. It can be further hypothesized that substitution in position 2 is not optimal and interferes with the binding mode of pramipexole derivatives. As confirmed **19**, as well as in the literature (Figure 46), pramipexole derivatives substituted with small, non-bulky

substituents in position 2 showed significantly higher affinity at D₃R. In addition, D₂R can exist in high and low-affinity forms, which can be another reason for low affinities of synthesized compounds **20-24** at D₂R/D₃R. There are significant changes in binding affinities of dopamine and apomorphine when binding to the different isoforms, resulting in lower binding affinities when bound to low affine isoform, due to different orientation of aspartate residue which is responsible for binding.⁶⁰³ These results further indicate that 4-phenylpiperazine moiety (as observed in **12-17**) interacts with OBS while pramipexole moiety binds to the SBP, which needs to be confirmed with MD simulations. Bioisosteric replacement of a methylene groups by ether did not lead to significant improvement. However, compounds **19-23** showed slight tendency to D₃R and can be further modified to synthesize selective D₃R ligands since they do not show affinity at D₂R. All compounds were further evaluated to examine their drug-like properties (Table 17).

Table 17: Drug-like properties of the compounds **18-24**.

No.	MW	cLogP	cLog S	Drug-likeness	HAC	HDO	PSA	Ro5 Ø	TSA	Mut.	Tum.
18	230.72	2.042	-3.055	1.13	3	1	70.23	0	165.13	no	No
19	317.29	4.092	-3.649	2.04	2	0	44.37	0	216.73	no	No
20	416.63	5.832	-4.748	-2.53	4	0	62.83	1	346.66	no	No
21	446.65	5.762	-4.766	-2.46	5	0	72.06	1	368.92	no	No
22	404.57	4.635	-4.558	-4.15	5	1	80.85	0	330.30	no	No
23	440.77	6.919	-4.024	-78.73	4	0	62.83	1	358.35	no	No
24	326.50	3.986	-3.297	-3.76	4	1	73.83	0	269.49	no	No

*HAC: H-bond acceptors; HDO: H-bond donors; PSA-Polar Surface Area; Ro5Ø-Lipinski's rule violation; TSA: Total Surface Area; Mut.-mutagenic potential; Tum: tumorigenic potential.

None of the obtained compounds expressed mutagenic or tumorigenic potential. However, only compounds **18** and **19** have a positive drug-like score. Compounds **20-23** are not predicted as good drug-like candidates, possibly due to their high lipophilicity (cLog P values > 5 and poor aqueous solubility cLogS < -4). The drug-likeness score is determined by comparing molecule structure with fragments in commercially available drugs. Therefore, it can express limitations by compounds containing novel chemical entities (e.g., silyl moiety in **23** that expressed very low drug-like score (-78.734)). Even though silicon is the second most abundant element on earth, it is not part of commercially available drugs, as organisms cannot directly use it. Therefore, there is almost none commercially available drug with silicon moiety. From this compound set can be concluded that linker prolongation and substitution in the eastern part of the molecule with bulky

aliphatic or small polar substituent negatively interfere with the binding mode. These results correlate with *in vitro* obtained data.

4.8 Structure-Activity Relationships of Multitargeting D_{2/3}R and H₃R Ligands

Recent analysis confirmed that around 85% of medial spiny neurons in the *dorsal* and *ventral striatum* that contain D₁R and D₂R also contain H₃R, confirming their proximity.³²⁶ In *striatum*, H₃R is mainly postsynaptically located in GABA dynorphinergic and enkephalinergic neurons, which enables interaction with postsynaptically located dopamine receptors. H₃R can form heterodimers with D₁R and D₂R, confirmed *in vitro* and *in vivo* (in reserpinized mice). In this species H₃R antagonist thioperamide potentiated synergistic effects and locomotor activation induced by D₁R agonist SKF 38393 and D₂R agonist quinpirole.⁶⁰⁴ Moreover, existence of antagonistic D₂R/H₃R intramembrane reaction was confirmed. H₃R agonism significantly lower the binding of D₂R agonist to the receptor of interest, suggesting direct protein-protein interaction between these two receptor subtypes. This interaction and improving of locomotor activity can be particularly beneficial in PD patients. In order to address symptoms of this multifactorial neurological disease, multitargeting ligands that target both of receptor of interest should be developed. Design and synthesis of MTDLs present potential therapeutic alternatives that can significantly impact patients' compliance. Administering one instead of multiple drugs, can improve pharmacokinetic, pharmacodynamic, and safety profile of a drug, as described in Section 1.6. Therefore, MTDLs targeting both dopamine D_{2/3}R and H₃R can be designed, and potentially resolve some of crucial factors in a multifactorial disease etiology. To rationally design MTDLs, pharmacophores need to be carefully chosen and coupled with appropriate length linker, merged, or fused, which will grant binding to both receptor of interest (Figure 16)

To obtain compounds **25-37**, pramipexole derivatives were coupled with 1-(3-chloropropyl)piperidine moiety to obtain linked D_{2/3}R-H₃R multitargeting ligands. New non-imidazole H₃R ligands contain amine instead of imidazole moiety. Non-imidazole moiety is not a CYP isoenzyme substrate and therefore is a safer therapeutic alternative than imidazole moieties. This moiety is coupled via a spacer that contributes to rigidity to the central core (Figure 47). The central core, either aromatic or aliphatic moiety, forms π - π interactions with the H₃R receptor, while basic moiety forms salt bridges with aspartate residues.^{605,606} This part is essential for binding to the receptor domain. In the eastern part of the molecule, various groups can be introduced that can impact functional selectivity.

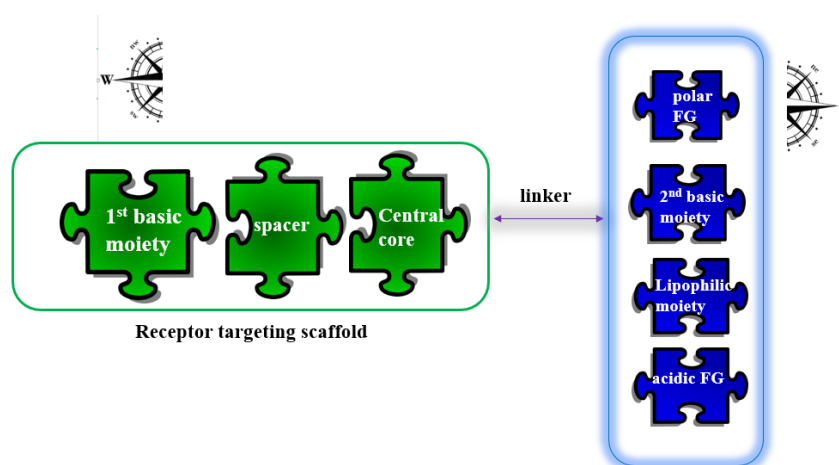


Figure 47: General pharmacophore of non-imidazole H₃R ligands. The western part of the molecule is characterized as the receptor targeting scaffold, while modifications at the eastern part of the molecule impact functional selectivity. Adapted from Walter et al.⁶⁰⁶

H₃R pharmacophore can be coupled with different moieties leading to developing highly potent mono- or multitargeting ligands.^{385,388,607} 1-(3-Chloropropyl)piperidine moiety has been so far coupled with different neuroleptics, to overcome their side effects as weight gain or extrapyramidal syndrome, which are consequences of their off-target effects (von Coburg et al., Figure 16). Antagonism and inverse agonism on H₃R reduced side effects of neuroleptics in several mouse models as shown by Ligneau et al.⁶⁰⁸ Moreover, hyperactivity of both histaminergic and dopaminergic system is observed in schizophrenia.⁶⁰⁹ In contrast to binding D₂R agonist, H₃R antagonism does not impact binding of D₂R antagonist, and therefore enables interaction on both receptor subtypes. Recently reported ST-2223 showed ameliorative effects on autism spectrum

disorder.⁴⁶⁰ While multitargeting derivatives containing H₃R antagonist and D₂R antagonist moieties were described, there is only a few patents where D₂R agonists were coupled with H₃R pharmacophore.

Therefore, moieties were coupled with the two- to the six-methylene groups as spacer. The methylene group spacer was chosen over the ether spacer due to the results described in Section 4.7, where ether derivatives did not show affinity at D₂/D₃R. Additionally, effects of primary, secondary, and tertiary amines to binding affinity at H₃R and D_{2/3}R was examined (Figure 48).

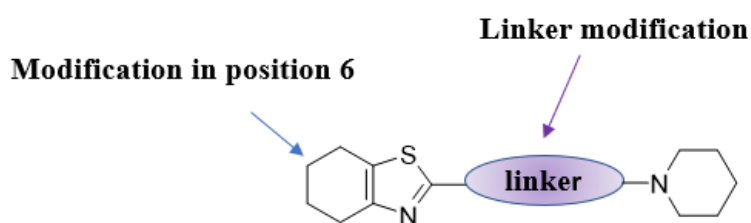
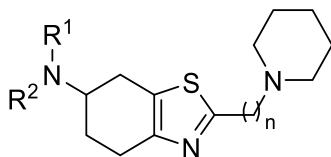


Figure 48: Modifications in position 6 and the linker in compounds 25-37.

All synthesized compounds were *in vitro* examined to estimate binding affinity at D₂R, D₃R, and H₃R. Few compounds were chosen to examine their antioxidative capacity (Table 18).

Table 18: Binding affinities of compounds 25-37.

No.	n	R ¹	R ²	K _i (D ₂ R) [μM] [95% CI]	K _i (D ₃ R) [μM] [95% CI]	K _i (H ₃ R) [nM] [95% CI]	ORAC-value [μM] ± SD
25	3	H	Ac	>10	>10	904 [552; 1480]	n.d.
26	4	H	Ac	>10	>10	538 [382; 757]	-1.23 ± 0.93
27	5	H	Ac	>10	>10	280 [69.8; 1122]	-1.27 ± 0.23
28	6	H	Ac	>10	>10	166 [24.8; 1105]	-0.23 ± 0.79
29	4	H	H	8.59 [1945 - 37967]	9.93 [3593 - 27440]	174 [63.5; 476]	n.d.
30	5	H	H	>10	>10	76.2 [41.2 ; 141]	-2.06
31	6	H	H	5.83 [1429; 23830]	6.49 [1812; 23289]	149 [84.2; 264]	-1.55
32	3	<i>n</i> -Pr	<i>n</i> -Pr	>10	>10	15.3 [10.0; 23.3]	n.d.
33	4	<i>n</i> -Pr	<i>n</i> -Pr	>10	>10	14.3 [3.42; 60.0]	-1,17 ± 0.37
34	5	<i>n</i> -Pr	<i>n</i> -Pr	>10	>10	37.3 [8.71; 160]	-1,76 ± 0.65
35	6	<i>n</i> -Pr	<i>n</i> -Pr	>10	>10	39.4 [10.3; 151]	n.d.*
36	4	H	<i>n</i> -Pr	>10	>10	141 [47.5; 141]	-1.04 ± 0.98
37	5	H	<i>n</i> -Pr	>10	>10	70.4 [11.3; 438]	-1,02 ± 0.69

*n.d not determined, CI: confidence interval, SI, selectivity index, SD, standard deviation, ORAC value: net protection produced by 1 μM Trolox.⁵⁷⁵

Unfortunately, this compound set did not result in affine D₂R and D₃R compounds ($K_i > 10 \mu\text{M}$), indicating that substitution with the bulky moieties in position 2 is not optimal for obtaining the

reaction within the binding pocket. Steric hindrance is observed for orthosteric and allosteric binding in other GPCRs as in serotonergic receptors.⁶¹⁰ In contrast, compounds showed low to moderate H₃R in nanomolar concentration ranges whereby compounds **32** and **33** showed a tendency to the highest H₃R affinity (**32**: $pK_i(\text{H}_3\text{R}) = 7.82$; **33**: $pK_i(\text{H}_3\text{R}) = 7.84$). These compounds contain tertiary amine in position 6 in the western part of the molecule, propyl and butyl linkers. With linker prolongation affinity tends to decrease, as observed in compounds **34** and **35**, but remains in the nanomolar concentration range. (**34**: $pK_i(\text{H}_3\text{R}) = 7.43$; **35**: $pK_i(\text{H}_3\text{R}) = 7.40$). Compounds **32-35** all contain tertiary amine in position 6, indicating that substitution with the bulky substituent can contribute to the interaction with H₃R. Substitution pattern with neutral moiety as in **25-28** show tendency to the affinity decrease.

Compounds were tested to examine their antioxidant capacity. They showed lower (negative) values than Trolox, reference compound. However, compound **28** containing six methylene groups linker and acetyl moiety in position 6 shows the closest values to Trolox (-0.23). The tendency of better antioxidant profile with linker prolongation was confirmed in compounds **37** and **31** that showed less negative values when compared to their analogues **36** and **30** that contain one methylene group less in the linker.

In line with these results, it can be concluded that substitution with bulkier dipropylamino substituents in position 6 was favorable for binding to the H₃R as those compounds showed tendency to higher affinity compared to their monopropylamino or acetamido analogues. Short length linker (three methylene groups) was favored when compared to a longer length linker (five or six methylene groups). Compounds **25-37** showed no significant affinity neither at D₂R nor at D₃R, indicating that substitution with a bulkier substituent in position 2 can negatively interfere with the binding mode. However, ligands that contain longer linkers showed a tendency to higher affinity at D₃R, confirming this hypothesis. Linker prolongation positively impacted antioxidative capacity and can be considered for possible further modification. MTDLs can be further modified as reported heterodimeric bitopic ligands, with very long linkers (more than 30 carbons, as reported by Ulman et al. Figure 4) to avoid steric hindrance. In addition, as a possible reason, the proximity of histamine and dopamine receptors and their distribution in the brain can be considered, as it described that H₃Rs form heterodimers with D₁R and D₂R in the human brain, especially in *striatum*.³²⁶ Coupling two pharmacophores with short linkers and their consequent lack of affinity

can explain that these receptor subtypes are not very close to one another, which needs to be confirmed with bioimaging studies.

Compounds from **25-37** were examined to estimate their drug-like properties (Table 19).

Table 19: Drug-like properties of compounds **25-37**.

No.	MW	cLogP	cLog S	Drug-likeness	HAC	HDO	PSA	Ro5 Ø	TSA	Mut.	Tum.
25	321.49	2.581	-2.599	3.11	4	1	73.47	0	256.59	no	no
26	335.51	3.036	-2.869	3.11	4	1	73.47	0	270.35	no	no
27	349.54	3.490	-3.139	0.78	4	1	73.47	0	284.11	no	no
28	363.57	3.945	-3.409	0.78	4	1	73.47	0	297.87	no	no
29	293.48	2.628	-2.671	3.35	3	1	70.39	0	237.40	no	no
30	307.50	3.082	-2.941	1.02	3	1	70.39	0	251.16	no	no
31	321.53	3.536	-3.211	1.02	3	1	70.39	0	264.92	no	no
32	363.61	4.513	-3.095	4.21	3	0	47.61	0	304.98	no	no
33	377.64	4.967	-3.365	4.21	3	0	47.61	0	318.74	no	no
34	391.67	5.421	-3.635	1.88	3	0	47.61	1	332.50	no	no
35	405.69	5.876	-3.905	1.88	3	0	47.61	1	346.26	no	no
36	335.56	3.839	-3.157	4.07	3	1	56.40	0	280.12	no	no
37	349.58	4.294	-3.427	1.74	3	1	56.40	0	293.88	no	no

*HAC: H-bond acceptors; HDO: H-bond donors; PSA-Polar Surface Area; Ro5Ø-Lipinski's rule violation; TSA: Total Surface Area; Mut.-mutagenic potential; Tum: tumorigenic potential.

None of the compounds expressed mutagenic or tumorigenic potential. All the compounds have PSA values under 90, indicating that they will cross BBB and exert their action in the CNS. Compounds **32-37** have PSA values under 60, which means that they will be entirely absorbed. Compounds **34** and **35** violate once Lipinski Ro5 due to their high lipophilicity ($\log P > 5$). This violation is associated with substitution with a tertiary amine in position 6, which leads to an increase in lipophilicity. Even though compounds **32-36** have clogP values slightly above or beyond 5, they are soluble in water ($c\text{LogS} > -4$) and can be considered for developing drug-like candidates. Compounds **32** and **33** have a high drug-like score (4.21) and can be considered for further modification for developing potent dopamine or histamine ligands, as well as for examination on the other biological targets. Short linkers (propyl or butyl) are favored compared to longer-length linkers due to increased solubility and permeability, as confirmed in drug-like

calculations. All compounds expressed moderate to good drug-like scores, which encourages further examination to the other targets.

4.9 Structure-Activity Relationships of Multitargeting D₃R and H₃R Ligands

In order to further increase affinity and optimize the synthesis of multitargeting ligands, D₃R pharmacophore was introduced and coupled with H₃R pharmacophore. As described in Section 4.8, compounds **25-37** did not show affinity at the D₂R or D₃R. Therefore, modifications were made to improve affinities at dopamine receptor of interest (Figure 49). Firstly, pramipexole moiety in the western part of the molecule was replaced with 4-phenylpiperazine moiety, a well-described D₃R privileged scaffold (Section 4.5). Secondly, pramipexole moiety was replaced with a spiro scaffold coupled with a tertiary amine to provide the necessary salt bridge interaction with the receptor. Spiro moiety increases rigidity in the molecule, leading to specific conformational orientation and interaction with the biological target. Moreover, potent D₃R ligand Buspirone contains spiro moiety (Section 1.1.5) in the western part of the molecule and served as a blueprint to synthesize this compound.⁶¹¹ The third modification in the western part of the molecule was introducing 1-(3-pyridinyl)piperazine moiety. Pyridine derivatives were recognized as a potential scaffold for obtaining both dopamine and histamine receptor affinity and selectivity.^{484,612,613} Replacement of 4-phenylpiperazine ($pK_a \sim 9$) by 1-(3-pyridinyl)piperazine ($pK_a \sim 8$) coupled with tertiary amine as a basic moiety can be used to examine the basicity required for the interaction with the receptor, and if slight modifications can interfere with the binding mode. These moieties were coupled with H₃R pharmacophore, 1-(3-phenoxypropyl)piperidine moiety to obtain high affine ligands. In these compounds linker was expanded with aromatic moiety that acts as a central core (Figure 47). Aromatic substituents increase lipophilicity and lead to better permeability in the CNS, and this linker is present in a high affine H₃R antagonist/inverse agonist pitolisant.

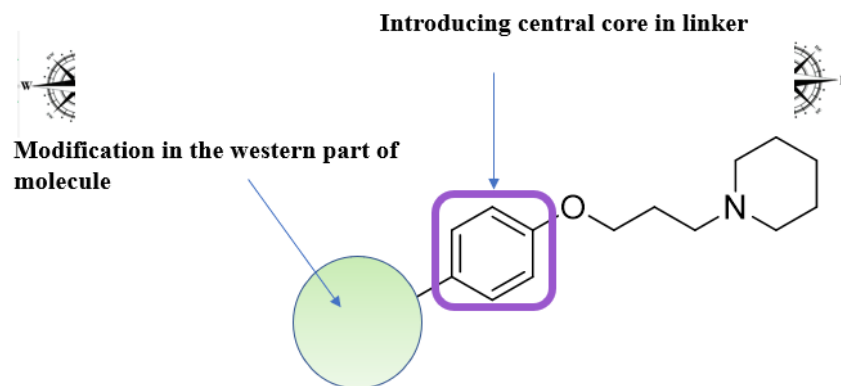
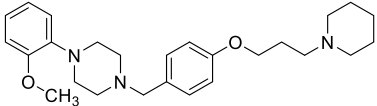
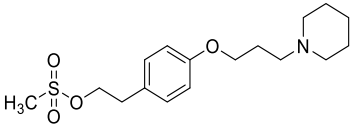
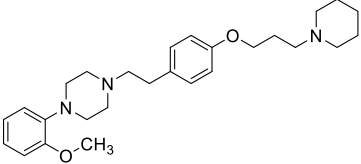
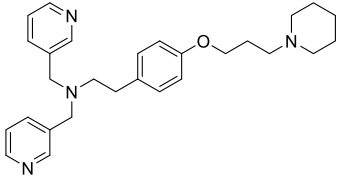


Figure 49: Modifications of multitargeting D₃R-H₃R ligands

All obtained compounds were *in vitro* examined to determine their affinities at dopamine D₂R, D₃R, and histamine H₃R (Table 20). Compounds that contain only H₃R pharmacophore (**38** and **41**) were tested only on this receptor.

Table 20: Binding affinities of compounds **38-43**.

No.	Structure	K_i (D ₂ R) [nM] [95% CI]	K_i (D ₃ R) [nM] [95%CI]	K_i (H ₃ R) [nM] [95%CI]
Pramipexole		3.3 ± 0.3*	0.5 ± 0.1*	n.d.
Pitolisant		n.d.	n.d.	5.25 [7.74; 8.82]
38		n.d.	n.d.	45.9 [18.5; 114]
39		n.d.	>10 μM	2.47 [1.87; 3.28]

40		212 [112; 400]	175 [81.7; 375]	2.89 [0.392; 23.1]
41		n.d.	n.d.	6.33 [2.43; 16.5]
42		26.8 [12.5; 57.5]	50 [22.9; 109]	9.46 [2.81; 31.8]
43		>10 μ M	>10 μ M	13.3 [7.82; 22.8]

*n.d not determined, K_i inhibition constant, CI, confidence interval.

All compounds showed low to very low nanomolar affinity at H₃R and can be considered potent H₃R ligands. Introducing aromatic moiety as a central core led to the design of potent H₃R ligands. Compound **39** showed a tendency to the highest affinity at H₃R (pK_i (H₃R) = 8.61), suggesting that rigidity in the structure can lead to conformational changes that can positively impact binding to the H₃R. Replacement with spiro moiety in the western part of the molecule did not diminish affinity at H₃R. However, this compound did not show affinity at D₃R (> 10 μ M). Lack of affinity can be explained by the steric hindrance that impacts the binding or affinity states of the D₂R receptor (high and low affinity). This moiety cannot substitute privileged D₃R scaffold. In compound **43**, highly lipophilic 1-(3-pyridinyl)piperazine moiety was incorporated in the western part of the molecule, and affinity at H₃R remained in nanomolar concentrations ranges (pK_i (H₃R) = 7.87). This further indicates that potency regulating moiety in H₃R is robust and tolerates incorporating highly lipophilic substituent as in **43**. Robustness of H₃R pharmacophore was confirmed with compounds **38** and **41**, where affinity remained in the nanomolar concentration range (**38**: pK_i (H₃R) = 7.34; **41**: pK_i (H₃R) = 8.2) when small substituents were introduced as *tert*-butyl or mesyl moiety, respectively. Compound **43**, however, did not show affinity at D₂R or D₃R, indicating that dopamine receptors are 1-(3-pyridinyl)piperazine moiety cannot successfully replace 1-(2-methoxyphenyl)piperazine or 1-(2,3-dichlorophenyl)piperazine as D₃R privileged

scaffold.. Even though basicity in the western part of the molecule remained, affinity was diminished. This once more emphasized that changes in the part of the molecule bind to OBS are highly sensitive. On the other hand, compounds **40** and **42** that contain this privileged scaffold showed nanomolar affinities at D₂R, D₃R, and H₃R and can be considered potent multitargeting ligands. 1-(2-Methoxyphenyl)piperazine moiety enables interaction in OBS. Compound **42** contains phenylethyl linker, showed preference 10-fold higher affinity at D₂R ($pK_i(D_2R) = 7.57$) and tendency to 3-fold higher affinity to D₃R ($pK_i(D_3R) = 7.30$) when compared to compound **40** that contain benzyl liker ($pK_i(D_2R) = 6.67$; $pK_i(D_3R) = 6.76$). Compounds **42** showed a slight preference for D₂R, whereby compound **40** showed a preference for D₃R and a slight tendency to higher affinity at H₃R. (**40**: $pK_i(H_3R) = 8.54$; **42**: $pK_i(H_3R) = 8.02$). These results indicate that phenylethyl linker is favored over benzyl linker for achieving optimal interaction with all of three receptor subtypes. All compounds were examined to estimate their drug-likeness (Table 21).

Table 21: Drug-like properties of compounds **38-43**.

No.	MW	cLogP	cLog S	Drug-likeness	HAC	HDO	PSA	Ro5 Ø	TSA	Mut.	Tum.
38	362.51	4.069	-3.655	-52.03	5	1	50.80	0	304.06	no	no
39	444.66	4.499	-3.739	-3.79	5	0	34.17	0	366.21	no	no
40	423.59	4.003	-3.229	4.02	5	0	28.18	0	348.06	no	no
41	341.47	2.685	-2.633	2.70	5	0	64.22	0	268.5	high	high
42	437.63	4.433	-3.341	5.38	5	0	28.18	0	361.82	no	no
43	444.62	3.764	-2.965	1.02	5	0	41.49	0	372.52	no	no

*HAC: H-bond acceptors; HDO: H-bond donors; PSA-Polar Surface Area; Ro5Ø-Lipinski's rule violation; TSA: Total Surface Area; Mut.-mutagenic potential; Tum: tumorigenic potential.

In this compound set, the first and only compound of all with high mutagenic and tumorigenic potential **41** was recognized. This recognition occurred due to the alkylating properties of this compound (mesyl derivative).⁶¹⁴ All compounds expressed PSA values lower than 90, and all, except **41**, lower than 60, indicating that these compounds will be entirely absorbed and express good permeability. All compounds, except **38** and **41**, expressed positive drug-like scores. Particularly low drug-likeness of compound **38**(-52.03) can be justified with the *tert*-butyl group that is not stable under acidic conditions (e.g., in stomach) which can lead to rapid degradation. However, this group can be used in prodrug development.^{615,616} None of the compounds violate Lipinski's Ro5.

Compounds **40** and **42** showed highest drug-likeness score, as well as highest *in vitro* affinity to the receptor of interest. Both compounds have good aqueous solubility (cLogS > -4), low PSA score (< 30), and it can be stated that both compounds are highly promising drug-like candidates. (drug-like score > 4).

To summarize, this compound set (**38-43**) confirmed robustness to changes in H₃R and dopamine D₂R and D₃R sensitivity to changes. Introducing spiro moiety or pyridine derivatives as potential primary pharmacophores were not well-tolerated in terms of D_{2/3}R affinity. This compound set grants two highly potent multitargeting ligands, characterized also as promising drug-like candidates by Data Warrior. Compound **42** with phenylethyl linker showed higher affinity to dopamine receptors and is chosen as a lead compound from this set.

4.10 Structure-Activity Relationships of Fluorescent Ligands

In recent years, various efforts have been made to enlighten cell signaling via GPCR. Fluorescent probes represent valuable tools for studying receptor ligand interactions and can be used for a broad range of experiments, from single molecule spectroscopy to cutting edge technologies as FRET or BRET (Section 2.7.1).^{617,618} Even though dopamine involvement in several neurological disease has been well documented, up to date only several fluorescent dopamine receptor ligands have been developed (Figure 50). In the late 80s Monsma et al. synthesized D₁R fluorescent derivative based on D₁R ligand SCH-23390 and D₂R fluorescent derivative based on N-(*p*-aminophenethyl)piperone.⁶¹⁹ Shortly after Barton et al., introduced new fluorophores as Cascade blue and Texas red and coupled them with the same pharmacophores. The affinities remained in low nanomolar concentration range.⁴⁹² Unfortunately since the beginning of nineties surprisingly few fluorescent, novel dopamine receptor derivatives were reported. Revelation of crystal structures dopamine D₂-like receptors in the last decade, encouraged scientist for pursuing further design of dopamine receptor fluorescent ligands. In 2020 Allikalt et al., reported dansyl-labeled D₂R/D₃R derivatives. Molecular docking studies confirmed that fluorophores do not hinder binding of pharmacophore into OBS in both receptors, hypothesizing that bulky scaffolds can be directly coupled to pharmacophores.⁴⁹⁴

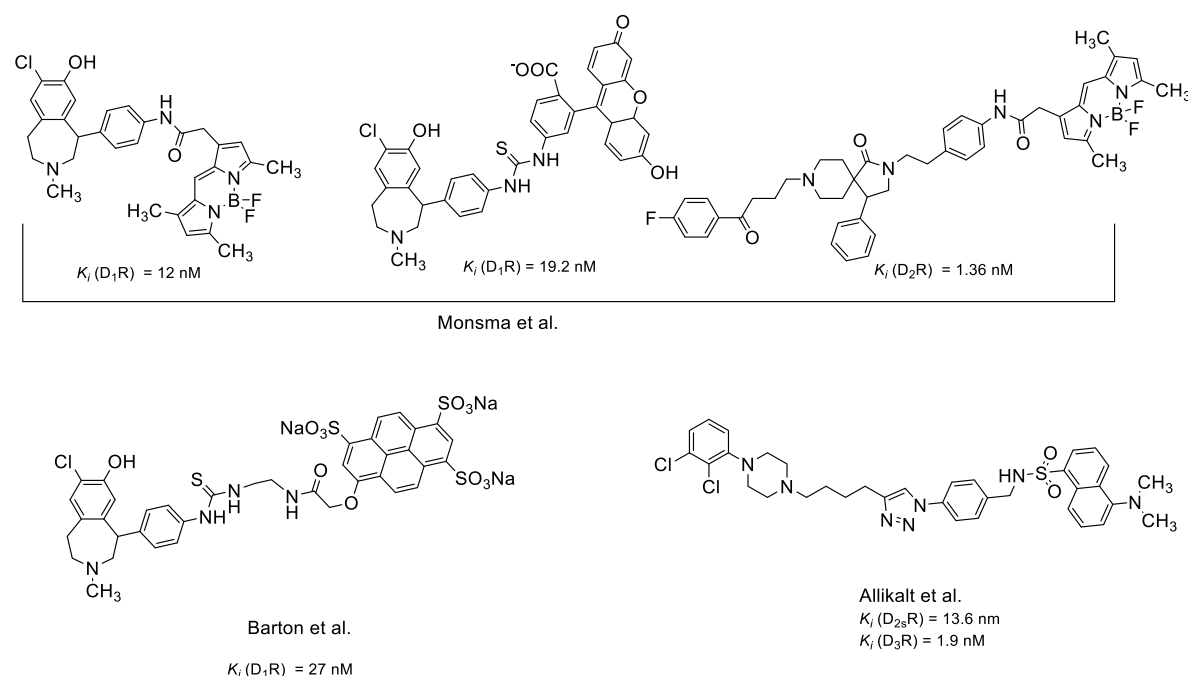


Figure 50: Dopamine receptor fluorescent ligands.

Although it was confirmed that dopamine D_3R is relatively limited distributed, selective D_3R ligands that can be used for imaging this receptor subtype have not yet been developed. Therefore, precise dopamine D_3R localization and distribution remained to be determined. By determination of receptor localization, their involvement in the disease etiology or pathology could be revealed. Fluorescent derivatives were developed to estimate receptor distribution and localization, dopamine and histamine receptor. Modifying BODIPY fluorophore ultimately led to designing BOPPY fluorophore (Section 2.7.2), a chemically and thermally stable alternative with excellent spectral characteristics. Therefore, BOPPY and its derivatives were coupled to the privileged dopamine scaffolds, 4-phenylpiperazine derivatives, and for the first-time BOPPY derivatives were coupled with GPCR. As described previously, a butyl linker granted compounds with the highest affinities at the receptor of interest and was chosen as a spacer for coupling dopamine receptor pharmacophore and BOPPY (Section 2.2). As primary pharmacophores, well-characterized 1-(2-methoxyphenyl)piperazine and 1-(2,3-dichlorophenyl) piperazine were introduced in the eastern part of the molecule^{392,395} (Figure 51). BOPPY core was modified by substitution in position 3 as in compounds **46** and **47** or by expanding with another aromatic ring, forming indole derivative as in compound **48**. Compounds were further in vitro examined (Table 22).

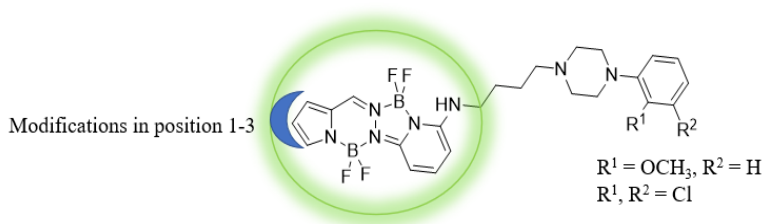


Figure 51: Modifications on dopamine receptor fluorescent ligands

Table 22 Binding affinities of dopamine receptor fluorescent ligands 44-48.

No.	Structure	MW	K_i [nM]	(D ₂ R) [95% CI]	K_i (D ₃ R) [nM] [95% CI]	SI
44		609.21	328 [185; 585]	22.5 [12.7; 39.9]	14.6	
45		571.24	81.1 [45.5; 145]	27.2 [12.6; 58.8]	3.0	
46		599.29	309 [182; 524]	34.3 [19.7; 59.7]	9.0	
47		637.25	497.3 [121; 2044]	52.19 [32.3; 84.2]	9.5	
48		593.29	182 [129; 258]	16.7 [5.57; 49.8]	10.9	

MW, molecular weight; K_i inhibition constant; CI, confidence interval; SI, selectivity index ($K_i(D_2)/K_i(D_3)$)

All five obtained compounds expressed moderate to low nanomolar affinities at both D₂R and D₃R with a slight preference at D₃R. Compound **48** contains an indole ring and tends to show the highest affinity at D₃R, with over 10-fold selectivity to D₃R ($pK_i(D_3R) = 7.78$) when compared to D₂R ($pK_i(D_2R) = 6.74$, SI = 10.9). Compounds **46** and **47** contain ethyl substituent in position 3 and show a tendency to higher affinity at D₃R (**46**: $pK_i(D_3R) = 7.47$; **47**: $pK_i(D_3R) = 7.28$) when compared to compounds with non-substituted **44** and **45**. (**44**: $pK_i(D_3R) = 7.65$ **45**: $pK_i(D_3R) = 7.57$). Replacement of 1-(2-methoxyphenyl)piperazine with 1-(2,3-dichlorophenyl)piperazine moiety did not diminish D₃R affinity. This is in line with reported results, as this scaffold presents another D₃R primary pharmacophore. Introducing aromatic moiety in the western part of the molecule, as in compound **48**, showed a tendency to highest affinity. However, this compound expressed a very low quantum yield (0.03), and therefore cannot be considered a potential fluorescent marker. On the other hand, introducing ethyl substituent in position 3, as in compounds **46** and **47**, tends to have a higher affinity at D₃R and excellent quantum yields: 0.63 and 0.69, respectively (Section 2.7.2). This substitution pattern can be beneficial for interaction with the receptor, as compounds **46** and **47** show more than 9-fold selectivity at D₃R and can be further utilized in bioimaging for binding kinetic experiments or bioimaging studies.

In contrast to already reported fluorescent dopamine receptor ligands, where no selective derivative has yet been described, the design of H₃R fluorescent derivatives led to the synthesis of very potent compounds with beneficial fluorescent properties (Figure 52). Amon et al. reported a three-step synthetic route for obtaining isoindole H₃R fluorescent derivatives with moderate to low nanomolar H₃R affinities (K_i ranges between 11 nM - 178 nM) and emission maxima in ranges 350 - 500 nm, depending on the substitution pattern.⁵³² The same working group reported one year later different fluorophores coupled with non-imidazole, 3-(phenoxypropyl)piperidine moiety, which is incorporated in pitolisant.⁵³³ Even though different fluorophores were introduced, affinity at H₃R remained in low nanomolar to picomolar concentration range. Emission maxima were in range of 350 – 530 nm, and quantum yields of those compounds were not reported. These efforts further resulted in reporting **Bodilisant** by coupling H₃R pharmacophore with BODIPY, up to than most stable and versatile fluorescent agent. Bodilisant shows high nanomolar affinity to H₃R ($K_i(H_3R) = 6.3$ nM), high subtype selectivity, express very high quantum yield (0.92),⁴⁹⁶ and can be further used in *in vivo* bioimaging. The emission maximum of Bodilisant is at 486 nm. In 2020 Bartole et al. reported imidazole derivative **UR-DEBa242**, a Py-5-labeled H₃R antagonist and H₄R

inverse agonist, shedding light on possible resolving of signal cascades involving these two receptor subtypes.⁵³⁴

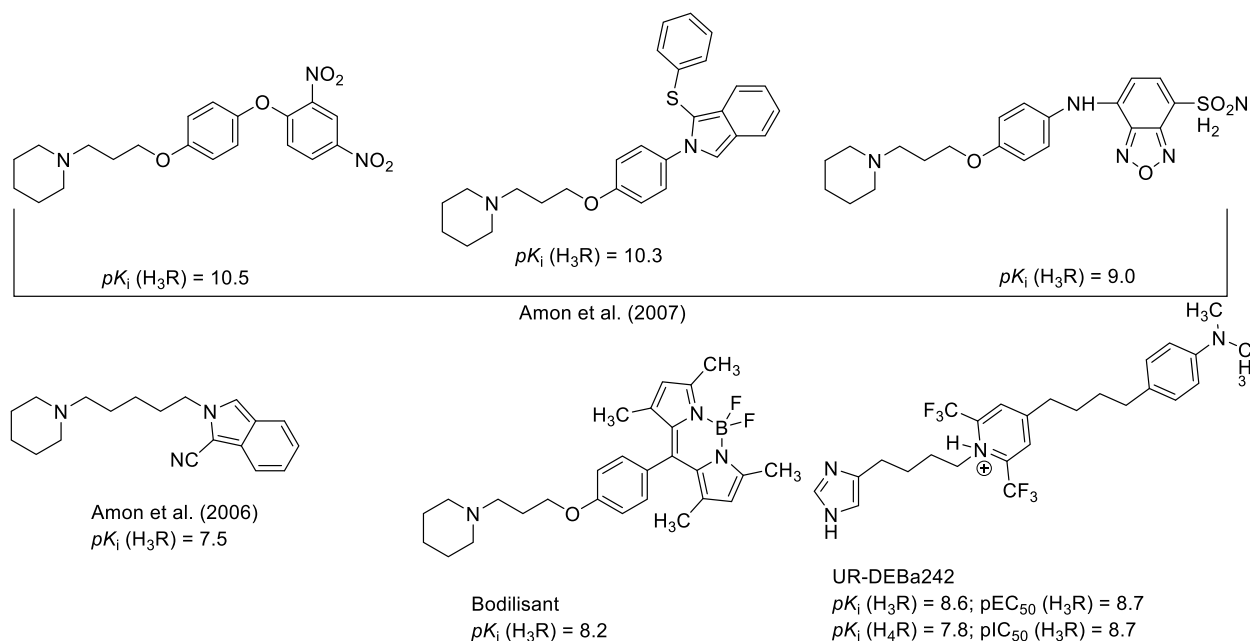
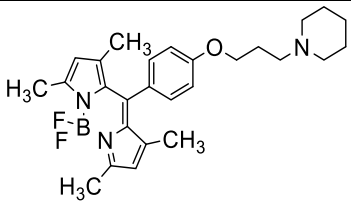
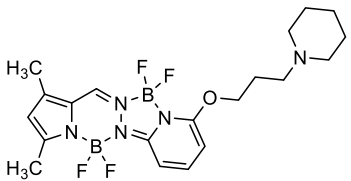
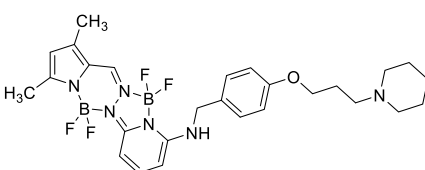


Figure 52: Histamine receptor fluorescent ligands.

However, due to advantages shown in comparison to BODIPY (e.g., higher stability, expressing fluorescence in solid-state), as well as its novelty developing new histamine H₃R fluorescent derivatives was the main objective. Incorporating an electron-rich moiety as a central core in the H₃R pharmacophore can lead to π - π interactions with the receptor of interest. Two ligands were developed to examine the effects of central core effects on the binding affinity. Therefore, H₃R pharmacophore was introduced, whereby compound **49** was direct coupled via ether to BOPPY fluorophore. BOPPY fluorophore in the case of **49** represents an expanded central core that can further interact with the H₃R. Compound **50** was connected via amine, and the linker was extended with benzyl moiety compared to compound **49**. *In vitro* obtained results are summarized in Table 23.

Table 23: Binding affinities of H₃R fluorescent ligands **49-50**.

No.	Structure	MW	K_i (H ₃ R) [nM] [95%CI]
Bodilisant		465.4	6.51 ± 3.31*
49		451.08	2000 [4000; 9400]
50		556.22	150 [70; 350]

*Data are expressed as mean value ± standard deviation, obtained from Tomasch et al.⁴⁹⁶ MW, molecular weight; K_i inhibition constant; CI, confidence interval.

Compound **50** that contains aromatic moiety as a central core expressed 13-fold higher affinity at H₃R (pK_i (H₃R) = 6.82) when compared to **49** (pK_i (H₃R) = 5.70). Compounds **49** and **50** showed comparable quantum yields, 0.60 and 0.56, respectively. Even though different groups may be introduced and affinity H₃R was not diminished (Sections 4.8 and 4.9), bulky BOPPY substituents cannot act as the central core, leading to diminishing affinity compared to small benzyl moiety as the central core. Therefore, compound **50** is favored and can be further used in bioimaging studies. Even though compound **50** expressed lower quantum yield and affinity to H₃R when compared to Bodilisant, this compound can be chosen as a potential alternative over Bodilisant in bioimaging studies due to the higher stability of this fluorophore. Additionally, this compound can be chosen for further optimization to obtain more affine H₃R fluorescent ligands. This is the first time to report that BOPPY fluorophore was coupled with GPCR, and it is the first biological application of this novel fluorophore.

5 Summary

Numerous neurological diseases have multifactorial etiology and are up-to-date only symptomatically treated. Even though dopamine has been recognized as an independent neurotransmitter over half a century ago, it represents an interesting target due to its involvement in disorders like PD, ADHD, schizophrenia, addictive behavior, restless legs syndrome, Huntington chorea. So far, most marketed dopamine ligands used in the treatment of these diseases express moderate to severe side effects, resulting in low patient adherence. Dopamine D₃ receptor was cloned at the beginning of the nineties and sparked interest due to its relatively focal localization, in the limbic region, indicating that this subtype can be involved in diseases associated with the mesolimbic dopamine pathway in the brain. Due to the high homology level between dopamine receptor subtypes, especially between D₂-like receptors, no selective dopamine D₃R drug was introduced to the market. Up to date, **BP 897** is D₃R preferring partial agonist that has entered several clinical trials (for schizophrenia, addictive behavior, ADHD) and served as a blueprint for the first compound set's design and synthesis (**1-10**).

In first compound set (**1-10**) modifications are made in the second pharmacophore and the linker that couples primary and second pharmacophore. Structure-activity relationships studies confirmed that the optimal linker length for synthesis is the butyl linker. Aryl amide moiety was replaced with coumarin, 3-bromo-4-methoxyphenyl, or SF₅ moiety. Introducing SF₅ substituents was particularly interesting as this novel moiety was not yet fully characterized. Compounds **1-10** showed moderate to low nanomolar affinities at D₂R and D₃R with preference to D₃R. Compound **9**, *p*-substituted pentafluorosulfanylphenyl derivative, showed the highest affinity at D₃R and highest preference over D₂R (SI = 20.5) in this compound set. Molecular docking simulations were performed to estimate this compound's precise binding mode to the D₂R and D₃R. *In silico* calculation confirmed that lower affinity at D₂R may be due to the steric hindrance of this voluminous lipophilic moiety in the *p*-position. Therefore, substitution patterns with highly lipophilic substituents can favor the synthesis of D₃R preferring ligands.

Compounds **11-17** were designed as bitopic dopamine D₂/D₃ receptor ligands their functional selectivity needs to be further determined. Bitopic ligands can target one receptor or homo- and heterodimers and lead to specific cellular responses. Rationally designed bitopic ligands can selectively target concrete cascade and consequently resolve the signaling pathway. By coupling orthosteric binding ligand with allosteric modulator, highly selective ligands for receptor subtype

can be developed. Compounds **11-17** contain both dopamine D₂R and D₃R pharmacophores, pramipexole analogues and 4-phenylpiperazine moiety. Each step of the six-step synthesis was optimized, resulting in an overall yield of over 20%. It was confirmed that brominating resulted in the highest yield when bromine was added at once and that HANTZSCH THIAZOLE synthesis should be conducted in DMF, stirring at room temperature for one hour and at 80 °C for another two hours, to obtain higher yields. Higher temperature, or longer reaction time, resulted in numerous side products (e.g., paracetamol or elimination products). This optimized synthesis resulted in **11-17** as well as in **25-37**, and in an overall yield of 18%. Compounds **12-17** represent highly promising biotopic ligands with affinities at D₂R and D₃R in low nanomolar concentration range. Drug-likeness was exceptionally high for **15** and **17** that showed *in vitro* nanomolar highest affinities at the receptor of interest. Moreover, every compound of this set expressed high ORAC values, indicating that these compounds have antioxidative properties and can be considered as potential neuroprotective agents. Optimization of linker and modification in position six led to compound **15** as hit compound from this series and highly promising drug-like ligand, as predicted by drug-like score.

In compounds **18-24** the linker was modified via bioisosteric replacement of methylene groups with ether derivatives. D₃R pharmacophore was replaced with aryl, bulky, and non-bulky aliphatic substituents in the western part of the molecule to examine their effects on the binding affinity. These modifications resulted in a loss of affinity in comparison to compounds **12-17**. Nevertheless, compounds **20-23** expressed slight D₃R preference and can be further modified as potential D₃R ligands. The synthesis of bioisosteric ligands was optimized and resulted in an overall yield of 30%.

Histamine H₃R receptor was cloned at the end of millennia and it was confirmed that this receptor subtype is associated with a sleep-wake disorder, Alzheimer's disease, cognitive impairment, alcohol abuse, or epilepsy. H₃R forms heterodimers with D₂R, especially in *striatum*. In reserpinized mice H₃R antagonist thioperamide potentiated synergistic effects and locomotor activation induced by D₁R and D₂R agonists.⁶⁰⁴ Moreover, H₃R agonism significantly lower the binding of D₂R agonist to the receptor of interest, suggesting direct protein-protein intramembrane interaction between these two receptor subtypes. This interaction and improving of locomotor activity can be particularly beneficial in PD patients, as well as effects of H₃R ligands on sleep

disturbances often observed in PD patients. Therefore, multitargeting ligands D_{2/3}R/H₃R ligands were designed (**25-43**). In compounds **25-37** H₃R pharmacophore 1-(3chloropropyl)piperidine was coupled with dopamine D_{2/3}R pharmacophore, pramipexole derivative and in **38-43** H₃R with D₃R pharmacophore 4-phenylpiperazine, spiro or pyridinepyrazine derivatives. Modifications were made with linker length, position 6 to examine basicity impact, and the western part of the molecule to replace primary pharmacophore. Compounds **25-37** express moderate to low affinity at H₃R. Compounds with longer linker (five or six methylene groups) tended to higher D_{2/3}R affinity compared to compounds with shorter linkers (three or four methylene groups), while compounds with short linkers were favored for optimal interaction with histamine H₃R. Substitution in position 2 negatively interfered with binding at D_{2/3}R OBS due to the steric hindrance, as showed by linker prolongation that resulted in more affine ligands. In compound set **38-43** compounds **40** and **42** stood out as the most promising multitargeting ligands. They expressed nanomolar affinity at D₂R, D₃R, and H₃R. Compound **42** showed a high affinity in low nanomolar concentration range at all receptors of interest and good drug-likeness parameter. Compound **39**, containing a spiro scaffold, showed the overall highest affinity at H₃R, indicating that substitution with a rigid scaffold can be favored for increasing H₃R affinity.

Dopamine and histamine receptor pharmacophores were coupled with, to date most stable fluorophore with excellent spectral characteristics - BOPPY. Developing fluorescent ligands can give insight into receptor distribution and localization and, consequently, determine their role or enable binding and kinetic studies. BOPPY fluorophore was developed only recently and is exceptionally chemically and thermally stable. It was first time reported that BOPPY fluorophore is coupled with GPCR. Dopamine receptor (**44-48**) and histamine receptor (**49-50**) fluorescent ligands were developed. Exceptionally high quantum yield expressed compounds **46** and **47**. Since they express nanomolar affinity at D₂R and D₃R with a preference for D₃R can be considered potent fluorescent ligands that can be further used in bioimaging studies. Stability was confirmed by LC-MS measurement, where compounds remained stable for five months. Compound **50** expressed nanomolar affinity at H₃R, and good quantum yield can be considered potent fluorescent histamine receptor ligand.

To summarize, 50 ligands were developed, and all conducted syntheses were optimized. In each compound set one-lead compound was chosen for potential further examination, based on *in vitro*,

in silico results, predicted drug-like score, or determination of fluorescent properties (Figure 53). Chosen compounds represent very promising potent novel dopamine and histamine receptor ligands, which can be further examined. The synthetic approach and observed Structure-activity relationships shed light on favoring substitution patterns and prerequisites to obtain affinity with the receptors of interest.

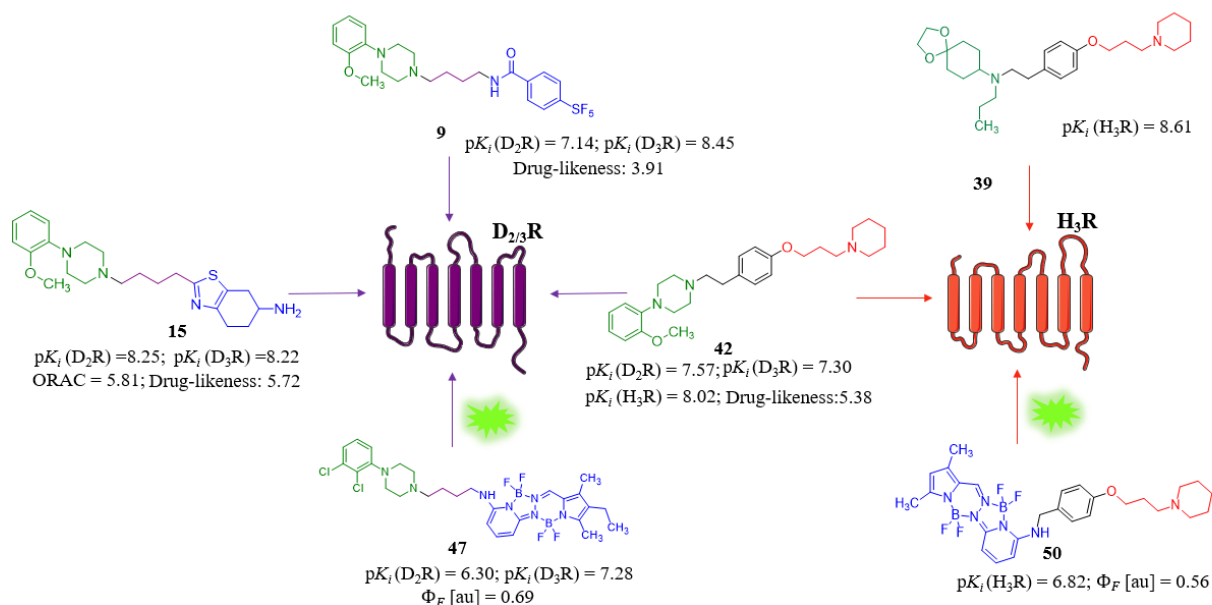


Figure 53: Lead compounds and their *in vitro*, drug-like and fluorescent properties. Φ_F : quantum yield ORAC value: net protection produced by 1 μ M Trolox. Positive values indicate superior antioxidant capacity compared to Trolox. Drug-likeness score, positive values indicate good drug-like properties calculated with equation that sums up score values of fragments that are present in the molecule under investigation

6 Experimental Section

6.1 Chemical Experiments

Chemicals:

All starting materials have been obtained from Acros Organics (Geel, Belgium), Apollo Scientific (Cheshire, UK), Sigma Aldrich (part of Merck KGa Group, Darmstadt, Germany), VWR (Darmstadt, Germany), and were used without further purification. The chemicals have been measured at New classic MR, ML 204 (Mettler Toledo, Columbus, Ohio, USA). Compounds were solubilized with VWR lab dancer and Ultrasonic cleaner USC-THD (VWR, Darmstadt, Germany).

Evaporation of solvents:

Solvents were evaporated at Rotavapor R II (Büchi, Flawil, Switzerland) with PC 3001 VARIO Chemie-Vacuum pump (Vacuubrand, Wertheim, Germany) and CVC 3000 Vacuum controlling system. The compounds were dried at the high-vacuum pump (Vacuubrand Chemie- Hybrid-Pumpe RC 6 (Vacuubrand, Wertheim, Germany).

Thin-layer chromatography:

Analytical thin-layer chromatography was carried out on pre-coated TLC sheets ALUGRAM® Xtra SIL G/UV₂₅₄ 20x20 cm (Macherey-Nagel, Dueren, Germany) and TLC Silica gel 60 NH₂ F₂₅₄ S 20x20 cm (Merck, Darmstadt, Germany).

Eluent for the TLC Chromatography were mixtures of dichloromethane, methanol, methanol saturated with ammonia, hexane, and ethyl acetate in different ratios. Detection: visualization under UV light at 254 nm or 356 nm (Biostep GmbH, Burckhartsdorf, Germany). TLC reagent sprayer potassium permanganate solution (2.5 g KMnO₄, 17 g K₂CO₃, 4.2 mL NaOH (5%) in 250 ml water), ninhydrin solution (2 g ninhydrin in 100 mL EtOH), phosphomolybdic acid solution (10 g phosphomolybdic acid in 100 mL EtOH) and 2,4-dinitrophenylhydrazin solution (12 g 2,4-dinitrophenylhydrazine, 60 ml concentrated sulfuric acid, 80 mL water, 200 mL 96% EtOH).

Column chromatography:

Sorbent: Kieselgel 60 (0.04-0.063 mm) for column chromatography (Macherey-Nagel, Düren, Deutschland, Acros Organics, Geel, Belgien).

Flash chromatography:

Biotage Isolera™ Spektra Systems with ACI™ and Assist (Biotage, Uppsala, Sweden) Stationary phase: Snap KP-Sil, Snap KP-Sil ULTRA, Sfaer KP-Amino D, Sfaer Silica D (Biotage, Uppsala, Sweden). Column capacity: 10g, 25g, 50g, 100g. Mobile phase: Mixture of dichloromethane, methanol, hexane, ethyl acetate in different ratios.

Mass spectroscopy:

Mass spectra were determined using Advion Mass Express (Advion, Ithaca, USA). The expression CMS uses Edwards RV12 rotary vane pump and The CETAC ASX-7000 auto-sampler platform. Atmospheric-pressure chemical ionization (APCI) (constant current 0 – 15 μ A) and electrospray ionization (ESI) (constant voltage 0 – 5kV) were used as a method of ionization, operating in both positive and negative mode. Data are shown as $[M+H]^+$ and $[M-H]^+$. Footprint - Width: 27 cm (10.6 in); Depth: 54.9 cm (21.6 in) rate range: Expression CMS :10 μ L/min to 0.5 mL/min (ESI), 10 μ L/min to 1.0 mL/min (APCI), nebulization gas: 0.5 L/min, heated desolvation/APCI gas: 1 to 10 L/min. Mass calibration stability of ± 0.1 Da over the defined mass range (10 – 1200 for S systems and 10-2000 for L systems) over 12 hours. Linear dynamic range of 5×10^3 . The abundance of naturally occurring isotopes is accurately produced from the full-scan mass spectra. The expression CMS system Voltage: 100 - 240 VA, Frequency: 50 -60 Hz CMS Fuse: 6 Amps, Max Power Consumption: 600 VA.

Melting point determination:

Melting points were determined at Büchi Schmelzpunkt M-565 (Büchi, Flawil, Switzerland) with an open capillary tube and are uncorrected.

NMR spectroscopy:

^1H and ^{13}C NMR spectra of compounds of interest were measured at Bruker Avance III - 300 (Year 2010) and Bruker Avance III - 600 (Year 2011) Bruker, Germany. As NMR solvents were used CDCl_3 and $\text{DMSO-}d_6$ and tetramethylsilane was used as a standard. Chemical shifts are given as parts per million (ppm) and been reported as: s (singlet), brs (broaden singlet), d (doublet), dd (double of doublets), ddd (double of double of doublets), dt (double of triplets), t (triplet), q (quartet), quint (quintet) sxt (sextet) or m (multiplet), Coupling constant (J) were given in Hertz (Hz). Number and assignment of protons (BP, BOPPY; BrMeOPh, 3-Bromo-4-methoxy)phenyl; coum, coumarine or 6 methoxy coumarine; diClPh, 1-(2,3-dichlorophenyl)piperazine; MeOPh, 1-(2-methoxy)phenyl; phth, phthalimide; pip, piperdine; Ph, phenyl; ppz, piperazine; pyr, pyridine; thia, thiazole.

Elemental analysis:

Compounds purity was determined by elemental analysis Vario MICRO cube Elemental Analyzer (Elementar Analysensysteme, Hanau, Germany). Measured valued were within $\pm 0.4\%$ of the theoretical and calculated values for the final compounds.

Liquid chromatography coupled with mass spectroscopy (LC-MS):

Purity of compounds was determined by LC-MS. Elute SP (HPG 700) Bruker Daltronics and amaZon speed ion Trap LC/MSn System (ESI-MS), Method: Alternating ion-Polarity :on; Scan Range: m/z: 80-1200; Nebulizer: Nitrogen, 15 Psi; Dry Gas: Nitrogen, 8 l/min, 200°C; Mass range Mode: UltraScan; Column: Intensity Solo 2 C18 (100 mm * 2.1 mm); Temperature: 50°C; Mobile phase: A. water hypergrade for LC-MS with 0.1 % formic acid (v/v) (Merck); B. Acetonitrile hypergrade for LC-MS (for LC-MS); Flow: 0.2 mL/min; Method of Analysis: 0- 4 min 98 % A, 4-5 min gradient 95% A, 5-9 min 95 % A, 9-16 min gradient 5% A, 16-17 min. gradient to 0% A, reconditioning: 17-18 min. gradient to 98 % A, 18-21 min 98 % A. For all the final compounds purity was > 95%.

Freeze drying:

Compounds were lyophilized with CHRIST ALPHA 1-4 LD Plus and ALPHA 2-4 D plus (Christ, Osterode am Harz, Germany). Ice condenser capacity: max 4 kg/24 h. Ice condenser temperature: -55°C. Ice condenser chamber volume: 6.5 l.

Low-temperature reaction bath with magnetic stirrer:

Thermo Haake® immersion coolers EK 90 (Haake, Karlsruhe, Germany) AC/DC input 230 V AC, temperature (-90) -(-40) °C. Acetone was used as immersion cooling liquid.

Microwave irradiation:

Initiator+ Microwave System EU (Biotage, Uppsala, Schweden). Temperature range: 40–300 °C. Pressure range 0–302 bar (3 MPa; 435 psi). Power range 0–400 W from magnetron at 2.45 GHz.

Hydrogenation:

Hydrogenation was carried out in autoclave model IV, 500 mL (Roth, Germany).

UV/Vis and fluorescence spectroscopy:

UV/Vis spectra were recorded at TECAN® Infinite 1000 Pro multi-use-reader (Tecan Group, Maennedorf, Switzerland); in MeOH and 293 K and on Perkin–Elmer UV/Vis/NIR Lambda 19 spectrometer in dichloromethane. Emission spectra were recorded dichloromethane at 293 K on a Hitachi F-7000 spectrometer using the instrument manufacturer's emission correction curve. Emission spectra were not corrected for the wavelength-dependent spectral responsivity of the fluorometer. All solution spectra were recorded with dyes dissolved in spectroscopic grade solvents at 298 K using 1 cm-quartz cuvette from Hellma GmbH. The molar extinction coefficients of dye solutions of known dye concentration were measured in a multipoint setup.

Cell centrifugation and homogenization:

Ultraturrax® Homogenizer (IKA®-Werke GmbH & Co. KG, Staufen, Germany).

Cell harvesting:

Inotech AG Cell harvester (Inotech, Nabburg, Germany).

Pipetting robot:

Tecan Freedom Evo 100 base unit. Serial number 1406004944 (Tecan, Maendorf, Switzerland).

Microplate multimode reader:

Tacan Infinite M100 Pro (Tecan, Maendorf, Switzerland).

Radioactivity counter:

Radioactivity was determined by liquid scintillation counting. B-counter Micro β trilux. Model Number TRILUX1DET1450024. (Perkin Elmer LAS, Rodgau Germany).

Data analysis:

In vitro assays were analyzed with Prism 6 (GraphPad Software Inc., San Diego, CA).

6.2 General Procedures

N- and *O*-alkylation (A)

To a stirred suspension of an alkyl halide (1.1-1.2 eq.) or nitrile (2 eq.) in acetone or acetonitrile anhydrous potassium carbonate (6-12 eq.) and a catalytic amount of potassium iodide (KI) corresponding amines, phenols or alcohols (1-1.2 eq.) were added. Depending on the leaving group, the reaction mixture was stirred at reflux temperature between 10-72h. After cooling down the reaction mixture to room temperature, inorganic salts were filtered off, and the filtrate was evaporated under reduced pressure. The crude reaction mixture was partitioned between EtOAc/DCM and water. The organic layer was separated, the remaining aqueous layer was extracted with EtOAc/DCM (3x) and washed with saturated solution sodium bicarbonate and brine. The combined organic layers were dried over anhydrous MgSO₄, filtered, and concentrated under reduced pressure. The crude mixture has been purified by flash column chromatography or by distillation.^{620,621}

Cleavage of Phthalimide Protection Group (B)

To a stirred solution of *N*-(ω -alkyl)phthalimide (1 eq.) in 30 mL of MeOH was added 0.5 mL of hydrazine monohydrate (64-65% aq. solution) and stirred upon reflux for 2 hours. After 2 hours, 5 mL 2M HCl was added to the hot solution, and the reaction mixture was stirred at a reflux temperature for another hour. After cooling down to room temperature, the reaction mixture was filtrated, and the filtrate was evaporated under reduced pressure. It was consequently diluted with 20 mL 2M NaOH, and residues were washed with water. The organic layer was separated, the remaining aqueous layer was extracted between EtOAc (3x) and washed with brine. The combined organic layers were dried over anhydrous MgSO₄, filtered, and concentrated under reduced pressure. Crude oils were further purified with column chromatography.^{621,622}

Reduction of Nitriles with Raney Ni (C)

Suitable nitriles (1 eq.) in 50 mL ammonia solution in methanol were consequently subjected to catalytic hydrogenation using freshly prepared Raney Nickel (from 500 mg of aluminum nickel alloy as previously described).⁴⁰⁵ The reaction mixture was reduced with H₂ at 5 bar pressure

overnight. The reaction mixture was filtered off through celite, and the filtrate was evaporated under reduced pressure on the following day. The obtained amines were used without further purification into the next reaction step.⁶²¹

Amide Synthesis (D)

To a stirred solution of amines (1 eq.) and corresponding acid in DCM were added HOBt (1.1 eq.) and EDC (1.1 eq.). The reaction mixture was stirred at room temperature overnight. Into the reaction mixture, saturated solution NaHCO_3 was added for quenching, and it was stirred for another 15 minutes. The crude product was partitioned between DCM (3x) and water. The combined organic layers were washed with saturated solution NaHCO_3 , brine, dried over anhydrous MgSO_4 , filtered, and concentrated under reduced pressure. The crude mixtures have been purified by flash column chromatography modified.^{406,623}

Reductive Amination of Aldehydes and Ketones (E)

To a stirring solution of corresponding aldehyde or ketone (1 eq.) in DCE, amine (1-10 eq.) was added, and starting material were stirred at room temperature for 0.5 -1h. Consequently, $\text{Na}[\text{BH}(\text{CH}_3\text{COO})_3]$ (1-10 eq.) in one portion and CH_3COOH (1-3 eq., only by reductive amination of ketones) were added. Depending on the starting materials, the reaction mixture was left to stir 2h-16h. TLC was used for the control. Upon the disappearance of the starting materials, the reaction was quenched by adding saturated solution NaHCO_3 and stirring at room temperature 15-30 minutes. The reaction mixture was partitioned between DCM and water. The combined organic layers were washed with a saturated solution of NaHCO_3 brine and dried over anhydrous MgSO_4 . Crude products were consequently purified with flash chromatography.⁴³⁰

Synthesis of Thioamides (F)

To a nitrile's solution (1 eq.) n in 4 M HCl in 1,4-dioxane or 4M HCl in EtOAc *O,O'*-diethyl-dithiophosphate (1.1. eq.) was added and left stir at room temperature for 10h. The reaction mixture was filtered off, evaporated with toluene at least three times, and dried on the high vacuum pump overnight. Obtained thioamides were used without further purification.

Synthesis of 6 acetamido 4,5,6,7 tetrahydrobenzothiazole Derivatives (G)

To a stirring solution of *N*-(4-oxocyclohexyl)acetamide (1.2-1.5 eq.) in chloroform (10-50 mL) was added all bromine (1.2-1.6 eq.) at once. The reaction mixture was stirred at room temperature until discoloration (observed after 15-20 minutes, depending on the derivative). The reaction mixture was evaporated under reduced pressure and co-evaporated with toluene (3x). Consequently, a concentrated reaction mixture was dissolved in DMF, and thioamide derivative (1 eq.) was added. The reaction mixture was stirred at room temperature for 1h, then heated up to 80 °C and stirred for another two hours. DMF was evaporated, and the reaction mixture was extracted with 5M NaOH solution and DCM (3x). Organic layers were collected, washed with water, brine, dried over anhydrous MgSO₄, and evaporated under reduced pressure. Crude oil was purified with column chromatography.

***N*-Deacetylation (H)**

Obtained amides (1 eq.) were dissolved in concentrated HBr or HCl. The solutions were heated up to reflux temperature and stirred 36-48 h, depending on the amine. TLC was used for the reaction control. The reaction mixture was left to cool down to room temperature and subsequently poured into ammonia solution at 0 °C (ice bath). The reaction mixture was extracted with DCM and water (3x). Combined organic layers were washed with brine and dried over anhydrous MgSO₄. The filtrate was evaporated under reduced pressure. Crude oils were further purified with column chromatography.

Synthesis of Diamino and Monoamino 4,5,6,7-tetrahydrobenzothiazols (I)

Corresponding acetals (1 eq.) were hydrolyzed in concentrated HBr at room temperature for 48h. Elementary bromine (1 eq.) was added dropwise until the solution was discolored. The reaction mixture was stirred for another 0.5 h-1 h after addition. After 2-3 h reaction became foggy, and thiourea (1 eq.) was added in portions. It was heated up to 90 °C and stirred for another 1.5 h. The reaction mixture was cooled to the room temperature and evaporated to dryness. The concentrate was recrystallized with ethanol.

Deamination of 2-amino-4,5,6,7-tetrahydrobenzothiazoles (J)

2-Amino 4,5,6,7-tetrahydrobenzothiazoles (1 eq.) were dissolved in DMSO, and the solution was cooled down to 0 °C. To the solution was portion wise added CuBr₂ (1.5 eq.) and the reaction mixture was left to stir for 15 minutes. Consequently, *tert*-butyl nitrite or *iso*-pentyl nitrite (1.5 eq.) was added dropwise over 30 minutes while keeping the temperature at 0 °C. The reaction mixture was left to heat up to room temperature and stirred overnight. On the following day, the reaction was quenched by adding saturated solution NH₄Cl, and DMSO was evaporated. The remaining solution was partitioned between DCM and H₂O. Organic layers were separated, washed with a saturated solution of NaHCO₃, brine, dried over MgSO₄, and evaporated under reduced pressure. Crude products were purified by flash column chromatography.⁶²⁴

Aromatic Nucleophilic Substitution on 2-bromothiazoles, Ether Synthesis (K)

To a THF solution of PMB alcohol (2 eq.) was added NaH ($\omega=60\%$, 3 eq.) in portions at room temperature. The reaction mixture was stirred at 40 °C for 2 hours. Consequently, 2-bromothiazole derivative (1 eq.) was added, and the reaction mixture was refluxed overnight. On the following day, the reaction was quenched by adding sat sol NaHCO₃, by stirring for 15 minutes. Organic layers were combined, washed with saturated solution NaHCO₃, brine, dried over anhydrous MgSO₄, and evaporated under reduced pressure. Crude oil was purified by column chromatography.

Synthesis of BOPPY Fluorophore (L)

To the solution of hydrazine pyridine chloride (1.1 eq.) and corresponding pyrrole-2-aldehyde (1 eq.) derivative in 1,2-dichloroethane (DCE) was added *p*-toluene sulfonic acid. The reaction mixture was refluxed overnight. On the following day, 3 mL of diisopropylethylamine (DIPEA) was added to the reaction mixture and stirred another 15-20 min. Consequently, boron trifluoride diethyl etherate (BF₃·Et₂O) was added, and the reaction mixture was refluxed for another four hours. TLC was used for reaction control. The reaction mixture was cooled down to room temperature, 50 mL of dichloromethane (DCM) was poured into the reaction mixture, and all of it was poured into 100-150 mL of water. The organic phase was extracted with DCM, washed three times with water, brine, and dried over anhydrous MgSO₄. The reaction mixture was evaporated under reduced pressure. The crude product was purified using flash column chromatography.⁴⁸⁸

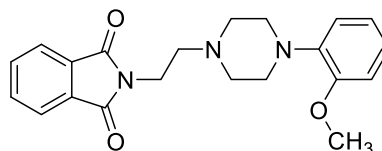
Aromatic Nucleophilic Substitution on Fluorophore (M)

To a stirring solution of fluorophores (1 eq.) and corresponding amines (3-9 eq.) in DCE, triethylamine (Et₃N) was added. The reaction mixture was stirred between 3 – 10h at 40 °C. TLC was used for the control. Consequently, reaction mixture was poured into 50 mL water and extracted three times with DCM. Organic layers were collected, washed with water, saturated brine, and dried over anhydrous MgSO₄. Crude product was purified using flash column chromatography.

2-{2-[4-(2-Methoxyphenyl)piperazin-1-yl]ethyl}isoindoline-1,3-dione: P8^{400,621}

According to procedure A, to a solution of 2-(2-bromoethyl)isoindoline-1,3-dione (**P2**, 4.68 mmol, 1.19 g), 1-(2-methoxyphenyl)piperazine (**P1**, 5.20 mmol, 1 g), 5,00 g K₂CO₃ and a catalytic amount of KI were added. The crude product was purified with flash column chromatography (sorbent SiO₂, eluent: DCM: MeOH 97:3). Yellow solid. Yield: 42%.

Chemical formula: C₂₁H₂₃N₃O₃
 Mr: 365.43
 Internal code: ME 003

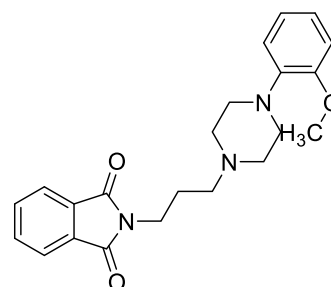


¹H NMR (300 MHz, DMSO-*d*₆) δ 7.93 – 7.81 (m, 4H, Phth), 6.97 – 6.79 (m, 4H, MeOPh), 3.75 (s, 3H, -OCH₃), 3.72 (t, *J* = 6.5 Hz, 2H, PhthN-CH₂), 2.88-3.0 (m, 4H, 2,6ppz), 2.62 – 2.52 (m, 6H, 3,5ppz, N-CH₂)
 MS (APCI(+)): m/z [M+H]⁺: calculated: 366.2 found: 366.1

2-{3-[4-(2-Methoxyphenyl)piperazin-1-yl]propyl}isoindoline-1,3-dione: P9^{400,621}

According to procedure A, to a solution of 2-(3-bromopropyl)isoindoline-1,3-dione (**P3**, 3.72 mmol, 1.00 g), 1-(2-methoxyphenyl)piperazine (**P1**, 3.11 mmol, 597mg), 5,00 g K₂CO₃ and a catalytic amount of KI were added. The crude product was purified with flash column chromatography. (sorbent SiO₂, eluent: DCM: MeOH 97:3). Yellow solid. Yield: 51%.

Chemical formula: C₂₂H₂₅N₃O₃
 Mr: 379.46
 Internal code: ME 001



¹H NMR (300 MHz, DMSO-*d*₆) δ 7.93 – 7.77 (m, 4H, Phth), 6.96 – 6.75 (m, 3H, 3,4,5 MeOPh), 6.68 (dd, *J* = 7.6, 1.5 Hz, 1H, 6MeOPh), 3.72 (s, 3H, -OCH₃), 3.67 (t, *J* = 6.7 Hz, 2H, PhthN-CH₂), 2.75 – 2.62 (m, 4H, 2,6ppz), 2.44 – 2.33 (m, 6H, 3,5ppz, ppzN-CH₂), 1.77 (quin, *J* = 6.6 Hz, 2H, ppzN-CH₂-CH₂)
 MS (APCI(+)): m/z [M+H]⁺: calculated: 380.1 found: 380.3

2-[4-[4-(2-Methoxyphenyl)piperazin-1-yl]butyl]isoindoline-1,3-dione: P10^{400,621}

According to procedure **A**, to a solution of 2-(4-bromobutyl)isoindoline-1,3-dione (**P4**, 3.54 mmol, 1.00 g), 1-(2-methoxyphenyl)piperazine (**P1**, 2.95 mmol, 567 mg), 5.00 g K₂CO₃ and a catalytic amount of KI were added. The crude product was purified with flash column chromatography (sorbent SiO₂, eluent: DCM: MeOH 95:5). Yellow solid. Yield: 96%.

Chemical formula:

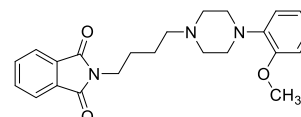
C₂₃H₂₇N₃O₃

Mr:

393.49

Internal code:

ME 002

¹H NMR (300 MHz, DMSO-*d*₆)

δ 7.93 – 7.78 (m, 4H, Phth), 6.99 – 6.79 (m, 4H, MeOPh.), 3.75 (s, 3H, -OCH₃), 3.59 (t, *J* = 6.9 Hz, 2H, PhthN-CH₂), 2.97 – 2.87 (m, 4H, 2,6ppz), 2.48 – 2.41 (m, 4H, 3,5ppz), 2.32 (t, *J* = 7.2 Hz, 2H, ppzN-CH₂), 1.61 (quin, 2H, PhthN-CH₂-CH₂), 1.45 (quin, *J* = 7.3 Hz, 2H, ppzN-CH₂-CH₂).

MS (APCI-(+)) *m/z* [M+H]⁺

calculated: 394.2 found: 394.24

4-[4-(2-Methoxyphenyl)piperazin-1-yl]butannitrile: P11^{400,625,626}

According to procedure **A**, to a solution of 4-bromobutanenitrile (**P6**, 13.5 mmol, 2.000 g), 2-methoxyphenylpiperazine (**P1**, 13.5 mmol, 2.598 g), 10.00 g K₂CO₃, and a catalytic amount of KI were added. Crude oil was purified with flash column chromatography (sorbent SiO₂, eluent: DCM: MeOH 95:5). Yellow solid. Yield: 69%.

Chemical formula:

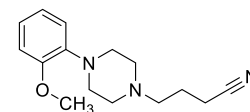
C₁₅H₂₁N₃O

Mr:

259.35

Internal code:

ME 178

¹H NMR (300 MHz, DMSO-*d*₆)

δ 7.00 – 6.85 (m, 4H, MeOPh), 3.78 (s, 3H, -OCH₃), 2.97-3.02 (br s, 4H, 2,6ppz), 2.47-2.50 (m, 6H, 3,5ppz, ppzN-CH₂), 2.41 (t, *J* = 6.9 Hz, 2H, CH₂-CN), 1.76 (quin, *J* = 7.0 Hz, 2H, ppzN-CH₂-CH₂).

MS (APCI-(+)) *m/z* [M+H]⁺

calculated: 260.2 found: 260.4

4-[4-(2,3-Dichlorophenyl)piperazin-1-yl]butannitrile: P12^{400,626}

According to procedure **A**, 4-bromobutanenitrile (**P6**, 6.75 mmol, 1.000 g) 1-(2,3-dichlorophenyl)piperazine (**P5**, 7.43 mmol, 1.988 g), 10.00 g K₂CO₃, and a catalytic amount of KI were added. Crude oil was purified with flash column chromatography (sorbent SiO₂, eluent: DCM: MeOH 95:5). Yellow solid. Yield: 95%.

Chemical formula:

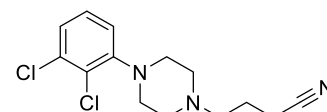
C₁₄H₁₇Cl₂N₃

Mr:

298.21

Internal code:

ME 069

¹H NMR (300 MHz, DMSO-*d*₆)

δ 7.34 – 7.27 (m, 2H, 5,6diClPh), 7.14 (dd, *J* = 6.2, 3.5 Hz, 1H, 4diClPh), 3.04 – 2.91 (br s, 4H, 2,6ppz), 2.57 – 2.52 (m, 4H, 3,5ppz), 2.50-2.51 (m, 2H, ppzNCH₂), 2.42 (t, *J* = 6.8 Hz, 2H, CH₂-CN), 1.75 (p, *J* = 6.9 Hz, 2H, CH₂-CH₂-CH₂).

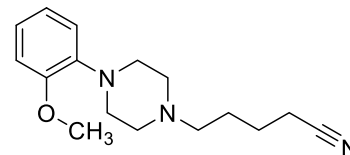
MS (APCI-(+)) *m/z* [M+H]⁺:

calculated: 298.1;300.1 found: 299.0; 300.0.

5-[4-(2-Methoxyphenyl)piperazin-1-yl]pentannitrile: P13^{400,627}

According to procedure **A**, 5-bromovaleronitrile (**P7**, 6.17 mmol, 1.000 g) 1-(2-methoxyphenyl)piperazine (**P1**, 6.17 mmol, 1.186 g), 5.000 g K₂CO₃, and a catalytic amount of KI were added. Crude oil was purified with flash column chromatography (sorbent SiO₂, eluent: DCM: MeOH 95:5). Transparent oil. Yield: 88%.

Chemical formula: C₁₆H₂₃N₃O
Mr: 273.38
Internal code: ME 063

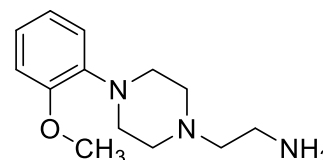


¹H NMR (300 MHz, DMSO-*d*₆) δ 7.05 – 6.80 (m, 4H, MeOPh), 3.77 (s, 3H, -OCH₃), 3.00 – 2.91 (br s, 4H, 2,6ppz), 2.56 – 2.52 (m, 2H, ppzN-CH₂), 2.46-2.50 (m, 4H, 3,5ppz), 2.34 (t, *J* = 6.5 Hz, 2H, CH₂-CN), 1.70 – 1.47 (m, 4H, CH₂-CH₂-CN)
MS (APCI(+)) *m/z* : [M+H]⁺: calculated: 274.2 found: 274.1

4-[4-(2-Methoxyphenyl)piperazin-1-yl]ethan-1-amine: P14^{400,625,628}

According to the procedure **B**, from **P8** (0.76 mmol, 290 mg). Crude oil was used in the next reaction step without further purification. Yellow oil. Yield: 85%.

Chemical formula: C₁₃H₂₁N₃O
Mr: 235.33
Internal code: ME 009

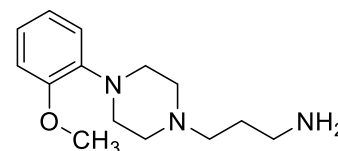


¹H NMR (300 MHz, DMSO-*d*₆) δ 6.97 – 6.83 (m, 4H, MeOPh), 3.77 (s, 3H, -OCH₃), 3.01 – 2.87 (br s, 4H, 2,6ppz), 2.61 – 2.53 (m, 2H, NH₂), 2.44-2.52 (m, 4H, 3,5ppz), 2.30 (t, *J* = 7.2 Hz, 2H, CH₂-NH₂), 1.53 – 1.30 (m, 2H, Nppz-CH₂)
MS (APCI(+)) *m/z* : [M+H]⁺: calculated: 264.2 found: 265.2

3-(4-(2-Methoxyphenyl)piperazin-1-yl)propan-1-amine: P15^{400,628}

According to procedure **B**, from **P9** (2.37 mmol, 635 mg). Crude oil was used in the next reaction step without further purification. Light yellow solid. Yield: 59%.

Chemical formula: C₁₄H₂₃N₃O
Mr: 249.36
Internal code: ME 025

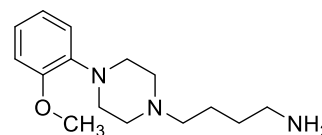


¹H NMR (300 MHz, DMSO-*d*₆) δ 7.12 – 6.78 (m, 4H, MeOPh), 3.76 (s, 3H, OCH₃), 2.95-3.00 (br s, 4H, 2,6ppz), 2.84 – 2.75 (m, 2H, NH₂), 2.42 – 2.32 (m, 2H, CH₂-NH₂), 2.01 – 1.60 (m, 8H, 4H, 3,5ppz, Nppz-CH₂CH₂)
MS (APCI(+)) *m/z* : [M+H]⁺: calculated: 250.2 found: 250.4

4-[4-(2-Methoxyphenyl)piperazin-1-yl]butan-1-amine: P16^{400,629,630}

According to procedure **B**, from **P10** (2.82 mmol, 1.110 g). Crude oil was purified with column chromatography (sorbent SiO₂, eluent: DCM: MeOH(NH₃) 95:5) and, according to procedure **C** from **P11** (9.35 mmol 2.426 g), used in the next step without further purification. Light yellow solid. Yield: 85%.

Chemical formula: C₁₅H₂₅N₃O
Mr: 263.39
Internal code: ME 181

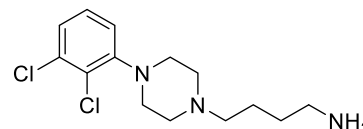


¹H NMR (300 MHz, DMSO-*d*₆) δ 7.02 – 6.71 (m, 4H, MeOPh), 3.77 (s, 3H, OCH₃), 3.00-2.85 (br s 4H, 2,6ppz) 2.53 (m, 8H, 3,5ppz, -CH₂-NH₂), 2.30 (t, *J* = 7.2 Hz, ppzN-CH₂), 1.55 – 1.25 (m, 4H, Nppz-CH₂-CH₂-CH₂-CN).
MS (APCI(+)) *m/z* : [M+H]⁺: calculated: 264.4 found: 264.4

4-[4-(2,3-Dichlorophenyl)piperazin-1-yl]butan-1-amine: P17^{400,631,632}

According to procedure **C** from **P12** (2.682 mmol, 0.800 g), Crude product was used without further purification Light yellow solid. Yield: 59%.

Chemical formula: C₁₄H₂₁Cl₂N₃
Mr: 302.24
Internal code: ME 198

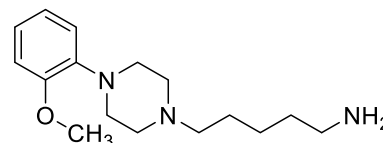


¹H NMR (300 MHz, DMSO-*d*₆) δ 7.34 – 7.24 (m, 2H, 4,5diClPh), 7.13 (dd, *J* = 6.3, 3.3 Hz, 1H, 6diClPh), 3.02 – 2.92 (br s, 4H, 2,6ppz), 2.62 – 2.51 (m, 4H, 3,5ppz), 2.45-2.47 (m, 4H, CH₂NH₂), 2.31 (t, *J* = 7.1 Hz, 2H, ppzN-CH₂), 1.55 – 1.28 (m, 4H, ppzN-CH₂-CH₂-CH₂).
MS (APCI(+)) *m/z* : [M+H]⁺: calculated: 302.1; 304.1 found: 302.4 304.4.

5-[4-(2-Methoxyphenyl)piperazin-1-yl]pentan-1-amine: P18^{400,633}

According to procedure **C** from **P13** (5.10 mmol, 1.395 g). The crude product was used without further purification. Yellow oil. Yield: 79%.

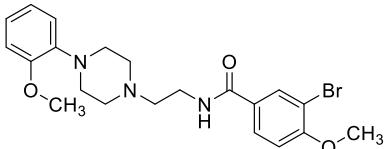
Chemical formula: C₁₆H₂₇N₃O
Mr: 277.41
Internal code: ME 067



¹H NMR (300 MHz, DMSO-*d*₆) δ 7.03 – 6.79 (m, 4H, MeOPh), 3.76 (s, 3H, -OCH₃), 3.07 – 2.85 (br s, 4H, 2,6ppz), 2.58 – 2.52 (m, 2H, NH₂), 2.40-2.46 (m, 4H, 3,5ppz), 2.29 (t, *J* = 8.0, 6.5 Hz, 2H, CH₂-NH₂), 1.52 – 1.20 (m, 8H, ppzN-CH₂-CH₂-CH₂-CH₂).
MS (APCI(+)) *m/z* : [M+H]⁺: calculated 278.2 found: 278.5

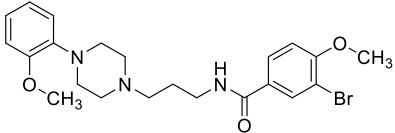
3-Bromo-4-methoxy-*N*-{2-[4-(2-methoxyphenyl)piperazin-1-yl]ethyl}benzamid (ST-2177): 1⁴⁰⁰

P14 (0.79 mmol, 187 mg) was dissolved in DCM. Into the solution was slowly added 3-bromo-4-methoxybenzoic acid (0.87 mmol, 202 mg), HOBt (0.8735 mmol, 134 mg), and EDC (0.8735 mmol, 136 mg), according to the procedure **D**. Crude product was purified by crystallization in acetone. Light yellow solid. Yield: 22%.

Chemical formula:	C ₂₁ H ₂₆ BrN ₃ O ₃	
Mr:	448.36	
Melting point:	163.4 °C	
Internal code:	ME 010	
¹ H NMR (300 MHz, DMSO- <i>d</i> ₆)	δ 8.42 (t, <i>J</i> = 5.6 Hz, 1H, 2BrMeOPh), 8.09 (d, <i>J</i> = 2.2 Hz, 1H, 4BrMeOPh), 7.88 (dd, <i>J</i> = 8.6, 2.2 Hz, 1H, 5BrMeOPh), 7.19 (d, <i>J</i> = 8.7 Hz, 1H, 6 MeOPh), 6.97 – 6.82 (m, 4H, 3,4,5MeOPh), 3.90 (s, 3H, -OCH ₃ (BrMeOPh)), 3.77 (s, 3H, -OCH ₃ (MeOPh)), 3.40 (m, 4H, ppzN-CH ₂ -CH ₂), 3.02 – 2.88 (br s, 4H, 2,6ppz), 2.63 – 2.54 (m, 4H, 3,5ppz).	
¹³ C NMR (75 MHz, DMSO- <i>d</i> ₆)	δ 164.28 (C=O), 157.47(4C BrPh), 151.93 (2C MeOPh), 141.21 (1C MeOPh), 131.75 (2C BrPh), 128.41 (1C BrPh), 127.95 (5C MeOPh), 122.31 (4C MeOPh), 120.79 (6C BrPh), 117.85(3C MeOPh), 112.07 (3C BrPh), 111.86 (5CBrPh), 110.23 (6C MeOPh), 57.01 (2C 6C ppz), 56.48 (3C 5C ppz), 55.27 (OCH ₃ MeOPh), 53.01 (OCH ₃ BrPh), 50.01,(ppzN-C) 36.86. (C-NH)	
MS (APCI(+)): <i>m/z</i> [M+H] ⁺	calculated	449.1;450.1; found: 449.0; 451.0
Elemental analysis	calculated	%C 56.26 %H 5.85 %N 9.37
	found:	%C 55.75 %H 5.87 %N 9.50;

3-Bromo-4-methoxy-*N*-{3-[4-(2-methoxyphenyl)piperazin-1-yl]propyl}benzamide (ST-2199): 2⁴⁰⁰

P15 (0.56 mmol, 140 mg) was dissolved in DCM. Into the solution were added 3-bromo-4-methoxybenzoic acid (0.61mmol. 143 mg), HOBt (0.61 mmol, 95 mg), and EDC (0.61 mol, 96 mg) in portions and the mixture was stirred at room temperature, according to the procedure **D**. Crude product was purified with column chromatography (sorbent SiO₂, eluent: DCM: MeOH 95:5). White solid. Yield: 30%.

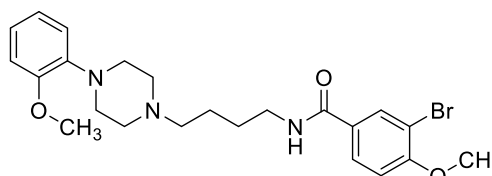
Chemical formula:	C ₂₂ H ₂₈ BrN ₃ O ₃	
Mr:	462.39	
Melting point:	127.6 °C	
Internal code:	ME 027	
¹ H NMR (300 MHz, DMSO- <i>d</i> ₆)	δ 8.49 (t, <i>J</i> = 5.5 Hz, 1H, CONH), 8.08 (d, <i>J</i> = 2.2 Hz, 1H, 3BrMeOPh), 7.88 (dd, <i>J</i> = 8.6, 2.2 Hz, 1H, 6BrMeOPh), 7.18 (d, <i>J</i> = 8.7 Hz, 1H, 5BrMeOPh), 6.99 – 6.81 (m, 4H, MeOPh), 3.90 (s, 3H, -OCH ₃ (BrMeOPh)), 3.76 (s, 3H, -OCH ₃ (MeOPh)), 3.32 – 3.24 (t, 2H, CH ₂ -CONH), 3.00 – 2.90 (m, 4H, 2,6ppz), 2.50-2.60 (m, 4H, 3,5ppz), 2.38 (t, <i>J</i> = 7.0 Hz, 2H, ppzN-CH ₂), 1.70 (quin, <i>J</i> = 7.0 Hz, 2H, ppzN-CH ₂ -CH ₂ -).	
¹³ C NMR (75 MHz, DMSO- <i>d</i> ₆)	δ 164.25 (C=O), 157.42 (4C BrMeOPh), 151.93(2C MeOPh), 141.21(1C MeOPh), 131.67 (2C BrMeOPh),,128.41 (1C BrMeOPh),, 128.05 (5C MeOPh), 122.30 (4C MeOPh), 120.79 (6C	

	BrMeOPh),, 117.86 (3C MeOPh), 112.04 (3C BrMeOPh), 111.86 (5C BrPh), 110.21 (6C MeOPh), 56.47 (2C, 6C ppz), 55.79 (3C, 5C ppz), 55.27 (OCH ₃ MeOPh). 53.02 (OCH ₃ BrMeOPh), 50.04 (ppz N-C), 37.96 (C-NH), 26.14 (PpzN-C-C).		
MS-(APCI(+)): m/z [M+H] ⁺	calculated	462.1;464.1;	Found 462.1;464.1;
Elemental Analysis	calculated:	%C 57.15	%H 6.10 %N 9.09
	found:	%C 56.70	%H 6.06 %N 8.82

3-Bromo-4-methoxy-*N*-{4-[4-(2-methoxyphenyl)piperazin-1-yl]butyl}benzamide (ST-2176): **3**⁴⁰⁰

P16 (1.93 mmol, 510 mg), was dissolved in DCM. To a solution, 3-bromo-4-methoxybenzoic acid (2.13 mmol, 492mg), HOBt (2.13 mmol, 326 mg), and EDC (2.13 mmol, 339 mg) were added according to procedure **D**. Crude product was purified by crystallization in acetone. White solid. Yield: 44%.

Chemical formula:	C ₂₃ H ₃₀ BrN ₃ O ₃
Mr:	476.42
Melting point:	162.0 °C
Internal code:	ME 007



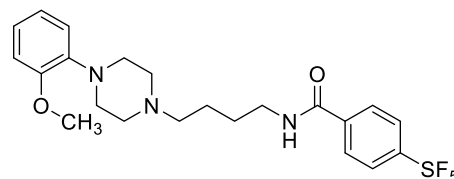
¹ H NMR (300 MHz, DMSO- <i>d</i> ₆)	δ 8.50 (t, <i>J</i> = 5.6 Hz, 1H, CONH), 8.15 (d, <i>J</i> = 2.2 Hz, 1H, 2 BrMeOPh), 7.94 (dd, <i>J</i> = 8.6, 2.2 Hz, 1H, 6BrMeOPh), 7.24 (d, <i>J</i> = 8.7 Hz, 1H, 5BrMeOPh), 7.06 – 6.90 (m, 4H, MeOPh), 3.96 (s, 3H, -OCH ₃ (BrMeOPh)), 3.82 (s, 3H, -OCH ₃ MeOPh), 3.32 (t, <i>J</i> = 6.3, 5.8 Hz, 2H, CH ₂ -NH), 3.00 (br s, 4H, 2,6ppz), 2.56-2.52 (m, 4H, 3,5ppz) 2.40 (t, <i>J</i> = 6.7 Hz, 2H, ppzN-CH ₂), 1.72 – 1.48 (m, 4H, ppzN-CH ₂ -CH ₂ -).		
¹³ C NMR (75 MHz, DMSO- <i>d</i> ₆)	δ 164.21 (C=O), 157.40 (4C BrMeOPh), 151.93 (2C MeOPh), 141.26 (1C MeOPh), 131.72 (2C BrMeOPh),, 128.40 (1C BrMeOPh), 128.08 (5C MeOPh), 122.27 (4C MeOPh), 120.79 (6C BrMeOPh), 117.82 (3C MeOPh), 112.03 (3C BrMeOPh), 111.87 (5CBrMeOPh), 110.20 (6C MeOPh), 57.60(2C 6C ppz), 56.46 (3C 5C ppz), 55.27 (OCH ₃ MeOPh), 53.01 (OCH ₃ BrMeOPh), 50.04,(ppzN-C), 27.04, (ppzN-C-C), 23.80. (ppzN-C-C-C).		
MS (APCI (+)): m/z [M+H] ⁺	calculated:	476.2; 478.2	found: 476.0; 478.0
Elemental Analysis	calculated:	%C 57.99	%H 6.35 %N 8.82
	found:	%C 57.83	%H 6.38 %N 8.68

***N*-{4-[4-(2-Methoxyphenyl)piperazin-1-yl]butyl}-4-(pentafluoro- λ^6 -sulfaneyl)benzamide (ST-2200):**
4⁴⁰⁰

P16 (0.36 mmol, 96 mg) was dissolved in DCM. To a solution, 4-(pentafluoro- λ^6 -sulfaneyl)benzoic acid (0.40 mmol, 100 mg) HOBt (0.40 mmol, 62 mg) EDC (0.40 mmol, 62 mg) were added according to the procedure **D**. Crude product was purified with column chromatography (Sorbent SiO₂ Eluent: DCM: MeOH 95:5). White solid. Yield: 46%.

Chemical formula: C₂₂H₂₈F₅N₃O₂S

Mr: 493.54
 Melting point: 137.7 °C
 Internal code: ME 041



¹H NMR(300 MHz, DMSO-*d*₆) δ 8.74 (t, *J* = 5.7 Hz, 1H, CONH), 8.02 (s, 4H, SF₅Ph), 6.95 – 6.83 (m, 4H, MeOPh), 3.76 (s, 3H, -OCH₃Ph), 3.29 (t, *J* = 6.4, 5.1 Hz, 2H, -CH₂NH), 3.01 – 2.88 (br s, 4H, 2,6ppz), 2.45-2.50 (m, 4H, 3,4ppz), 2.35 (d, *J* = 8.5 Hz, 2H, ppzN-CH₂), 1.64 – 1.45 (m, 4H, ppzN-CH₂-CH₂).

¹³C NMR (75 MHz, DMSO-*d*₆) δ 164.43, (C=O), 157.10 (4C SF₅Ph), 151.93 (2C MeOPh), 141.24 (1C SF₅Ph), 138.17 (1C MeOPh), 128.27 (5C MeOPh) 125.94 (2C 6C SF₅Ph), 122.28 (3C 5C SF₅Ph), 120.7 (6C MeOPh), 117.82 (4C MeOPh), 111.87 (3C MeOPh), 57.55 (2C 6C ppz), 55.27 (3C 5C ppz), 52.9 (OCH₃), 50.02 (C-NH), 40.0 (ppz N-C), 26.90 (C-CN), 23.74 (ppzNC-C)

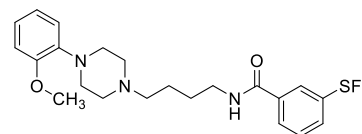
MS- (APCI(+)) : m/z [M+H]⁺
 calculated: 494.2 found: 494.9.
 Elemental Analysis
 calculated: %C 53.54 %H 5.72 %N 8.51 %S 6.50
 found: %C 53.50 %H 5.68 %N 8.38 %S 6.34

***N*-{4-[4-(2-Methoxyphenyl)piperazin-1-yl]butyl}-3-(pentafluoro- λ^6 -sulfaneyl)benzamide (ST-2201):**
5⁴⁰⁰

P16 (0.73 mmol, 193 mg) was dissolved in DCM. To a solution were added, 3-(pentafluoro- λ^6 -sulfaneyl)benzoic acid (0.81 mmol, 200 mg), HOBt (0.81 mmol, 123 mg) and EDC (0.81 mmol, 125 mg), according to the procedure **D**. Crude product was purified with column chromatography (Sorbent SiO₂ Eluent: DCM: MeOH 95:5). White solid. Yield: 41%.

Chemical formula: C₂₂H₂₈F₅N₃O₂S

Mr: 493.54
 Melting point: 123.2 °C
 Internal code: ME 043



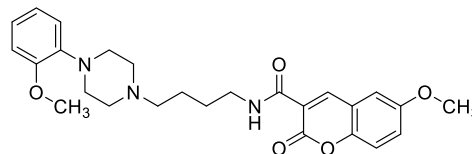
¹H NMR (300 MHz, DMSO-*d*₆) δ 8.82 (t, *J* = 5.6 Hz, 1H, CONH), 8.32 (t, *J* = 1.9 Hz, 1H, 2SF₅Ph), 8.19 – 8.02 (m, 2H, 4,6 SF₅Ph), 7.73 (t, *J* = 8.0 Hz, 1H, 5SF₅Ph), 6.99 – 6.83 (m, 4H, MeOPh), 3.76 (s, 3H, -OCH₃), 3.33 – 3.28 (m, 2H, CH₂-NH), 3.02 – 2.88 (br s, 4H, 2,6ppz), 2.52-2.60 (m, 4H, 3,5ppz) 2.38 (t, *J* = 6.8 Hz, 2H, ppzN-CH₂), 1.64 – 1.45 (m, 4H, ppzN-CH₂-CH₂-CH₂-).

^{13}C NMR (75 MHz, DMSO- d_6)	δ 164.01 (C=O), 152.78 (3C SF ₅ Ph), 151.92 (2C MeOPh), 141.16 (1C MeOPh), 135.66 (1C SF ₅ Ph), 131.06 (6C SF ₅ Ph), 129.77 (5C SF ₅ Ph), 128.21 (4C SF ₅ Ph), 124.28 (5C MeOPh), 122.33 (2 C SF ₅ Ph), 120.7 (4C MeOPh), 117.82 (3C MeOPh), 111.86 (6C MeOPh), 57.44 (2C 6C ppz), 55.25 (3C 5C ppz), 52.9 (OCH ₃) 49.89 (ppzN-C) 40.03 (C-NH), 26.86 (ppz NC-C-C) 23.64 (ppz NC-C);				
MS- (APCI-+): m/z [M+H] ⁺	calculated:	494.2	found:	494.9	
Elemental Analysis	calculated:	%C53.54	%H5.72	%N8.51	%S6.50
	found:	%C53.24	%H5.87	%N8.25	%S6.24

6-Methoxy-*N*-{4-[4-(2-methoxyphenyl)piperazin-1-yl]butyl}-2-oxo-2*H*-chromene-3-carboxamide (ST-2221): 6⁴⁰⁰

P16 (0.93 mmol, 245 mg) was dissolved in DCM. To a solution were added 6-methoxy-2-oxo-2*H*-chromene-3-carboxylic acid (0.45 mmol, 100 mg), HOBt (0.54 mmol, 84 mg) and EDC (0.54 mmol, 8 mg, according to the procedure **D**). Crude product was purified with column chromatography (sorberent SiO₂, eluent: DCM: MeOH 95:5). Light orange solid. Yield: 67%.

Chemical formula :	C ₂₆ H ₃₁ N ₃ O ₅
Mr:	465.55
Melting point:	140.4°C
Internal code:	ME 049

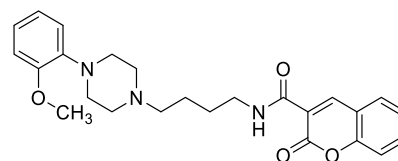


^1H NMR(300 MHz, DMSO- d_6)	δ 8.82 (s, 1H, 4coum), 8.73 (t, J = 5.7 Hz, 1H, CONH), 7.56 (d, J = 3.0 Hz, 1H, 8coum), 7.46 (d, J = 9.1 Hz, 1H, 5coum), 7.34 (dd, J = 9.1, 3.0 Hz, 1H, 7coum), 6.99 – 6.81 (m, 4H, MeOPh), 3.82 (s, 3H, -OCH ₃ (MeOPh)), 3.76 (s, 3H, -OCH ₃ (coum)), 3.36 (m, 2H, CH ₂ NH), 2.95 (br s, 2,6ppz), 2.51 (m, 4H, 3,5ppz) 2.36 (m, 2H, ppzN-CH ₂ -CH ₂ -CH ₂ -)			
^{13}C NMR (75 MHz, DMSO- d_6)	δ 161.03 (C=O), 160.53(2C coum), 155.92 (10C coum), 151.93 (2C MeOPh), 148.31 (1C MeOPh), 147.11 (4C coum), 128.11 (6C coum), 122.30 (8C coum) 121.86 (7C coum), 120.79 (5C MeOPh), 119.24 (5C coum), 117.84 (6c MeOPh), 117.23 (4C MeOPh), 117.05 (3C coum), 111.86 (9C coum), 56.65 (2C 6C ppz), 55.82(3C 5C ppz), 55.25 (ppzN-C), 52.95(C-NH).49.98 (OCH ₃ MeOPh), 40.54 (OCH ₃ coum), 26.90 (ppzNC-C),23.60(C-C-NH).			
MS-(APCI-+): m/z [M+H] ⁺	calculated:	466.2;	found:	466.3;
Elemental Analysis:	calculated:	%C 67.08	%H 6.71	%N 9.03
	found:	%C 66.81	%H 6.67	%N 8.90

***N*-{4-[4-(2-Methoxyphenyl)piperazin-1-yl]butyl}-2-oxo-2*H*-chromene-3-carboxamide (ST-2220):**7^{400,621,634}

P16 (0.51 mmol, 134 mg) was dissolved in DCM. To a solution were added, 2-oxo-2*H*-chromene-3-carboxylic acid (0.56 mmol, 107 mg), HOBt (0.56 mmol, 86 mg) and EDC (0.56 mmol, 86 mg) according to the procedure **D**. Crude product was purified with column chromatography (sorberent SiO₂, eluent: DCM: MeOH 95:5). Yellow powder. Yield: 39%.

Chemical formula: C₂₅H₂₉N₃O₄
 Mr: 435.52
 Melting point: 122.5 °C
 Internal code: ME 058



¹H NMR (300 MHz, DMSO-*d*₆) δ 8.85 (s, 1H, 4coum), 8.69 (t, *J* = 5.8 Hz, 1H, CONH), 7.99 (dd, *J* = 7.8, 1.6 Hz, 1H, 5coum), 7.75 (td, *J* = 8.7, 7.3, 1.7 Hz, 1H, 7coum), 7.54 – 7.39 (m, 2H, 6,8coum), 6.97 – 6.79 (m, 4H, MeOPh), 3.76 (s, 3H, -OCH₃ (MeOPh)), 3.35-3.40 (t, 7.3 Hz 2H, CH₂CONH), 2.99 – 2.89 (br s, 4H, 2,6ppz), 2.45-2.50 (m, 4H, 3,5ppz), 2.35 (t, *J* = 6.7 Hz, 2H, ppzN-CH₂), 1.62 – 1.38 (m, 4H, ppzN-CH₂-CH₂-CH₂-).

¹³C NMR (75 MHz, DMSO-*d*₆) δ 161.01 (C=O), 160.38 (2C coum), 153.81 (10C coum), 151.93 (2C MeOPh), 147.19 (1C MeOPh), 141.24 (5C coum), 133.97 (6C coum), 130.18 (8C coum), 125.09 (7C coum), 122.28 (5C MeOPh), 120.79 (4C MeOPh), 119.20 (6c MeOPh), 118.47 (4C coum), 117.83 (3C MeOPh), 116.10 (3C coum), 111.87 (9C coum), 57.50 (2C 6C ppz), 55.27 (3C 5C ppz), 52.99 (ppzN-C), 50.03 (C-NH), 40.03 (OCH₃), 26.95 (ppzNC-C), 23.65 (C-CN)

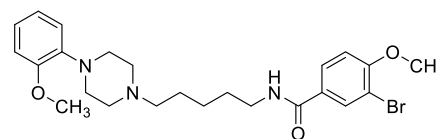
MS- (APCI-+): (m/z) [M+H]⁺ calculated: 436.2; found: 436.1;

LC-MS (ESI-+) m/z [M+H]⁺ 97.14% (436.14)

3-Bromo-4-methoxy-*N*-{5-[4-(2-methoxyphenyl)piperazin-1-yl]pentyl}benzamide (ST-2219): 8⁴⁰⁰

P16 (4.04 mmol, 1.121 g) was dissolved in DCM. To a solution were added 3-bromo-4-methoxybenzoic acid (4.46 mmol, 1.030 g) HOBt (4.46 mmol, 0.610 g) and EDC (4.46 mmol, 0.690 g), according to the procedure **D**. Crude product was purified with column chromatography (Sorberent SiO₂ Eluent: DCM:MeOH 95:5). White solid. Yield: 30%.

Chemical formula: C₂₄H₃₂BrN₃O₃
 Mr: 490.44
 Melting point: 110.7 °C
 Internal code: ME 068



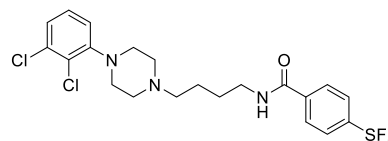
¹H NMR (600 MHz, DMSO-*d*₆) δ 8.42 (t, *J* = 5.6 Hz, 1H, CONH), 8.09 (d, *J* = 2.2 Hz, 1H, 2BrMeOPh), 7.88 (dd, *J* = 8.6, 2.2 Hz, 1H, 6BrMeOPh), 7.18 (d, *J* = 8.7 Hz, 1H, 5BrMeOPh), 6.96 – 6.80 (m, 4H, MeOPh), 3.90 (s, 3H, -OCH₃ (BrMeOPh)), 3.76 (s, 3H, -OCH₃ (MeOPh)), 3.24 (m, 2H, CH₂CONH), 3.00 – 2.87 (br s, 4H, 2,6ppz), 2.45-2.50 (m, 4H, 3,5ppz), 2.32 (bs, 2H, ppzN-CH₂), 1.58 – 1.44 (m, 4H, HN-CH₂-CH₂-CH₂), 1.36 – 1.27 (m, 2H, ppzN-CH₂-CH₂).

^{13}C NMR (151 MHz, DMSO- d_6)	δ 164.68 (C=O), 157.91 (4C BrMeOPh), 152.43, (2C MeOPh), 141.73 (1C MeOPh), 132.22 (2C BrMeOPh), 128.91 (1C BrMeOPh), 128.59 (5C MeOPh), 122.79 (4C MeOPh), 121.29 (6C BrMeOPh), 118.32 (3C MeOPh), 112.52 (3C BrMeOPh), 112.37 (5C BrMeOPh), 110.71 (6C MeOPh), 58.27 (2C 6C ppz), 56.97 (3C 5C ppz) 55.77 (OCH ₃ MeOPh), 53.49 (OCH ₃ BrMeOPh), 50.47 (ppzN-C), 40.54 (NH-C), 29.42 (ppzNC-C), 26.39 (C-CN _H), 24.81(ppzNCC-C)-
MS (APCI(+)) m/z [M+H] ⁺	calculated: 490.2; 492.2 found: 490.2; 492.1
LC-MS (ESI(+))	95.08%
m/z [M+2H] ²⁺ . [M+H] ⁺	(245.38;492.04)

***N*-{4-[4-(2,3-Dichlorophenyl)piperazin-1-yl]butyl}-4-(pentafluoro- λ^6 -sulfaneyl)benzamide (ST-2236): **9**⁴⁰⁰**

P16 (0.66 mmol, 200 mg) was dissolved in DCM. To a solution were added, 4-(pentafluoro- λ^6 -sulfaneyl)benzoic acid (0.73 mmol, 181 mg), HOBT (0.73 mmol, 111 mg) and EDC (0.73 mmol, 113 mg) according to the procedure **D**. Crude product was purified with column chromatography (Sorberent SiO₂ Eluent: DCM: MeOH 95:5). White solid. Yield: 30%.

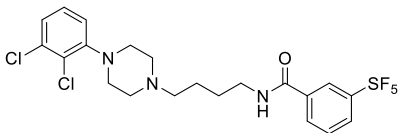
Chemical formula:	C ₂₁ H ₂₄ Cl ₂ F ₅ N ₃ OS
Mr:	532.40
Melting point:	129.0 °C
Internal code	ME 073



^1H NMR (300 MHz, DMSO- d_6)	δ 8.73 (t, J = 5.4 Hz, 1H, CONH), 8.02 (br s, 4H, SF ₅ Ph), 7.36 – 7.25 (m, 2H, 5,6diClPh), 7.13 (dd, J = 6.0, 3.6 Hz, 1H, 4diClPh), 3.29 (t, 2H, CH ₂ -NH), 3.04 – 2.92 (br s, 4H, 2,6ppz), 2.5-2.60(m, 4H, 3,5ppz), 2.37 (t, J = 6.7 Hz, 2H, ppzN-CH ₂), 1.63 – 1.44 (m, 4H, ppz N-CH ₂ -CH ₂ -CH ₂).
^{13}C NMR (151 MHz, DMSO- d_6)	δ 164.96 (C=O), 151.68 (1C diClppz), 138.67 (4C SF ₅ Ph), 133.08 (3C diClppz), 128.91 (1C SF ₅ Ph), 128.78 (5C SF ₅ Ph), 126.46 (3CF ₃ Ph), 126.46 (5C diClppz), 124.79 (2C diClppz), 119.99 (4C diClppz), 57.89 (2C 6C ppz), 53.26 (3C 5C ppz) 51.41 (ppzN-C), 40.52 (C-NH ₂), 27.37 (C-CN _H), 24.20.1 (ppzN-C-C)
MS- (APCI(+)): m/z [M+H] ⁺	calculated: 532.1; 534.1 found: 532.1; 534.1
LC-MS (ESI(+)) m/z [M+H] ⁺	96.80% (531.95)

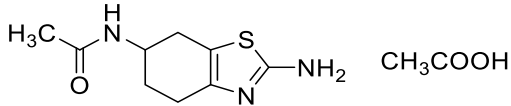
***N*-{4-[4-(2,3-Dichlorophenyl)piperazin-1-yl]butyl}-3-(pentafluoro- λ^6 -sulfaneyl)benzamide (ST-2237): 10⁴⁰⁰**

P16 (0.66 mmol, 200 mg) was dissolved in DCM To a solution were added 3-(pentafluoro- λ^6 -sulfaneyl)benzoic acid (0.73 mmol, 181 mg) HOBT (0.73 mmol 111 mg) and EDC (0.73 mmol, 113 mg), according to the procedure **D**. Crude product was purified with column chromatography (Sor bent SiO₂ Eluent: DCM: MeOH 97:3). Beige solid. Yield: 39%.

Chemical formula:	C ₂₁ H ₂₄ Cl ₂ F ₅ N ₃ OS	
Mr:	532.40	
Melting point:	104.8°C	
Internal code:	ME 074	
¹ H NMR (300 MHz, DMSO- <i>d</i> ₆)	δ 8.80 (t, <i>J</i> = 5.3 Hz, 1H, CONH), 8.31 (d, <i>J</i> = 2.1 Hz, 1H, 2SF ₅ Ph), 8.22 – 8.02 (m, 2H, 4,6SF ₅ Ph), 7.72 (t, <i>J</i> = 8.0 Hz, 1H, 5SF ₅ Ph), 7.34 – 7.24 (m, 2H, 5,6diClPh), 7.17 – 7.06 (m, 1H; 4diClPh), 3.30 (t, <i>J</i> = 5.9 Hz, 2H, CH ₂ -CONH), 3.06 – 2.89 (br s, 4H, 2,6ppz), 2.51-2.55 (m, 4H, 3,5ppz) 2.36 (t, <i>J</i> = 6.7 Hz, 2H, ppzN-CH ₂), 1.68 – 1.41 (m, 4H, CH ₂ -CH ₂ -NH).	
¹³ C NMR (75 MHz, DMSO- <i>d</i> ₆)	δ 164.01 (C=O), 153.13 (2C SF ₅ Ph), 151.18 (1C diClPh), 135.67 (3C diClPh), 132.58 (1C SF ₅ Ph), 131.0 (6C F ₅ Ph), 129.77 (5C SF ₅ Ph), 128.38 (4C SF ₅ Ph), 128.21, (6C SF ₅ Ph), 125.96 (5C diClPh), 124.50 (4C diClPh) 124.29 (2C diClPh), 119.45 (6C diClPh), 57.39 (2C 6C ppz), 52.77 (3C 5C ppz), 50.91 (ppzN-C), 40.03 (C-NH), 26.88 (ppzNC-C) 23.75.(C-CNH)	
MS- APCI-(+) m/z [M+H] ⁺ :	calculated: 532.1;534.1	found: 532.1;534.1
LC-MS (ESI-(+)) m/z [M+H] ⁺ :	95.63% (531.96)	

***N*-(2-Amino-4,5,6,7-tetrahydrobenzo[*d*]thiazol-6-yl)acetamide: P20⁶³⁵**

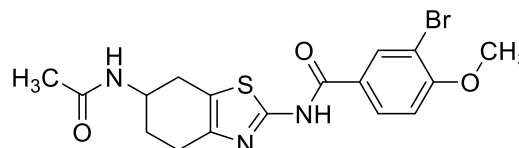
N-(4-Oxocyclohexyl)acetamide (**P19**) was dissolved in 10 mL CH₃COOH. The solution was heated up to 65 °C. Bromine was added dropwise, until reaction mixture changed color from red to yellow. Upon bromine addition, the reaction mixture was stirred at room temperature for another hour. Consequently, thiourea was added and the reaction mixture was refluxed for 3 hours. The reaction mixture was filtered, evaporated under reduced pressure, and dried under high vacuum overnight. On the following day, precipitate was suspended in water and lyophilized (2x) to remove CH₃COOH rest, resulting in **P20**. Light grey powder. Yield: 70%.

Chemical formula:	C ₁₁ H ₁₇ N ₃ O ₃ S	
Mr (free base):	211.28	
Mr (salt):	271.34	
Internal code:	ME 077	
¹ H NMR (300 MHz, DMSO- <i>d</i> ₆)	δ 9.11 (s, 1H, NH ₃ ⁺), 7.99 (d, <i>J</i> = 7.6 Hz, 1H, NH-CO), 4.13 – 3.95 (m, 1H, 6thiaCH), 2.77 (dd, <i>J</i> = 16.3, 5.2 Hz, 1H, 4thiaCH) 2.70-2.65 (m, 2H, 4thia CH, 7thiaCH), 2.41 – 2.22 (m, 1H, 7thia CH), 1.94-1.84 (m, 1H, 5thiaCH), 1.82 (s, 3H, CH ₃), 1.71 (ddd, <i>J</i> = 16.2, 13.6, 7.2 Hz, 1H, 5thiaCH).	
MS- (APCI-(+)): m/z [M+H] ⁺ :	calculated: 212.1	found: 211.9

***N*-(6-Acetamido-4,5,6,7-tetrahydrobenzo[*d*]thiazol-2-yl)-3-bromo-4-methoxybenzamide (ST-2304): 11**

P20 (1.94 mmol, 412 mg) was dissolved in DCM. To a solution, 3-bromo-4-methoxybenzoic (2.13 mmol, 494 mg), HOBt (2.13 mmol, 288 mg) and EDC (2.13 mmol, 331 mg) were added, according to the procedure **D**. Crude product was purified by flash column chromatography (sorberent: SiO₂, eluent DCM:MeOH 95:5) White solid. Yield: 29%.

Chemical formula: C₁₇H₁₈BrN₃O₃S
Mr: 424.31
Melting point: 264.7 °C
Internal code: ME 119



¹H NMR (300 MHz, DMSO- *d*₆) δ 12.5 (bs, 1H, NHCO-BrMeOPh) 8.34 (d, *J* = 2.2 Hz, 1H, -CONH thia), 8.13 (dd, *J* = 8.7, 2.2 Hz, 1H, 6BrMeOPh), 7.98 (d, *J* = 7.6 Hz, 1H; 2BrMeOPh), 7.25 (d, *J* = 8.8 Hz, 1H, 3BrMeOPh), 4.04 (t, 1H; 6thiaCH), 3.94 (s, 3H -OCH₃), 2.94 (dd, *J* = 16.0, 5.3 Hz, 1H; 4thiaCH), 2.70 (q, *J* = 8.6, 7.1 Hz, 1H, 4thiaCH), 2.61 – 2.52 (m, 2H, 7thia CH₂), 2.00 – 1.84 (m, 1H, 5thiaCH), 1.82 (s, 3H; -CH₃), 1.81 – 1.71 (m, 1H 5thiaCH).

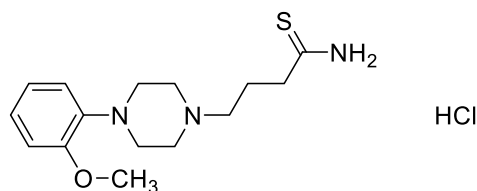
¹³C NMR (75 MHz, DMSO- *d*₆) δ 168.72 (C=O thia), 166.80 (C=O, thia), 158.52 (9C thia), 132.74 (4C BrPh) 129.47 (1C BrPh), 119.55 (2C thia), 112.29 (2C BrPh), 110.54 (3C BrPh), 56.66 (6Cthia) 44.6 (OCH₃) 28.37 (5Cthia), 28.15 (7Cthia), 23.96 (4Cthia), 22.68 (CH₃).

MS- (APCI(+)): *m/z* [M+H]⁺: calculated 424.0; 426.0 found: 423.7; 425.8
LC-MS (ESI(+)) *m/z* [M+H]⁺: 96.49%(423.99)

4-[4-(2-Methoxyphenyl)piperazin-1-yl]butanethioamide hydrochloride: P21

P11 (15.2 mmol, 3.9652 g) and *O,O'*-diethyl-dithiophosphate (15.2 mmol, 2.8473 g) were dissolved in 4M HCl in 1,4-dioxane, according to the procedure **F**. White solid. Yield: 71%.

Chemical formula: C₁₅H₂₄ClN₃OS
Mr (free base): 293.43
Mr (salt): 329.89
Internal code: ME 253



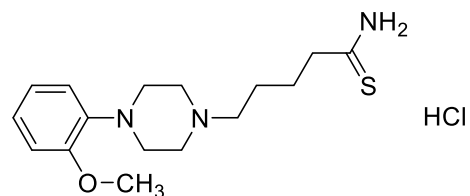
¹H NMR (300 MHz, DMSO- *d*₆) δ 10.88 (s, 1H NH₃⁺), 6.42 – 6.15 (m, 4H, MeOPh), 5.02 (br s, 2H NH₂), 3.09 (s, 3H, -OCH₃), 2.84 – 2.68 (m, 6H, 2:6ppz, ppzN-CH₂, CH₂-CS), 2.5-2.60 (br.s 4H, 3; 5ppz) 1.69 – 1.19 (m, 2H, ppzNC-CH₂).

MS (APCI(-)): *m/z* [M-H]⁺: calculated: 292.2; 293.5 found: 292.5 ; 293.6

5-[4-(2-Methoxyphenyl)piperazin-1-yl]pentanethioamide hydrochloride: P22⁶³⁶

Compound **P13** (14.8 mmol, 4.0326 g) and *O,O'*-Diethyl-dithiophosphate (14.8 mmol, 2.7562 g) were dissolved in 4M HCl in 1,4-dioxane, according to the procedure **F**. White solid. Yield: 50%.

Chemical formula: C₁₆H₂₆ClN₃OS
 Mr (free base): 307.46
 Mr (salt): 343.96
 Internal code: ME 255

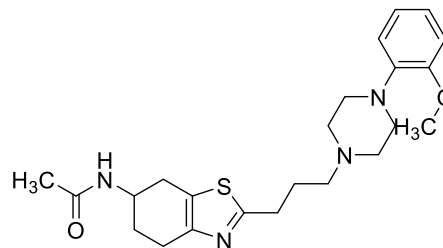


¹H NMR (300 MHz, DMSO *d*₆) δ 11.28 (s, 1H, NH₃⁺), 7.14 – 6.80 (m, 4H MeOPh), 4.76 (s, 2H, NH₂), 3.80 (s, 3H, OCH₃), 3.52 – 3.38 (m, 4H, 2;6ppz) 2.50-2.90 (m, 8H, 3;5ppz, ppzN-CH₂, CH₂-CS), 1.99 – 1.60 (m, 4H ppzNC-CH₂CH₂).
 MS (APCI(+)): m/z [M+H]⁺: calculated: 308.1;309.1 found: 308.4;309.4

***N*-{2-[3-(4-(2-Methoxyphenyl)piperazin-1-yl)propyl]-4,5,6,7-tetrahydrobenzo[*d*]thiazol-6-yl}acetamide (ST-2410): 12**

According to the procedure **G**, from *N*-(4-oxocyclohexyl)-acetamide (**P19**, 13.6 mmol, 2.1139 g), bromine (13.6 mmol, 2.1735 g, 0.7 mL) and **P11**(10.88 mol, 3.5892 g). Crude product was purified with column chromatography (sorbent SiO₂, eluent DCM:MeOH(NH₃)93:7) Yellow solid. Yield: 22%.

Chemical formula: C₂₃H₃₂N₄O₂S
 Mr: 428.60
 Internal code: ME 257

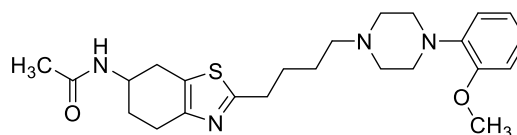


¹H NMR (300 MHz, DMSO *d*₆) δ 7.97 (d, *J* = 7.4 Hz, 1H, CONH), 6.99 – 6.82 (m, 4H, MeOPh), 4.12 – 3.93 (m, 1H 6thiaCH), 3.76 (s, 3H, -OCH₃), 3.03 – 2.86 (m, 7H, 2,6ppz, 2thiaCH₂, 4thiaCH), 2.82 – 2.64 (m, 2H, 4thiaCH, 7thiaCH), 2.52-2.60 (m, 2H, 7thiaCH, 5thiaCH), 2.45-2.50 (m, 4H, 3,5ppz), 2.39 (t, *J* = 7.0 Hz, 2H, N-CH₂), 1.92 – 1.83 (m, 2H, ppzNC-CH₂), 1.81 (s, 3H, -CH₃), 1.78 – 1.69 (m, 1H, 5thiaCH).
¹³C NMR (75 MHz, DMSO *d*₆) δ 168.74, (C=O), 167.36 (9Cthia), 151.94 (2C MeOPh), 148.43 (1C MeOPh), 141.25 (2Cthia), 125.32 (8Cthia), 122.29 (5C MeOPh), 120.81 (6C MeOPh), 117.85 (4C MeOPh), 111.87 (3C MeOPh), 56.79, (ppzN-C) 55.27 (OCH₃), 52.94 (2C 6C ppz) 50.06 (3C 5C ppz), 44.73 5C (6Cthia), 30.65 (2Cthia-C), 28.90 (5Cthia), 28.09 9(7Cthia), 26.53 (4C thia), 24.30 (ppzNC-C), 22.67 (CH₃).
 MS (APCI(+)): m/z [M+H]⁺: calculated: 429.2, 430.3 found: 429.3;430.3
 LC-MS (ESI(+)) m/z 100%
 [M+2H]²⁺ [M+H]⁺: (215.06; 429.29)

***N*-(2-{4-[4-(2-Methoxyphenyl)piperazin-1-yl]butyl}-4,5,6,7-tetrahydrobenzo[*d*]thiazol-6-yl)acetamide (ST-2411): 13**

According to the procedure **G** from *N*-(4-oxocyclohexyl) acetamide (**P19**, 13.6 mol 2.1139 g), bromine (13.6 mmol, 2.1735 g, 0.7 mL) and **P22** (10.2 mol, 2.3906 g) Crude product was purified with column chromatography (sorbent SiO₂, eluent DCM:MeOH(NH₃)95:5) Yellow solid. Yield: 22%.

Chemical formula: C₂₄H₃₄N₄O₂S
Mr: 442.62
Internal code: ME 256



¹H NMR (300 MHz, DMSO- *d*₆) δ 7.97 (d, *J* = 7.4 Hz, 1H, CONH), 6.99 – 6.82 (m, 4H, MeOPh), 4.11 – 3.95 (m, 1H, 6thiaCH), 3.77 (s, 3H, -OCH₃), 3.04 – 2.83 (m, 7H, 4H 2,6ppz, 2thiaCH₂, 4CthiaCH), 2.80 – 2.53 (m, 3H, 4thiaCH, ppzN-CH₂), 2.41 – 2.20 (m, 4H, 3,5ppz), 2.06 – 1.83 (m, 2H, 7thiaCH₂), 1.82 (s, 3H, -CH₃), 1.76 – 1.47 (m, 6H, 5thiaCH₂, 2thiaC-CH₂-CH₂).

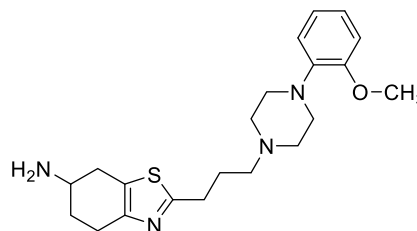
¹³C NMR (75 MHz, DMSO *d*₆) δ 168.73 (C=O), 167.52(9C thia), 151.93 (2C MeOPh), 148.42 (1C MeOPh), 141.26, (2C thia), 125.26 (5C MeOPh), 122.27 (4C MeOPh), 120.80 (6C MeOPh), 117.84 (3C MeOPh), 111.87 (8C thia), 55.27 (ppzN-C), 53.01 (2C, 6C ppz), 50.06 (3C, 5C ppz) 44.72 (OCH₃), 38.45 (6Cthia), 32.47 (2Cthia-C), 31.08 (7Cthia), 28.90 (ppzNC-C), 28.07 (5Cthia), 27.30 (4Cthia), 25.62(ppz NCC-C), 22.67 (CH₃)

MS (APCI(+)) *m/z* [M+H]⁺: calculated 443.2; 444.2 found 443.8; 444.8
LC-MS (ESI(+))
m/z [M+2H]²⁺: [M+H]⁺: 98.21%
(222.08, 443.32)

2-{3-[4-(2-Methoxyphenyl)piperazin-1-yl]propyl}-4,5,6,7-tetrahydrobenzo[*d*]thiazol-6-amine (ST-2412): 14

Compound **12** (2.095 mmol, 898 mg) was dissolved in concentrated HCl (37 %) and treated according to the procedure **H**. Crude product was purified with column chromatography (sorbent SiO₂, eluent DCM:MeOH(NH₃) 93:7). Yellow solid. Yield: 61%.

Chemical formula: C₂₁H₃₀N₄OS
Mr: 386.56
Internal code: ME 259



¹H NMR (300 MHz, DMSO *d*₆) δ 7.02 – 6.82 (m, 4H, MeOPh), 3.76 (s, 3H, -OCH₃), 3.13 – 3.02 (m, 1H, 6thiaCH), 3.02 – 2.82 (m, 7H, 4thiaCH₂, 7thiaCH, 2,6ppz), 2.82 – 2.57 (m, 3H, ppzN-CH₂, 7thiaCH), 2.45-2.50 (m, 4H, 3,5ppz); 2.38 (m, 4H, NH₂, 2CthiaCH₂), 1.95 – 1.74 (m, 2H, 5thiaCH₂), 1.66 – 1.41 (m, 2H, CH₂-CNppz).

¹³C NMR (75 MHz, DMSO *d*₆) δ 166.87 (9Cthia), 151.94 (2C MeOPh), 148.60 (2C thia), 141.25 (1C MeOPh), 126.10 (5C MeOPh), 122.29 (6C MeOPh), 120.81 (4C MeOPh), 117.85 (3C MeOPh), 111.88, (8C thia) 56.81 (ppzN-C), 55.28 (2C, 6C ppz), 52.94(3C 5C ppz) 50.06 (6C thia), 47.36

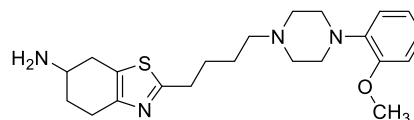
	(OCH ₃), 32.43 (2thiaC-C), 32.06 (5C thia)2, 30.48,(7C thia)
	26.56,(4C thia) 24.67 ppz (NC-C)
MS (APCI(+)): m/z [M+H] ⁺ :	Calculated 387.2;388.2 Found 387.3;388.3
LC-MS (ESI(+))	95.56%
m/z [M+2H] ²⁺ [M+H] ⁺ :	(185.54; 387.26)

2-{4-[4-(oxyphenyl)piperazin-1-yl]butyl}-4,5,6,7-tetrahydrobenzo[d]thiazol-6-amine (ST-2413): 15

Compound **13** (1.615 mmol, 714 mg), was reflux in HCl (37%) according to the procedure **H**. Crude product was purified with column chromatography (Sorbent SiO₂ Eluent DCM:MeOH(NH₃)93:7). Yellow solid.

Yield: 38%.

Chemical formula:	C ₂₂ H ₃₂ N ₄ OS
Mr:	400.59
Internal code:	ME 258

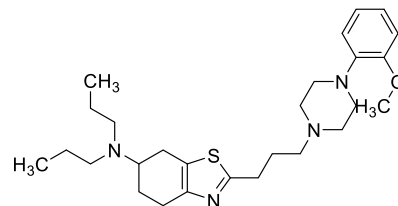


¹ H NMR (300 MHz, DMSO <i>d</i> ₆)	δ 7.00 – 6.72 (m, 4H, MeOPh), 3.76 (s, 3H, -OCH ₃), 3.16 – 3.04 (m, 2H, 2thia-CH ₂), 3.01 – 2.81 (m, 8H, 4thiaCH ₂ , 2,6ppz, 7thiaCH), 2.78 – 2.57 (m, 3H, 7thia CH, ppzN-CH ₂), 2.47 (s, 4H,3,5ppz), 2.33 (t, <i>J</i> = 7.1 Hz, 2H, NH ₂), 1.95 – 1.83 (m, 1H, 5thiaCH), 1.75 – 1.44 (m, 5H, 5thiaCH, 2thiaCH ₂ -CH ₂ -CH ₂)
¹³ C NMR (75 MHz, DMSO <i>d</i> ₆)	δ 167.12 (9C thia), 151.94 (2C MeOPh), 148.56 (2C thia), 141.26 (1C MeOPh), 125.89 (5C MeOPh), 122.28 (6C MeOPh), 120.80 (4C MeOPh), 117.84 (3C MeOPh), 111.87 (8C thia), 57.40 (ppzN-C), 55.27 (2C, 6C ppz), 53.01 (3C, 5C ppz), 50.06 (6C thia), 47.30 (OCH ₃), 32.47 (2Cthia-C), 32.10 (7C thia), 31.60 (5C thia), 27.32 (4C thia), 25.60(ppzNC-C), 24.61 (ppzNCC-C).
MS (APCI(+)): m/z [M+H] ⁺ :	Calculated 401.2; 402.2 found 401.3 402.3
LC-MS (ESI(+))	95.14%
m/z [M+2H] ²⁺ [M+H] ⁺ :	(192.54; 401:27)

2-{3-[4-(2-Methoxyphenyl)piperazin-1-yl]propyl}-*N,N*-dipropyl-4,5,6,7-tetrahydrobenzo[d]thiazol-6-amine (ST-2414): 16

Compound **14** (1.02 mmol, 396.9 mg) propionaldehyde (10.27 mmol, 593.6 mg) and Na[BH(CH₃COO)₃] (7.19 mmol, 1.523 g) were treated according to the procedure **E**. The crude product was purified with column chromatography (Sorbent SiO₂ Eluent DCM; MeOH(NH₃)95:5). Yellow oil. Yield: 48%.

Chemical formula:	C ₂₇ H ₄₂ N ₄ OS
Mr:	470.72
Internal code:	ME 266



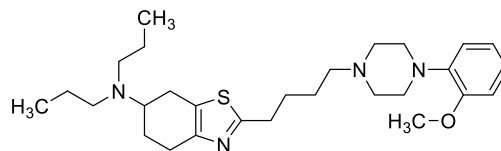
¹ H NMR (600 MHz, DMSO <i>d</i> ₆)	δ 6.96 – 6.83 (m, 4H, MeOPh), 3.76 (s, 3H, -OCH ₃), 3.17 (d, <i>J</i> = 5.2 Hz, 1H, 6thiaCH), 2.98 – 2.91 (m, 4H, 2,6ppz), 2.88 (t, <i>J</i> = 7.5 Hz, 2H, ppzN-CH ₂), 2.80 – 2.72 (m, 2H, 2thiaCH ₂), 2.68 – 2.55 (m, 4H, 3,5ppz), 2.50 – 2.46 (m, 6H, thiaN-CH ₂ , 4thiaCH ₂), 2.45 – 2.33 (m, 2H, 7thiaCH ₂), 1.94 – 1.88 (m, 1H, 5thiaCH), 1.83 (quin, <i>J</i> = 7.3 Hz,
---	--

^{13}C NMR (151 MHz, DMSO d_6)	2H, $\text{CH}_2\text{-CNppz}$), 1.71 – 1.61 (m, 1H, 5thiaCH), 1.37 (hept, $J = 7.2$ Hz, 4H, 2($\text{CH}_3\text{-CH}_2$)), 0.83 (m, 6H, 2 CH_3).
MS (APCI-(+)) m/z [$\text{M}+\text{H}^+$] $^+$:	δ 167.78 (9Cthia), 152.45 (2C MeOPh), 149.28 (2Cthia), 141.76 (1C MeOPh), 127.30 (5C MeOPh), 122.80 (6C MeOPh), 121.31 (4C MeOPh), 118.33 (3C MeOPh), 112.39 (8Cthia), 57.30 (ppzN-C), 55.78 (2C, 6C ppz), 53.43 (3C, 5C ppz), 52.40 (2thiaN-C), 50.56 (OCH_3), 31.02 (6C thia), 27.07(2Cthia-C), 26.71(7C thia), 25.81 (5C thia), 25.33 (ppzNC-C), 22.32 ($\text{CH}_3\text{C-C}$), 21.63 ($\text{CH}_3\text{-C}$), 12.18 (CH_3).
LC-MS (ESI-(+))	calculated 471.3;472.3 Found 471.5;472.5
m/z [$\text{M}+2\text{H}^+$] $^{2+}$ [$\text{M}+\text{H}^+$] $^+$:	96.86% (236.08; 471.34)

2-{4-[4-(2-Methoxyphenyl)piperazin-1-yl]butyl}-*N,N*-dipropyl-4,5,6,7-tetrahydrobenzo[d]thiazol-6-amine (ST-2415): 17

Compound **15** (0.75 mmol, 300 mg), propionaldehyde (7.49 mmol, 435 mg, 0.54 mL) and $\text{Na}[\text{BH}(\text{CH}_3\text{COO})_3]$ (5.24 mmol, 1.1111 g) were treated according to procedure **E**. Crude product was purified with column chromatography (sorbent SiO_2 , eluent $\text{DCM}:\text{MeOH}(\text{NH}_3)$ 93:7). Yellow oil. Yield: 24%.

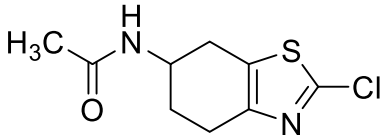
Chemical formula:	$\text{C}_{28}\text{H}_{44}\text{N}_4\text{OS}$
Mr:	484.75
Internal code:	ME 263



^1H NMR (300 MHz, DMSO- d_6)	δ 6.96 – 6.82 (m, 4H, MeOPh), 3.76 (s, 3H, OCH_3), 2.94 (br s, 4H, 2,6ppz), 2.87 (t, $J = 7.4$ Hz, 2H, ppzN- CH_2), 2.81 – 2.71 (m, 1H, 6thiaCH), 2.48 – 2.44 (m, 3H, 4thiaCH, 2thia- CH_2), 2.45 – 2.37 (m, 5H, 4H 3,5ppz, 4thiaCH), 2.33 (t, $J = 7.1$ Hz, 2H, 7thia CH_2), 1.91 (d, $J = 12.4$ Hz, 1H, 4thiaCH), 1.73 – 1.62 (m, 3H, 2thiaC-C- CH_2 , 5thiaCH), 1.57 – 1.45 (m, 3H, 5thiaCH), 1.37 (m, 6H, 2thiaC- CH_2 , (CH_3CH_2) $_2$), 0.84 (t, $J = 7.3$ Hz, 6H, (CH_3) $_2$).
^{13}C NMR (75 MHz, DMSO- d_6)	δ 167.41 (9Cthia), 151.93 (2C MeOPh), 148.77 (2C thia), 141.25, (1C MeOPh) 126.75 (5C MeOPh), 122.28 (6C MeOPh), 120.79 (4C MeOPh), 117.83 (3C MeOPh), 111.87 (8C thia), 57.41(ppzN-C), 56.66 (2C, 6C ppz), 55.26 (3C, 5C ppz), 53.00 (2thia-C), 51.89 (OCH_3), 50.05 (thiaN-C), 32.5 (6C thia), 27.35 (2thiaC-C), 26.7 (7C thia) 26.19 (5C thia), 25.56 (4C thia), 24.82 (ppzNC-C), 21.81($\text{CH}_3\text{-C}$), 11.68 (CH_3).
MS (APCI-(+)): m/z [$\text{M}+\text{H}^+$] $^+$:	calculated: 485.3;486.3 found: 485.5; 486.5
LC-MS (ESI-(+))	97.68%
m/z [$\text{M}+2\text{H}^+$] $^{2+}$ [$\text{M}+\text{H}^+$] $^+$:	(243.12;485.38)

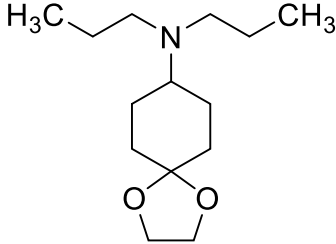
***N*-(2-Chloro-4,5,6,7-tetrahydrobenzo[*d*]thiazol-6-yl)acetamide: 18**

P20 (4.73 mmol, 1.00 g) was dissolved in concentrated HCl (37%). The solution was cooled down to -30°C. NaNO₂ solution (1M) was slowly added over 30 minutes. The reaction mixture was vigorously stirred for another hour at -30°C. Consequently, H₃PO₂ (50% in H₂O) was dropwise added and the reaction mixture was stirred overnight at -4°C. The reaction mixture was cooled down to -30°C and NaOH solution (40 %) was added on the following day. The reaction mixture was slowly heated up to the room temperature. It was further portioned between CHCl₃ and EtOH (5:1), dried over anhydrous MgSO₄ and evaporated under reduced pressure. Brown oil. Yield 10%.⁶³⁷

Chemical formula:	C ₉ H ₁₁ ClN ₂ OS			
Mr:	230.71			
Internal code:	ME 289			
¹ H NMR (300 MHz, DMSO- <i>d</i> ₆)	δ 7.99 (d, <i>J</i> = 7.4 Hz, 1H, CONH), 4.05 (m, 1H, 6thiaCH), 3.06 – 2.92 (m, 2H, 4thiaCH ₂), 2.78 – 2.70 (m, 2H, 7thia CH ₂), 1.95 – 1.85 (m, 2H, 5thiaCH ₂), 1.82 (s, 3H, CH ₃).			
¹³ C NMR (75 MHz, DMSO- <i>d</i> ₆) δ	168.77 (C=O), 148.33 (9Cthia), 129.45 (2C thia), 116.2 (8Cthia), 44.08 (6Cthia), 28.82 (5CThia), 27.56 (7Cthia), 24.03 (4Cthia), 22.64 (CH ₃).			
MS (APCI(+)): <i>m/z</i> [M+H] ⁺ :	calculated	231.0;232.0	found	231.0;232.1
LC-MS (ESI(+)) <i>m/z</i> [M+H] ⁺ :	99.32% (230.97)			

***N,N*-Dipropyl-1,4-dioxaspiro[4.5]decan-8-amine: P25⁶³⁸**

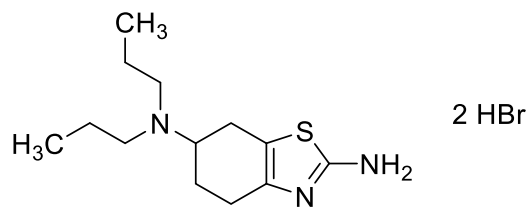
Compound **P24** (44.82 mmol, 7.00 g), dipropylamine (134.45 mmol, 13.45 g), and Na[BH(CH₃COO)₃] (67.23 mmol, 14.25 g) were treated according to the procedure **E**. The crude product was used without further purification. Yellow solid, Yield: 87%.

Chemical formula:	C ₁₄ H ₂₇ NO ₂			
Mr:	241.38			
Internal code:	ME 298			
¹ H NMR (300 MHz, DMSO- <i>d</i> ₆)	δ 3.82 (s, 4H, 4,5 spiroCH ₂), 2.46 (d, <i>J</i> = 7.3 Hz, 1H, 8spirpCH), 2.32 (t, <i>J</i> = 7.6 Hz, 4H, N-(CH ₂ CH ₂ CH ₃) ₂), 1.73 – 1.52 (m, 4H, 2,6spiroCH ₂), 1.51 – 1.39 (m, 4H, 1,7CH ₂), 1.38 – 1.26 (m, 4H, N(CH ₂ CH ₂ CH ₃) ₂), 0.82 (t, <i>J</i> = 7.3 Hz, 6H, N-(CH ₂ CH ₂ CH ₃) ₂).			
MS (APCI(+)): <i>m/z</i> [M+H] ⁺ :	calculated:	242.3	found:	242.5

***N,N*-Dipropyl-4,5,6,7-tetrahydrobenzo[*d*]thiazole-2,6-diamine dihydro bromide: P26⁶³⁹**

Compound **P25** (44.8 mmol, 10.8193g), bromine (44.8 mmol, 7.163g, 2.3 mL), and thiourea (44.8mmol, 3.4127g) were treated according to procedure **I**. Crude product was purified by crystallization in EtOH.

Chemical formula: C₁₃H₂₅Br₂N₃S
 Mr (free base): 253.41
 Mr (salt): 415.23
 Internal code: ME 300

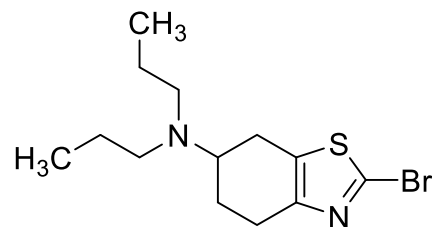


¹H NMR (300 MHz, DMSO *d*₆) δ 9.48 (bs, 2H, NH⁺, 2thia-NH₃⁺), 9.17 (bs, 2H, NH₂), 3.51 (m, 1H, 6thiaCH), 3.03 – 2.73 (m, 5H 4thia CH, N-(CH₂CH₂CH₃)₂), 2.72 – 2.54 (m, 1H, 4thiaCH), 2.47 – 2.34 (m, 2H 7thia CH₂), 2.11 (m, 1H, 5thiaCH), 1.82 – 1.63 (m, 1H, 5thiaCH), 1.60 – 1.39 (m, 4H, N-(CH₂CH₂CH₃)₂), 0.65 (t, *J* = 7.0 Hz, 6H, N-(CH₂CH₂CH₃)₂)
 MS (APCI(+)): m/z [M+H]⁺: calculated : 254.2;255.2 Found 254.4,254.5

2-Brom-*N,N*-dipropyl-4,5,6,7-tetrahydrobenzo[*d*]thiazol-6-amine: 19

Compound **P26** (7.42 mmol, 3.0657 g), CuBr₂ (11.13 mmol, 4.8522 g) and *tert*-butyl isonitrite (11.13 mmol, 1.1475 g) were treated according to the procedure **J**. Crude oil was purified with flash chromatography (sorbent SiO₂, eluent DCM:MeOH 95:5). Brown oil. Yield: 10%.

Chemical formula: C₁₃H₂₁BrN₂S
 Mr: 317.29
 Internal code: ME 358



¹H NMR (300 MHz, CDCl₃) δ 2.98 (m, 1H, 6thiaCH), 2.88 – 2.50 (m, 4H, 4thiaCH₂, 7thiaCH₂), 2.38 (m, 4H N-(CH₂CH₂CH₃)₂), 1.90-2.01 (m, 1H, 5thiaCH) 1.66 (dd, *J* = 12.1, 5.2 Hz, 1H, 5thiaCH), 1.39 (m, 4H N-(CH₂CH₂-CH₃)₂) .
¹³C NMR (75 MHz, DMSO-*d*₆) δ 150.24 (9C thia), 132.47 (2C thia), 132.01 (8C thia), 56.21 (thiaN-C), 51.83 (6C thia), 26.05 (5C thia), 25.09 (7C thia), 24.76 (4C thia), 21.72 (CH₃-C), 11.64 (CH₃).
 MS (APCI(+)): m/z [M+H]⁺: calculated: 317.1;319.1 found 317.1;319.1
 LC-MS (ESI(+)) m/z [M+H]⁺: 100% (317.00)

2-[4-(Benzyloxy)butoxy]-*N,N*-dipropyl-4,5,6,7-tetrahydrobenzo[*d*]thiazol-6-amine (ST-2469): 20

To the benzyloxyalcohol (9.93 mmol, 1.79 g) solution in 1,4-dioxane at room temperature NaH ($\omega=60\%$, 9.93 mmol, 238.4 mg) was added portionwise at room temperature. The reaction mixture was left to stir at room temperature for the next three hours. Consequently, to the reaction mixture was added **19** (3.15 mmol, 1.00 g) dissolved in 15 mL 1,4-dioxane solution, and the reaction mixture was stirred at 40°C overnight. On the following day, reaction was quenched by adding sat. solution of NH₄Cl (stirred for 15 minutes), evaporated under reduced pressure, and partitioned between DCM and H₂O. Organic layers were combined, washed with saturated NaHCO₃ solution, brine, dried over anhydrous MgSO₄ and evaporated under reduced pressure. Crude oil was purified by column chromatography (sorbent SiO₂, eluent DCM :MeOH(NH₃) 98:2). Yellow oil. Yield:15%.

Chemical formula:

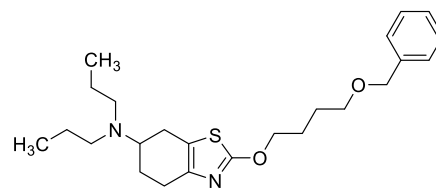
C₂₄H₃₆N₂O₂S

Mr:

416.62

Internal code:

ME 337

¹H NMR (300 MHz, CDCl₃)

δ 7.31 – 7.24 (m, 5H, Ph), 4.43 (s, 2H, O-CH₂-Ph), 4.26 (t, $J = 6.4$ Hz, 2thiaO-CH₂), 3.45 (td, $J = 6.0, 1.9$ Hz, 2H, PhCO-CH₂), 3.01 – 2.87 (m, 1H, 6thiaCH), 2.72 – 2.45 (m, 4H, 4thiaCH₂, 7thiaCH₂) 2.37 (dt $J = 7.2, 5.3$ Hz, 4H, N-(CH₂CH₂CH₃)₂), 1.93 (m, 1H, 5thiaCH), 1.87 – 1.75 (m, 2H, 2thiaOCC-CH₂), 1.74 – 1.58 (m, 3H, 5thiaCH, 2thiaOC-CH₂), 1.38 (sxt, 4H, N-(CH₂CH₂CH₃)₂), 0.81 (t, $J = 7.3$ Hz, 6H, N-(CH₂CH₂CH₃)₂).

¹³C NMR (75 MHz, DMSO-*d*₆)

δ 172.42 (2C thia), 143.26 (9C thia), 138.49 (2C Ph), 128.37 (2C, 6C Ph), 127.72 (4C Ph), 127.62 (3C,5C Ph), 127.53 (8C thia), 72.93 9 (Ph-C), 71.00 (PhCO-C), 69.74 (2thiaCO-C), 57.26 (N-C), 52.76 (6Cthia), 26.95 (5C thia), 26.16 (7C thia), 25.96 (4C thia), 25.79 (2thiaCOCC-C), 25.09(2thiaCOC-C), 22.31 (C-CH₃), 11.86 9 (CH₃).

MS (APCI(+)): m/z [M+H]⁺:

calculated 417.2;418.2 found 417.2;418.2

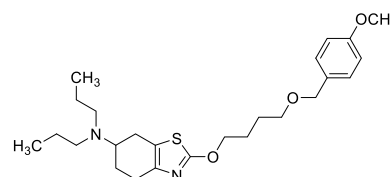
LC-MS (ESI(+)) m/z [M+H]⁺:

100% (417.24)

2-{4-[(4-Methoxybenzyl)oxy]butoxy}-*N,N*-dipropyl-4,5,6,7-tetrahydrobenzo[*d*]thiazol-6-amine (ST-2474): 21

According to procedure **K**, from PMB alcohol (1.15 mmol, 243 mg), NaH ($\omega=60\%$) (1.73 mmol, 42 mg), and consequently **19** (0.56 mmol, 180 mg) was added, and the reaction mixture was refluxed overnight. Crude oil was purified by column chromatography (sorberent SiO₂, eluent DCM :MeOH (NH₃) 95: 5). Yellow oil. Yield: 18%.

Chemical formula: C₂₅H₃₈N₂O₃S
Mr: 446.65
Internal code: ME 354-1



¹H NMR (600 MHz, CDCl₃) δ 7.25 (d, $J = 2.2$ Hz, 2H, 2,6Ph), 6.89 – 6.85 (m, 2H, 3,5Ph), 4.43 (s, 2H, Ph-CH₂-O), 4.32 (t, $J = 6.5$ Hz, 2H, 2thiaO-CH₂), 3.80 (s, 3H, -OCH₃), 3.49 (t, $J = 6.4$ Hz, 2H, PhCO-CH₂), 3.01 (m, 1H, 6thiaCH), 2.76 – 2.50 (m, 5H, 4thiaCH, N-(CH₂CH₂CH₃)₂), 2.49 – 2.37 (m, 4H, 4thiaCH, 7thia CH₂, 5thiaCH), 1.99 (m, 1H, 5thiaCH), 1.86 (tt, $J = 8.6, 6.6$ Hz, 2H, 2thiaOCC-CH₂), 1.76 – 1.72 (m, 2H, 2thiaOCC-CH₂), 1.44 (sxt, 4H, N-(CH₂CH₂CH₃)₂), 0.88 (t, $J = 7.3$ Hz, 6H, N-(CH₂CH₂CH₃)₂).

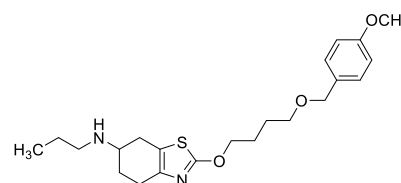
¹³C NMR (100 MHz, CDCl₃) δ 158.12 (4C Ph), 142.20 (9C thia), 141.40 (2C thia), 131.24 (1C MeOPh), 129.59 (2C, 6C Ph), 128.22 (4C Ph), 112.76 (3C, 5C Ph), 71.56 (Ph-C), 69.98 (thiO-C), 68.41 (PhCO-C), 56.22 (6C thia), 54.26 (OCH₃), 51.74 (thiaN-C), 25.9 (5C thia), 25.13 (thiaOC-C), 24.97 (thiaOCC-C), 24.77 (7C thia), 24.08 (4C thia), 21.32 (C-CH₃), 10.8 (CH₃).

MS (APCI(+)): m/z [M+H]⁺: Calculated; 447.2; 448.2; Found: 447.1; 448.
LC-MS (ESI(+)) m/z [M+H]⁺: 97.0% (447.25)

2-{4-[(4-Methoxybenzyl)oxy]butoxy}-*N*-propyl-4,5,6,7-tetrahydrobenzo[*d*]thiazol-6-amine (ST-2473): 22

According to the procedure **K**, from PMB alcohol (1.15 mmol, 243 mg), NaH ($\omega=60\%$) (1.73 mmol, 42 mg), and consequently **19** (0.56 mmol, 180 mg) was added, and the reaction mixture was refluxed overnight. Crude oil was purified by column chromatography (sorberent SiO₂, eluent DCM: MeOH(NH₃) 95: 5). Yellow oil. Yield: 18%.

Chemical formula: C₂₂H₃₂N₂O₃S
Mr: 404.57
Internal code: ME 354-2



¹H NMR (300 MHz, DMSO *d*₆) δ 7.23 (d, $J = 8.3$ Hz, 2H, 2,6Ph), 6.89 (d, $J = 8.3$ Hz, 2H, 3,5Ph), 4.36 (s, 2H, Ph-CH₂), 4.29 (t, $J = 6.4$ Hz, 2H, 2thiaO-CH₂), 3.73 (s, 3H, -OCH₃), 3.2-3.35 (m, 2H, 6thiaCH, NH), 3.06 (bs, 2H, PhCO-CH₂), 2.90 (dd, $J = 15.7, 5.1$ Hz, 1H, 4thiaCH), 2.65 (m,

^{13}C NMR (75 MHz, DMSO d_6)	3H, 4thiaCH, N-CH ₂), 2.61 – 2.52 (m, 2H, 7thiaCH ₂), 2.13 – 1.93 (m, 1H, 5thiaCH), 1.83 – 1.69 (m, 2H, 2thiaOC-CH ₂), 1.67 – 1.55 (m, 3H, 2thiaOCC-CH ₂ , 5thiaCH), 1.48 (sxt, 2H, N-CH ₂ CH ₂ CH ₃), 0.89 (t, $J = 7.4$ Hz, 3H, N-CH ₂ CH ₂ CH ₃).
MS (APCI(+)): m/z [M+H] ⁺ :	δ 158.60 (4C Ph) 149.10 (9C thia), 143.01 (2C thia), 130.48 (1C Ph) 129.07 (2C, 6C Ph), 117.30 (4C Ph), 113.57 (3C, 5C Ph), 71.45 (Ph-C), 70.97 (PhO-C), 68.7 (thiO-C), 54.99 (OCH ₃), 53.13 (6C thia), 48.03 (N-C), 28.0 (thiOCC-C), 27.50 (5C thia), 25.56, (7C thia) 25.31 (4C thia), 24.58 (thiOC-C) 21.65 (C-CH ₃), 11.57 (CH ₃).
LC-MS (ESI(+)) m/z [M+H] ⁺ :	calculated 405.2; 406.2 found 405.2; 406.2
	96.7% (405.19)

2-{4-[(*Tert*-butyldimethylsilyl)oxy]butoxy}-*N,N*-dipropyl-4,5,6,7-tetrahydrobenzo[*d*]thiazol-6-amine (ST-2470): 23

tert-Butyl-dimethylsilanol (4.81 mmol, 984 mg) was dissolved in 20 mL THF. Consequently, NaH ($\omega=60\%$) (7.2 mmol, 174) mg was portionwise added, and the reaction mixture was stirred at room temperature for four hours. Afterward, **19** (1.6 mmol, 509 mg), was added, and the reaction mixture was refluxed for 48 hours. The reaction was quenched with a saturated solution of NH₄Cl, stirred for 15 minutes, and partitioned between DCM and water (3x). Organic layers were combined, washed with saturated solution NaHCO₃, brine, dried over anhydrous MgSO₄, and evaporated under reduced pressure. Crude oil was purified by column chromatography (sorberent SiO₂, eluent DCM :MeOH (NH₃) 98: 2). Yellow oil. Yield: 18%.

Chemical formula:

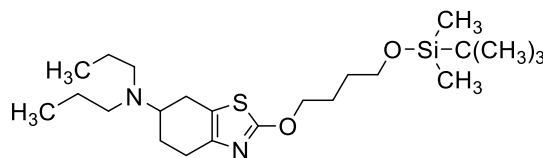
C₂₃H₄₄N₂O₂SSi

Mr:

440.76

Internal code:

ME 360



^1H NMR (300 MHz, CDCl₃)

δ 4.58 (t, $J = 6.5$ Hz, 2H -CH₂-OTBDMS), 3.97 – 3.85 (m, 4H, N-(CH₂CH₂CH₃)₂), 3.05 – 2.80 (m, 3H, 6thiaCH, 2thiaO-CH₂), 2.78 – 2.66 (m, 3H, 4thiaCH₂, 7thiaCH), 2.24 (s, 1H, 7thiaCH), 2.15 – 2.01 (m, 2H, CH₂ COTBDMS), 1.95 – 1.83 (m, 4H, N-(CH₂CH₂CH₃)₂), 1.70 (m, 2H, 5thiaCH₂), 1.19 – 1.12 (m, 17H, (t-Bu), 2thiaOC-CH₂, N-(CH₂CH₂CH₃)₂), 0.29 (s, 6H OSi-(t-Bu)(CH₃)₂).

^{13}C NMR (75 MHz, CDCl₃)

δ 143.27 (9C thia), 142.90 (2C thia), 105.6 (8C thia) 71.20 (thiaO-C), 63.35 (C-OSi), 62.80 (6C thia), 62.57, 52.76 (N-C), 30.28 (5C thia), 29.90 (C-COSi), 29.10 (7C thia), 25.95 (t-Bu), 25.91 (4C thia), 25.47 (thiaOC-C), 11.84(CH₃-C), -5.30, (Si-C CH₃).

MS (APCI(+)): m/z [M+H]⁺:

calculated: 441.3;442.1 found: 441.3;442.4

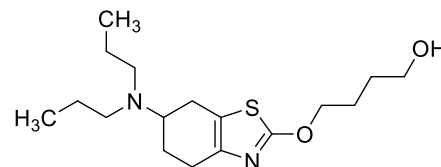
LC-MS (ESI(+)) m/z [M+H]⁺:

95.2% (441.31)

4-((6-(Dipropylamino)-4,5,6,7-tetrahydrobenzo[d]thiazol-2-yl)oxy)butan-1-ol (ST-2471): 24

To a solution of **23** (41.88 mmol, 185 mg) in 20 mL THF was added TBAF (1M THF solution, 83.76 mmol, 0.84 mL) over 15 minutes. The reaction mixture was stirred at room temperature for 10 hours. On the following day the reaction mixture was evaporated under reduced pressure and partitioned between EtOAc and H₂O. Organic layers were collected, washed with brine, dried over anhydrous MgSO₄, and evaporated under reduced pressure. Crude oil was purified by column chromatography. (sorberent SiO₂, eluent DCM: MeOH 9: 1). Yellow oil. Yield: 60%.

Chemical formula: C₁₇H₃₀N₂O₂S
Mr: 326.50
Internal code: ME 365



¹H NMR (300 MHz, DMSO-*d*₆) δ 4.45 (t, *J* = 5.1 Hz, 1H, OH), 4.28 (t, *J* = 6.6 Hz, 2H, 2thiaO-CH₂), 3.42 (td, *J* = 6.3, 5.0 Hz, 2H, HO-CH₂), 2.94 (m, 1H, 6thiaCH), 2.57 (m, 4H, N-(CH₂CH₂CH₃)₂), 2.41 (m, 4H, CH₃-CH₂)₂, 1.88 (m, 1H, 4thiaCH), 1.73 (m, 3H 4thiaCH, 7thiaCH₂), 1.49 (m, 3H thiaOC-CH₂, 5thiaCH), 1.39 (m, 3H, CH₂ COH, 5thiaCH), 0.85 (t, *J* = 7.3 Hz, 6H, N-(CH₂CH₂CH₃)₂).

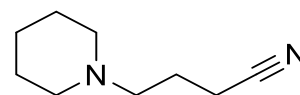
¹³C NMR (75 MHz, DMSO-*d*₆) δ 153.0 (9C thia), 143.05 (2C thia), 99.50 (8C thia), 71.04 (thiaO-C), 60.19 (C-OH), 56.0, (6C thia), 51.89 (N-C), 34.5 (5C thia), 28.68 (7C thia), 26.35 (4C thia), 25.1 (C-CCOH), 24.50 (C-COH), 21.50 (CH₃-C) 11.6 (CH₃).

MS (APCI(+)): *m/z* [M+H]⁺: calculated: 327.2; 328.2 found: 327.2; 328.3
LC-MS (ESI(+)) *m/z* [M+H]⁺: 95.1% (327.20)

4-(Piperidin-1-yl)butanenitrile: P29⁶⁴⁰

Piperidine (0.24 mol, 20.00 g, 23 mL), 4-bromobutanenitrile (**P6** 0.12 mol, 17.38 g), and 10.00 g K₂CO₃ were refluxed in acetone according to procedure A. Crude oil was purified by distillation. Transparent oil. Yield 41%.

Chemical formula: C₉H₁₆N₂
Mr: 152.24
Internal code: ME 087



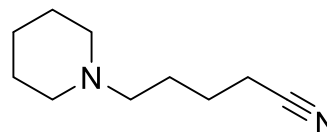
¹H NMR (300 MHz, DMSO *d*₆) δ 2.46 (t, *J* = 7.1 Hz, 2H, pip-CH₂), 2.33 – 2.26 (m, 6H 2,6pipCH₂, CH₂-CN), 1.70 (p, *J* = 7.0 Hz, 2H pipCH₂-CH₂), 1.50 (dq, *J* = 10.7, 5.0 Hz, 4H, 3,5pipCH₂), 1.43 – 1.29 (m, 2H, 4pipCH₂).

MS(APCI(+)): *m/z* [M+H]⁺: calculated: 153.2 found: 153.1

5-(Piperidin-1-yl)pentanenitrile: P30^{454,532}

Piperidine (0.12 mol, 10.51 g, 12.19 mL), 5-bromovaleronitrile (**P7**, 0.06 mol, 10.00 g), 10.00 g K₂CO₃ were refluxed in acetone according to the procedure **A**. Crude oil was purified by distillation. Transparent oil. Yield 73%.

Chemical formula: C₁₀H₁₈N₂
Mr: 166.27
Internal code: ME 230



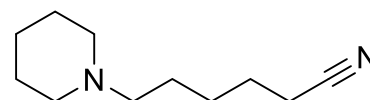
¹H NMR (300 MHz, DMSO- *d*₆) δ 2.49 (t, *J* = 4.1 Hz, 2H, pip-CH₂), 2.28 – 2.18 (m, 6H, CH₂CN, 2,6 pip CH₂), 1.53 (m, 8H, pipC-CH₂-CH₂-, 3,5 pipCH₂), 1.42 – 1.28 (m, 2H, 4 pipCH₂).

MS (APCI(+)): m/z [M+H]⁺: Calculated 167.2 found: 167.3

6-(Piperidin-1-yl)hexanenitrile: P31⁵³²

Piperidine (0.11 mol, 8.959 g, 11.22 mL), 6-bromohexanenitrile (**P24**, 0.05 mol, 10.00 g), 10.00 g K₂CO₃ and catalytic amount of KI were refluxed in acetone according to the procedure **A**. Crude oil was purified by distillation. Transparent oil. Yield: quantitative.

Chemical formula: C₁₁H₂₀N₂
Mr: 180.30
Internal code: ME 233



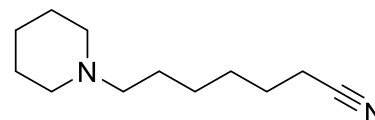
¹H NMR (300 MHz, DMSO- *d*₆) δ 2.47 (t, *J* = 7.1 Hz, 2H, pip-CH₂), 1.63 – 1.52 (m, 2H, CH₂CN), 1.47 (m, 6H, 2,6 pip CH₂CH₂-CCN), 1.43 – 1.37 (m, 4H, pipC-CH₂CH₂), 1.41 – 1.29 (m, 6H, 3,4,5 pipCH₂).

MS (APCI(+)): m/z [M+H]⁺: Calculated 181.2 Found 181.4

7-(Piperidin-1-yl)heptanenitrile: P32¹⁸¹

Piperidine (0.11 mol, 8.959 g, 10.38 mL), 7-bromovaleronitrile (**P24**, 52.6 mmol, 10.00 g), 10.00 g K₂CO₃ and catalytic amount of KI were refluxed in acetone, according to the procedure **A**. Crude oil was purified by distillation. Transparent oil. Yield 55%.

Chemical formula: C₁₂H₂₂N₂
Mr: 194.32
Internal code: ME 226



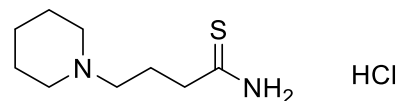
¹H NMR (600 MHz, DMSO- *d*₆) δ 2.47 (t, *J* = 7.1 Hz, 2H, pip-CH₂), 2.34 – 2.22 (m, 4H, CH₂-CH₂-CCN), 2.19 (t, *J* = 7.5 Hz, 2H, CH₂-CN), 1.54 (m, 2H, pipC-CH₂), 1.48 (p, *J* = 5.6 Hz, 4H, 3,5 pipCH₂), 1.43 – 1.32 (m, 4H, 2,6 pipCH₂), 1.30 – 1.23 (m, 2H, 4 pipCH₂).

MS (APCI(+)): m/z [M+H]⁺: calculated: 195.2 found: 195.4

4-(Piperidin-1-yl)butanethioamide hydrochloride: P33

P29 (21.7 mmol, 3.33 g) and *O,O'*-diethyl-dithiophosphate (26.1 mmol, 4.872 g) were dissolved in 4M HCl in 1,4-dioxane, according to the procedure **F**. Crude product was used in the next step without further purification. Yellow solid. Yield: 20%.

Chemical formula: C₉H₁₉ClN₂S
 Mr(free base): 186.32
 Mr(salt): 222.78
 Internal code: ME 089



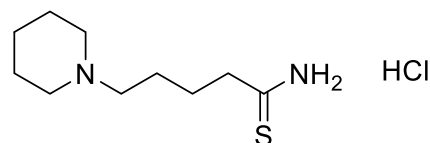
¹H NMR (300 MHz, DMSO- *d*₆) δ 10.82 (d, *J* = 23.0 Hz, 1H, NH₃⁺), 7.92 – 6.96 (m, 2H, NH₂), 3.07 – 2.68 (m, 2H, pip-CH₂), 2.33 – 2.00 (m, 4H, 3,5pipCH₂), 2.00 – 1.51 (m, 4H, 2,6pipCH₂), 1.46 – 1.27 (m, 2H CH₂CS), 1.19 (q, *J* = 6.3 Hz, 2H, 4pipCH₂).

MS (APCI(+)): *m/z* [M+H]⁺: calculated 187.1 Found 187.2

5-(Piperidin-1-yl)pentanethioamide hydrochloride: P34

P30 (44.62 mmol, 7.4195 g) and *O,O'*-diethyl-dithiophosphate (44.62mmol, 8.3102 g) were dissolved in 4M HCl in 1,4-dioxane, according to the procedure **F**. Crude product was used without further purification. Yellow solid. Yield: 95%.

Chemical formula: C₁₀H₂₁ClN₂S
 Mr(free base): 200.34
 Mr(salt): 236.8
 Internal code: ME 232



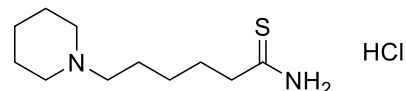
¹H NMR (300 MHz, DMSO *d*₆) δ 9.34 (d, *J* = 16.1 Hz, 1H, pipNH⁺), 3.38 (d, *J* = 12.1 Hz, 2H, NH₂), 3.05 – 2.69 (m, 2H, pip-CH₂), 2.5-2.65 (m, 8H, pip-CH₂CH₂, 3,5pipCH₂), 1.95 – 1.50 (m, 4H, 2,6pipCH₂), 1.55 – 0.91 (m, 2H, 4pipCH₂).

MS (APCI(+)): *m/z* [M+H]⁺: calculated 201.3 found 201.7

6-(Piperidin-1-yl)hexanethioamide hydrochloride: P35⁶⁴¹

P31 (7.48 mmol, 1.35 g), *O,O'*-diethyl-dithiophosphate (7.48 mmol, 1.3944 g) were dissolved in 4M HCl in 1,4-dioxane, according to the procedure **F**. Crude product was used without further purification. Yellow solid. Yield: 79%.

Chemical formula: C₁₁H₂₃ClN₂S
 Mr(free base): 214.37
 Mr(salt): 250.83
 Internal code: ME 222

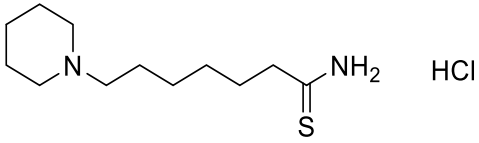


¹H NMR (300 MHz, DMSO *d*₆) δ 10.42 (s, 1H pipNH⁺), 9.31 (d, *J* = 25.5 Hz, 2H, NH₂), 3.37 (d, *J* = 12.1 Hz, 2H, CH₂-CS), 2.99 – 2.89 (m, 2H pip-CH₂), 2.87 – 2.71 (m, 2H CH₂-CCS), 1.90 – 1.58 (m, 10H 2,3,5,6pipCH₂, pipC-CH₂), 1.47 – 1.12 (m, 4H, pipCC-CH₂, 4pipCH₂).

MS (APCI(+)): *m/z* [M+H]⁺: calculated 215.1;216.1 found: 215.3;216.2

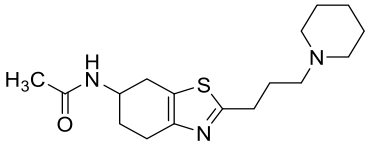
7-(Piperidin-1-yl)heptanethioamide hydrogen chloride: P36

P32 (53.2 mmol, 10.340 g) *O,O'*-diethyl-dithiophosphate (53.2 mmol, 9.909 g) were dissolved in 4M HCl in 1,4-dioxane, according to the procedure F. Crude product was used without further purification. Yellow solid. Yield: 95%.

Chemical formula:	$C_{12}H_{25}ClN_2S$	
Mr(free base):	228.40	
Mr(salt):	264.86	
Internal code:	ME 229	
1H NMR (300 MHz, DMSO d_6)	δ 10.49 (s, 1H, pipNH ⁺), 9.30 (d, J = 23.1 Hz, 2H, NH ₂), 3.37 (d, J = 12.1 Hz, 2H, pip-CH ₂), 3.02 – 2.71 (m, 2HCH ₂ -CCS), 2.47 (d, J = 7.5 Hz, 2H, CH ₂ -CS), 1.93 – 1.64 (m, 10H, 2,3,5,6 CH ₂ , pip, pipC-CH ₂), 1.50 – 1.14 (m, 6H, pipCC-CH ₂ CH ₂ , 4pipCH ₂).	
MS (APCI(+)): m/z [M+H ⁺] ⁺ :	Calculated: 229.2	found: 229.7

***N*-[2-(3-(Piperidin-1-yl)propyl)-4,5,6,7-tetrahydrobenzo[*d*]thiazol-6-yl]-acetamide (ST-2305): 25**

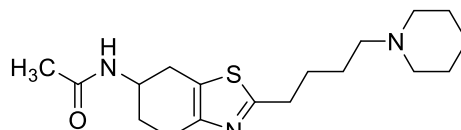
N-(4-Oxocyclohexyl)acetamide (**P19**) (9.65 mmol, 1.50 g) was dissolved in chloroform, and bromine (9.69 mmol, 1.55g, 0.5 mL) was dropwise added at room temperature. The solution was heated up to 60 °C and stirred until discoloration. The reaction mixture was evaporated under reduced pressure. Consequently, concentrate **P33** (7.29 mmol, 1.3577 g) was dissolved in DMF (40 mL), was added and the reaction mixture was refluxed for two hours. Crude oil was purified with column chromatography (Sorbet: SiO₂, Eluent DCM:MeOH/NH₃ 9:1 and 95:5). Yellow oil. Yield: 18%.

Chemical formula:	$C_{17}H_{27}N_3OS$	
Mr:	321.48	
Internal code:	ME 125	
1H NMR (300 MHz, DMSO- d_6)	δ 7.96 (d, J = 7.5 Hz, 1H CONH), 4.10 – 3.92 (m, 1H, 6thiaCH), 3.02 – 2.91 (m, 1H, 4thiaCH), 2.86 (t, J = 7.6 Hz, 2H, 2thia-CH ₂), 2.82 – 2.53 (m, 3H, 4thia CH, 7thiaCH ₂), 2.34 – 2.22 (m, 6H, 2,6pipCH ₂ , pipN-CH ₂), 1.95 – 1.84 (m, 1H, 5thiaCH), 1.81 (s, 3H, -CH ₃), 1.80 – 1.68 (m, 3H, 2Cthia-CH ₂ , 5thiaCH), 1.47 (p, J = 5.5 Hz, 4H, 3,5pipCH ₂), 1.40 – 1.33 (m, 2H, 4pipCH ₂).	
^{13}C NMR (75 MHz, DMSO- d_6)	δ 168.72 (C=O) 167.43 (9C thia), 148.40 (2C thia), 125.28 (8C thia), 57.43 (pipN-C), 53.96 (2C, 6C pip), 44.71 (6C thia), 30.49 (7C thia), 28.89 (pipNC-C), 28.08 (4C pip), 26.65 (3C,5C pip), 25.58 (5C thia), 24.28 (2thiaC-C), 24.14 (4C thia), 22.67 (CH ₃)	
MS- (APCI(+)): (m/z) [M+H ⁺] ⁺ :	calculated 322.2 ; 323.2	found 322.7;323.8
LC-MS (ESI(+)) m/z [M+H ⁺] ⁺ :	97.35% (322.13)	

***N*-{2-[4-(Piperidin-1-yl)butyl]-4,5,6,7-tetrahydrobenzo[*d*]thiazol-6-yl}acetamide (ST-2438): 26**

N-(4-Oxocyclohexyl)acetamide (**P19**) (13.6 mmol, 2.1139 g), bromine (13.6 mmol, 2.1777 g, 0.7 mL) and **P34** (10.88 mmol, 2.1797 g) were treated according to the procedure **G**. Crude oil was purified with column chromatography (Sorbent: SiO₂ Eluent: DCM:MeOH (NH₃) 93:7) Yellow oil. Yield: 32%.

Chemical formula: C₁₈H₂₉N₃OS
Mr: 335.51
Internal code: ME 239



¹H NMR (300 MHz, DMSO- *d*₆) δ 7.97 (d, *J* = 7.5 Hz, 1H, CONH), 4.12 – 3.96 (m, 1H, 6thiaCH), 2.97 (dd, *J* = 16.0, 5.4 Hz, 1H, 4thiaCH), 2.87 (t, *J* = 7.5 Hz, 1H, 4thiaCH), 2.83 – 2.55 (m, 3H, 2thiaCH₂, 7thiaCH), 2.35 – 2.15 (m, 6H, pipN-CH₂, pip 3,5pipCH₂), 2.00 – 1.84 (m, 1H, 7thiaCH), 1.82 (s, 3H, CH₃), 1.79 – 1.59 (m, 4H, pipNC-CH₂, 5thiaCH₂), 1.56 – 1.30 (m, 8H, 2Cthia-CH₂, 2,4,6pipCH₂).

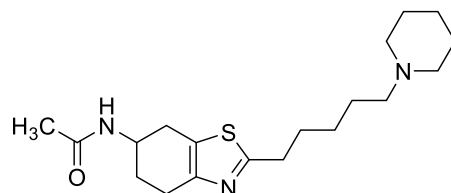
¹³C NMR (75 MHz, DMSO- *d*₆) δ 168.73 (C=O), 167.53 (9C thia), 148.40 (2C thia) 125.24 (8C thia), 58.09 (pipN-C), 54.03 (2C,6Cpip), 44.71 (6C thia), 32.47 (7C thia), 28.90 (3C, 5Cpip) 28.07 (pip NC-C), 27.36 (4C pip), 25.71 (CH₃), 25.56 (5C thia), 24.27 (4C thia), 24.14 (2thiaC-C), 22.67 (2thia CC-C).

MS (APCI(+)): *m/z* [M+H]⁺: calculated: 336.2 found: 336.7
LC-MS (ESI(+)): *m/z* [M+H]⁺: 96.82% (336.19)

***N*-{2-[5-(Piperidin-1-yl)pentyl]-4,5,6,7-tetrahydrobenzo[*d*]thiazol-6-yl}acetamide (ST-2439): 27**

N-(4-oxocyclohexyl)acetamide (**P19**) (13.6 mmol, 2.1139 g), bromine (13.6 mmol, 3.1770 g, 0.7 mL), and **P35** (8.69 mmol, 2.1797 g) were treated according to the procedure **G**. Crude product was purified with column chromatography (Sorbent SiO₂, Eluent DCM:MeOH(NH₃) 93:7). Yellow oil. Yield: 52%.

Chemical formula: C₁₉H₃₁N₃OS
Mr: 349.54
Internal code: ME 240



¹H NMR (300 MHz, DMSO- *d*₆) δ 7.96 (d, *J* = 7.5 Hz, 1H, CONH), 4.08 – 3.94 (m, 1H, 6thiaCH), 2.96 (dd, *J* = 16.2, 5.4 Hz, 1H, 4thiaCH), 2.85 (t, *J* = 7.6 Hz, 2H, 2thia-CH₂), 2.79 – 2.53 (m, 3H, 4thiaCH, 7thiaCH₂), 2.26 (s, 4H, 2,6 pipCH₂), 2.18 (t, *J* = 7.1 Hz, 2H, pipN-CH₂), 1.95 – 1.86 (m, 1H, 5thiaCH, pipC-CH₂), 1.81 (s, 3H, CH₃), 1.78 – 1.60 (m, 3H, 5thiaCH), 1.51 – 1.26 (m, 10H, 3,4,5pip-CH₂, pipCC-CH₂CH₂).

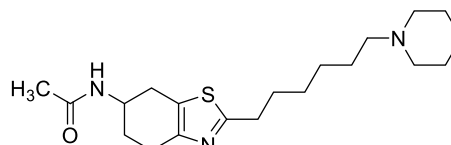
¹³C NMR (75 MHz, DMSO-*d*₆) δ 168.72 (C=O), 167.52 (9C thia), 148.39 (2C thia), 125.24 (8C thia) 58.47 (pipN-C), 54.06 (2C,6Cpip), 44.72 (6C thia), 32.56 (5C thia) 29.33(2Cthia-C) 28.90 (pipNC-C), 28.08 (7C thia), 26.41(CH₃), 26.02 (3C,5Cpip), 25.58 (4C pip), 24.28, (pipNCC-C), 24.19 (2thiaCC-C) 22.67 (4C thia)

MS (APCI(+)): *m/z* [M+H]⁺: calculated 350.2; 351.2 found: 350.7;351.7
LC-MS (ESI(+)) *m/z* [M+H]⁺: 97.74% (350.22)

***N*-{2-[6-(Piperidin-1-yl)hexyl]-4,5,6,7-tetrahydrobenzo[d]thiazol-6-yl}acetamide (ST-2443): 28**

N-(4-oxocyclohexyl)acetamide (**P19**) (13.6 mmol, 2.1105 g) bromine (13.6 mmol, 2.1777g, 0.7 mL) and **P36** (10.88 mmol, 2.4849 g) were treated according to the procedure **G**. Crude product was purified with column chromatography (sorbent SiO₂, eluent DCM: MeOH/NH₃ 93:7). Yellow oil which crystallizes upon storage. Yield: 29%.

Chemical formula: C₂₀H₃₃N₃OS
Mr: 363.56
Internal code: ME 247



¹H NMR (300 MHz, DMSO- *d*₆) δ 8.03 (d, *J* = 7.5 Hz, 1H, CONH), 4.15 – 4.01 (m, 1H, 6thiaCH), 3.03 (dd, *J* = 16.2, 5.4 Hz, 1H, 4thiaCH), 2.91 (t, *J* = 7.6 Hz, 2H, 2thia-CH₂), 2.87 – 2.61 (m, 3H, 4thiaCH, 7thiaCH₂), 2.40 – 2.28 (m, 4H, 2,6pipCH₂), 2.24 (t, *J* = 7.2 Hz, 2H pipN- CH₂), 2.01 – 1.92 (m, 1H, 5thia CH), 1.87 (s, 3H, CH₃), 1.70 (m, 2H, pipNC-CH₂), 1.58 – 1.47 (m, 5H, 5thiaCH, pipNCC-CH₂-CH₂), 1.47 – 1.31 (m, 8H, 2thiaC- CH₂, 3,4,5 pipCH₂)

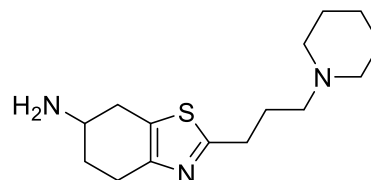
¹³C NMR (151 MHz, DMSO- *d*₆) δ 169.2 (C=O), 168.02 (9C thia), 148.91 (2C thia), 125.73 (8C thia), 59.09(pipN-C), 54.58 (2C 6C pip), 45.23 (6Cthia), 33.05 (5C thia), 31.16 (4C pip), 29.85 (pipNC-C), 29.40 (3C; 5C pip), 28.84 (2thiaC-C), 28.59 (2thiaCC-C), 27.16 (C-CCpip), 26.71 (2thiaCC-C), 26.08 (7C thia), 24.79 (4C thia), 24.69(CH₃).

MS (APCI(+)): *m/z* [M+H]⁺: Calculated 364.2;365.2 found: 364.8;365.7
LC-MS (ESI(+)) 99.76%
m/z [M+2H]²⁺ [M+H]⁺: (153.04;364.24)

2-(3-(Piperidin-1-yl)propyl)-4,5,6,7-tetrahydrobenzo[d]thiazol-6-amine: P37

Compound **25** (0.48mmol, 157 mg) was treated according to the procedure **F** for 36 hours. Crude product was used without further purification.

Chemical formula: C₁₅H₂₅N₃S
Mr: 279.45
Internal code: ME 131

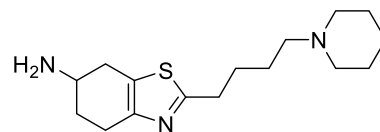


¹H NMR (300 MHz, DMSO- *d*₆) δ 3.75 (m, 1H, 6thiaCH), 2.86 (m, 4H, 2thia-CH₂, 4thiaCH₂), 2.78 – 2.64 (m, 3H, pipN-CH₂, 7thiaCH), 2.66 – 2.55 (m, 2H, NH₂), 2.28 (m, 5H, 2,6 pipCH₂, 7thia CH), 1.79 (m, 4H, pipNC-CH₂, 5thiaCH₂), 1.49 (m, 4H, 3,5pipCH₂), 1.38 (m, 2H, 4pipCH₂).

2-[4-(Piperidin-1-yl)butyl]-4,5,6,7-tetrahydrobenzo[d]thiazol-6-amine (ST-2467): 29

Compound **26** (2.52 mmol, 845 mg) was treated according to the procedure **F**. Crude product was purified with column chromatography (sorbent Silica gel 60 NH₂, eluent DCM: MeOH 98:2) Dark green oil. Yield: 15 %.

Chemical formula: C₁₆H₂₇N₃S
Mr: 293.47
Internal code: ME 241



¹H NMR (300 MHz, DMSO-*d*₆) δ 3.2 (m, 2H, NH₂), 3.14 – 3.01 (m, 1H, 6thiaCH), 2.92 – 2.79 (m, 3H, 2thiaCH₂, 4thiaCH), 2.80 – 2.54 (m, 2H, 4thiaCH, 7thiaCH), 2.51-2.54 (m, 2H, pipN-CH₂), 2.36 (dd, *J* = 15.9, 8.3 Hz, 1H, 7thiaCH), 2.30 – 2.17 (m, 4H, 2,6pipCH₂), 1.93 – 1.81 (m, 1H, 5thiaCH) 1.70-1.55 (m, 4H, 2 thiaC-CH₂-CH₂), 1.51 – 1.29 (m, 7H, 5thiaCH, 3,4,5pipCH₂).

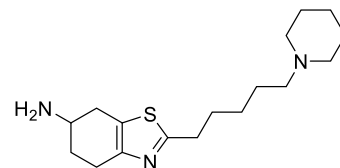
¹³C NMR (151 MHz, DMSO-*d*₆) δ 167.05 (9C thia), 148.57 (2C thia), 126.02 (8C thia), 58.13 (pipN-C), 54.05 (2C, 6C pip), 47.36 (6C thia), 32.49 (5C thia), 32.42 (2thia-C), 32.05 (7C thia), 27.40 (3C, 5C pip) 25.74 (4C pip), 25.59 (pipNC-C), 24.66 (2thiaC-C), 24.18 (4C thia)

MS (APCI(+)) *m/z* [M+H]⁺: calculated: 294.2 found: 294.6
LC-MS (ESI(+)) *m/z* [M+H]⁺: 95.25% (294.15)

2-[5-(Piperidin-1-yl)pentyl]-4,5,6,7-tetrahydrobenzo[d]thiazol-6-amine (ST-2437): 30

Compound **27** (0.3 mmol, 106 mg) was treated according to the procedure **F**. Crude product was further purified with flash column chromatography (sorbent Silica gel 60 NH₂, eluent DCM:MeOH 98:2). Dark green oil. Yield: 75%.

Chemical formula: C₁₇H₂₉N₃S
Mr: 307.50
Internal code: ME 234



¹H NMR (300 MHz, Chloroform-*d*) δ 3.22 (m, 1H, 6thiaCH), 2.98 – 2.87 (m, 1H, 4thiaCH), 2.87 – 2.79 (m, 3H, 4 thiaCH, 2thiaCH₂), 2.78 – 2.57 (m, 2H, pipN-CH₂), 2.29 (m, 3H, 7thiaCH₂, 5thiaCH), 1.76 – 1.63 (m, 4H, 2,6pipCH₂), 1.63 – 1.46 (m, 8H, 3,5pipCH₂, CH₂C-pipN, 2thiaC-CH₂), 1.45 – 1.27 (m, 5H, 5thiaCH, -NH₂, 4pipCH₂), 1.22 – 1.09 (m, 2H, pipCC-CH₂).

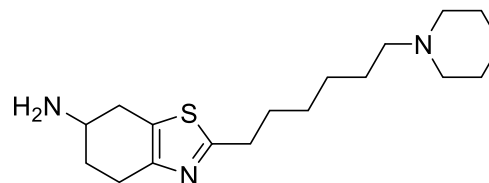
¹³C NMR (75 MHz, DMSO-*d*₆) δ 163.4(9C thia), 143.47 (2C thia), 120.60 (8C thia), 53.78 (pipN-C), 49.14 (2C, 6C pip), 42.40 (6C thia), 28.18 (4C pip), 27.86 (3C, 5C pip), 27.28 (2thia-C), 24.77(5C thia), 21.86 (7C thia) 20.83 (4C thia), 20.16 (2thiaC-C), 19.56 (pipNC-C) 18.86 (pipNCC-C).

MS (APCI(+)): *m/z* [M+H]⁺: Calculated 308.2 found: 308.4
LC-MS (ESI(+)): 95.66%
m/z [M+2H]²⁺[M+H]⁺ (145.99; 308.15)

2-[6-(Piperidin-1-yl)hexyl]-4,5,6,7-tetrahydrobenzo[d]thiazol-6-amine (ST-2444): 31

Compound **28** (2.43 mmol, 885 mg) was treated according to the procedure **F**. Crude product was purified with flash column chromatography (sorbent Silica gel 60 NH₂, eluent: DCM MeOH 98:2). Dark green oil. Yield: 57%.

Chemical formula: C₁₈H₃₁N₃S
Mr: 321.53
Internal code: ME 248



¹H NMR (300 MHz, DMSO- *d*₆) δ 3.14 – 3.04 (m, 3H, 6thiaCH, 2thiaCH₂), 2.91 (d, *J* = 5.1 Hz, 1H, 4thiaCH), 2.88 – 2.79 (m, 2H, 4thiaCH, 7thiaCH), 2.6-2.7 (m, 2H, 2thiaCH-CH₂) 2.38 (ddt, 1H, *J* = 16.0, 8.3, 2.1 Hz, 1H, 7thiaCH), 2.27 (m, 4H, 2,6pipCH₂), 2.18 (t, 2H, *J* = 7.1 Hz, pipN-CH₂), 1.98 – 1.83 (m, 1H 5thiaCH) 1.52-1.63 (m, 4H, pipN-CH₂, -NH₂), 1.50- 1.20 (m, 11H, 3,5pip-CH₂, 5thiaCH, pipN-CH₂-CH₂-CH₂)

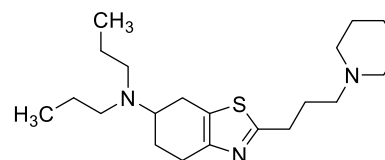
¹³C NMR (75 MHz, DMSO- *d*₆) δ 167.06 (9C thia), 148.57 (2C thia), 125.96 (8C thia), 58.60 (pipN-C), 54.08 (2C, 6C pip), 47.35 (6C thia), 32.55 (5C thia), 32.31 (2thia-C), 31.95 (4C pip), 29.38 (3C, 5C pip), 28.33 (pipNC-C), 26.66 (7C thia) 26.21 (2thiaC-C), 25.58 (2thiaCC-C), 24.6(C-CCpip), 24.19 (4Ct hia).

MS (APCI(+)):m/z [M+H]⁺: calculated: 322.2;323.2 found: 322.7;323.8
LC-MS (ESI(+)) 96.60%
m/z [M+2H]²⁺ [M+H]⁺: (153.05;322.22)

2-[3-(Piperidin-1-yl)propyl]-N,N-dipropyl-4,5,6,7-tetrahydrobenzo[d]thiazol-6-amine (ST-2303):**32**

P37 (0.56 mmol, 157 mg), propionaldehyde (0.31 mmol, 87 mg) and Na[BH(CH₃COO)₃] (0.94 mmol, 199 mg) were treated according to the procedure **E**. Crude product was purified with column chromatography (sorbent SiO₂, eluent DCM: MeOH (NH₃) 95:5. Yellow oil. Yield: 44%.

Chemical formula: C₂₁H₃₇N₃S
Mr: 363.61
Internal code: ME 135



¹H NMR (300 MHz, DMSO- *d*₆) δ 2.94 (t, *J* = 5.9 Hz, 1H, 6thiaCH), 2.84 (t, *J* = 7.5 Hz, 2H, 2thiaCH₂), 2.74 (t, *J* = 3.9 Hz, 2H, pipN-CH₂), 2.70 – 2.55 (m, 2H, 4thiaCH₂), 2.40 (m, 4H, N-(CH₂)₂), 2.28 (m, 6H, 7thiaCH₂, 2,6 pipCH₂), 1.97 – 1.85 (m, 1H, 5thiaCH), 1.78 (p, *J* = 7.4 Hz, 2H, pipC-CH₂), 1.71 – 1.54 (m, 1H, 5thiaCH), 1.53 – 1.29 (m, 10H, 2 (CH₂-CH₃), 3,4,5 pipCH₂), 0.84 (t, *J* = 7.3 Hz, 6H, (-CH₃)₂).

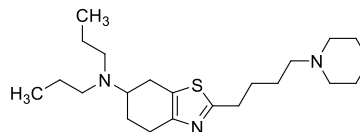
¹³C NMR (75 MHz, DMSO- *d*₆) δ 167.29 (9C thia), 148.76 (2C thia), 126.77 (8C thia), 57.40 (pipN-C), 56.64 (2C, 6C pip), 53.94(thiaN-C), 51.89 (6C thia), 30.49 (5C thia), 26.66(4C pip), 26.18 (3C, 5C pip) 25.53 (pipNC-C) 25.29 (7C thia), 24.81(2thiaC-C), 24.10 (4Ct hia) 21.80 (C-CH₃), 11.67 (CH₃)

MS- (APCI(+)): (m/z) [M+H]⁺: calculated 364.3;365.3 found: 364.9;365.9
LC-MS (ESI(+)) 97.81%
m/z [M+2H]²⁺ [M+H]⁺: (182.56; 364.27)

2-(4-(Piperidin-1-yl)butyl)-N,N-dipropyl-4,5,6,7-tetrahydrobenzo[d]thiazol-6-amine (ST 2466): 33

Compound **29** (1.02 mmol, 300 mg), propionaldehyde (10.22 mmol, 593 mg), and Na[BH(CH₃COO)₃] (7.115 mmol, 1.516 g) were treated according to the procedure **E**. The crude product was purified with column chromatography (sorberent SiO₂, eluent: DCM:MeOH(NH₃) 95:5). Yellow oil which crystalizes upon storage. Yield: 23%.

Chemical formula: C₂₂H₃₉N₃S
Mr: 377.64
Internal code: ME 245



¹H NMR (300 MHz, CDCl₃) δ 3.11 – 2.97 (m, 1H, 6thiaCH), 2.97 – 2.86 (m, 3H, 2thiaCH₂, 4thiaCH), 2.86 – 2.54 (m, 3H, 4thiaCH, pipN-CH₂), 2.54 – 2.31 (m, 10H, 7thiaCH₂, N-(CH₂)₂ 2,6pip-CH₂), 2.11 – 1.98 (m, 1H, 5thiaCH), 1.83 – 1.55 (m, 9H, 5thiaCH, pipN-CH₂-CH₂ 2(CH₃-CH₂), 1.46 (m, 6H, 3,4,5pipCH₂), 0.88 (t, *J* = 7.3 Hz, 6H, (-CH₃)₂).

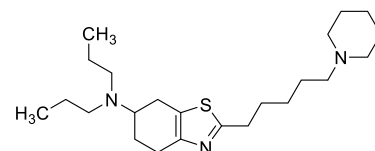
¹³C NMR (75 MHz, CDCl₃) δ 168.47 (9C thia), 149.16 (2C thia), 127.32 (8C thia), 59.00 (pipN-C), 57.43 (2C, 6C pip) 54.57 (6C thia), 52.77 (thiaN-C), 33.41, (5C thia) 28.31 (pipNC-C), 26.72 (3C, 5C pip), 26.25 (7C thia), 25.8 (2thiaCC-C), 25.40 (2thiaC-C), 24.36 (4C thia), 22.32 (C-CH₃) 11.86 (CH₃).

MS (APCI(+)): *m/z* [M+H⁺]⁺: calculated: 378.3;379.3 found: 378.3;379.3
LC-MS (ESI(+)) 99.22%
m/z [M+2H⁺]²⁺ [M+H⁺]⁺: (189.56; 378.32)

2-[5-(Piperidin-1-yl)pentyl]-N,N-dipropyl-4,5,6,7-tetrahydrobenzo[d]thiazol-6-amine (ST-2440): 34

Compound **31** (0.65 mmol, 200 mg) propionaldehyde (2.60 mmol, 151 mg), and Na[BH(CH₃COO)₃] (1.95 mmol, 414 mg) were treated according to the procedure **E**. Crude product was purified with hand column (sorberent SiO₂, eluent DCM:MEOH (NH₃) 99:1) and flash column chromatography (sorberent: Silica gel 60 NH₂, eluent DCM:MEOH 98:2). Green oil. Yield: 20%.

Chemical formula: C₂₃H₄₁N₃S
Mr: 391,66
Internal code: ME 244-1



¹H NMR (300 MHz, CDCl₃) δ 3.12 – 2.97 (m, 1H, 6thiaCH), 2.99 – 2.84 (m, 3H, 2thiaCH₂, 4ThiaCH), 2.83 – 2.53 (m, 4H, N-(CH₂)₂), 2.54 – 2.32 (m, 9H, 4thiaCH, 7thiaCH₂, pipN-CH₂, 2,6 pipCH₂), 2.09 – 1.99 (m, 1H, 5thiaCH), 1.82 – 1.54 (m, 9H, 5thia CH, CH₂CH₂CH₂-Npip, 4pipCH₂), 1.53 – 1.33 (m, 8H, 3,5 pipCH₂ -N(CH₂ CH₃)₂), 0.88 (t, *J* = 7.3 Hz, 6H, (CH₃)₂)

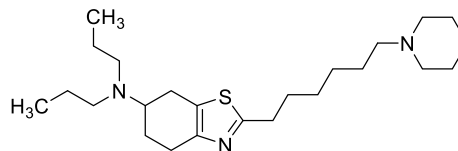
¹³C NMR (75 MHz, CDCl₃) δ 168.55 (9C thia), 149.15 (2C thia), 127.27 (8C thia), 58.98 (pipN-C), 57.42 (2C, 6C pip), 54.34 (6C thia), 52.76 (thiaN-C), 33.45 (5C thia), 30.04 (2Cthia-C), 27.07 (3C, 5C pip), 26.71 (4C pip), 25.97 (pipNC-C), 25.82 (2thiaC-C), 25.37 (7C thia), 25.30 (4C thia), 24.04 (2thiaCC-C), 22.29 (C-CH₃), 11.87 (CH₃).

MS (APCI(+)): *m/z* [M+H⁺]⁺: calculated: 392.3;393.3 found: 392.8;393.9
LC-MS (ESI(+)) 95.83%
m/z [M+2H⁺]²⁺ [M+H⁺]⁺: (196.56;392.32)

2-[6-(Piperidin-1-yl)hexyl]-*N,N*-dipropyl-4,5,6,7-tetrahydrobenzo[*d*]thiazol-6-amine (ST 2445): 35

Compound **31** (0.58 mmol, 186 mg), propionaldehyde (5.79 mmol, 337 mg), and Na[BH(CH₃COO)₃] (4.06 mmol, 860 mg) were treated according to the procedure **E**. The crude product was purified with column chromatography (sorbent SiO₂, eluent DCM: MeOH(NH₃) 95:5). Yield: 30%.

Chemical formula: C₂₄H₄₃N₃S
Mr: 405.69
Internal code: ME 250



¹H NMR (300 MHz, CDCl₃) δ 3.74 (m, 1H, 6thiaCH), 3.50 (m, 2H, 2thiaCH₂), 3.15 – 2.95 (m, 4H, N-(CH₂)₂), 2.95 – 2.79 (m, 8H, 4thiaCH₂, pipN-CH₂, 2,6pipCH₂), 2.74 – 2.45 (m, 2H, 7thiaCH₂), 2.34 – 2.19 (m, 7H, pipN-CH₂, 5thiaCH, 2thiaC-CH₂, CH₂-CNpip), 2.07 (m, 7H, 5thiaCH, CH₂-CCNpip, 3,5pipCH₂), 1.88 (d, *J* = 15.2 Hz, 4H, N-(CH₂-CH₃)₂), 1.62 – 1.52 (m, 2H, CH₂-CCCN), 1.45 (m, 2H, 4pipCH₂), 1.01 (t, *J* = 6.1 Hz, 6H - (CH₃)₂).

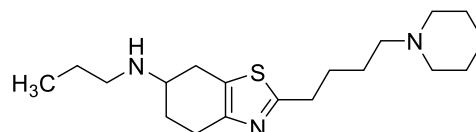
¹³C NMR (75 MHz, CDCl₃) δ 170.27 (9C thia), 147.95 (2C thia), 123.80 (8C thia), 59.45 (pipN-C), 57.38 (2C, 6C pip), 53.20 (thiaN-C), 52.60 (6C thia), 32.90 (5C thia), 29.51 (2thia-C), 28.02 (pipNC-C), 26.43 (7C thia), 25.36 (2thiaC-C), 24.70 (2thiaCC-C), 24.54 (C-CCpip), 22.55 (4C thia), 17.98 (C-CH₃), 11.46 (CH₃).

MS (APCI(+)): m/z [M+H]⁺: calculated: 406.3;407.3 found: 406.4 407.4
LC-MS (ESI(+)) 96.15%
m/z [M+2H]²⁺ [M+H]⁺: (203.57; 406.33)

2-[4-(Piperidin-1-yl)butyl]-*N*-propyl-4,5,6,7-tetrahydrobenzo[*d*]thiazol-6-amine (ST-2442): 36

Compound **29** (1.03 mmol, 304mg), propionaldehyde (1.03 mmol, 60 mg), and Na[BH(CH₃COO)₃] (1.55 mmol, 329.2 mg) were treated according to the procedure **E**. Crude product was purified with column chromatography (sorbent SiO₂, eluent DCM: MeOH(NH₃) 95:5). Yellow oil. Yield: 30%.

Chemical formula: C₁₉H₃₃N₃S
Mr: 335.55
Internal code: ME 246



¹H NMR (300 MHz, CDCl₃) δ 3.08 – 2.97 (m, 1H, 6thiaCH), 2.93 (t, *J* = 7.5 Hz, 2H, 2thiaCH₂), 2.87 – 2.74 (m, 2H, 7thiaCH, 4thiaCH), 2.66 (m, 2H, 7thiaCH, 4thiaCH), 2.61 – 2.26 (m, 6H, pipN-CH₂, thiaN-CH₂, CH₂-CCN), 2.05 (tt, *J* = 6.8, 6.3 Hz, 1H, 5thiaCH), 1.75 (m, 4H, 2,6pipCH₂), 1.63 (bs, 6H, 3,4,5pipCH₂), 1.53 (m, 3H, 5thiaCH, CH₂CH₃), 1.47 (s, 2H, NH₂), 0.94 (t, *J* = 7.4 Hz, 3H, -CH₃).

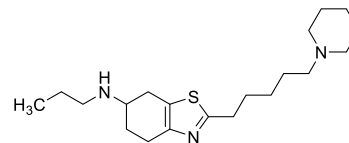
¹³C NMR (75 MHz, CDCl₃) δ 168.40 (9C thia), 149.05 (2C thia), 126.11 (8C thia), 58.97 (pipN-C), 54.55 (2C, 6C pip), 53.94 (thiaN-C), 49.31 (6C thia), 33.38 (5C thia), 30.41 (2Cthia-C), 29.56 (4C pip), 28.27 (3C, 5C pip), 26.21 (7C thia), 25.76 (4C thia), 25.03 (pipNC-C), 24.33 (pipNCC-C), 23.52 (C-CH₃), 11.86 (CH₃).

MS (APCI(+)): m/z [M+H]⁺: calculated: 336.2;337.2 found: 336.7;337.7
LC-MS (ESI(+)) 95.74%
m/z [M+2H]²⁺ [M+H]⁺: (168.55; 336.26)

2-[5-(Piperidin-1-yl)pentyl]-N-propyl-4,5,6,7-tetrahydrobenzo[d]thiazol-6-amine (ST-2441): 37

Compound **30** (0.65 mmol, 200 mg), propionaldehyde (2.60 mmol, 151 mg), and Na[BH(CH₃COO)₃] (1.95 mmol, 414 mg) were treated according to the procedure **E**. The crude product was purified with column chromatography (sorbent SiO₂, eluent DCM: MeOH(NH₃) 95:5). Light green oil. Yield: 22%.

Chemical formula: C₂₀H₃₅N₃S
Mr: 349.58
Internal code: ME 244-2



¹H NMR (300 MHz, CDCl₃) δ 3.08 – 2.97 (m, 2H, 2thia CH₂), 2.90 (t, *J* = 7.7 Hz, 2H pipN-CH₂), 2.82-2.71 (m, 1H, 6thiaCH), 2.65-2.65 (t, *J* = 7.5 Hz, 2H, 7thiaCH₂), 2.58 – 2.46 (m, 1H, 4thiaCH), 2.43 – 2.26 (m, 7H, 2thia-CH₂, 4thiaCH, -CH₂CH₂-C-pip), 2.12 – 2.00 (m, 1H, NH), -1.85 – 1.68 (m, 4H, 2,6pip CH₂), 1.67 – 1.49 (m, 10H, 2thiaCC-CH₂, 5thiaCH₂, CH₃-CH₂, 3,5pipCH₂), 1.41 – 1.34 (m, 2H, 4pipCH₂), 0.93 (t, *J* = 7.4 Hz, 3H, -CH₃).

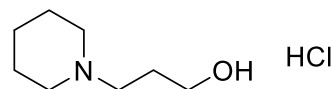
¹³C NMR (75 MHz, CDCl₃) δ 168.64 (9C thia), 149.05 (2C thia), 126.05 (8C thia), 59.26 (pipN-C), 54.55 (2C, 6C pip), 53.95 (thiaN-C), 49.31 (6C thia), 33.51 (5C thia), 30.42 (2thiaC-C), 30.13 (7C thia), 29.57 (C-CNH), 27.25 (3C, 5Cpip), 26.44 (4C pip), 25.76 (C-CCN), 25.04 (2thiaCC-C), 24.35 (4C thia), 23.52 (C-CH₃), 11.86 (CH₃).

MS (APCI- (+)): m/z [M+H]⁺: calculated 350.2;351.2 found: 350.8;351.8
LC-MS (ESI- (+)) 96.49%
m/z [M+2H]²⁺ [M+H]⁺: (175.55;350.29)

3-(Piperidin-1-yl)propan-1-ol: P38^{361,606}

Piperidine (10 g, 0.12 mol, 11.6 mL) and 3-chloro-1propanol (0.12 mol, 11.34 g), 10 g K₂CO₃ and a catalytic amount of KI were treated according to procedure **A**. The crude product was purified by distillation and crystallization as hydrochloride salt from 2-propanol. White solid. Yield: 80%.

Chemical formula: C₈H₁₈ClNO
Mr (free base): 143.23
Mr (salt): 179.69
Internal code: ME 306

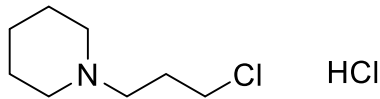


¹H NMR (600 MHz, DMSO-*d*₆) δ 10.43 (s, 1H, pipNH⁺), 4.80 (s, 1H, OH), 3.46 (t, *J* = 6.0 Hz, 2H, CH₂OH), 3.37 (d, *J* = 13.7 Hz, 2H pipN-CH₂), 3.0- 2.90 (m, pipNC-CH₂), 1.99 – 1.57 (m, 8H, 2,3,5,6pipCH₂), 1.37 (m, 2H, 4pipCH₂).

MS (APCI-(+)) m/z [M+H]⁺: calculated 144.1 Found 144.1

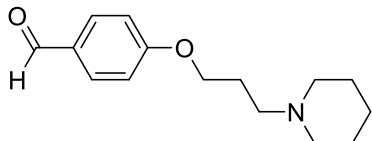
1-(3-Chloropropyl)piperidine hydrochloride: P39⁶⁴²

Alcohol **P38** (34.9 mmol, 6.271 g) was dissolved in toluene, and consequently, thionyl chloride was added (70 mmol, 8.327 g, 5.1 mL) under nitrogen atmosphere at 0 °C. Reaction mixture was stirred for 3h at room temperature. Precipitate filtered, and washed with ether. The crude product was recrystallized with ethanol. White solid. Yield: 90%.

Chemical formula:	C ₈ H ₁₇ Cl ₂ N	
Mr: (free base):	161.67	
Mr (salt):	198.13	
Internal code:	ME 158	
¹ H NMR (600 MHz, DMSO- <i>d</i> ₆)	δ 10.92 (s, 1H, pipNH ⁺ (CH ₂)), 3.75 (t, <i>J</i> = 6.4 Hz, 2H, pipN-CH ₂), 3.17 – 3.01 (m, 2H, pipCH ₂), 2.85 (m, 4H, 2,6pipCH ₂), 2.33 – 2.12 (m, 2H, pipNC-CH ₂), 1.98 – 1.61 (m, 4H, 3,5 pip CH ₂), 1.38 (m, 2H, 4pipCH ₂).	
MS (APCI(+)) m/z [M+H] ⁺ :	Calculated	162.1 found 162.1

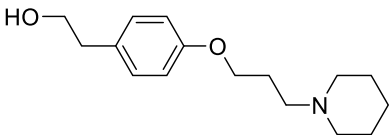
4-[3-(Piperidin-1-yl)propoxy]benzaldehyde: P40³⁸⁵

According to the procedure **A** from 4-hydroxy-benzaldehyde (15.1 mmol, 1.844 g), **P39** (10.1 mmol, 2g), 10.00 g K₂CO₃ and catalytic amount KI. Crude product was used into the next reaction step without further purification. Yellow oil. Yield: 90%.

Chemical formula:	C ₁₅ H ₂₁ NO ₂	
Mr:	247.34	
Internal code:	ME 159	
¹ H NMR (300 MHz, DMSO <i>d</i> ₆)	9.87 (s, 1H, CHO), 7.95 – 7.79 (d, <i>J</i> = 8,3 Hz, 2H, 3,5Ph), 7.19 – 7.02 (d, 2H, <i>J</i> = 8.5 Hz 2,6Ph), 4.12 (t, <i>J</i> = 6.4 Hz, 2H, O-CH ₂), 2.46 – 2.21 (m, 6H, pipN-CH ₂ , 2,6pipCH ₂), 2.00 – 1.76 (m, 2H, pipNC-CH ₂), 1.57 – 1.39 (m, 4H, 3,5pipCH ₂), 1.39 – 1.24 (m, 2H, 4pipCH ₂).	
MS (APCI(+)) m/z [M+H] ⁺ :	calculated	248.2 found 248.9

2-[4-3-(Piperidin-1-yl)propoxy]phenylethanol: P41⁶⁴³

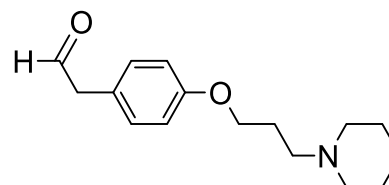
4-(2-hydroxyethyl)phenol (18.64 mmol, 2.5765 g), **P39** (9.32 mmol, 1.8474 g), 10.00 g K₂CO₃, and catalytic amount of KI were treated according to the procedure **A**. The crude product was used without further purification.

Chemical formula:	C ₁₆ H ₂₅ NO ₂	
Mr:	263.38	
Internal code:	ME 372	
¹ H NMR (300 MHz, DMSO- <i>d</i> ₆)	δ 7.23 – 6.99 (d, 2H, <i>J</i> = 8.3 Hz, 2,6 Ph CH), 6.91 – 6.69 (d, <i>J</i> = 8.9 Hz, 2H, 3,5Ph), 4.5-4.6 (bs, 1H, OH), 3.92 (t, <i>J</i> = 6.4 Hz, 2H PhO-CH ₂), 3.52 (t, <i>J</i> = 7.2 Hz, 2H, CH ₂ -OH), 2.62 (t, <i>J</i> = 7.2 Hz, 2H, pipN-CH ₂), 2.40 – 2.21 (m, 6H, Ph -CH ₂ , 2,6pip CH ₂), 1.91 – 1.70 (m, 2H, 4pipCH ₂), 1.55 – 1.41 (m, 4H, 3,5pipCH ₂), 1.41 – 1.26 (m, 2H, pipNC-CH ₂).	
MS (APCI(+)) m/z [M+H] ⁺ :	Calculated	264.2 Found 264.1

2-{4-[3-(Piperidin-1-yl)propoxy]phenyl}acetaldehyde: P42

Under nitrogen atmosphere, oxalyl chloride (3.12 mmol, 395 mg, 0.39 mL) was dissolved in DMSO and the reaction mixture was cooled down to -80 °C and stirred for 3 hours. Consequently, 0.6 mL DMSO in 2 mL DCM was added and the reaction was stirred for another 15 minutes. **P41** (2.83 mmol, 746 mg) was dissolved in 2 mL DCM and portionwise added into the reaction mixture over 5 minutes. The reaction mixture was stirred 15 minutes and 2.5 mL Et₃N was added and stirred for another 5 minutes. The reaction mixture was left to heat up to the room temperature and the reaction was quenched by adding water and stirring for 15 minutes. Reaction mixture was portioned between DCM and water (3x). Organic layers were combined, washed with saturated solution NaHCO₃, brine, dried over anhydrous MgSO₄ and evaporated under reduced pressure. LC MS measurements confirmed 50% of the product and crude product was used in the next reaction step without further purification. Yellow oil. Yield: 50%.^{471,644}

Chemical formula: C₁₆H₂₃NO₂
Mr: 241.37
Internal code: ME 383

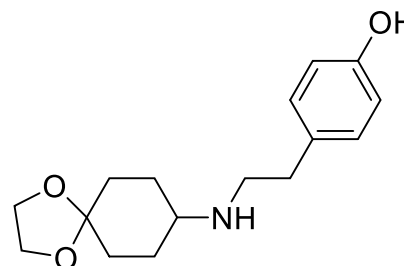


LC-MS (ESI-+)) 50.5%

4-(2-((1,4-Dioxaspiro[4.5]decan-8-yl)amino)ethyl)phenol: P43

Compound **P24** (6.4 mmol, 1.00 g), tyramine hydrochloride (6.4 mmol, 1.1118 g), Na[BH(CH₃COO)₃] (9.6 mol, 2.035 g) and CH₃COOH (6.4 mmol, 384 mg) were treated according to the procedure E. Crude product was purified with column chromatography (sorbent: SiO₂, eluent: DCM:MeOH 9:1). Yellow solid. Yield: 8%.

Chemical formula: C₁₆H₂₃NO₃
Mr: 277.36
Internal code: ME 201



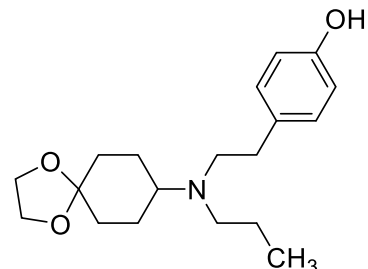
¹H NMR (300 MHz, DMSO-*d*₆) δ 9.5 (bs, 1H, OH) 7.09 – 6.92 (d, *J*=8.6 Hz 2H, 3,5 Ph), 6.74 – 6.60 (d, 2H, *J*=8.6 Hz, 2,6 Ph), 3.85 (s, 4H, 4,5spiroCH₂), 2.79 (dd, *J*=8.7, 6.4 Hz, 2H, N-CH₂), 2.64 (t, *J*=5.5 Hz, 2H, Ph-CH₂), 1.81 (m, 3H, 8spiroCH, NC-CH₂), 1.67 (m, 2H, 2,6spiroCH₂), 1.51 – 1.25 (m, 5H, NH, 1,7spiroCH₂).

MS (APCI-+): m/z [M+H]⁺: Calculated 278.2 Found 278.5

4-(2-(Propyl(1,4-dioxaspiro[4.5]decan-8-yl)amino)ethyl)phenol: P44

Compound **P43** (45.93 mmol, 127.4 mg), propionaldehyde (1.38 mmol, 80 mg), Na[BH(CH₃COO)₃] (68.89 mmol, 146 mg) were treated according to procedure E. The crude product was used in the next reaction step without further purification. Yellow solid. Yield: 69%.

Chemical formula: C₁₉H₂₉NO₃
Mr: 319.45
Internal code: ME 203

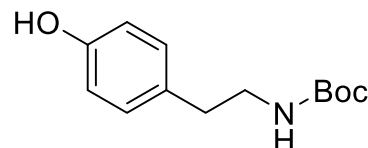


¹H NMR (300 MHz, DMSO-*d*₆) δ 9.10 (s, 1H, OH), 6.99 (d, *J* = 8.1 Hz, 2H 2, 6 Ph), 6.75 – 6.60 (m, 2H 3,5 Ph), 3.84 (s, 4H, 4,5spiroCH₂), 2.5–2.7 (m, 4H, 2,6 spiro CH₂), 1.40 (m, 2H Ph-CH₂), 1.66 (t, *J* = 12.0 Hz, 4H, 2 N-CH₂), 1.49 – 1.32 (m, 6H CH₂-CH₃, 1,7spiroCH₂), 0.94 – 0.68 (m, 3H CH₃).
MS (APCI(+)): *m/z* [M+H]⁺: Calculated 320.2 Found 320.2

***Tert*-butyl (4-hydroxyphenethyl)carbamate: P45**

Tyramine hydrochloride (17.27 mmol, 3.00 g) was dissolved in MeOH/H₂O (2:1) and di-*tert*-butyl dicarbonate (25.9 mmol, 5.66 g) and NaHCO₃ (51.81 mmol, 4.352 g) was added, and the reaction was stirred at room temperature for 3 hours. TLC was used for control. Consequently, the reaction was evaporated to dryness and partitioned in between EtOAc and H₂O. Organic layers were collected, washed with brine, dried over anhydrous MgSO₄, and evaporated under reduced pressure. The crude product was used in the next reaction step without further purification. White solid. Yield: 95%.

Chemical formula: C₁₃H₁₉NO₃
Mr: 237.30
Internal code: ME 262

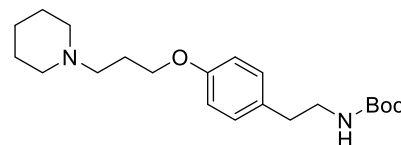


¹H NMR (300 MHz, DMSO *d*₆) δ 9.15 (s, 1H, OH), 6.97 (d, *J* = 7.9 Hz, 2H, 3,5 Ph), 6.82 (t, *J* = 4.5, 0.7 Hz, 1H, NH), 6.67 (d, *J* = 8.7 Hz, 2H, 2,6 Ph), 3.13 – 3.00 (m, 2H, CH₂-NH), 2.62 – 2.53 (m, 2H, Ph-CH₂), 1.37 (s, 9H, Boc).
MS (APCI(-)): *m/z* [M-H]⁻: calculated : 236.1 Found 236.0

Tert-butyl {4-[3-(piperidin-1-yl)propoxy]phenethyl}carbamate: 38

Compound **P44** (10.5 mmol, 2.5 g), **P39** (11.58 mmol, 2.1969 g) 10 g K_2CO_3 , and catalytic amount KI were treated according to procedure **A**. The crude product was purified with column chromatography (Sorbent SiO_2 , eluent DCM; MeOH (NH_3) 95: 5) Red solid. Yield: 81%.

Chemical formula: $C_{21}H_{34}N_2O_3$
Mr: 362.51
Internal code: ME 388



1H NMR (300 MHz, DMSO- d_6) δ 7.08 (d, J = 8.4 Hz, 2H, 3,5 Ph), 6.82 (m, 3H, NH, 2,6Ph), 3.94 (t, J = 12.8 Hz, 2H, O- CH_2), 3.08 (dt, J = 8.2, 6.1 Hz, 2H, CH_2 -NH), 2.60 (t, J = 7.4 Hz, 2H, pipN- CH_2), 2.42 – 2.19 (m, 6H, pipNC- CH_2 , 2,6pip CH_2), 1.91 – 1.74 (m, 2H, Ph- CH_2), 1.52 – 1.44 (m, 4H, 3,5pip CH_2), 1.36 (bs, 11H, Boc, 4pip CH_2).

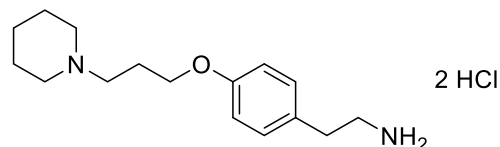
^{13}C NMR (75 MHz, DMSO) δ 156.99 (4C Ph), 155.45 (C=O), 129.48 (1C Ph), 119.22 (2, 6C Ph), 114.23 (3C, 5C Ph), 77.37 (C-t-Bu), 65.75 (O-C), 55.11 (2C, 6C pip), 54.04 (pipN-C), 41.77 (C-NBoc), 32.05 (Ph-C), 29.55 (3C, 5C pip), 28.21 (4C pip), 24.06 (CH_3 -Boc).

MS (APCI(+)): m/z $[M+H]^+$: calculated 363.3 found: 363.3;
LC-MS (ESI(+)) m/z $[M+H]^+$: 100% (363.21)

2-(4-(3-(Piperidin-1-yl)propoxy)phenyl)ethan-1-amine hydrochloride: P46

BOC-protected amine (**38**) was dissolved in 4M HCl in 1,4-dioxane and stirred at room temperature overnight. The reaction mixture was evaporated to dryness and co-evaporated at least three times with toluene or diethyl ether. Amines obtained as salts were used in the next step without further purification.

Chemical formula: $C_{16}H_{28}N_2ClO$
Mr (free base): 262.40
Mr (salt):
Internal code: ME 390



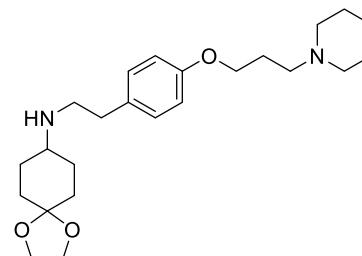
1H NMR (300 MHz, DMSO- d_6) δ 10.85 (s, 1H, NH-(CH_2) $^+$), 8.22 (s, 1H, NH_3^+), 7.35 – 7.08 (d, J = 8.8 Hz, 2H, 3,5 Ph), 7.02 – 6.77 (d, 2H, J = 5.2 Hz, 2,6 Ph), 4.03 (t, J = 6.1 Hz, 2H, O- CH_2), 3.21 – 3.01 (m, 2H, NH_2), 2.90 (m, 6H, pipN- CH_2 , 2,6pip CH_2), 2.35 – 2.10 (m, 4H, Ph CH_2 - CH_2), 2.05 – 1.61 (m, 6H, OC- CH_2 , 3,5pip CH_2), 1.40 (s, 2H, 4pip CH_2).

MS (APCI(+)): m/z $[M+H]^+$: Calculated 263.2 Found 263.1

***N*-{4-[3-(Piperidin-1-yl)propoxy]phenethyl}-1,4-dioxaspiro[4.5]decan-8-amine: P47**

Compound **P46** (2.79 mmol, 692 mg), **P35** (2.78 mmol, 435 mg), Na[BH(CH₃COO)₃] (4.19 mmol, 886 mg) and CH₃COOH (2.78 mmol, 167 mg) were treated according to the procedure **E**. Crude product was used without further purification in the next reaction step. Yellow solid. Yield: 82%.

Chemical formula: C₂₄H₃₈N₂O₃
Mr: 402.58
Internal code: ME 339



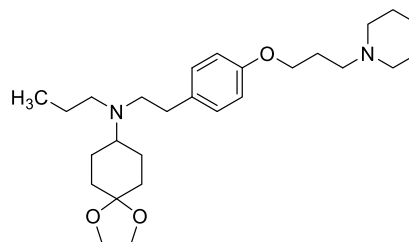
¹H NMR (300 MHz, DMSO- *d*₆) δ 7.27 – 7.17 (d, *J*=8.8 Hz, 2H, 3,5Ph), 6.90 – 6.80 (d, *J*=9.0 Hz, 2H, 2,6Ph), 4.00 – 3.91 (m, 2H, O-CH₂), 3.83 (d, *J*= 1.9 Hz, 4H, 4,5 spiroCH₂), 3.64 (s, 2H, pipN-CH₂), 2.44 – 2.32 (m, 4H, 2,6pipCH₂), 2.01 – 1.60 (m, 8H, 1,2,6,7 CH₂), 1.49 (m, 4H, 3,5pipCH₂), 1.37 (m, 4H, pipNC- CH₂, 4pipCH₂).

MS (APCI(+)): *m/z* [M+H]⁺: calculated 403.3 found:403.6

***N*-{4-[3-(Piperidin-1-yl)propoxy]phenethyl}-*N*-propyl-1,4-dioxaspiro[4.5]decan-8-amine (ST-2377): 39**

According to procedure **A** from **P44** (31.3 mmol, 100 mg), **P39** (62.6 mmol, 124 mg), 5.00 g K₂CO₃, and catalytic amount KI. The crude product was purified by column chromatography (sorberent SiO₂, eluent DCM: MeOH(NH₃) 95:5). Transparent oil. Yield: 21%.

Chemical formula: C₂₇H₄₄N₂O₃
Mr: 444.34
Internal code: ME 205



¹H NMR (300 MHz, CDCl₃) δ 7.16 – 7.08 (d, *J*=8.7 Hz, 2H, 3,5 PhCH), 6.85 – 6.76 (d, *J*=8.6 Hz, 2H, 2,6PhCH), 4.02 (t, *J* = 5.8 Hz, 2H, PhO-CH₂), 3.93 (s, 4H, 4,5spiroCH₂), 2.88 (bs, 11H, 8CH, spiroN-(CH₂)₂, 2,6spiro-CH₂ pipN- CH₂), 2.35 – 2.18 (m, 2H, Ph-CH₂), 1.95-1.2(bs, 4H, 2,6pipCH₂), 1.85 – 1.49 (m, 12H, 1,7spiro-CH₂ pipNC-CH₂, 3,4,5 pipCH₂, -CH₂CH₃), 0.92 (t, *J* = 7.3 Hz, 3H, CH₃).

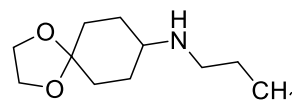
¹³C NMR (75 MHz, CDCl₃) δ 157.24 (4C Ph), 129.82 (1C Ph), 114.52 (2C, 6C Ph), 107.80 (3C 5C Ph), 65.53 (O-CC-O), 64.46 (PhO-C), 64.32, (pipN-C), 55.61 (2C 6C Ph), 53.88 (spiroN-C), 53.02 (1C, 7C spiro), 52.77 (spiroN-C), 33.79 (Ph-C), 24.6 (pipNC-C), 24.9 (2C, 6C spiro), 24.60 (C-CpipN), 23.71 (4C pip), 22.90 (3C 5C pip), 20.57 (CH₃-C), 11.72 (CH₃).

MS (APCI(+)): *m/z* [M+H]⁺: calculated 445.3 Found 446.0
LC-MS(ESI(+)): *m/z* 100%
[M+2H]²⁺[M+H]⁺: (223.01;445.28)

N-Propyl-1,4-dioxaspiro[4.5]decan-8-amine: P48⁶⁴⁵

P35 (22.41 mmol, 3.50 g) and propylamine (33.61 mmol, 1.986 g, 2.76 mL) were dissolved in 50 mL methanol. The reaction mixture was reduced with H₂ at 5 bar for ten h, in the presence of palladium on carbon. After 12 h, the mixture was filtrated through celite, and the filtrate was evaporated under reduced pressure. The crude product was used in the next reaction step without further purification. Red oil. Yield: 50%.⁶²⁹

Chemical formula: C₁₁H₂₁NO₂
Mr: 199.29
Internal code: ME 386

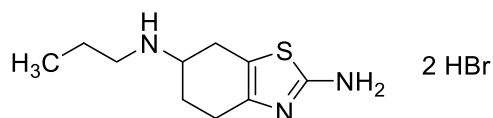


¹H NMR (300 MHz, DMSO-*d*₆) δ 3.82 (s, 4H, 4,5spiroCH₂), 2.48 – 2.39 (m, 3H, 8 CH, N-CH₂), 1.79 – 1.60 (m, 4H, 2,6spiroCH₂), 1.50 – 1.20 (m, 7H, 1,7spiroCH₂, NH, CH₂-CH₃), 0.85 (t, *J* = 7.4 Hz, 3H, -CH₃).
MS (APCI(+)): *m/z* [M+H]⁺: Calculated 200.1 found: 200.1

N⁶-Propyl-4,5,6,7-tetrahydrobenzo[d]thiazole-2,6-diamine dihydrobromide: P49^{448,646}

Compound **P48** (4.22 mmol, 841 mg), bromine (4.22 mmol, 674 mg, 4.22 mL) and thiourea (4.22 mmol, 322 mg) were treated according to the procedure **I**. White solid. Yield: 20%.

Chemical formula: C₁₀H₁₉Br₂N₃S
Mr (free base): 211.33
Mr (salt): 373.15
Internal code: ME 375

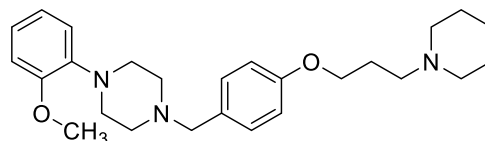


¹H NMR (300 MHz, DMSO *d*₆) δ 9.23 (bs, 1H, NH⁺) 8.80 (bs, 2H, thia-NH₂⁺), 3.09 – 2.83 (m, 4H, N-CH₂, 6thiaCH, 4thiaCH), 2.80 – 2.50 (m, 4H, 4thia CH, 7thia CH₂), 2.29 – 2.15 (m, 1H, 5thiaCH), 2.05 – 1.80 (m, 1H, 5thiaCH), 1.66 (sxt, 2H, NH-CH₂-CH₂CH₃), 0.93 (t, *J* = 7.3 Hz, 3H, CH₃).
MS (APCI(+)): *m/z* [M+H]⁺: calculated: 212.1;213.1 found:212.1,213.0

1-(2-Methoxyphenyl)-4-{4-[3-(piperidin-1-yl)propoxy]benzyl}piperazine (ST-2365): 40

Compound **P40** (10.09 mmol, 2.4967 g), 1-(2-methoxyphenyl)piperazine (**P1**, 10.9 mol, 1.9407 g) Na[BH(CH₃COO)₃] (17.4 mol, 3.6960 g) were treated according to the procedure from **E**. The crude product was purified with column chromatography (sorbent: SiO₂, eluent DCM: MeOH(NH₃) 98:2). Yellow oil, crystallizes upon storage. Yield: 13%.

Chemical formula: C₂₆H₃₇N₃O₂
Mr: 423.60
Internal code: ME 160



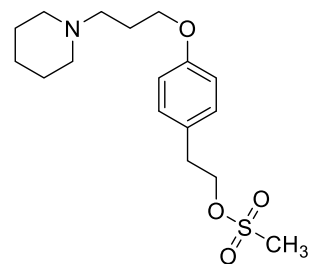
¹H NMR 300 MHz, DMSO-*d*₆) δ 7.27 – 7.15 (d, *J*=8.4 Hz, 2H, 3,5Ph), 6.97 – 6.81 (m, 6H, MeOPh, 2,6Ph), 3.97 (t, *J* = 6.4 Hz, 2H, O-CH₂), 3.75 (s, 3H, -OCH₃), 2.93 (br s, 4H, 2,6ppz), 2.50-2.52 (br s, 4H, 3,5ppz) 2.48 – 2.32 (m, 8H, pipN-CH₂, ppzN-CH₂, 2,6pipCH₂), 1.87 (m, 2H, PhOC-CH₂), 1.50 (m, 4H, 3,5pipCH₂), 1.45 – 1.32 (m, 2H, 4pipCH₂).

^{13}C NMR (75 MHz, DMSO- d_6)	δ 157.68 (4C Ph), 152.02 (2C MeOPh), 141.34 (1C MeOPh), 130.11 (1C Ph), 129.84 (2C, 6C Ph), 122.27 (4C MeOPh), 120.83 (5C MeOPh), 117.93 (3C, 5C Ph), 114.12 (6C MeOPh), 112.07 (3C MeOPh), 65.84 (O-C), 61.56 (pipN-C), 55.33 (2C, 6Cpip), 55.01 (3C,5Cpip), 53.94 (OCH ₃), 52.68 (ppzN-C), 50.06 (2C, 6Cpip), 26.16 (pipNC-C) 25.36 (4C pip), 23.9 (3C, 5Cpip).			
MS- (APCI-+): m/z [M+H] ⁺	calculated	424.3	found	424.9
LC-MS (ESI-+) m/z	95.55%			
[M+2H] ²⁺ : [M+H] ⁺ :	(212.56; 424.30)			

4-[3-(Piperidin-1-yl)propoxy]phenethyl methanesulfonate (ST-2472): 41

To a solution of **P41** (3.79 mmol, 1.00 g) in dichloromethane at 0-5 °C (ice bath temperature) was dropwise added triethylamine (5.69 mmol, 57.63 mg, 0.8 mL). The reaction mixture was stirred at 0 °C for 30 minutes. Consequently, methane sulfonyl chloride (4.17 mmol, 478 mg) was added dropwise over 15 minutes and stirred at the same temperature for another 30 minutes. The reaction was quenched with a saturated solution of NaHCO₃, stirring for 15 min. The reaction mixture was extracted with dichloromethane and water. The organic layers were combined, washed with a saturated solution of NaHCO₃, brine, dried over anhydrous MgSO₄, and concentrated under the reduced pressure (water bath temperature did not exceed 40 °C during evaporation).⁴⁸³ Yellow solid. Yield: 85%.

Chemical formula:	C ₁₇ H ₂₇ NO ₄ S
Mr:	341.47
Internal code:	ME 379

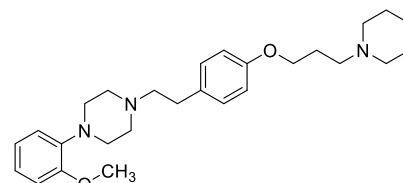


^1H NMR (300 MHz, DMSO- d_6)	δ 7.18 (d, $J=8.5$ Hz, 2H, 3,5 Ph), 6.86 (d, $J=6.1$ Hz, 2H, 2,6 Ph), 4.35 (t, $J=6.8$ Hz, 2H, PhO-CH ₂), 3.96 (t, $J=6.4$ Hz, 2H, CH ₂ -OS), 3.1 (s, 3H, CH ₃) 2.91 (t, $J=6.8$ Hz, 2H, Ph-CH ₂), 2.44 – 2.25 (m, 6H, pipN- CH ₂ , 2,6pipCH ₂), 1.84 (quin, $J=6.7$ Hz, 2H, pipC- CH ₂), 1.58 – 1.45 (m, 4H, 3,5pipCH ₂), 1.45 – 1.31 (m, 2H, 4pipCH ₂).			
^{13}C NMR (75 MHz, DMSO- d_6)	δ 157.37 (1C Ph), 129.94 (4C Ph), 128.57 (3C, 5C Ph), 114.35 (2C, 6C Ph), 70.80 (C-OSO ₃ H), 65.73 (PhO-C), 55.00 (2C, 6C pip), 53.93 (pipN-C), 36.52 (Si-CH ₃), 33.80 (Ph-C), 26.07 (4C pip), 25.33 (3C, 5C pip), 23.88.(pipNC-C).			
MS (APCI-+): m/z [M+H] ⁺ :	calculated	342.2; 343.2	found:	342.2; 343.2
LC-MS (ESI-+) m/z [M+H] ⁺ :	97.6% (342.14)			

1-(2-Methoxyphenyl)-4-{4-[3-(piperidin-1-yl)propoxy]phenetyl}piperazine (ST-2366): 42

Compound **41** (5.36 mmol, 1.8311 g), 1-(2-methoxyphenyl)piperazine (**P1**, 26.81 mmol, 5.1458 g), 10.00 g K_2CO_3 , and a catalytic amount of KI in 75 mL ACN were treated according to procedure **A**. The crude product was purified with column chromatography (sorbent SiO_2 , eluent DCM: MeOH(NH_3) 95:5). White oil which crystalize upon storage. Yield: 36%.

Chemical formula: $C_{27}H_{39}N_3O_2$
Mr: 437.63
Internal code: ME 165



1H NMR (300 MHz, DMSO- d_6) δ 7.16 – 7.08 (d, $J=8,6$ Hz, 2H, 3,5Ph CH), 6.96 – 6.78 (m, 6H, 4H MeOPh, 2,6Ph), 3.94 (t, $J=6.4$ Hz, 2H, O-CH₂), 3.76 (s, 3H, -OCH₃), 2.96 (br s, 4H, 2,6ppz), 2.68 (t, $J=9.5$, 2H, pip N-CH₂), 2.55 (br s, 4H, 3,5ppz), 2.51-2.53 (m, 2H, ppzN CH₂), 2.41 – 2.28 (m, 6H, 2,6pipCH₂, PhCH₂), 1.84 (p, 2H, OC- CH₂), 1.48 (p, $J=5.3$ Hz, 4H, 3,5pipCH₂), 1.43 – 1.32 (m, 2H, 4pipCH₂).

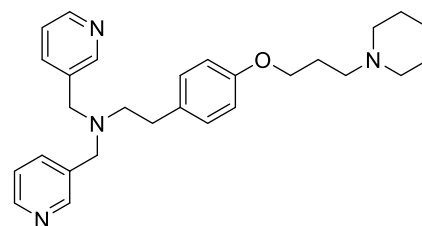
^{13}C NMR (75 MHz, DMSO- d_6) δ 156.88 (4C Ph), 152.02 (2C MeOPh), 141.36 (1C MeOPh), 132.26 (1C Ph), 129.47 (2,6C Ph), 122.24 (4C MeOPh), 120.86 (5C MeOPh), 117.88 (3,5C Ph), 114.30 (6C MeOPh), 112.10 (3C MeOPh), 65.9 (O-C), 60.04 (2C, 6C ppz), 55.34 (3C, 5C ppz) 55.12 (OCH₃), 54.05 (2C, 6C pip), 52.97 (pipN-C), 50.05 (ppzN-C), 31.84 (ppzNC-C), 26.34 (pipC-C), 25.54 pip(3C, 5C pip), 24.04 (4C pip).

MS- (APCI-+): (m/z) $[M+H]^+$: calculated: 438.4 found: 438.7
LC-MS (ESI-+) m/z 95.12%
 $[M+2H]^{2+}$: $[M+H]^+$: (219.57; 438.32)

2-{4-[3-(Piperidin-1-yl)propoxy]phenyl}-N,N-bis(pyridin-3-ylmethyl)ethan-1-amine (ST-2409): 43

Compound **P46** (1.04 mmol, 350 mg) pyridine-3-aldehyde (1.04 mmol, 111.7 mg), $Na[BH(CH_3COO)_3]$ (1.56 mmol, 332 mg) were treated according to the procedure **E**. The crude product was purified with column chromatography (sorbent: SiO_2 , eluent: DCM:MeOH(NH_3) 95:5). Orange solid. Yield: 20%.

Chemical formula: $C_{28}H_{36}N_4O$
Mr: 444.62
Internal code: ME 270



1H NMR (300 MHz, DMSO d_6) δ 8.47 (d, $J=2.2$ Hz, 2H, 2pyrCH), 8.43 (dd, $J=4.8, 1.7$ Hz, 2H, 6pyrCH), 7.64 (dt, $J=7.8, 2.0$ Hz, 2H, 4pyrCH), 7.30 (dd, $J=7.8, 4.7$ Hz, 2H, 5pyrCH), 7.03 – 6.92 (d, $J=8.7$ Hz, 2H, 3,5Ph), 6.82 – 6.74 (d, $J=8.5$ Hz, 2H, 2,6Ph), 3.93 (t, $J=6.4$ Hz, 2H, PhO-CH₂), 3.65 (s, 4H, N-(CH₂)₂), 2.71 (t, $J=8.8, 5.8$ Hz, 2H, pipN-CH₂), 2.62 – 2.53 (m, 2H, Ph-CH₂), 2.42 – 2.24 (m, 6H, N-CH₂CPh, 2,6pipCH₂), 1.82 (quin, $J=6.6$ Hz, 2H, pipNC-CH₂), 1.48 (m, 4H, 3,5pipCH₂), 1.43 – 1.31 (m, 2H, 4pipCH₂).

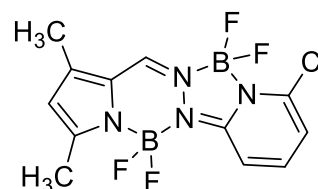
^{13}C NMR (75 MHz, DMSO d_6)	δ 156.83 (4C Ph), 149.71 (2C pyr), 148.16 (6C pyr), 136.11(4C pyr), 134.57 (1C pyr), 132.2 (1C Ph), 131.90 (4C pyr), 129.47 (3C pyr), 123.35 (5C pyr), 114.18 (2C; 6C Ph), 113.52 (3C, 5C Ph), 65.79 (O-C), 55.12 (pipN-C), 54.67 (N-C), 54.54, 54.05, 31.45 (Ph-C), 26.25(OC-C), 25.51 (3C, 5C pip), 24.07 (4C pip).
MS (APCI(+)): m/z $[\text{M}+\text{H}]^+$:	calculated 445.3 Found 445.4;
LC-MS (ESI(+))	96.35%
m/z $[\text{M}+2\text{H}]^{2+}$: $[\text{M}+\text{H}]^+$:	(223.11; 445.33)

10-Chloro-5,5,12,12-tetrafluoro-1,3-dimethyl-5*H*,12*H*-5 λ^4 ,6 λ^4 ,12 λ^4 ,13 λ^4 -

pyrido[1',2':4,5][1,2,4,3]triazaborolo[2,1-*a*]pyrrolo[1,2-*d*][1,2,4,3]triazaborinine: P53⁴⁸⁸

3,5-Dimethylpyrrole-2-carboxaldehyde (**P50**, 2 mmol, 246 mg), 2-chloro-6-hydrazinopyridine (2.1 mmol, 302 mg), and *p*-toluene sulfonic acid (0.05 mol, 87 mg) were treated according to the procedure L. The crude product was purified with flash column chromatography (sorberent SiO₂, eluent: Hex: EtOAc 1:1). Yellow solid. Yield: 30%.

Chemical formula:	C ₁₂ H ₁₁ B ₂ ClF ₄ N ₄
Mr:	344.31
Internal code:	ME 174



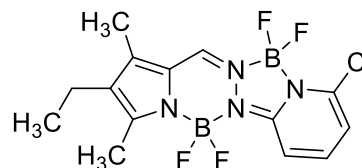
^1H NMR (600 MHz, DMSO- d_6)	δ 8.64 (s, 1H, 13 <i>H</i>), 8.12 (dd, $J = 8.9, 7.5$ Hz, 1H, 7 <i>H</i>), 7.36 (d, $J = 8.9$ Hz, 1H, 8 <i>H</i>), 7.31 (d, $J = 7.5$ Hz, 1H, 9 <i>H</i>), 6.31 (s, 1H 2 <i>H</i>), 2.40 (s, 3H, 1-CH ₃), 2.34 (s, 3H, 3-CH ₃).
MS (APCI(+)) m/z $[\text{M}+\text{H}]^+$:	Hz, 1H), 6.31 (s, 1H), 2.40 (s, 3H 1-CH ₃), 2.34 (s, 3H 3-CH ₃). calculated: 345.1; 346.1 found 345.4; 346.5

10-Chloro-2-ethyl-5,5,12,12-tetrafluoro-1,3-dimethyl-5*H*,12*H*-5 λ^4 ,6 λ^4 ,12 λ^4 ,13 λ^4 -

pyrido[1',2':4,5][1,2,4,3]triazaborolo[2,1-*a*]pyrrolo[1,2-*d*][1,2,4,3]triazaborinine: P54⁵²⁴

4-Ethyl-3,5-dimethyl-1*H*-pyrrole-2-carbaldehyde (**P51**, 4 mmol, 605mg), 2-chloro-6-hydrazinopyridine (4.2 mmol, 603mg), *p*-toluene sulfonic acid (0.1 mmol, 174 mg) were treated according to the procedure L. Crude product was purified with flash column chromatography (sorberent SiO₂, eluent: Hex: EtOAc 1:1). Yellow solid. Yield: 52%.

Chemical formula:	C ₁₄ H ₁₅ B ₂ ClF ₄ N ₄
Mr:	372.37
Internal code:	ME 186



^1H NMR (600 MHz, DMSO- d_6)	δ 8.56 (s, 1H, 13 <i>H</i>), 8.09 (dd, $J = 8.9, 7.5$ Hz, 1H, 7 <i>H</i>), 7.34 (d, $J = 8.9$ Hz, 1H, 8 <i>H</i>), 7.27 (dd, $J = 7.5, 0.7$ Hz, 1H, 9 <i>H</i>), 2.43 (q, $J = 7.5$ Hz, 2H, -CH ₃ -CH ₂), 2.37 (s, 3H, 1-CH ₃), 2.28 (s, 3H-3-CH ₃), 1.03 (t, $J = 7.6$ Hz, 3H, CH ₂ -CH ₃).
--	---

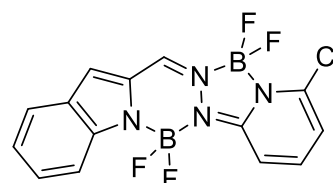
MS (APCI-(+)) m/z [M+H]⁺: calculated; 372.1;374.1 found; 373.6;374.6.

11-Chloro-6,6,13,13-tetrafluoro-6H,13H-6λ⁴,7λ⁴,13λ⁴,14λ⁴-

pyrido[1'',2'':4',5']][1,2,4,3]triazaborolo[2',1':1,2][1,2,4,3]triazaborinino[4,5-*a*]indole: P55⁵²⁴

According to the procedure **L** from Indole 2-carboxy aldehyde (**P52** 2.0 mmol, 290mg) 2-Chloro-6-hydrazinopyridine (2.1 mmol, 302 mg), *p*-toluene sulfonic acid (0.05 mmol, 87 mg) the Crude product was purified with flash column chromatography (Sorbent SiO₂, Eluent: Hex: EtOAc 1:1). Orange solid. Yield: 15%.

Chemical formula: C₁₄H₉B₂ClF₄N₄
Mr: 366.32
Internal code: ME 180



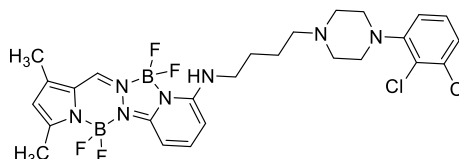
¹H NMR (300 MHz, DMSO-*d*₆) δ 9.23 (s, 1H, 14H), 8.27 (dd, *J* = 8.9, 7.7 Hz, 1H, 4H), 7.84 (dt, *J* = 8.3, 1.1 Hz, 1H, 2H), 7.67 (d, *J* = 8.4 Hz, 1H, 14H), 7.60 (s, 1H, 10H), 7.55 – 7.42 (m, 3H, 8H,9H, 16H), 7.21 (ddd, *J* = 8.0, 6.9, 0.9 Hz, 1H, 3H).

MS (APCI-(+)) m/z [M+H]⁺: calculated 366.1;367.1; Found 367.0.;367.9.

***N*-{4-[4-(2,3-Dichlorophenyl)piperazin-1-yl]butyl}-5,5,12,12-tetrafluoro-1,3-dimethyl-5H,12H-5λ⁴,6λ⁴,12λ⁴,13λ⁴-pyrido[1',2':4,5][1,2,4,3]triazaborolo[2,1-*a*]pyrrolo[1,2-*d*][1,2,4,3]triazaborinin-10-amine (ST-2371): 44**

Compound **P53** (0.246 mmol, 85 mg), 4-[4-(2,3-dichlorophenyl)piperazin-1-yl]butan-1-amine. (0.981 mmol, 297 mg) and Et₃N (0.71 mmol, 73 mg) were treated according to the procedure **M**. The crude product was purified with flash column chromatography (sorbent SiO₂, eluent:DCM: MeOH 98:2). Yellow solid. Yield: 85%.

Chemical formula: C₂₆H₃₁B₂Cl₂F₄N₇
Mr: 610.10
Melting point: 160.9 °C
Internal code: ME 175



¹H NMR (300 MHz, DMSO- *d*₆) δ 8.38 (s, 1H, 13HBP), 7.79 (t, *J* = 8.3 Hz, 1H, NH), 7.39 – 7.26 (m, 2H, 7HBP, 8HBP), 7.14 (dd, *J* = 5.9, 3.9 Hz, 1H, 9HBP), 6.91 (d, *J* = 6.5 Hz, 1H, 4H diClPh), 6.37 (m, 2H, 5,6 diClPh), 6.21 (s, 1H,2HBP), 3.45-3.35 (m, 4H, ppz,N-CH₂, NH-CH₂) 2.98 (s, 4H, 2,6ppz), 2.50-2.55 (bs, 4H, 3,5ppz) 2.36 (s, 3H, 1-CH₃), 2.31 (s, 3H, 3-CH₃), 1.68 – 1.43 (m, 4H, PipNC-CH₂-CH₂).

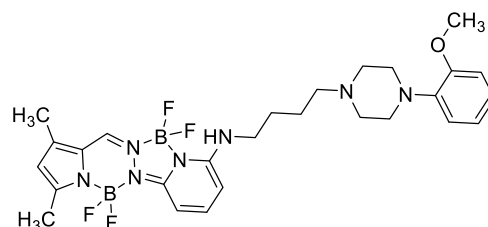
¹³C NMR (151 MHz, CDCl₃) δ 151.50 (6C BP), 146.14 (3C BP), 144.64 (1C diClPh), 141.20 (13C BP), 135.10 (3C diClPh), 134.05 (8C BP), 127.47 (5C diClppz), 127.10 (2C diClPh), 124.59 (4C diClPh), 122.57 (1C BP), 118.61 (2C BP), 117.50 (7C BP), 96.50 (14C BP), 94.51 (9C BP), 57.81

	(ppzN-C), 53.35 (2C, 6C ppz), 53.18 (3C, 5C ppz), 51.34 (NH-C), 26.72 (ppzNC-C), 23.92, (NHC-C) 13.94(3-CH ₃), 10.90 (1-CH ₃).
MS (APCI(+)): m/z [M+H] ⁺ :	calculated 610.1;612.2 found 610.3;611.3;
	609.2 : 612.4
LC-MS (ESI(+)) m/z [M+H] ⁺ :	95.48% (610.20)

5,5,12,12-Tetrafluoro-N-{4-[4-(2-methoxyphenyl)piperazin-1-yl]butyl}-1,3-dimethyl-5H,12H-5 λ^4 ,6 λ^4 ,12 λ^4 ,13 λ^4 -pyrido[1',2':4,5][1,2,4,3]triazaborolo[2,1-a]pyrrolo[1,2-d][1,2,4,3]triazaborinin-10-amine (ST 2364): 45

According to the procedure **M** from **P53** (0.26 mmol, 90 mg) 1-(2-methoxyphenyl)piperazine butanamine (**P16**, 1.83 mmol, 481 mg) and Et₃N (0.72 mmol, 72.6 mg) Crude product was purified with flash column chromatography (sorbent SiO₂, eluent DCM :MeOH 95:5). Yellow-green powder. Yield: 88%.

Chemical formula:	C ₂₇ H ₃₅ B ₂ F ₄ N ₇ O
Mr:	571.24
Melting point:	198.2 °C
Internal code:	ME 177



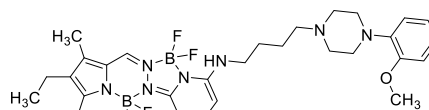
¹ H NMR (300 MHz, DMSO- <i>d</i> ₆)	δ 8.37 (s, 1H, 13HBP), 7.78 (t, <i>J</i> = 8.3 Hz, 1H, NH), 7.04 – 6.81 (m, 5H, MeOPh, 7H BP), 6.36 (dd, <i>J</i> = 21.8, 8.3 Hz, 2H, 8,9HBP), 6.21 (s, 1H, 2BP), 3.76 (s, 3H -OCH ₃), 3.35-3.30 (m, 2H, NH-CH ₂), 2.99 – 2.86 (m, 4H, 2,6ppz), 2.48 (s, 4H, 3,5ppz), 2.36 (s, 3H, 1-CH ₃), 2.30 (s, 3H, 3-CH ₃), 1.74 – 1.38 (m, 4H, ppzN-CH ₂ -CH ₂), 1.34 – 1.15 (m, 2H, NHC-CH ₂).
¹³ C NMR (75 MHz, DMSO- <i>d</i> ₆)	δ 152.01 (2C MeOPh), 151.39 (13C BP), 149.24 (1C MeOPh), 145.07 (14C BP), 144.11 (6C BP), 141.35 (8C BP), 134.58 (1C BP), 128.56 (2C BP), 122.25 (4C MeOPh), 120.86 (3C MeOPh), 117.88 (5C MeOPh), 116.78 (6C MeOPh), 112.09 (7C BP), 96.08 (10C BP), 93.27 (9C BP), 57.21 (ppzN-C), 55.33 (OCH ₃), 52.95 (2C 6C ppz), 50.07 (3C 5C ppz), 41.83 (NH-C), 26.54 (ppz NC-C) 25.85 (ppzNCC-C), 13.47 (3-CH ₃), 10.50(1 CH ₃).
MS (APCI(+)): m/z [M+H] ⁺ :	calculated: 572.3, 571.3, 5 found: 570.4;571.4
LC-MS (ESI(+)) m/z [M+H] ⁺ :	95.59% (572.28)

2-Ethyl-5,5,12,12-tetrafluoro-N-{4-[4-(2-methoxyphenyl)piperazin-1-yl]butyl}-1,3-dimethyl-5H,12H-5 λ^4 ,6 λ^4 ,12 λ^4 ,13 λ^4 -pyrido[1',2':4,5][1,2,4,3]triazaborolo[2,1-a]pyrrolo[1,2-d][1,2,4,3]triazaborinin-10-amine (ST-2379): 46

Compound **P54** (0.40mmol, 150 mg), 1-(2-methoxyphenyl)piperazine butanamine (**P16**, 1.41 mmol, 372.3 mg) and Et₃N (1mmol, 101.1 mg) were treated according to the procedure **M**. Crude product was purified with flash column chromatography (Sorbent SiO₂, Eluent DCM MeOH 95:5). Yellow solid. Yield: 52%.

Chemical formula:	C ₂₉ H ₃₉ B ₂ F ₄ N ₇ O
Mr:	599.29
Melting point:	201.7 °C

Internal code: ME 187



^1H NMR (300 MHz, DMSO- d_6) δ 8.31 (s, 1H, 13HBP), 7.77 (t, J = 8.3 Hz, 1H, NH), 7.01 – 6.77 (m, 5H, 4HMeOPh, 7HBP), 6.39 (d, J = 8.1 Hz, 1H, 8HBP), 6.31 (d, J = 8.5 Hz, 1H, 9HBP), 3.76 (s, 3H, -OCH₃), 3.41 – 3.34 (m, 2H, NH-CH₂), 2.94 (bs, 4H, 2,6ppz), 2.45-2.50 (m, 6H, 3,5ppz, pipN-CH₂), 2.44 – 2.36 (m, 2H, CH₃-CH₂), 2.33 (s, 3H 1-CH₃), 2.25 (s, 3H 3-CH₃), 1.66 – 1.44 (m, 4H NHC-CH₂-CH₂), 1.02 (t, J = 7.5 Hz, 3H, CH₃-CH₂).

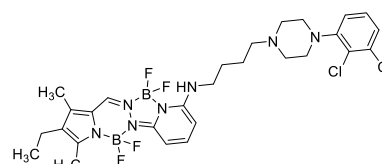
^{13}C NMR (75 MHz, DMSO- d_6) δ 152.52 (2C MeOPh), 151.86 (13C BP), 145.44 (14C BP), 141.85 (1C MeOPh), 132.25 (3C BP), 129.78 (1C BP), 128.53 (8C BP), 122.74 (4C MeOPh) 123.5 (3C MeOPh), 121.37 (6C MeOPh), 118.39 (5C MeOPh), 112.60 (10C BP), 96.32 (7C BP), 93.80 (9C BP), 57.71 (OCH₃), 55.84 (ppz 2C 6C), 53.46 (3C, 5C ppz), 50.57 (ppzN-C) 42.32 (HN-C), 26.36 (ppzNC-C), 23.64(CH₃-C), 17.12 (NHC-C), 15.21(CH₃-C) 11.99, (3-CH₃), 9.11 (1-CH₃).

MS (APCI(+)): m/z [M+H]⁺: calculated: 599.3, 601.3 found 599.9, 601.0
 LC-MS (ESI(+)) m/z [M+H]⁺: 100.0% (600.32)

***N*-{4-[4-(2,3-Dichlorophenyl)piperazin-1-yl]butyl}-2-ethyl-5,5,12,12-tetrafluoro-1,3-dimethyl-5*H*,12*H*-5 λ^4 ,6 λ^4 ,12 λ^4 ,13 λ^4 -pyrido[1',2':4,5][1,2,4,3]triazaborolo[2,1-*a*]pyrrolo[1,2-*d*][1,2,4,3]triazaborinin-10-amine (ST-2379): 47**

According to the procedure **M** from **P54** (0.23 mmol, 88 mg) 4-[4-(2,3-dichlorophenyl)piperazin-1-yl]butan-1-amine (**P17**, 0.71 mmol, 214 mg) and Et₃N (73 mg). Crude product was purified with flash column chromatography (sorbent SiO₂, eluent DCM MeOH 98:2). Yellow solid. Yield: 39%.

Chemical formula: C₂₈H₃₅B₂Cl₂F₄N₇
 Mr: 638.15
 Melting point: 176.0 °C
 Internal code: ME 200



^1H NMR (300 MHz, DMSO- d_6) δ 8.34 (s, 1H, 13HBP), 7.80 (t, J = 8.3 Hz, 1H, NH), 7.31 (d, J = 3.7 Hz, 2H, 5,6diClPh), 7.22 – 7.06 (m, 1H, 7HBP), 6.89 (m, 1H, 8HBP), 6.37 (m, 3H, 2,9HBP, 4diClPh), 3.00 (s, 3H, 1-CH₃), 2.50-2.60 (m, 4H, ppzN-CH₂ NH-CH₂), 2.45-2.50 (m, 4H, 2,6ppz), 2.44 – 2.35 (m, 4H, 3,5ppz), 2.36 (s, 3H, 3-CH₃), 2.27 (m, 2H, ppzNC-CH₂), 1.72 – 1.38 (m, 4H CH₃-CH₂, CH₂-CNH), 1.05 (t, J = 7.5 Hz, 3H, CH₃-CH₂).

^{13}C NMR (75 MHz, DMSO- d_6) δ 151.31 (13C BP), 151.19 (1C diClPh), 145.00 (3C BP), 132.58 (3C diClPh), 131.74 (8C BP), 129.28 (1C BP), 128.44 (2C BP), 125.97 (5C diClPh), 124.31 (4C diClPh), 121.34 (6C diClPh), 119.53 (6C diClppz), 95.88 (10C BP), 93.20 (9C BP), 57.05 (ppzN-C), 52.72 (2C, 6C ppz), 50.96 (3C, 5C ppz), 41.74 (NH-C), 25.78 (ppzNCC-C) 23.11 (ppzNC-C), 16.65 (CH₃-C) 14.81 (CH₃-C), 11.54 (3-CH₃), 8.74 (1-CH₃).

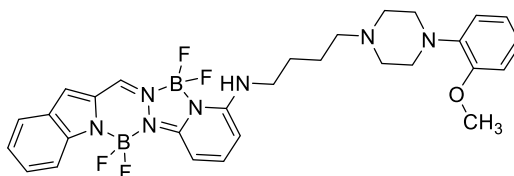
MS (APCI(+)): m/z [M+H]⁺: Calculated 638.3; 640.3 found 638.6; 640.4

LC-MS (ESI(+)) m/z [M+H]⁺: 95.11% (638.24)

6,6,12,12-Tetrafluoro-*N*-{4-[4-(2-methoxyphenyl)piperazin-1-yl]butyl}-6*H*,12*H*-6 λ^4 ,12 λ^4 ,13 λ^4 -**benzo[4',5']-[1,2,3]diazaborolo[2',1':1,2][1,2,4,3]triazaborinino[4,5-*a*]indol-11-amine (ST-2363): 48**

Compound **P55** (0.25mmol, 92mg), 1-(2-methoxyphenyl)piperazine butanamine (**P16**, 0.70mmol, 185.4 mg) and 0.1 ml Et₃N were treated according to the procedure **M**. Crude product was purified with flash column chromatography (sorberent SiO₂, eluent DCM MeOH 95:5). Orange solid. Yield: 40%.

Chemical formula: C₂₉H₃₃B₂F₄N₇O
Mr: 593.24
Melting point: 197.8 °C
Internal code: ME 182/2



¹H NMR (300 MHz, DMSO- *d*₆) δ 8.94 (s, 1H 16*HBP*), 7.90 (t, *J* = 8.3 Hz, 1H, NH), 7.80 (dd, *J* = 8.2, 1.2 Hz, 1H, 4*HBP*), 7.67 (d, *J* = 8.4 Hz, 1H, 14*HBP*), 7.46 – 7.31 (m, 3H, 1*H*, 2*H*, 8*HBP*), 7.18 (ddd, *J* = 8.1, 6.9, 1.0 Hz, 1H, 3*HBP*), 6.98 – 6.82 (m, 4H, MeOPh), 6.54 (dd, *J* = 8.4, 5.7 Hz, 2H 10*H*,9*HBP*), 3.76 (s, 3H, -OCH₃), 3.40 (d, *J* = 6.5 Hz, 2H, ppzN-CH₂), 2.90-3.00 (bs, 4H, 2,6ppz), 2.45 (m, 4H 3,5ppz) 2.37 (bs, 2H NH-CH₂), 1.68 – 1.45 (m, 4H ppzN CH₂-CH₂).

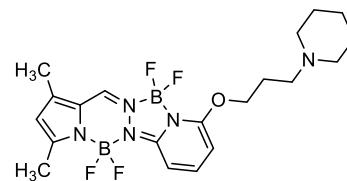
¹³C NMR (75 MHz, DMSO- *d*₆) δ 152.02 (6C BP), 151.75, (3C BP) 145.92 (2C MeOPh), 132.67 (1C MeOPh), 129.16 (13C BP), 126.47 (8C BP), 122.67 (6C MeOPh), 122.27 (5C MeOPh) 121.30 (4C MeOPh) 120.87 (1C BP), 117.90 (2C BP), 114.48 (3C MeOPh),, 113.30 (7C BP), 112.10 (14C BP), 98.39 (9C BP), 57.18 (ppzN-C), 55.35, (OCH₃), 52.96 (2C, 6C ppz), 50.06 (3C, 5C ppz), 41.95(NH-C) 25.83, (ppzNC-C), 23.09.(ppzNCC-C)

MS (APCI(+)): *m/z* [M+H]⁺: calculated 593.3, 594.3 found: 593.8;594.5
LC-MS (ESI(+)) *m/z* [M+H]⁺: 96.93% (594.29)

5,5,12,12-Tetrafluoro-1,3-dimethyl-10-[3-(piperidin-1-yl)propoxy]-5*H*,12*H*-5 λ^4 ,6 λ^4 ,12 λ^4 ,13 λ^4 -**pyrido[1',2':4,5][1,2,4,3]triazaborolo[2,1-*a*]pyrrolo[1,2-*d*][1,2,4,3]triazaborinine (ST-2468): 49**

To a solution of **P38** (1.12 mmol, 161.1 mg) in THF was portion wise added NaH (ω =60%, 1.12 mmol, 26.99 mg) and the reaction mixture was stirred at 40 °C 3 hours. Consequently, **P53** (78.73 mmol, 27.11 mg) was added and the reaction was left to stir at 40°C overnight. The reaction was quenched by adding saturated solution NH₄Cl and stirring for 15 minutes. The reaction mixture was further portioned between DCM and H₂O. Organic layers were combined, washed with brine, dried over anhydrous MgSO₄, and evaporated under reduced pressure. The crude product was purified by column chromatography (sorberent SiO₂, eluent DCM MeOH 9:1.) Green solid. Yield: 19%.

Chemical formula: C₂₀H₂₇B₂F₄N₅O
Mr: 451.08
Internal code: ME 307

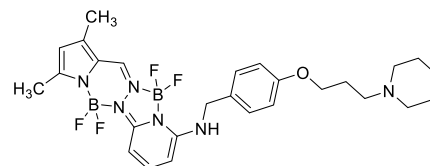


^1H NMR (300 MHz, DMSO d_6)	δ 8.46 (s, 1H, 13HBP), 8.12 (t, $J = 8.4$ Hz, 1H, 7HBP), 6.90 (d, $J = 8.5$ Hz, 1H, 8HBP), 6.66 (d, $J = 8.1$ Hz, 1H, 2HBP), 6.24 (s, 1H, 9HBP), 4.41 (t, $J = 6.0$ Hz, 2H O-CH ₂), 2.77 (bs, 6H 2,6pipCH ₂ , pipN-CH ₂), 2.37 (s, 3H 1-CH ₃), 2.31 (s, 3H 3-CH ₃), 2.15 – 2.02 (m, 2H, CH ₂ -CpipN), 1.63 (bs, 4H, 3,5pipCH ₂), 1.46 (bs, 2H, 4pipCH ₂)
^{13}C NMR (151 MHz, DMSO- d_6)	δ 158.73 (6C BP), 150.70 (3C BP), 148.34 (14C BP), 145.7 (13 C BP), 142.26 (8C BP), 136.43 (7C BP), 122.8 (2C BP), 101.22 (1C BP), 96.43 (9C BP), 68.45 (O-C), 53.88 (N-C), 53.57 (2C, 6C pip), 24.46 (C-CN) 27.10. (4C pip) 25.073 (3C, 5C pip) 14.05 (3-CH ₃), 11.041 (1-CH ₃).
MS (APCI(+)): [M+H] ⁺ +	calculated 452.2; 451.2; 453.2 found 451.5; 452.6; 453.6
LC-MS (ESI(+)) m/z [M+H] ⁺ +	99.58% (452.22)

5,5,12,12-Tetrafluoro-1,3-dimethyl-N-{4-[3-(piperidin-1-yl)propoxy]benzyl}-5H,12H-5 λ^4 ,6 λ^4 ,12 λ^4 ,13 λ^4 -pyrido[1',2':4,5][1,2,4,3]triazaborolo[2,1-a]pyrrolo[1,2-d][1,2,4,3]triazaborinin-10-amine (ST-2416): 50

Compound **P53** (0.29 mmol, 100 mg), **P46** (1.16 mmol, 392.2 mg) and Et₃N (0.87 mmol, 88.17 mg) were treated according to the procedure **M**. Crude product was purified by flash column chromatography (Sorbent SiO₂ Eluent: DCM MeOH 93:7). Yellow-green solid. Yield: 19%.

Chemical formula:	C ₂₇ H ₃₄ B ₂ F ₄ N ₆ O
Mr:	556.22
Internal code	ME 251



^1H NMR (300 MHz, CDCl ₃)	δ 7.61 – 7.47 (m, 2H 2,6Ph), 7.23 (d, $J = 2.1$ Hz, 1H, 14HBP), 6.96 – 6.85 (m, 2H 3,5 Ph), 6.69 (d, $J = 8.4$ Hz, 1H, 2HBP), 6.13 (s, 1H, 7H BP), 5.90 (d, $J = 8.2$ Hz, 1H, 8HBP), 5.59 (t, $J = 5.5$ Hz, 1H, 9HBP), 4.42 (d, $J = 5.5$ Hz, 2H Ph-CH ₂), 4.02 (t, $J = 6.2$ Hz, 2H O-CH ₂), 2.74 – 2.50 (m, 5H NH, 3,5pipCH ₂), 2.48 (s, 3H 1-CH ₃), 2.29 (s, 3H CH ₃), 1.57-2.0 (br s, 4H pipN-CH ₂ CH ₂), 1.26 (brs, 4H 2,6pipCH ₂), 0.93 – 0.78 (m, 2H, 4pipCH ₂).
^{13}C NMR (75 MHz, CDCl ₃)	δ 158.75 (6C BP), 153.8 (4C Ph), 144.68 (3C BP), 135.06 (14 CBP), 128.27 (13 C BP), 127.98 (1C Ph), 127.09 (8C BP), 122.3 (2C ,6 C Ph), 117.04 (10C BP), 115.04 (3C, 5C Ph), 95.07 (7C BP), 95.01 (9C BP), 66.05 (O-C), 55.85 (2C, 6C pip), 54.44 (N-C), 46.27 (Ph-C), 29.71 (C-Cpip), 23.99 (3C 5C pip), 13.93 (3-CH ₃), 10.89. (1-CH ₃)
MS(APCI(-)): m/z [M-H] ⁺ :-	calculated 555.25; 556.3 Found: 556.7; 557.8
LC-MS (ESI(+)) m/z [M+H] ⁺ +	97.44% (557.34)

6.3 Molecular Docking Simulation

Molecular docking simulations were performed using GOLD 5.6.3 software (CDCC, Cambridge, United Kingdom). Into co-crystal structures of D₃R (PDB ID: 3PBL and D₂R (PDB ID: 6CM4) test ligand of the first series have been docked.⁴⁰⁰

6.3.1 Protein Preparation

Protein preparation represents a crucial step in molecular docking and enables the assigning of titration places and optimizing hydrogen bonds. Protein was prepared as long these lines: firstly, hydrogen atoms were added to the molecule (Playmolecule ProteinPrepare procedure (Accelerate labs, Barcelona, Spain)⁶⁴⁷ lysozyme residues were manually removed, and 7 alanine residues were inserted in the molecule via Modelersoftware⁶⁴⁸ (maintenance: Benn Webb, USCF, San Francisco, USA). For inserting proteins in phosphatidylcholine membrane, CHARM-GUI membrane builder was used (maintenance: Dr. Im WG, Lehigh University, Bethlehem).⁶⁴⁹ Proteins underlaid the steepest descent energy minimization protocol, using GAFF2 force fields and Amber ff14sb in AMBER 2018 software (maintenance: Rashaan Lyons Mission Bay Campus, San Francisco, USA)⁶⁵⁰ For all of the ligands, dominant microspecies at physiological pH were selected in Marvin Sketch 5.5.1.0 (ChemAxon, Budapest, Hungary). Consequently, obtained forms were pre-optimized with semiempirical Parameterized Model revision three methods in Chem 3D (ChemOffice, Perkin Elmer Woltam, Massachusetts USA) and refined with Hartree-Fock/3-21G method. With Gaussian Ultra 7 Software(incorporated in Chem3D).⁶⁵¹ Binding site was defined as residues within 6Å from co-crystal ligands, number of genetic algorithm runs was set to 30 with maximum flexibility accounted for ligands. As scoring function Goldscore was chosen (regarding to the lowest RMSD). 2D interaction plots were generated with LigPlot+ software⁶⁵² (maintenance: Roman Laskowski, European Bioinformatics Institute, Cambridge, UK).

6.3.2 QM/MM Calculations

System was equilibrated minimum through 6 steps, with standard Amber protocol, generated by CHARM-GUI which led to energy minimization. In each equilibration step until the fore last ligands position restraints were keep constant (10 kcal/mol/Å²) while step position restraints on protein were gradually reduced (starting from 10 kcal/mol/Å²). In the last two equilibration steps QM/MM approach was used: (ligand restraints = 10 kcal/mol/Å² and protein restraints = 0.5 kcal/mol/Å²; ligand restraints = 0 kcal/mol/Å² and protein restraints = 0.1 kcal/mol/Å²

respectively. QM region was treated with semi-empirical PM3 Hamiltonian (sander suite of Amber 2018). The rest was classically treated with Amber ff14sb. Upon equilibration end, positions restraints were removed production run (100 ps) with same protocol. Each frame from last 20 ps of trajectory was additionally minimized on the same semi-empirical PM3 level, and the complex with the minimal total energy was further optimized using QM/MM approach on the higher level of theory (DFT M06-2X functional with def2-TZUP basis set).⁶⁵³ For each minimization cycle 200 cycles of steepest descent and conjugated gradient were conducted. DFT QM/MM minimization was performed with Orca 4.21 (part of Amber 2018).⁶⁵⁴ An electronic embedding scheme was used to treat simulations non-periodically. The SHAKE algorithm was applied on H atoms in QM region, and PME approach was used to calculate long-range electrostatics.

6.3.3 Non-Covalent Interaction Calculations

Interactions between **9** and receptors of interest were interpreted by NCI plot 4.0 software.^{400,556} This software predict and analysis reduced density gradients (s) which are simple function of electronic density (ρ) and its gradient ($s(r) = \frac{1}{C_s} \frac{|\nabla\rho(r)|}{\rho(r)^{4/3}}$). Reduced gradient describes local non homogeneity of electron. Density in the molecule and in regions far from the molecule, the density exponentially decays to zero and will consequently be strong positive. However, values of RDS approaches zero in the cases of covalent bonds and non-covalent interactions. NCI is commonly associated with small gradient followed by low density while covalent bonds are associated with high density and small gradient. Type of NCI is determined using Laplacian of the density. Different types of NCI (hydrogen bonds, π -interactions, Van der Waals interaction) can be differentiated with the sign of the second eigenvalues of the Hessian matrix (λ_2). Strong stabilizing interactions, commonly observed at hydrogen bonds express negative (λ_2) value higher ρ values (> 0.01 a.u.) and weak delocalized interactions like Van der Waals interactions have ρ values close to 0. Strong repulsive interactions express positive λ_2 and ρ values larger than 0.01 Higher densities correspond to stronger interactions, both stabilizing and destabilizing, depending on λ_2 . NCIs were analyzed in the terms of the 2D NCI plots of s vs $\rho \cdot \text{sign} \lambda_2$, 3D NCI plots (isosurfaces), and integrals of electron density ($\int \rho^2$). Cut-off value of $s \leq 0.3$ was used to plot gradients in 3D space and to generate isosurfaces of well-defined density values. Self-consistent field method was conducted to examine SF₅ interaction moiety with the receptor of interest while promolecular approach was used to determine interaction of entire ligands with protein residues. integrals of

promolecular densities ($\int \rho^2$) of three specific regions ($\text{sign}(\lambda^2)\rho(r)$ between -0.05 and -0.01 ; $\text{sign}(\lambda^2)\rho(r)$ between -0.01 and 0.01 and $\text{sign}(\lambda^2)\rho(r)$ between 0.01 and 0.05) across QM/MM trajectory were used to quantitatively assess convergence of QM/MM simulations.^{655, 656}

6.4 Pharmacological Experiments

6.4.1 Cell Culture and Membrane Preparation of CHO-K1 Cells expressing the hD_{2s}R and the hD₃R

Chinese hamster ovary (CHO-K1) cell lines that stably express either the short splicing variant of D₂R human (D_{2short}) or the D₃ receptor were firstly grown at 37 °C in a humidified (95%) atmosphere of 5% CO₂ in Dulbecco's Modified Eagle Medium-high glucose (DMEM), with 4500 mg/L glucose and sodium bicarbonate, without *L*-glutamine and sodium pyruvate, liquid, sterile-filtered, suitable for cell culture, suitable for hybridoma.⁵³⁹ DMEM medium represents a widely used basal medium for culturing mammal cells, and for this cell cultivation was supplemented for D₂R cells with 1% glutamine, 10% fetal bovine serum (FBS), and 1% penicillin/streptomycin, and for D₃R with 1% glutamine, 10% dialyzed FBS. After medium removal, CHO-D₂ cells were collected in 10 mL phosphate-buffered saline buffer (DBS w/o: Ca and Mg, product number: P04-36500) and CHO-D₃ cells in medium. Consequently, cell membrane homogenate was centrifuged at 3000xg for 10 minutes at 4 °C. Afterward, the cells were resuspended in a binding buffer that contains 120 mM NaCl, 1 mM CaCl₂, 5 mM KCl, 120 mM NaCl and 50 mM Tris, pH 7.4) with Ultraturrax® Homogenizer (Ika-MWerke GmbH) disrupted and centrifuged at 23 000 x g for 30 minutes at the same temperature. The pellet was stored in ice-cold binding buffer at -80 °C.⁵⁶⁰

6.4.2 Radioligand Displacement Assay at D_{2short}R and D₃R on CHO-K1 Cell Line Preparation

The affinity at the human isoform dopamine D_{2s}R and D₃R receptor were determined by radioligand displacement assays, as reported previously by this working group with slight modifications.^{559,560} Membrane preparations of CHO-K1 cell line firmly expressing the short splicing variant hD_{2s}R and hD₃R were used for performing displacement assay. Before the experiment started, cells were thawed, diluted, sonicated at 4 °C, and stored in ice-cold binding buffer. For binding experiments, 96well microtiter plates were used (TPP Techno Plastic Products AG, Trasadingen, Switzerland). Membrane fractions (D_{2s}R: 25 µg/200 µL; D₃R: 20 µg/200 µL, final concentrations) were co-incubated with [³H]spiperone ($K_d = 0.2$ nM, PerkinElmer Life, and

Analytical Sciences, Rodgau, Germany) and test ligand for 120 min at room temperature. Stock solutions (10 mM) of test ligands, prepared in pure DMSO. Stock solutions were further diluted in binding buffer (2 mM CaCl₂, 1 mM MgCl₂, 120 mM NaCl, 5 mM KCl, 50 mM TRIS/HCl, pH 7.4). Samples were incubated with 10 μM haloperidol to determine non-specific binding. Filtration was performed using a 96-well cell harvester with deionized water (Inotech AG, Dottikon, Switzerland). The assay was terminated by rapid filtration through GF/B glass fiber filters (PerkinElmer Life Sciences, Rodgau, Germany) pre-treated with 0.3% polyethyleneimine (Sigma–Aldrich, Taufkirchen, Germany) using an Inotech cell harvester (Inotech AG, Dottikon, Switzerland). The system was washed three times with 0.3 ml/well of demineralized water to remove the unbound ligand. Filter was dried at 54 °C for one hour in drying cabinet, and radioactivity was determined by liquid scintillation counting, using 1450 MicroBeta Trilux scintillation counter (PerkinElmer Life Sciences, Rodgau, Germany). The data was obtained in triplicate in at least three independent experiments. The data analysis was performed with GraphPad Prism 6.1 (San Diego, CA, USA) using non-linear regression (one-site competition). The IC₅₀ values were transformed to K_i values by using the CHENG-PRUSOFF equation.⁵⁶⁶ K_i is reported with corresponding confidence interval (95%), while pK_i is interpreted as mean value ± standard error of the mean (S.E.M). In contrast, the c.p.m in graphs were given as mean ± standard deviation.

6.4.3 hH₃R [³H]-N^α-methylhistamine Binding Assay on HEK-293 Cell Membrane Preparation

The assay was conducted as previously reported by this working group, with slight modification.⁵⁶⁷⁶⁰⁷ Human embryo kidney (HEK-293) cell line was washed and homogenized with an Ultraturrax® homogenizer and stored in ice-cold H₃R binding buffer (100 mM NaCl, 12.5 mM MgCl₂, and 75 mM Tris/HCl, pH 7.4). Membrane fractions were centrifuged (20,000 xg, 20 min, 4 °C), resuspended in the binding buffer, and stored at -80 °C until further use. Before the experiment started, cell membranes were thawed, sonicated at 4 °C, and kept in ice-cold binding buffer. Competition binding experiments were carried out along these lines: crude membrane extracts (20-25 μg/well in a final volume of 200 μL binding buffer were firstly incubated with [³H]N^α-methylhistamine(2 nM; K_d = 3.08 nM, determined by saturation binding experiments, PerkinElmer Life and Analytical Sciences, Rodgau Germany) and different concentration range to the respective test ligand. The assay was conducted in a concentration range 0.01 nM-100 μM of

the test compound (seven to eleven concentrations) in 96-well microtiter plates (TPP Techno Plastic Products AG, Trasadingen, Switzerland) with a final assay volume of 200 μL per well. Ligands were incubated while continuously shaking, at room temperature for 90 minutes. In presence of selective 10 μM H_3 inverse agonist/antagonist pitolisant, nonspecific binding was determined. Bound radio ligand was further filtrated from free radioligand through GF/B filters which were pre-treated with 0.3% (m/v) polyethyleneimine using an Inotech cell harvester. Unbound ligand was further removed by washing with ice cold demineralized water (0.3mL per well). Assay were carried out at least in duplicates in minimum three separate experiments., Radioactivity was determined by liquid scintillation counting, 1450 MicroBeta Trilux scintillation counter (PerkinElmer Life Sciences, Rodgau, Germany). Specific binding were analyzed by non-linear square fit by Graphpad Prism 6.1 (San Diego, USA) Affinities to the receptor of interest (K_i) were expressed as with corresponding confidence interval. were calculated from the IC_{50} values using the CHENG-PRUSOFF equation.

6.4.4 Oxygen Radical Absorbance Capacity Assay

Oxygen Radical Absorbance Capacity (ORAC) assay was established and performed in Stark's lab to examine antioxidative properties of chosen compounds. The method was based as previously described by Ou et al.⁵⁷⁷ In our setup, the ORAC indicates the concentration of a compound to which its antioxidant capacity is equivalent to 1 μM . Assay establishment: radical generator (AAPH) concentration, 100 μL of fluorescein was incubated at 37 $^\circ\text{C}$ for 15 minutes (excitation and emission wavelengths 492 and 516 nm, respectively, were used for initial reading) to determine bleaching in presence of free radical only. As negative control potassium-phosphate buffer was used while as positive control served 100 μL of AAPH. The 96-well plates were shaken for 10 seconds. The signal was measured in 61 cycles in a 1-minute interval at 492 nm and 516 nm (excitation and emission wavelength, respectively). The measurement was conducted with 50 flashes with 400 Hz and an integration time of 20 μs . The total volume assay was 200 μL . The bleaching of fluorescein by 75 mM AAPH was reached after less than 20 minutes, and this concentration of free radical generator were chosen for further assay conduction. A linear correlation was established between net AUC and Trolox concentration from 1.25 μM and 20 μM ($R^2 = 0.996$). BHA (1 mM), caffeic acid, and quercetin (0.5 mM) were used as references for Trolox concentration of 2 mM. Experiments were conducted at least seven times.

Assay conduction in brief: fluorescein (100 nM) was incubated with examined compounds (concentration range Trolox: 1.25, 2.5, 5, 10 and 20 μM , BHA: 0.625, 1.25, 2.5, 5 and 10 μM , caffeic acid and quercetin: 0.3125, 0.625, 1.25, 2.5 and 5 μM) for 15 minutes. Consequently, 75 mM of AAPH was added at 37 °C for 61 min to 91 min, and fluorescence decrease was measured. The net AUC values were calculated and plotted against concentration the Trolox concentrations ($R^2 > 0.95$).

$$\text{net AUC} = \text{slope [1/}\mu\text{M]}_{\text{Trolox}} * C_{\text{Trolox}} [\mu\text{M}] + \text{y-intercept}_{\text{Trolox}}$$

Consequently, from net AUC values, ORAC values of each independent experiment were calculated and plotted against the concentration of the substance on the calibration curve.

$$\text{ORAC } [\mu\text{M}] = \text{net AUC}_{\text{sample}} - \text{y-intercept}_{\text{Trolox}} / \text{slope [1/}\mu\text{M]}_{\text{Trolox}}$$

The mean values of ORAC from seven experiments were plotted against reference compounds (BHA, caffeic acid, and quercetin), and a 1 μM concentration of examined compound was inserted in this calibration curve. ORAC values of the substances have been determined from this calibration curve. Data were analyzed with GraphPad Prism 7.1. and are presented as mean value \pm standard deviation

7 References

- (1) Mannich C.; Jacobsohn W. Uber Oxyphenyl-Alkylamine Und Dioxyphenyl-Alkylamine. *Mitteilung aus Pharm. Institut der Univ. Berlin* **1910**.
- (2) Daubner, S. C.; Le, T.; Wang, S. Tyrosine Hydroxylase and Regulation of Dopamine Synthesis. *Arch. Biochem. Biophys.* **2011**, *508* (1), 1–12.
- (3) Dunkley, P. R.; Bobrovskaya, L.; Graham, M. E.; Von Nagy-Felsobuki, E. I.; Dickson, P. W. Tyrosine Hydroxylase Phosphorylation: Regulation and Consequences. *J. Neurochem.* **2004**, *91* (5), 1025–1043.
- (4) Nagatsu T., Levitt M., Udenfriend S. Tyrosine Hydroxylase. the Initial Step in Norepinephrine Biosynthesis. *J. Biol. Chem.* **1964**, *239* (9), 2910–2917.
- (5) Cho, S.; Neff, N. H.; Hadjiconstantinou, M. Regulation of Tyrosine Hydroxylase and Aromatic L-Amino Acid Decarboxylase by Dopaminergic Drugs. *Eur. J. Pharmacol.* **1997**, *323* (2–3), 149–157.
- (6) Berry, M. D.; Juorio, A. V.; Li, X. M.; Boulton, A. A. Aromatic L-Amino Acid Decarboxylase: A Neglected and Misunderstood Enzyme. *Neurochem. Res.* **1996**, *21* (9), 1075–1087.
- (7) Hadjiconstantinou, M.; Neff, N. H. Enhancing Aromatic L-Amino Acid Decarboxylase Activity: Implications for L-DOPA Treatment in Parkinson's Disease. *CNS Neurosci. Ther.* **2008**, *14* (4), 340–351.
- (8) Green, A. L. The Inhibition of Dopamine- β -Oxidase by Chelating Agents. *BBA - Enzymol. Subj.* **1964**, *81* (2), 394–397.
- (9) Weinsihilboum R.M.; Nguuyen B. T.; Johnsos D.G.; Kopin J.I.; Axelrod J. Proportioanl release of Norepinephrine and Dopamine- β -hydroxilase form Sympatic Nerves. *Science* **1971**, *174*, 1349–1352.
- (10) Molinoff, P. B.; Axelrod J; Biochemistry of catecholamines, *Annu. Rev. Biochem.* **1971**, *40*, 465-500.
- (11) Meiser, J.; Weindl, D.; Hiller, K. Complexity of Dopamine Metabolism. *Cell Commun. Signal* **2013**, *11* (1), 1–18.
- (12) Pugh, C. E. M.; Quastel, J. H. Oxidation of Aliphatic Amines by Brain and Other Tissues. *Biochem. J.* **1937**, *31* (2), 286–291.
- (13) Resnick, O.; Elmadjian, F. The metabolism of epinephrine containing isotopic carbon in man, *J. Clin. Endocrinol. Metabol.* **1958**, *18*, 28-35.
- (14) Bach, A. W.; Lan, N. C.; Johnson, D. L.; Abell, C. W.; Bembenek, M. E.; Kwan, S. W.; Seeburg, P. H.; Shih, J. C. CDNA Cloning of Human Liver Monoamine Oxidase A and B: Molecular Basis of Differences in Enzymatic Properties. *Proc. Natl. Acad. Sci. U. S. A.* **1988**, *85* (13), 4934–4938.
- (15) Kwan, S. W.; Bergeron, J. M.; Abell, C. W. Molecular Properties of Monoamine Oxidases A and B. *Psychopharmacology (Berl)*. **1992**, *106*, 1–5.
- (16) Da Prada, M.; Kettler, R.; Keller, H. H.; Burkard, W. P.; Muggli-Maniglio, D.; Haefely, W. E. Neurochemical Profile of Moclobemide, a Short-Acting and Reversible Inhibitor of Monoamine Oxidase Type A. *J. Pharmacol. Exp. Ther.* **1989**, *248* (1), 400–414.
- (17) Axelrod A. O-Methylation of Epinephrine and Other Catechols in vitro and in vivo, *Science*, **1957**, *126*, 7–9.
- (18) Labrosse E.H.; Axelrod J.; O-methylation, the Principal Route of Metabolism of Epinephrine in Man. *Science*, **1958**, *128* (7), 593–595.
- (19) Akil, M.; Kolachana, B. S.; Rothmond, D. A.; Hyde, T. M.; Weinberger, D. R.; Kleinman, J. E. Catechol-O-Methyltransferase Genotype and Dopamine Regulation in the Human Brain. *J. Neurosci.* **2003**, *23* (6), 2008–2013.
- (20) Morimoto, S.; Takao, M.; Hatsuta, H.; Nishina, Y.; Komiya, T.; Sengoku, R.; Nakano, Y.; Uchino, A.; Sumikura, H.; Saito, Y.; Kanemaru, K.; Murayama, S. Homovanillic Acid and 5-Hydroxyindole Acetic Acid as Biomarkers for Dementia with Lewy Bodies and Coincident Alzheimer's Disease: An Autopsy-Confirmed Study. *PLoS One* **2017**, *12* (2), 1–11.
- (21) Hiroi, T.; Imaoka, S.; Funae, Y. Dopamine from tyramine. *Biochem. Biophys. Res. Commun* **1998**, *843* (249), 838–843.
- (22) Bromek, E.; Haduch, A.; Gołembowska, K.; Daniel, W. A. Cytochrome P450 Mediates Dopamine Formation in the Brain in Vivo. *J. Neurochem.* **2011**, *118* (5), 806–815.
- (23) Iuga, C.; Alvarez-Idaboy, J. R.; Vivier-Bunge, A. ROS Initiated Oxidation of Dopamine under Oxidative Stress Conditions in Aqueous and Lipidic Environments. *J. Phys. Chem. B* **2011**, *115* (42), 12234–12246.
- (24) Guo, J. D.; Zhao, X.; Li, Y.; Li, G. R.; Liu, X. L. Damage to Dopaminergic Neurons by Oxidative Stress in Parkinson's Disease (Review). *Int. J. Mol. Med.* **2018**, *41* (4), 1817–1825.
- (25) Kopin I.J. Technique for the Study of Alternate Metabolic Pathways ; Epinephrine Metabolism in Man, *Science*, **1960**, *131*,1372-1374.
- (26) Sun, Y.; Pham, A. N.; Waite, T. D. Elucidation of the Interplay between Fe(II), Fe(III), and Dopamine with

- Relevance to Iron Solubilization and Reactive Oxygen Species Generation by Catecholamines. *J. Neurochem.* **2016**, 955–968.
- (27) Segura-Aguilar, J.; Paris, I.; Muñoz, P.; Ferrari, E.; Zecca, L.; Zucca, F. A. Protective and Toxic Roles of Dopamine in Parkinson's Disease. *J. Neurochem.* **2014**, *129* (6), 898–915.
- (28) Sulzer, D.; Bogulavsky, J.; Larsen, K. E.; Behr, G.; Karatekin, E.; Kleinman, M. H.; Turro, N.; Krantz, D.; Edwards, R. H.; Greene, L. A.; Zecca, L. Neuromelanin Biosynthesis Is Driven by Excess Cytosolic Catecholamines Not Accumulated by Synaptic Vesicles. *Proc. Natl. Acad. Sci. U. S. A.* **2000**, *97* (22), 11869–11874.
- (29) Bergquist, J.; Tarkowski, A.; Ekman, R.; Ewing, A. Discovery of Endogenous Catecholamines in Lymphocytes and Evidence for Catecholamine Regulation of Lymphocyte Function via an Autocrine Loop. *Proc. Natl. Acad. Sci. U. S. A.* **1994**, *91* (26), 12912–12916.
- (30) Jose, P. A.; Eisner, G. M.; Felder, R. A. Role of Dopamine Receptors in the Kidney in the Regulation of Blood Pressure. *Curr. Opin. Nephrol. Hypertens.* **2002**, *11* (1), 87–92.
- (31) Eisenhofer, G.; Goldstein, D. S. Peripheral Dopamine Systems. *Prim. Auton. Nerv. Syst. Second Ed.* **2004**, 176–177.
- (32) Quickel, K. E.; Feldman, J. M.; Lebovitz, H. E. Inhibition of Insulin Secretion by Serotonin and Dopamine: Species Variation. *Endocrinology* **1971**, *89* (5), 1295–1302.
- (33) Snider, S. R.; Kuchel, O. Dopamine: An Important Neurohormone of the Sympathoadrenal System. Significance of Increased Peripheral Dopamine Release for the Human Stress Response and Hypertension. *Endocr. Rev.* **1983**, *4* (3), 291–309.
- (34) German, D. C.; Manaye, K. F. Midbrain Dopaminergic Neurons (Nuclei A8, A9, and A10): Three-dimensional Reconstruction in the Rat. *J. Comp. Neurol.* **1993**, *331* (3), 297–309.
- (35) Zhou, F. M.; Lee, C. R. Intrinsic and Integrative Properties of Substantia Nigra Pars Reticulata Neurons. *Neuroscience* **2011**, *198*, 69–94.
- (36) Tepper, J. M.; Martin, L. P.; Anderson, D. R. GABA(A) Receptor-Mediated Inhibition of Rat Substantia Nigra Dopaminergic Neurons by Pars Reticulata Projection Neurons. *J. Neurosci.* **1995**, *15* (4), 3092–3103.
- (37) Celada, P.; Paladini, C. A.; Tepper, J. M. GABAergic Control of Rat Substantia Nigra Dopaminergic Neurons: Role of Globus Pallidus and Substantia Nigra Pars Reticulata. *Neuroscience* **1999**, *89* (3), 813–825.
- (38) Gibb, W. R. G.; Lees, A. J. The Relevance of the Lewy Body to the Pathogenesis of Idiopathic Parkinson's Disease. *J. Neurol. Neurosurg. Psychiatry.* **1988**, 745–752.
- (39) Kegeles, L. S.; Abi-Dargham, A.; Frankle, W. G.; Gil, R.; Cooper, T. B.; Slifstein, M.; Hwang, D. R.; Huang, Y.; Haber, S. N.; Laruelle, M. Increased Synaptic Dopamine Function in Associative Regions of the Striatum in Schizophrenia. *Arch. Gen. Psychiatry* **2010**, *67* (3), 231–239.
- (40) Abi-Dargham, A.; Rodenhiser, J.; Printz, D.; Zea-Ponce, Y.; Gil, R.; Kegeles, L. S.; Weiss, R.; Cooper, T. B.; Mann, J. J.; Van Heertum, R. L.; Gorman, J. M.; Laruelle, M. Increased Baseline Occupancy of D2 Receptors by Dopamine in Schizophrenia. *Proc. Natl. Acad. Sci. U. S. A.* **2000**, *97* (14), 8104–8109.
- (41) Howes, O. D.; Williams, M.; Ibrahim, K.; Leung, G.; Egerton, A.; McGuire, P. K.; Turkheimer, F. Midbrain Dopamine Function in Schizophrenia and Depression: A Post-Mortem and Positron Emission Tomographic Imaging Study. *Brain* **2013**, *136* (11), 3242–3251.
- (42) Schultz, W. Predictive Reward Signal of Dopamine Neurons. *J. Neurophysiol.* **1998**, *80* (1), 1–27.
- (43) Anstrom, K. K.; Miczek, K. A.; Budygin, E. A. Increased Phasic Dopamine Signaling in the Mesolimbic Pathway during Social Defeat in Rats. *Neuroscience* **2009**, *161* (1), 3–12.
- (44) Blythe, S. N.; Wokosin, D.; Atherton, J. F.; Bevan, M. D. Cellular Mechanisms Underlying Burst Firing in Substantia Nigra Dopamine Neurons. *J. Neurosci.* **2009**, *29* (49), 15531–15541.
- (45) Mamelì-Engvall, M.; Evrard, A.; Pons, S.; Maskos, U.; Svensson, T. H.; Changeux, J. P.; Faure, P. Hierarchical Control of Dopamine Neuron-Firing Patterns by Nicotinic Receptors. *Neuron* **2006**, *50* (6), 911–921.
- (46) Dahan, L.; Astier, B.; Vautrelle, N.; Urbain, N.; Kocsis, B.; Chouvet, G. Prominent Burst Firing of Dopaminergic Neurons in the Ventral Tegmental Area during Paradoxical Sleep. *Neuropsychopharmacology* **2007**, *32* (6), 1232–1241.
- (47) Floresco, S. B.; West, A. R.; Ash, B.; Moorel, H.; Grace, A. A. Afferent Modulation of Dopamine Neuron Firing Differentially Regulates Tonic and Phasic Dopamine Transmission. *Nat. Neurosci.* **2003**, *6* (9), 968–973.
- (48) Gorwood, P.; Le Strat, Y.; Ramoz, N.; Dubertret, C.; Moalic, J. M.; Simonneau, M. Genetics of Dopamine Receptors and Drug Addiction. *Hum. Genet.* **2012**, *131* (6), 803–822.
- (49) Thomas, M. J.; Kalivas, P. W.; Shaham, Y. Neuroplasticity in the Mesolimbic Dopamine System and Cocaine

- Addiction. *Br. J. Pharmacol.* **2008**, *154* (2), 327–342.
- (50) Contreras-Rodríguez, O.; Albein-Urios, N.; Perales, J. C.; Martínez-Gonzalez, J. M.; Vilar-López, R.; Fernández-Serrano, M. J.; Lozano-Rojas, O.; Verdejo-García, A. Cocaine-Specific Neuroplasticity in the Ventral Striatum Network Is Linked to Delay Discounting and Drug Relapse. *Addiction* **2015**, *110* (12), 1953–1962.
- (51) Carlsson, A. Antipsychotic Drugs, Neurotransmitters, and Schizophrenia. *Am. J. Psychiatry* **1978**, *135* (2), 164–173.
- (52) Weinstein, J. J.; Chohan, M. O.; Slifstein, M.; Kegeles, L. S.; Moore, H.; Abi-Dargham, A. Review Pathway-Specific Dopamine Abnormalities in Schizophrenia, Historical perspective on dopamine research in schizophrenia *Biol Psychiatry*. **2016**, *81* (1), 31–42.
- (53) Floresco, S. B.; Magyar, O. Mesocortical Dopamine Modulation of Executive Functions: Beyond Working Memory. *Psychopharmacology (Berl)*. **2006**, *188* (4), 567–585.
- (54) Tanaka, M.; Sun, F.; Li, Y.; Mooney, R. A Mesocortical Dopamine Circuit Enables the Cultural Transmission of Vocal Behaviour. *Nature* **2018**, *563* (7729), 117–120.
- (55) Gorelova, N.; Mulholland, P. J.; Chandler, L. J.; Seamans, J. K. The Glutamatergic Component of the Mesocortical Pathway Emanating from Different Subregions of the Ventral Midbrain. *Cereb. Cortex* **2012**, *22* (2), 327–336.
- (56) Bostwick, J. R.; Pharm, D.; Guthrie, S. K.; Pharm, D.; Ellingrod, V. L.; Pharm, D. Antipsychotic-Induced Hyperprolactinemia. *Pharmacotherapy* **2009**, *29*, 64–73.
- (57) Nakamura, M.; Nagamine, T. Hypoprolactinemia and Extrapyramidal Symptoms in Male Schizophrenia or Psychotic Affective Disorder Patients Treated with Aripiprazole. *Clin. Neuropsychopharmacol. Ther.* **2012**, *3*, 18–22.
- (58) Llinás, R.; Steinberg, I. Z.; Walton, K. Relationship between Presynaptic Calcium Current and Postsynaptic Potential in Squid Giant Synapse. *Biophys. J.* **1981**, *33* (3), 323–351.
- (59) Gringard P. The Neurobiology of Slow Synaptic Transmission *Science* **2001** *294*, 1024–1030.
- (60) German, C. L.; Baladi, M. G.; McFadden, L. M.; Hanson, G. R.; Fleckenstein, A. E. Regulation of the Dopamine and Vesicular Monoamine Transporters: Pharmacological Targets and Implications for Disease. *Pharmacol. Rev.* **2015**, *67* (4), 1005–1024.
- (61) Erickson, J. D.; Eiden, L. E.; Hoffman, B. J. Expression Cloning of a Reserpine-Sensitive Vesicular Monoamine Transporter. *Proc. Natl. Acad. Sci. U. S. A.* **1992**, *89* (22), 10993–10997.
- (62) Finn, J. P.; Edwards, R. H. Individual Residues Contribute to Multiple Differences in Ligand Recognition between Vesicular Monoamine Transporters 1 and 2. *J. Biol. Chem.* **1997**, *272* (26), 16301–16307.
- (63) Uhl, G. R. Dopamine Transporter: Basic Science and Human Variation of a Key Molecule for Dopaminergic Function, Locomotion, and Parkinsonism. *Mov. Disord.* **2003**, *18*, S71–S80.
- (64) Hilger, D.; Masureel, M.; Kobilka, B. K. Structure and Dynamics of GPCR Signaling Complexes. *Nat. Struct. Mol. Biol.* **2018**, *25* (1), 4–12.
- (65) Andersen, P. H.; Gingrich, J. A.; Bates, M. D.; Dearry, A.; Falardeau, P.; Senogles, S. E.; Caron, M. G. Dopamine Receptor Subtypes: Beyond the D1/D2 Classification. *Trends Pharmacol. Sci.* **1990**, *11* (6), 231–236.
- (66) Sibley, D. R.; Monsma, F. J. Molecular Biology of Dopamine Receptors. *Trends Pharmacol Sci.* **1992**, *13*, 61–69.
- (67) Robertson, C. L.; Ishibashi, K.; Mandelkern, M. A.; Brown, A. K.; Ghahremani, D. G.; Sabb, F.; Bilder, R.; Cannon, T.; Borg, J.; London, E. D. Striatal D1- and D2-Type Dopamine Receptors Are Linked to Motor Response Inhibition in Human Subjects. *J. Neurosci.* **2015**, *35* (15), 5990–5997.
- (68) Ayano, G. Dopamine: Receptors, Functions, Synthesis, Pathways, Locations and Mental Disorders: Review of Literatures. *J. Ment. Disord. Treat.* **2016**, *2* (2), 2–5.
- (69) Undie, A. S.; Friedman, E. Stimulation of a Dopamine D1 Receptor Enhances Inositol Phosphates Formation in Rat Brain. *J. Pharmacol. Exp. Ther.* **1990**, *253* (3), 987–992.
- (70) Missale, C.; Russel Nash, S.; Robinson, S. W.; Jaber, M.; Caron, M. G. Dopamine Receptors: From Structure to Function. *Physiol. Rev.* **1998**, *78* (1), 189–225.
- (71) O’Dowd, B. F. Structures of Dopamine Receptors. *J. Neurochem.* **1993**, *60* (3), 804–816.
- (72) Miyamoto, Y.; Katayama, S.; Shigematsu, N.; Nishi, A.; Fukuda, T. Striosome-Based Map of the Mouse Striatum That Is Conformable to Both Cortical Afferent Topography and Uneven Distributions of Dopamine D1 and D2 Receptor-Expressing Cells. *Brain Struct. Funct.* **2018**, *223* (9), 4275–4291.
- (73) Levey, A. I.; Hersch, S. M.; Rye, D. B.; Sunahara, R. K.; Niznik, H. B.; Kitt, C. A.; Price, D. L.; Maggio, R.; Brann, M. R.; Ciliax, B. J. Localization of D1 and D2 Dopamine Receptors in Brain with Subtype-Specific

- Antibodies. *Proc. Natl. Acad. Sci. U. S. A.* **1993**, *90* (19), 8861–8865.
- (74) Civelli, O.; Bunzow, J. R.; Grandy, D. K. Molecular Diversity of the Dopamine Receptors. *Annu. Rev. Pharmacol. Toxicol.* **1993**, *33*, 281–307.
- (75) Ariano, M. A.; Sibley, D. R. Dopamine Receptor Distribution in the Rat CNS: Elucidation Using Anti-Peptide Antisera Directed against D1A and D3 Subtypes. *Brain Res.* **1994**, *649* (1–2), 95–110.
- (76) Zhang, J. X. B. X. Z. and A. Z. Dopamine D1 Receptor Ligands: Where Are We Now and Where Are We Going. *Med. Res. Rev.* **2008**, *29* (2), 272–294.
- (77) Neumeyer, J. L.; Kula, N. S.; Bergman, J.; Baldessarini, R. J. Receptor Affinities of Dopamine D1 Receptor-Selective Novel Phenylbenzazepines. *Eur. J. Pharmacol.* **2003**, *474* (2–3), 137–140.
- (78) Van Tol, H. H. M.; Bunzow, J. R.; Guan, H. C.; Sunahara, R. K.; Seeman, P.; Niznik, H. B.; Civelli, O. Cloning of the Gene for a Human Dopamine D4 Receptor with High Affinity for the Antipsychotic Clozapine. *Nature* **1991**, *350* (6319), 610–614.
- (79) Ciliax, B. J.; Nash, N.; Heilman, C.; Sunahara, R.; Hartney, A.; Tiberi, M.; Rye, D. B.; Caron, M. G.; Niznik, H. B.; Levey, A. I. Dopamine D5 Receptor Immunolocalization in Rat and Monkey Brain. *Synapse* **2000**, *37* (2), 125–145.
- (80) Khan, Z. U.; Gutiérrez, A.; Martín, R.; Peafiel, A.; Rivera, A.; De La Calle, A. Dopamine D5 Receptors of Rat and Human Brain. *Neuroscience* **2000**, *100* (4), 689–699.
- (81) Kimura, K.; Sela, S.; Bouvier, C.; Grandy, D. K.; Sidhu, A. Differential Coupling of D1 and D5 Dopamine Receptors to Guanine Nucleotide Binding Proteins in Transfected GH4C1 Rat Somatomammotrophic Cells. *J. Neurochem.* **1995**, *64* (5), 2118–2124.
- (82) Passani, M. B.; Benetti, F.; Blandina, P.; Furini, C. R. G.; de Carvalho Myskiw, J.; Izquierdo, I. Histamine Regulates Memory Consolidation. *Neurobiol. Learn. Mem.* **2017**, *145*, 1–6.
- (83) Rangel-Barajas, C.; Coronel, I.; Florán, B. Dopamine Receptors and Neurodegeneration. *Aging Dis.* **2015**, *6* (5), 349–368.
- (84) Greif, G. J.; Lin, Y. J.; Liu, J. C.; Freedman, J. E. Dopamine-Modulated Potassium Channels on Rat Striatal Neurons: Specific Activation and Cellular Expression. *J. Neurosci.* **1995**, *15* (6), 4533–4544.
- (85) Ariano, M. A.; Hee Chol Kang; Haugland, R. P.; Sibley, D. R. Multiple Fluorescent Ligands for Dopamine Receptors. II. Visualization in Neural Tissues. *Brain Res.* **1991**, *547* (2), 208–222.
- (86) De Mei C., Ramos M., Iitaka C., Borelli E. Getting Specialized: Presynaptic and Postsynaptic Dopamine D2 Receptors. **2009**, *9* (1), 53–58.
- (87) Martel, J. C.; Gatti McArthur, S. Dopamine Receptor Subtypes, Physiology and Pharmacology: New Ligands and Concepts in Schizophrenia. *Front. Pharmacol.* **2020**, *11*, 1–17.
- (88) Maramai, S.; Gemma, S.; Brogi, S.; Campiani, G.; Butini, S.; Stark, H.; Brindisi, M. Dopamine D3 Receptor Antagonists as Potential Therapeutics for the Treatment of Neurological Diseases. *Front. Neurosci.* **2016**, *10*, 451.
- (89) Van Tol, H. H. M.; Wu, C. M.; Guan, H. C.; Ohara, K.; Bunzow, J. R.; Civelli, O.; Kennedy, J.; Seeman, P.; Niznik, H. B.; Jovanovic, V. Multiple Dopamine D4 Receptor Variants in the Human Population. *Nature* **1992**, *358* (6382), 149–152.
- (90) Tarazi, F. I.; Florijn, W. J.; Creese, I. Differential Regulation of Dopamine Receptors after Chronic Typical and a Typical Antipsychotic Drug Treatment. *Neuroscience* **1997**, *78* (4), 985–996.
- (91) Oak, J. N.; Oldenhof, J.; Van Tol, H. H. M. The Dopamine D4 Receptor: One Decade of Research. *Eur. J. Pharmacol.* **2000**, *405* (1–3), 303–327.
- (92) Bonaventura, J.; Quiroz, C.; Cai, N. S.; Rubinstein, M.; Tanda, G.; Ferré, S. Key Role of the Dopamine D4 Receptor in the Modulation of Corticostriatal Glutamatergic Neurotransmission. *Sci. Adv.* **2017**, *3* (1), 1–9.
- (93) Arnsten, A. F. T.; Murphy, B.; Merchant, K. The Selective Dopamine D4 Receptor Antagonist, PNU-101387G, Prevents Stress-Induced Cognitive Deficits in Monkeys. *Neuropsychopharmacology* **2000**, *23* (4), 405–410.
- (94) Zhou Y.; Cao.C.; He L.; Wang X.; Zhang X.C. Crystal Structure of dopamine D4 Dopamine Receptor bound to the Subtype selective L745870. *eLife* **2019**, *8*, e48822.
- (95) Dearry, A.; Gingrich, J. A.; Falardeau, P.; Fremeau Jr, R. T.; Bates, M. D.; Caron, M. G. Molecular Cloning and Expression of the Gene for a Human D1 Dopamine Receptor. *Nature* **1990**, *347*, 72–76.
- (96) Bunzow, J. R.; Van Tol, H. H. M.; Grandy, D. K.; Albert, P.; Salon, J.; Christie, M.; Machida, C. A.; Neve, K. A.; Civelli, O. Cloning and Expression of a Rat D2 Dopamine Receptor cDNA. *Nature* **1988**, *336* (6201), 783–787.
- (97) Sokoloff, P.; Giros, B.; Martres, M. P.; Bouthenet, M. L.; Schwartz, J. C. Molecular Cloning and Characterization of a Novel Dopamine Receptor (D3) as a Target for Neuroleptics. *Nature* **1990**, *347* (6289),

- 146–151.
- (98) Sunahara R.K.; Guan H.C.; O'Dowd B.H.; Seeman P.; Laurier L.G.; Torchia J.; Van Toel H.H.M.; Niznik H.B. Cloning of the gene for a human dopamine D5 receptor with higher affinity for dopamine than D1. *Nature* **1991**, *350*, 610–614.
- (99) Alkorta, I.; Villar, H. O. Considerations on the Recognition of the D1 Receptor by Agonists. *J. Comput. Aided. Mol. Des.* **1993**, *7* (6), 659–670.
- (100) Andersen, P. H.; Jansen, J. A. Dopamine Receptor Agonists: Selectivity and Dopamine D1 Receptor Efficacy. *Eur. J. Pharmacol. Mol. Pharmacol.* **1990**, *188* (6), 335–347.
- (101) Kotani, M.; Kiyoshi, A.; Murai, T.; Nakako, T.; Matsumoto, K.; Matsumoto, A.; Ikejiri, M.; Ogi, Y.; Ikeda, K. The Dopamine D1 Receptor Agonist SKF-82958 Effectively Increases Eye Blinking Count in Common Marmosets. *Behav. Brain Res.* **2016**, *300*, 25–30.
- (102) Mierau, J.; Schneider, F. J.; Ensinger, H. A.; Chio, C. L.; Lajiness, M. E.; Huff, R. M. Pramipexole Binding and Activation of Cloned and Expressed Dopamine D2, D3 and D4 Receptors. *Eur. J. Pharmacol. Mol. Pharmacol.* **1995**, *290* (1), 29–36.
- (103) Vallone, D.; Picetti, R.; Borrelli, E. Structure and Function of Dopamine Receptors. *Neurosci. Biobehav. Rev.* **2000**, *1*, 125–32.
- (104) Cox, B. F. BP 897, a Selective Dopamine D3 Receptor Ligand with Therapeutic Potential for the Treatment of Cocaine-Addiction. *CNS Drug. Rev.* **2003**, *9* (2), 141–158.
- (105) Moritz, A. E.; Free, R. B.; Weiner, W. S.; Akano, E. O.; Gandhi, D.; Abramyan, A.; Keck, T. M.; Ferrer, M.; Hu, X.; Southall, N.; Steiner, J.; Aubé, J.; Shi, L.; Frankowski, K. J.; Sibley, D. R. Discovery, Optimization, and Characterization of ML417: A Novel and Highly Selective D3 Dopamine Receptor Agonist. *J. Med. Chem.* **2020**, *63* (10), 5526–5567.
- (106) Gómez-jeria, J. S.; López-aravena, R. A Theoretical Analysis of the Relationships between Electronic Structure and Dopamine D4 Receptor Affinity in a Series of Compound Based on the Classical A Theoretical Analysis of the Relationships between Electronic Structure and Dopamine D4 Receptor *J. Chem. Res.* **2020**, *5* (6), 1–9.
- (107) Bernaerts, P.; Tirelli, E. Facilitatory Effect of the Dopamine D4 Receptor Agonist PD168,077 on Memory Consolidation of an Inhibitory Avoidance Learned Response in C57BL/6J Mice. *Behav. Brain Res.* **2003**, *142* (1–2), 41–52.
- (108) Leng, Z. G.; Lin, S. J.; Wu, Z. R.; Guo, Y. H.; Cai, L.; Shang, H. B.; Tang, H.; Xue, Y. J.; Lou, M. Q.; Zhao, W.; Le, W. D.; Zhao, W. G.; Zhang, X.; Wu, Z. B. Activation of DRD5 (Dopamine Receptor D5) Inhibits Tumor Growth by Autophagic Cell Death. *Autophagy* **2017**, *13* (8), 1404–1419.
- (109) Haney, M.; Ward, A. S.; Foltin, R. W.; Fischman, M. W. Effects of Ecopipam, a Selective Dopamine D1 Antagonist, on Smoked Cocaine Self-Administration by Humans. *Psychopharmacology (Berl)*. **2001**, *155* (4), 330–337.
- (110) Billard, W.; Ruperto, V.; Crosby, G.; Iorio, L. C.; Barnett, A. Characterization of the Binding of 3H-SCH 23390, a Selective D-1 Receptor Antagonist Ligand, in Rat Striatum. *Life Sci.* **1984**, *35* (18), 1885–1893.
- (111) Garnock-Jones, K. P. Cariprazine : A Review in Schizophrenia. *CNS Drugs* **2017**, *31* (6), 513–525.
- (112) Di Ciano, P.; Underwood, R. J.; Hagan, J. J.; Everitt, B. J. Attenuation of Cue-Controlled Cocaine-Seeking by a Selective D3 Dopamine Receptor Antagonist SB-27701 1-A. *Neuropsychopharmacology* **2003**, *28* (2), 329–338.
- (113) Slifstein, M.; Abi-Dargham, A.; Girgis, R. R.; Suckow, R. F.; Cooper, T. B.; Divgi, C. R.; Sokoloff, P.; Leriche, L.; Carberry, P.; Oya, S.; Joseph, S. K.; Guiraud, M.; Montagne, A.; Brunner, V.; Gaudoux, F.; Tonner, F. Binding of the D3-Preferring Antipsychotic Candidate F17464 to Dopamine D3 and D2 Receptors: A PET Study in Healthy Subjects with [¹¹C]-(+)-PHNO. *Psychopharmacology (Berl)*. **2020**, *237* (2), 519–527.
- (114) Bristow, L. J.; Kramer, M. S.; Kulagowski, J.; Patel, S.; Ragan, C. I.; Seabrook, G. R. Schizophrenia and L-745,870, a Novel Dopamine D4 Receptor Antagonist. *Trends Pharmacol. Sci.* **1997**, *18* (6), 186–188.
- (115) Demchyshyn, L. L.; McConkey, F.; Niznik, H. B. Dopamine D5 Receptor Agonist High Affinity and Constitutive Activity Profile Conferred by Carboxyl-Terminal Tail Sequence. *J. Biol. Chem.* **2000**, *275* (31), 23446–23455.
- (116) Wang, S.; Che, T.; Levit, A.; Shoichet, B. K.; Wacker, D.; Roth, B. L. Structure of the D2 Dopamine Receptor Bound to the Atypical Antipsychotic Drug Risperidone. *Nature* **2018**, *555* (7695), 269–273.
- (117) Chien, E. Y. T.; Liu, W.; Zhao, Q.; Katritch, V.; Han, G. W.; Hanson, M. A.; Shi, L.; Newman, A. H.; Javitch, J. A.; Cherezov, V.; Stevens, R. C. Structure of the Human Dopamine D3 Receptor in Complex with a D2/D3 Selective Antagonist. *Science* **2010**, *330* (6007), 1091–1095

- (118) Yin, J.; Chen, K. Y. M.; Clark, M. J.; Hijazi, M.; Kumari, P.; Bai, X. chen; Sunahara, R. K.; Barth, P.; Rosenbaum, D. M. Structure of a D2 Dopamine Receptor–G-Protein Complex in a Lipid Membrane. *Nature* **2020**, *584* (7819), 125–129.
- (119) Seeman, P.; Schwarz, J.; Chen, J. F.; Szechtman, H.; Perreault, M.; McKnight, G. S.; Roder, J. C.; Quirion, R.; Boksa, P.; Srivastava, L. K.; Yanai, K.; Weinshenker, D.; Sumiyoshi, T. Psychosis Pathways Converge via D2High Dopamine Receptors. *Synapse* **2006**, *60* (4), 319–346.
- (120) Seeman, P. All Roads to Schizophrenia Lead to Dopamine Supersensitivity and Elevated Dopamine D2High Receptors. *CNS Neurosci. Ther.* **2011**, *17* (2), 118–132.
- (121) Lefkowitz, R. J.; Shenoy, S. K. Transduction of Receptor Signals. *Science* **2005**, *308*, 512–518.
- (122) Beaulieu, J.; Gainetdinov, R. R. The Physiology, Signaling, and Pharmacology of Dopamine Receptors. *Pharmacol. Rev.* **2011**, *63* (1), 182–217.
- (123) Guidice, T. Del; Lemasson, M.; Beaulieu, J. Role of Beta-Arrestin 2 Downstream of Dopamine Receptors in the Basal Ganglia. *Front. Neuroanat.* **2011**, *5*, 1–11.
- (124) Gastel, J. Van; Hendrickx, J. O.; Leysen, H.; Santos-otte, P.; Salomone, S. β -Arrestin Based Receptor Signaling Paradigms : Potential Therapeutic Targets for Complex Age-Related Disorders. *Front. Pharmacol.* **2018**, *9*, 1369.
- (125) Beaulieu, J.; Sotnikova, T. D.; Yao, W.; Kockeritz, L.; Woodgett, J. R.; Gainetdinov, R. R.; Caron, M. G. Lithium Antagonizes Dopamine-Dependent Behaviors Mediated by an AKT Glycogen Synthase Kinase 3 Signaling Cascade. *PNAS*, *101* (14), 5099–5104.
- (126) Beaulieu, J.; Sotnikova, T. D.; Marion, S.; Lefkowitz, R. J.; Gainetdinov, R. R.; Caron, M. G.; Carolina, N.; Carolina, N. An Akt / β -Arrestin 2 / PP2A Signaling Complex Mediates Dopaminergic Neurotransmission and Behavior. *Cell* **2005**, *122*, 261–273.
- (127) Sun W.L, Quizon P.M., Zhu J. Molecular Mechanism: ERK Signaling, Drug Addiction and Behavioral Effects. *Prog Mol Biol Transl Sci.* **2016**, *137*, 1–40.
- (128) Neve, K. A.; Seamans, J. K.; Trantham-Davidson, H. Dopamine Receptor Signaling. *J. Recept. Signal Transduct.* **2004**, *24* (3), 165–205.
- (129) Van Holstein, M.; Aarts, E.; Van Der Schaaf, M. E.; Geurts, D. E. M.; Verkes, R. J.; Franke, B.; Van Schouwenburg, M. R.; Cools, R. Human Cognitive Flexibility Depends on Dopamine D2 Receptor Signaling. *Psychopharmacology (Berl)*. **2011**, *218* (3), 567–578.
- (130) Seeman, P. Targeting the Dopamine D2 Receptor in Schizophrenia. *Expert Opin. Ther. Targets* **2006**, *10* (4), 515–531.
- (131) Seeman P.; Lee T.; Wong C.; Wong K. Antipsychotic Drug Doses and Neuroleptic / Dopamine Receptors. *Nature* **1976**, *261*, 717.
- (132) Ullmann, T.; Gienger, M.; Budzinski, J.; Hellmann, J.; Hübner, H.; Gmeiner, P.; Weikert, D. Homobivalent Dopamine D2Receptor Ligands Modulate the Dynamic Equilibrium of D2Monomers and Homo- and Heterodimers. *ACS Chem. Biol.* **2021**, *16*, 371–379.
- (133) Liu, C.; Bonaventure, P.; Lee, G.; Nepomuceno, D.; Kuei, C.; Wu, J.; Li, Q.; Joseph, V.; Sutton, S. W.; Eckert, W.; Yao, X.; Yieh, L.; Dvorak, C.; Carruthers, N.; Coate, H.; Yun, S.; Dugovic, C.; Harrington, A.; Lovenberg, T. W. GPR139, an Orphan Receptor Highly Enriched in the Habenula and Septum, Is Activated by the Essential Amino Acids L-Tryptophan and L-Phenylalanine S. *Mol. Pharmacol.* **2015**, *88* (5), 911–925.
- (134) Wang, L.; Lee, G.; Kuei, C.; Yao, X.; Harrington, A.; Bonaventure, P.; Lovenberg, T. W.; Liu, C. GPR139 and Dopamine D2 Receptor Co-Express in the Same Cells of the Brain and May Functionally Interact. *Front. Neurosci.* **2019**, *13*, 1–14.
- (135) Nyberg, L.; Karalija, N.; Salami, A.; Andersson, M.; Wählin, A.; Kaboovand, N.; Köhneke, Y.; Axelsson, J.; Rieckmann, A.; Papenberg, G.; Garrett, D. D.; Riklund, K.; Lövdén, M.; Lindenberger, U.; Bäckman, L. Dopamine D2 Receptor Availability Is Linked to Hippocampal–Caudate Functional Connectivity and Episodic Memory. *Proc. Natl. Acad. Sci. U. S. A.* **2016**, *113* (28), 7918–7923.
- (136) Wang, M.; Pei, L.; Fletcher, P. J.; Kapur, S.; Seeman, P.; Liu, F. Schizophrenia, Amphetamine-Induced Sensitized State and Acute Amphetamine Exposure All Show a Common Alteration: Increased Dopamine D2 Receptor Dimerization. *Mol. Brain* **2010**, *3* (1), 1–9.
- (137) Baik, J. H.; Picetti, R.; Saiardi, A.; Thiriet, G.; Dierich, A.; Depaulis, A.; Le Meur, M.; Borrelli, E. Parkinsonian-like Locomotor Impairment in Mice Lacking Dopamine D2 Receptors. *Nature* **1995**, *377* (6548), 424–428.
- (138) Rinne, J. O.; Laihinen, A.; Rinne, U. K.; Nägren, K.; Bergman, J.; Ruotsalainen, U. PET Study on Striatal Dopamine D2 Receptor Changes during the Progression of Early Parkinson’s Disease. *Mov. Disord.* **1993**, *8* (2), 134–138.

- (139) Tinsley, R. B.; Bye, C. R.; Parish, C. L.; Tziotis-Vais, A.; George, S.; Culvenor, J. G.; Li, Q. X.; Masters, C. L.; Finkelstein, D. I.; Horne, M. K. Dopamine D2 Receptor Knockout Mice Develop Features of Parkinson Disease. *Ann. Neurol.* **2009**, *66* (4), 472–484.
- (140) Yang, P.; Knight, W. C.; Li, H.; Guo, Y.; Perlmutter, J. S.; Benzinger, T. L. S.; Morris, J. C.; Xu, J. Dopamine D1 + D3 Receptor Density May Correlate with Parkinson Disease Clinical Features. *Ann. Clin. Transl. Neurol.* **2021**, *8* (1), 224–237.
- (141) Masellis, M.; Collinson, S.; Freeman, N.; Tampakeras, M.; Levy, J.; Tchelet, A.; Eyal, E.; Berkovich, E.; Eliaz, R. E.; Abler, V.; Grossman, I.; Fitzer-Attas, C.; Tiwari, A.; Hayden, M. R.; Kennedy, J. L.; Lang, A. E.; Knight, J. Dopamine D2 Receptor Gene Variants and Response to Rasagiline in Early Parkinson's Disease: A Pharmacogenetic Study. *Brain* **2016**, *139* (7), 2050–2062.
- (142) Volkow, N. D.; Gur, R. C.; Wang, G. J.; Fowler, J. S.; Moberg, P. J.; Ding, Y. S.; Hitzemann, R.; Smith, G.; Logan, J. Association between Decline in Brain Dopamine Activity with Age and Cognitive and Motor Impairment in Healthy Individuals. *Am. J. Psychiatry* **1998**, *155* (3), 344–349.
- (143) Kegeles, L. S.; Slifstein, M.; Frankle, W. G.; Xu, X.; Hackett, E.; Bae, S. A.; Gonzales, R.; Kim, J. H.; Alvarez, B.; Gil, R.; Laruelle, M.; Abi-Dargham, A. Dose-Occupancy Study of Striatal and Extrastriatal Dopamine D2 Receptors by Aripiprazole in Schizophrenia with PET and [18F] Fallypride. *Neuropsychopharmacology* **2008**, *33* (13), 3111–3125.
- (144) Newman, A. H.; Grundt, P.; Cyriac, G.; Deschamps, J. R.; Taylor, M.; Kumar, R.; Ho, D.; Luedtke, R. R. N-(4-(4-(2,3-Dichloro- or 2-Methoxyphenyl)Piperazin-1-yl)Butyl) Heterobiarylcarboxamides with Functionalized Linking Chains as High Affinity and Enantioselective D3 Receptor Antagonists. *J. Med. Chem.* **2009**, *52* (8), 2559–2570.
- (145) Fan, L.; Tan, L.; Chen, Z.; Qi, J.; Nie, F.; Luo, Z.; Cheng, J.; Wang, S. Haloperidol Bound D2 Dopamine Receptor Structure Inspired the Discovery of Subtype Selective Ligands. *Nat. Commun.* **2020**, *11* (1), 1–11.
- (146) Kühhorn, J.; Hübner, H.; Gmeiner, P. Bivalent Dopamine D2 Receptor Ligands: Synthesis and Binding Properties. *J. Med. Chem.* **2011**, *54* (13), 4896–4903.
- (147) Vangveravong, S.; Zhang, Z.; Taylor, M.; Bearden, M.; Xu, J.; Cui, J.; Wang, W.; Luedtke, R. R.; MacH, R. H. Synthesis and Characterization of Selective Dopamine D2 Receptor Ligands Using Aripiprazole as the Lead Compound. *Bioorg. Med. Chem.* **2011**, *19* (11), 3502–3511.
- (148) Shen, Y.; McCorvy, J. D.; Martini, M. L.; Rodriguiz, R. M.; Pogorelov, V. M.; Ward, K. M.; Wetsel, W. C.; Liu, J.; Roth, B. L.; Jin, J. D2 Dopamine Receptor G Protein-Biased Partial Agonists Based on Cariprazine. *J. Med. Chem.* **2019**, *62* (9), 4755–4771.
- (149) Allen, J. A.; Yost, J. M.; Setola, V.; Chen, X.; Sassano, M. F.; Chen, M.; Peterson, S.; Yadav, P. N.; Huang, X. P.; Feng, B.; Jensen, N. H.; Che, X.; Bai, X.; Frye, S. V.; Wetsel, W. C.; Caron, M. G.; Javitch, J. A.; Roth, B. L.; Jin, J. Discovery of β -Arrestin-Biased Dopamine D2 Ligands for Probing Signal Transduction Pathways Essential for Antipsychotic Efficacy. *Proc. Natl. Acad. Sci. U. S. A.* **2011**, *108* (45), 18488–18493.
- (150) Guillin, O.; Diaz, J.; Carroll, P.; Griffon, N.; Schwartz, J. C.; Sokoloff, P. BDNF Controls Dopamine D3 Receptor Expression and Triggers Behavioural Sensitization. *Nature* **2001**, *411* (6833), 86–89.
- (151) Heidbreder, C. A.; Newman, A. H. Current Perspectives on Selective Dopamine D3 Receptor Antagonists as Pharmacotherapeutics for Addictions and Related Disorders. *Ann. N. Y. Acad. Sci.* **2010**, *1187*, 4–34.
- (152) Sokoloff, P.; Foll, B. Le. The Dopamine D3 Receptor, a Quarter Century Later *Eur. J. Neurosci.* **2017**, *45*, 2–19.
- (153) Sokoloff, P.; Martres, M. P.; Giros, B.; Bouthenet, M. L.; Schwartz, J. C. The Third Dopamine Receptor (D3) as a Novel Target for Antipsychotics. *Biochem. Pharmacol.* **1992**, *43* (4), 659–666.
- (154) Shi, L.; Javitch, J. A. The Binding Site of Aminergic G Protein-Coupled Receptors: The Transmembrane Segments and Second Extracellular Loop. *Annu. Rev. Toxicol. Pharmacol.* **2002**, *42*, 437–467.
- (155) Prieto, G. A. Abnormalities of Dopamine D3 Receptor Signaling in the Diseased Brain *J. Cent. Nerv. Syst. Dis.* **2017**, *9*, 1–8.
- (156) Landwehrmeyer, B.; Mengod, G.; Palacios, J. M. Dopamine D3 Receptor mRNA and Binding Sites in Human Brain. *Molecular Brain Research* **1993**, *18*, 187–192.
- (157) Kim, A.; Nigmatullina, R.; Zalyalova, Z.; Soshnikova, N.; Krasnov, A. Upgraded Methodology for the Development of Early Diagnosis of Parkinson's Disease Based on Searching Blood Markers in Patients and Experimental Models. *Mol. Neurobiol.* **2019**, *56* (5) 3437–3450.
- (158) Pacheco, R.; Prado, C. E.; Barrientos, M. J.; Bernales, S. Role of Dopamine in the Physiology of T-Cells and Dendritic Cells. *J. Neuroimmunol.* **2009**, *216* (1–2), 8–19.
- (159) Cosentino, M.; Fietta, A. M.; Ferrari, M.; Rasini, E.; Bombelli, R.; Carcano, E.; Saporiti, F.; Meloni, F.; Marino, F.; Lecchini, S. Human CD4⁺CD25⁺ Regulatory T Cells Selectively Express Tyrosine Hydroxylase

- and Contain Endogenous Catecholamines Subserving an Autocrine/Paracrine Inhibitory Functional Loop. *Blood* **2007**, *109* (2), 632–642.
- (160) Contreras, F.; Prado, C.; González, H.; Franz, D.; Osorio-Barrios, F.; Osorio, F.; Ugalde, V.; Lopez, E.; Elgueta, D.; Figueroa, A.; Lladser, A.; Pacheco, R. Dopamine Receptor D3 Signaling on CD4+ T Cells Favors Th1- and Th17-Mediated Immunity. *J. Immunol.* **2016**, *196* (10), 4143–4149.
- (161) Franz, D.; Contreras, F.; González, H.; Prado, C.; Elgueta, D.; Figueroa, C.; Pacheco, R. Dopamine Receptors D3 and D5 Regulate CD4+T-Cell Activation and Differentiation by Modulating ERK Activation and CAMP Production. *J. Neuroimmunol.* **2015**, *284*, 18–29.
- (162) Elgueta, D.; Contreras, F.; Prado, C.; Montoya, A.; Ugalde, V.; Chovar, O.; Villagra, R.; Henríquez, C.; Abellanas, M. A.; Aymerich, M. S.; Franco, R.; Pacheco, R. Dopamine Receptor D3 Expression Is Altered in CD4+ T-Cells from Parkinson's Disease Patients and Its Pharmacologic Inhibition Attenuates the Motor Impairment in a Mouse Model. *Front. Immunol.* **2019**, *10*, 1–17.
- (163) Solís, O.; Garcia-Montes, J. R.; González-Granillo, A.; Xu, M.; Moratalla, R. Dopamine D3 Receptor Modulates L-DOPA-Induced Dyskinesia by Targeting D1 Receptor-Mediated Striatal Signaling. *Cereb. Cortex* **2017**, *27* (1), 435–446.
- (164) Elgueta, D.; Aymerich, M. S.; Contreras, F.; Montoya, A.; Celorrio, M.; Rojo-Bustamante, E.; Riquelme, E.; González, H.; Vásquez, M.; Franco, R.; Pacheco, R. Pharmacologic Antagonism of Dopamine Receptor D3 Attenuates Neurodegeneration and Motor Impairment in a Mouse Model of Parkinson's Disease. *Neuropharmacology* **2017**, *113*, 110–123.
- (165) Boileau, I.; Guttman, M.; Rusjan, P.; Adams, J. R.; Houle, S.; Tong, J.; Hornykiewicz, O.; Furukawa, Y.; Wilson, A. A.; Kapur, S.; Kish, S. J. Decreased Binding of the D3 Dopamine Receptor-Preferring Ligand [¹¹C]-(+)-PHNO in Drug-Nave Parkinsons Disease. *Brain* **2009**, *132* (5), 1366–1375.
- (166) Schwartz, J. C.; Diaz, J.; Pilon, C.; Sokoloff, P. Possible Implications of the Dopamine D3 Receptor in Schizophrenia and in Antipsychotic Drug Actions. *Brain Res. Rev.* **2000**, *31* (2–3), 277–287.
- (167) Silfstein, M.; van de Giessen, E.; Van Snellenburg, J.; Thompson, J. L.; Narendran, R.; Gil, R.; Hackett, E.; Girgis, R. R.; Ojeil, N.; Moore, H.; D'Souza, D.; Malison, R. T.; Huang, Y.; Lim, K.; Nabulsi, N.; Carson, R. E.; Lieberman, J. A.; Abi-Dargham, A. Deficits in Prefrontal Cortical and Extra-Striatal Dopamine Release in Schizophrenia: A PET FMRI Study. *JAMA Psychiatry* **2015**, *72* (4), 316–324.
- (168) Gallezot, J. D.; Beaver, J. D.; Gunn, R. N.; Nabulsi, N.; Weinzimmer, D.; Singhal, T.; Slifstein, M.; Fowles, K.; Ding, Y. S.; Huang, Y.; Laruelle, M.; Carson, R. E.; Rabiner, E. A. Affinity and Selectivity of [¹¹C]-(+)-PHNO for the D3 and D2 Receptors in the Rhesus Monkey Brain in Vivo. *Synapse* **2012**, *66* (6), 489–500.
- (169) Doot, R. K.; Dubroff, J. G.; Labban, K. J.; Mach, R. H. Selectivity of Probes for PET Imaging of Dopamine D3 Receptors. *Neurosci. Lett.* **2019**, *691*, 18–25.
- (170) Wilson, A. A.; McCormick, P.; Kapur, S.; Willeit, M.; Garcia, A.; Hussey, D.; Houle, S.; Seeman, P.; Ginovart, N. Radiosynthesis and Evaluation of [¹¹C]-(+)-4-Propyl-3,4,4a,5,6,10b-Hexahydro-2H-Naphtho[1,2-b][1,4]Oxazin-9-ol as a Potential Radiotracer for in Vivo Imaging of the Dopamine D2 High-Affinity State with Positron Emission Tomography. *J. Med. Chem.* **2005**, *48* (12), 4153–4160.
- (171) Narendran, R.; Slifstein, M.; Guillin, O.; Hwang, Y.; Hwang, D. R.; Scher, E.; Reeder, S.; Rabiner, E.; Laruelle, M. Dopamine (D2/3) Receptor Agonist Positron Emission Tomography Radiotracer [¹¹C]-(+)-PHNO Is a D3 Receptor Preferring Agonist in Vivo. *Synapse* **2006**, *60* (7), 485–495.
- (172) Girgis, R. R.; Slifstein, M.; D'Souza, D.; Lee, Y.; Periclou, A.; Ghahramani, P.; Laszlovszky, I.; Durgam, S.; Adham, N.; Nabulsi, N.; Huang, Y.; Carson, R. E.; Kiss, B.; Kapás, M.; Abi-Dargham, A.; Rakhit, A. Preferential Binding to Dopamine D3 over D2 Receptors by Cariprazine in Patients with Schizophrenia Using PET with the D3/D2 Receptor Ligand [¹¹C]-(+)-PHNO. *Psychopharmacology (Berl.)* **2016**, *233* (19–20), 3503–3512.
- (173) Boneberg, E. M.; Von Seydlitz, E.; Pröpster, K.; Watzl, H.; Rockstroh, B.; Illges, H. D3 Dopamine Receptor mRNA Is Elevated in T Cells of Schizophrenic Patients Whereas D4 Dopamine Receptor mRNA Is Reduced in CD4+T Cells. *J. Neuroimmunol.* **2006**, *173* (1–2), 180–187.
- (174) Torrisi, S. A.; Salomone, S.; Geraci, F.; Caraci, F.; Bucolo, C.; Drago, F.; Leggio, G. M. Buspirone Counteracts MK-801-Induced Schizophrenia-like Phenotypes through Dopamine D3 Receptor Blockade. *Front. Pharmacol.* **2017**, *8*, 1–13.
- (175) Neisewander, J. L.; Fuchs, R. A.; Tran-Nguyen, L. T. L.; Weber, S. M.; Coffey, G. P.; Joyce, J. N. Increases in Dopamine D3 Receptor Binding in Rats Receiving a Cocaine Challenge at Various Time Points after Cocaine Self-Administration: Implications for Cocaine-Seeking Behavior. *Neuropsychopharmacology* **2004**, *29* (8), 1479–1487.
- (176) Le Foll, B.; Francès, H.; Diaz, J.; Schwartz, J. C.; Sokoloff, P. Role of the Dopamine D3 Receptor in Reactivity

- to Cocaine-Associated Cues in Mice. *Eur. J. Neurosci.* **2002**, *15* (12), 2016–2026.
- (177) Khaled, M. A. T. M.; Farid Araki, K.; Li, B.; Coen, K. M.; Marinelli, P. W.; Varga, J.; Gaál, J.; Le Foll, B. The Selective Dopamine D3 Receptor Antagonist SB 277011-A, but Not the Partial Agonist BP 897, Blocks Cue-Induced Reinstatement of Nicotine-Seeking. *Int. J. Neuropsychopharmacol.* **2010**, *13* (2), 181–190.
- (178) Leggio, G. M.; Camillieri, G.; Platania, C. B. M.; Castorina, A.; Marrazzo, G.; Torrisi, S. A.; Nona, C. N.; D'Agata, V.; Nobrega, J.; Stark, H.; Bucolo, C.; Le Foll, B.; Drago, F.; Salomone, S. Dopamine D3 Receptor Is Necessary for Ethanol Consumption: An Approach with Bupirone. *Neuropsychopharmacology* **2014**, *39* (8), 2017–2028.
- (179) Lv, Y.; Hu, R. rong; Jing, M.; Zhao, T. yun; Wu, N.; Song, R.; Li, J.; Hu, G. Selective Dopamine D3 Receptor Antagonist YQA14 Inhibits Morphine-Induced Behavioral Sensitization in Wild Type, but Not in Dopamine D3 Receptor Knockout Mice. *Acta Pharmacol. Sin.* **2019**, *40* (5), 583–588.
- (180) Damsma G, Bottema T, Westerink B.H.C, Tepper P.G.,Dijkstra D., Pugsley T.A, MacKenzie R.G, Heffner T.G. and Wikstrom H. Pharmacological Aspects of R-(+)-7-OH-DPAT, a Putative Dopamine D3 Receptor Ligand. *Eur. J.Pharmacol.*, **1993**, *249*, 9–10.
- (181) Hackling, A. E.; Stark, H. Dopamine D3 Receptor Ligands with Antagonist Properties. *ChemBioChem* **2002**, *3* (10), 946–961.
- (182) Michino, M.; Boateng, C. A.; Donthamsetti, P.; Yano, H.; Bakare, O. M.; Bonifazi, A.; Ellenberger, M. P.; Keck, T. M.; Kumar, V.; Zhu, C.; Verma, R.; Deschamps, J. R.; Javitch, J. A.; Newman, A. H.; Shi, L. Toward Understanding the Structural Basis of Partial Agonism at the Dopamine D3 Receptor. *J. Med. Chem.* **2017**, *60* (2), 580–593.
- (183) Cussac, D.; Newman-Tancredi, A.; Sezgin, L.; Millan, M. J. The Novel Antagonist, S33084, and GR218,231 Interact Selectively with Cloned and Native, Rat Dopamine D3 Receptors as Compared with Native, Rat Dopamine D2 Receptors. *Eur. J. Pharmacol.* **2000**, *394* (1), 47–50.
- (184) Gilbert, J. G.; Newman, A. H.; Gardner, E. L.; Ashby, C. R.; Heidbreder, C. A.; Pak, A. C.; Peng, X. Q.; Xi, Z. X. Acute Administration of SB-277011A, NGB 2904, or BP 897 Inhibits Cocaine Cue-Induced Reinstatement of Drug-Seeking Behavior in Rats: Role of Dopamine D3 Receptors. *Synapse* **2005**, *57* (1), 17–28.
- (185) Gadhiya, S.; Cordone, P.; Pal, R. K.; Gallicchio, E.; Wickstrom, L.; Kurtzman, T.; Ramsey, S.; Harding, W. W. New Dopamine D3-Selective Receptor Ligands Containing a 6-Methoxy-1,2,3,4-Tetrahydroisoquinolin-7-Ol Motif. *ACS Med. Chem. Lett.* **2018**, *9* (10), 990–995.
- (186) Tan, L.; Zhou, Q.; Yan, W.; Sun, J.; Kozikowski, A. P.; Zhao, S.; Huang, X. P.; Cheng, J. Design and Synthesis of Bitopic 2-Phenylcyclopropylmethylamine (Pcpma) Derivatives as Selective Dopamine D3 Receptor Ligands. *J. Med. Chem.* **2020**, *63* (9), 4579–4602.
- (187) Kumar, V.; Bonifazi, A.; Ellenberger, M. P.; Keck, T. M.; Pommier, E.; Rais, R.; Slusher, B. S.; Gardner, E.; You, Z. B.; Xi, Z. X.; Newman, A. H. Highly Selective Dopamine D3 Receptor (D3R) Antagonists and Partial Agonists Based on Eticlopride and the D3R Crystal Structure: New Leads for Opioid Dependence Treatment. *J. Med. Chem.* **2016**, *59* (16), 7634–7650.
- (188) Appiah-Kubi, P.; Olotu, F. A.; Soliman, M. E. S. Exploring the Structural Basis and Atomistic Binding Mechanistic of the Selective Antagonist Blockade at D3 Dopamine Receptor over D2 Dopamine Receptor. *J. Mol. Recognit.* **2021**, 1–15.
- (189) Sun, X.; Gou, H. Y.; Li, F.; Lu, G. Y.; Song, R.; Yang, R. F.; Wu, N.; Su, R. Bin; Cong, B.; Li, J. Y-QA31, a Novel Dopamine D3 Receptor Antagonist, Exhibits Antipsychotic-like Properties in Preclinical Animal Models of Schizophrenia. *Acta Pharmacol. Sin.* **2016**, *37* (3), 322–333.
- (190) Chen, J.; Levant, B.; Wang, S. High-Affinity and Selective Dopamine D3 Receptor Full Agonists. *Bioorg. Med. Chem. Lett.* **2012**, *22* (17), 5612–5617.
- (191) Garcia-Ladona, F. J.; Cox, B. F. BP 897, a Selective Dopamine D3 Receptor Ligand with Therapeutic Potential for the Treatment of Cocaine-Addiction. *CNS Drug Rev.* **2003**, *9* (2), 141–158.
- (192) Heidler, P.; Zohrabi-Kalantari, V.; Calmels, T.; Capet, M.; Berrebi-Bertrand, I.; Schwartz, J. C.; Stark, H.; Link, A. Parallel Synthesis and Dopamine D3/D2 Receptor Screening of Novel {4-[4-(2-Methoxyphenyl)Piperazin-1-Yl]Butyl}carboxamides. *Bioorg. Med. Chem.* **2005**, *13* (6), 2009–2014.
- (193) Ágai-csongor, É.; Domány, G.; Nógrádi, K.; Galambos, J.; Vágó, I.; Greiner, I.; Laszlovszky, I.; Gere, A.; Schmidt, É.; Kiss, B.; Vastag, M.; Tihanyi, K.; Sággy, K.; Laszy, J.; Gyertyán, I.; Zájér-balázs, M.; Gémesi, L.; Kapás, M.; Szombathelyi, Z. Discovery of Cariprazine (RGH-188): A Novel Antipsychotic Acting on Dopamine D3 / D2 Receptors. *Bioorg. Med. Chem. Lett.* **2012**, *22*, 3437–3440.
- (194) Campbell, R. H.; Diduch, M.; Gardner, K. N.; Thomas, C. Review of Cariprazine in Management of Psychiatric Illness. *Mental Health Clinician* **2017**, *7* (5) 1–9.

- (195) Diefenderfer, L. A.; Iuppa, C. Brexpiprazole: A Review of a New Treatment Option for Schizophrenia and Major Depressive Disorder. *Ment. Heal. Clin.* **2017**, *7* (5), 207–212.
- (196) Di Sciascio, G.; Riva, M. A. Aripiprazole: From Pharmacological Profile to Clinical Use. *Neuropsychiatr. Dis. Treat.* **2015**, *11*, 2635–2647.
- (197) Reavill, C.; Taylor, S. G.; Wood, M. D.; Ashmeade, T.; Austin, N. E.; Avenell, K. Y.; Boyfield, I.; Branch, C. L.; Cilia, J.; Coldwell, M. C.; Hadley, M. S.; Hunter, A. J.; Jeffrey, P.; Jewitt, F.; Johnson, C. N.; Jones, D. N. C.; Medhurst, A. D.; Middlemiss, D. N.; Nash, D. J.; Riley, G. J.; Routledge, C.; Stemp, G.; Thewlis, K. M.; Trail, B.; Vong, A. K. K.; Hagan, J. J. Pharmacological Actions of a Novel, High-Affinity, and Selective Human Dopamine D3 Receptor Antagonist, SB-277011-A. *J. Pharmacol. Exp. Ther.* **2000**, *294* (3), 1154–1165.
- (198) Xi, Z. X.; Gardner, E. L. Pharmacological Actions of NGB 2904, a Selective Dopamine D3 Receptor Antagonist, in Animal Models of Drug Addiction. *CNS Drug Rev.* **2007**, *13* (2), 240–259.
- (199) Xiong Xi Z., Gilbert G.G., Pak A.C., Ashby R.C., Heidbreder C.A, and Gardner E.L. Selective Dopamine D3 Receptor Antagonism by SB-277011A Attenuates Cocaine Reinforcement as Assessed by Progressive- Ratio and Variable-Cost-Variable-Payoff Fixed-Ratio Cocaine Self- Administration in Rats. *Eur. J. Neurosci.* **2005**, *21* (12), 3427–3438.
- (200) Cosi, C.; Martel, J. C.; Auclair, A. L.; Collo, G.; Cavalleri, L.; Heusler, P.; Leriche, L.; Gaudoux, F.; Sokoloff, P.; Moser, P. C.; Gatti-McArthur, S. Pharmacology Profile of F17464, a Dopamine D3 Receptor Preferential Antagonist. *Eur. J. Pharmacol.* **2021**, *890*, 173635.
- (201) Bitter, I.; Lieberman, J. A.; Gaudoux, F.; Sokoloff, P.; Groc, M.; Chavda, R.; Delsol, C.; Barthe, L.; Brunner, V.; Fabre, C.; Fagard, M.; Montagne, A.; Tonner, F. Randomized, Double-Blind, Placebo-Controlled Study of F17464, a Preferential D3 Antagonist, in the Treatment of Acute Exacerbation of Schizophrenia. *Neuropsychopharmacology* **2019**, *44* (11), 1917–1924.
- (202) Redden, L.; Rendenbach-Mueller, B.; Abi-Saab, W. M.; Katz, D. A.; Goenjian, A.; Robieson, W. Z.; Wang, Y.; Goss, S. L.; Greco, N.; Saltarelli, M. D. A Double-Blind, Randomized, Placebo-Controlled Study of the Dopamine D 3 Receptor Antagonist ABT-925 in Patients with Acute Schizophrenia. *J. Clin. Psychopharmacol.* **2011**, *31* (2), 221–225.
- (203) Bhathena, A.; Wang, Y.; Kraft, J. B.; Idler, K. B.; Abel, S. J.; Holley-Shanks, R. R.; Robieson, W. Z.; Spear, B.; Redden, L.; Katz, D. A. Association of Dopamine-Related Genetic Loci to Dopamine D3 Receptor Antagonist ABT-925 Clinical Response. *Transl. Psychiatry* **2013**, *3* (4), e245-4.
- (204) Graff-Guerrero, A.; Redden, L.; Abi-Saab, W.; Katz, D. A.; Houle, S.; Barsoum, P.; Bhathena, A.; Palaparthi, R.; Saltarelli, M. D.; Kapur, S. Blockade of [¹¹C](+)-PHNO Binding in Human Subjects by the Dopamine D3 Receptor Antagonist ABT-925. *Int. J. Neuropsychopharmacol.* **2010**, *13* (3), 273–287.
- (205) Murphy, A.; Nestor, L. J.; McGonigle, J.; Paterson, L.; Boyapati, V.; Ersche, K. D.; Flechais, R.; Kuchibatla, S.; Metastasio, A.; Orban, C.; Passeti, F.; Reed, L.; Smith, D.; Suckling, J.; Taylor, E.; Robbins, T. W.; Lingford-Hughes, A.; Nutt, D. J.; Deakin, J. F. W.; Elliott, R. Acute D3 Antagonist GSK598809 Selectively Enhances Neural Response during Monetary Reward Anticipation in Drug and Alcohol Dependence. *Neuropsychopharmacology* **2017**, *42* (5), 1049–1057.
- (206) Appel, N. M.; Li, S. H.; Holmes, T. H.; Acri, J. B. Dopamine D3 Receptor Antagonist (GSK598809) Potentiates the Hypertensive Effects of Cocaine in Conscious, Freely-Moving Dogs. *J. Pharmacol. Exp. Ther.* **2015**, *354* (3), 484–492.
- (207) Micheli, F. Recent Advances in the Development of Dopamine D3 Receptor Antagonists: A Medicinal Chemistry Perspective. *ChemMedChem* **2011**, *6* (7), 1152–1162.
- (208) American Psychiatric Association -.*Diagnostic And Statistical Manual Of Mental Disorders*, (5th Edition) **2013**.
- (209) Avramopoulos, D. Recent Advances in the Genetics of Schizophrenia. *Mol. neuropsychiatry* **2018**, *4*, 35–51.
- (210) Rees, E.; O'Donovan, M. C.; Owen, M. J. Genetics of Schizophrenia. *Curr. Opin. Behav. Sci.* **2015**, *2*, 8–14.
- (211) Cannon, T. D.; Kaprio, J.; Lönnqvist, J.; Huttunen, M.; Koskenvuo, M. The Genetic Epidemiology of Schizophrenia in a Finnish Twin Cohort: A Population-Based Modeling Study. *Arch. Gen. Psychiatry* **1998**, *55* (1), 67–74.
- (212) Vierbuchen, T.; Ostermeier, A.; Pang, Z. P.; Kokubu, Y.; Südhof, T. C.; Wernig, M. Direct Conversion of Fibroblasts to Functional Neurons by Defined Factors. *Nature* **2010**, *463* (7284), 1035–1041.
- (213) Cong L., Ann Ran, F., Cox D., Lin, S., Barretto R., Habib N., Hsu P.D., Wu X., Jiang W., Marraffini L.A., and Zhang F.. Multiplex Genome Engineering Using CRISPR / Cas Systems. *Science*, **2013**, 819–824.
- (214) Henssler, J.; Brandt, L.; Müller, M.; Liu, S.; Montag, C.; Sterzer, P.; Heinz, A. Migration and Schizophrenia: Meta-Analysis and Explanatory Framework. *Eur. Arch. Psychiatry Clin. Neurosci.* **2020**, *270* (3), 325–335.

- (215) Dealberto, M. J. Ethnic Origin and Increased Risk for Schizophrenia in Immigrants to Countries of Recent and Longstanding Immigration. *Acta Psychiatr. Scand.* **2010**, *121* (5), 325–339.
- (216) McDonald, C.; Murray, R. M. Interactive Report Early and Late Environmental Risk Factors for Schizophrenia *Brain Res. Rev.* **2000**, *31*, 130–137.
- (217) Eyles, D. W.; Trzaskowski, M.; Vinkhuyzen, A. A. E.; Mattheisen, M.; Meier, S.; Gooch, H.; Anggono, V.; Cui, X.; Tan, M. C.; Burne, T. H. J.; Jang, S. E.; Kvaskoff, D.; Hougaard, D. M.; Nørgaard-Pedersen, B.; Cohen, A.; Agerbo, E.; Pedersen, C. B.; Børglum, A. D.; Mors, O.; Sah, P.; Wray, N. R.; Mortensen, P. B.; McGrath, J. J. The Association between Neonatal Vitamin D Status and Risk of Schizophrenia. *Sci. Rep.* **2018**, *8* (1), 1–8.
- (218) Kočovská, E.; Gaughran, F.; Krivoy, A.; Meier, U. C. Vitamin-D Deficiency as a Potential Environmental Risk Factor in Multiple Sclerosis, Schizophrenia, and Autism. *Front. Psychiatry* **2017**, *8*, 1–11.
- (219) Chiang, M.; Natarajan, R.; Fan, X. Vitamin D in Schizophrenia: A Clinical Review. *Evid. Based. Ment. Health* **2016**, *19* (1), 6–9.
- (220) Haddad, L.; Schäfer, A.; Streit, F.; Lederbogen, F.; Grimm, O.; Wüst, S.; Deuschle, M.; Kirsch, P.; Tost, H.; Meyer-Lindenberg, A. Brain Structure Correlates of Urban Upbringing, an Environmental Risk Factor for Schizophrenia. *Schizophr. Bull.* **2015**, *41* (1), 115–122.
- (221) Plana-Ripoll, O.; Bøcker Pedersen C.; McGrath J.J. Urbanicity and Risk of Schizophrenia—New Studies and Old Hypotheses Oleguer. *JAMA Psychiatry* **2018**, *75* (7), 678–686.
- (222) Fusar-Poli, P.; Tantardini, M.; De Simone, S.; Ramella-Cravaro, V.; Oliver, D.; Kingdon, J.; Kotlicka-Antczak, M.; Valmaggia, L.; Lee, J.; Millan, M. J.; Galderisi, S.; Balottin, U.; Ricca, V.; McGuire, P. Deconstructing Vulnerability for Psychosis: Meta-Analysis of Environmental Risk Factors for Psychosis in Subjects at Ultra High-Risk. *Eur. Psychiatry* **2017**, *40*, 65–75.
- (223) Babulas, V.; Factor-Litvak, P.; Goetz, R.; Schaefer, C. A.; Brown, A. S. Prenatal Exposure to Maternal Genital and Reproductive Infections and Adult Schizophrenia. *Am. J. Psychiatry* **2006**, *163* (5), 927–929.
- (224) McCutcheon, R. A.; Abi-Dargham, A.; Howes, O. D. Schizophrenia, Dopamine and the Striatum: From Biology to Symptoms. *Trends Neurosci.* **2019**, *42* (3), 205–220.
- (225) Beck, K.; Hindley, G.; Borgan, F.; Ginestet, C.; McCutcheon, R.; Brugger, S.; Driesen, N.; Ranganathan, M.; D’Souza, D. C.; Taylor, M.; Krystal, J. H.; Howes, O. D. Association of Ketamine With Psychiatric Symptoms and Implications for Its Therapeutic Use and for Understanding Schizophrenia: A Systematic Review and Meta-Analysis. *JAMA Netw. open* **2020**, *3* (5), e204693.
- (226) Patel, K. R.; Cherian, J.; Gohil, K.; Atkinson, D. Schizophrenia: Overview and Treatment Options. *P T* **2014**, *39* (9), 638–645.
- (227) Marsman, A.; Van Den Heuvel, M. P.; Klomp, D. W. J.; Kahn, R. S.; Luijten, P. R.; Hulshoff Pol, H. E. Glutamate in Schizophrenia: A Focused Review and Meta-Analysis of IH-MRS Studies. *Schizophr. Bull.* **2013**, *39* (1), 120–129.
- (228) Bell, K. F. S.; Bennett, D. A.; Cuello, A. C. Paradoxical Upregulation of Glutamatergic Presynaptic Boutons during Mild Cognitive Impairment. *J. Neurosci.* **2007**, *27* (40), 10810–10817.
- (229) Insel, T. R. Rethinking Schizophrenia. *Nature* **2010**, *468* (7321), 187–193.
- (230) Cerveri, G.; Gesi, C.; Mencacci, C. Pharmacological Treatment of Negative Symptoms in Schizophrenia: Update and Proposal of a Clinical Algorithm. *Neuropsychiatr. Dis. Treat.* **2019**, *15*, 1525–1535.
- (231) Seeman, P.; Tallerico, T. Rapid Release of Antipsychotic Drugs from Dopamine D2 Receptors: An Explanation for Low Receptor Occupancy and Early Clinical Relapse upon Withdrawal of Clozapine or Quetiapine. *Am. J. Psychiatry* **1999**, *156* (6), 876–884.
- (232) Seeman, P. Atypical Antipsychotics Mechanism of Action. *Can. J. Psychiatry* **2002**, *47*, 27–38.
- (233) Hirsch, L.; Patten, S. B.; Bresee, L.; Jette, N.; Pringsheim, T. Second-Generation Antipsychotics and Metabolic Side-Effects: Canadian Population-Based Study. *BJPsych Open* **2018**, *4* (4), 256–261.
- (234) Townsend, L. K.; Peppler, W. T.; Bush, N. D.; Wright, D. C. Obesity Exacerbates the Acute Metabolic Side Effects of Olanzapine. *Psychoneuroendocrinology* **2018**, *88*, 121–128.
- (235) Roerig, J. L.; Steffen, K. J.; Mitchell, J. E. Atypical Antipsychotic-Induced Weight Gain: Insights into Mechanisms of Action. *CNS Drugs* **2011**, *25* (12), 1035–1059.
- (236) Pirmohamed, M.; Park, K. Mechanism of Clozapine-Induced Agranulocytosis. Current Status of Research and Implications for Drug Development. *CNS Drugs* **1997**, *7* (2), 139–158.
- (237) Durgam, S.; Earley, W.; Li, R.; Li, D.; Lu, K.; Laszlovszky, I.; Fleischhacker, W. W.; Nasrallah, H. A. Long-Term Cariprazine Treatment for the Prevention of Relapse in Patients with Schizophrenia: A Randomized, Double-Blind, Placebo-Controlled Trial. *Schizophr. Res.* **2016**, *176* (2–3), 264–271.
- (238) Suehs, B.; Argo, T. R.; Bendele, S. D.; Crismon, M. L.; Trivedi, M. H. Texas Medication Algorithm Project

- Procedural Manual Major Depressive Disorder Algorithms, **2008**.
- (239) Tysnes, O. B.; Storstein, A. Epidemiology of Parkinson's Disease. *J. Neural. Transm.* **2017**, *124* (8), 901–905.
- (240) Lonneke M L de Lau, M. M. B. B. The Epidemiology of Parkinson's Disease. *Lancet Neurol.* **2006**, *5* (6), 525–535.
- (241) Nussbaum, R. L.; Ellis, C. E. Alzheimer's Disease and Parkinson's Disease. *N. Engl. J. Med* **2021**, *348* (14), 1356-1364.
- (242) De Rijk M.C.; Tzourio C.; Breteler M.M.B.; Dartigues J.F.; Amaducci L.; Lopez-Pousa S.; Manubens-Bertran J.M.; Alperovitch A.; Rocca W.A. Prevalence of Parkinsonism and Parkinson's Disease in Europe: The EUROPARKINSON Collaborative Study. *J. Neurol. Neurosurgery Psychiatry* **1997**, *62*, 10–15.
- (243) Przedborski, W. D. S. Parkinson's Disease: Mechanisms and Models. *Neuron* **2003**, *39*, 889–909.
- (244) Schultz, W. Depletion of Dopamine in the Striatum as an Experimental Model of Parkinsonism: Direct Effects and Adaptive Mechanisms. *Prog. Neurobiol.* **1982**, *18* (2–3), 121–166.
- (245) Leng, A.; Mura, A.; Hengerer, B.; Feldon, J.; Ferger, B. Effects of Blocking the Dopamine Biosynthesis and of Neurotoxic Dopamine Depletion with 1-Methyl-4-Phenyl-1,2,3,6-Tetrahydropyridine (MPTP) on Voluntary Wheel Running in Mice. *Behav. Brain Res.* **2004**, *154* (2), 375–383.
- (246) Sveinbjornsdottir, S. The Clinical Symptoms of Parkinson's Disease. *J. Neurochem.* **2016**, *139*, 318–324.
- (247) Schwarz, S. T.; Xing, Y.; Tomar, P.; Bajaj, N.; Auer, D. P. In Vivo Assessment of Brainstem Depigmentation in Parkinson Disease: Potential as a Severity Marker for Multicenter Studies. *Radiology* **2017**, *283* (3), 789–798.
- (248) Ball, N.; Teo, W.-P.; Chandra, S.; Chapman, J. Parkinson's Disease and the Environment. *Front. Neurol.* **2019**, *10*.
- (249) Polymeropoulos, M. H.; Higgins, J. J.; Golbe, L. I.; Johnson, W. G.; Ide, S. E.; Di Iorio, G.; Sanges, G.; Stenroos, E. S.; Pho, L. T.; Schaffer, A. A.; Lazzarini, A. M.; Nussbaum, R. L.; Duvoisin, R. C. Mapping of a Gene for Parkinson's Disease to Chromosome 4q21-Q23. *Science*, **1996**, *274* (5290), 1197–1199.
- (250) Chang, D.; Nalls, M. A.; Hallgrímsson, I. B.; Hunkapiller, J.; Brug, M. van der; Cai, F.; Kerchner, G. A.; Ayalon, G.; Bingol, B.; Sheng, M.; Hinds, D.; Behrens, T. W.; Singleton, A. B.; Bhangale, T. R.; Graham, R. R. A Meta-Analysis of Genome-Wide Association Studies Identifies 17 New Parkinson's Disease Risk Loci. *Nat. Genet.* **2017**, *49* (10), 1511–1516.
- (251) LeWitt, P. A.; Rezai, A. R.; Leehey, M. A.; Ojemann, S. G.; Flaherty, A. W.; Eskandar, E. N.; Kostyk, S. K.; Thomas, K.; Sarkar, A.; Siddiqui, M. S.; Tatter, S. B.; Schwalb, J. M.; Poston, K. L.; Henderson, J. M.; Kurlan, R. M.; Richard, I. H.; Van Meter, L.; Sapan, C. V.; Doring, M. J.; Kaplitt, M. G.; Feigin, A. AAV2-GAD Gene Therapy for Advanced Parkinson's Disease: A Double-Blind, Sham-Surgery Controlled, Randomised Trial. *Lancet Neurol.* **2011**, *10* (4), 309–319.
- (252) Bartus, R. T.; Weinberg, M. S.; Samulski, R. J. Parkinson's Disease Gene Therapy: Success by Design Meets Failure by Efficacy. *Mol. Ther.* **2014**, *22* (3), 487–497.
- (253) Axelsen, T. M.; Woldbye, D. P. D. Gene Therapy for Parkinson's Disease, an Update. *J. Parkinsons. Dis.* **2018**, *8* (2), 195–215.
- (254) Jackson-Lewis, V.; Przedborski, S. Protocol for the MPTP Mouse Model of Parkinson's Disease. *Nat. Protoc.* **2007**, *2* (1), 141–151.
- (255) Ritz B., Acherio A., Chechoway H., Marder K., Nelson L.M., Rocca W.A., Ross W., Strickland D., Van den Eeden S.V.K. and Gorell J. Pooled Analysis of Tobacco Use and Risk of Parkinson Disease. *Arch. Neurol.* **2007**, *64* (7), 990–997.
- (256) Liu, R.; Guo, X.; Park, Y.; Huang, X.; Sinha, R.; Freedman, N. D.; Hollenbeck, A. R.; Blair, A.; Chen, H. Caffeine Intake, Smoking, and Risk of Parkinson Disease in Men and Women. *Am. J. Epidemiol.* **2012**, *175* (11), 1200–1207.
- (257) Gallo, V.; Vineis, P.; Cancellieri, M.; Chiodini, P.; Barker, R. A.; Brayne, C.; Pearce, N.; Vermeulen, R.; Panico, S.; Bueno-De-Mesquita, B.; Vanacore, N.; Forsgren, L.; Ramat, S.; Ardanaz, E.; Arriola, L.; Peterson, J.; Hansson, O.; Gavrila, D.; Sacerdote, C.; Sieri, S.; Kühn, T.; Katzke, V. A.; Van Der Schouw, Y. T.; Kyrozi, A.; Masala, G.; Mattiello, A.; Perneczky, R.; Middleton, L.; Saracci, R.; Riboli, E. Exploring Causality of the Association between Smoking and Parkinson's Disease. *Int. J. Epidemiol.* **2019**, *48* (3), 912–925.
- (258) Hernán, M. A.; Takkouche, B.; Caamaño-Isorna, F.; Gestal-Otero, J. J. A Meta-Analysis of Coffee Drinking, Cigarette Smoking, and the Risk of Parkinson's Disease. *Ann. Neurol.* **2002**, *52* (3), 276–284.
- (259) Park, A.; Stacy, M. Non-Motor Symptoms in Parkinson's Disease. *J. Neurol.* **2009**, *256*, 293–298.
- (260) Postuma, R. B.; Berg, D.; Stern, M.; Poewe, W.; Olanow, C. W.; Oertel, W.; Obeso, J.; Marek, K.; Litvan, I.

- Lang, A. E.; Halliday, G.; Goetz, C. G.; Gasser, T.; Dubois, B.; Chan, P.; Bloem, B. R.; Adler, C. H.; Deuschl, G. MDS Clinical Diagnostic Criteria for Parkinson's Disease. *Mov. Disord.* **2015**, *30* (12), 1591–1601.
- (261) Zheng, K. S.; Dorfman, B. J.; Christos, P. J.; Khadem, N. R.; Henchcliffe, C.; Piboolnurak, P.; Nirenberg, M. J. Clinical Characteristics of Exacerbations in Parkinson Disease. *Neurologist* **2012**, *18* (3), 120–124.
- (262) Calabresi, P.; Picconi, B.; Parnetti, L.; Di Filippo, M. A Convergent Model for Cognitive Dysfunctions in Parkinson's Disease: The Critical Dopamine-Acetylcholine Synaptic Balance. *Lancet Neurol.* **2006**, *5* (11), 974–983.
- (263) Vanle, B.; Olcott, W.; Jimenez, J.; Bashmi, L.; Danovitch, I.; Ishak, W. W. NMDA Antagonists for Treating the Non-Motor Symptoms in Parkinson's Disease. *Transl. Psychiatry* **2018**, *8* (117).
- (264) Politis, M.; Niccolini, F. Serotonin in Parkinson's Disease. *Behav. Brain Res.* **2015**, *277*, 136–145.
- (265) Poewe, W.; Antonini, A.; Zijlmans, J. C.; Burkhard, P. R.; Vingerhoets, F. Levodopa in the Treatment of Parkinson's Disease: An Old Drug Still Going Strong. *Clin. Interv. Aging* **2010**, *5*, 229–238.
- (266) Tran, T. N.; Vo, T. N. N.; Frei, K.; Truong, D. D. Levodopa-Induced Dyskinesia: Clinical Features, Incidence, and Risk Factors. *J. Neural Transm.* **2018**, *125* (8), 1109–1117.
- (267) Chen, J. J.; Pharm, D.; Swope, D. M. Pharmacotherapy for Parkinson's Disease. *Pharmacotherapy* **2007**, 161–173.
- (268) Obering, C. D.; Chen, J. J.; Swope, D. M. Update on Apomorphine for the Rapid Treatment of Hypomobility ("off") Episodes in Parkinson's Disease. *Pharmacotherapy* **2006**, *26* (6 I), 840–852.
- (269) Wiggins J.; Skinner C. Bromocriptine. Induced Pleuropulmonary Fibrosis. *Thorax*, **1986**, 328–330.
- (270) Alberti, C. Drug-Induced Retroperitoneal Fibrosis: Short Aetiopathogenetic Note, from the Past Times of Ergot-Derivatives Large Use to Currently Applied Bio-Pharmacology. *G. di Chir.* **2015**, *36* (4), 187–191.
- (271) Klietz, M.; Greten, S.; Wegner, F.; Höglinger, G. U. Safety and Tolerability of Pharmacotherapies for Parkinson's Disease in Geriatric Patients. *Drugs and Aging* **2019**, *36* (6), 511–530.
- (272) Santangelo, G.; Barone, P.; Trojano, L.; Vitale, C. Pathological Gambling in Parkinson's Disease. A Comprehensive Review. *Park. Relat. Disord.* **2013**, *19* (7), 645–653.
- (273) Wilson, S. M.; Wurst, M. G.; Whatley, M. F.; Daniels, R. N. Classics in Chemical Neuroscience: Pramipexole. *ACS Chem. Neurosci.* **2020**, *11* (17), 2506–2512.
- (274) Deutschländer, A.; La Fougère, C.; Boetzel, K.; Albert, N. L.; Gildehaus, F. J.; Bartenstein, P.; Xiong, G.; Cumming, P. Occupancy of Pramipexole (Sifrol) at Cerebral Dopamine D2/3 Receptors in Parkinson's Disease Patients. *NeuroImage Clin.* **2016**, *12*, 41–46.
- (275) Zhang, W.; Wang, Y.; Cong, S. Y.; Nao, J. F.; Feng, J.; Bi, G. R. Efficacy and Tolerability of Pramipexole for the Treatment of Primary Restless Leg Syndrome: A Meta-Analysis of Randomized Placebo-Controlled Trials. *Neuropsychiatr. Dis. Treat.* **2013**, *9*, 1035–1043.
- (276) Benbir, G.; Guillemainault, C. Pramipexole: New Use for an Old Drug - The Potential Use of Pramipexole in the Treatment of Restless Legs Syndrome. *Neuropsychiatr. Dis. Treat.* **2006**, *2* (4), 393–405.
- (277) You, X.; Wu, W.; Xu, J.; Jiao, Z.; Ke, M.; Huang, P.; Lin, C. Development of a Physiologically Based Pharmacokinetic Model for Prediction of Pramipexole Pharmacokinetics in Parkinson's Disease Patients With Renal Impairment. *J. Clin. Pharmacol.* **2020**, *60* (8), 999–1010.
- (278) Dooley, M.; Markham, A. Pramipexole. A Review of Its Use in the Management of Early and Advanced Parkinson's Disease. *Drugs and Aging* **1998**, *12* (6), 495–514.
- (279) Li, C.; Guo, Y.; Xie, W.; Li, X.; Janokovic, J.; Le, W. Neuroprotection of Pramipexole in UPS Impairment Induced Animal Model of Parkinson's Disease. *Neurochem. Res.* **2010**, *35* (10), 1546–1556.
- (280) Wang, Y.; Yu, X.; Zhang, P.; Ma, Y.; Wang, L.; Xu, H.; Sui, D. Neuroprotective Effects of Pramipexole Transdermal Patch in the MPTP-Induced Mouse Model of Parkinson's Disease. *J. Pharmacol. Sci.* **2018**, *138* (1), 31–37.
- (281) Holloway, R. G. Pramipexole vs Levodopa as Initial Treatment for Parkinson Disease: A 4-Year Randomized Controlled Trial. *Arch. Neurol.* **2004**, *61* (7), 1044–1053.
- (282) Bxarone, P.; Poewe, W.; Albrecht, S.; Debieuvre, C.; Massey, D.; Rascol, O.; Tolosa, E.; Weintraub, D. Pramipexole for the Treatment of Depressive Symptoms in Patients with Parkinson's Disease: A Randomised, Double-Blind, Placebo-Controlled Trial. *Lancet Neurol.* **2010**, *9* (6), 573–580.
- (283) Corrigan, M. H.; Denahan, A. Q.; Eugene Wright, C.; Ragual, R. J.; Evans, D. L. Comparison of Praahpexole, Fluoxetine, and Placebo in Patients with Major Depression. *Depress. Anxiety* **2000**, *11* (2), 58–65.
- (284) Fawcett, J.; Rush, A. J.; Vukelich, J.; Diaz, S. H.; Dunklee, L.; Romo, P.; Yarns, B. C.; Escalona, R. Clinical Experience with High-Dosage Pramipexole in Patients with Treatment-Resistant Depressive Episodes in Unipolar and Bipolar Depression. *Am. J. Psychiatry* **2016**, *173* (2), 107–111.
- (285) Enna, S. J.; Bylund, D. B. Saffinamide. *xPharm Compr. Pharmacol. Ref.* **2007**, *4*, 1–2.

- (286) Ramsay, R. R.; Basile, L.; Maniquet, A.; Hagenow, S.; Pappalardo, M.; Saija, M. C.; Bryant, S. D.; Albrecht, A.; Guccione, S. Parameters for Irreversible Inactivation of Monoamine Oxidase. *Molecules* **2020**, *25* (24),5908.
- (287) Borgohain, R.; Szasz, J.; Stanzione, P.; Meshram, C.; Bhatt, M.; Chirilineau, D.; Stocchi, F.; Lucini, V.; Giuliani, R.; Forrest, E.; Rice, P.; Anand, R.; Illiyas Sahadulla, M.; Kardan, U.; Keshava, B. S.; Kishore, A.; Kothari, S. S.; Krishna Murthy, J. M.; Kumar, S.; Kumar Pal, P.; Mehta, N.; Prabhakar, S.; Prabhakar, S. K.; Pradhan, S.; Roy, A. K.; Sankhla, C.; Sethi, P. K.; Shah, A. B.; Shankar, N.; Shukla, R.; Sowani, A.; Srinivasa, R.; Varma, M.; Vasudevan, D.; Vavilikolanu Sreenivas, P.; Velmurugendran, C. U.; Vijayan, K.; Bajenaru, O.; Bulboaca, A.; Campeanu, A.; Chirileanu, D.; Muresanu, D.; Panea, C.; Popescu, C.; Simu, M.; Ticmeanu, M.; Avarello, T.; Bonuccelli, U.; Eleopra, R.; Onofrj, M.; Quatrале, R. Randomized Trial of Saffinamide Addition to Levodopa in Parkinson's Disease with Motor Fluctuations. *Mov. Disord.* **2014**, *29* (2), 229–237.
- (288) Bette, S.; Shpiner, D. S.; Singer, C.; Moore, H. Saffinamide in the Management of Patients with Parkinson's Disease Not Stabilized on Levodopa: A Review of the Current Clinical Evidence. *Ther. Clin. Risk Manag.* **2018**, *14*, 1737–1745.
- (289) Deeks, E. D. Saffinamide: First Global Approval. *Drugs* **2015**, *75* (6), 705–711.
- (290) Smith, K. S.; Smith, P. L.; Heady, T. N.; Trugman, J. M.; Harman, W. D.; Macdonald, T. L. In Vitro Metabolism of Tolcapone to Reactive Intermediates: Relevance to Tolcapone Liver Toxicity. *Chem. Res. Toxicol.* **2003**, *16* (2), 123–128.
- (291) Olanow, C. W.; Watkins, P. B. Tolcapone: An Efficacy and Safety Review (2007). *Clin. Neuropharmacol.* **2007**, *30* (5), 287–294.
- (292) Sawada, H.; Oeda, T.; Kuno, S.; Nomoto, M.; Yamamoto, K.; Yamamoto, M.; Hisanaga, K.; Kawamura, T. Amantadine for Dyskinesias in Parkinson's Disease: A Randomized Controlled Trial. *PLoS One* **2010**, *5* (12), 6–12.
- (293) Dale H.H., Histamine Shock. *J. Physiol.* **1919**, 355–390.
- (294) Huang, H.; Li, Y.; Liang, J.; Finkelman, F. D. Molecular Regulation of Histamine Synthesis. *Front. Immunol.* **2018**, *9*, 1–7.
- (295) Panula, P.; Chazot, P. L.; Cowart, M.; Gutzmer, R.; Leurs, R.; Liu, W. L. S.; Stark, H.; Thurmond, R. L.; Haas, H. L. International Union of Basic and Clinical Pharmacology. XCVIII. Histamine Receptors. *Pharmacol. Rev.* **2015**, *67* (3), 601–655.
- (296) Haas, H. L.; Sergeeva, O. A.; Selbach, O. Histamine in the Nervous System. *Physiol. Rev.* **2008**, *88* (3), 1183–1241.
- (297) Haas, H. L.; Schwartz, J. C. Electrophysiology of Histamine-Receptors. *Receptor Biochemistry and Methodology*, **1992** *16*, 161–177.
- (298) Martinez-Mir, M. I.; Pollard, H.; Moreau, J.; Arrang, J. M.; Ruat, M.; Traiffort, E.; Schwartz, J. C.; Palacios, J. M. Three Histamine Receptors (H1, H2 and H3) Visualized in the Brain of Human and Non-Human Primates. *Brain Res.* **1990**, *526* (2), 322–327.
- (299) Tagawa, M.; Kano, M.; Okamura, N.; Higuchi, M.; Matsuda, M.; Mizuki, Y.; Arai, H.; Iwata, R.; Fujii, T.; Komemushi, S.; Ido, T.; Itoh, M.; Sasaki, H.; Watanabe, T.; Yanai, K. Neuroimaging of Histamine H1-Receptor Occupancy in Human Brain by Positron Emission Tomography (PET): A Comparative Study of Ebastine, a Second-Generation Antihistamine, and (+)-Chlorpheniramine, a Classical Antihistamine. *Br. J. Clin. Pharmacol.* **2001**, *52* (5), 501–509.
- (300) Sadek, B.; Stark, H. Cherry-Picked Ligands at Histamine Receptor Subtypes. *Neuropharmacology* **2016**, *106*, 56–73.
- (301) Morse K.L.; Behan J.; Laz T.M.; West R.E.; Greenfeder S.E.; Anthes J.C.; Umland S.; Wan Y.; Hipkin R.W.; Gonsiorek W.; Shin N.; Gustafson E.L.; Qiao X.; Wang S.; Hendrick J.A; Green J. Cloning, Expression, and Pharmacological Characterization of a Novel Human Histamine Receptor. *J. Pharmacol. Exp. Ther.* **2001**, *59* (3), 434–441.
- (302) Nakamura, T.; Itadani, H.; Hidaka, Y.; Ohta, M.; Tanaka, K. Molecular Cloning and Characterization of a New Human Histamine Receptor, HH4R. *Biochem. Biophys. Res. Commun.* **2000**, *279* (2), 615–620.
- (303) Black, J. W.; Duncan, W. A. M.; Durant, C. J.; Ganellin, C. R.; Parsons, E. M. Definition and Antagonism of Histamine H2-Receptors. *Nature* **1972**, *236* (5347), 385–390.
- (304) Arrang, J.M.; Garbarg, M.; Schwartz, J.C. Auto-Inhibition of Brain Histamine Release Mediated by a Novel Class (H3) of Histamine Receptor. *Nature* **1983**, *302*, 3–8.
- (305) Clark, R.A.F.; Sandler, J.A.; Gallin, J.I.; Kaplan, A.P. Histamine Modulation of Eosinophil Migration Richard. *J. Immunol.* **1977**, *118*, 137–145.
- (306) Yamashita, M.; Fukui, H.; Sugama, K.; Horio, Y.; Ito, S.; Mizuguchi, H.; Wada, H. Expression Cloning of a

- CDNA Encoding the Bovine Histamine H1 Receptor. *Proc. Natl. Acad. Sci. U. S. A.* **1991**, *88* (24), 11515–11519.
- (307) De Backer, M. D.; Gommeren, W.; Moereels, H.; Nobels, G.; Van Gompel, P.; Leysen, J. E.; Luyten, W. H. M. L. Genomic Cloning, Heterologous Expression and Pharmacological Characterization of a Human Histamine H1 Receptor. *Biochem. Biophys. Res. Comm.* **1993**, *197* (3), 1601–1608.
- (308) Gantz, I.; Munzert, G.; Tashiro, T.; Schäffer, M.; Wang, L.; DelValle, J.; Yamada, T. Molecular Cloning of the Human Histamine H2 Receptor. *Biochem. Biophys. Res. Commun.* **1991**, *178* (3), 1386–1392.
- (309) Lovenberg, T. W.; Roland, B. L.; Wilson, S. J.; Jiang, X.; Pyati, J.; Huvar, A.; Jackson, M. R.; Erlander, M. G. Cloning and Functional Expression of the Human Histamine H3 Receptor. *Mol. Pharmacol.* **1999**, *55* (6), 1101–1107.
- (310) Adami, M.; Micheloni, C.; Grandi, D.; Stark, H. Differential Effects of Functionally Different Histamine H4 Receptor Ligands on Acute Irritant Dermatitis in Mice. *Naunyn. Schmiedeberg's Arch. Pharmacol.* **2018**, *391* (12), 1387–1397.
- (311) Gschwandtner, M.; Stark, H.; Gutzmer, R. Profiling of Histamine H4 Receptor Agonists in Native Human Monocytes. *Br. J. Pharmacol.* **2013**, *170* (1), 136–143.
- (312) Galeotti, N.; Sanna, M. D.; Ghelardini, C. Pleiotropic Effect of Histamine H4 Receptor Modulation in the Central Nervous System. *Neuropharmacology* **2013**, *71*, 141–147.
- (313) Syed, Y. Y. Pitolisant: First Global Approval. *Drugs* **2016**, *76* (13), 1313–1318.
- (314) Fox, G. B.; Esbenshade, T. A.; Pan, J. B.; Radek, R. J.; Krueger, K. M.; Yao, B. B.; Browman, K. E.; Buckley, M. J.; Ballard, M. E.; Komater, V. A.; Miner, H.; Zhang, M.; Faghhi, R.; Rueter, L. E.; Bitner, R. S.; Drescher, K. U.; Wetter, J.; Marsh, K.; Lemaire, M.; Porsolt, R. D.; Bennani, Y. L.; Sullivan, J. P.; Cowart, M. D.; Decker, M. W.; Hancock, A. A. Pharmacological Properties of ABT-239 [4-(2-{2-[(2R)-2-Methylpyrrolidinyl] Ethyl}-Benzofuran-5-Yl)Benzonitrile]: II. Neurophysiological Characterization and Broad Preclinical Efficacy in Cognition and Schizophrenia of a Potent and Selective Histamine H3 R. *J. Pharmacol. Exp. Ther.* **2005**, *313* (1), 176–190.
- (315) Eissa, N.; Jayaprakash, P.; Azimullah, S.; Ojha, S. K.; Al-Houqani, M.; Jalal, F. Y.; Łażewska, D.; Kieć-Kononowicz, K.; Sadek, B. The Histamine H3R Antagonist DL77 Attenuates Autistic Behaviors in a Prenatal Valproic Acid-Induced Mouse Model of Autism. *Sci. Rep.* **2018**, *8* (1), 1–15.
- (316) Rosethorne, E. M.; Charlton, S. J. Agonist-Biased Signaling at the Histamine H4 Receptor: JNJ7777120 Recruits β -Arrestin without Activating G Proteins. *Mol. Pharmacol.* **2011**, *79* (4), 749–757.
- (317) Petremann, M.; Gueguen, C.; Delgado Betancourt, V.; Wersinger, E.; Dyhrfeld-Johnsen, J. Effect of the Novel Histamine H4 Receptor Antagonist SENS-111 on Spontaneous Nystagmus in a Rat Model of Acute Unilateral Vestibular Loss. *Br. J. Pharmacol.* **2020**, *177* (3), 623–633.
- (318) Thurmond, R. L.; Chen, B.; Dunford, P. J.; Greenspan, A. J.; Karlsson, L.; La, D.; Ward, P.; Xu, X. L. Clinical and Preclinical Characterization of the Histamine H4 Receptor Antagonist JNJ-39758979s. *J. Pharmacol. Exp. Ther.* **2014**, *349* (2), 176–184.
- (319) Cogé, F.; Guénin, S.; Audinot, V.; Renouard-Try, A.; Beauverger, P.; Macia, C.; Ouvry, C.; Nagel, N.; Rique, H.; Boutin, J. A.; Galizzi, J. Genomic Organization and Characterization of Splice Variants of the Human Histamine H3 Receptor. *Biochem. J.* **2001**, *355* (2), 279–288.
- (320) Leurs, R.; Hoffmann, M.; Wieland, K.; Timmerman, H. Receptor Gene Is Cloned at Last. *Trends Pharmacol. Sci.* **2000**, *21* (1), 11–12.
- (321) Drutel, G.; Peitsaro, N.; Karlstedt, K.; Wieland, K.; Smit, M. J.; Timmerman, H.; Panula, P.; Leurs, R. Identification of Rat H3 Receptor Isoforms with Different Brain Expression and Signaling Properties. *Mol. Pharmacol.* **2001**, *59* (1), 1–8.
- (322) Berlin, M.; Boyce, C. W.; De Lera Ruiz, M. Histamine H3 Receptor as a Drug Discovery Target. *J. Med. Chem.* **2011**, *54* (1), 26–53.
- (323) Wellendorph, P.; Goodman, M. W.; Burstein, E. S.; Nash, N. R.; Brann, M. R.; Weiner, D. M. Molecular Cloning and Pharmacology of Functionally Distinct Isoforms of the Human Histamine H3 Receptor. *Neuropharmacology* **2002**, *42* (7), 929–940.
- (324) Nieto-alamilla, G.; Márquez-gómez, R. The Histamine H3 Receptor : Structure , Pharmacology , and Function. *Mol. Pharmacol.*, **2016**, *90*, 649–673.
- (325) Silver, R. B.; Poonwasi, K. S.; Seyedi, N.; Wilson, S. J.; Lovenberg, T. W.; Levi, R. Decreased Intracellular Calcium Mediates the Histamine H3-Receptor-Induced Attenuation of Norepinephrine Exocytosis from Cardiac Sympathetic Nerve Endings. *Proc. Natl. Acad. Sci. U. S. A.* **2002**, *99* (1), 501–506.
- (326) Ellenbroek, B. A.; Ghiabi, B. The Other Side of the Histamine H3 Receptor. *Trends Neurosci.* **2014**, *37* (4), 191–199.

- (327) Kooistra, A. J.; Kuhne, S.; De Esch, I. J. P.; Leurs, R.; De Graaf, C. A Structural Chemogenomics Analysis of Aminergic GPCRs: Lessons for Histamine Receptor Ligand Design. *Br. J. Pharmacol.* **2013**, *170* (1), 101–126.
- (328) Arrang, J. M.; Morisset, S.; Gbahou, F. Constitutive Activity of the Histamine H3 Receptor. *Trends Pharmacol. Sci.* **2007**, *28* (7), 350–357.
- (329) Gomez-Ramirez, J.; Ortiz, J.; Blanco, I. Presynaptic H3 Autoreceptors Modulate Histamine Synthesis through Camp Pathway. *Mol. Pharmacol.* **2002**, *61* (1), 239–245.
- (330) Giovannini, M. G.; Efoudebe, M.; Passani, M. B.; Baldi, E.; Bucherelli, C.; Giachi, F.; Corradetti, R.; Blandina, P. Improvement in Fear Memory by Histamine-Elicited ERK2 Activation in Hippocampal CA3 Cells. *J. Neurosci.* **2003**, *23* (27), 9016–9023.
- (331) Lai, X.; Ye, L.; Liao, Y.; Jin, L.; Ma, Q.; Lu, B.; Sun, Y.; Shi, Y.; Zhou, N. Agonist-Induced Activation of Histamine H3 Receptor Signals to Extracellular Signal-Regulated Kinases 1 and 2 through PKC-, PLD-, and EGFR-Dependent Mechanisms. *J. Neurochem.* **2016**, *137* (2), 200–215.
- (332) Bongers, M. (2008) Signal Transduction of the Histamine H3 Receptor. Doctoral Dissertation. Vrije Universiteit Amsterdam.
- (333) Silver, R. B.; Mackins, C. J.; Smith, N. C. E.; Koritchneva, I. L.; Lefkowitz, K.; Lovenberg, T. W.; Levi, R. Coupling of Histamine H3 Receptors to Neuronal Na⁺/H⁺ Exchange: A Novel Protective Mechanism in Myocardial Ischemia. *Proc. Natl. Acad. Sci. U. S. A.* **2001**, *98* (5), 2855–2859.
- (334) Bongers, G.; Bakker, R. A.; Leurs, R. Molecular Aspects of the Histamine H3 Receptor. *Biochem. Pharmacol.* **2007**, *73* (8), 1195–1204.
- (335) Panula, P.; Eriksson, K. S.; Sallmen, T. Neuronal histamine deficit in Alzheimer's disease *Neuroscience* **1998**, *82* (4), 993–997.
- (336) Rizk A., Curley J., Robertson J. and Raber J.. Anxiety and Cognition in Histamine H 3 Receptor À / À Mice. *Eur. J. Neuroscience* **2004**, *19*, 1992–1996.
- (337) Brioni, J. D.; Esbenshade, T. A.; Garrison, T. R.; Bitner, S. R.; Cowart, M. D. Discovery of Histamine H 3 Antagonists for the Treatment of Cognitive Disorders and Alzheimer ' s Disease. *J. Pharmacol.. Exp. Ther.* **2016**, *336* (1), 38–46.
- (338) Millán-Guerrero, R. O.; Isais-Millán, R.; Benjamín, T. H.; Tene, C. E. N α -Methyl Histamine Safety and Efficacy in Migraine Prophylaxis: Phase III Study. *Can. J. Neurol. Sci.* **2006**, *33* (2), 195–199.
- (339) Krause, M.; Rouleau, A.; Stark, H.; Luger, P.; Lipp, R.; Garbarg, M.; Schwartz, J. C.; Schunack, W. Synthesis, X-Ray Crystallography, and Pharmacokinetics of Novel Azomethine Prodrugs of (R)- α -Methylhistamine: Highly Potent and Selective Histamine H3 Receptor Agonists. *J. Med. Chem.* **1995**, *38* (20), 4070–4079.
- (340) Rouleau, A.; Garbarg, M.; Ligneau, X.; Mantion, C.; Lavie, P.; Advenier, C.; Lecomte, J. M.; Krause, M.; Stark, H.; Schunack, W.; Schwartz, J. C. Bioavailability, Antinociceptive and Antiinflammatory Properties of BP 2-94, a Histamine H 3 Receptor Agonist Prodrug. *J. Pharmacol. Exp. Ther.* **1997**, *281* (3), 1085–1094.
- (341) Ito, S.; Yoshimoto, R.; Miyamoto, Y.; Mitobe, Y.; Nakamura, T. Detailed Pharmacological Characterization of GT-2331 for the Rat Histamine H 3 Receptor. *Eur.J.Pharmacol.* **2006**, *529*, 40–46.
- (342) Schwartz, J. C. The Histamine H3 Receptor: From Discovery to Clinical Trials with Pitolisant. *Br. J. Pharmacol.* **2011**, *163* (4), 713–721.
- (343) Shi, Y.; Sheng, R.; Zhong, T.; Xu, Y.; Chen, X.; Yang, D.; Sun, Y.; Yang, F.; Hu, Y.; Zhou, N. Identification and Characterization of ZEL-H16 as a Novel Agonist of the Histamine H3 Receptor. *PLoS One* **2012**, *7* (8), e24185.
- (344) Yokoyama H., Onodera K, Inuma K., Watanabe T. Effect of Thioperamide , a Histamine H3 Receptor Antagonist , on Electrically Induced Convulsions in Mice. *Eur. J. Pharmacol.* **1993**, *234*, 129–133.
- (345) Komater, V. A.; Browman, K. E.; Curzon, P.; Hancock, A. A.; Decker, M. W.; Fox, G. B. H3 Receptor Blockade by Thioperamide Enhances Cognition in Rats without Inducing Locomotor Sensitization. *Psychopharmacology*, **2003**, *167*, 363–372.
- (346) Lim, H. D.; Istyastono, E. P.; van de Stolpe, A.; Romeo, G.; Gobbi, S.; Schepers, M.; Lahaye, R.; Menge, W. M. B. P.; Zuiderveld, O. P.; Jongejan, A.; Smits, R. A.; Bakker, R. A.; Haaksma, E. E. J.; Leurs, R.; de Esch, I. J. P. Clobenpropit Analogs as Dual Activity Ligands for the Histamine H3 and H4 Receptors: Synthesis, Pharmacological Evaluation, and Cross-Target QSAR Studies. *Bioorg. Med. Chem.* **2009**, *17* (11), 3987–3994.
- (347) Yokoyama H., Onodera K., Maeyama K., Sakurai E., Clobenpropit (VUF-9153), a New Histamine Receptor Antagonist, Inhibits Electrically Induced Convulsions in Mice. *Eur.J.Pharmacol.* **1994**, *260*, 23–28.
- (348) Femenía, T.; Magara, S.; DuPont, C. M.; Lindskog, M. Hippocampal-Dependent Antidepressant Action of the H3 Receptor Antagonist Clobenpropit in a Rat Model of Depression. *Int. J. Neuropsychopharmacol.* **2015**, *18*

- (9), 1–11.
- (349) Ligneau, X.; Lin, J. S.; Vanni-Mercier, G.; Jouvett, M.; Muir, J. L.; Ganellin, C. R.; Stark, H.; Elz, S.; Schunack, W.; Schwartz, J. C. Neurochemical and Behavioral Effects of Ciproxifan, a Potent Histamine H₃-Receptor Antagonist. *J. Pharmacol. Exp. Ther.* **1998**, *287* (2), 658–666.
- (350) Barbier, A. J.; Berridge, C.; Dugovic, C.; Laposky, A. D.; Wilson, S. J.; Boggs, J.; Aluisio, L.; Lord, B.; Mazur, C.; Pudiak, C. M.; Langlois, X.; Xiao, W.; Apodaca, R.; Carruthers, N. I.; Lovenberg, T. W. Acute Wake-Promoting Actions of JNJ-5207852, a Novel, Diamine-Based H₃ Antagonist. *Br. J. Pharmacol.* **2004**, *143* (5), 649–661.
- (351) Bonaventure, P.; Letavic, M.; Dugovic, C.; Wilson, S.; Aluisio, L.; Pudiak, C.; Lord, B.; Mazur, C.; Kamme, F.; Nishino, S.; Carruthers, N.; Lovenberg, T. Histamine H₃ Receptor Antagonists: From Target Identification to Drug Leads. *Biochem. Pharmacol.* **2007**, *73* (8), 1084–1096.
- (351) Bonaventure, P.; Letavic, M.; Dugovic, C.; Wilson, S.; Aluisio, L.; Pudiak, C.; Lord, B.; Mazur, C.; Kamme, F.; Nishino, S.; Carruthers, N.; Lovenberg, T. Histamine H₃ Receptor Antagonists: From Target Identification to Drug Leads. *Biochem. Pharmacol.* **2007**, *73* (8), 1084–1096.
- (352) Bahi, A.; Sadek, B.; Schwed, S. J.; Walter, M.; Stark, H. Influence of the Novel Histamine H₃ Receptor Antagonist ST1283 on Voluntary Alcohol Consumption and Ethanol-Induced Place Preference in Mice. *Psychopharmacology (Berl)*. **2013**, *228* (1), 85–95.
- (353) Sadek, B.; Saad, A.; Subramanian, D.; Shafiullah, M.; Łazewska, D.; Kieć-Kononowicz, K. Anticonvulsant and Pro-cognitive Properties of the Non-Imidazole Histamine H₃ Receptor Antagonist DL77 in Male Adult Rats. *Neuropharmacology* **2016**, *106*, 46–55.
- (354) Eissa, N.; Khan, N.; Ojha, S. K.; Lazewska, D.; Kieć-Kononowicz, K.; Sadek, B. The Histamine H₃ Receptor Antagonist DL77 Ameliorates MK801-Induced Memory Deficits in Rats. *Front. Neurosci.* **2018**, *12*, 1–11.
- (355) Szczepańska, K.; Karcz, T.; Siwek, A.; Kuder, K. J.; Latacz, G.; Bednarski, M.; Szafarz, M.; Hagenow, S.; Lubelska, A.; Olejarz-Maciej, A.; Sobolewski, M.; Mika, K.; Kotańska, M.; Stark, H.; Kieć-Kononowicz, K. Structural Modifications and in Vitro Pharmacological Evaluation of 4-Pyridyl-Piperazine Derivatives as an Active and Selective Histamine H₃ Receptor Ligands. *Bioorg. Chem.* **2019**, *91*, 103071.
- (356) Szczepańska, K.; Karcz, T.; Kotańska, M.; Siwek, A.; Kuder, K. J.; Latacz, G.; Mogilski, S.; Hagenow, S.; Lubelska, A.; Sobolewski, M.; Stark, H.; Kieć-Kononowicz, K. Optimization and Preclinical Evaluation of Novel Histamine H₃ Receptor Ligands: Acetyl and Propionyl Phenoxyalkyl Piperazine Derivatives. *Bioorg. Med. Chem.* **2018**, *26* (23–24), 6056–6066.
- (357) Medhurst, S. J.; Collins, S. D.; Billinton, A.; Bingham, S.; Dalziel, R. G.; Brass, A.; Roberts, J. C.; Medhurst, A. D.; Chessell, I. P. Novel Histamine H₃ Receptor Antagonists GSK189254 and GSK334429 Are Efficacious in Surgically-Induced and Virally-Induced Rat Models of Neuropathic Pain. **2008**, *138*, 61–69.
- (358) Lamb, Y. N. Pitolisant: A Review in Narcolepsy with or without Cataplexy. *CNS Drugs* **2020**, *34* (2), 207–218.
- (359) Dutilleul, P. C.; Ryvlin, P.; Kahane, P.; Vercueil, L.; Semah, F.; Biraben, A.; Schwartz, J. C.; De Seze, J.; Hirsch, E.; Collongues, N. Exploratory Phase II Trial to Evaluate the Safety and the Antiepileptic Effect of Pitolisant (BF2.649) in Refractory Partial Seizures, given as Adjunctive Treatment during 3 Months. *Clin. Neuropharmacol.* **2016**, *39* (4), 188–193.
- (360) Kotańska, M.; Kuder, K. J.; Szczepańska, K.; Sapa, J.; Kieć-Kononowicz, K. The Histamine H₃ Receptor Inverse Agonist Pitolisant Reduces Body Weight in Obese Mice. *Naunyn. Schmiedeberg's. Arch. Pharmacol.* **2018**, *391* (8), 875–881.
- (361) Sadek, B.; Saad, A.; Sadeq, A.; Jalal, F.; Stark, H. Histamine H₃ Receptor as a Potential Target for Cognitive Symptoms in Neuropsychiatric Diseases. *Behav. Brain Res.* **2016**, *312*, 415–430.
- (362) Ghergan, A.; Coupaye, M.; Leu-Semenescu, S.; Attali, V.; Oppert, J. M.; Arnulf, I.; Poitou, C.; Redolfi, S. Prevalence and Phenotype of Sleep Disorders in 60 Adults with Prader–Willi Syndrome. *Sleep* **2017**, *40* (12), 1–10.
- (363) Overeem, S.; Mignot, E.; GertvanDijk, J.; Lammers, G. J. Narcolepsy: Clinical Features, New Pathophysiologic Insights, and Future Perspectives. *J. Clin. Neurophysiol.* **2001**, *18* (2), 78–105.
- (364) Dauvilliers, Y. Treatment Options for Narcolepsy. *CNS Drugs*, **2016**, *30* (1), 369–379.
- (365) Barateau, L.; Chenini, S.; Evangelista, E.; Jaussent, I.; Lopez, R.; Dauvilliers, Y. Clinical Autonomic Dysfunction in Narcolepsy Type 1. *Sleep* **2019**, *42* (12), 1–9.
- (366) Baumann-Vogel, H.; Schreckenbauer, L.; Valko, P. O.; Werth, E.; Baumann, C. R. Narcolepsy Type 2: A Rare, yet Existing Entity. *J. Sleep Res.* **2020**, 1–4.
- (367) Dauvilliers, Y.; Arnulf, I.; Mignot, E. Seminar Narcolepsy with Cataplexy. *Lancet*, **2007**, *369*, 499–511.
- (368) Lin, J.-S.; Sergeeva, O. A.; Haas, H. L. Histamine H₃ Receptors and Sleep-Wake Regulation Histamine's

- Role in Waking. *J. Pharmacol. Exp. Ther.* **2011**, *336* (1), 17–23.
- (369) Kanbayashi, T.; Kodama, T.; Kondo, H.; Satoh, S.; Inoue, Y.; Chiba, S.; Shimizu, T.; Nishino, S. CSF Histamine Contents in Narcolepsy, Idiopathic Hypersomnia and Obstructive Sleep Apnea Syndrome. *Sleep* **2009**, *32* (2), 181–187.
- (370) Ozen Barut, B.; Tascilar, N.; Varo, A., Sleep Disturbances in Essential Tremor and Parkinson Disease: A Polysomnographic Study. *J. Clin. sleep Med.* **2015**, *11* (6).
- (371) Thannickal, T. C.; Lai, Y. Y.; Siegel, J. M. Hypocretin (Orexin) Cell Loss in Parkinson's Disease. *Brain* **2007**, *130* (6), 1586–1595.
- (372) Breen, D. P.; Vuono, R.; Nawarathna, U.; Fisher, K.; Shneerson, J. M.; Reddy, A. B.; Barker, R. A. Sleep and Circadian Rhythm Regulation in Early Parkinson Disease. *JAMA Neurol.*, **2014**, *71* (5), 589-595.
- (373) Gunn, D. G.; Naismith, S. L.; Lewis, S. J. G. Sleep Disturbances in Parkinson Disease and Their Potential Role in Heterogeneity. *Psychiatry Neurol.* **2010**, *23* (2), 131–137.
- (374) Anighoro, A.; Rastelli, G. Polypharmacology: Challenges and Opportunities in Drug Discovery. *J. Med. Chem* **2014**, *57*, 7874-7887.
- (375) Camacho-arroyo, I.; Gonzalez-covarrubias, V.; Morales-pacheco, M.; Trujillo-bornios, S. I. New Approaches in Oncology for Repositioning Drugs : The Case of PDE5 Inhibitor Sildenafil *Front. Oncol.* **2021**, *11*, 1–13.
- (376) Proschak, E.; Stark, H.; Merk, D. Polypharmacology by Design: A Medicinal Chemist's Perspective on Multitargeting Compounds. *J. Med. Chem.* **2019**, *62* (2), 420–444.
- (377) Morphy, R.; Rankovic, Z. Designed Multiple Ligands. An Emerging Drug Discovery Paradigm. *J. Med. Chem.* **2005**, *48* (21), 6523-6543.
- (378) Treibs, A.; Kreuzer, F. -H. Difluorboryl-Komplexe von Di- Und Tripyrrylmethenen. *Liebigs Ann.* **1968**, *718* (1), 208–223.
- (379) Pedrosaa O., Marques Duarte da Cruz R., de Oliveira Viana J., Olímpio de Mouraa R., Mitsugu I., Barbosa Filhoc J.M., Dinize M.M.F.M, Scottic M.T., Scottic L. and Mendonda F.J.B. Hybrid Compounds as Direct Multitarget Ligands: A Review. *Curr. Top. Med. Chem.*, **2017**, *17*, 1044–1079.
- (380) Ramsay, R. R.; Popovic-Nikolic, M. R.; Nikolic, K.; Uliassi, E.; Bolognesi, M. L. A Perspective on Multi-Target Drug Discovery and Design for Complex Diseases. *Clin. Transl. Med.* **2018**, *7* (1):3.
- (381) Nikolic, K.; Mavridis, L.; Djikic, T.; Vucicevic, J.; Agbaba, D.; Yelekci, K.; Mitchell, J. B. O. Drug Design for CNS Diseases: Polypharmacological Profiling of Compounds Using Cheminformatic, 3D-QSAR and Virtual Screening Methodologies. *Front. Neurosci.* **2016**, *10*.
- (382) Besnard, J., Ruda, G.F., Setola, V., Abecassis K., Rodriguiz, R.M., Huang, X.P., Norval S., Sassano M.F., Shin A.I., Webster, L.A., Simeons, F.R.C., Stojanovski, L., Prat, A., Seidah, N.G., Constam, D.B., Bickerton, G.R., Read, K.D., Wetsel W.C., Gilbert, I.H., Roth, B.L., Hopkins, A.L. Automated Design of Ligands to Polypharmacological Profiles. *Nature* **2012**, *492*, 215-222.
- (383) Bolea I.; Juárez-Jim nez J.; de los Rí C.; Chioua M.; Pouplana P.; Luque F.; Unzeta M.; Marco-Contelles J.; Samadi A. Synthesis, Biological Evaluation, and Molecular Modeling of Donepezil and *N*-[(5-(Benzyloxy)-1-Methyl-1H-Indol-2-yl)Methyl]-*N*- Methylprop-2-yn-1-Amine Hybrids as New Multipotent Cholinesterase/Monoamine Oxidase Inhibitors for the T. *J. Med. Chem.* **2011**, *54* (24),8251-8270.
- (384) Jaiteh, M.; Zeifman, A.; Saarinen, M.; Svenningsson, P.; Bréa, J.; Loza, M. I.; Carlsson, J. Docking Screens for Dual Inhibitors of Disparate Drug Targets for Parkinson's Disease. *J. Med. Chem.* **2018**, *61* (12), 5269–5278.
- (385) Von Coburg, Y.; Kottke, T.; Weizel, L.; Ligneau, X.; Stark, H. Potential Utility of Histamine H3 Receptor Antagonist Pharmacophore in Antipsychotics. *Bioorg. Med. Chem. Lett.* **2009**, *19* (2), 538–542.
- (386) Männel, B.; Jaiteh, M.; Zeifman, A.; Randakova, A.; Möller, D.; Hübner, H.; Gmeiner, P.; Carlsson, J. Structure-Guided Screening for Functionally Selective D2 Dopamine Receptor Ligands from a Virtual Chemical Library. *ACS Chem. Biol.* **2017**, *12* (10), 2652–2661.
- (387) Koch, P.; Brunschweiler, A.; Namasivayam, V.; Ullrich, S. Probing Substituents in the 1- and Annelated Water-Soluble Xanthine Derivatives as Multi-Target Drugs With Potent Adenosine Receptor Antagonistic Activity. *Front.Chem.*, **2018**, *6*, 1–28.
- (388) Cao, X.; Zhang, Y.; Chen, Y.; Qiu, Y.; Yu, M.; Xu, X.; Liu, X.; Liu, B. F.; Zhang, L.; Zhang, G. Synthesis and Biological Evaluation of Fused Tricyclic Heterocycle Piperazine (Piperidine) Derivatives As Potential Multireceptor Atypical Antipsychotics. *J. Med. Chem.* **2018**, *61* (22), 10017–10039.
- (389) Boeckler, F.; Lanig, H.; Gmeiner, P. Modeling the Similarity and Divergence of Dopamine D2-like Receptors and Identification of Validated Ligand-Receptor Complexes. *J. Med. Chem.* **2005**, *48* (3), 694–709.
- (390) Garcia-Ladona, F. J.; Cox, B. F. BP 897, a Selective Dopamine D3 Receptor Ligand with Therapeutic Potential for the Treatment of Cocaine-Addiction. *CNS Drug Rev.* **2003**, *9* (2), 141–158.

- (391) Chu, W.; Tu, Z.; McElveen, E.; Xu, J.; Taylor, M.; Luedtke, R. R.; MacH, R. H. Synthesis and in Vitro Binding of N-Phenyl Piperazine Analogs as Potential Dopamine D3 Receptor Ligands. *Bioorg. Med. Chem.* **2005**, *13* (1), 77–87.
- (392) Banala A. K.; Levy B. A.; Khatr, S. S.; Furman C. A.; Roof R. A.; Mishra Y.; Gri S. A.; Sibley D. R.; Luedtke R. R.; Newman A. H.. *J. Med. Chem* **2011**, *54*, 3581–3594.
- (393) Feng, Z.; Hou, T.; Li, Y. Selectivity and Activation of Dopamine D3R from Molecular Dynamics. *J. Mol. Model.* **2012**, *18* (12), 5051–5063.
- (394) Lane, J. R.; Chubukov, P.; Liu, W.; Canals, M.; Cherezov, V.; Abagyan, R.; Stevens, R. C.; Katritch, V. Structure-Based Ligand Discovery Targeting Orthosteric and Allosteric Pockets of Dopamine Receptors. *Mol. Pharmacol.* **2013**, *84* (6), 794–807.
- (395) Newman, A. H.; Beuming, T.; Banala, A. K.; Donthamsetti, P.; Pongetti, K.; Labounty, A.; Levy, B.; Cao, J.; Michino, M.; Luedtke, R. R.; Javitch, J. A.; Shi, L. Molecular Determinants of Selectivity and Efficacy at the Dopamine D3 Receptor. *J. Med. Chem.* **2012**, *55* (15), 6689–6699.
- (396) Vida, N.; Vaclavik, J.; Beier, P. Synthesis and Reactivity of Aliphatic Sulfur Pentafluorides from Substituted (Pentafluorosulfanyl)Benzenes. *Beilstein J. Org. Chem.* **2016**, *12*, 110–116.
- (397) Das, P.; Tokunaga, E.; Shibata, N. Recent Advancements in the Synthesis of Pentafluorosulfanyl (SF₅-) Containing Heteroaromatic Compounds. *Tetrahedron Lett.* **2017**, *58* (52), 4803–4815.
- (398) Sowaileh, M. F.; Hazlitt, R. A.; Colby, D. A. Application of the Pentafluorosulfanyl Group as a Bioisosteric Replacement. *ChemMedChem* **2017**, *12* (18), 1481–1490.
- (399) Hose, A.; Tareque, R.K., Mortensen, M., Legay, R., Coles, S.J., Tizzard, G.J., Greenland B.W., Smart, T.V., Bagley M.C., Spencer, J. Synthesis and biological evaluation of benzodiazepines containing a pentafluorosulfanyl group *Tetrahedron* **2021**, *85*, 135907.0.
- (400) Elek, M.; Djokovic, N.; Frank, A.; Oljacic, S.; Zivkovic, A.; Nikolic, K.; Stark, H. Synthesis , in Silico , and in Vitro Studies of Novel Dopamine D2 and D3 Receptor Ligands. *Arch. Pharm.*, **2021**, *354* (6), 2000486.
- (401) Finkelstein, H. Darstellung Organischer Jodide Aus Den Entsprechenden Bromiden Und Chloriden. *Mitteilung nus dem Chemischen Institut der Universitrat Straßburg* **1910**.
- (402) Gabriel S.Über eine Darstellungsweise primärer Amine aus den entsprechenden Halogenverbindungen. *Aus den I Berliner Universitäts-Laboratorium*, **1887**.
- (403) Gibson, M. S.; Bradshaw, R. W. The Gabriel Synthesis of Primary Amines. *Angew. Chemie Int. Ed. English* **1968**, *7* (12), 919–930.
- (404) Khan, M. N. Kinetic Evidence for the Occurrence of a Stepwise Mechanism in Hydrazinolysis of Phthalimide. *J. Org. Chem.* **1995**, *7*, 1129–1134.
- (405) Dominguez, X. A.; Lopez, I. C.; Franco, R. Notes: Simple Preparation of a Very Active Raney Nickel Catalyst. *J. Org. Chem.* **1961**, *26* (5), 1625.
- (406) Montalbetti, C. A. G. N.; Falque, V. Amide Bond Formation and Peptide Coupling. *Tetrahedron* **2005**, *61* (46), 10827–10852.
- (407) Valeur, E.; Bradley, M. Amide Bond Formation: Beyond the Myth of Coupling Reagents. *Chem. Soc. Rev.* **2009**, *38* (2), 606–631.
- (408) Sahlholm, K.; Agren, R.; Zeberg, H.; Stepniewski, T. M. I.; Benjamin Free, R.; Reilly, S. W.; Luedtke, R. R.; Arhem, P.; Ciruela, F.; Sibley, D. R.; Mach, R. H.; Selent, J.; Nilsson, J. Ligand with Two Modes of Interaction with the Dopamine D2 Receptor-an Induced-Fit Mechanism of Insurmountable Antagonism. *ACS Chem. Neurosci.* **2020**, *11* (19), 3130–3143.
- (409) Jacobson, K. A. New Paradigms in GPCR Drug Delivery. *Biochem Pharmacol.* **2015**, *98* (4), 541–555.
- (410) Lane, J. R.; Sexton, P. M.; Christopoulos, A. Bridging the Gap: Bitopic Ligands of G-Protein-Coupled Receptors. *Trends Pharmacol. Sci.* **2013**, *34* (1), 59–66.
- (411) Hubble, J. P. Pre-Clinical Studies of Pramipexole: Clinical Relevance. *Eur. J. Neurol.* **2000**, *7*, 15–20.
- (412) Yang, P.; Perlmutter, J. S.; Benzinger, T. L. S.; Morris, J. C.; Xu, J. Dopamine D3 Receptor: A Neglected Participant in Parkinson Disease Pathogenesis and Treatment? *Ageing Res. Rev.* **2020**, *57*, 100994.
- (413) Constantinescu, R. Update on the Use of Pramipexole in the Treatment of Parkinson's Disease. *Neuropsychiatr. Dis. Treat.* **2008**, *4* (2), 337–352.
- (414) Laboratories Limited, M. L. Improved Process for the Preparation of (S)-2-Amino-4,5,6,7-Tetrahydro- 6-(Propylamino)Benzothiazole and Its Pharmaceutically Acceptable Salts WO 2011/021214 A2. **2011**.
- (415) Bramley, Dupplin, Goberdhan, M. The Hantzsch Thiazole Synthesis under Acidic Conditions: Change of Regioselectivity. *J. Chem. Soc.* **1987**, *6*, 639-643.
- (416) Egan R, Tadanier J, Garmaise, D. G. A. Intermediates in The Hantzsch Thiazole Synthesis. *J. Org. Chem.* **1968**, *731* (6), 2511–2513.

- (417) Ghosh, T.; Si, A.; Kumar Misra, A. Facile Transformation of Nitriles into Thioamides: Application to C-Glycosyl Nitrile Derivatives. *ChemistrySelect* **2017**, *2* (4), 1366–1369.
- (418) Liboska, R.; Zyka, D.; Bobek, M. Synthesis of Primary Thioamides from Nitriles and Hydrogen Sulfide Catalyzed by Anion-Exchange Resin. *Synthesis (Stuttg)*. **2002**, *12*, 1649–1651.
- (419) Curphey, T. J. Thionation of Esters and Lactones with the Reagent Combination of Phosphorus Pentasulfide and Hexamethyldisiloxane. *Tetrahedron Lett.* **2002**, *43* (3), 371–373.
- (420) Gauthier, J. Y.; Lebel, H. A Remarkably Simple Conversion of Nitriles to Thioamides. *Phosphorus. Sulfur. Silicon Relat. Elem.* **1994**, *95* (1–4), 325–326.
- (421) Varma, R. S.; Kumar, D. Microwave-Accelerated Solvent-Free Synthesis of Thioketones, Thiolactones, Thioamides, Thionoesters, and Thioflavonoids. *Org. Lett.* **1999**, *1* (5), 697–700.
- (422) Imanishi, N.; Iwaoka, K.; Koshio, H.; Nagashima, S. Y.; Kazuta, K. I.; Ohta, M.; Sakamoto, S.; Ito, H.; Akuzawa, S.; Kiso, T.; Tsukamoto, S. I.; Mase, T. New Thiazole Derivatives as Potent and Selective 5-Hydroxytryptamine 3 (5-HT₃) Receptor Agonists for the Treatment of Constipation. *Bioorg. Med. Chem.* **2003**, *11* (7), 1493–1502.
- (423) Kaboudin, B.; Yarahmadi, V.; Kato, J. Y.; Yokomatsu, T. A Simple and Novel Method for the Direct Conversion of Carboxylic Acids into Thioamides. *RSC Adv.* **2013**, *3* (18), 6435–6441.
- (424) Bachman Stephan, Flohr Alexander, Groebke K; Koerner M.; Kuhn B.; Peters J.U.; Rudolph M. (2012) PDE 10 Modulators WO 2013/034506 A1.
- (425) Yadav, A. K.; Srivastava, V. P.; Yadav, L. D. S. O,O-Diethyl Dithiophosphoric Acid Mediated Direct Synthesis of Thioamides from Aldehydes and Ketones. *Tetrahedron Lett.* **2012**, *53* (52), 7113–7116.
- (426) Wuts, P. G. M. *Green's Protective Groups in Organic*, 9, 5th Ed. Wiley **1999**.
- (427) Sultane, P. R.; Mete, T. B.; Bhat, R. G. Chemoselective N-Deacetylation under Mild Conditions. *Org. Biomol. Chem.* **2014**, *12* (2), 261–264.
- (428) Shimizu, Y.; Morimoto, H.; Zhang, M.; Ohshima, T. Microwave-Assisted Deacylation of Unactivated Amides Using Ammonium-Salt-Accelerated Transamidation. *Angew. Chemie - Int. Ed.* **2012**, *51* (34), 8564–8567.
- (429) Hoyos, L. J.; Primet, M.; Pralialud, H. Sulfur Poisoning and Regeneration of Palladium-Based Catalysts. *J. Chem. Soc. Faraday Trans.* **1992**, *88* (1), 113–119.
- (430) Abdel-Magid, A. F.; Carson, K. G.; Harris, B. D.; Maryanoff, C. A.; Shah, R. D. Reductive Amination of Aldehydes and Ketones with Sodium Triacetoxyborohydride. Studies on Direct and Indirect Reductive Amination Procedures. *J. Org. Chem.* **1996**, *61* (11), 3849–3862.
- (431) Mirza-Aghayan, M.; Tavana, M. M.; Rahimifard, M.; Boukherroub, R. Palladium on Activated Carbon Catalyzed Reductive Amination of Aldehydes and Ketones by Triethylsilane. *Appl. Organomet. Chem.* **2014**, *28* (2), 113–115.
- (432) Sanders, M. L.; Donkor, I. O. A Novel Series of Urea-Based Peptidomimetic Calpain Inhibitors. *Bioorg. Med. Chem. Lett.* **2006**, *16* (7), 1965–1968.
- (433) Shokrolahi, A.; Zali, A.; Keshavarz, M. H. Reductive Amination of Aldehydes and Ketones by NaBH₄ Using Carbon-Based Solid Acid (CBSA) as Catalyst. *Green Chem. Lett. Rev.* **2011**, *4* (3), 195–203.
- (434) Stark H.; Leppanen M.; Saur O.; Kottke T.; Michael P. (2009) Tetrahydrobenzothiazole Derivatives with Dopamine Receptor Activity WO2009/056805.
- (435) Addison CCJ.; Lewis, J.; The chemistry of the nitrosyl group (NO) *Q. Rev. Chem. Soc.* **1955**, *9*, 115–149.
- (436) Misra, R. N.; Xiao, H. Y.; Williams, D. K.; Kim, K. S.; Lu, S.; Keller, K. A.; Mulheron, J. G.; Batorsky, R.; Tokarski, J. S.; Sack, J. S.; Kimball, S. D.; Lee, F. Y.; Webster, K. R. Synthesis and Biological Activity of N-Aryl-2-Aminothiazoles: Potent Pan Inhibitors of Cyclin-Dependent Kinases. *Bioorg. Med. Chem. Lett.* **2004**, *14* (11), 2973–2977.
- (437) Hao M.; Gray N. S.; Zhang T.; Kwiatkowski. N. P. (2016) Inhibitors of cyclic dependent kinases, WO2017044858A3.
- (438) Kozikowski, A. P.; Tuckmantel, W.; Thunb, L. Synthesis of the Thiazolone Analogue of the Acetylcholinesterase. *Helvetica* **1994**, *77* (5), 1256–1266.6.
- (439) Doyle, M. P.; Dellaria, J. F.; Siegfried, B.; Bishop, S. W. Reductive Deamination of Arylamines by Alkyl Nitrites in N,N-Dimethylformamide. A Direct Conversion of Arylamines to Aromatic Hydrocarbons. *J. Org. Chem.* **1977**, *42* (22), 3494–3498.
- (440) Ek, F.; Axelsson, O.; Wistrand, L. G.; Frejd, T. Aromatic Allylation via Diazotization: Metal-Free C-C Bond Formation. *J. Org. Chem.* **2002**, *67* (18), 6376–6381.
- (441) Perosa, A.; Tundo, P.; Zinovyev, S. Mild Catalytic Multiphase Hydrogenolysis of Benzyl Ethers. *Green Chem.* **2002**, *4* (5), 492–494.
- (442) Weinreb, S. M.; Epling, G. A.; Comi, R.; Reitano, M. Efficacious Cleavage of the Benzyl Ether Protecting

- Group by Electrochemical Oxidation. *J. Org. Chem.* **1975**, *40* (9), 1356–1358.
- (443) Ikeuchi, K.; Murasawa, K.; Ohara, K.; Yamada, H. P-Methylbenzyl Group: Oxidative Removal and Orthogonal Alcohol Deprotection. *Org. Lett.* **2019**, *21* (17), 6638–6642.
- (444) Glaus, F.; Dedić, D.; Tare, P.; Nagaraja, V.; Rodrigues, L.; Aínsa, J. A.; Kunze, J.; Schneider, G.; Hartkoorn, R. C.; Cole, S. T.; Altmann, K. H. Total Synthesis of Ripostatin B and Structure-Activity Relationship Studies on Ripostatin Analogs. *J. Org. Chem.* **2018**, *83* (13), 7150–7172.
- (445) Horita, K.; Yoshioka, T.; Tanaka, T.; Oikawa, Y.; Yonemitsu, O. On the Selectivity of Deprotection of Benzyl, Mpm (4-Methoxybenzyl) and Dmpm (3,4-Dimethoxybenzyl) Protecting Groups for Hydroxy Functions. *Tetrahedron* **1986**, *42* (11), 3021–3028.
- (446) Tucker, J. W.; Narayanam, J. M. R.; Shah, P. S.; Stephenson, C. R. J. Oxidative Photoredox Catalysis: Mild and Selective Deprotection of PMB Ethers Mediated by Visible Light. *Chem. Commun.* **2011**, *47* (17), 5040–5042.
- (447) Cavedon, C.; Sletten, E. T.; Madani, A.; Niemeyer, O.; Seeberger, P. H.; Pieber, B. Visible-Light-Mediated Oxidative Debzilylation Enables the Use of Benzyl Ethers as Temporary Protecting Groups. *Org. Lett.* **2021**, 514–518.
- (448) Muzzi, M.; Gerace, E.; Buonvicino, D.; Coppi, E.; Resta, F.; Formentini, L.; Zecchi, R.; Tigli, L.; Guasti, D.; Ferri, M.; Camaioni, E.; Masi, A.; Pellegrini-Giampietro, D. E.; Mannaioni, G.; Bani, D.; Pugliese, A. M.; Chiarugi, A. Dextramipexole Improves Bioenergetics and Outcome in Experimental Stroke. *Br. J. Pharmacol.* **2018**, *175* (2), 272–283.
- (449) Gleich, G. J. Dextramipexole: A New Antieosinophil Drug? *Blood* **2018**, *132* (5), 461–462.
- (450) Cudkowicz, M.; Bozik, M. E.; Ingersoll, E. W.; Miller, R.; Mitsumoto, H.; Shefner, J.; Moore, D. H.; Schoenfeld, D.; Mather, J. L.; Archibald, D.; Sullivan, M.; Amburgey, C.; Moritz, J.; Gribkoff, V. K. The Effects of Dextramipexole (KNS-760704) in Individuals with Amyotrophic Lateral Sclerosis. *Nat. Med.* **2011**, *17* (12), 1652–1656.
- (451) Patschinski, P.; Zhang, C.; Zipse, H. The Lewis Base-Catalyzed Silylation of Alcohols—a Mechanistic Analysis. *J. Org. Chem.* **2014**, *79* (17), 8348–8357.
- (452) Enders, D.; Nguyen, D. Synthesis of Enantioenriched Substituted Tetrahydrofurans and Tetrahydropyrans via Iron-Mediated Chirality Transfer and Ring Closure. *Synthesis (Stuttg.)* **2000**, *14*, 2092–2098.
- (453) Hüls, A.; Purand, K.; Stark, H.; Reidemeister, S.; Ligneau, X.; Arrang, J. M.; Schwartz, J. C.; Schunack, W. Novel Histamine H₃-Receptor Antagonists with Benzyl Ether Structure or Related Moieties: Synthesis and Structure-Activity Relationships. *Arch. Pharm. (Weinheim)* **1996**, *329* (8–9), 379–385.
- (454) Graßmann, S.; Apelt, J.; Ligneau, X.; Pertz, H. H.; Arrang, J. M.; Ganellin, C. R.; Schwartz, J. C.; Schunack, W.; Stark, H. Search for Histamine H₃ Receptor Ligands with Combined Inhibitory Potency at Histamine N-Methyltransferase: ω- Piperidinoalkamine Derivatives. *Arch. Pharm. (Weinheim)* **2004**, *337* (10), 533–545.
- (455) Toullec, J., El-Alaoui M., Kinetics and Mechanism of the Acid-Catalyzed Bromination of Ring-Substituted Acetophenones in Methanol. Thermodynamics of the Ketone-Acetal-Enol Ether System in Methanol and Water. *J. Org. Chem.* **1986**, *51* (21), 4054–4061.
- (456) Sato, M.; Nagano, S.; Seki, T. A Photoresponsive Liquid Crystal Based on (1-Cyclohexenyl)Phenyldiazene as a Close Analogue of Azobenzene. *Chem. Commun.* **2009**, *25*, 3792–3794.
- (457) Denonne F.; Sylvain C.; Laurent P.; Defays S. (2007) Fused oxazoles and thiazoles as histamine H₃ receptor ligands W2008/012010.
- (458) Gilpin, R. K.; Zhou, W. Studies of the Thermal Degradation of Acetaminophen Using a Conventional HPLC Approach and Electrospray Ionization-Mass Spectrometry. *J. Chromatogr. Sci.* **2004**, *42* (1), 15–20.
- (459) Chen, X.; Ni, F.; Liu, Y.; Fu, L.; Li, J. A New and Practical Synthesis of Cariprazine through the Facile Construction of 2-[Trans -4-(3,3-Dimethylureido)Cyclohexyl]Acetic Acid. *Synth.* **2016**, *48* (18), 3120–3126.
- (460) Eissa, N.; Venkatachalam, K.; Jayaprakash, P.; Falkenstein, M.; Dubiel, M.; Frank, A.; Reiner-link, D.; Stark, H.; Sadek, B. The Multi-Targeting Ligand ST-2223 with Histamine H₃ Receptor and Dopamine D₂ / D₃ Receptor Antagonist Properties Mitigates Autism-Like Repetitive Behaviors and Brain Oxidative Stress in Mice. *Int.J.Mol.Sci.* **2021**, *22*, 1947.
- (461) Szczepanska, K.; Kuder, K.; Kiec-Kononowicz, K. Histamine H₃ Receptor Ligands in the Group of (Homo)Piperazine Derivatives. *Curr. Med. Chem.* **2017**, *25* (14), 1609–1626.
- (462) Meier, G.; Apelt, J.; Reichert, U.; Graßmann, S.; Ligneau, X.; Elz, S.; Leurquin, F.; Ganellin, C. R.; Schwartz, J. C.; Schunack, W.; Stark, H. Influence of Imidazole Replacement in Different Structural Classes of Histamine H₃-Receptor Antagonists. *Eur. J. Pharm. Sci.* **2001**, *13* (3), 249–259.
- (463) Sadek, B.; Saad, A.; Latacz, G.; Kuder, K.; Olejarz, A.; Karcz, T.; Stark, H.; Kiec-Kononowicz, K. Non-Imidazole-Based Histamine H₃ Receptor Antagonists with Anticonvulsant Activity in Different Seizure

- Models in Male Adult Rats. *Drug Des. Devel. Ther.* **2016**, *10*, 3879–3898.
- (464) Isensee, K.; Amon, M.; Galaparti, A.; Ligneau, X.; Camelin, J. C.; Capet, M.; Schwartz, J. C.; Stark, H. Fluorinated Non-Imidazole Histamine H3 Receptor Antagonists. *Bioorg Med. Chem. Lett.* **2009**, *19* (8), 2172–2175.
- (465) Thomasch, M.; Stephan Schwed, J.; Weizel, L.; Stark, H. Novel Chalcone-Based Fluorescent Human Histamine H3 Receptor Ligands as Pharmacological Tools. *Front. Syst. Neurosci.* **2012**, *6*, 1–16.
- (466) Fuhrmann, E.; Talbiersky, J. Synthesis of Alkyl Aryl Ethers by Catalytic Williamson Ether Synthesis with Weak Alkylation Agents. *Org. Process Res. Dev.* **2005**, *9* (2), 206–211.
- (467) Mandal, S.; Mandal, S.; Ghosh, S. K.; Sar, P.; Ghosh, A.; Saha, R.; Saha, B. A Review on the Advancement of Ether Synthesis from Organic Solvent to Water. *RSC Adv.* **2016**, *6* (73), 69605–69614.
- (468) Dueno, E. E.; Chu, F.; Kim, S. I.; Kyung Woon Jung. Cesium Promoted O-Alkylation of Alcohols for the Efficient Ether Synthesis. *Tetrahedron Lett.* **1999**, *40* (10), 1843–1846.
- (469) Diamanti, A.; Ganase, Z.; Grant, E.; Armstrong, A.; Piccione, P. M.; Rea, A. M.; Richardson, J.; Galindo, A.; Adjiman, C. S. Mechanism, Kinetics and Selectivity of a Williamson Ether Synthesis: Elucidation under Different Reaction Conditions. *React. Chem. Eng.* **2021**, *6*, 1195–1211.
- (470) Weissberg, A.; Dahan, A.; Portnoy, M. Williamson Ether Synthesis on Solid Support: Substitution versus Elimination. *J. Comb. Chem.* **2001**, *3* (2), 154–156.
- (471) Mancuso, A. J.; Huang, S. L.; Swern, D. Oxidation of Long-Chain and Related Alcohols to Carbonyls by Dimethyl Sulfoxide “Activated” by Oxalyl Chloride. *J. Org. Chem.* **1978**, *43* (12), 2480–2482.
- (472) Zi-Tao Zhua, Adam C. Munhalla, and Steven W. Johnson. a, b. Tyramine Excites Rat Subthalamic Neurons in Vitro by a Dopamindependent Mechanism. *Neurpharmacology* **2007**, *52* (4), 1169–1178.
- (473) Angelina, E.; Andujar, S.; Moreno, L.; Garibotto, F.; Párraga, J.; Peruchena, N.; Cabedo, N.; Villecco, M.; Cortes, D.; Enriz, R. D. 3-Chlorotyramine Acting as Ligand of the D2 Dopamine Receptor. Molecular Modeling, Synthesis and D2 Receptor Affinity. *Mol. Inform.* **2015**, *34* (1), 28–43.
- (474) Neelarapu, Raghupathi, P. A. P. A One-Pot Selective Synthesis of N-Boc Protected Secondary Amines: Tandem Direct Reductive Amination/N-Boc Protection. *Tetrahedron* **2012**, *68* (35), 7056–7062.
- (475) George, N.; Ofori, S.; Parkin, S.; Awuah, S. G. Mild Deprotection of the: N-Tert -Butyloxycarbonyl (N -Boc) Group Using Oxalyl Chloride. *RSC Adv.* **2020**, *10* (40), 24017–24026.
- (476) Marcantoni, E.; Massaccesi, M.; Bartoli, G.; Bosco, M.; Sambri, L. Selective Deprotection of N-Boc-Protected Tert -Butyl Ester Amino Acids by the CeCl₃ · 7H₂O - NaI System in Acetonitrile NaI System Promotes the Carbon - Carbon Bond Formation between R -Halogeno Ketones and Carbonyl Compounds under Anhydrous Condition. *Annu. Rep. Prog. Chem. Soc* **2002**, *98*, 41–60
- (477) Han G.; Tamaki, M.; Hrubby, V. J. Fast , Efficient and Selective Deprotection of the Group Using HCl / Dioxane. *J. Pept. Res.* **2001**, *58*, 338–341.
- (478) Zheng, Y.; Tice, C. M.; Singh, S. B. The Use of Spirocyclic Scaffolds in Drug Discovery. *Bioorg. Med. Chem. Lett.* **2014**, *24* (16), 3673–3682.
- (479) Sean W. Reillya, Suzy Griffinc, Michelle Taylorc, Kristoffer Sahlholma, Chi-Chang Wenga, Kuiying Xua, Daniel A. Jacomeb, Robert R. Luedtkec, and R. H. M. Highly Selective Dopamine D3 Receptor Antagonists with Arylated Diazaspiro Alkane Cores. *J. Med. Chem.* **2017**, *60* (23), 9905–9910.
- (480) Genin, M. J.; Mishra, R. K.; Johnson, R. L. Dopamine Receptor Modulation by a Highly Rigid Spiro Bicyclic Peptidomimetic of Pro-Leu-Gly-NH₂. *J. Med. Chem.* **1993**, *36* (22), 3481–3483.
- (481) Klinkenberg, J. L.; Hartwig, J. F. Catalytic Organometallic Reactions of Ammonia. *Angew. Chemie - Int. Ed.* **2011**, *50* (1), 86–95.
- (482) Berdini, V.; Cesta, M. C.; Curti, R.; Anniballe, G. D.; Bello, D.; Nano, G.; Nicolini, L.; Allegretti, M. A Modified Palladium Catalysed Reductive Amination Procedure Valerio. *Tetrahedron* **2002**, *58*, 5669–5674.
- (483) Crossland, R. K.; Servis, K. L. A Facile Synthesis of Methanesulfonate Esters. *J. Org. Chem.* **1970**, *35* (9), 3195–3196.
- (484) Löber, S.; Aboul-Fadl, T.; Hübner, H.; Gmeiner, P. Di- and Trisubstituted Pyrazolo[1,5-a]Pyridine Derivatives: Synthesis, Dopamine Receptor Binding and Ligand Efficacy. *Bioorg. Med. Chem. Lett.* **2002**, *12* (4), 633–636.
- (485) Boens, N.; Leen, V.; Dehaen, W. Fluorescent Indicators Based on BODIPY. *Chem. Soc. Rev.* **2012**, *41* (3), 1130–1172.
- (486) Loudet, A.; Burgess, K. BODIPY Dyes and Their Derivatives: Syntheses and Spectroscopic Properties. *Chem. Rev.* **2007**, *107* (11), 4891–4932.
- (487) Tamgho, I. S.; Hasheminasab, A.; Engle, J. T.; Nemykin, V. N.; Ziegler, C. J. A New Highly Fluorescent and Symmetric Pyrrole-BF₂ Chromophore: BOPHY. *J. Am. Chem. Soc.* **2014**, *136* (15), 5623–5626.

- (488) Yu, C.; Huang, Z.; Wang, X.; Miao, W.; Wu, Q.; Wong, W. Y.; Hao, E.; Xiao, Y.; Jiao, L. A Family of Highly Fluorescent and Unsymmetric Bis(BF₂) Chromophore Containing Both Pyrrole and N-Heteroarene Derivatives: BOPPY. *Org. Lett.* **2018**, *20* (15), 4462–4466.
- (489) Geier, G. R.; Lindsey, J. S. Investigation of Porphyrin-Forming Reactions. Part 1. Pyrrole + Aldehyde Oligomerization in Two-Step, One-Flask Syntheses of Meso-Substituted Porphyrins. *J. Chem. Soc.* **2001**, *5*, 677–686.
- (490) Murray, A. M.; Ryoo, H. L.; Gurevich, E.; Joyce, J. N. Localization of Dopamine D3 Receptors to Mesolimbic and D2 Receptors to Mesostriatal Regions of Human Forebrain. *Proc. Natl. Acad. Sci. U. S. A.* **1994**, *91* (23), 11271–11275.
- (491) Gurevich, E. V.; Joyce, J. N. Distribution of Dopamine D3 Receptor Expressing Neurons in the Human Forebrain Comparison with D2 Receptor Expressing Neurons. *Neuropsychopharmacology* **1999**, *20* (1), 60–80.
- (492) Barton, A. C.; Kang, H. C.; Rinaudo, M. S.; Monsma, F. J.; Stewart-Fram, R. M.; Macinko, J. A.; Haugland, R. P.; Ariano, M. A.; Sibley, D. R. Multiple Fluorescent Ligands for Dopamine Receptors. I. Pharmacological Characterization and Receptor Selectivity. *Brain Res.* **1991**, *547* (2), 199–207.
- (493) Madras, B. K.; Canfield, D. R.; Pfaelzer, C.; Vittimberga, F. J.; Difiglia, M.; Aronin, N.; Bakthavachalam, V.; Baindur, N.; Neumeier, J. L. Fluorescent and Biotin Probes for Dopamine Receptors: D1 and D2 Receptor Affinity and Selectivity. *Mol. Pharmacol.* **1990**, *37* (6), 833–839.
- (494) Allikalt, A.; Purkayastha, N.; Flad, K.; Schmidt, M. F.; Tabor, A.; Gmeiner, P.; Hübner, H.; Weikert, D. Fluorescent Ligands for Dopamine D2/D3 Receptors. *Sci. Rep.* **2020**, *10* (1), 21842.
- (495) Hayashi, Y.; Obata, N.; Tamaru, M.; Yamaguchi, S.; Matsuo, Y.; Saeki, A.; Seki, S.; Kureishi, Y.; Saito, S.; Yamaguchi, S.; Shinokubo, H. Facile Synthesis of Biphenyl-Fused BODIPY and Its Property. *Org. Lett.* **2012**, *14* (3), 866–869.
- (496) Tomasch, M.; Schwed, J. S.; Paulke, A.; Stark, H. Bodilisant, A Novel Fluorescent, Highly Affine Histamine H₃ Receptor Ligand. *Med. Chem. Lett.* **2013**, (4) 269–273.
- (497) Sun, X. Y.; Liu, T.; Sun, J.; Wang, X. J. Synthesis and Application of Coumarin Fluorescence Probes. *RSC Adv.* **2020**, *10* (18), 10826–10847.
- (498) Toseland, C. P. Fluorescent Labeling and Modification of Proteins. *J. Chem. Biol.* **2013**, *6* (3), 85–95.
- (499) Dean, K. M.; Palmer, A. E. Advances in Fluorescence Labeling Strategies for Dynamic Cellular Imaging. *Nat. Chem. Biol.* **2014**, *10* (7), 512–523.
- (500) Wolfbeis, O. S. An Overview of Nanoparticles Commonly Used in Fluorescent Bioimaging. *Chem. Soc. Rev.* **2015**, *44* (14), 4743–4768.
- (501) Berney, C.; Danuser, G. FRET or No FRET: A Quantitative Comparison. *Biophys. J.* **2003**, *84* (6), 3992–4010.
- (502) Piston, D. W.; Kremers, G. J. Fluorescent Protein FRET: The Good, the Bad and the Ugly. *Trends Biochem. Sci.* **2007**, *32* (9), 407–414.
- (503) Zhou, Z.; Li, N.; Tong, A. A New Coumarin-Based Fluorescence Turn-on Chemodosimeter for Cu²⁺ in Water. *Anal. Chim. Acta* **2011**, *702* (1), 81–86.
- (504) Wallace, M. B.; Meining, A.; Canto, M. I.; Fockens, P.; Miehle, S.; Roesch, T.; Lightdale, C. J.; Pohl, H.; Carr-Locke, D.; Löhr, M.; Coron, E.; Filoche, B.; Giovannini, M.; Moreau, J.; Schmidt, C.; Kiesslich, R. The Safety of Intravenous Fluorescein for Confocal Laser Endomicroscopy in the Gastrointestinal Tract. *Aliment. Pharmacol. Ther.* **2010**, *31* (5), 548–552.
- (505) Ulrich, G.; Ziessel, R.; Harriman, A. The Chemistry of Fluorescent Bodipy Dyes: Versatility Unsurpassed. *Angew. Chemie - Int. Ed.* **2008**, *47* (7), 1184–1201.
- (506) Boyer, J. H.; Haag, A. M.; Sathyamoorthi, G.; Pavlopoulos, T. G. Pyrromethene-BF₂ Complexes *Heteroat. Chem.* **1993**, *4* (1), 39–49.
- (507) Wu, L.; Burgess, K. A New Synthesis of Symmetric Boraindacene (BODIPY) Dyes. *Chem. Commun.* **2008**, *40*, 4933–4935.
- (508) McCusker, C.; Carroll, J. B.; Rotelo, V. M. Cationic Polyhedral Oligomeric Silsesquioxane (POSS) Units as Carriers for Drug Delivery Processes. *Chem. Commun.* **2005**, *1* (8), 996–998.
- (509) Ray, C.; Schad, C.; Moreno, F.; Maroto, B. L.; Bañuelos, J.; Arbeloa, T.; García-Moreno, I.; Villafuerte, C.; Muller, G.; De La Moya, S. BCl₃-Activated Synthesis of COO-BODIPY Laser Dyes: General Scope and High Yields under Mild Conditions. *J. Org. Chem.* **2020**, *85* (7), 4594–4601.
- (510) Kaur, P.; Singh, K. Recent Advances in the Application of BODIPY in Bioimaging and Chemosensing. *J. Mater. Chem. C*, **2019**, *7* (37), 11361–11405.
- (511) Spangenburg, E. E.; Pratt, S. J. P.; Wohlers, L. M.; Lovering, R. M. Use of BODIPY (493/503) to Visualize

- Intramuscular Lipid Droplets in Skeletal Muscle. *Biomed.Res.Int.* **2011**, 598358.
- (512) Rudin, M.; Weissleder, R. Molecular Imaging in Drug Discovery and Development. *Nat. Rev. Drug Discov.* **2003**, 2 (2), 123–131.
- (513) Ortiz, M. J.; Garcia-Moreno, I.; Agarrabeitia, A. R.; Duran-Sampedro, G.; Costela, A.; Sastre, R.; López Arbeloa, F.; Bañuelos Prieto, J.; López Arbeloa, I. Red-Edge-Wavelength Finely-Tunable Laser Action from New BODIPY Dyes. *Phys. Chem. Chem. Phys.* **2010**, 12 (28), 7804–7811.
- (514) Chen, J.; Burghart, A.; Derecskei-Kovacs, A.; Burgess, K. 4,4-Difluoro-4-Bora-3a,4a-Diaza-s-Indacene (BODIPY) Dyes Modified for Extended Conjugation and Restricted Bond Rotations. *J. Org. Chem.* **2000**, 65 (10), 2900–2906.
- (515) Kim, H.; Burghart, A.; Welch, M. B.; Reibenspies, J.; Burgess, K. Synthesis and Spectroscopic Properties of a New 4-Bora-3a, 4a-Diaza-s-Indacene. *Chem. Comm* **1999**, 18, 1889–1890.
- (516) Yu, C.; Xu, Y.; Jiao, L.; Zhou, J.; Wang, Z.; Hao, E. Isoindole-BODIPY Dyes as Red to near-Infrared Fluorophores. *Chem. - A Eur. J.* **2012**, 18 (21), 6437–6442.
- (517) Kim, D.; Ma, D.; Kim, M.; Jung, Y.; Kim, N. H.; Lee, C.; Cho, S. W.; Park, S.; Huh, Y.; Jung, J.; Ahn, K. H. Fluorescent Labeling of Protein Using Blue-Emitting 8-Amino-BODIPY Derivatives. *J. Fluoresc.* **2017**, 27 (6), 2231–2238.
- (518) Yu, C.; Jiao, L.; Zhang, P.; Feng, Z.; Cheng, C.; Wei, Y.; Mu, X.; Hao, E. Highly Fluorescent BF₂ Complexes of Hydrazine-Schiff Base Linked Bispyrrole. *Org. Lett.* **2014**, 16 (11), 3048–3051.
- (519) Rurack, K.; Kollmannsberger, M.; Daub, J. Molecular Switching in the near Infrared (NIR) with a Functionalized Boron-Dipyromethene Dye. *Angew. Chemie - Int. Ed.* **2001**, 40 (2), 385–387.
- (520) Itoh, N.; Cao, J.; Chen, Z. H.; Yoshida, Y.; Niki, E. Advantages and Limitation of BODIPY as a Probe for the Evaluation of Lipid Peroxidation and Its Inhibition by Antioxidants in Plasma. *Bioorg. Med. Chem. Lett.* **2007**, 17 (7), 2059–2063.
- (521) Bakthavachalam, V.; Neumeyer, J. L.; Baidur, N.; Neumeyer, J. L.; Madras, B. K. Fluorescent Probes for Dopamine Receptors: Synthesis and Characterization of Fluorescein and 7-Nitrobenz-2-Oxa-1,3-Diazol-4-Yl Conjugates of D-1 and D-2 Receptor Ligands. *J. Med. Chem.* **1991**, 34 (11), 3235–3241.
- (522) Sykes, D. A.; Moore, H.; Stott, L.; Holliday, N.; Javitch, J. A.; Robert Lane, J.; Charlton, S. J. Extrapyramidal Side Effects of Antipsychotics Are Linked to Their Association Kinetics at Dopamine D2 Receptors. *Nat. Commun.* **2017**, 8 (1), 1–11.
- (523) Elgemeie, G. H.; Ahmed, K. A.; Ahmed, E. A.; Helal, M. H.; Masoud, D. M. A Simple Approach for the Synthesis of Coumarin Fluorescent Dyes under Microwave Irradiation and Their Application in Textile Printing. *Pigment Resin Technol.* **2016**, 45 (4), 217–224.
- (524) Yu, C.; Huang, Z.; Wang, X.; Miao, W.; Wu, Q.; Wong, W. Y.; Hao, E.; Xiao, Y.; Jiao, L. A Family of Highly Fluorescent and Unsymmetric Bis(BF₂) Chromophore Containing Both Pyrrole and N-Heteroarene Derivatives: BOPPY. *Org. Lett.* **2018**, 20 (15), 4462–4466.
- (525) Kaur, N.; Kaur, P.; Bhatia, G.; Singh, K.; Singh, J. Indole-BODIPY: A "turn-on" Chemosensor for Hg²⁺ with Application in Live Cell Imaging. *RSC Adv.* **2016**, 6 (86), 82810–82816.
- (526) Doose, S.; Neuweiler, H.; Sauer, M. Fluorescence Quenching by Photoinduced Electron Transfer: A Reporter for Conformational Dynamics of Macromolecules. *ChemPhysChem* **2009**, 10 (9–10), 1389–1398.
- (527) Kowalczyk, T.; Lin, Z.; Van Voorhis, T. Fluorescence Quenching by Photoinduced Electron Transfer in the Zn²⁺ Sensor Zinpyr-1: A Computational Investigation. *J. Phys. Chem. A.* **2010**, 114 (38), 10427–10434.
- (528) Buncel, E.; Rajagopal, S. Solvatochromism and Solvent Polarity Scales. *Acc. Chem. Res.* **1990**, 23 (7), 226–231.
- (529) Caar P.W., Solvatochromism, Linear Solvataion Energy Relationships and Chromatography *Microchem. Jour.* **1993**, 48, 4-23.
- (530) Marini, A.; Muñoz-Losa, A.; Biancardi, A.; Mennucci, B. What Is Solvatochromism? *J. Phys. Chem. B.* **2010**, 114 (51), 17128–17135.
- (531) Cowart, M.; Pratt, J. K.; Stewart, A. O.; Bennani, Y. L.; Esbenshade, T. A.; Hancock, A. A. A New Class of Potent Non-Imidazole H3 Antagonists: 2-Aminoethylbenzofurans. *Bioorg. Med. Chem. Lett.* **2004**, 14 (3), 689–693.
- (532) Amon, M.; Ligneau, X.; Schwartz, J. C.; Stark, H. Fluorescent Non-Imidazole Histamine H3 Receptor Ligands with Nanomolar Affinities. *Bioorg. Med. Chem. Lett.* **2006**, 16 (7), 1938–1940.
- (533) Amon, M.; Ligneau, X.; Camelin, J. C.; Berrebi-Bertrand, I.; Schwartz, J. C.; Stark, H. Highly Potent Fluorescence-Tagged Nonimidazole Histamine H3 Receptor Ligands. *ChemMedChem* **2007**, 2 (5), 708–716.
- (534) Bartole, E.; Grätz, L.; Littmann, T.; Wifling, D.; Seibel, U.; Buschauer, A.; Bernhardt, G. UR-DEBa242: A Py-5-Labeled Fluorescent Multipurpose Probe for Investigations on the Histamine H3 and H4 Receptors. *J.*

- Med. Chem.* **2020**, *63* (10), 5297–5311.
- (535) Echenique, P.; Alonso, J. L. A Mathematical and Computational Review of Hartree-Fock SCF Methods in Quantum Chemistry. *Mol. Phys.* **2007**, *105* (23–24), 3057–3098.
- (536) Li, H.; Zeng, X. C. Wetting and Interfacial Properties of Water Nanodroplets in Contact with Graphene and Monolayer Boron-Nitride Sheets. *ACS Nano* **2012**, *6* (3), 2401–2409.
- (537) Johnson, B. R. The Renormalized Numerov Method Applied to Calculating Bound States of the Coupled-Channel Schroedinger Equation. *J. Chem. Phys.* **1978**, *69* (10), 4678–4688.
- (538) Sukumar, N.; Das, S.; Sukumar, N. Current Trends in Virtual High Throughput Screening Using Ligand-Based and Structure-Based Methods. *Comb. Chem. High Throughput Screen.* **2011**, *14* (10), 872–888.
- (539) Sokoloff, P.; Andrieux, M.; Besançon, R.; Pilon, C.; Martres, M. P.; Giros, B.; Schwartz, J. C. Pharmacology of Human Dopamine D3 Receptor Expressed in a Mammalian Cell Line: Comparison with D2 Receptor. *Eur. J. Pharmacol. Mol. Pharmacol.* **1992**, *225* (4), 331–337.
- (540) Moritz, A. E.; Free, R. B.; Sibley, D. R. Advances and Challenges in the Search for D2 and D3 Dopamine Receptor-Selective Compounds. *Cell Signal* **2018**, *41*, 75–81.
- (541) Ananthan, S.; Saini, S. K.; Zhou, G.; Hobrath, J. V.; Padmalayam, I.; Zhai, L.; Bostwick, J. R.; Antonio, T.; Reith, M. E. A.; McDowell, S.; Cho, E.; McAleer, L.; Taylor, M.; Luedtke, R. R. Design, Synthesis, and Structure-Activity Relationship Studies of a Series of [4-(4-Carboxamidobutyl)]-1-Arylpiperazines: Insights into Structural Features Contributing to Dopamine D3 versus D2 Receptor Subtype Selectivity. *J. Med. Chem.* **2014**, *57* (16), 7042–7060.
- (542) Bueschbell, B.; Barreto, C. A. V.; Preto, A. J.; Schiedel, A. C.; Moreira, I. S. A Complete Assessment of Dopamine Receptor-Ligand Interactions through Computational Methods. *Molecules* **2019**, *24* (7), 1–26.
- (543) Ferruz, N.; Doerr, S.; Vanase-Frawley, M. A.; Zou, Y.; Chen, X.; Marr, E. S.; Nelson, R. T.; Kormos, B. L.; Wager, T. T.; Hou, X.; Villalobos, A.; Sciabola, S.; De Fabritiis, G. Dopamine D3 Receptor Antagonist Reveals a Cryptic Pocket in Aminergic GPCRs. *Sci. Rep.* **2018**, *8* (1), 1–10.
- (544) Lane, J. R.; Abramyan, A. M.; Adhikari, P.; Keen, A. C.; Lee, K. H.; Sanchez, J.; Verma, R. K.; Lim, H. D.; Yano, H.; Javitch, J. A.; Shi, L. Distinct Inactive Conformations of the Dopamine D2 and D3 Receptors Correspond to Different Extents of Inverse Agonism. *Elife* **2020**, *9*, 1–26.
- (545) Wang, Z.; Sun, H.; Yao, X.; Li, D.; Xu, L.; Li, Y.; Tian, S.; Hou, T. Comprehensive Evaluation of Ten Docking Programs on a Diverse Set of Protein-Ligand Complexes: The Prediction Accuracy of Sampling Power and Scoring Power. *Phys. Chem. Chem. Phys.* **2016**, *18* (18), 12964–12975.
- (546) Alberts, G. L.; Pregonzer, J. F.; Im, W. Bin. Contributions of Cysteine 114 of the Human D3 Dopamine Receptor to Ligand Binding and Sensitivity to External Oxidizing Agents. *Br. J. Pharmacol.* **1998**, *125* (4), 705–710.
- (547) Ericksen, S. S.; Cummings, D. F.; Teer, M. E.; Amdani, S.; Schetz, J. A. Ring Substituents on Substituted Benzamide Ligands Indirectly Mediate Interactions with Position 7.39 of Transmembrane Helix 7 of the D4 Dopamine Receptor. *J. Pharmacol. Exp. Ther.* **2012**, *342* (2), 472–485.
- (548) Warshel, A.; Levitt, M. Theoretical Studies of Enzymic Reactions: Dielectric, Electrostatic and Steric Stabilization of the Carbonium Ion in the Reaction of Lysozyme. *J. Mol. Biol.* **1976**, *103* (2), 227–249.
- (549) Zhang, Y. Pseudobond Ab Initio QM/MM Approach and Its Applications to Enzyme Reactions. *Theor. Chem. Acc.* **2006**, *116* (1–3), 43–50.
- (550) Zhao, Y.; Truhlar, D. G. The M06 Suite of Density Functionals for Main Group Thermochemistry, Thermochemical Kinetics, Noncovalent Interactions, Excited States, and Transition Elements: Two New Functionals and Systematic Testing of Four M06-Class Functionals and 12 Other Function. *Theor. Chem. Acc.* **2008**, *120* (1–3), 215–241.
- (551) Stewart, J. J. P. Optimization of Parameters for Semiempirical Methods I. Method. *J. Comput. Chem.* **1989**, *10* (2), 209–220.
- (552) Husch, T.; Reiher, M. Comprehensive Analysis of the Neglect of Diatomic Differential Overlap Approximation. *J. Chem. Theory Comput.* **2018**, *14* (10), 5169–5179.
- (553) Walker, M.; Harvey, A. J. A.; Sen, A.; Dessent, C. E. H. Performance of M06, M06-2X, and M06-HF Density Functionals for Conformationally Flexible Anionic Clusters: M06 Functionals Perform Better than B3LYP for a Model System with Dispersion and Ionic Hydrogen-Bonding Interactions. *J. Phys. Chem. A.* **2013**, *117* (47), 12590–12600.
- (554) Wang, Y.; Verma, P.; Zhang, L.; Li, Y.; Liu, Z.; Truhlar, D. G.; He, X. M06-SX Screened-Exchange Density Functional for Chemistry and Solid-State Physics. *Proc. Natl. Acad. Sci. U. S. A.* **2020**, *117* (5), 2294–2301.
- (555) Li, A.; Muddana, H. S.; Gilson, M. K. Quantum Mechanical Calculation of Noncovalent Interactions: A Large-Scale Evaluation of PMx, DFT, and SAPT Approaches. *J. Chem. Theory Comput.* **2014**, *10* (4), 1563–

- 1575.
- (556) Contreras-García, J.; Johnson, E. R.; Keinan, S.; Chaudret, R.; Piquemal, J. P.; Beratan, D. N.; Yang, W. NCIPLOT: A Program for Plotting Noncovalent Interaction Regions. *J. Chem. Theory Comput.* **2011**, *7* (3), 625–632.
- (558) Dalvit, C.; Vulpetti, A. Fluorine-Protein Interactions and ¹⁹F NMR Isotropic Chemical Shifts: An Empirical Correlation with Implications for Drug Design. *ChemMedChem* **2011**, *6* (1), 104–114. 12.
- (559) Schübler, M.; Sadek, B.; Kottke, T.; Weizel, L.; Stark, H. Synthesis, Molecular Properties Estimations, and Dual Dopamine D2 and D3 Receptor Activities of Benzothiazole-Based Ligands. *Front. Chem.* **2017**, *5*, 1–19.
- (560) Frank, A.; Kiss, D. J.; Keserü, G. M.; Stark, H. Binding Kinetics of Cariprazine and Aripiprazole at the Dopamine D3 Receptor. *Sci. Rep.* **2018**, *8* (1), 1–9.
- (561) McKinney, M.; Raddatz, R. Practical Aspects of Radioligand Binding. *Curr. Protoc. Pharmacol.* **2006**, *Chapter 1* (1), 1–42.
- (562) Bylund, D. B.; Toews, M. L. Radioligand Binding Methods Practical Guide and Tips. *Am. J. Physiol.* **1993**, *265* (5), 421–429.
- (563) Mendel, C. M.; Mendel, D. B. “Non-Specific” Binding. The Problem, and a Solution. *Biochem. J.* **1985**, *228* (1), 269–272.
- (564) Motulsky, H. J.; Neubig, R. R. Analyzing Binding Data. *Curr. Protoc. Neurosci.* **2010**, *52*, 1–55.
- (565) Rosenthal, H. E. A Graphic Method for the Determination and Presentation of Binding Parameters in a Complex System. *Anal. Biochem.* **1967**, *20* (3), 525–532.
- (566) Yung-Chi, C.; Prusoff, W. H. Relationship between the Inhibition Constant (KI) and the Concentration of Inhibitor Which Causes 50 per Cent Inhibition (I50) of an Enzymatic Reaction. *Biochem. Pharmacol.* **1973**, *22* (23), 3099–3108.
- (567) Kottke, T.; Sander, K.; Weizel, L.; Schneider, E. H.; Seifert, R.; Stark, H. Receptor-Specific Functional Efficacies of Alkyl Imidazoles as Dual Histamine H3/H4 Receptor Ligands. *Eur. J. Pharmacol.* **2011**, *654* (3), 200–208.
- (568) Katoch, N.; Kaur, P.; Kashyap, P.; Gupta, S.; Dahiya, R. S. Role of Oxidative Stress in Cardiovascular Diseases. *Res. J. Pharm. Biol. Chem. Sci.* **2013**, *4* (3), 870–881.
- (569) Kirkham, P. A.; Barnes, P. J. Oxidative Stress in COPD. *Chest* **2013**, *144* (1), 266–273.
- (570) Chung, S. S. M.; Ho, E. C. M.; Lam, K. S. L.; Chung, S. K. Contribution of Polyol Pathway to Diabetes-Induced Oxidative Stress. *J. Am. Soc. Nephrol.* **2003**, *14*, 233–236.
- (571) Russo, G.; Curcio, F.; Bulli, G.; Aran, L.; Della-morte, D.; Testa, G.; Cacciatore, F.; Bonaduce, D.; Abete, P. Oxidative Stress and Diseases. *Clin. Interv. Aging.* **2012**, *757–772*.
- (572) Moylan, J. S.; Reid, M. B. Oxidative Stress, Chronic Disease, and Muscle Wasting. *Muscle and Nerve* **2007**, *35* (4), 411–429.
- (573) Patel, M. Targeting Oxidative Stress in Central Nervous System Disorders. *Trends Pharmacol. Sci.* **2016**, *37* (9), 768–778.
- (574) Pizzino, G.; Irrera, N.; Cucinotta, M.; Pallio, G.; Mannino, F.; Arcoraci, V.; Squadrito, F.; Altavilla, D.; Bitto, A. Oxidative Stress: Harms and Benefits for Human Health. *Oxid. Med. Cell. Longev.* **2017**, 8416763.
- (575) Cao, G.; Alessio, H. M.; Cutler, R. G. Oxygen-Radical Absorbance Capacity Assay for Antioxidants. *Free Radic. Biol. Med.* **1993**, *14* (3), 303–311.
- (576) DeLange, R. J.; Glazer, A. N. Phycoerythrin Fluorescence-Based Assay for Peroxy Radicals: A Screen for Biologically Relevant Protective Agents. *Anal. Biochem.* **1989**, *177* (2), 300–306.
- (577) Ou, B.; Hampsch-Woodill, M.; Prior, R. L. Development and Validation of an Improved Oxygen Radical Absorbance Capacity Assay Using Fluorescein as the Fluorescent Probe. *J. Agric. Food Chem.* **2001**, *49* (10), 4619–4626.
- (578) Sander, T.; Freyss, J.; Von Korff, M.; Rufener, C. DataWarrior: An Open-Source Program for Chemistry Aware Data Visualization and Analysis. *J. Chem. Inf. Model.* **2015**, *55* (2), 460–473.
- (579) Benet L., Hosey C.M., Ursu O., and. Oprea T.I., BDDCS, the Rule of 5 and Drugability. *Adv Drug Deliv Rev* **2016**, *101*, 89–98.
- (580) Lipinski, C. A.; Lombardo, F.; Dominy, B. W.; Feeney, P. J. Experimental and Computational Approaches to Estimate Solubility and Permeability in Drug Discovery and Development Settings. *Adv. Drug Deliv. Rev.* **2001**, *46*, 3–21.
- (581) Ursu, O.; Rayan, A.; Goldblum, A.; Oprea, T. I. Understanding Drug-Likeness. *Wiley Interdiscip. Rev. Comput. Mol. Sci.* **2011**, *1* (5), 760–781.
- (582) Van De Waterbeemd, H.; Camenisch, G.; Folkers, G.; Chretien, J. R.; Raevsky, O. A. Estimation of Blood-

- Brain Barrier Crossing of Drugs Using Molecular Size and Shape, and H-Bonding Descriptors. *J. Drug Target.* **1998**, *6* (2), 151–165.
- (583) Veber, D.F., Johnson, S.R., Yuan Cheng, H., Smith B.R., Ward K.W. and K. D. K.; Departments. Molecular Properties That Influence the Oral Bioavailability of Drug Candidates. *J. Med. Chem.* **2002**, *45*, 2615–2623.
- (584) Pajouhesh, H.; Lenz, G. R. Medicinal Chemical Properties of Successful Central Nervous System Drugs. *NeuroRx* **2005**, *2* (4), 541–553.
- (585) Ostrowska, K. Coumarin-Piperazine Derivatives as Biologically Active Compounds. *Saudi Pharm. J.* **2020**, *28* (2), 220–232.
- (586) Teran, C., Santana L., Uriarte E., Fall, Y., Unelius L. and Ragnar-Tolf B. Phenylpiperazine Derivatives with Strong Affinity For 5HT1A; D2A and D3 Receptors. *Bioorg. Med. Chem. Lett.* **1998**, *8* (24), 3567–3570.
- (587) Lee, S. P.; O'Dowd, B. F.; Rajaram, R. D.; Nguyen, T.; George, S. R. D2 Dopamine Receptor Homodimerization Is Mediated by Multiple Sites of Interaction, Including an Intermolecular Interaction Involving Transmembrane Domain 4. *Biochemistry* **2003**, *42* (37), 11023–11031.
- (588) Guo, W.; Shi, L.; Filizola, M.; Weinstein, H.; Javitch, J. A. Crosstalk in G Protein-Coupled Receptors: Changes at the Transmembrane Homodimer Interface Determine Activation. *Proc. Natl. Acad. Sci. U. S. A.* **2005**, *102* (48), 17495–17500.
- (589) Borroto-Escuela, D. O.; Pintsuk, J.; Schäfer, T.; Friedland, K.; Ferraro, L.; Tanganelli, S.; Liu, F.; Fuxe, K. Multiple D2 Heteroreceptor Complexes: New Targets for Treatment of Schizophrenia. *Ther. Adv. Psychopharmacol.* **2016**, *6* (2), 77–94.
- (590) Erez M, Takemori A.E.; Porthogese P.S. Narcotic Antagonistic Potency of Bivalent Ligands Which Contain 0-Naltrexamine. Evidence for Bridging between Proximal Recognition Sites., *J. Med. Chem.* **1982**, *25* (7), 847–849.
- (591) Carli M.; Kolachalam S.; Arighieri S.; Rossi M.; Giovanni L.; Maggio R.; Scarselli M. Dopamine D2 Receptors Dimers. How can we Pharmacologically Target Them? *Curr. Neuropharmacol.* **2018**, *16* (2).
- (592) Newman, A. H.; Battiti, F. O.; Bonifazi, A. 2016 Philip S. Portuguese Medicinal Chemistry Lectureship: Designing Bivalent or Bitopic Molecules for G-Protein Coupled Receptors. The Whole Is Greater Than the Sum of Its Parts. *J. Med. Chem.* **2020**, *63* (5), 1779–1797.
- (593) Fronik, P.; Gaiser, B. I.; Sejer Pedersen, D. Bitopic Ligands and Metastable Binding Sites: Opportunities for G Protein-Coupled Receptor (GPCR) Medicinal Chemistry. *J. Med. Chem.* **2017**, *60* (10), 4126–4134.
- (594) Bonifazi, A.; Yano, H.; Guerrero, A. M.; Kumar, V.; Hoffman, A. F.; Lupica, C. R.; Shi, L.; Newman, A. H. Novel and Potent Dopamine D2 Receptor Go-Protein Biased Agonists. *ACS Pharmacol. Transl. Sci.* **2019**, *2* (1), 52–65.
- (595) Kumar, V.; Moritz, A. E.; Keck, T. M.; Bonifazi, A.; Ellenberger, M. P.; Sibley, C. D.; Free, R. B.; Shi, L.; Lane, J. R.; Sibley, D. R.; Newman, A. H. Synthesis and Pharmacological Characterization of Novel Trans-Cyclopropylmethyl-Linked Bivalent Ligands That Exhibit Selectivity and Allosteric Pharmacology at the Dopamine D3 Receptor (D3R). *J. Med. Chem.* **2017**, *60* (4), 1478–1494.
- (596) Silvano, E.; Millan, M. J.; La Cour, C. M.; Han, Y.; Duan, L.; Griffin, S. A.; Luedtke, R. R.; Aloisi, G.; Rossi, M.; Zazzeroni, F.; Javitch, J. A.; Maggio, R. The Tetrahydroisoquinoline Derivative SB269,652 Is an Allosteric Antagonist at Dopamine D3 and D2 Receptors. *Mol. Pharmacol.* **2010**, *78* (5), 925–934.
- (597) Zou, M. F.; Keck, T. M.; Kumar, V.; Donthamsetti, P.; Michino, M.; Burzynski, C.; Schweppe, C.; Bonifazi, A.; Free, R. B.; Sibley, D. R.; Janowsky, A.; Shi, L.; Javitch, J. A.; Newman, A. H. Novel Analogues of (R)-5-(Methylamino)-5,6-Dihydro-4H-Imidazo[4,5,1-l]Quinolin-2(1H)-One (Sumanitrole) Provide Clues to Dopamine D2/D3 Receptor Agonist Selectivity. *J. Med. Chem.* **2016**, *59* (7), 2973–2988.
- (598) Le, W. D.; Jankovic, J.; Xie, W.; Appel, S. H. Antioxidant Property of Pramipexole Independent of Dopamine Receptor Activation in Neuroprotection. *J. Neural Transm.* **2000**, *107* (10), 1165–1173.
- (599) Danzeisen, R.; Schwalenstoecker, B.; Gillardon, F.; Buerger, E.; Krzykalla, V.; Klinder, K.; Schild, L.; Hengerer, B.; Ludolph, A. C.; Dorner-Ciossek, C.; Kusmaul, L. Targeted Antioxidative and Neuroprotective Properties of the Dopamine Agonist Pramipexole and Its Nondopaminergic Enantiomer SND919CL2x [(+)-2-Amino-4,5,6,7-Tetrahydro-6-L-Propylamino-Benzothiazole Dihydrochloride]. *J. Pharmacol. Exp. Ther.* **2006**, *316* (1), 189–199.
- (600) Langdon, S. R.; Ertl, P.; Brown, N. Bioisosteric Replacement and Scaffold Hopping in Lead Generation and Optimization. *Mol. Inform.* **2010**, *29* (5), 366–385.
- (601) Brown, N. Bioisosteres and Scaffold Hopping in Medicinal Chemistry. *Mol. Inform.* **2014**, *33* (6–7), 458–462.
- (602) Stark H.; Leppanen M.; Sasse B.; Saur O.; Kottke T.; Peters M. (2009) Tetrahydrobenzothiazole Derivatives with Dopamine Receptor Activity Wo 2009/056811.
- (603) Durdagi, S.; Salmas, R. E.; Stein, M.; Yurtsever, M.; Seeman, P. Binding Interactions of Dopamine and

- Apomorphine in D2 High and D2 Low States of Human Dopamine D2 Receptor Using Computational and Experimental Techniques. *ACS Chem. Neurosci.* **2016**, *7* (2), 185–195.
- (604) Ferrada, C.; Ferré, S.; Casadó, V.; Cortés, A.; Justinova, Z.; Barnes, C.; Canela, E. I.; Goldberg, S. R.; Leurs, R.; Lluís, C.; Franco, R. Interactions between Histamine H3 and Dopamine D2 Receptors and the Implications for Striatal Function. *Neuropharmacology* **2008**, *55* (2), 190–197.
- (605) Celanire, S.; Wijtman, M.; Talaga, P.; Leurs, R.; De Esch, I. J. P. Keynote Review: Histamine H3 Receptor Antagonists Reach out for the Clinic. *Drug Discov. Today* **2005**, *10* (23–24), 1613–1627.
- (606) Walter, M.; Isensee, K.; Kottke, T.; Ligneau, X.; Camelin, J. C.; Schwartz, J. C.; Stark, H. Azole Derivatives as Histamine H3 Receptor Antagonists, Part 2: C-C and C-S Coupled Heterocycles. *Bioorg. Med. Chem. Lett.* **2010**, *20* (19), 5883–5886.
- (607) Bautista-Aguilera, Ó. M.; Hagenow, S.; Palomino-Antolin, A.; Farré-Alins, V.; Ismaili, L.; Joffrin, P. L.; Jimeno, M. L.; Soukup, O.; Janočková, J.; Kalinowsky, L.; Proschak, E.; Iriepa, I.; Moraleda, I.; Schwed, J. S.; Romero Martínez, A.; López-Muñoz, F.; Chioua, M.; Egea, J.; Ramsay, R. R.; Marco-Contelles, J.; Stark, H. Multitarget-Directed Ligands Combining Cholinesterase and Monoamine Oxidase Inhibition with Histamine H3R Antagonism for Neurodegenerative Diseases. *Angew. Chemie - Int. Ed.* **2017**, *56* (41), 12765–12769.
- (608) Ligneau, X.; Landais, L.; Perrin, D.; Piriou, J.; Uguen, M.; Denis, E.; Robert, P.; Parmentier, R.; Anaclet, C.; Lin, J. S.; Burbán, A.; Arrang, J. M.; Schwartz, J. C. Brain Histamine and Schizophrenia: Potential Therapeutic Applications of H3-Receptor Inverse Agonists Studied with BF2.649. *Biochem. Pharmacol.* **2007**, *73* (8), 1215–1224.
- (609) Humbert-Claude, M.; Morisset, S.; Gbahou, F.; Arrang, J. M. Histamine H3 and Dopamine D2 Receptor-Mediated [35S]GTPγ[S] Binding in Rat Striatum: Evidence for Additive Effects but Lack of Interactions. *Biochem. Pharmacol.* **2007**, *73* (8), 1172–1181.
- (610) Plenge, P.; Shi, L.; Beuming, T.; Te, J.; Newman, A. H.; Weinstein, H.; Gether, U.; Loland, C. J. Steric Hindrance Mutagenesis in the Conserved Extracellular Vestibule Impedes Allosteric Binding of Antidepressants to the Serotonin Transporter. *J. Biol. Chem.* **2012**, *287* (47), 39316–39326.
- (611) New, J. S.; Yevich, J. P.; Eison, M. S.; Taylor, D. P.; Riblet, L. A.; VanderMaelen, C. P.; Temple, D. L. Bupirone Analogues. 2. Structure-Activity Relationships of Aromatic Imide Derivatives. *J. Med. Chem.* **1986**, *29* (8), 1476–1482.
- (612) Prante, O.; Tietze, R.; Hocke, C.; Löber, S.; Hübner, H.; Kuwert, T.; Gmeiner, P. Synthesis, Radiofluorination, and in Vitro Evaluation of Pyrazolo[1,5-a]Pyridine-Based Dopamine D4 Receptor Ligands: Discovery of an Inverse Agonist Radioligand for PET. *J. Med. Chem.* **2008**, *51* (6), 1800–1810.
- (613) Kitbunnadaj, R.; Zuiderveld, O. P.; Christophe, B.; Hulscher, S.; Menge, W. M. P. B.; Gelens, E.; Snip, E.; Bakker, R. a; Celanire, S.; Gillard, M.; Talaga, P.; Timmerman, H.; Leurs, R. Identification of 4-(1H - Imidazol-4 (5)-methyl)Pyridine (Immethridine) as a Novel , Potent , and Highly Selective Histamine H3 Receptor Agonist Histamine Is a Biogenic Amine with Multiple Physiological Effects. *J. Med. Chem.* **2004**, *47*, 2414–2417.
- (614) Committee on Acute Exposure Guideline Levels; Committee on Toxicology; Board on Environmental Studies and Toxicology; Division on Earth and Life Studies; National Research Council, Acute Exposure Guideline Levels;. (2016) Acute Exposure Guideline Levels for Selected Airborne Chemicals. 14th Ed. National Academy Press.
- (615) Veinberg, G.; Shestakova, I.; Vorona, M.; Kanepe, I.; Domrachova, I.; Lukevics, E. Doxorubicin Prodrug on the Basis of Tert-Butyl Cephalosporanate Sulfones. *Bioorg. Med. Chem. Lett.* **2004**, *14* (4), 1007–1010.
- (616) Tan, X.; Boudinot, F. D.; Chu, C. K.; Egron, D.; Perigaud, C.; Gosselin, G.; Imbach, J. L. Pharmacokinetics of Bis(t-Butyl-SATE)-AZTMP, a Bispivaloylthioethyl Prodrug for Intracellular Delivery of Zidovudine Monophosphate, in Mice. *Antivir. Chem. Chemother.* **2000**, *11* (3), 203–211.
- (617) Chavez-Abiega, S.; Goedhart, J.; Bruggeman, F. J. Physical Biology of GPCR Signalling Dynamics Inferred from Fluorescence Spectroscopy and Imaging. *Curr. Opin. Struct. Biol.* **2019**, *55*, 204–211.
- (618) Soave, M.; Bridson, S. J.; Hill, S. J.; Stoddart, L. A. Fluorescent Ligands: Bringing Light to Emerging GPCR Paradigms. *Br. J. Pharmacol.* **2020**, *177* (5), 978–991.
- (619) Monsma, F. J.; Barton, A. C.; Chol Kang, H.; Brassard, D. L.; Haugland, R. P.; Sibley, D. R. Characterization of Novel Fluorescent Ligands with High Affinity for D1 and D2 Dopaminergic Receptors. *J. Neurochem.* **1989**, *52* (5), 1641–1644.
- (620) Lachmann, D.; Studte, C.; Männel, B.; Hübner, H.; Gmeiner, P.; König, B. Photochromic Dopamine Receptor Ligands Based on Dithienylethenes and Fulgides. *Chem. - A Eur. J.* **2017**, *23* (54), 13423–1343.
- (621) Hackling, A.; Ghosh, R.; Perachon, S.; Mann, A.; Hölting, H. D.; Wermuth, C. G.; Schwartz, J. C.; Sippl, W.;

- Sokoloff, P.; Stark, H. *N*-(ω)-(4-(2-Methoxyphenyl)Piperazin-1-yl)Alkyl)Carboxamides as Dopamine D2 and D3 Receptor Ligands. *J. Med. Chem.* **2003**, *46* (18), 3883–3899.
- (622) Gao, M.; Mock, B. H.; Hutchins, G. D.; Zheng, Q. H. Synthesis and Initial PET Imaging of New Potential Dopamine D3 Receptor Radioligands (E)-4,3,2-[¹¹C]Methoxy-*N*-4-(4-(2-Methoxyphenyl) Piperazin-1-yl)Butyl-Cinnamoylamides. *Bioorg. Med. Chem.* **2005**, *13* (22), 6233–6243.
- (623) Valeur, E.; Bradley, M. Amide Bond Formation: Beyond the Myth of Coupling Reagents. *Chem. Soc. Rev.* **2009**, *38* (2), 606–631.
- (624) Ramakrishna N.; Shinde A.L.; Kambhamati R.; Namala R.; Dwarbapudi A.R.; Laxman K.; Gampa M.; Kodru P.; Tiriveedhi T.; Kandikere V.M.; Muddana N.R.; Saralaya R.S.; Jayaran P.; Shamugahantan D.; Ahmad I.; Jasti V. (2012) Heterocyclic compounds as histamine H3 ligands, WO2012/029070.
- (625) Khatri, M.; Rai, S. K.; Ranbhor, R.; Kishore, K.; Tiwari, M. Synthesis and Pharmacological Evaluation of [(4-Arylpiperazin-1-yl) - Alkyl] -Carbamic Acid Ethyl Ester Derivatives as Potential Anxiolytic Agents. **2012**, *35* (7), 1143–1152.
- (626) Jean, M.; Renault, J.; Levoine, N.; Danvy, D.; Calmels, T.; Berrebi-bertrand, I.; Robert, P.; Schwartz, J. C.; Lecomte, J. M.; Uriac, P.; Capet, M. Lett., Synthesis and Evaluation of Amides Surrogates of Dopamine D3 Receptor Ligands. **2010**, *Bioorg. Med. Chem. Lett.* *20*, 5376–5379.
- (627) Muñoz-Osses, M.; Godoy, F.; Fierro, A.; Gómez, A.; Metzler-Nolte, N. New Organometallic Imines of Rhenium(i) as Potential Ligands of GSK-3 β : Synthesis, Characterization and Biological Studies. *Dalt. Trans.* **2018**, *47* (4), 1233–1242.
- (628) Pirzer, A. S.; Lasch, R.; Friedrich, H.; Hu, H.; Gmeiner, P.; Heinrich, M. R. Benzyl Phenylsemicarbazides: A Chemistry-Driven Approach Leading to G Protein-Biased Dopamine D4 Receptor Agonists with High Subtype Selectivity. *J. Med. Chem.* **2019**, *62*, 9658–6679.
- (629) Chen, P.; Taylor, M.; Griffin, S. A.; Amani, A.; Hayatshahi, H.; Korzekwa, K.; Ye, M.; Mach, R. H.; Liu, J.; Luedtke, R. R.; Gordon, J. C.; Blass, B. E. (Thiophen-3-yl) Benzamides as Selective Dopamine D3 Receptor Ligands. *Bioorg. Med. Chem. Lett.* **2019**, *29* (18), 2690–2694.
- (631) De Simone, A.; Russo, D.; Ruda, G. F.; Micoli, A.; Ferraro, M.; Di Martino, R. M. C.; Ottonello, G.; Summa, M.; Armirotti, A.; Bandiera, T.; Cavalli, A.; Bottegoni, G. Design, Synthesis, Structure-Activity Relationship Studies, and Three-Dimensional Quantitative Structure-Activity Relationship (3D-QSAR) Modeling of a Series of O-Biphenyl Carbamates as Dual Modulators of Dopamine D3 Receptor and Fatty Acid Amide Hydrolase. *J. Med. Chem.* **2017**, *60* (6), 2287–2304.
- (632) Cao, Y.; Min, C.; Acharya, S.; Kim, K. M.; Cheon, S. H. Design, Synthesis and Evaluation of Bitopic Arylpiperazinephenyl-1,2,4-Oxadiazoles as Preferential Dopamine D3 Receptor Ligands. *Bioorg. Med. Chem.* **2016**, *24* (2), 191–200.
- (633) Liégeois, R. Synthesis and in Vitro Binding Studies of Piperazine-Alkyl-Naphthamides: Impact of Homology and Sulphonamide / Carboxamide Bioisosteric. *Bioorg. Med. Chem. Lett.* **2010**, *20*, 5199–5202.
- (634) Leopoldo, M.; Lacivita, E.; De Giorgio, P.; Colabufo, N. A.; Niso, M.; Berardi, F.; Perrone, R. Design, Synthesis, and Binding Affinities of Potential Positron Emission Tomography (PET) Ligands for Visualization of Brain Dopamine D3 Receptors. *J. Med. Chem.* **2006**, *49* (1), 358–365.
- (635) Prasanna, D. S.; Kavitha, C. V.; Raghava, B.; Vinaya, K.; Ranganatha, S. R.; Raghavan, S. C.; Rangappa, K. S. Synthesis and Identification of a New Class of (S)-2,6-Diamino-4,5,6,7-Tetrahydrobenzo[d]Thiazole Derivatives as Potent Antileukemic Agents. *Invest. New Drugs* **2010**, *28* (4), 454–465.
- (636) Perronel R., Berardil F., Colabufol NA., Fornaretto MG, Caccia C, MC Arthur R.M. Synthesis of Arylpiperazines with a Terminal Naphthothiazole Group and Their Evaluation on 5-HT, DA and a Receptor. *Eur. J. Med. Chem.*, **1997**, *32*, 739–746.
- (637) Oliveira, C. B.; Maher, C. G.; Pinto, R. Z.; Traeger, A. C.; Lin, C. W. C.; Chenot, J. F.; van Tulder, M.; Koes, B. W. Clinical Practice Guidelines for the Management of Non-Specific Low Back Pain in Primary Care: An Updated Overview. *Eur. Spine J.* **2018**, *27* (11), 2791–2803.
- (638) Saur O., (2007) Dopamin D2 und D3 Rezeptorliganden als pharmakologische Werkzeuge und potentielle Arzneistoffe. Doctoral Dissertation. Goethe Universität Frankfurt am Mein.
- (639) Glase, S. A.; Corbin, A. E.; Pugsley, T. A.; Heffner, T. G.; Wise, L. D. Synthesis and Dopaminergic Activity of Pyridine Analogs of 5-Hydroxy-2-(Di-n-Propylamino)Tetralin. *J. Med. Chem.* **1995**, *38* (16), 3132–3137.
- (640) Wang, Y. D.; Bao, X. Q.; Xu, S.; Yu, W. W.; Cao, S. N.; Hu, J. P.; Li, Y.; Wang, X. L.; Zhang, D.; Yu, S. S. A Novel Parkinson's Disease Drug Candidate with Potent Anti-Neuroinflammatory Effects through the Src Signaling Pathway. *J. Med. Chem.* **2016**, *59* (19), 9062–9079.
- (641) Archibald J.L., Curran A.C.W., 68-1-piperidino-thiocarpoamides, US3917618-A, **1976**.
- (642) Sander, K.; Kottke, T.; Hoffend, C.; Walter, M.; Weizel, L.; Camelin, J.; Ligneau, X.; Schneider, E. H.; Seifert,

- R.; Schwartz, J.; Stark, H. First Metal-Containing Histamine H₃ Receptor Ligands. *Org. Lett.* **2010**, *12* (11), 2578–2581.
- (643) Labeeuw, O.; Levoine, N.; Poupardin-Olivier, O.; Calmels, T.; Ligneau, X.; Berrebi-Bertrand, I.; Robert, P.; Lecomte, J. M.; Schwartz, J. C.; Capet, M. Novel and Highly Potent Histamine H₃ Receptor Ligands. Part 3: An Alcohol Function to Improve the Pharmacokinetic Profile. *Bioorg. Med. Chem. Lett.* **2013**, *23* (9), 2548–2554.
- (644) Lee, C. K.; Loh, T. Gram-Scale Synthesis of (–)-Epibatidine. *Org. Lett.* **2005**, *5*, 10–12.
- (645) Modi, G.; Antonio, T.; Reith, M.; Dutta, A. Structural Modifications of Neuroprotective Anti-Parkinsonian N₆-(2-(4-(Biphenyl-4-yl)Piperazin-1-yl)-Ethyl)-N⁶-Propyl-4,5,6,7-Tetrahydrobenzo[d]Thiazole-2,6-Diamine (D-264): An Effort toward the Improvement of in Vivo Efficacy of the Parent Molecule. *J. Med. Chem.* **2014**, *57* (4), 1557–1572.
- (646) Weichert, D.; Stanek, M.; Hübner, H.; Gmeiner, P. Structure-Guided Development of Dual B₂ Adrenergic/Dopamine D₂ Receptor Agonists. *Bioorg Med. Chem.* **2016**, *24* (12), 2641–2653.
- (647) Martínez-Rosell, G.; Giorgino, T.; De Fabritiis, G. PlayMolecule ProteinPrepare: A Web Application for Protein Preparation for Molecular Dynamics Simulations. *J. Chem. Inf. Model.* **2017**, *57* (7), 1511–1516.
- (648) Webb, B.; Sali, A. Comparative Protein Structure Modeling Using MODELLER. *Curr. Protoc. Bioinforma.* **2016**, *54*, 5.6.1-5.6.37.
- (649) Lee, J.; Cheng, X.; Swails, J. M.; Yeom, M. S.; Eastman, P. K.; Lemkul, J. A.; Wei, S.; Buckner, J.; Jeong, J. C.; Qi, Y.; Jo, S.; Pande, V. S.; Case, D. A.; Brooks, C. L.; MacKerell, A. D.; Klauda, J. B.; Im, W. CHARMM-GUI Input Generator for NAMD, GROMACS, AMBER, OpenMM, and CHARMM/OpenMM Simulations Using the CHARMM36 Additive Force Field. *J. Chem. Theory Comput.* **2016**, *12* (1), 405–413.
- (650) Vassetzki, D.; Pagliai, M.; Procacci, P. Assessment of GAFF2 and OPLS-AA General Force Fields in Combination with the Water Models TIP3P, SPCE, and OPC3 for the Solvation Free Energy of Druglike Organic Molecules. *J. Chem. Theory Comput.* **2019**, *15* (3), 1983–1995.
- (651) Wiberg B.K., *J. Comput. Chem.* Ab Initio Molecular Orbit Theory, **1986**, *7* (3), 379–383.
- (652) Laskowski, R.A., Swindelis, M.B., LigPlot+: Multiple Ligand-Protein Interaction Diagrams for Drug Discovery. *J. Chem. Inf. Model.* **2011**, *51* (10), 2778–2786.
- (653) Weigend, F.; Ahlrichs, R. Balanced Basis Sets of Split Valence, Triple Zeta Valence and Quadruple Zeta Valence Quality for H to Rn: Design and Assessment of Accuracy. *Phys. Chem. Chem. Phys.* **2005**, *7* (18), 3297–3305.
- (654) Neese, F. Software Update: The ORCA Program System, Version 4.0. *Wiley Interdiscip. Rev. Comput. Mol. Sci.* **2018**, *8* (1), 4–9.
- (655) Chaudret, R.; De Courcy, B.; Contreras-García, J.; Gloaguen, E.; Zehnacker-Rentien, A.; Mons, M.; Piquemal, J. P. Unraveling Non-Covalent Interactions within Flexible Biomolecules: From Electron Density Topology to Gas Phase Spectroscopy. *Phys. Chem. Chem. Phys.* **2014**, *16* (21), 9876–9891.
- (650) Laplaza, R.; Peccati, F.; A. Boto, R.; Quan, C.; Carbone, A.; Piquemal, J. P.; Maday, Y.; Contreras-García, J. NCIPLOT and the Analysis of Noncovalent Interactions Using the Reduced Density Gradient. *Wiley Interdiscip. Rev. Comput. Mol. Sci.* **2020**, 1–18.

8 List of Publications

Milica Elek, Nemanja Djokovic, Annika Frank, Slavica Oljadic, Aleksandra Zivkovic, Katarina Nikolic and Holger Stark. Synthesis, in silico, and in vitro studies of novel dopamine D₂ and D₃ receptor ligands. *Archiv der Pharmazie*, (2021) 354 (6), e2000486 (open access).

Markus Falkenstein, Milica Elek and Holger Stark, Chemical probes for histamine receptor subtypes. *Current Topics in Behavioral Neurosciences*, in press (2021).

Michael Dietrich, Christina Hecker, Milica Elek, Markus Falkenstein, Andrea Issberner, Sven Meuth, Holger Stark and Philipp Albrecht Evaluierung der protektiven Eigenschaften von Natriumkanalblockern, Monoaminoxidase-B-Inhibitoren und Histamin-H3-Rezeptor-Antagonisten in präklinischen Modellen retinaler Neurodegeneration. (2021)

Milica Elek and Holger Stark, *Deutscher Apotheker Zeitung* Nr. 48 Paracetamol, wie war das noch? (2019).

In preparation:

Milica Elek, Laura Meyer, Mariam Dubiel, Aleksandra Zivkovic, Thomas J.J. Müller and Holger Stark, Design and synthesis of dopaminergic D₂R and D₃R receptor ligands

Milica Elek and Holger Stark, Aktuelle Dopamin-Therapeutika zur Behandlung der Parkinson-Krankheit (Pharmakon)

Awards:

Best multimedia poster, MedChem2019 a pan-European network meeting for Medicinal Chemistry Catanzaro (Italy), June 13th-15th

9 Curriculum Vitae



MILICA ELEK

PhD candidate

Curious, adaptive, single-minded, highly motivated, initiative, go-getter. Ambitious, professional with proven cross-cultural agility, strong skills in communication, negotiation, and presentation, enthusiastic traveler. Team player leaning naturally to leadership roles.

LANGUAGES

- Serbian - Native
- English - Highly proficient
- German - Highly proficient
- Spanish - Working knowledge

SKILLS

- MS Office
- ChemOffice
- MestreNova
- Origin
- Pentacle
- Gold

OTHER INTERESTS

- Traveling, reading, hiking
- Member of World Scout Organization

CONTACT DETAILS

- 📞 +4917667659381
- @ milica.elek@hhu.de
- 📍 Hüttenstraße 48, 40215, Düsseldorf

CAREER HISTORY

University Teaching Assistant | 06/2018 - present

Heinrich-Heine University Düsseldorf, Düsseldorf

- Teaching Assistant in lab course "Arzneistoffanalytik unter besonderer Berücksichtigung der Arzneibücher" (particular focus on drug analytics. Techniques: HPLC, GC, LC-MS, IR, NMR, TLC, UV-VIS.)

Quality Assurance | 12/2016 - 06/2017

Hemofarm A.D. (Member of STADA group), Vrsac, Serbia

- Expert Associate for Internal and External Audits (particular focus on implementing GMP guidelines)

Intern | 06/2016 - 12/2016

Pharmacy: Higija, Bajina Basta, Serbia

Intern | 07/2015 - 08/2015

Pharmacy: Farmacia Alianca, Porto

- Student internships during Student Exchange Program

ACADEMIC HISTORY

Heinrich-Heine University Düsseldorf, Düsseldorf
PhD Education | 2017-2021 (expected)

Pharmaceutical and Medicinal Chemistry (Design and synthesis of novel multifunctional dopamine and histamine ligands)

Approbation für Apotheker

Licensed as pharmacist | 2020

Faculty of Pharmacy, Belgrade University, Belgrade

Master Education | 2011 - 2016 (SUMMA CUM LAUDE)

CERTIFICATES

TELC Deutsch B2, 2019

Fachsprachprüfung für Apotheker C1, 2019

Certificate in Advanced English C1, 2016

iGRAD : Good Scientific Practice,

Leadership skills, Success in Companies,

Writing paper in Life Sciences, 2018-2019

SCHOLARSHIPS

- Research Grants- Doctoral Programs in Germany, 2017/2018, German Academic Exchange Service (DAAD, 2017-2021)
- Scholarship for the best students at the universities of the member states of the European Union and the European Free Trade Association, Government of Republic of Serbia (2018)
- Scholarship for top talented students, Government of Republic of Serbia (2014-2016)